City of San Diego
PUBLIC UTILITIES
Water & Wastewater

Application For Renewal of NPDES CA0107409 and 301(h) Modified Secondary Treatment Requirements

POINT LOMA OCEAN OUTFALL

Volume VI
Appendices E thru H

January 2015

THE CITY OF SAN DIEGO PUBLIC UTILITIES DEPARTMENT

Application for Renewal of NPDES CA0107409

301(h) Modified Secondary Treatment Requirements for Biochemical Oxygen Demand and Total Suspended Solids

POINT LOMA OCEAN OUTFALL &

POINT LOMA WASTEWATER TREATMENT PLANT

Submitted pursuant to
Sections 301(h) and 301(j)(5) of the Clean Water Act

City of San Diego
Public Utilities Department
9192 Topaz Way
San Diego, CA 92123
(858) 292-6401

January 2015

APPLICATION FOR RENEWAL OF NPDES CA0107409
301(h) MODIFIED SECONDARY TREATMENT REQUIREMENTS

Point Loma Ocean Outfall
Point Loma Wastewater Treatment Plant

VOLUME VI
APPENDICES E thru H

Appendix E **Sources of PCB Contamination**

Appendix F **Point Loma Ocean Outfall Plume Behavior Study**

Appendix G **Kelp Forest Ecosystem Monitoring Report**

Appendix H **Coastal Remote Sensing Annual Reports**

LIST OF VOLUMES

Volume I	**Executive Summary**	
Volume II	**Part 1 - Basis of Application** **Part 2 - NPDES Application Forms** **Part 3 - Antidegradation Analysis**	
Volume III	**Large Applicant Questionnaire**	
Volume IV	**Appendix A**	**Existing Metro System Facilities and Operations**
	Appendix B	**Future Metro System Facilities** ***B.1 Planned Metro System Facilities Improvements*** ***B.2 2012 Recycled Water Study*** ***B.3 Water Purification Demonstration Project Report***
Volume V	**Appendix C**	**Ocean Benthic Conditions** ***C.1 Benthic Sediments, Invertebrates and Fishes*** ***C.2 San Diego Benthic Tolerance Intervals*** ***C.3 San Diego Regional Sediment Quality Contour Plots*** ***C.4 San Diego Sediment Mapping Study*** ***C.5 Deep Benthic Habitat Assessment Study***
	Appendix D	**Bioaccumulation Assessment**
Volume VI	**Appendix E**	**Sources of PCB Contamination**
	Appendix F	**Point Loma Ocean Outfall Plume Behavior Study**
	Appendix G	**Kelp Forest Ecosystem Monitoring Report**
	Appendix H	**Coastal Remote Sensing Annual Reports**
Volume VII	**Appendix I**	**Beneficial Use Assessment** ***I.1 Beneficial Use Evaluation*** ***I.2 Compliance with Recreational Body Contact Standards***
	Appendix J	**Endangered Species**
	Appendix K	**Essential Fish Habitat Assessment**
	Appendix L	**Proposed Monitoring Program**
Volume VIII	**Appendix M**	**2013 Annual Biosolids Report**
Volume IX	**Appendix N**	**Source Control Program**
	Appendix O	**2013 Annual Pretreatment Report**
Volume X	**Appendix P**	**Oceanography**
	Appendix Q	**Initial Dilution Simulation Models**
	Appendix R	**Re-entrainment**
	Appendix S	**Dissolved Oxygen Demand**
	Appendix T	**Analysis of Ammonia**
	Appendix U	**2012 California Ocean Plan**
	Appendix V	**Correspondence**

Appendix E
SOURCES OF PCB CONTAMINATION

Renewal of NPDES CA0107409

APPENDIX E

SOURCES OF PCB CONTAMINATION

January 2015

APPENDIX E

Sources of PCB Contamination

Table of Contents

APPENDIX E.1 – PCBs in PLWTP Wastewater

Meyer, S., and J. McAnally. 2008. PCB Congeners in the Point Loma Wastewater Treatment Plant and other Metro waste streams – Fall 2007. City of San Diego Wastewater Chemistry Section Technical Report (February 13, 2008), p. 17.

APPENDIX E.2 – PCBs in San Diego Fishes

Parnell, P.E., A.K. Groce, T.D. Stebbins, and P.K. Dayton. 2008. Discriminating sources of PCB contamination in fish on the coastal shelf off San Diego, California (USA). Marine Pollution Bulletin, 56: 1992–2002.

Appendix E.1

PCBs in PLWTP Wastewater

THE CITY OF SAN DIEGO
MAYOR JERRY SANDERS

TECHNICAL REPORT

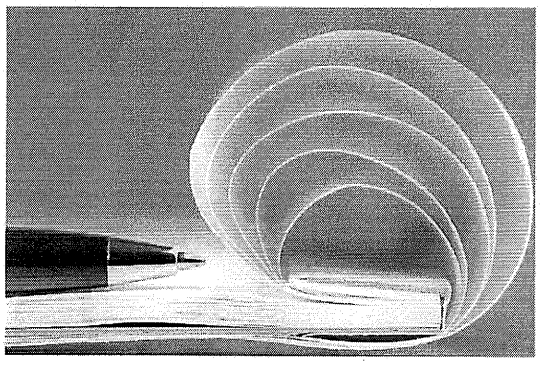

PCB Congeners in the Point Loma Wastewater Treatment Plant & Other Metro Waste Streams - Fall 2007

DATE: Feb 13 2008

By: Jeffrey McAnally, Associate Chemist, MWWD,EMTS,WCS
Steve Meyer, Senior Chemist

City of San Diego
Wastewater Chemistry Section
Environmental Monitoring and Technical Services Division
5530 Kiowa Drive * Mail Station 85A * La Mesa * CA 91942
Tel (619) 6668-3215 * Fax (619) 668-3284
Email: jmcanally@sandiego.gov
Email: smeyer@sandiego.gov

Contents:

1. Executive Summary 3
2. Background 3
3. Methodology 4
4. Results 5
5. Conclusions 5
Appendix A, Summary Data Tables 6
Appendix B – QC and Batch Data Sheet 16
Endnotes: 17

1. Executive Summary

In this study our goal was to determine if target[1] PCB congeners were present in Pt Loma Wastewater Treatment Plant (WWTP) influent and effluent. A total of 28 Influent and effluent samples were taken between September and December 2007. No PCB congeners were identified in any sample. It is highly unlikely that PCBs are a significant pollutant, if present at all, in wastewater streams at the Pt. Loma WWTP.

An additional 17 samples from the Metro system plants were also analyzed for PCB congeners including SBWRP and NCWRP influents, effluents, reclaimed water, and other treatment products (e.g. primary effluent, raw and digested sludge, etc.). No PCB congeners were detected in any sample.

2. Background[2]

Metro began analyzing for PCBs in wastewater as Total PCBs in 1978, although we did not identify individual aroclors or congeners. Improved technology and methods introduced in 1985 resulted in more sensitive and robust analyses and we began monitoring and reporting aroclors in 1986. The prior positive results occasionally determined were not reproducible in subsequent analyses. No PCB aroclors have been identified in influent or effluent at Pt. Loma WWWTP for over 21-years (1986-today) nor from SBWRP since monitoring began in 2002.

Ocean monitoring for PCBs began many years ago in ocean sediments (began in 1985) and fish tissue (began in-house analyses in late 1995). Originally PCB determinations in sediments, as in effluent, were for aroclors. In 1998 the NPDES permit was changed, stipulating congeners be determined vs. aroclors. This aligned the Monitoring and Reporting Programs (MRP) for sediments and fish tissue so that PCBs were determined as congeners in all ocean samples [although not for influent and effluent monitoring]. Determinations are for the 41 (out of 209) congeners that was developed jointly with the scientific and regulatory community as those identified as having significance to the Southern California Bight and were included in the MRPs for both Pt. Loma and SBWRP (South Bay Water Reclamation Plant).

Current analytical methodology provides high sensitivity and specificity in the determination of PCB congeners to low parts per billion (ppb) and parts per trillion (ppt) levels. Detection limits in fish tissue determinations are somewhat ambiguous due to the highly variable nature of fish tissue from species to species and tissue type. MDLS (Method Detection Limits) for Aroclors in wastewater range from <1 ppb to 4 ppb. No

---

[1] There are 209 individual PCB congeners, however certain congeners are in much higher percentages for each Aroclor and can serve as markers. This study follows the Southern California Bight Study consensus list of 40-congeners that represent the range of significant potential environmental pollutants. This list is based upon history of use, expectation of toxicity, chlorination level, and previous detected presence in the environment.

[2] Also see the White Paper of October 1, 2007 by Steve Meyer.

empirical work on MDLs in wastewater has been done for congeners, it would be a reasonable estimate that MDLs would be an order of magnitude lower, along with significantly greater confidence in qualitative identification (i.e. less change of a false positive).

Wastewater MRPs still stipulate monitoring for aroclors rather than congeners for effluent, while the ocean monitoring is strictly on congeners. Direct comparison is impossible at this point and I would note that any guess is speculation, but it is possible that we might see PCB congeners in influent or effluent if we apply the same methodology.

Beginning in September 2007 the regularly sampled influent and effluent wastewaters from Point Loma Wastewater Treatment plant were analyzed for PCB's as congeners in addition to our regular testing for Aroclor's. Our normal EPA Method 608 is capable of allowing single peak PCB congener identification to take place during the normal course of chlorinated pesticide testing. The necessary modification was simply an instrumental software adjustment using a method from our existing congener analysis in sediments and fish.

3. Methodology

Samples for these determinations were taken on regular monitoring schedule between September 2007 and December 2007. A one liter aliquot of each regular monitoring sample from the Pt. Loma WWTP were extracted with methylene chloride using the standard procedure for EPA Method 608. The solvent is exchanged with hexane. The sample extract is concentrated by distillation in a TurboVap 500 apparatus. A Florisil clean-up procedure is performed using hexane-ether. After the Florisil clean-up, a final concentration is done with a TurboVap 500 apparatus and then diluted to ten milliliters. To remove sulfur, a mercury clean-up procedure is performed to the concentrated sample. The clean extract was analyzed by GC/ECD/MS (Gas Chromatography/Electron Capture Detector and Mass Selective Detector). For these determinations, the sample aliquots were treated with PCB congener surrogates and a separate aliquot of the 608 concentrated extract was run on GC-ECD/MSD.

The method is adapted from the procedures in EPA Method 608 and SW-846 Method 8082A. Qualitative determination was made with a Varian 3800 Ion Trap Mass Spectrometer following separation by capillary column gas chromatography. This instrument , methods, and operating conditions mirrored those in use for congener determinations as regularly performed for all congener analysis methods used in the lab. The industry standard DBXLB column was used and mated with and Electron Capture Detector and an Ion Trap Mass Spectrometer.

A low level PCB congener standard (0.625 ppb) containing all of the target congeners was analyzed and chromatographic data from the influent and effluent samples was evaluated against the standard information. Peaks at relative retention times and presence of parent and daughter ions were the qualitative criteria used to judge detection. While a

complete Method Detection Limit experiment was not performed for this study, estimated detectable concentrations for the most abundant congeners (in wastewater) range from 0.4 – 0.8 ppb.

4. Results

No PCB congeners were found in either the influent or effluent samples.

5. Conclusions

This study captured a significantly broad time span and at sufficiently low levels (0.4-0.8 ppb) that PCB congeners, if present, would have been identified. It is highly unlikely that PCBs are a significant pollutant, if present at all, in wastewater streams at the Pt. Loma WWTP.

Although limited, the studies included samples from critical system waste streams that would be likely to show the presence of PCB congeners if any were present. The raw and digested sludge (sewage solids) samples also serve as concentrators of pollutants and no PCBs were detected in those streams.

There is no approved method published in the Federal Register or acknowledged by California DHS, ELAP for PCB congener determinations in wastewater. However, the methodology used for this study is robust enough to be used on a regular basis if necessary.

Appendix A, Summary Data Tables

Point Loma Special Study
PCB Congeners in Effluent and Influent

PCB Congeners							
Sample ID	**P397986**	**P397986**	**P397989**	**P398940**	**P398940**	**P398943**	
Sample Source	**P.Loma Effluent**	**P.Loma Effluent**	**P. Loma Influent**	**P.Loma Effluent**	**P.Loma Effluent**	**P.Loma Influent**	
Sample Date	**PLE 3-Sep-07**	**PLE DUP 3-Sep-07**	**PLR 3-Sep-07**	**PLE 11-Sep-07**	**PLE DUP 11-Sep-07**	**PLR 11-Sep-07**	
Analyte							
PCB 18	nd	nd	nd	nd	nd	nd	
PCB 28	nd	nd	nd	nd	nd	nd	
PCB 52	nd	nd	nd	nd	nd	nd	
PCB 49	nd	nd	nd	nd	nd	nd	
PCB 44	nd	nd	nd	nd	nd	nd	
PCB 37	nd	nd	nd	nd	nd	nd	
PCB 74	nd	nd	nd	nd	nd	nd	
PCB 70	nd	nd	nd	nd	nd	nd	
PCB 66	nd	nd	nd	nd	nd	nd	
PCB 101	nd	nd	nd	nd	nd	nd	
PCB 99	nd	nd	nd	nd	nd	nd	
PCB 119	nd	nd	nd	nd	nd	nd	
PCB 87	nd	nd	nd	nd	nd	nd	
PCB 110	nd	nd	nd	nd	nd	nd	
PCB 81	nd	nd	nd	nd	nd	nd	
PCB 151	nd	nd	nd	nd	nd	nd	
PCB 77	nd	nd	nd	nd	nd	nd	
PCB 149	nd	nd	nd	nd	nd	nd	
PCB 123	nd	nd	nd	nd	nd	nd	
PCB 118	nd	nd	nd	nd	nd	nd	
PCB 114	nd	nd	nd	nd	nd	nd	
PCB 153/168	nd	nd	nd	nd	nd	nd	
PCB 105	nd	nd	nd	nd	nd	nd	
PCB 138	nd	nd	nd	nd	nd	nd	
PCB 158	nd	nd	nd	nd	nd	nd	
PCB 187	nd	nd	nd	nd	nd	nd	
PCB 183	nd	nd	nd	nd	nd	nd	
PCB 126	nd	nd	nd	nd	nd	nd	
PCB 128	nd	nd	nd	nd	nd	nd	
PCB 167	nd	nd	nd	nd	nd	nd	
PCB 177	nd	nd	nd	nd	nd	nd	
PCB 156	nd	nd	nd	nd	nd	nd	
PCB 157	nd	nd	nd	nd	nd	nd	
PCB 180	nd	nd	nd	nd	nd	nd	
PCB 170	nd	nd	nd	nd	nd	nd	
PCB 201	nd	nd	nd	nd	nd	nd	
PCB 169	nd	nd	nd	nd	nd	nd	
PCB 189	nd	nd	nd	nd	nd	nd	
PCB 194	nd	nd	nd	nd	nd	nd	
PCB 206	nd	nd	nd	nd	nd	nd	

Point Loma Special Study
PCB Congeners in Effluent and Influent

PCB Congeners							
Sample ID	**P400006**	**P400006**	**P400009**				
Sample Source	**P.Loma Effluent**	**P.Loma Effluent**	**P. Loma Influent**				
Sample Date	**PLE 19-Sep-07**	**PLE DUP 19-Sep-07**	**PLR 19-Sep-07**				
Analyte							
PCB 18	nd	nd	nd				
PCB 28	nd	nd	nd				
PCB 52	nd	nd	nd				
PCB 49	nd	nd	nd				
PCB 44	nd	nd	nd				
PCB 37	nd	nd	nd				
PCB 74	nd	nd	nd				
PCB 70	nd	nd	nd				
PCB 66	nd	nd	nd				
PCB 101	nd	nd	nd				
PCB 99	nd	nd	nd				
PCB 119	nd	nd	nd				
PCB 87	nd	nd	nd				
PCB 110	nd	nd	nd				
PCB 81	nd	nd	nd				
PCB 151	nd	nd	nd				
PCB 77	nd	nd	nd				
PCB 149	nd	nd	nd				
PCB 123	nd	nd	nd				
PCB 118	nd	nd	nd				
PCB 114	nd	nd	nd				
PCB 153/168	nd	nd	nd				
PCB 105	nd	nd	nd				
PCB 138	nd	nd	nd				
PCB 158	nd	nd	nd				
PCB 187	nd	nd	nd				
PCB 183	nd	nd	nd				
PCB 126	nd	nd	nd				
PCB 128	nd	nd	nd				
PCB 167	nd	nd	nd				
PCB 177	nd	nd	nd				
PCB 156	nd	nd	nd				
PCB 157	nd	nd	nd				
PCB 180	nd	nd	nd				
PCB 170	nd	nd	nd				
PCB 201	nd	nd	nd				
PCB 169	nd	nd	nd				
PCB 189	nd	nd	nd				
PCB 194	nd	nd	nd				
PCB 206	nd	nd	nd				

Point Loma Special Study
PCB Congeners in Effluent and Influent

October PCB Congeners							
Sample ID	**P399261**	**P399266**	**P399281**	**P399286**	**P399291**	**P399296**	**P403205**
Sample Source	**P.Loma Effluent**	**P.Loma Influent**	**N01 PS Influent**	**N01 PEN[i] Influent**	**N10 [ii]Effluent**	**N34 Rec[iii] Water**	**P.Loma Effluent**
Sample Date	**Oct-02-07**	**Oct-02-07**	**Oct-02-07**	**Oct-02-07**	**Oct-02-07**	**Oct-02-07**	**Oct-13-07**
Analyte							
PCB 18	nd	nd	nd	nd	nd	nd	nd
PCB 28	nd	nd	nd	nd	nd	nd	nd
PCB 52	nd	nd	nd	nd	nd	nd	nd
PCB 49	nd	nd	nd	nd	nd	nd	nd
PCB 44	nd	nd	nd	nd	nd	nd	nd
PCB 37	nd	nd	nd	nd	nd	nd	nd
PCB 74	nd	nd	nd	nd	nd	nd	nd
PCB 70	nd	nd	nd	nd	nd	nd	nd
PCB 66	nd	nd	nd	nd	nd	nd	nd
PCB 101	nd	nd	nd	nd	nd	nd	nd
PCB 99	nd	nd	nd	nd	nd	nd	nd
PCB 119	nd	nd	nd	nd	nd	nd	nd
PCB 87	nd	nd	nd	nd	nd	nd	nd
PCB 110	nd	nd	nd	nd	nd	nd	nd
PCB 81	nd	nd	nd	nd	nd	nd	nd
PCB 151	nd	nd	nd	nd	nd	nd	nd
PCB 77	nd	nd	nd	nd	nd	nd	nd
PCB 149	nd	nd	nd	nd	nd	nd	nd
PCB 123	nd	nd	nd	nd	nd	nd	nd
PCB 118	nd	nd	nd	nd	nd	nd	nd
PCB 114	nd	nd	nd	nd	nd	nd	nd
PCB 153/168	nd	nd	nd	nd	nd	nd	nd
PCB 105	nd	nd	nd	nd	nd	nd	nd
PCB 138	nd	nd	nd	nd	nd	nd	nd
PCB 158	nd	nd	nd	nd	nd	nd	nd
PCB 187	nd	nd	nd	nd	nd	nd	nd
PCB 183	nd	nd	nd	nd	nd	nd	nd
PCB 126	nd	nd	nd	nd	nd	nd	nd
PCB 128	nd	nd	nd	nd	nd	nd	nd
PCB 167	nd	nd	nd	nd	nd	nd	nd
PCB 177	nd	nd	nd	nd	nd	nd	nd
PCB 156	nd	Nd	nd	nd	nd	nd	nd
PCB 157	nd	Nd	nd	nd	nd	nd	nd
PCB 180	nd	Nd	nd	nd	nd	nd	nd
PCB 170	nd	Nd	nd	nd	nd	nd	nd
PCB 201	nd	Nd	nd	nd	nd	nd	nd
PCB 169	nd	Nd	nd	nd	nd	nd	nd
PCB 189	nd	Nd	nd	nd	nd	nd	nd
PCB 194	nd	Nd	nd	nd	nd	nd	nd
PCB 206	nd	Nd	nd	nd	nd	nd	nd

Point Loma Special Study
PCB Congeners in Effluent and Influent

October PCB Congeners							
Sample ID	**P403208**	**P403958**	**P403961**	**P404936**	**P404939**	**P399377**	**P399372**
Sample Source	**P.Loma Influent**	**P.Loma Effluent**	**P.Loma Influent**	**P.Loma Effluent**	**P.Loma Influent**	**South B[iv]. Outfall**	**South B. Influent**
Sample Date	**Oct-13-07**	**Oct-21-07**	**Oct-21-07**	**Oct-29-07**	**Oct-29-07**	**Oct-02-07**	**Oct-02-07**
Analyte							
PCB 18	nd	nd	nd	nd	nd	nd	nd
PCB 28	nd	nd	nd	nd	nd	nd	nd
PCB 52	nd	nd	nd	nd	nd	nd	nd
PCB 49	nd	nd	nd	nd	nd	nd	nd
PCB 44	nd	nd	nd	nd	nd	nd	nd
PCB 37	nd	nd	nd	nd	nd	nd	nd
PCB 74	nd	nd	nd	nd	nd	nd	nd
PCB 70	nd	nd	nd	nd	nd	nd	nd
PCB 66	nd	nd	nd	nd	nd	nd	nd
PCB 101	nd	nd	nd	nd	nd	nd	nd
PCB 99	nd	nd	nd	nd	nd	nd	nd
PCB 119	nd	nd	nd	nd	nd	nd	nd
PCB 87	nd	nd	nd	nd	nd	nd	nd
PCB 110	nd	nd	nd	nd	nd	nd	nd
PCB 81	nd	nd	nd	nd	nd	nd	nd
PCB 151	nd	nd	nd	nd	nd	nd	nd
PCB 77	nd	nd	nd	nd	nd	nd	nd
PCB 149	nd	nd	nd	nd	nd	nd	nd
PCB 123	nd	nd	nd	nd	nd	nd	nd
PCB 118	nd	nd	nd	nd	nd	nd	nd
PCB 114	nd	nd	nd	nd	nd	nd	nd
PCB 153/168	Nd	nd	nd	nd	nd	nd	nd
PCB 105	nd	nd	nd	nd	nd	nd	nd
PCB 138	nd	nd	nd	nd	nd	nd	nd
PCB 158	nd	nd	nd	nd	nd	nd	nd
PCB 187	nd	nd	nd	nd	nd	nd	nd
PCB 183	nd	nd	nd	nd	nd	nd	nd
PCB 126	nd	nd	nd	nd	nd	nd	nd
PCB 128	nd	nd	nd	nd	nd	nd	nd
PCB 167	nd	nd	nd	nd	nd	nd	nd
PCB 177	nd	nd	nd	nd	nd	nd	nd
PCB 156	nd	nd	nd	nd	nd	nd	nd
PCB 157	nd	nd	nd	nd	nd	nd	nd
PCB 180	nd	nd	nd	nd	nd	nd	nd
PCB 170	nd	nd	nd	nd	nd	nd	nd
PCB 201	nd	nd	nd	nd	nd	nd	nd
PCB 169	nd	nd	nd	nd	nd	nd	nd
PCB 189	nd	nd	nd	nd	nd	nd	nd
PCB 194	nd	nd	nd	nd	nd	nd	nd
PCB 206	nd	nd	nd	nd	nd	nd	nd

Point Loma Special Study
PCB Congeners in Effluent and Influent

October PCB Congeners							
Sample ID Sample Source Sample Date	P399382 South B. ITP Comb[v] Oct-02-07	P399387 South B. PRIEFF Oct-02-07	P399392 SB SEC Effluent Oct-02-07	P399315 Digested Composite[vi] Oct-02-07	P399301 Raw Composite[vii] Oct-02-07	P399276 MBC Comb[viii] Oct-02-07	P399328 MBC NC RSL Oct-02-07
Analyte							
PCB 18	nd	nd	nd	nd	nd	nd	nd
PCB 28	nd	nd	nd	nd	nd	nd	nd
PCB 52	nd	nd	nd	nd	nd	nd	nd
PCB 49	nd	nd	nd	nd	nd	nd	nd
PCB 44	nd	nd	nd	nd	nd	nd	nd
PCB 37	nd	nd	nd	nd	nd	nd	nd
PCB 74	nd	nd	nd	nd	nd	nd	nd
PCB 70	nd	nd	nd	nd	nd	nd	nd
PCB 66	nd	nd	nd	nd	nd	nd	nd
PCB 101	nd	nd	nd	nd	nd	nd	nd
PCB 99	nd	nd	nd	nd	nd	nd	nd
PCB 119	nd	nd	nd	nd	nd	nd	nd
PCB 87	nd	nd	nd	nd	nd	nd	nd
PCB 110	nd	nd	nd	nd	nd	nd	nd
PCB 81	nd	nd	nd	nd	nd	nd	nd
PCB 151	nd	nd	nd	nd	nd	nd	nd
PCB 77	nd	nd	nd	nd	nd	nd	nd
PCB 149	nd	nd	nd	nd	nd	nd	nd
PCB 123	nd	nd	nd	nd	nd	nd	nd
PCB 118	nd	nd	nd	nd	nd	nd	nd
PCB 114	nd	nd	nd	nd	nd	nd	nd
PCB 153/168	nd	nd	nd	nd	nd	nd	nd
PCB 105	nd	nd	nd	nd	nd	nd	nd
PCB 138	nd	nd	nd	nd	nd	nd	nd
PCB 158	nd	nd	nd	nd	nd	nd	nd
PCB 187	nd	nd	nd	nd	nd	nd	nd
PCB 183	nd	nd	nd	nd	nd	nd	nd
PCB 126	nd	nd	nd	nd	nd	nd	nd
PCB 128	nd	nd	nd	nd	nd	nd	nd
PCB 167	nd	nd	nd	nd	nd	nd	nd
PCB 177	nd	nd	nd	nd	nd	nd	nd
PCB 156	nd	nd	nd	nd	nd	nd	nd
PCB 157	nd	nd	nd	nd	nd	nd	nd
PCB 180	nd	nd	nd	nd	nd	nd	nd
PCB 170	nd	nd	nd	nd	nd	nd	nd
PCB 201	nd	nd	nd	nd	nd	nd	nd
PCB 169	nd	nd	nd	nd	nd	nd	nd
PCB 189	nd	nd	nd	nd	nd	nd	nd
PCB 194	nd	nd	nd	nd	nd	nd	nd
PCB 206	nd	nd	nd	nd	nd	nd	nd

Point Loma Special Study
PCB Congeners in Effluent and Influent

October PCB Congeners							
Sample ID **Sample Source** **Sample Date**	**P399330** **MBC NC** **DSL** **Oct-02-07**	**P399404** **South B.** **RSL 10** **Oct-02-07**					
Analyte							
PCB 18	nd	nd					
PCB 28	nd	nd					
PCB 52	nd	nd					
PCB 49	nd	nd					
PCB 44	nd	nd					
PCB 37	nd	nd					
PCB 74	nd	nd					
PCB 70	nd	nd					
PCB 66	nd	nd					
PCB 101	nd	nd					
PCB 99	nd	nd					
PCB 119	nd	nd					
PCB 87	nd	nd					
PCB 110	nd	nd					
PCB 81	nd	nd					
PCB 151	nd	nd					
PCB 77	nd	nd					
PCB 149	nd	nd					
PCB 123	nd	nd					
PCB 118	nd	nd					
PCB 114	nd	nd					
PCB 153/168	nd	nd					
PCB 105	nd	nd					
PCB 138	nd	nd					
PCB 158	nd	nd					
PCB 187	nd	nd					
PCB 183	nd	nd					
PCB 126	nd	nd					
PCB 128	nd	nd					
PCB 167	nd	nd					
PCB 177	nd	nd					
PCB 156	nd	nd					
PCB 157	nd	nd					
PCB 180	nd	nd					
PCB 170	nd	nd					
PCB 201	nd	nd					
PCB 169	nd	nd					
PCB 189	nd	nd					
PCB 194	nd	nd					
PCB 206	nd	nd					

Point Loma Special Study
PCB Congeners in Effluent and Influent

PCB Congeners							
Sample ID	**P405770**	**P405770**	**P405548**	**P405773**	**P406880**	**P406880**	**P406883**
Sample Source	**P. Loma Effluent**	**P. Loma Effluent DUP**	**S. Bay Outfall**	**P. Loma Influent**	**P. Loma Effluent**	**P. Loma Effluent DUP**	**P. Loma Influent**
Sample Date	**Nov-06-07**	**Nov-06-07**	**Nov-07-07**	**Nov-06-07**	**Nov-14-07**	**Nov-14-07**	**Nov-14-07**
Analyte							
PCB 18	nd	nd	nd	nd	nd	nd	nd
PCB 28	nd	nd	nd	nd	nd	nd	nd
PCB 52	nd	nd	nd	nd	nd	nd	nd
PCB 49	nd	nd	nd	nd	nd	nd	nd
PCB 44	nd	nd	nd	nd	nd	nd	nd
PCB 37	nd	nd	nd	nd	nd	nd	nd
PCB 74	nd	nd	nd	nd	nd	nd	nd
PCB 70	nd	nd	nd	nd	nd	nd	nd
PCB 66	nd	nd	nd	nd	nd	nd	nd
PCB 101	nd	nd	nd	nd	nd	nd	nd
PCB 99	nd	nd	nd	nd	nd	nd	nd
PCB 119	nd	nd	nd	nd	nd	nd	nd
PCB 87	nd	nd	nd	nd	nd	nd	nd
PCB 110	nd	nd	nd	nd	nd	nd	nd
PCB 81	nd	nd	nd	nd	nd	nd	nd
PCB 151	nd	nd	nd	nd	nd	nd	nd
PCB 77	nd	nd	nd	nd	nd	nd	nd
PCB 149	nd	nd	nd	nd	nd	nd	nd
PCB 123	nd	nd	nd	nd	nd	nd	nd
PCB 118	nd	nd	nd	nd	nd	nd	nd
PCB 114	nd	nd	nd	nd	nd	nd	nd
PCB 153/168	nd	nd	nd	nd	nd	nd	nd
PCB 105	nd	nd	nd	nd	nd	nd	nd
PCB 138	nd	nd	nd	nd	nd	nd	nd
PCB 158	nd	nd	nd	nd	nd	nd	nd
PCB 187	nd	nd	nd	nd	nd	nd	nd
PCB 183	nd	nd	nd	nd	nd	nd	nd
PCB 126	nd	nd	nd	nd	nd	nd	nd
PCB 128	nd	nd	nd	nd	nd	nd	nd
PCB 167	nd	nd	nd	nd	nd	nd	nd
PCB 177	nd	nd	nd	nd	nd	nd	nd
PCB 156	nd	nd	nd	nd	nd	nd	nd
PCB 157	nd	nd	nd	nd	nd	nd	nd
PCB 180	nd	nd	nd	nd	nd	nd	nd
PCB 170	nd	nd	nd	nd	nd	nd	nd
PCB 201	nd	nd	nd	nd	nd	nd	nd
PCB 169	nd	nd	nd	nd	nd	nd	nd
PCB 189	nd	nd	nd	nd	nd	nd	nd
PCB 194	nd	nd	nd	nd	nd	nd	nd
PCB 206	nd	nd	nd	nd	nd	nd	nd

Point Loma Special Study
PCB Congeners in Effluent and Influent

PCB Congeners							
Sample ID	**P407920**	**P407920**	**P407923**	**P408859**	**P408859**	**P408862**	
Sample Source	**P. Loma Effluent**	**P. Loma Effluent**	**P. Loma Influent**	**P. Loma Effluent**	**P. Loma Effluent**	**P. Loma Influent**	
Sample Date	**Nov-22-07**	**Nov-22-07**	**Nov-22-07**	**Nov-30-07**	**Nov-30-07**	**Nov-30-07**	
Analyte							
PCB 18	nd	nd	nd	nd	nd	nd	nd
PCB 28	nd	nd	nd	nd	nd	nd	nd
PCB 52	nd	nd	nd	nd	nd	nd	nd
PCB 49	nd	nd	nd	nd	nd	nd	nd
PCB 44	nd	nd	nd	nd	nd	nd	nd
PCB 37	nd	nd	nd	nd	nd	nd	nd
PCB 74	nd	nd	nd	nd	nd	nd	nd
PCB 70	nd	nd	nd	nd	nd	nd	nd
PCB 66	nd	nd	nd	nd	nd	nd	nd
PCB 101	nd	nd	nd	nd	nd	nd	nd
PCB 99	nd	nd	nd	nd	nd	nd	nd
PCB 119	nd	nd	nd	nd	nd	nd	nd
PCB 87	nd	nd	nd	nd	nd	nd	nd
PCB 110	nd	nd	nd	nd	nd	nd	nd
PCB 81	nd	nd	nd	nd	nd	nd	nd
PCB 151	nd	nd	nd	nd	nd	nd	nd
PCB 77	nd	nd	nd	nd	nd	nd	nd
PCB 149	nd	nd	nd	nd	nd	nd	nd
PCB 123	nd	nd	nd	nd	nd	nd	nd
PCB 118	nd	nd	nd	nd	nd	nd	nd
PCB 114	nd	nd	nd	nd	nd	nd	nd
PCB 153/168	nd	nd	nd	nd	nd	nd	nd
PCB 105	nd	nd	nd	nd	nd	nd	nd
PCB 138	nd	nd	nd	nd	nd	nd	nd
PCB 158	nd	nd	nd	nd	nd	nd	nd
PCB 187	nd	nd	nd	nd	nd	nd	nd
PCB 183	nd	nd	nd	nd	nd	nd	nd
PCB 126	nd	nd	nd	nd	nd	nd	nd
PCB 128	nd	nd	nd	nd	nd	nd	nd
PCB 167	nd	nd	nd	nd	nd	nd	nd
PCB 177	nd	nd	nd	nd	nd	nd	nd
PCB 156	nd	nd	nd	nd	nd	nd	nd
PCB 157	nd	Nd	nd	nd	nd	nd	nd
PCB 180	nd	Nd	nd	nd	nd	nd	nd
PCB 170	nd	Nd	nd	nd	nd	nd	nd
PCB 201	nd	Nd	nd	nd	nd	nd	nd
PCB 169	nd	Nd	nd	nd	nd	nd	nd
PCB 189	nd	Nd	nd	nd	nd	nd	nd
PCB 194	nd	Nd	nd	nd	nd	nd	nd
PCB 206	nd	Nd	nd	nd	nd	nd	nd

Point Loma Special Study
PCB Congeners in Effluent and Influent

PCB Congeners							
Sample ID	**P409640**	**P409640**	**P409104**	**P409643**	**P410668**	**P410668**	**P410671**
Sample Source	**P.Loma Effluent**	**P.Loma Effluent DUP**	**S.Bay Outfall**	**P.Loma Influent**	**P.Loma Effluent**	**P.Loma Effluent DUP**	**P.Loma Influent**
Sample Date	**Dec-08-07**	**Dec-08-07**	**Dec-05-07**	**Dec-08-07**	**Dec-16-07**	**Dec-16-07**	**Dec-16-07**
Analyte							
PCB 18	nd	nd	nd	nd	nd	nd	nd
PCB 28	nd	nd	nd	nd	nd	nd	nd
PCB 52	nd	nd	nd	nd	nd	nd	nd
PCB 49	nd	nd	nd	nd	nd	nd	nd
PCB 44	nd	nd	nd	nd	nd	nd	nd
PCB 37	nd	nd	nd	nd	nd	nd	nd
PCB 74	nd	nd	nd	nd	nd	nd	nd
PCB 70	nd	nd	nd	nd	nd	nd	nd
PCB 66	nd	nd	nd	nd	nd	nd	nd
PCB 101	nd	nd	nd	nd	nd	nd	nd
PCB 99	nd	nd	nd	nd	nd	nd	nd
PCB 119	nd	nd	nd	nd	nd	nd	nd
PCB 87	nd	nd	nd	nd	nd	nd	nd
PCB 110	nd	nd	nd	nd	nd	nd	nd
PCB 81	nd	nd	nd	nd	nd	nd	nd
PCB 151	nd	nd	nd	nd	nd	nd	nd
PCB 77	nd	nd	nd	nd	nd	nd	nd
PCB 149	nd	nd	nd	nd	nd	nd	nd
PCB 123	nd	nd	nd	nd	nd	nd	nd
PCB 118	nd	nd	nd	nd	nd	nd	nd
PCB 114	nd	nd	nd	nd	nd	nd	nd
PCB 153/168	nd	nd	nd	nd	nd	nd	nd
PCB 105	nd	nd	nd	nd	nd	nd	nd
PCB 138	nd	nd	nd	nd	nd	nd	nd
PCB 158	nd	nd	nd	nd	nd	nd	nd
PCB 187	nd	nd	nd	nd	nd	nd	nd
PCB 183	nd	nd	nd	nd	nd	nd	nd
PCB 126	nd	nd	nd	nd	nd	nd	nd
PCB 128	nd	nd	nd	nd	nd	nd	nd
PCB 167	nd	nd	nd	nd	nd	nd	nd
PCB 177	nd	nd	nd	nd	nd	nd	nd
PCB 156	nd	nd	nd	nd	nd	nd	nd
PCB 157	nd	nd	nd	nd	nd	nd	nd
PCB 180	nd	nd	nd	nd	nd	nd	nd
PCB 170	nd	nd	nd	nd	nd	nd	nd
PCB 201	nd	nd	nd	nd	nd	nd	nd
PCB 169	nd	nd	nd	nd	nd	nd	nd
PCB 189	nd	nd	nd	nd	nd	nd	nd
PCB 194	nd	nd	nd	nd	nd	nd	nd
PCB 206	nd	nd	nd	nd	nd	nd	nd

Point Loma Special Study
PCB Congeners in Effluent and Influent

PCB Congeners							
Sample ID	**P411681**	**P411681**	**P411684**	**P411681**			
Sample Source	**P.Loma Effluent**	**P.Loma Effluent DUP**	**P.Loma Influent**	**P.Loma Effluent**			
Sample Date	**Dec-24-07**	**Dec-24-07**	**Dec-24-07**	**Dec-24-07**			
Analyte							
PCB 18	7.9	10	22	nd			
PCB 28	nd	Nd	nd	nd			
PCB 52	nd	Nd	nd	nd			
PCB 49	nd	Nd	nd	nd			
PCB 44	nd	Nd	nd	nd			
PCB 37	nd	Nd	nd	nd			
PCB 74	nd	Nd	nd	nd			
PCB 70	nd	Nd	nd	nd			
PCB 66	nd	Nd	nd	nd			
PCB 101	nd	Nd	nd	nd			
PCB 99	nd	Nd	nd	nd			
PCB 119	nd	Nd	nd	nd			
PCB 87	nd	Nd	nd	nd			
PCB 110	nd	nd	nd	nd			
PCB 81	nd	nd	nd	nd			
PCB 151	nd	nd	nd	nd			
PCB 77	nd	nd	nd	nd			
PCB 149	nd	nd	nd	nd			
PCB 123	nd	nd	nd	nd			
PCB 118	nd	nd	nd	nd			
PCB 114	nd	nd	nd	nd			
PCB 153/168	nd	nd	nd	nd			
PCB 105	nd	nd	nd	nd			
PCB 138	nd	nd	nd	nd			
PCB 158	nd	nd	nd	nd			
PCB 187	nd	nd	nd	nd			
PCB 183	nd	nd	nd	nd			
PCB 126	nd	nd	nd	nd			
PCB 128	nd	nd	nd	nd			
PCB 167	nd	nd	nd	nd			
PCB 177	nd	nd	nd	nd			
PCB 156	nd	nd	nd	nd			
PCB 157	nd	nd	nd	nd			
PCB 180	nd	nd	nd	nd			
PCB 170	nd	nd	nd	nd			
PCB 201	nd	nd	nd	nd			
PCB 169	nd	nd	nd	nd			
PCB 189	nd	nd	nd	nd			
PCB 194	nd	nd	nd	nd			
PCB 206	nd	nd	nd	nd			

Appendix B – QC and Batch Data Sheet

Pesticide Group Analysis Evaluation

Batch/Analysis date: 073502P_C77/10-10-07 073777P_C83/11-14-07
073618P_C80/10-11-07 073778P_C87/11-16-07
073619P_C85/10-11-07 073792P_C33/11-15-07
073628P_C91/10-11-07 073798P_C36/11-20-07
073806P_C41/11-16-07 073837P_C71/1-16-08
073812P_C34/1-18-08 08021P_C31/1-18-08
073825P_C40/1-18-08 073461P_C40/1-17-08
073832P_C90/1-18-08 073604P_C64/1-17-08

1. ANALYSIS: (circle one)
Chlorinated Pesticides
Organophosphorus
Organotin Compounds
PCB
PAH
Lipids
(Congeners)

2. SAMPLE INFORMATION
Month/Year Sep/07, Oct/07, Nov/07, Dec/07
Sample Size 1.00 Liter

3. MATRIX (circle one)
(Wastewater)
Fish Tissue
Sludge
Ocean Sediment
Grit
Other

4. EXTRACTION AND CONCENTRATION
Extraction Date 9/7, 9/12, 9/26, 10/9, 10/19, 10/25, 10/30, 10/25, 11/5, 11/21, 11/28, 12/3, 12/10, 12/17, 12/26
Extracted Within Holding Time (Y) N
Analyzed Within Holding Time * (Y) N

5. CHROMATOGRAPHIC ANALYSIS
Rerun: Y (N)

INSTRUMENT
GC/ECD
GC/FPD
(GC/MS)
LC

COLUMNS	
DB-XLB	Quantitative
	Qualitative

MS ion trap Saturn 2000 (qualitative)

MS CONFIRMATION ON HITS: (YES) NO

COELUTED COMPONENTS

Column	Analytes		
* DB-XLB	PCB 18/PAC-9	PCB 41/OP-DDD	PCB 136/OP-DDT
	PCB 66/Heptachlor	PCB 64/Endo-B	
	PP-DDMS/PCB 101	PCB 153/PCB 168	

6. QC INFORMATION

RECOVERIES	LOW	HIGH
CP MIX	—	—
MX-5	—	—
CARP-1	—	—
INT CHK	—	—
ERA QC	—	—
SPIKE	—	—
DUP SPIKE	—	—
BLANK	no PCB's	surrogate

# of Calibration Points Used: 3 (Ø)

R^2	
High	—
Low	—

% Breakdown	
o,p-DDT	—
Endrin	—

7. LOG BOOK INFORMATION

	Standard Used	Book #	Page #
	Spike Solution	No spike	
	Surrogate Solution	No surrogate	
	Standards	WCL-N-157	28 & 83
	Ext Chk Sample	—	—

Extracted by: SV
GC Operated by: SV
Reviewed by:

NOTES

* Samples from batches extracted on 11/2, 11/8, and 11/21 were injected after 40 days of extraction date. However, there is no holding time established for congeners.
(Ø) Used 0.625, 1.25, and 5.0 ppb stds to calibrate. Since the PCB analysis was qualitative, the linearity was not essential.
* Identification of PCBs is not a problem in the MS, even if coelution involving PCB's are present in the GC column DB-XLB.

Endnotes:

---

[i] N01 PEN ≡ North City Water Reclamation Plant (NCWRP) Influent
[ii] N10 Effluent ≡ NCWRP primary effluent.
[iii] N34 Rec Water ≡ NCWRP Reclaimed water.
[iv] SBWRP (South Bay Water Reclamation Plant) effluent to ocean outfall.
[v] International WWTP and SBWRP combined effluent sample.
[vi] PLWWTP Digested sludge composited from aliquots of each digester at the PLWWTP.
[vii] PLWWTP raw sludge composited from samples to primary digesters.
[viii] MBC (Metro Biosolids Center) Return Stream.

Appendix E.2

PCBs in San Diego Fishes

Marine Pollution Bulletin 56 (2008) 1992–2002

Contents lists available at ScienceDirect

Marine Pollution Bulletin

journal homepage: www.elsevier.com/locate/marpolbul

Discriminating sources of PCB contamination in fish on the coastal shelf off San Diego, California (USA)

P. Ed Parnell [a,*], Ami K. Groce [b], Timothy D. Stebbins [b], Paul K. Dayton [a]

[a] Scripps Institution of Oceanography, Integrative Oceanography Division, University of California, San Diego, Mail Code 0227, 9500 Gilman Drive, La Jolla, CA 92093-0227, United States

[b] City of San Diego Marine Biology Laboratory, Metropolitan Wastewater Department, 2392 Kincaid Road, San Diego, CA 92101-0811, United States

ARTICLE INFO

Keywords:
PCB
Pollution
Bioaccumulation
Fish
Wastewater
Dredge disposal

ABSTRACT

Management of coastal ecosystems necessitates the evaluation of pollutant loading based on adequate source discrimination. Monitoring of sediments and fish on the shelf off San Diego has shown that some areas on the shelf are contaminated with polychlorinated biphenyls (PCBs). Here, we present an analysis of PCB contamination in fish on the shelf off San Diego designed to discriminate possible sources. The analysis was complicated by the variability of species available for analysis across the shelf, variable affinities of PCBs among species, and non-detects in the data. We utilized survival regression analysis to account for these complications. We also examined spatial patterns of PCBs in bay and offshore sediments and reviewed more than 20 years of influent and effluent data for local wastewater treatment facilities. We conclude that most PCB contamination in shelf sediments and fish is due to the ongoing practice of dumping contaminated sediments dredged from San Diego Bay.

1. Introduction

Polychlorinated biphenyls (PCBs) are a class of stable, synthetic chlorinated hydrocarbons manufactured and used in the US beginning in 1929 with production peaking in the 1960s. Although their manufacture ended in 1979 due to environmental and human health concerns, PCBs persist as legacy pollutants whose chronic toxicity represents a serious environmental risk. Sediments and food webs in many industrialized bays and watersheds are contaminated with PCBs – a problem that will persist indefinitely due to the stability of PCBs. For example, the marine food webs of all major ports in California are contaminated, and tissues of fish living within these areas typically exhibit PCB concentrations that exceed limits recommended for human consumption (Brown et al., 2006; Davis et al., 2007). Open coastal habitats are generally less impacted because of their higher energy climate and more remote setting. However, practices such as offshore sewage discharge and disposal of sediments dredged from bays and harbors (dredge disposal) are effective highways for contamination of coastal shelves with PCBs and other pollutants.

The major non-advective sources of PCBs to the marine environment during the height of their manufacture and use included aerial deposition, ocean dumping, wastewater discharge, vessel coatings, rainfall, and surface runoff (Mearns et al., 1991). For just the southern California shelf, these PCB sources combined for an estimated total discharge of 44 metric tons in 1971 (SCCWRP, 1973). Presently, source control practices by sewage treatment facilities have drastically reduced PCB concentrations in wastewater to below detection limits (Lyon et al., 2006). However, the discharge of effluent containing low levels of PCBs may still represent an environmental risk. Additionally, mobilization of PCBs from legacy reservoirs within bays or near some ocean outfalls continues to be chronic sources of contamination to shelf food webs (e.g., Zeng et al., 1998).

The presence of PCBs in benthic sediments and fishes collected off San Diego, California (USA) has been observed in studies conducted by the City of San Diego as part of discharge monitoring requirements for operating two ocean outfalls (e.g., see City of San Diego, 2007a,b) or during larger regional surveys of the Southern California Bight (e.g., Allen et al., 1998, 2002a; Noblet et al., 2002; Schiff et al., 2006). Identification of the source(s) of PCB contamination on the San Diego shelf is critical for developing future management decisions with regard to sewage treatment levels, watershed management and sediment disposal practices.

Possible sources of PCBs off San Diego include dispersal of contaminated sediments from San Diego Bay via tidal exchange, wastewater discharge via ocean outfalls, offshore disposal of sediments dredged from the Bay, and surface runoff from local watersheds. PCB contamination of sediments, mussels, and fish within San Diego Bay is well documented (Mearns et al., 1991; Fairey

* Corresponding author.
E-mail addresses: edparnell@ucsd.edu (P. Ed Parnell), agroce@sandiego.gov (A.K. Groce), tstebbins@sandiego.gov (T.D. Stebbins), pkd@coast.ucsd.edu (P.K. Dayton).

0025-326X/$ - see front matter © 2008 Elsevier Ltd. All rights reserved.
doi:10.1016/j.marpolbul.2008.08.023

et al., 1996, 1998; City of San Diego 2003). Wastewater discharge off San Diego is principally through two large ocean outfalls: (a) the Point Loma Ocean Outfall (PLOO), which discharges treated effluent from the Point Loma Wastewater Treatment Plant; (b) the South Bay Ocean Outfall (SBOO), which discharges commingled effluent from the South Bay Water Reclamation Plant and the International Wastewater Treatment Plant. Discharge via the PLOO has impacted two different areas over time. From 1963 through late 1993, wastewater was discharged approximately 3.9 km offshore at a depth of ~60 m. The PLOO was extended further offshore with construction completed in November 1993, at which time discharge was transferred to the present deeper site (~100 m) about 7.2 km west of Point Loma. The SBOO is located just north of the USA/Mexico border, with the outfall terminating approximately 5.6 km offshore at a depth of ~27 m. The USEPA-designated LA-5 dredge materials disposal site is located ~6 km SSW from the end of PLOO at depths between ~125 and 200 m. Although designed to be non-dispersive and situated deep enough to minimize sediment resuspension from surface waves, significant dumping has occurred well inshore (and shallower) of the LA-5 boundaries (see Gardner et al., 1998a,b). These short dumps represent an increased risk of contaminant exposure off Point Loma. Additionally, the presence of the now defunct LA-4 disposal site SSE of LA-5 may be another source of contaminants. The input of PCBs to the coastal shelf via surface runoff has not been well studied for San Diego watersheds. However, studies of stream plumes in Santa Monica Bay indicate that PCBs were detectable near the shoreline 2–4 km distant from the most urbanized stream source (Schiff and Bay, 2003). Watersheds of the most industrialized areas of San Diego County drain into San Diego Bay, which is itself contaminated by local inputs (e.g., shipyards, naval stations, abandoned dumpsites, port activities, transportation infrastructure). The nature of these various contaminant sources complicates efforts to evaluate the importance of surface runoff as a source of PCBs to the local marine environment.

The City of San Diego has monitored many constituents of concern in benthic sediments, the water column, and biota of the San Diego shelf for many years (see City of San Diego 2007a,b, and references therein). Some of these data have shown detectable levels of PCBs in sediments and in tissues of local fishes. For sediments, PCBs have been detected mostly in areas near LA-5 and the PLOO. There also appears to be a pattern of PCB bioaccumulation in fishes, but one that appears spatially broader than in sediments. One assessment showed higher PCB levels in fishes caught by hook and line near the PLOO than at a northern reference site, suggesting the outfall as a possible source of contamination. However, these results were inconsistent with other findings for trawl-caught fishes. Discriminating between such patterns is difficult and is confounded here by large numbers of non-detects in the data, the presence of mixed and/or different species assemblages, and differences in lipid content and the age of fish sampled over time and space. Therefore, the actual source of PCB contamination off San Diego is not well known at present. Here, we seek to discriminate among possible sources of PCBs in San Diego fishes utilizing statistical analyses that utilize non-detects in the data and that account for the dependency of PCB bioaccumulation on species and lipid content.

2. Methods

The City of San Diego's ocean monitoring program includes evaluation of contaminant loads in benthic sediments as well as their bioaccumulation in bottom dwelling (demersal) fishes to comply with permit requirements for discharging wastewater through the Point Loma and South Bay ocean outfalls (PLOO and SBOO, respectively). Fish analyzed for this study were collected using standard otter trawl or rig fishing (hook and line) gear at 15 locations throughout the San Diego coastal region (see Fig. 1). For the PLOO region, these include two rig fishing sites (RF1, RF2), two trawl sites (SD9, SD11), and four trawl zones (TF1–TF4). The designation of trawl zones occurred effective August 2003 with a permit change that redefined or combined areas for six previous sites (see City of San Diego, 2004): (a) TF1 represents combination of sites SD10 and SD12 surrounding the PLOO discharge point; (b) TF2 represents the area surrounding sites SD13 and SD14 north of the outfall; (c) TF3 represents the area surrounding site SD8 located NE of the LA-5 disposal site; (d) TF4 represents the area surrounding site SD7 located W of the LA-4 disposal site. Sampling locations for the SBOO region where fish liver tissues are collected include seven discreet sites designated SD15–SD21. For simplicity, all sampling locations are referred to as sites throughout this paper.

The present analysis was conducted using PCB congener data from fish collected over a 12 year period from 1995 through 2006 (see Table 1). Prior to 1995, PCBs were measured as Aroclors rather than congeners, and therefore the data are not comparable. All analyses presented herein are for liver tissues. Specific details concerning field sampling, tissue processing, and chemical analysis can be found in City of San Diego (2007a,b).

2.1. PCBs in San Diego fishes

2.1.1. Analytical rationale

Discrimination of PCB sources contaminating fish populations off San Diego is complicated by the fact that different species

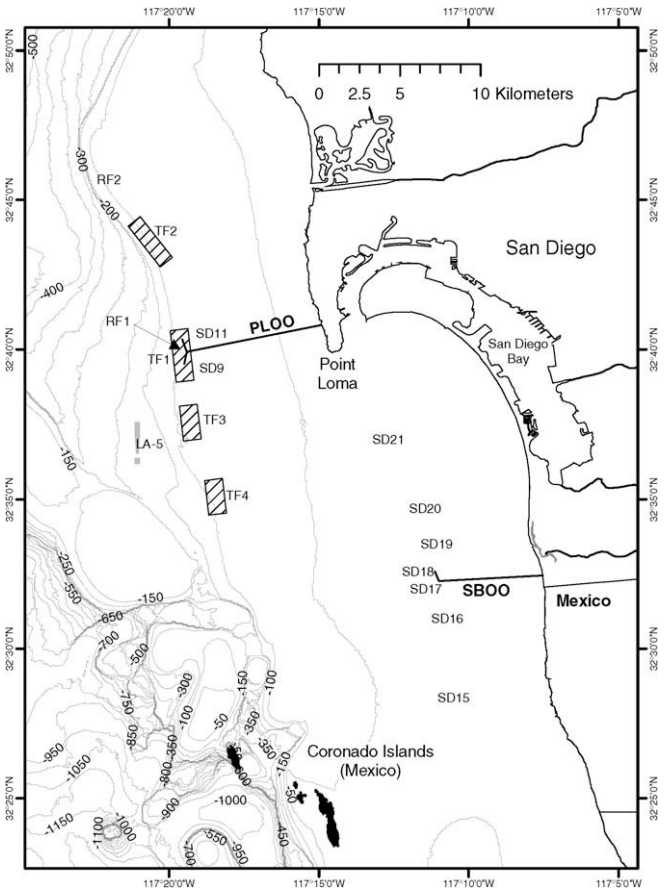

Fig. 1. Map of the San Diego shelf showing locations of trawl and rig fishing sites, the Point Loma Ocean Outfall (PLOO), the South Bay Ocean Outfall (SBOO), and the LA-5 dredge disposal site.

Table 1
Table of study site names, affiliation with monitoring project (PLOO or SBOO), depth, collection method (trawl vs. rig fishing) and years that data were available for analysis

Zone	Outfall	Gear	Depth (m)	Sample period
RF1	PLOO	Rig	100	1995–2003
Rf2	PLOO	Rig	100	1995–2003
SD9	PLOO	Trawl	90	1995–2003
SD11	PLOO	Trawl	90	1995–2003
TF1	PLOO	Trawl	100	1995–2006
TF2	PLOO	Trawl	100	1995–2006
TF3	PLOO	Trawl	100	1995–2006
TF4	PLOO	Trawl	100	1995–2006
SD15	SBOO	Trawl	30	1996–2006
SD16	SBOO	Trawl	30	1995–2006
SD17	SBOO	Trawl	30	1995–2006
SD18	SBOO	Trawl	30	1995–2006
SD19	SBOO	Trawl	30	1995–2006
SD20	SBOO	Trawl	30	1995–2006
SD21	SBOO	Trawl	30	1995–2006

See text for additional information on site designations over time.

assemblages were sampled among sites (species problem) and by the percentage of non-detects in the data (non-detect problem). The affinities of PCBs to accumulate in fish tissues are both a function of tissue type and the composition and class of lipid within tissues (Mearns et al., 1991). The amount of lipid present (i.e., lipid content) in different tissues can vary greatly among species (see Phillips, 1995). Therefore, these differences must be accounted for, if possible, to facilitate meaningful comparisons of PCB contamination in fish among areas. Non-detects are also problematic for among site comparisons because they mask the true distribution of contaminants at each site, decrease the sample size available for statistical comparisons among sites if excluded, and/or possibly bias results if substituted values are instead used in the analysis. It is presently a common practice to use substituted values, such as half the detection limit, in analyses of environmental data (Helsel, 2005, p. 11). We have addressed both the 'species' and 'non-detect' problems using a combination of survival analysis and linear regression models. Survival analysis was developed for applications where data are right censored, such as individual human life spans in which study subjects are still alive upon completion of the study (e.g., >82 years old). Environmental data, on the other hand, in which non-detects are common, present the opposite problem in which non-detects must be quantified as less than the detection limit (e.g., <1 ppb).

Our analysis was conducted in two phases. The first included all species at all sites (rig fishing and trawling) in an effort to determine spatial patterns of PCB contamination that corresponded with potential contaminant sources (e.g., naturally forced export of PCBs from San Diego Bay to the shelf, the disposal of bay sediments at or near the LA-5 disposal site, and the two ocean outfalls). The results of the first phase ruled out naturally forced export from the Bay as well as the SBOO as likely sources, but were insufficient to adequately discriminate between other possible sources such as the PLOO or LA-5. Therefore, the second phase focused on the PLOO and LA-5 areas. For this phase we included data from trawling sites only since the species assemblages were similar. These assemblages were dominated by paralicthyids (e.g., sanddabs) allowing us to focus on this particular functional group (as per Allen et al., 2002b).

For both phases, PCB congeners were only included in the analyses if their sample sizes were $\geqslant$30 and the percentage of non-detects was $\leqslant$80%. These are commonly applied thresholds for survival analysis (Helsel, 2005). All statistical analyses were conducted using *R* (utilizing the 'NADA', 'survival', 'ca', 'multcomp', and 'vegan' libraries).

2.1.1.1. Phase I. Distribution parameters for PCB congeners were first estimated and plotted using the nonparametric Kaplan–Meier method (Helsel, 2005) with combined censored and non-censored data (see Fig. 2). Detrended correspondence analysis (Legendre and Legendre, 1998) was applied to the number of samples in a cross-tabulation of species and sites to facilitate visualization of species compositions among sites. Species were then grouped by trophic guild and/or lipid type because sample sizes for individual species were too low among sites for meaningful statistical comparisons.

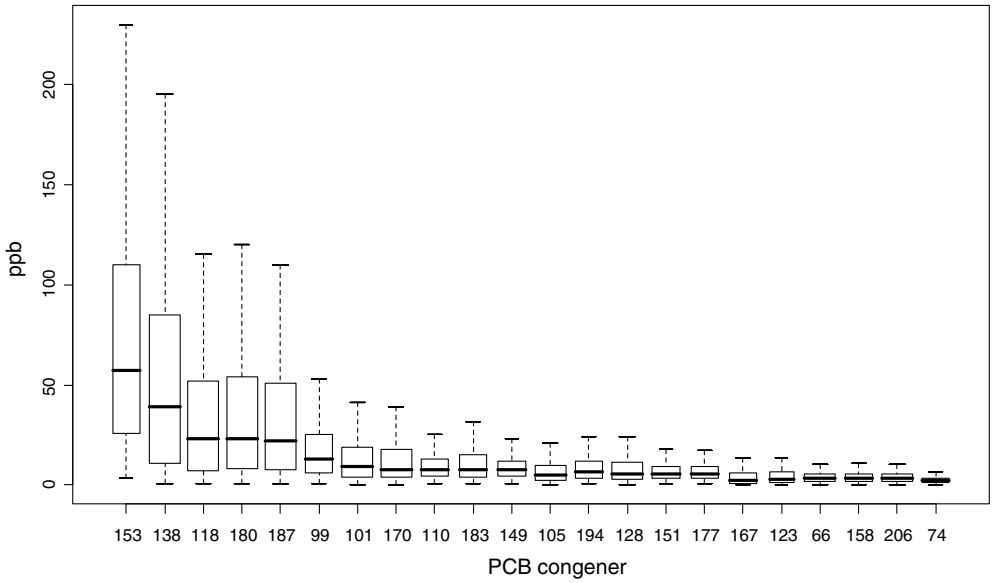

Fig. 2. Boxplots showing the distribution of PCB concentrations by congener for fish livers. Plot is for all species sampled as part of the South Bay Ocean Outfall and Point Loma Ocean Outfall monitoring programs. Distributions were estimated from pooled detect and non-detect data using Kaplan–Meier survival analysis (see text for details). Bars indicate medians, boxes enclose the 25th–75th percentiles, and whiskers indicate 5th and 95th percentiles. Box widths indicate relative sample sizes among congeners. PCB 153 includes congeners 153 and 168, which were not distinguished analytically. Congener boxplots are ordered by means.

Table 2
Table of species whose liver tissues were analyzed for PCBs as part of the Point Loma and South Bay ocean outfall monitoring programs

Species name	Common name	Species abbreviation	Species group
Paralicthyids			
Citharichthys sordidus	Pacific sanddab	PacSD	Sd
Citharichthys xanthostigma	Longfin sanddab	LfSD	Sd
Citharichthys spp.	Mixed sanddabs	CitSp	Sd
Hippoglossina stomata	Bigmouth sole	BmSol	Trbt
Pleuronectids			
Microstomus pacificus	Dover sole	DvSol	Trbt
Pleuronectes vetulus	English sole	EnSol	Trbt
Pleuronichthys verticalis	Horneyhead turbot	HnTrb	Trbt
Scianids			
Cheilotrema saturnum	White croaker	WC	Crk
Scorpaenids			
Scorpaena guttata	California scorpionfish	Scul	RF
Sebastes auriculatus	Brown rockfish	BrRF	RF
Sebastes caurinus	Copper rockfish	CuRF	RF
Sebastes chlorostictus	Greenspotted rockfish	GsRF	RF
Sebastes constellatus	Starry rockfish	StarRF	RF
Sebastes flavidus	Yellowtail rockfish	YelRF	RF
Sebastes helvomaculatus	Rosethorn rockfish	RtRF	RF
Sebastes hopkinsi	Squarespot rockfish	SsRF	RF
Sebastes miniatus	Vermillion rockfish	VRF	RF
Sebastes ovalis	Speckled rockfish	SpRF	RF
Sebastes paucipinus	Bocaccio	Boc	RF
Sebastes pinniger	Canary rockfish	CaRF	RF
Sebastes rosenblatti	Greenblotched rockfish	GbRF	RF
Sebastes rubrivinctus	Flag rockfish	FRF	RF
Sebastes saxicola	Stripetail rockfish	StrpRF	RF
Sebastes semicinctus	Halfbanded rockfish	HlfRF	RF
Sebastes serriceps	Treefish	Tree	RF
Sebastes umbrosus	Honeycomb rockfish	HonRf	RF
Sebastes spp.	Mixed rockfish	RF	RF

The species and species groups are listed in Table 2. Detrended correspondence analysis was conducted on the grouped species to visualize species groupings among study sites.

Each PCB congener was then analyzed using regression for parametric (lognormal) survival. The model formula consisted of PCB concentration as a function of percent lipid nested within the species groups. The nesting of species groups was removed from the survival regression models for congeners whose species groups were not significant. Standardized residuals were then plotted in probability plots to check the assumed lognormal model for each congener. Residuals for congeners yielding significant regressions were then summed for subsequent multiple comparison analysis (c.f., total PCBs) among sites. Multiple comparisons were conducted using Tukey's honest significant difference test, which accounts for stepwise error rates inherent in multiple testing (Yandell, 1997). The result is the set of confidence intervals for pairwise multiple comparisons. These values were then transformed to logical vectors of *p*-values for visualization using '*T*' depiction of undifferentiated classes (Donaghue, 2004). Principal component analysis was also conducted on the means (by site) of the residuals to further visualize possible site groupings and congener residual composition among the sites. The resultant biplot aided the interpretation of the data because sites were separated among congeners.

2.1.1.2. Phase II. The analytical approach used in Phase II was similar to that in Phase I except that only Pacific and longfin sanddabs were included in the analyses. The results of Phase I indicated that PCB contamination was greatest in fish captured near the PLOO and the LA-5 disposal site. However, the most likely source was not apparent due to a lack of significant spatial differences among sites that would lead to a clear interpretation of source based on proximity. Therefore, only PLOO monitoring sites were included in Phase II. Sanddabs were chosen in an effort to refine the survival regression models tested in Phase I, because they were the most numerous group of fishes among the sites, and because their lipid physiology and affinity for PCBs has been well studied (see Groce, 2002).

2.2. Regional sediment monitoring

In order to assess the distribution of PCBs in benthic sediments off San Diego as a possible source of contamination to fishes, we evaluated results of (a) 12 regional surveys conducted by the City of San Diego between 1995 and 2006 at sites ranging from northern Baja California to northern San Diego County, and (b) repeated monitoring at fixed sites surrounding the PLOO and SBOO between 1991 and 2006. The regional surveys of 1995–1997, 1999–2002 and 2005–2006 were conducted as part of the SBOO monitoring program (see City of San Diego, 2007b), while sampling in 1998 and 2003 was conducted as part of the Bight'98 and Bight'03 surveys of the entire Southern California Bight (see Noblet et al., 2002; Schiff et al., 2006). Bight'98 included sites in San Diego Bay as well as in offshore coastal habitats. All of the above surveys were based on arrays of randomly selected stations using the probability-based EMAP design. Regional data for 2004 were collected utilizing a different mapping design for the PLOO and SBOO regions (see Stebbins et al., 2004; Ritter and Leecaster, 2007). Between 1995 and 2006, a total of 681 regional samples from 574 sites were collected and analyzed. Of these, 630 samples (523 sites) were from offshore habitats, while 51 samples (51 sites) were from San Diego Bay. Monitoring at fixed sites was conducted quarterly or semiannually at 50 additional sites, including 23 PLOO sites (1991–2006) and 27 SBOO sites (1995–2006). Combined, these account for more than 2500 additional sediment samples for the offshore shelf.

3. Results

3.1. PCBs in San Diego fishes

3.1.1. Phase I

Twenty-three congeners satisfied the non-detect thresholds of $n \geqslant 30$ and percent non-detects $\leqslant 80\%$ (see Fig. 2 for a list of these congeners). Congeners 153 and 168 were not distinguished analytically and were therefore pooled (hereafter referred to as congener 153/168). Congeners 153/168, 138, 118, 180 and 187 contributed the greatest to total liver loadings. The distribution of species among sites is indicated in Fig. 3. Rig fishing sites were clearly dominated by rockfish, while trawl sites were composed of a mix of flatfish (paralicthyids and pleuronectids), rockfish, and white croaker. The composition of species groups among sites (see Table 2 for groupings) is indicated in Fig. 4. Clearly, there were large differences in species and species group composition among sites. Longfin sanddabs, white croaker and scorpionfish dominated the SBOO trawl stations. Longfin sanddabs were common at PLOO stations SD9 and SD11, but not at the deeper PLOO trawl sites (see Table 1). Pacific sanddabs, which typically occur more deeply than longfins, dominated the deeper sites. Different species compositions among the shallower and deeper sites are important and were a focus of statistical analyses performed as part of Phase II.

The survival regression models for individual PCB congeners as a function of percent lipid were significant ($p < 0.05$) for most congeners, with the only exceptions being congeners 74, 123, 158 and 167. Concentrations of these four congeners were low relative to most others (see Fig. 2). The coefficients of percent lipid nested by species groups were significant ($p < 0.05$) for congeners 153, 138, 180, 187 and 199. Coefficients for percent lipid nested within species groups were not significant ($p > 0.5$) for the remaining congeners, which indicated that lipids were significantly related to congener concentration. However, this relationship did not differ among species groups. The relationship was significantly different among species groups for congeners 153, 138, 180, 187 and 199. The small range of concentrations for most other congeners was the likely reason for the lack of significant difference among species groups for the remaining congeners. Congener 118 was the sole exception in that it had a relatively large range of concentrations (Fig. 2), but regression coefficients did not differ among species groups.

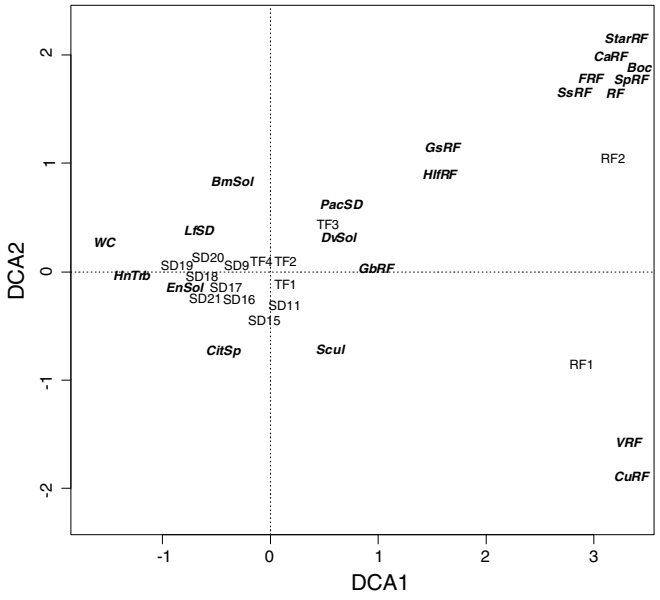

Fig. 3. Graph of detrended correspondence analysis showing composition of species (bold italics) analyzed for PCB contamination in livers among monitoring sites near the Point Loma and the South Bay ocean outfalls. See Table 2 for species codes.

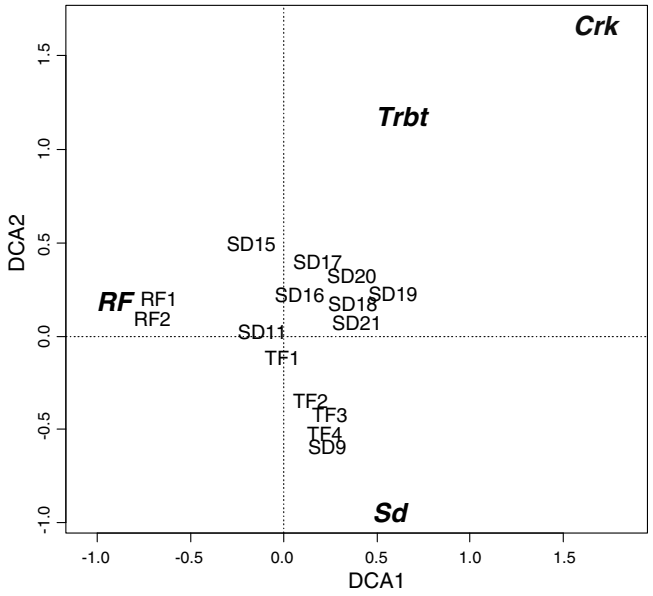

Fig. 4. Graph of detrended correspondence analysis showing composition of species groups (bold italics) analyzed for PCB contamination in livers among monitoring sites near the Point Loma and the South Bay ocean outfalls. 'RF' = pooled rockfish, 'Trbt' = turbots and soles, 'Sd' = sanddabs, 'Crk' = white croaker.

The results of multiple comparisons of summed residuals from the survival regression models are shown in Fig. 5. Boxplots show the distributions of residuals by site and are listed in order of increasing mean. The 'T' depiction of multiple comparisons (right panel; threshold $p = 0.05$) illustrates three robust significant groupings. The first is the southernmost SBOO trawl site (SD15); the second includes sites SD9 located just inshore of the PLOO southern diffuser leg and TF3 located just west of LA-5; the third group consists of the remaining PLOO and SBOO sites. The distribution of total PCB residuals is significantly the least at SD15, and significantly greatest at TF3 and SD9, with the remaining sites distributed in between. The biplot of the principle component analysis (PC1 and PC2, which accounted for >93% of the total variance) of residual PCB totals shows clear separation of the sites that had significantly different total residual distributions (SD15, SD9 and TF3), but it also indicates separation of the PLOO rig fishing sites and SD11. These separations appear to be due to the same congeners whose species groups were significant in the survival regression models. It therefore appears that at least some of the species group signal remains in the total PCB residual data. It should also be noted that the two PLOO rig fishing stations separate out on the same congener axes, and this is true for trawl sites SD9 and SD11 but along different congener axes. TF3, on the other hand, is not associated with the same congener axes as any other sites and therefore has its own unique composition of regression residuals. These differences are likely due to the residual effect of species group (i.e., different species' affinities among congeners), but they could also indicate different contaminant sources (see Fig. 6).

3.1.2. Phase II

The results of Phase I clearly indicate that the greatest PCB contamination of fish on the coastal shelf off San Diego occurs nearest LA-5 and the PLOO discharge site. These results however, are

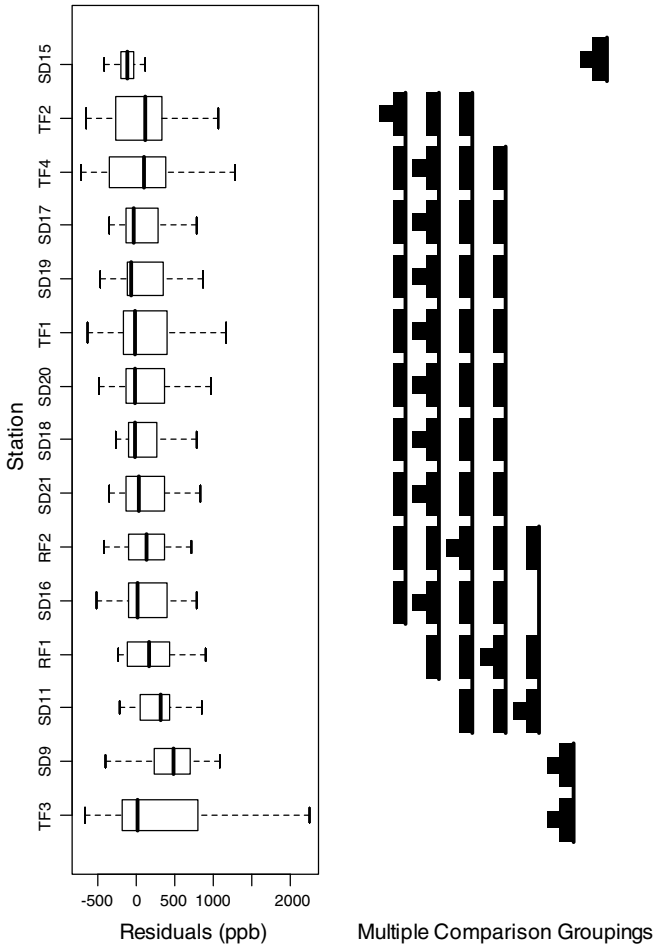

Fig. 5. Boxplots (left panel) of PCB residuals from survival regression analysis (Phase I) summed for each congener at a site (see text). The distribution of residuals indicates PCB concentrations not accounted for by the survival regression models which included effects for species group and percent lipid. Boxes are ordered by site means. Bars indicate medians, boxes enclose the 25th–75th percentiles, and whiskers indicate 5th and 95th percentiles. Box widths indicate relative sample sizes by congener. Right panel shows results of multiple comparison tests (Tukey HSD comparisons, $\alpha = 0.05$) among sites. The multiple comparison chart indicates sites that are significantly different from one another. Each column represents significant groupings. Linked sites indicate a lack of significant difference when site(s) indicated by 'T' shaped box is used as the base for comparison. Each column therefore represents significant groupings.

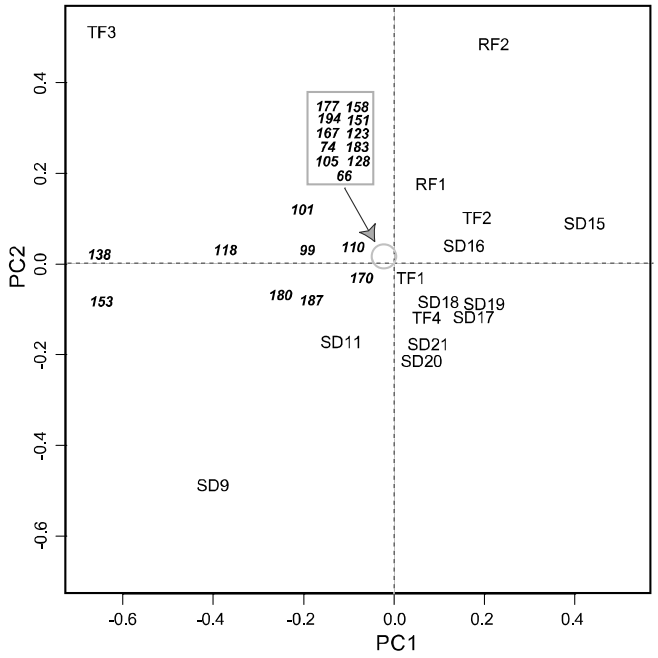

Fig. 6. Results of principle component analysis (PC1 and PC2) of mean PCB congener residuals (bold italics) among sites. Residuals are from a survival regression model relating [PCB] to lipid content and species groups (see text).

inconclusive as to the source(s) of PCB contamination. The results also indicate that the survival regression models did not appear to fully account for the differences in PCB affinities among species. Therefore we shifted our focus to analyze only trawling sites located north of the South Bay region in order to remove as much species specific effect as possible and because these encompass the area of greatest PCB contamination (i.e., PLOO sites SD9, SD11, TF1, TF2, TF3 and TF4). We further limit our analysis in this phase to Pacific and longfin sanddabs, and we do so for two reasons. First, these two species have similar lipid physiology and therefore similar affinities for PCBs, and second, these species dominate the demersal fish community at the PLOO trawling sites. Unfortunately, we could not limit our analysis to a single species because neither composed a large enough sample size among all the sites.

Percent lipid differed significantly among the two species at the PLOO sites (t-test, $p < 0.05$, see Fig. 7). The species composition among the different sites is shown in Fig. 8. The four deeper trawl sites (TF1, TF2, TF3 and TF4) had more Pacific sanddabs, while the shallower SD9 and SD11 sites were dominated by longfin sanddabs. PCB congener data were modeled similarly as in Phase I using survival regression models where PCB concentrations were modeled as a function of lipid nested within species. Congeners 153, 138, 118, 180 and 187 had significant coefficients ($p \ll 0.05$) for percent lipids nested within species, indicating that the two sanddab species had different slopes of PCB concentration as a function of lipid for these congeners. Recall that these congeners had the highest mean and median concentrations (Fig. 2). For the remaining congeners, species nesting was dropped from the model. The result was that all PCB congeners except for 167, 123, 66, 158

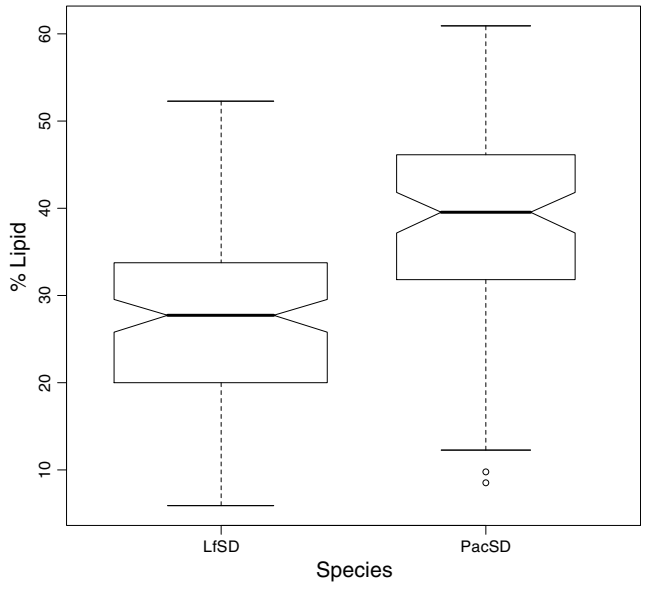

Fig. 7. Boxplots of liver lipid content for longfin sanddabs and Pacific sanddabs sampled as part of the Point Loma Ocean Outfall monitoring program. Notches indicate 95% confidence intervals, box widths indicate relative sample sizes.

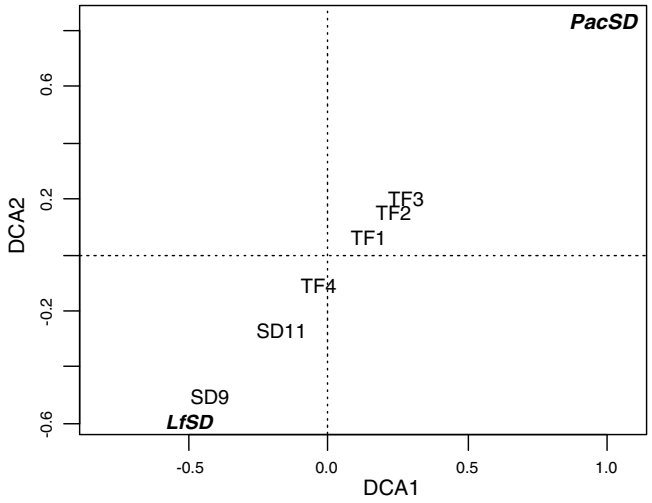

Fig. 8. Detrended correspondence analysis plot showing compositions of sanddab species whose livers were analyzed for PCBs as part of the Point Loma Ocean Outfall monitoring program ('PacSD' = pacific sanddab, 'LfSD' = longfin sanddab).

and 206 had significant coefficients for percent lipid. Residuals for congeners having significant coefficients for lipids nested by species and congeners having significant coefficients for lipids were summed as in Phase I to produce total residuals. Multiple comparisons and boxplots of these residuals are shown in Fig. 9. Total PCB residuals were significantly higher at TF3 than elsewhere. The median at TF3 is slightly greater than all other sites, although the 75th and 95th percentiles are much larger indicating that the most contaminated fish were sampled from TF3, the site nearest the LA-5 disposal site.

3.2. PCBs in San Diego sediments

Results from the regional monitoring activities are shown in Fig. 10. PCBs were detected in 12 regional sediment samples, which correspond to a detection rate of ~1.8% for the San Diego shelf region. These included samples from three sites located far north of the PLOO (i.e., off Mission Bay or La Jolla), one site just NE of LA-5 that is also monitored as part of fixed site sampling for the PLOO, two sites located about halfway between LA-5 and the mouth of San Diego Bay, five sites east or SSE of LA-5 and nearer to LA-4, and one site just south of the SBOO. PCBs were also detected in 12 sediment samples collected from San Diego Bay during Bight'98; however this corresponds to a much higher detection rate of ~24%.

Fixed site monitoring around the PLOO and SBOO yielded PCB detection rates similar to that for the regional offshore sites (i.e., <2%). PCBs were detected an additional 47 times out of the more than 2500 samples analyzed. Of these, most detects ($n = 39$) occurred at six sites in the area adjacent to LA-5 or between the disposal site and the PLOO; one of the sites near LA-5 was also sampled as part of the sediment mapping study included in the regional results described above. The remaining samples with detected PCBs represent single occurrences at eight different sites, including three PLOO sites north of the outfall and five sites in the SBOO region.

4. Discussion

Ocean monitoring programs are typically designed to evaluate the effects of discharge streams originating from a specific point source (e.g., municipal wastewater outfalls). In most cases, the regions monitored span multiple habitats (e.g., soft-bottom vs. rocky substrates) and may include different types of organisms in which bioaccumulation of contaminants may occur. Additionally, other point or non-point sources of contaminants are often not adequately considered in monitoring designs even though their presence can greatly influence the outcome of any study. Because contaminants such as PCBs, PAHs, pesticides and trace metals accumulate in marine sediments and can impact the environment in many ways, assessment of benthic conditions is an important component of monitoring programs. Benthic habitats are usually characterized by numerous, relatively immobile species of infaunal or epifaunal invertebrates (macrofauna) that are sensitive to sediment quality, and which have proven to be useful indicators of environmental impact. In turn, macrofauna are preyed upon by larger, more mobile species such as demersal fishes, which can concentrate contaminants in their tissues and transport them further up the food chain to higher level consumers (e.g., marine mammals, birds, and ultimately humans). Consequently, it is important for monitoring programs to include efforts to sample fish populations and to evaluate the bioaccumulation of contaminants.

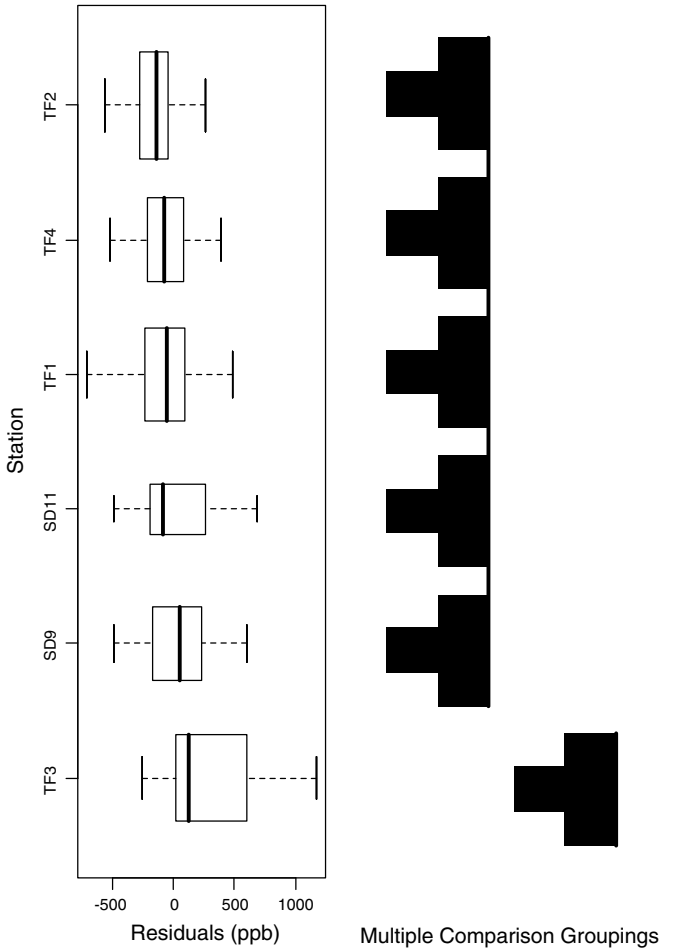

Fig. 9. Boxplots (left panel) of PCB residuals from survival regression analysis (Phase II) summed for each congener at a site (see text). The distribution of residuals indicates PCB concentrations not accounted for by the survival regression models which included effects for species group and percent lipid. Boxes are ordered by site means. Bars indicate medians, boxes enclose the 25th–75th percentiles, and whiskers indicate 5th and 95th percentiles. Box widths indicate relative sample sizes by congener. Right panel shows results of multiple comparison tests (Tukey HSD comparisons, $\alpha = 0.05$) among sites. The multiple comparison chart indicates sites that are significantly different from one another. Each column represents significant groupings. Linked sites indicate a lack of significant difference when site(s) indicated by 'T' shaped box is used as the base for comparison. Each column therefore represents significant groupings.

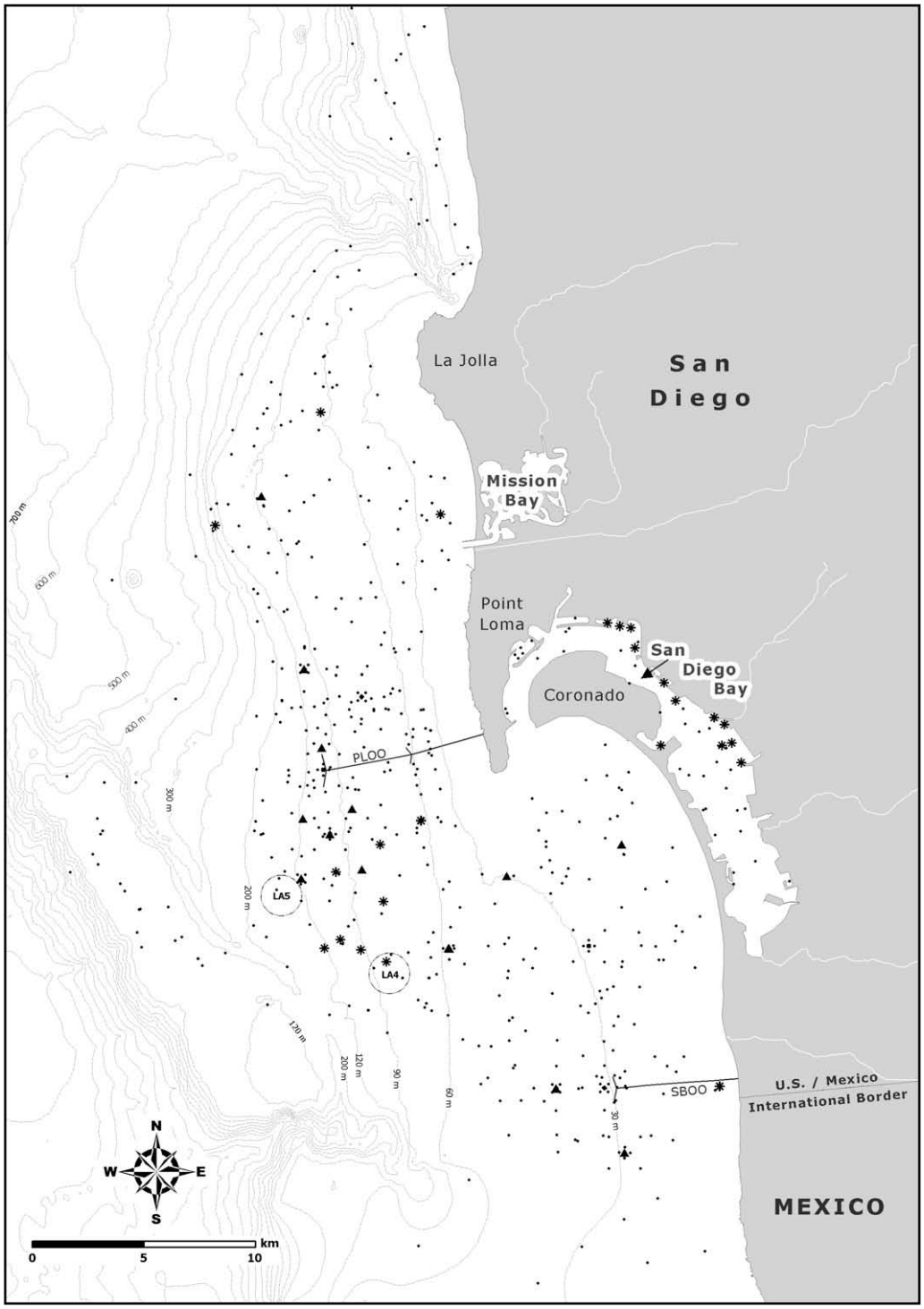

Fig. 10. Map of benthic sediment sites sampled off San Diego as part of: (a) annual regional surveys of randomly selected sites from 1995 to 2006 and (b) repeated quarterly or semiannual sampling of fixed sites for PLOO and SBOO regions; see text for additional details. * indicate regional sites where PCB concentrations were detected in sediments above detection limits; △ indicate fixed sites where PCBs were detected.

Analysis of PCB bioaccumulation in fish is complex due to the difficulty of sampling adequate numbers of the same species over broad spatial ranges that may include mixes of habitats from coastal shelves to enclosed bays and estuaries (see Allen et al., 1998). This is exemplified in the present data set for fishes sampled from the open coastal shelf off San Diego, southern California. Sample sizes for single species of fish were not adequate to model non-detect values in a meaningful manner, which is a common problem in fish bioaccumulation studies. The best synoptic view (Phase I) that we could produce was therefore based on all species sampled. The alternative of excluding non-detects was not an option because that would further reduce sample sizes and result in decreased statistical power and the loss of sites in the overall analysis.

Further complicating mixed-species analyses are mobility patterns both within and among species. For example, California scorpionfish often migrate dozens of kilometers to aggregate for

seasonal spawning (Hartmann, 1987). Such movements are much larger than the scale of our sites. Therefore, individual fish sampled at any of the study sites could have been feeding at any of the other study sites. Clearly this is suboptimal when attempting to match spatial patterns of bioaccumulation to contaminant sources. The only possible synoptic picture that we could produce included scorpionfish data by necessity because this species was the most common, accounting for ~30% of all fish sampled.

Results of the Phase I analysis indicated significant dependence of PCB concentration on lipid content for all congeners except those whose concentrations were low (medians <10–15 ppb) where this relationship was more likely to lose significance due to the narrow range of concentrations. Further, species groups significantly affected the dependence of PCB concentration on lipid content for congeners having the largest moments of central tendency (with the exception of PCB 118). Summed residuals from the survival regression models represent total PCB concentrations among the sites after accounting for effects of species groups and lipid content. Multiple comparisons of these residuals clearly demonstrate a spatial pattern of decreased PCB contamination in fish in the southernmost area south of the USA/Mexico border, and a large area of greater PCB contamination north of the border at all but two sites where PCB contamination is significantly greater than the rest. The latter include TF3 located near the LA-5 dredge disposal site, and SD9 located ~1.2 km inshore of the southern diffuser for the PLOO. This pattern of contamination is inconsistent with what would be expected if natural transport of PCBs from San Diego Bay or discharge via the SBOO were responsible for contamination of coastal fish. However, it does not exclude human transport of dredge materials from the Bay or wastewater discharge through the PLOO as sources of PCBs.

The above results could be explained if either wastewater discharged via the PLOO or dredge materials from San Diego Bay were the source of PCBs, and/or if the survival regression models were not adequate to fully account for the species effect. However, a study of influent/effluent streams for the Point Loma Wastewater Treatment Plant (PLWTP) indicate that the PLOO has been an unlikely source of PCBs for at least the last two decades and likely longer (see Meyer and McAnally, 2008). For example, no PCBs measured either as Aroclors (1986–present) or congeners (2007 special study) have been detected in influent or effluent at the PLWTP since the City began analyzing for them. Similar results were found for wastewater samples analyzed for the South Bay Water Reclamation Plant (2002–present), which discharges via the SBOO. Furthermore, if PCBs were ever discharged in significant quantities through the outfalls, there should be a pattern of legacy PCB accumulation in sediments near past or present discharge sites. No such patterns are evident for either the PLOO or SBOO regions (see Fig. 10 and below).

On the other hand, PCB contamination of demersal fishes via exposure to dredged bay sediments transported to coastal habitats is likely. For example, sediments and fish in San Diego Bay exhibit much higher levels of PCB contamination than those on the shelf (City of San Diego, 2003). Consequently, it is logical that such sediments deposited at offshore disposal sites have the potential to contaminate local fishes. Although LA-5 was designed to be far offshore and deep enough to serve as a non-dispersive disposal site in order to minimize contaminant exposure to the local biota, this can only be effective if dredge materials are actually deposited at the site. However, a multibeam bathymetric study conducted by the USGS (Gardner et al., 1998a,b) revealed over 250 piles of dredged material well inshore (and shallower) than the intended dump site

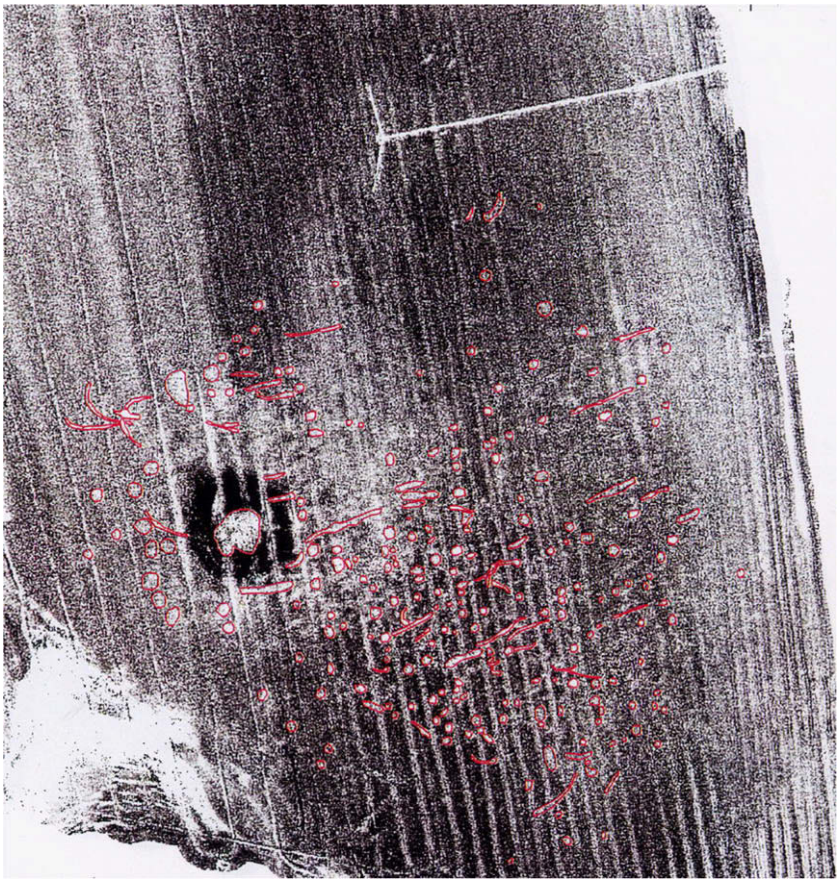

Fig. 11. Backscatter image showing spatial distribution of dredge disposal mounds (outlined in red). Dark circle with concentric lighter circle is the LA-5 dredge disposal site. The Point Loma Ocean Outfall is clearly visible. Survey from Gardner et al. (1998a,b).

that were attributed to the practice of dumping sediments closer to shore while en route to LA-5 (see Fig. 11). The distribution of these short dumps coincides well with the spatial pattern of PCBs detected in sediments on the San Diego shelf.

Analyses conducted during Phase II were designed to discriminate the source of fish PCB contamination on the Point Loma shelf. The most important aspects of this analysis were to eliminate as much species specific noise as possible and to determine if PCB bioaccumulation in fish at the shallower sites (SD9 and SD11) were comparable to the deeper TF3 site after application of a stricter accounting for species effect. Species composition at SD9 and SD11 (90 m deep) was quite different than at TF3 (100 m deep). Sites SD9 and SD11 were dominated by longfin sanddabs and California scorpionfish, whereas TF3 was dominated by Pacific sanddabs. This difference was likely due to species specific depth ranges and habitat. For example, longfins typically occur in shallower waters in southern California than Pacific sanddabs (Groce, 2002). Pacific sanddabs also undergo an ontogenetic migration preferring shallower depths as young fish and deeper depths later in life. Therefore, both species and age compositions differed among these sites. Scorpionfish also contributed to a difference in age compositions among sites because they are longer-lived and mature more slowly than sanddabs, thereby having a greater capacity for PCB contamination. The exclusion of scorpionfish from Phase II facilitated removal of a large possible source of noise from the data while not diminishing sample sizes to the point that statistical analyses would be excluded. However, observed differences in percent lipid between the sanddab species and possibly variable species specific affinities for PCB congeners were still important factors to account for in the analysis. Both lipids and species were found to be important independent sources of variability in PCB concentrations. After these factors were accounted for in the survival regression models, the pattern of differences in total PCB contamination among the sites became clear. PCB contamination was significantly greatest at TF3, the site nearest the LA-5 disposal site implicating dredge sediments from San Diego Bay as the most probable source of PCB contamination in fish off the Point Loma shelf.

Patterns of PCB contamination in the benthos based on over 3100 sediment samples from the San Diego region concur with prior studies that documented greater PCB contamination in San Diego Bay than in offshore areas (Mearns et al., 1991; City of San Diego, 2003). The spatial distribution of detects also supports the hypothesis that dredged bay sediments intended for disposal in deep waters are the most likely source of PCB contamination to the San Diego shelf. For example, 80% of all PCBs detected in offshore waters occurred south of the PLOO in areas relatively near the disposal sites or where short dumps intended for LA-5 have been documented. In contrast, sediments do not appear contaminated at current outfall discharge sites or near the original PLOO diffusers where wastewater was discharged for about 30 years (i.e., 1963–1993, including the peak period of PCB use). This supports the argument that wastewater discharge has not been a source of PCBs to the shelf. While this may be the case for Point Loma, it has not always been true for other outfalls (see Mearns et al., 1991). Finally, the paucity of PCBs detected in shallow waters along the coastline indicates that surface runoff from local watersheds also does not play a significant role in PCB transport to the coastal waters off San Diego.

While it is clear from this study that the main source of PCBs contaminating fish on the coastal shelf off San Diego is the disposal of contaminated sediments dredged from San Diego Bay, it is not clear whether this level of contamination significantly impacts fish populations or the ecosystems of which they are a part. Furthermore, there is no evidence that PCB contamination in San Diego fishes represents a human health issue. These concerns are outside the focus of this study. However, the practice of disposing dredged materials onto coastal shelf habitats warrants further scrutiny. The benefit of decontaminating bay and estuarine environments via such practices must be weighed carefully against the risk of contaminating more pristine shelf ecosystems. Dredge disposal practices have been well studied to determine methodologies that minimize environmental impacts during disposal (Jones-Lee and Lee, 2005). However, the fate of dredged contaminants to receiving environments over the long term – whether they enter the food chain readily or have such low bioavailability that they simply persist in sediments and slowly disperse through physical means – remains poorly understood and likely varies on a case by case basis.

5. Conclusions

The observation that fish on the coastal shelf of San Diego are contaminated with PCBs is of concern. We conclude that the most probable source of PCB contamination is the disposal of dredged sediments from San Diego Bay, and not the natural transport (outflow) of materials from the Bay, the discharge of wastewater through local ocean outfalls, or surface runoff from local watersheds. Further, the problem has likely been exacerbated by improper disposal practices where dredged sediments were dumped short of and in shallower waters than their intended target, thereby facilitating diffusion of PCBs and other contaminants over a wider area. We recommend increased scrutiny of such disposal practices and an examination of priorities for the protection of bay vs. shelf ecosystems. It is especially important to consider the trade-offs when dredge disposal is intended as a means of detoxifying contaminated bays and estuaries at the risk of toxifying shelf ecosystems.

Acknowledgements

We thank Jim Gardner and Pete Dartnell of the US Geological Survey for the use of their figure showing the spatial distribution of dredge disposal mounds off Point Loma (Fig. 11), and Dawn Olson of the City of San Diego for assistance mapping contaminant distributions off San Diego and for help preparing figures. We are grateful to Rick Gersberg of San Diego State University for first bringing this matter to our attention and for subsequent discussions during his review of the City's ocean monitoring data. PEP, TDS and AKG acknowledge support from the City of San Diego, Metropolitan Wastewater Department (Environmental Monitoring and Technical Services Division).

References

Allen, M.J., Moore, S.L., Schiff, K.C., Weisberg, S.B., Diener, D., Stull, J.K., Groce, A.K., Mubarak, J., Tang, C.L., Gartman, R., 1998. Southern California Bight 1994 Pilot Project: Chapter V. Demersal Fishes and Megabenthic Invertebrates. Southern California Coastal Water Research Project, Westminster, CA. p. 324.

Allen, M.J., Groce, A.K., Diener, D., Brown, J., Steinert, S.A., Deets, G., Noblet, J.A., Moore, S.L., Diehl, D., Jarvis, E.T., Raco-Rands, V., Thomas, C., Ralph, Y., Gartman, R., Cadien, D., Weisberg, S.B., Mikel, T., 2002a. Southern California Bight 1998 Regional Monitoring Program: V. Demersal Fishes and Megabenthic Invertebrates. Southern California Coastal Water Research Project, Westminster, CA, p. 548.

Allen, M.J., Moore, S.L., Weisberg, S.B., Groce, A.K., Leecaster, M.K., 2002b. Comparability of bioaccumulation within the sanddab guild in coastal Southern California. Marine Pollution Bulletin 44, 452–458.

Brown, F.R., Winklera, J., Visitaa, P., Dhaliwala, J., Petreasa, M., 2006. Levels of PBDEs, PCDDs, PCDFs, and coplanar PCBs in edible fish from California coastal waters. Chemosphere 64 (2), 276–286.

City of San Diego, 2003. An Ecological Assessment of San Diego Bay: A Component of the Bight'98 Regional Survey. City of San Diego Ocean Monitoring Program, Metropolitan Wastewater Department, Environmental Monitoring and Technical Services Division, San Diego, CA.

City of San Diego, 2004. Annual Receiving Waters Monitoring Report for the Point Loma Ocean Outfall, 2003. City of San Diego Ocean Monitoring Program,

Metropolitan Wastewater Department, Environmental Monitoring and Technical Services Division, San Diego, CA.
City of San Diego, 2007a. Annual Receiving Waters Monitoring Report for the Point Loma Ocean Outfall, 2006. City of San Diego Ocean Monitoring Program, Metropolitan Wastewater Department, Environmental Monitoring and Technical Services Division, San Diego, CA.
City of San Diego, 2007b. Annual Receiving Waters Monitoring Report for the South Bay Ocean Outfall (South Bay Water Reclamation Plant), 2006. City of San Diego Ocean Monitoring Program, Metropolitan Wastewater Department, Environmental Monitoring and Technical Services Division, San Diego, CA.
Davis, J.A., Hetzel, F., Oram, J.J., McKee, L.J., 2007. Polychlorinated biphenyls (PCBs) in San Francisco Bay. Environmental Research 105, 67–86.
Donaghue, J.R., 2004. Implementing Shaffer's multiple comparison procedure for a large number of groups. In: Benjamini Bretz, Sarkar, (Eds.), Recent Developments in Multiple Comparison Procedures, Institute of Mathematical Statistics Lecture Notes–Monograph Series, vol. 47.
Fairey, R., Bretz, C., Lamerdin, S., Hunt, J., Anderson, B., Tudor, S., Wilson, C.J., LeCaro, F., Stephenson, M., Puckett, M., Long, E.R., 1996. Chemistry, Toxicity, and Benthic Community Conditions in Sediments of the San Diego Bay Region. Final Report. State Water Resources Control Board, NOAA, California Department of Fish and Game, Marine Pollution Studies Laboratory, and Moss Landing Marine Lab. Sacramento, CA.
Fairey, R., Roberts, C., Jacobi, M., 1998. Assessment of sediment toxicity and chemical concentrations in the San Diego Bay region, California, USA. Environmental Toxicology and Chemistry 17 (8), 1570–1581.
Gardner, J.V., Dartnell, P., Torresan, M.E., 1998a. LA-5 Marine Disposal Site and Surrounding Area, San Diego, California: Bathymetry, Backscatter, and Volumes of Disposal Materials. Administrative Report, July 1998. US Geological Survey, Menlo Park, CA.
Gardner, J.V., Butman, P.B., Mayer, L.A., Clarke, J.H., 1998b. Mapping US continental shelves. Sea Technology 39 (6), 10–17.
Groce, A.K., 2002. Influence of Life History and Lipids on the Bioaccumulation of Organochlorines in Demersal Fishes. MS Thesis, San Diego State University, p. 115.
Hartmann, A.R., 1987. Movement of scorpionfishes (Scorpiniodae: *Sebastes* and *Scorpaena*) in the southern California Bight. California Fish and Game 73 (2), 68–79.
Helsel, D.R., 2005. Nondetects and Data Analysis, Statistics for Censored Environmental Data. John Wiley & Sons, Inc., Hoboken, New Jersey. p. 250.
Jones-Lee, A., Lee, G.F., 2005. Water quality aspects of dredged sediment management. In: Lehr, J.H., Keely, J. (Eds.), Water Encyclopedia: Water Quality and Resource Development. Wiley, Hoboken, NJ, pp. 122–127.
Legendre, P., Legendre, L., 1998. Numerical Ecology. Elsevier, Amsterdam. p. 853.
Lyon, G.S., Petschauer, D., Stein, E.D., 2006. Effluent discharges to the southern California Bight from large municipal wastewater treatment facilities in 2003 and 2004 In: Weisberg, S.B., Miller, K.A. (Eds.), Southern California Coastal Water Research Project Biennial Report 2005–2006. Southern California Coastal Water Research Project, Westminster, CA.
Mearns, A.J., Matta, M., Shigeneka, G., MacDonald, D., Buchman, M., Harris, H., Golas, J., Lauenstein, G., 1991. Contaminant trends in the southern California Bight: Inventory and Assessment. NOAA Technical Memorandum NOS ORCA 62. Seattle, WA, p. 448.
Meyer, S., McAnally, J., 2008. PCB congeners in the Point Loma Wastewater Treatment Plant and other Metro waste streams – Fall 2007. City of San Diego Wastewater Chemistry Section Technical Report (February 13, 2008), p. 17.
Noblet, J.A., Zeng, E.Y., Baird, R., Gossett, R.W., Ozretich, R.J., Phillips, C.R., 2002. Southern California Bight 1998 Regional Monitoring Program: VI. Sediment Chemistry. Southern California Coastal Water Research Project, Westminster, CA.
Phillips, D.J.H., 1995. The chemistries and environmental fates of trace metals and organochlorines in aquatic ecosystems. Marine Pollution Bulletin 31, 193–200.
Ritter, K.J., Leecaster, M.K., 2007. Multi-lag cluster designs for estimating the semivariogram for sediments affected by effluent discharges offshore in San Diego. Environmental and Ecological Statistics 14, 41–53.
Southern California Coastal Water Research Project, 1973. The ecology of the southern California Bight: Implications for water quality management. SCCWRP Technical Report 104. El Segundo, CA, p. 499.
Schiff, K., Bay, S., 2003. Impacts of stormwater discharges on the nearshore benthic environment of Santa Monica Bay. Marine Environmental Research 56, 225–243.
Schiff, K., Maruya, K., Christenson, K., 2006. Southern California Bight 2003 Regional Monitoring Program: II. Sediment Chemistry. Southern California Coastal Water Research Project, Westminster, CA.
Stebbins, T.D., Schiff, K.C., Ritter, K., 2004. San Diego Sediment Mapping Study: Workplan for Generating Scientifically Defensible Maps of Sediment Condition in the San Diego Region. City of San Diego Metropolitan Wastewater Department, San Diego, CA, and Southern California Coastal Water Research Project, Westminster, CA. p. 11.
Yandell, B.S., 1997. Practical Data Analysis for Designed Experiments. Chapman & Hall. p. 440.
Zeng, E.Y., Yu, C.C., Tran, K., 1998. In-Situ Measurements of Chlorinated Hydrocarbons in the Water Column off the Palos Verdes Peninsula, California. In: Weisberg, S.B., Miller, K.A. (Eds.), Southern California Coastal Water Research Project Biennial Report 1997–1998. Southern California Coastal Water Research Project, Westminster, CA.

Appendix F
POINT LOMA OCEAN OUTFALL PLUME BEHAVIOR STUDY

Renewal of NPDES CA0107409

APPENDIX F

POINT LOMA OCEAN OUTFALL PLUME BEHAVIOR STUDY

January 2015

Appendix F

Point Loma Ocean Outfall Plume Behavior Study

Rogowski, P., E. Terrill, M. Otero, L. Hazard, S.Y. Kim, P.E. Parnell, and P. Dayton. 2012. Final Report: Point Loma Ocean Outfall Plume Behavior Study. Prepared for City of San Diego Public Utilities Department by Scripps Institution of Oceanography, University of California, San Diego, CA.

Final Report

Point Loma Ocean Outfall Plume Behavior Study

Prepared For

City of San Diego Public Utilities Department

NOAA Award No. NA08NOS4730441
(UCSD Contract H094679)

Prepared By

Scripps Institution of Oceanography
University of California, San Diego
9500 Gilman Drive
La Jolla, CA 92093-0213

Principal Contact	Peter Rogowski, Postdoctoral Researcher
Principal Investigators	P. Edward Parnell, Associate Researcher Paul Dayton, Professor Eric Terrill, CORDC Director

September 14, 2012

Updated 11/14/12, T.D. Stebbins
(tstebbins@sandiego.gov)

Point Loma Ocean Outfall Plume Behavior Study

Peter Rogowski*, Eric Terrill, Mark Otero, Lisa Hazard, Sung Yong Kim
Coastal Observing Research and Development Center (CORDC)
Marine Physical Laboratory
Scripps Institution of Oceanography

P. Edward Parnell, Paul Dayton
Coastal Ecology Group
Integrative Oceanography Division
Scripps Institution of Oceanography

**lead author*

EXECUTIVE SUMMARY

The discharge of municipal wastewater into natural environments poses potential risks to ecosystems, public health, and the beneficial uses of these environments by humans. The practice of wastewater disposal into coastal environments in the U.S. has advanced tremendously over the last half century from discharging untreated or partly treated sewage effluent in shallow water close to shore (even within bays and estuaries) to the discharge of highly treated effluent through deep ocean outfalls engineered to achieve rapid dilution and prevent the wastewater plumes from surfacing. Surfacing wastewater plumes pose increased risks to public health and to beneficial uses because they are more likely to contact the shoreline due to the typical pattern of daily onshore wind that is ubiquitous along coastlines worldwide. Most modern deep ocean outfalls achieve high rates of dilution and subsurface trapping by discharging through multiple diffuser ports distributed along long diffusers which are situated well below the oceanic thermocline which acts as a cap for the buoyant rising plume. Risk management of wastewater discharge is an evolving science that advances through the interplay of observation, monitoring, and engineering refinement. The present study focused on observation and monitoring of the Point Loma Ocean Outfall (PLOO), operated by the City of San Diego, to gauge its performance and to inform ongoing biological, sediment and water quality monitoring programs.

Specifically, we report the results of a study funded by an award to the City of San Diego by the National Oceanographic and Atmospheric Administration (NOAA Award No. NA08NOS4730441) that was designed to determine the characteristic fates of the wastewater plume emanating from the City's Point Loma Ocean Outfall (PLOO). The study focused on describing the physical oceanographic environment into which wastewater is discharged via the outfall and how that environment interacts with the resultant wastewater plume. This interaction determines how much the plume is diluted as it rises in the water column and mixes turbulently with ambient seawater, how high the plume rises, where the plume is

transported, and how quickly the plume is further diluted as it is transported downfield by currents. Thus, this study both informs on the performance of the Pt. Loma outfall as well as serves to identify specific areas of the coastal shelf off San Diego that are most likely to be affected by PLOO wastewater.

The study consisted of a combination of observational and modeling approaches. The observational component included observations of ocean currents and temperature intended to characterize the current and temperature structure of receiving ocean waters on the Pt. Loma shelf and to support of the use of an autonomous underwater vehicle (AUV) equipped with sensors capable of detecting the plume. The modeling component consisted of predicting plume rise height in the near field and post-hoc validation with AUV based observations of plume dilution.

Plume detection was facilitated using an optical sensor on the AUV that enabled the estimation of colored dissolved organic matter (CDOM). CDOM occurs naturally but exists in much greater concentrations in wastewater and thus serves as a useful tracer of wastefield dispersion in coastal environments. Ocean temperatures and currents estimated directly over the outfall discharge area and made available in real time via telemetry to shore, were used to pre-program the AUV to navigate the likely trajectory (horizontal movement and vertical position within the water column) given current and temperature structure. Upon deployment, the AUV navigated programmed tracklines oscillating in depth between the near-surface and several meters below the estimated trapping depth of the plume. Current meters were also deployed in shallower waters along the 35 m contour to resolve the most likely areas affected by wastewater plume incursion closer to shore.

The results of the study indicated that the PLOO wastefield never surfaced, and its shallowest depth during the observational period was 35 m. Further, given the hydrographic conditions of Pt. Loma shelf waters and the discharge characteristics of the outfall, the probability of the plume surfacing is highly unlikely. Observed rise heights were consistently less than modeled predictions indicating that the application of existing models to the PLOO overestimate the rise height by ~20%. This indicates that the PLOO performs better than predicted with respect to subsurface plume trapping. However, dilution rates were less than predicted since the greatest dilution rates occur as the plume rises. This was observationally confirmed as dilutions were typically 60-80% of prediction. Design parameters such as port spacing were likely the cause of these deviations from modeled predictions. Most importantly, we observed that the plume was advected mainly alongshore with only two instances where the plume moved toward shore but shoaled in waters deeper than the kelp forest (~30 m). Inshore current observations indicate that upwelling circulation, of tidal period or longer, are mostly associated with southeastward movement of the plume. The implication of this is that given the most likely plume shoaling conditions the PLOO wastefield is typically directed away from Pt. Loma and the kelp forest.

We also conclude that our hydrographic observations of currents and temperature at the outfall discharge site enabled adequate estimation of plume trajectory. Therefore, hydrographic observations alone are adequate to predict PLOO plume behavior. The most likely areas of shelf waters and sediments affected by the plume are oriented NNW to SSE as currents mainly alternate between these two directions. The plume was observed to extend

for more than 9 km from the diffusers in these dominant directions during several monitoring missions.

As a result of our findings, we propose the following recommendations to enhance and refine future receiving waters monitoring efforts for the PLOO discharge region.

Recommendation 1: Operation of a permanent oceanographic mooring system located near the terminal diffuser wye structure of the outfall (discharge site) designed to measure subsurface velocity and ocean stratification should be continued to document the state of the receiving waters into which the PLOO discharges.

Recommendation 2: The quarterly water quality sampling component of the City's ocean monitoring program for the PLOO region should be modified to use telemetered current meter/temperature data from a permanent mooring (see Rec 1) located near the outfall discharge site to design a more adaptive and optimized sampling grid pattern for each survey.

Recommendation 3: In order to measure plume location and dilution levels most effectively, operation of a mobile AUV as described herein should be in place and integrated with near-real-time reports of water column stratification and subsurface velocity.

Contents

EXECUTIVE SUMMARY i

List of Tables 2

List of Figures 3

I. INTRODUCTION 7

II. METHODS 8

A. Description of Study Area 8

B. Current and Temperature Observations 9

1. Telemetry Mooring 9

2. Nearshore ADCPs 14

C. Modeling Near-Field Plume 14

D. Autonomous Underwater Vehicle Deployments 15

1. Mission Planning 16

2. Colored Dissolved Organic Matter (CDOM) 18

III. RESULTS AND FINDINGS 20

A. Shelf Hydrographic Observations 20

1. Telemetry Mooring 20

2. Hydrography of the Inner Shelf 26

B. Modeling Plume Rise Height 35

C. AUV Plume Surveys 35

1. Summary of AUV Plume Survey Findings 37

2. Observed PLOO Plume Characteristics 44

IV. DISCUSSION 46

A. Example AUV Missions 46

B. Far-Field Mixing 46

C. Computing Plume Dispersion 48

D. Near- and Far-field Trends 49

E. Comparison with Analytical Mixing Model 50

F. Enhanced Far-Field Mixing and Plume Rise 51

V. CONCLUSIONS 57

A. Findings 58

B. Published Work 59

VI. MONITORING RECOMMENDATIONS 60

VII. ACKNOWLEDGMENTS 60

VIII. LITERATURE CITED 61

Appendix

1 Mission Summary

List of Tables

Table 1. Settings for the Acoustic Doppler Current Profiler (ADCP) used to monitor subsurface currents at the PLOO. 11

Table 2. A list of the parameters used in the NRFIELD plume model. a) Outfall configuration parameters. b) Model outputs. 15

Table 3. Onboard sensing capabilities of the REMUS vehicle and application to plume water detection. 18

Table 4. Means of current components at the inshore South and Central Pt. Loma ADCP 35m contour study sites. Means of signed components (indicating direction) and means of absolute values (in parenthesis) are listed (u – cross-shore, v – alongshore, w – vertica 27

Table 5. Loadings and eigenvalues resulting from EOF analysis of near bottom velocities (u,v,w) at the South Pt. Loma station. 27

Table 6. Summary of ocean conditions and observed plume ranges for days that REMUS surveys were conducted. 36

Table 7. REMUS survey summary including Froude number, minimum observed plume depth, and minimum observed dilution. 45

Table 8. Comparison of 8/3/2010 and 2/25/2011 background conditions and their effect on plume width. 47

Table 9. Comparison of REMUS field measurements and NRFIELD predictions for 8/3/2010 and 2/25/2011. 51

List of Figures

Figure 1. Location of the Point Loma Ocean Outfall (PLOO), the nearshore ADCP's and telemetered monitoring mooring (buoy). 8

Figure 2. Drawing and a photograph of the Scripps-designed coastal buoy system for measuring stratification and currents at the Point Loma Ocean Outfall. 10

Figure 3. Photograph of the deployed ocean buoy at the PLOO. The white cylinder on the right is a radar reflector and the cylinder on the left is a GPS tracking device. 11

Figure 4. Mooring diagram for the PLOO buoy. The diagram outlines the major mechanical components of the mooring used to keep the buoy in place for the duration of the supplemental monitoring program. 13

Figure 5. REMUS vehicle on boat prior to mission deployment (GPS, sidescan sonar, ADCP, CTD, backscatter, colored dissolved organic matter [CDOM]). 16

Figure 6. Near real-time PLOO plume trajectory estimated for depths between 60 – 90 m from the PLOO mooring indicating southerly flow. The dotted line denotes the horizontal PLOO REMUS mission programmed to capture plume signature. 17

Figure 7. CDOM calibration curve for successive dilutions of source effluent from the Point Loma Wastewater Treatment Plant. 19

Figure 8. Time series of ocean temperature. Top:Temperature time series during entire mooring sampling period. Bottom: Temperature time series from December 13-30, 2010 illustrating an observed down-welling event. The color bars indicate the temperature in Celsius. 22

Figure 9. Eastward, Northward, and Vertical Velocity profiles from December 20-25. A significant and consistent northwest current is seen in the hours preceding a downwelling event on December 22, at approximately 18:00. 23

Figure 10. Depth averaged currents for the north/south and east/west components at the PLOO mooring site. The blue line is hourly data while the red line is a 25-hour running average to remove the tides. 24

Figure 11. Depth averaged currents for the north/south and east/west components at the PLOO mooring site. The blue line is hourly data while the red line is a 25-hour running average to remove the tides. 25

Figure 12. Currents (top panel) throughout the water column and bottom temperature (bottom panel) at the South Pt. Loma ADCP study site – depth 33m from October 22, 2010 –

January 25, 2011. Colors indicate current direction, and intensity indicates magnitude (see legend). 28

Figure 13. Currents (top panel) throughout the water column and bottom temperature (bottom panel) at the South Pt. Loma ADCP study site – depth 33m from May 28, 2011 – September 1, 2011. Colors indicate current direction, and intensity indicates magnitude. . 29

Figure 14. Currents (top panel) throughout the water column and bottom temperature (bottom panel) at the South Pt. Loma ADCP study site for a 2-week period – water depth 33m, from August 8, 2011 – August 22, 2011. 30

Figure 15. Near bottom cross-shore (E-W) currents (mm $s^{-1)}$ at the Central (blue) and South (red) ADCP study sites for the entire study period. Cross-shore currents at the both the subtidal (pictured) and tidal frequencies were much greater at south Pt. Loma. 31

Figure 16. Probability density of Mode 1 currents indicating that Mode 1 was most frequently positive indicating southeastward and upward currents near the bottom at the South Pt. Loma ADCP study site. Moderate positive values were most frequent for Mode 1. 32

Figure 17. Time series of first mode of EOF of currents at South Pt. Loma near the bottom (green). Velocities were first filtered using a 5-day lowpass filter to eliminate higher frequency variability. The first mode captured >55% of the variability of cross- shore, alongshore, and vertical velocities. Bottom temperature (also lowpass filtered) is shown in blue. 33

Figure 18. Times series of near bottom currents and temperature (u,v,w, and T) observed at the central (blue) and southern (red) Pt. Loma 35m ADCP stations. Data were lowpass filtered to remove tidal frequencies. 34

Figure 19. Density structure at the PLOO from April 2010 to April 2011. Also shown are the rise height and plume base estimated using the NRFIELD buoyant plume model. The estimated time-dependent depth extents of the plume are bound by these two black lines. No surfacing events were evident. 35

Figure 20. a) REMUS vehicle mission track (red) extending approximately 5 km south of PLOO (shown in black) for sampling conducted on August 3, 2010. Colored lines indicate the estimated plume trajectory based on PLOO buoy velocity profiles. b) Elevated values of CDOM (>4 ppb) indicate high concentrations of organic matter in the PLOO plume. The PLOO is shown in black with the observed plume toward the south-southeast. The plume trajectory (colored lines) is estimated from the PLOO buoy velocity profiles. 37

Figure 21. Elevated values (>0.0013m-1) of optical backscatter at 650 nm indicate elevated turbidity in the PLOO plume. The PLOO is shown in black with the observed plume toward

the south-southeast. The plume trajectory (colored lines), estimated from the PLOO buoy velocity profiles, suggest the plume advects east until a depth of 60 m where the currents change to a southerly flow. 38

Figure 22. a) REMUS vehicle mission track (red) extending approximately 5 km south of PLOO (shown in black) for sampling conducted on February 25, 2011. Colored lines indicate the estimated plume trajectory based on PLOO buoy velocity profiles. b) Elevated values of CDOM (>4 ppb) indicate high concentrations of organic matter in the PLOO plume. The PLOO is shown in black with the observed plume toward the south. The plume trajectory (colored lines) is estimated from the PLOO buoy velocity profiles. 38

Figure 23. T-S diagram as a function of computed dilution ratios for the August 3, 2010 (a) and February 25, 2011 (b) PLOO missions. The dilution ratio (via CDOM measurements) clearly shows the plume's water mass properties as relatively fresh compared to ambient waters. The diagonal lines in each figure represent lines of constant density. 39

Figure 24. Horizontal (left) and vertical (right) distributions of the PLOO plume measured on August 3, 2010 (a) and February 25, 2011(b). Plume distributions are based on the number of samples with CDOM > 4.3 ppb and salinity < 33.65 ppt falling within each spatial bin (50 x 50 m horizontally and 1 m vertically) then normalized by the maximum number of samples observed in a single bin. On the horizontal distribution plot, the REMUS mission path is shown as a dotted black line, the estimated plume trajectory based on buoy velocity measurements are shown by colored lines and the PLOO outfall is shown in black. 41

Figure 25. Plume distributions are based on the number of samples with characteristic CDOM and salinity values within 1 meter vertical bins. The number of samples is then normalized by the maximum number of samples observed in a single bin for each mission. The relative temperature profile (temperature profile relative to bottom water temperature) is plotted in red. 42

Figure 26. Plume distributions are based on the number of samples with characteristic CDOM and salinity values within spatial bins of 50 x 50 meters. The number of samples is then normalized by the maximum number of samples observed in a single bin for each mission. The REMUS mission path is shown in grey, the estimated plume trajectory based on buoy velocity measurements is shown in pink dashed lines and the PLOO outfall wye is shown in black. 43

Figure 27. Density structure at the PLOO from April 2010 to April 2011. Also shown are the rise height and plume base estimated using the NRFIELD buoyant plume model. The estimated time-dependent depth extents of the plume are bound by these two black lines. No surfacing events were evident. 44

Figure 28. Cross-sectional dilution plots as a function of range from the outfall for (a) August 3, 2010 and (b) February 25, 2011 monitoring missions. The range is measured from the wye to each successive cross-section; (a) 2 km, 3 km, 4 km, 5 km and (b) 0.25 km, 0.75 km, 1.5 km. The figures show the distribution of the plume width and thickness as it progresses downstream. The sawtooth REMUS pattern is included in the 0.25 km cross-section, Figure 28b. 47

Figure 29. Median measured dilution ratios using the CDOM proxy as a function of time from PLOO. Data from missions with steady currents that were parallel to the diffusers (North/South) were combined to show the log-log trend in dilution as a function of time from the outfall. The trend based on missions performed in high Fr number regimes (defined as Fr > 0.11) compared to low Fr number regimes (F < 0.11) is also shown. 50

Figure 30. Profile plots of velocity shear and current velocity for August 3, 2010 (dotted line) and February 25, 2011 monitoring missions. The Ri profile plots of from the area of enhanced mixing seen in Figure 19b. 52

Figure 31. Normalized plume density plotted against depth for the 0.25 km cross-section (hollow bars) and the 1.5 km cross-section (black bars) illustrating a rise in plume height of 10 m in the far-field and profile plots of temperature, salinity and Ri number in the area of interest. 54

Figure 32. Observed isotherms at depths of (a) 2 m, 31 m, and 55 m from February 13, 2011 to February 29, 2011 and (b) 1 m, 13 m, 25 m, 38 m, 50 m, 62 m and 74 m from 20 July 2010 to 6 August 2010. 54

Figure 33. (a) Ocean temperature time series from December 13, 2010 to December 30, 2010. (b) Observed isotherms at depths of 19 m, 31 m, 54 m, 89 m from December 13, 2010 to December 30, 2010 55

Figure 34. Uniform alongshore current direction that intersects the Coronado Islands and affects the PLOO study area on December 22, 2010. 56

Figure 35. Online display of HF Radar derived surface currents in the South Bay on December 22, 2010. Sites maintained through this effort include Point Loma, Border Field State Park, and Coronado Islands. 57

I. INTRODUCTION

The Point Loma Ocean Outfall (PLOO) discharges an average of ~160 million gallons (~0.7 km^3) per day of treated sewage from the Point Loma Wastewater Treatment Plant (PLWTP) into the coastal shelf waters off San Diego. The effluent is treated to a level of advanced primary, wherein at least 85% of suspended solids are removed before being discharged into the Pacific Ocean through a diffusive outfall located ~7.2 km offshore of Point Loma in waters ~100 m deep. At the outset of our study, the behavior of the PLOO wastewater plume (wastefield) was not well known because it had not been studied with the necessary tools to map its three-dimensional extent in a Lagrangian manner over the time and space scales of initial and far-field secondary dilution. The behavior and spatial extent of ocean wastefields off San Diego are complex given the dynamic and complex ocean conditions on the San Diego shelf. Ocean conditions that affect plume behavior off San Diego are known to vary seasonally and are affected by larger scale ocean circulation within the southern California borderlands, local wind patterns, and winds located as far south as southern Baja California.

The purpose of the work presented here was to determine the behavior and dispersion of the PLOO plume using state-of-the-art methodology and equipment. The goals of our project are to address two primary concerns of operating the ocean outfall in its current configuration: (1) possible effects to beach and near-surface water quality and (2) its risk to the coastal marine environment. This study addresses beach and surface water quality concerns by determining whether the wastewater plume surfaces and encroaches upon beaches, and if so, to estimate the frequency of such events. It also supports efforts to address ecosystem concerns by determining the frequency of spatial occurrence (i.e. the temporal footprint) of the plume thereby helping to spatially focus current and future biological and water and sediment quality monitoring programs.

The work outlined here involved (1) tracking the wastefield using an autonomous underwater vehicle (AUV) whose daily track was based on telemetered buoy observations of currents and temperature structure at the end of the outfall, (2) modeling near-field plume behavior off Point Loma, and (3) observations of inner shelf bottom temperature and currents just offshore of the kelp forests using acoustic current profilers.

Information from these three major components supported the description of plume behavior across a broad spectrum of ocean conditions. The modeling effort consisted of using an EPA standard near-field model that describes the footprint, mixing and rising of the buoyant plume. The nearshore current meter and temperature data collected just offshore of the kelp forest provided information on the directionality of nearshore currents during upwelling events when conditions are most favorable for transporting the submerged wastefield into the kelp forest. Ocean circulation and temperature observations were conducted from December 2009 to February of 2012. AUV deployments were conducted from April 2010 to May 2011.

II. METHODS

A. Description of Study Area

The study area (Figure 1) is centered around the Y-shaped outfall that terminates in two 760 m diffuser legs oriented at an internal angle of roughly 151.5 degrees. The average volume of effluent discharged between 93 and 95 m is ~7.89 m^3/s. The bottom topography from the shore at Point Loma to the outfall discharge zone gently slopes to approximately 100 m. Beyond the 100 m isobaths there is a complex network of submarine canyons which make up the La Jolla Canyon Channel system. The currents in the region experience a variety of local driving mechanisms including barotropic tides, internal tides, and winds, as well as larger scale flows such as the seasonally northward flowing Davidson countercurrent and the

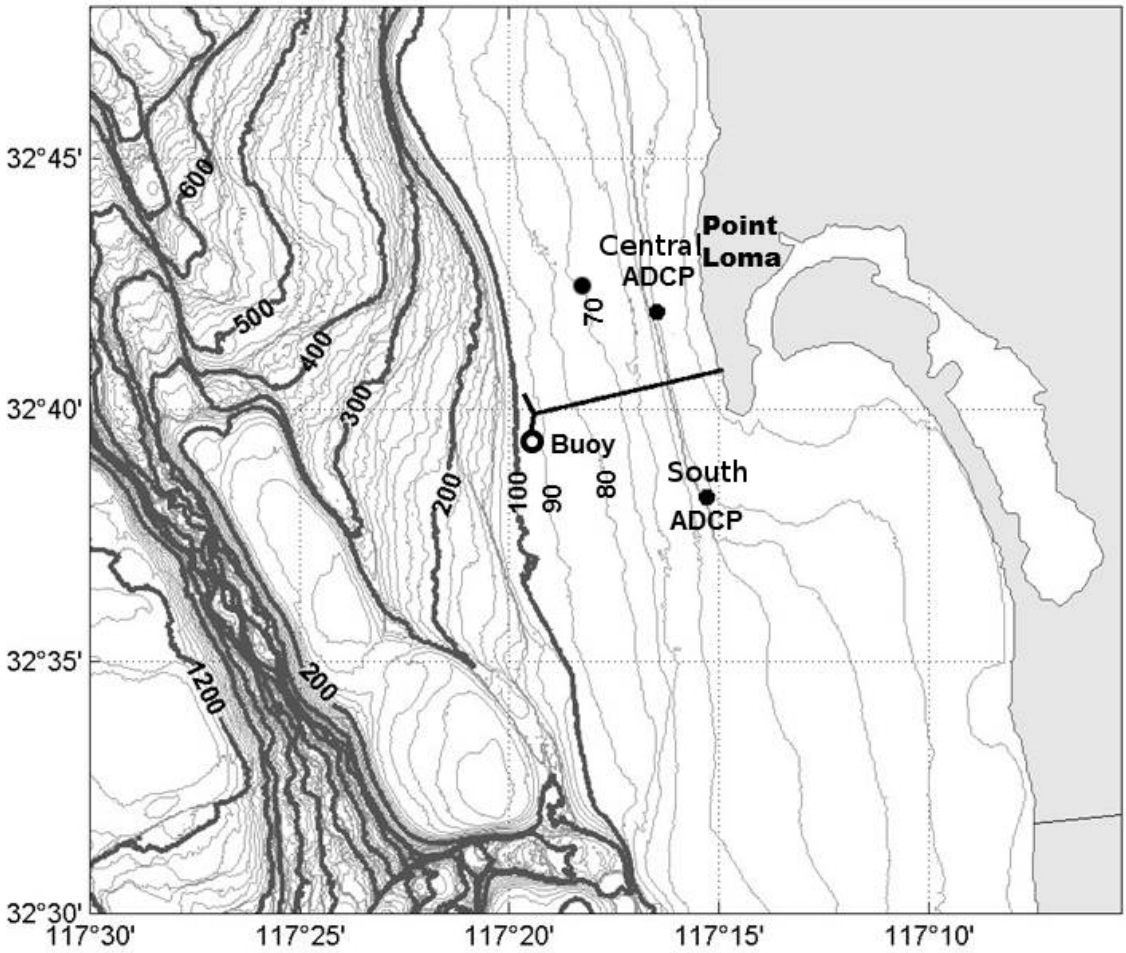

Figure 1. Location of the Point Loma Ocean Outfall (PLOO), the nearshore ADCP's and telemetered monitoring mooring (buoy).

southward flowing California Current. Tides are governed by a mixed diurnal-semidiurnal tidal forcing, with a dominant semidiurnal component [*Chadwick and Largier*, 1999].

The submarine topography associated with the Point Loma headland complicates the local current flow. The mean current direction adjacent to Point Loma is southward with typical alongshore flow speeds of 5 – 20 cm/s. As the water continues southward past the headland it separates from the coast and a vorticity maximum is observed west of Point Loma. The flow diverges from the coast at the tip of the headland, leading to upwelling of cold nutrient-rich deeper waters [*Hendricks and Christensen*, 1987, *Roughan et al., 2005*].

The seasonality of southern California is responsible for the stratification patterns of the local waters. Warmer waters and a more stratified ocean typically are present during the dry season (April through September), with the warmest temperatures occurring in August and September. Cooler waters and weak stratification characterize the ocean conditions during the wet season (October thorough March) [*Terrill*, 2009]. Typical stratification depths range between 30 - 40 m. Below these depths minimal variability in stratification depth is observed throughout the year.

The circulation feature most likely to transport the submerged wastefield emanating from the PLOO towards shore is the onshore progression of the internal tide. The internal tide propagates along the thermocline and is strongest during spring tidal conditions. The shoreward progression of the internal tide manifests as onshore currents predominating at subthermocline depths where the submerged wastefield is most likely trapped. The nearshore ADCP observations were thereby needed to determine the behavior of the internal tide over the inner shelf nearer the kelp forests and beaches.

B. Current and Temperature Observations

1. Telemetry Mooring

An oceanographic buoy designed and built by Scripps Institution of Oceanography for real-time monitoring of ocean conditions at POTW outfalls was used for this study. The mooring consisted of a surface buoy that contained an Acoustic Doppler Current Profiler (ADCP, TRDI Instruments, San Diego, CA) a temperature chain (Precision Measurement Engineering, Encinitas, CA), data logger, satellite telemetry unit, Global Positioning System (GPS) receiver, and a battery pack. The downward looking ADCP profiled ocean currents from 4.3 m deep to the seafloor. All mechanical aspects of the buoy, mooring, and anchoring system were fabricated by Scripps (Figures 2 and 3).

The system was designed for a nominal 6-month servicing interval to replace sensor batteries and offload data from the internal memory recorders. Due to mechanical wear and fatigue on the mooring components, major components of the mooring (swivels, chain, and shackles) were also replaced at this time.

Ocean currents were measured using the ADCP. The ADCP estimates currents by transmitting pulses of sound through the water column and measuring the Doppler shift of the signal scattered from particles moving with the ocean currents. The ADCP was oriented to be downward looking from the surface buoy and provides a profile of ocean currents from 4.3 m to the seafloor. The settings for the unit are listed in Table 1.

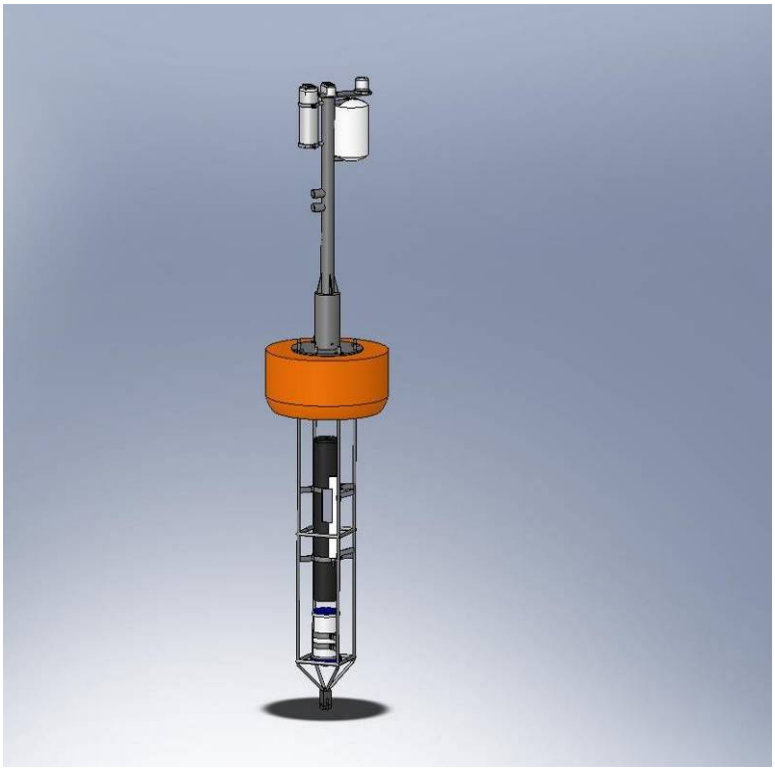

Figure 2. Drawing and a photograph of the Scripps-designed coastal buoy system for measuring stratification and currents at the Point Loma Ocean Outfall.

Figure 3. Photograph of the deployed ocean buoy at the PLOO. The white cylinder on the right is a radar reflector and the cylinder on the left is a GPS tracking device.

Table 1. Settings for the Acoustic Doppler Current Profiler (ADCP) used to monitor subsurface currents at the PLOO.

System Parameter	Setting
Acoustic frequency	300 kHz
Pings per ensemble	25
Ensemble interval	3 minutes
Range cell size	3 meter
Measurement standard deviation	1.4 cm/s
Number of depth cells	33

Measurements of water column stratification were made using temperature sensors located at different depths. For the PLOO buoy, a temperature chain was employed, which consisted of 13 nodes spaced across the water column, each measuring ocean temperature with accuracy of 0.01°C. Measurements at each depth were synchronized to provide a water column profile of stratification at one-hour intervals. Use of the interconnected temperature measurements provided consistent timing across different water depths and eliminated clock drift problems that often occur when individual, self-recording temperature probes are used. The depths of measurement were 2 m, 5.8 m, 7.7 m, 9.6 m, 11.5 m, 15.4 m, 19.2 m, 23.1 m, 30.8 m, 38.6 m, 54.2 m, 69.4 m, and 88.6 m.

Buoy position, currents, and ocean temperature data were transmitted to shore once each hour using an Iridium Satellite modem. Receiving the data in near-real-time allowed observation of present ocean conditions to estimate the rise height and the direction of the PLOO plume. The mooring was deployed just west of the diffuser wye at 32.665N, -117.325W at a depth of 95 m. The all-chain mooring was secured with a 900-lb anchor (Figure 4). The mooring was deployed on April 7, 2010, and subsequently serviced on November 4, 2010. Deployment and servicing were conducted using Scripps research vessels.

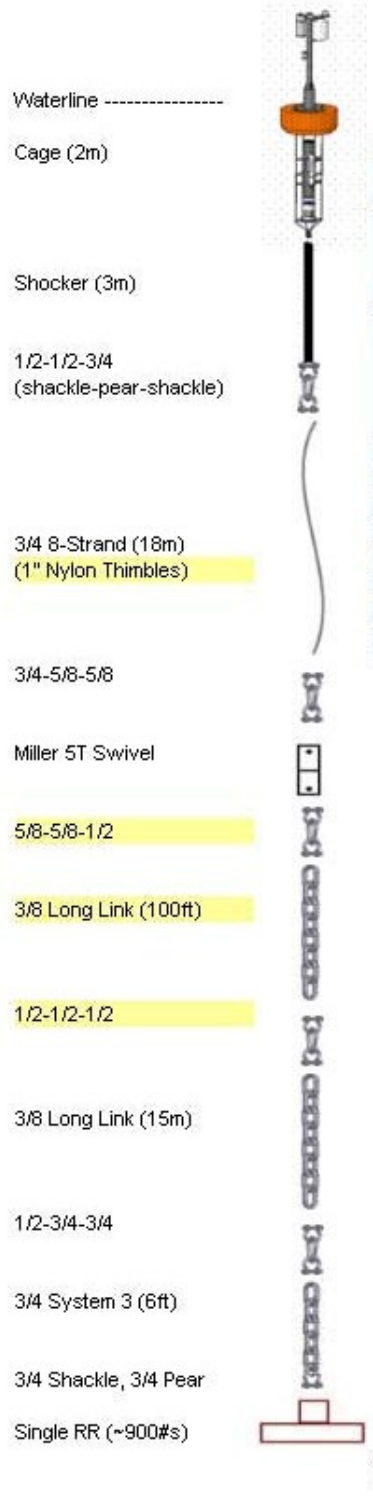

Figure 4. Mooring diagram for the PLOO buoy. The diagram outlines the major mechanical components of the mooring used to keep the buoy in place for the duration of the supplemental monitoring program.

2. Nearshore ADCPs

Two 600 kHz Teledyne Ryan ADCPs (Workhorse Sentinels) were deployed inshore of the PLOO diffuser wye along the 35 m contour (see Fig. 1 – Central and South ADCPs) to supplement the offshore current data generated at the telemetry mooring site. The nearshore ADCPs were deployed on the bottom looking upwards and data were internally stored. The ADCPs were retrieved and redeployed at approximately three-month intervals. Currents were binned at two meter intervals beginning from ~3 m off the bottom to the surface. The ADCPs were also equipped with a temperature sensor. Current and temperature sampling intervals were set to five minutes.

C. Modeling Near-Field Plume

The rise height of a buoyant discharge plume is controlled by the outfall design and density structure with depth in the near-field and ocean circulation in the far-field. The latter is controlled by winds, tides, along-shore pressure gradients, and internal waves. The U.S. EPA Roberts-Snyder-Baumgartner (RSB) plume model (renamed NRFIELD) was applied to the mooring data to predict the height of the plume and its potential to surface in the near-field (Roberts et al. 1989, Roberts 1999a, Roberts 1999b). The NRFIELD model is based on extensive experimental studies on multiport diffusers in density-stratified currents of arbitrary flow described in *Roberts et al*., [1989]. The experiments covered a wide range of parameters typical of ocean outfalls including jet momentum, buoyancy flux, port spacing, stratification, and current speed and direction [*Roberts*, 1999a]. Once these inputs are defined, the model predicts wastefield characteristics at the end of the initial mixing zone (near-field). These include near field dilution, plume rise height, thickness and length of the initial mixing zone. An extensive description of the model basis can be found in *Roberts et al*., [1989] and the model formulation is described in the EPA manual [*Baumgartner et al*., 1994]. The PLOO engineering parameters and the NRFIELD model output are listed in Tables 2a and 2b.

Table 2. A list of the parameters used in the NRFIELD plume model. a) Outfall configuration parameters. b) Model outputs.

(a)

Model inputs	**Input data**
Number of ports	208
Port diameter (m)	0.1
Port spacing (m)	7.32
Discharge depth (m)	93
Diffuser orientation (degrees)	15
Effluent density	0.997
Number of points in density profile	7

(b)

Model outputs
Minimum dilution at the end of the near-field
Rise height (m)
Plume Thickness (m)
Height to level of near-field dilution (m)
Length of the near-field (m)

Ocean density was not directly measured on the mooring. Instead density profiles were estimated using temperature data since the density stratification in Southern California has been found to be strongly dependent on temperature [*Winant and Bratkovich*, 1981, *Bratkovich, 1985*]. Density profiles were thus estimated from measured temperature profiles and climatological estimates of salinity (Millero and Poisson 1981, Fofonoff and Millard Jr. 1983).

D. Autonomous Underwater Vehicle Deployments

Primary mapping of the PLOO plume was performed by an Autonomous Underwater Vehicle (AUV) designed for coastal monitoring. The Remote Environmental Measuring UnitS (REMUS) manufactured by Hydroid LLC (Figure 5) utilizes onboard navigation for vehicle control and can be preprogrammed to map user-driven scenarios based on areas of interest. The vehicle is typically launched by two persons from the boat at a location nearest to the start position and receives a start command from an underwater acoustic control unit called a Ranger. At initial deployment, the vehicle always takes a Global Positioning System (GPS) fix and zeros the pressure sensor to initialize its horizontal and vertical navigation algorithms. After these fixes, the vehicle navigates using underwater transponders with fixed/known locations or by re-acquiring GPS throughout the deployment. Depth is monitored by a pressure sensor and altitude and speed of the vehicle over the seafloor is obtained with an ADCP bottom ping. The Ranger continually queries the vehicle throughout the deployment to gain system status. The vehicle has a 100-meter maximum operating depth and 22-hour battery capacity for surveying at an optimum

speed of 3 knots. This range decreases with increasing speed to eight hours of surveying at five knots. Upon completion of the mission, the vehicle is again recovered by two personnel.

Figure 5. REMUS vehicle on boat prior to mission deployment (GPS, sidescan sonar, ADCP, CTD, backscatter, colored dissolved organic matter [CDOM]).

The AUV includes an array of instrumentation for environmental monitoring. The combination of the CTD and optical sensors (the standard workhorse tools used by boat-based NPDES monitoring programs) placed onto a flexible platform such as REMUS, lends itself well to the problem of plume mapping through surveying changes in ocean properties. The REMUS has four main sections - a nose section, an RD Instruments 1200-kilohertz (kHz) ADCP, a mid-body and tail section. The nose section includes both the Ultra-Short BaseLine (USBL) and Long BaseLine (LBL) acoustic navigation transducers. The sensors used for these studies include a fast response, high resolution, Conductivity, Temperature, and Depth (CTD, Neil Brown Instruments, Falmouth, MA) sensor and an optical fluorometer calibrated to measure backscatter at 650 nm and 880 nm and CDOM with a sensitivity of 0.09 ppb (WET Labs ECO triplet, Philomath, OR). The parameters measured onboard the REMUS vehicle and their usage for discharge plume detection is listed in Table 3.

1. Mission Planning

A challenge in accurately tracking a wastewater plume is the design of an effective sampling plan which adapts to variable oceanographic conditions in the environment [*Ramos et al*., 2002]. For the PLOO, scientists utilized velocity and temperature profile sets to accurately program the REMUS to capture the plume signature. Datasets were reviewed daily to determine whether conditions indicated either northward or southward advection of the plume. The most probable missions would be planned prior to sampling based on near real-time oceanographic conditions at the outfall as monitored by the buoy coupled with plume model predictions.

In the days preceding a monitoring mission, model outputs using telemetered data from the moored buoy instrumentation were analyzed for vehicle path planning. Vertical sampling was constrained by estimates of the plume height and thickness using the U.S. EPA Roberts-Snyder-Baumgartner (RSB) plume model (now renamed NRFIELD) [*Roberts et al*., 1989, 1999a, 1999b]. The AUV was programmed to swim a sawtooth undulation pattern normal to the mean advection of the plume for a depth range based on the predicted rise height and thickness of the plume from NRFIELD outputs (typically between 40 – 90 m). This approach yielded an

approximate profile spacing of 500 m for resolving cross-sections of the plume at varying ranges from the discharge.

Horizontal sampling was constrained with the aid of trajectory estimates made from telemetered buoy ADCP data. Trajectories representing the bulk transport of the water for the entire water column were computed for 72 hours of data and updated on an automated basis with the receipt of the next hour of data (Figure 6). Trajectories were computed from the time series of *u* and *v* velocities from the buoy ADCP. This web-accessible spatial information served as a key decision aid for horizontal path planning of the survey to maximize chances of sampling the plume. When used in conjunction with a 5-hour averaged current profile, REMUS mission paths (dotted line) were developed to spatially optimize plume sampling and minimize measurements outside of the plume. Hourly current velocity profiles were also monitored in the hours leading up to the vehicle deployment to assess if the plume orientation was changing and determine if adjustments were necessary.

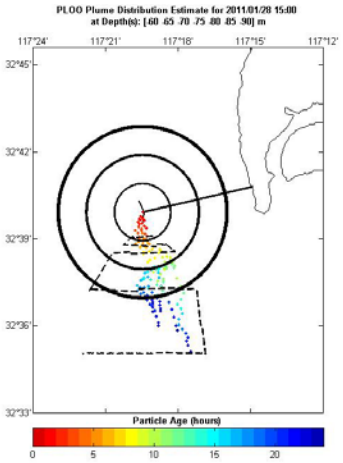

Figure 6. Near real-time PLOO plume trajectory estimated for depths between 60 – 90 m from the PLOO mooring indicating southerly flow. The dotted line denotes the horizontal PLOO REMUS mission programmed to capture plume signature.

Table 3. Onboard sensing capabilities of the REMUS vehicle and application to plume water detection.

Parameter	Ambient Values	Measured Plume Values	Measurement Value
Velocity	N/A	N/A	Subsurface velocity measurements can be used to calculate currents for comparison with fixed mooring assets and to assess changes in currents within the sampling region.
Conductivity (Salinity)	33.7 - 34.2 practical salinity units (psu)	PLOO ≤ .07 - 0.2 psu below ambient	Conductivity measurements are used to calculate salinity values and can measure the freshwater signal of plume water compared to background ocean levels.
Temperature	N/A	N/A	Water temperature measurements are used to estimate ocean stratification, which controls the rise height of a buoyant discharge plume.
Optical backscatter	bb(650) <0.001 bb(880) <0.003	PLOO bb(650) <0.003 bb(880) <0.006	Optical backscatter measured at two wavelengths (650 and 880 nanometers [nm]) is used as an indication of turbidity. The signal measured by this meter is directly correlated to particle concentrations. Higher turbidity measurements are indicative of plume water. The TJR plume is always clear in backscatter due to strong signal, but kelp can easily mask PLOO plume signature in the far field. Kelp forest has values bb(650) <0.01 and bb(880) <0.01. Ratios of the optical backscatter can serve as a proxy for the size distribution of ocean particles.
CDOM (Colored Dissolved Organic Matter)	≤ 4.0 parts per billion (ppb)	≥ 4.2 ppb	CDOM measurements serve as a clear indicator of plume water having values more elevated than ambient seawater.

2. Colored Dissolved Organic Matter (CDOM)

Use of fluorescence for distinguishing plume water from its receiving water has been addressed in earlier literature [Jones et al., 1993; Washburn et al., 1992; Wu et al., 1994]. The authors used chlorophyll fluorescence, a beam transmissometer, a current meter, and a CTD collectively to determine plume location. The work of Petrenko et al. [1997] complimented these findings by utilizing only elevated levels of fluorescence to detect plume waters through the use of a fluorometer with a excitation/emission (Ex/Em) wavelength pair of 228/340 nm. They concluded that such fluorescence (low Ex/Em wavelength) may be useful as a new in situ natural tracer of effluent discharges. The present work builds on this finding by using a compact form factor fluorometer calibrated to measure CDOM, with Ex/Em = 370/460 that is suitable for installation in the nose of an AUV. The sensor was calibrated in a black polyethelene tank (0.3 m diameter x 1.3 m high) through successive dilutions of source effluent from the Point Loma Wastewater Treatment Plant (PLWTP) using clean seawater obtained from the Scripps Pier. Seawater was chosen for the dilute to replicate field conditions. The CDOM fluorometer was suspended in the middle of the tank to eliminate any biases from optical reflections and the tank

was kept dark to prevent ambient light from influencing the sensor reading. Successive dilutions from 1:1 to 1:600 (by volume) were conducted, and the sensor was configured to sample at 1 Hz for several minutes between dilution levels. The source had a measured CDOM concentration of 121 ppb and the ambient seawater CDOM concentration was 3.96 ppb which was accounted for in the calibration. The CDOM calibration curve showed that the sensor has a well-behaved response to the range of dilutions used described by D = F(CDOM (ppb))

$$D = 2*10^{-5}*(CDOM)^2+6*10^{-3}*(CDOM) - 8*10^{-4} \qquad \text{(Eq. 1)}$$

with $R^2 = 0.99$, (plotted on log plot to show full range of dilution; Figure 7), with the detectability of the highest dilution ratio limited by the background seawater levels. For a dilution range of 50 - 600 (levels expected to be sensed in the field), the CDOM levels concentrations ranged from 0 – 2.5 ppb after the background CDOM concentration is accounted for. We note that effluent CDOM levels will vary from plant to plant due to varying levels of treatment, making this calibration specific to the PLWTP. The sensor calibration (eq. 1) was applied to the AUV-based CDOM measurements in order to infer plume dilution in the following sections.

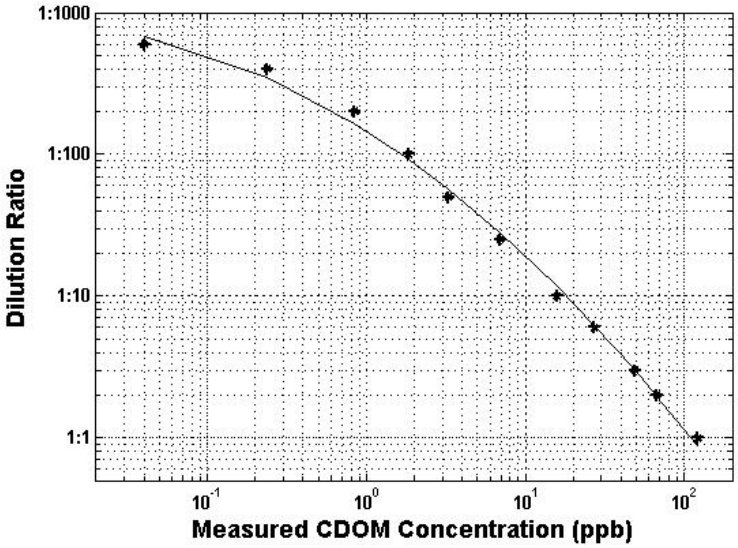

Figure 7. CDOM calibration curve for successive dilutions of source effluent from the Point Loma Wastewater Treatment Plant.

A principal challenge in tracking an outfall plume is the spatial and temporal variability of ocean currents and stratification in coastal waters which, without the aid of recent measurements, limits plume sampling far from the outfall due to uncertainty in the plume's location. Often the plume is missed by traditional *a priori* grid-shaped sampling designs due to the plume's spatial patchiness and the limited range of the freshwater signature of the plume. For example, *Terrill* [2009] shows that monthly sampling of a discharge offshore San Diego using traditional conductivity, temperature, and depth (CTD) sampling on pre-defined grids were able to detect the discharge plume only twice out of 16 monthly surveys. The work performed

on the South Bay Ocean Outfall (SBOO) determined that the plume had an elevated CDOM signature that proved to be a better natural tracer than traditional monitoring methods. CDOM exists naturally in seawater and freshwater environments and generally consists of decaying organic matter from living organisms. Nearshore CDOM has both marine and terrestrial sources due to riverine input. CDOM concentrations near shore may be further elevated by human activities such as logging, agriculture, and wastewater discharge. Based on this work, elevated CDOM levels from discharged wastewater were used as the primary plume tracker for PLOO monitoring missions.

III. RESULTS AND FINDINGS

A. Shelf Hydrographic Observations

1. Telemetry Mooring

A summary of the vertical structure of ocean temperature and water velocity is provided in this section. Figure 8 (top) presents a color contour plot of time records of ocean temperature at the outfall site. The contour is created by data from the 13 temperature probes that span the water column. The seasonality of the ocean temperatures is clearly evident in the upper water column (<30 m), with warmer waters and a stratified ocean present during the dry season (April through September) and remaining through the beginning of the wet season (October). Cooler waters and weak stratification characterize the ocean conditions in the upper water column during the remainder of the wet season (November through March). Below 30 m, the water column remains weakly stratified throughout the year. The only significant fluctuations in temperature occur at the end of December. Figure 8 (bottom) illustrates the temporal variability of the temperature time series from December 13-30, 2010 during an observed down-welling event. On December 22, 2010, the warmer surface water is advected down the length of the water column creating a well-mixed layer of warm water to a depth of approximately 80 m.

Alongshore winds are a common forcing mechanism of coastal upwelling and downwelling. When wind flows parallel to a long coastline for an extended period, a steady state develops and net transport of the surface waters will be 90^{o} to the right of the wind direction [*Ekman*, 1905]. Therefore, periods of wind-induced downwelling are associated with persistent southerly and onshore winds. However, the warming event observed on December 22, 2010, does not appear to be a result of wind induced downwelling as velocity profiles show a consistent northwest current in the hours preceding the downwelling event (Figure 9). If Ekman transport was causing the downwelling, an on-shore current would be evident in the study area. Also, no significant on-shore winds were measured during this time frame, eliminating the wind as a possible mechanism. From Figure 9, the maximum downward velocity (~ 0.5 m/s) occurs for only a 1-hour interval with lower velocities (~0.1 m/s) observed in the hour before and after. Similar maximum vertical velocities in the upward direction are seen 9 hours earlier, also for only a 1-hour interval. This pattern of high upward velocity followed by high downward velocity suggests the presence of an internal wave propagating through the study area. Internal waves will be discussed in more depth in a later section.

A way of assessing the general trends of the currents at the site is to examine the depth-averaged flow. For this analysis, the currents are vertically averaged and a 25-hour time averaging window is used to average out the tidal motion to make the subtidal motions more visible. The subtidal motions are most relevant for tracking plume behavior since tidal motions do not result in net transport. Figure 10 presents the depth and tidally filtered velocity records for the site. The figure shows the temporal variability of the currents from April 2010 to April 2011. However, graphically presenting the dense data over a 12-month period does not give one an indication of the shorter time-scale fluctuations in the ocean current. As an example of the variability of the regions currents, a time series of velocities for the time period from December 21-28, 2010, is provided in Figure 11. The figure illustrates the changes in the currents that can occur over a few days, with the flow dominant northward at the start of the record and changing to a southward flow in the period of 3 days.

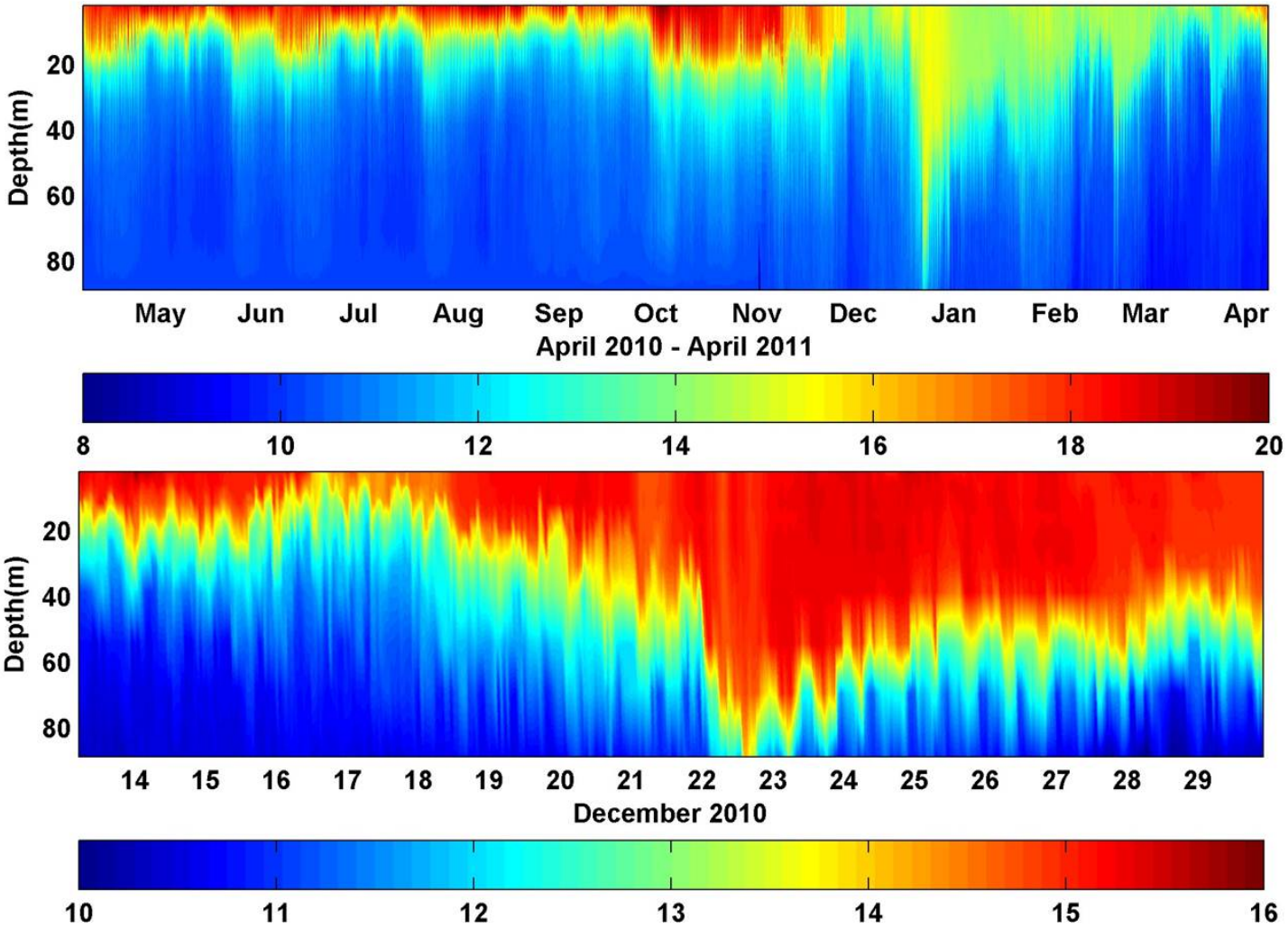

Figure 8. Time series of ocean temperature. Top:Temperature time series during entire mooring sampling period. Bottom: Temperature time series from December 13-30, 2010 illustrating an observed down-welling event. The color bars indicate the temperature in Celsius.

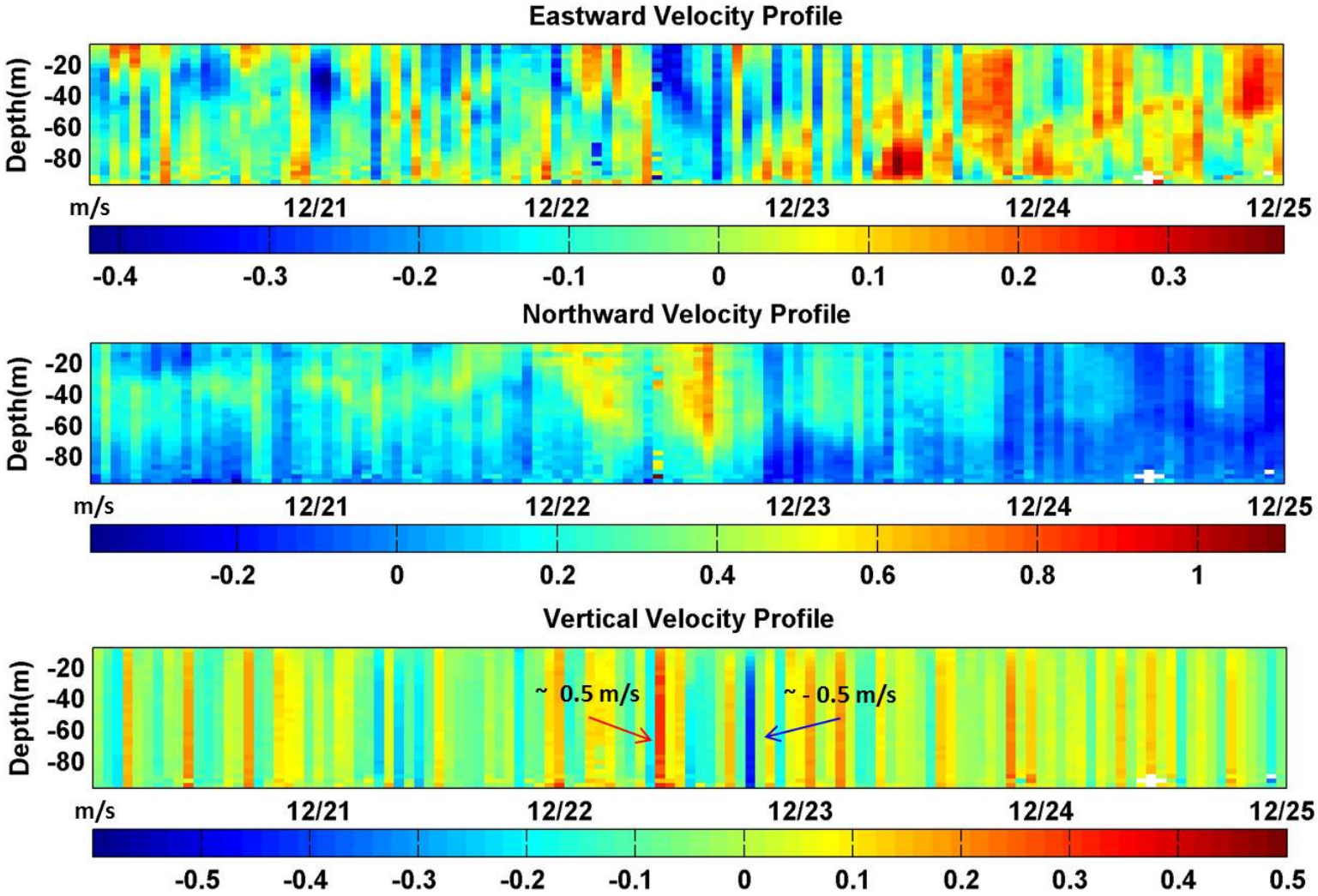

Figure 9. Eastward, Northward, and Vertical Velocity profiles from December 20-25. A significant and consistent northwest current is seen in the hours preceding a downwelling event on December 22, at approximately 18:00.

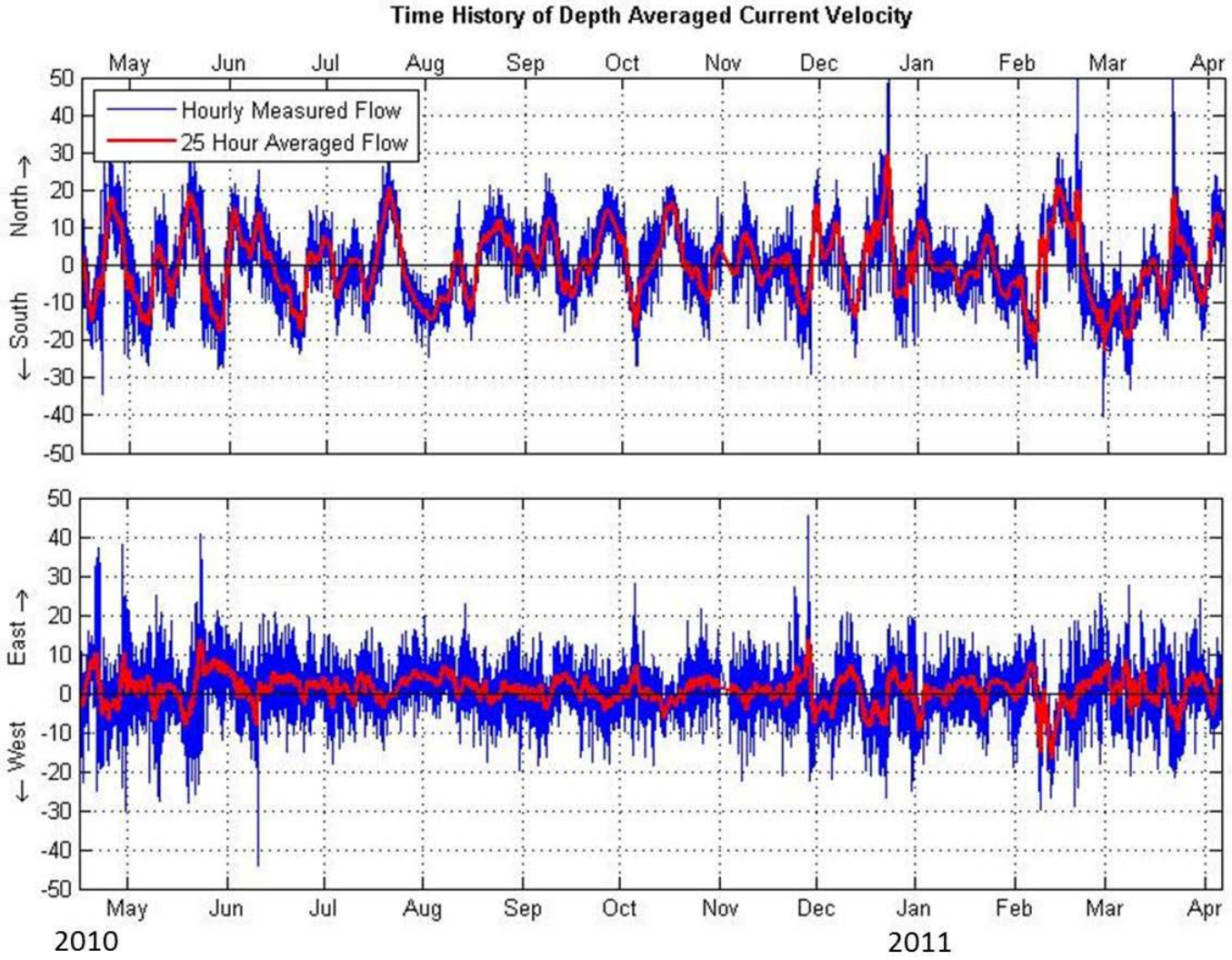

Figure 10. Depth averaged currents for the north/south and east/west components at the PLOO mooring site. The blue line is hourly data while the red line is a 25-hour running average to remove the tides.

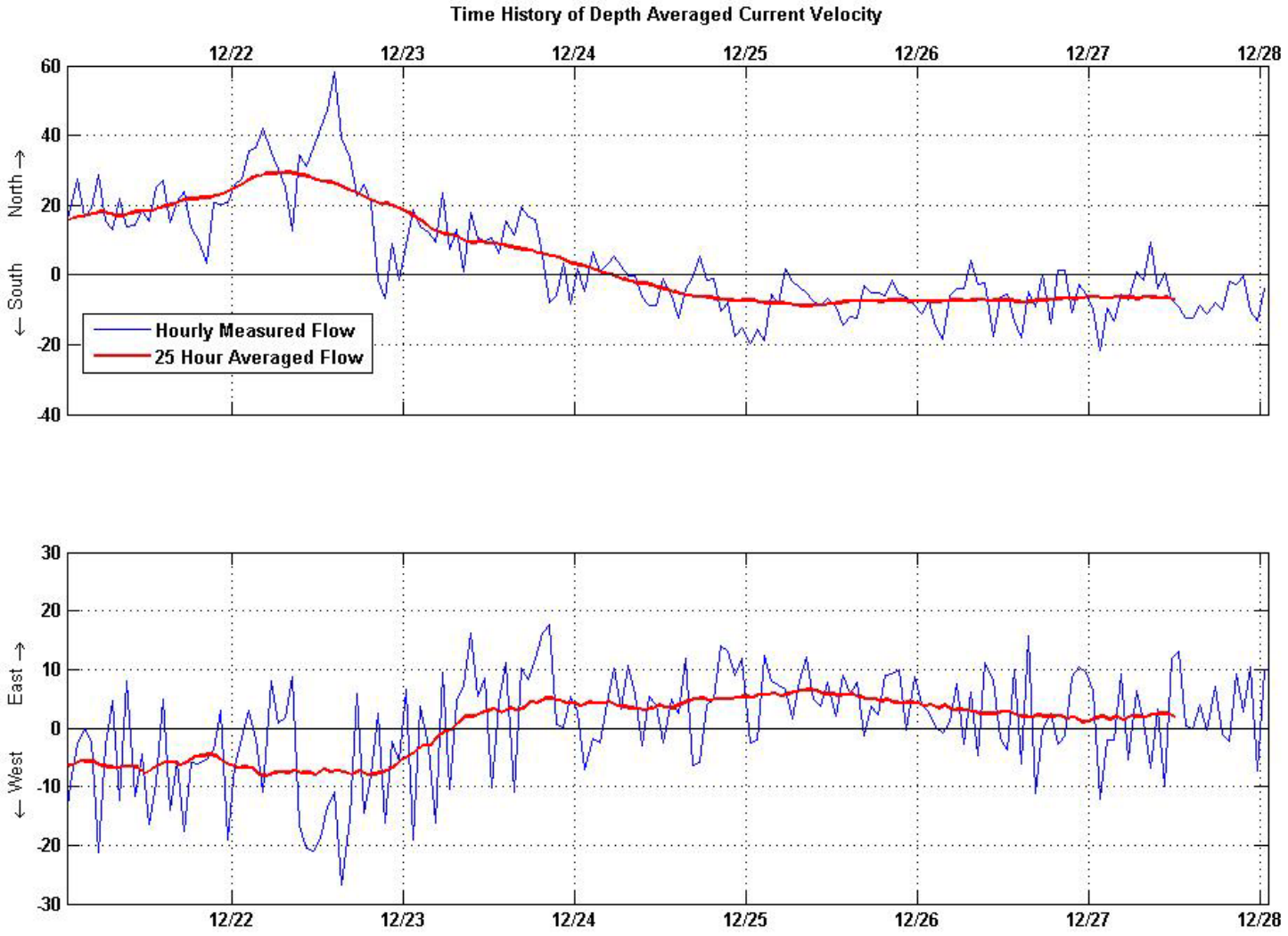

Figure 11. Depth averaged currents for the north/south and east/west components at the PLOO mooring site. The blue line is hourly data while the red line is a 25-hour running average to remove the tides.

2. Hydrography of the Inner Shelf

Currents over the inner shelf along the 35m contour (see ADCP locations in Figure 1), were similar to the currents observed over the outfall diffusers. The largest source of variability in the subtidal frequency band included alternating periods of approximately unidirectional alongshore flows (oriented northwest to southeast) throughout the water column persisting for periods of a few days to a little more than a week (Figures 12 and 13). Temperature increases at subtidal frequencies near the bottom typically coincided with northerly flows. Vertically sheared flows were typically observed during transitions between the low frequency northward and southward flows (Figure 14). There did not appear to be a seasonal pattern in the duration and frequency of the lower frequency oscillating flows. Near bottom tidal frequency currents were oriented mostly cross-shore, driven by the internal tide (Figure 15) with onshore currents observed just prior to, and during, temperature decreases indicating upwelling. The strong downwelling event observed at the mooring ADCP in December of 2010 was also observed at both the central and southern Pt. Loma 35 meter sites (Figure 15).

Currents among the two inner shelf study sites, while significantly correlated at most depths, exhibited notable differences. The largest difference was the magnitude of cross-shore flows in both the tidal and subtidal bands (Figure 15). Cross-shore currents in the middle and lower water column at the south site were typically two to three times as great as the central site (Table 4, Figure 16). Vertical velocities at the two sites indicate that the central site is an area of divergence with upward velocities near surface and downward velocities near bottom while the opposite is true for south Pt. Loma where vertical velocities appear convergent. Clearly, upward movement in the bottom of the water column at South Pt. Loma is greater than that for central Pt. Loma indicating that if the outfall plume broached the 35m contour and approached shore, the southern portion of the Pt. Loma nearshore shelf would be most impacted. This is further supported by the greater magnitude cross-shore velocities observed at South Pt. Loma. However, plume contact with this portion of the inner shelf is unlikely given observed and modeled plume trapping depths.

Horizontal and vertical velocities near the bottom at South Pt. Loma (tidal band) were analyzed using EOF analysis since it appears that the south Pt. Loma shelf is the most likely area to be impacted by the plume if it transgressed close to shore (see Table 5 for EOF loadings). The first mode accounted for ~55% of the overall variability among vertical and horizontal velocity constituents. Mode 1 was characterized as a combination of southeastward currents coincident with upward vertical velocities and conversely, northwestward currents coinciding with downward vertical velocities. Subtidal band currents exhibited similar behavior. Southeastward and upward vertical velocities predominated (Figure 17) during the study period of 2010-2012. The first had a strong effect on temperature, with temperature decreases slightly preceding and coinciding with increases in Mode 1 (Figure 18), further indicating that upwelling was accompanied by southeastward currents. Mode 1 was significantly negatively correlated with temperature changes ($r = -0.41$, $p<0.001$).

Table 4. Means of current components at the inshore South and Central Pt. Loma ADCP 35m contour study sites. Means of signed components (indicating direction) and means of absolute values (in parenthesis) are listed (u – cross-shore, v – alongshore, w – vertical

	Central			South		
	u	**v**	**w**	**u**	**v**	**w**
Near surface	237.2 (308.1)	-76.5 (291.9)	9.9 (19.0)	217.6 (417)	-133.8 (365)	-11.7 (24.7)
Midwater	1.2 (25.2)	10.2 (47.5)	0.1 (4.7)	3.06 (76.8)	3.6 (71.8)	1.3 (6.3)
Near bottom	-4.1 (28.9)	4.9 (33.1)	-0.8 (3.1)	-9.3 (54.2)	2.9 (45.3)	0.2 (4.3)

Table 5. Loadings and eigenvalues resulting from EOF analysis of near bottom velocities (u,v,w) at the South Pt. Loma station.

	Component	**Mode 1**	**Mode 2**
EOFs	**u**	0.65	~0
	v	-0.53	0.71
	w	0.54	0.70
	Eigenvalue	1.68	0.85

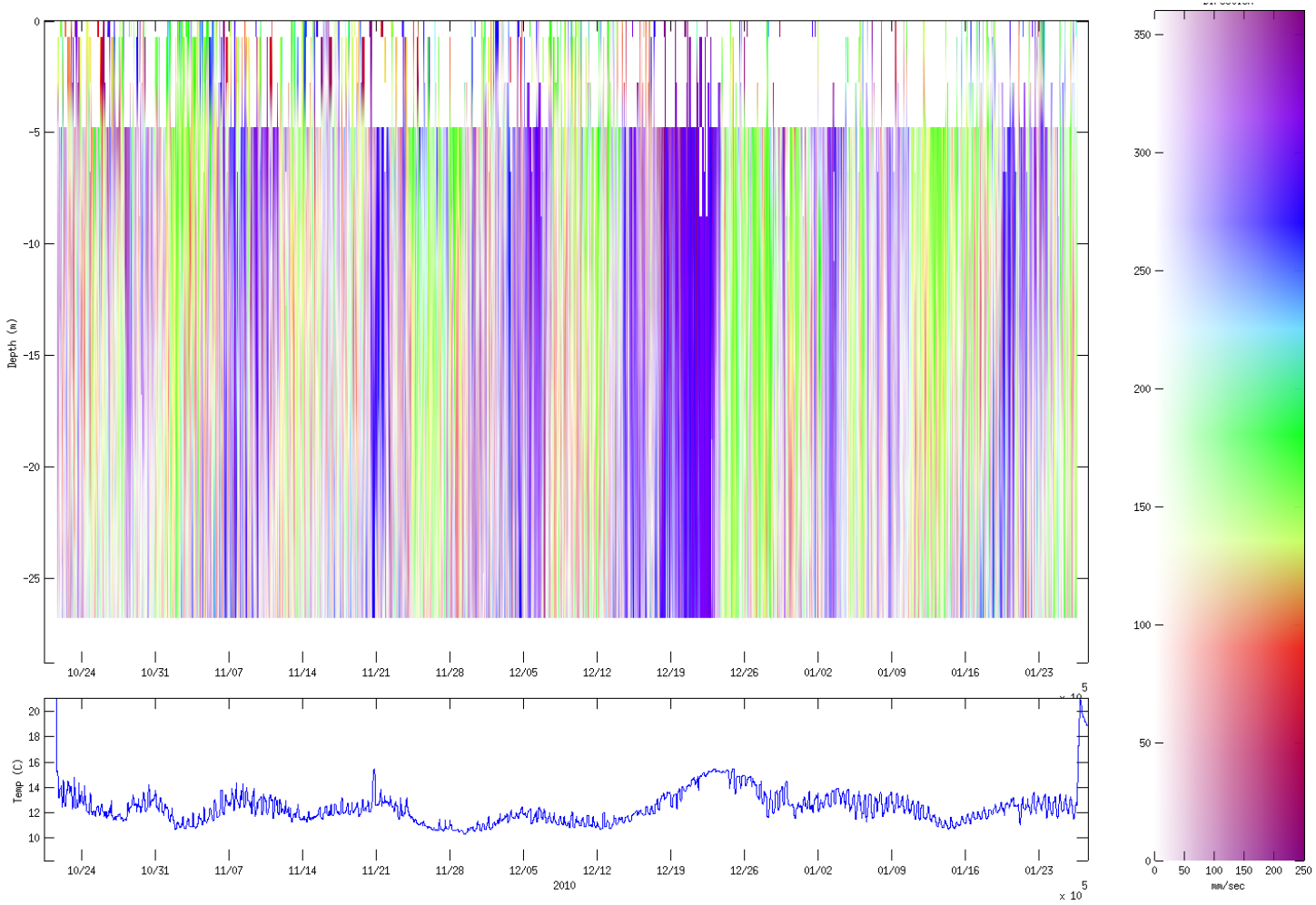

Figure 12. Currents (top panel) throughout the water column and bottom temperature (bottom panel) at the South Pt. Loma ADCP study site – depth 33m from October 22, 2010 – January 25, 2011. Colors indicate current direction, and intensity indicates magnitude (see legend).

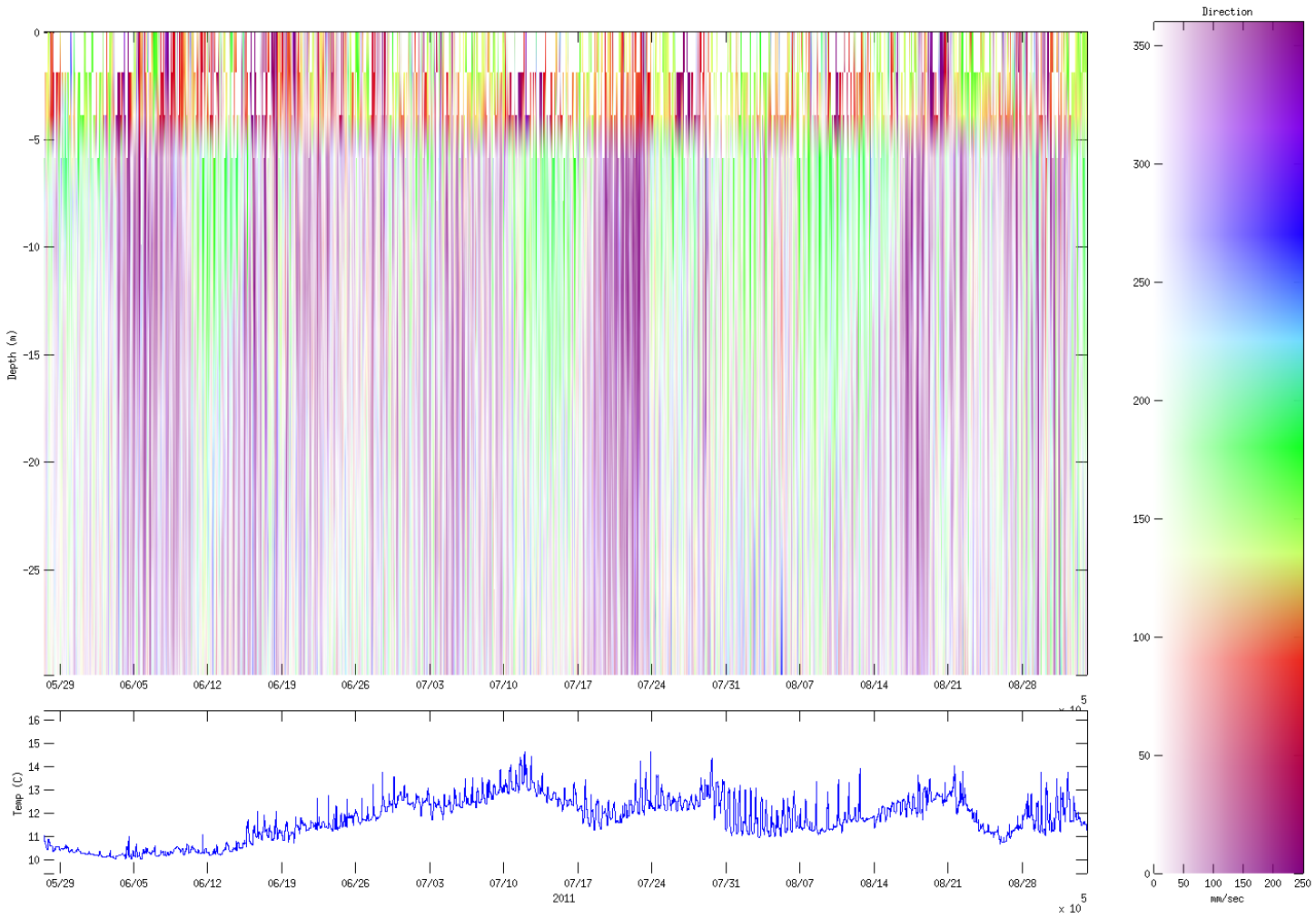

Figure 13. Currents (top panel) throughout the water column and bottom temperature (bottom panel) at the South Pt. Loma ADCP study site – depth 33m from May 28, 2011 – September 1, 2011. Colors indicate current direction, and intensity indicates magnitude.

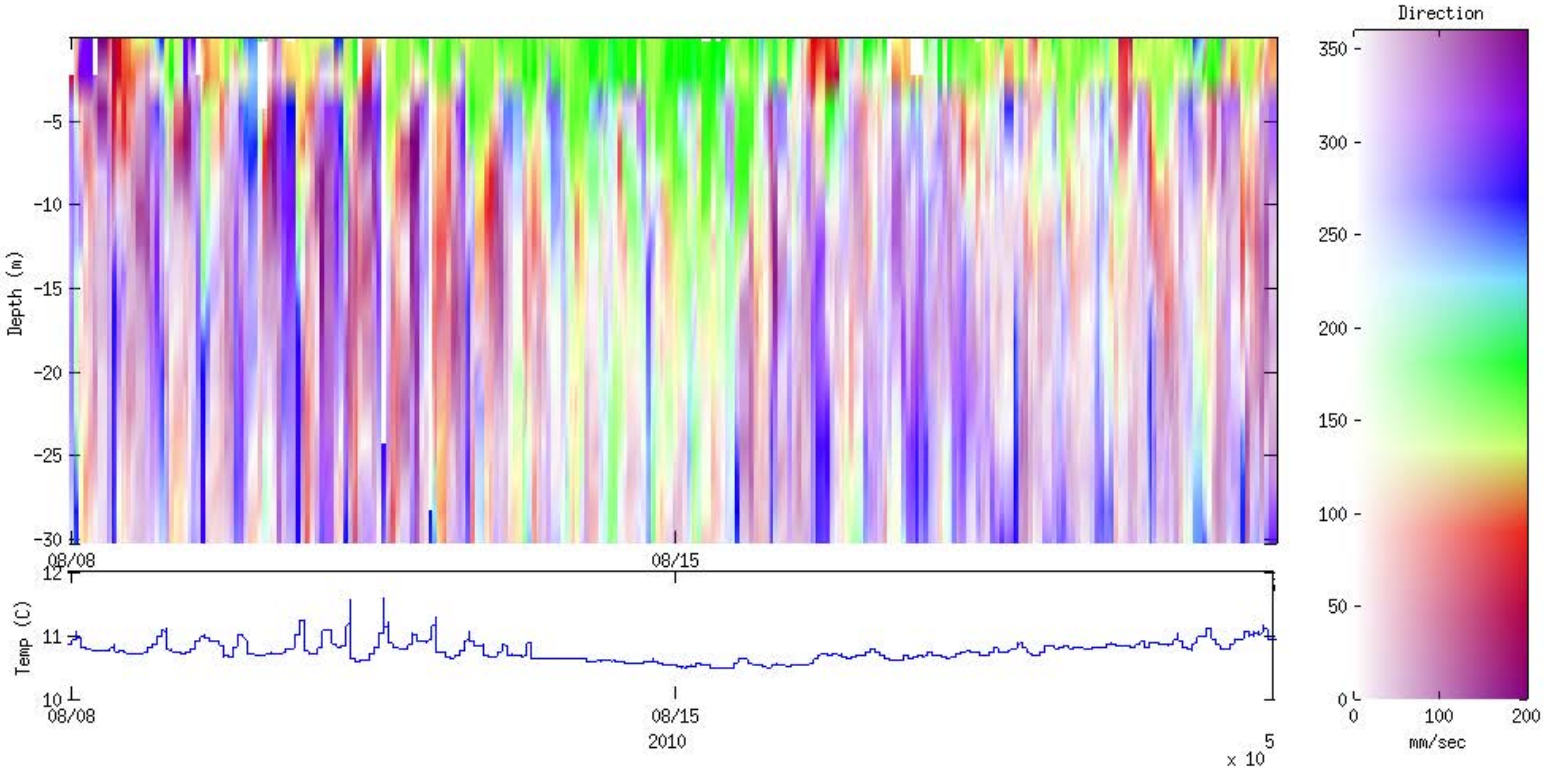

Figure 14. Currents (top panel) throughout the water column and bottom temperature (bottom panel) at the South Pt. Loma ADCP study site for a 2-week period – water depth 33m, from August 8, 2011 – August 22, 2011.

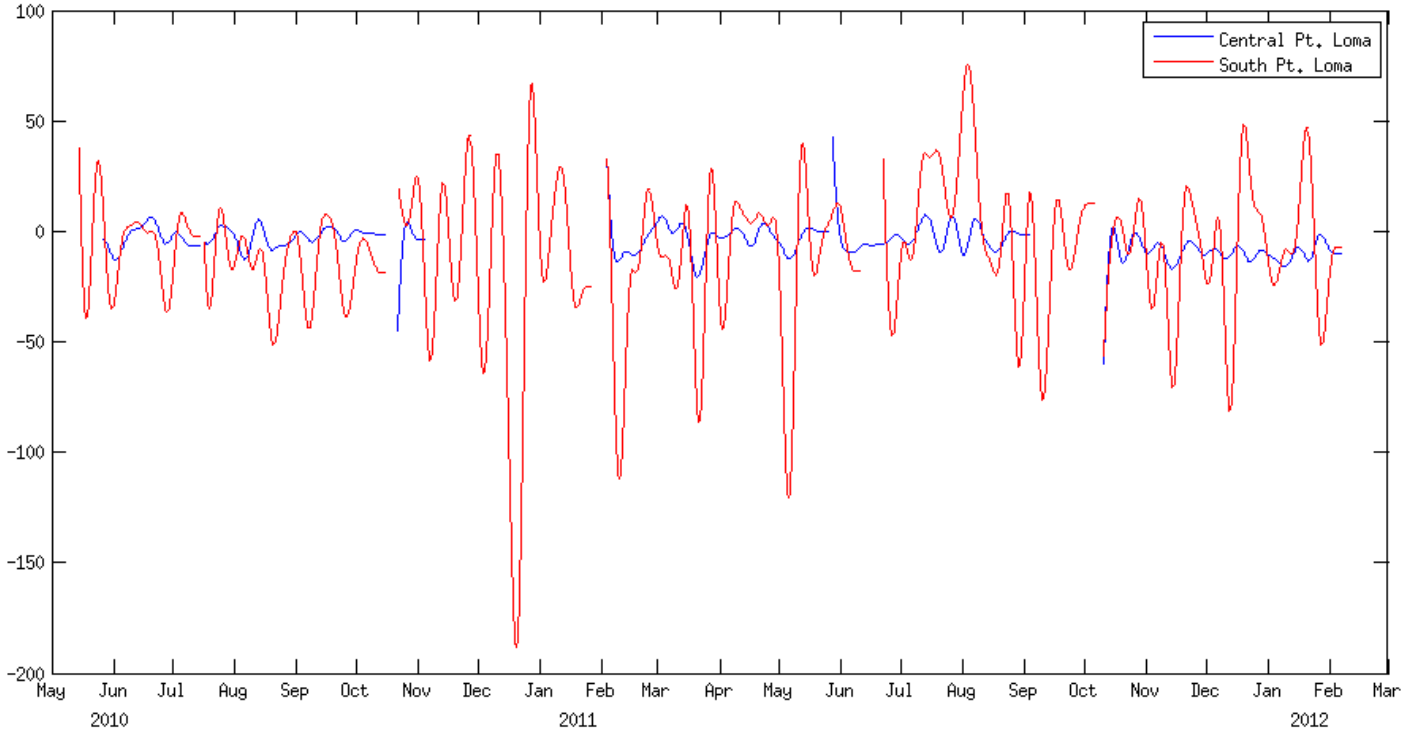

Figure 15. Near bottom cross-shore (E-W) currents (mm $s^{-1)}$ at the Central (blue) and South (red) ADCP study sites for the entire study period. Cross-shore currents at the both the subtidal (pictured) and tidal frequencies were much greater at south Pt. Loma.

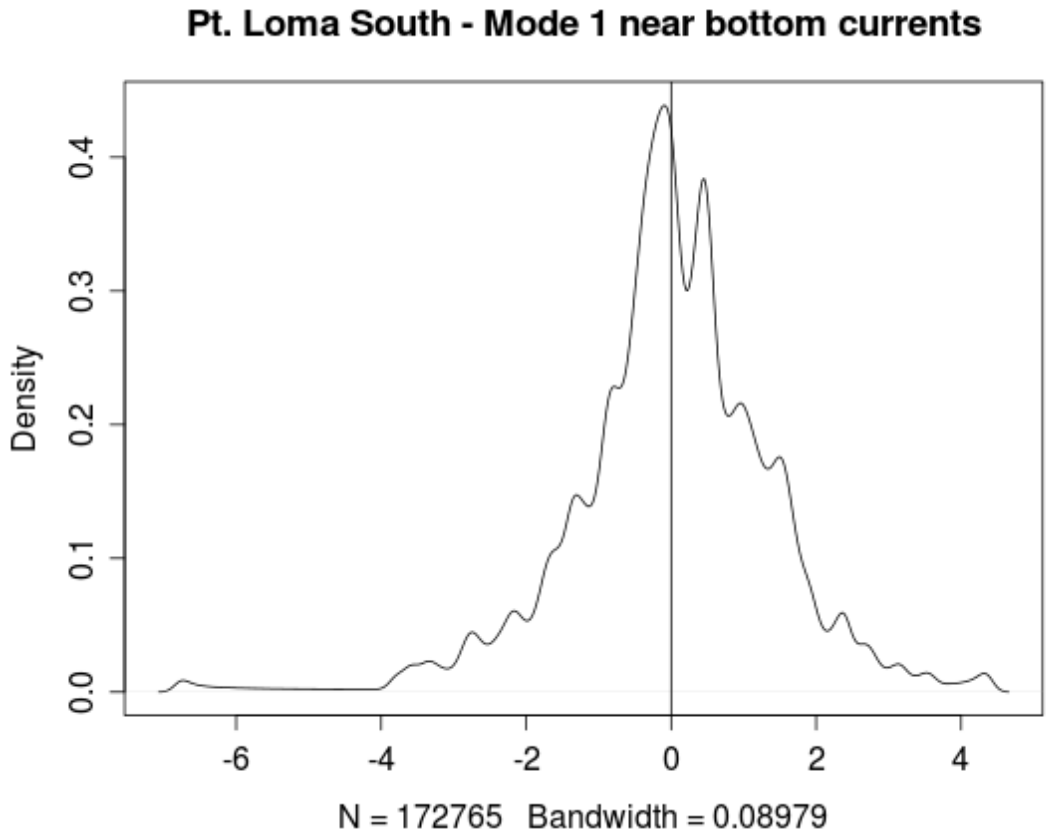

Figure 16. Probability density of Mode 1 currents indicating that Mode 1 was most frequently positive indicating southeastward and upward currents near the bottom at the South Pt. Loma ADCP study site. Moderate positive values were most frequent for Mode 1.

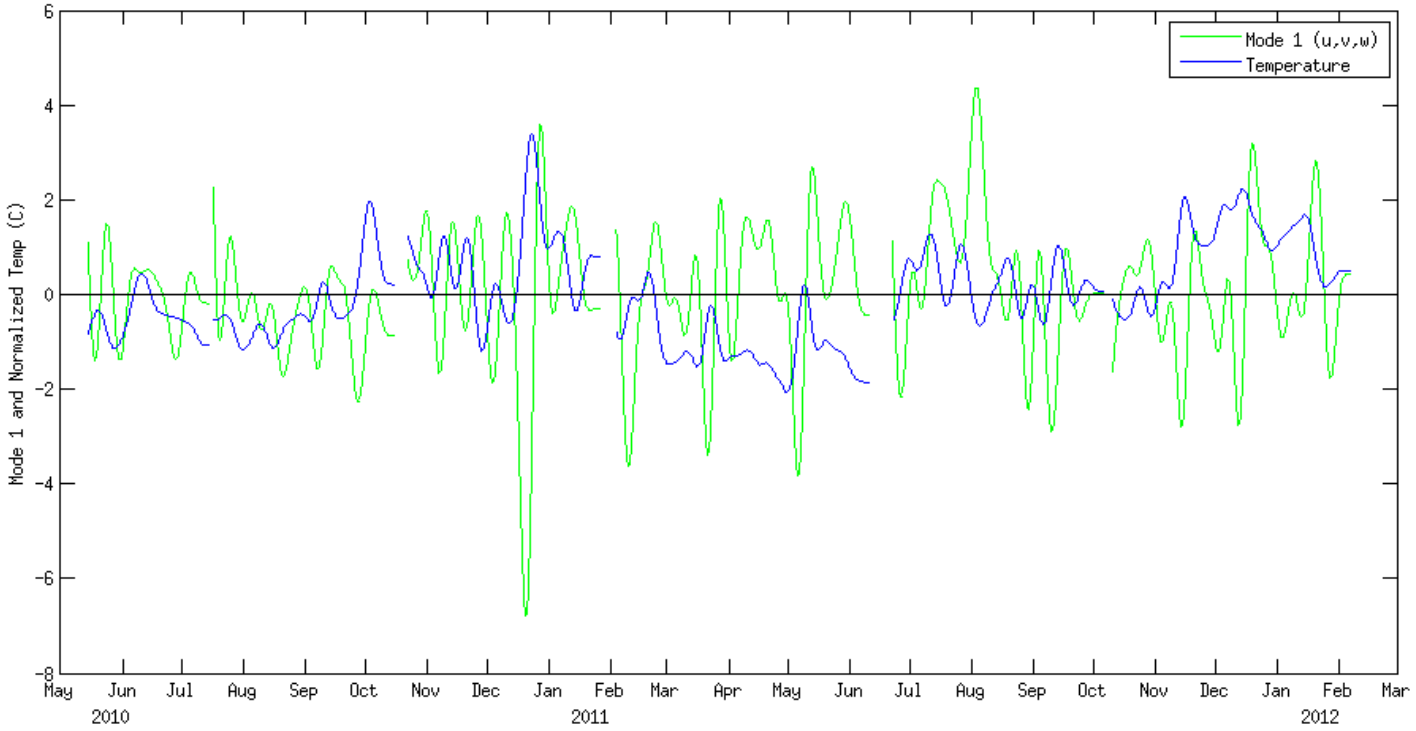

Figure 17. Time series of first mode of EOF of currents at South Pt. Loma near the bottom (green). Velocities were first filtered using a 5-day lowpass filter to eliminate higher frequency variability. The first mode captured >55% of the variability of cross- shore, alongshore, and vertical velocities. Bottom temperature (also lowpass filtered) is shown in blue.

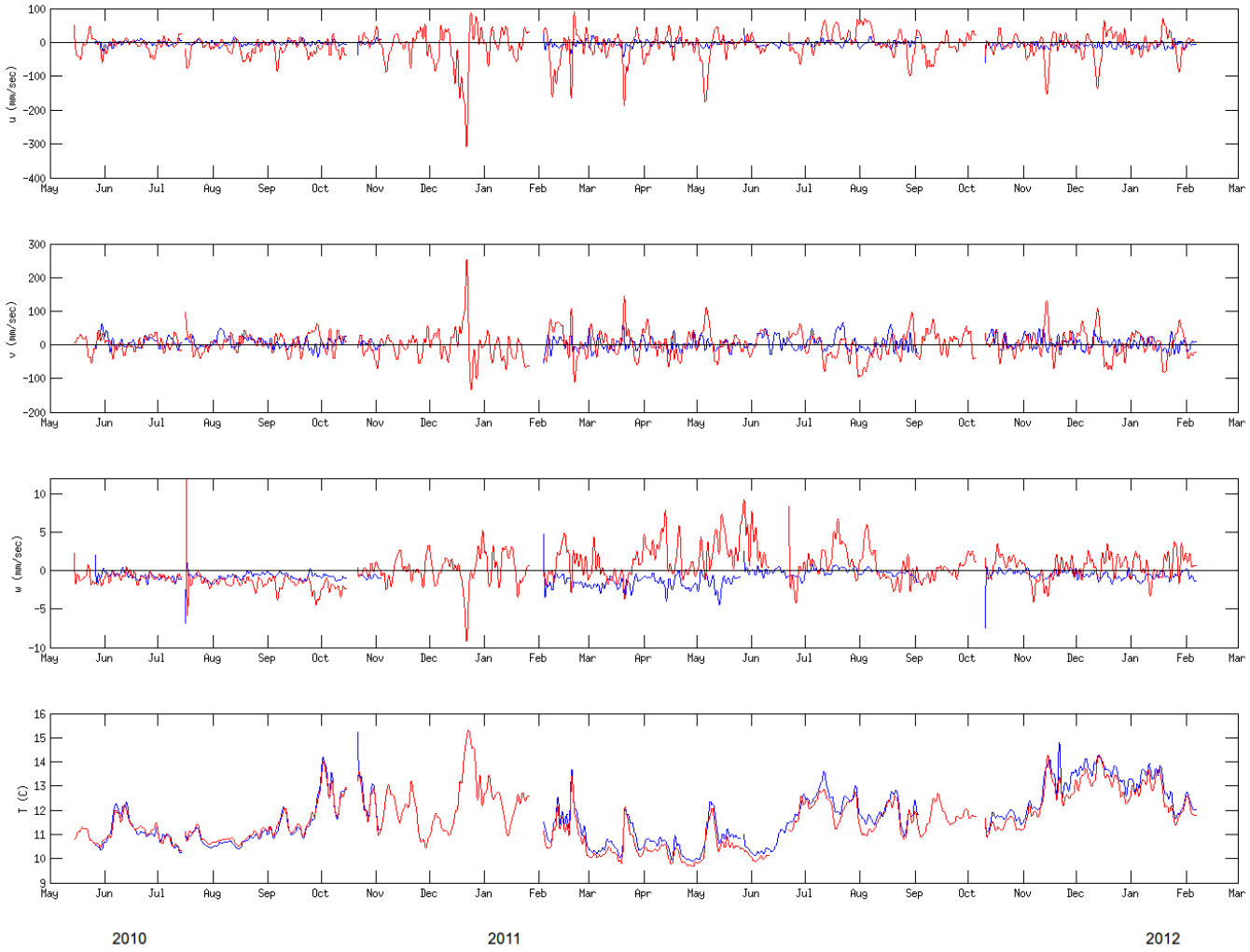

Figure 18. Times series of near bottom currents and temperature (u,v,w, and T) observed at the central (blue) and southern (red) Pt. Loma 35m ADCP stations. Data were lowpass filtered to remove tidal frequencies.

B. Modeling Plume Rise Height

The predicted rise height and bottom depth of the plume, computed hourly for the 12-month record, are shown superimposed with the ambient ocean density for the period of the program (Fig. 19). The plume height is highly dependent on the stratification. The model predicts the plume to rise through the weakly stratified bottom layer until it intersects with the strongly stratified upper layer. A range of rise heights between the depths of 20-30 m was typical during the months of April 2010 to October 2010, while warm waters extended to a depth of 30 m from October 2010 through November 2010 causing stronger stratification at these depths which suppresses the predicted rise height to a depth of approximately 40 m. During the downwelling event on December 22, 2010, the higher density water advected from the surface was predicted to limit rise height to a depth of 60 m.

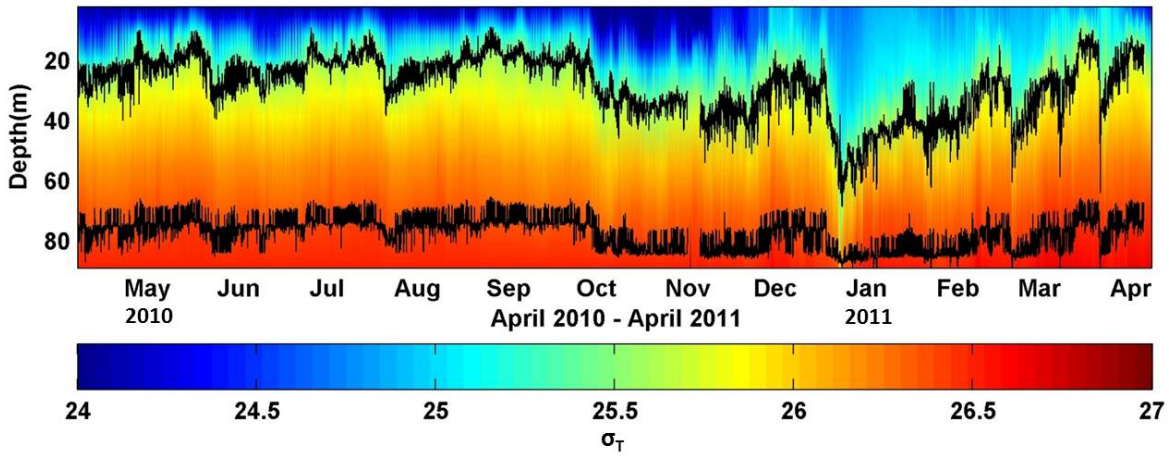

Figure 19. Density structure at the PLOO from April 2010 to April 2011. Also shown are the rise height and plume base estimated using the NRFIELD buoyant plume model. The estimated time-dependent depth extents of the plume are bound by these two black lines. No surfacing events were evident.

C. AUV Plume Surveys

A total of 21 AUV plume sampling missions were conducted between April 2010 and April 2011. Plume sampling dates and general ocean conditions are summarized in Table 6. Monitoring missions were performed on low wind/wave days to assist in deployment and recovery of the REMUS.

REMUS monitoring missions of the PLOO plume were performed when both high and low stratification conditions were present. Generally, the plume was advected either North or South for all missions, with exceptions for the February 28, 2011 and March 3, 2011 (minimal current), April 22, 2011 (variable - changing direction in the hours preceding a mission) and the June 16, 2010 and December 8, 2010 monitoring missions in which an onshore flow was observed (Table 6). The maximum observed plume range is directly dependent on REMUS path planning. Missions conducted on October 14, 2010 and October 28, 2010 included widely spaced transects that allowed for a final transect at approximately 10 km from the outfall diffusers. These missions were designed to capture the extent of the plume and its mixing far

from its source. Conversely, missions from February 25, 2011 through April 22, 2011 focus on the plume mixing nearer to the outfall.

Table 6. Summary of ocean conditions and observed plume ranges for days that REMUS surveys were conducted.

Date	Stratification			Dominant Along-shore Current	Dominant Cross-shore Current	Current Magnitude (m/s) *	Max Observed Plume Range ᵗ(km)
	Subjective	ΔT (°C)	mld (m)				
2010/04/15	Weak	4	5	**North**	**Minimal**	**0.07**	3.3
2010/05/19	Strong	6	3	**North**	**Off-shore**	**0.12**	3.3
2010/06/16	Strong	8.5	2	**Minimal**	**On-shore**	**0.1**	2.2
2010/06/25	Strong	7.5	1	**North**	**On-shore**	**0.1**	2.1
2010/07/14	Weak	4	5	**South**	**On-shore**	**0.1**	4
2010/08/03	Strong	6	4	**South**	**Off-shore**	**0.07**	5.1
2010/09/01	Strong	6	6	**North**	**Minimal**	**0.1**	7.3
2010/10/14	Strong	9	8	**North**	**Off-shore**	**0.17**	9.7
2010/10/28	Strong	8	11	**South**	**On-shore**	**0.11**	9.2
2010/11/16	Strong	6	11	**South**	**Off-shore**	**0.05**	2.9
2010/11/30	Weak	4	5	**North**	**Off-shore**	**0.15**	9.5
2010/12/08	Weak	4	10	**Minimal**	**On-shore**	**0.09**	1.9
2010/12/16	Weak	4	5	**North**	**Off-shore**	**0.05**	2.8
2011/01/21	Weak	4	12	**North**	**On-shore**	**0.13**	1.2
2011/01/28	Weak	4	11	**South**	**Minimal**	**0.18**	9
2011/02/08	Weak	5	3	**North**	**Off-shore**	**0.11**	8.4
2011/02/25	Weak	5	8	**South**	**On-shore**	**0.16**	1.7
2011/02/28	Weak	4	13	**Minimal**	**Minimal**	**0.03**	2.2
2011/03/03	Weak	4.5	7	**Minimal**	**Minimal**	**0.03**	1
2011/04/15	Strong	6	11	**South**	**Minimal**	**0.15**	0.3
2011/04/22	Strong	7	4	**Variable**	**Variable**	**0.07**	1.4

ᵗ Range taken from Intermediate Diffuser Wye

* Average current magnitude between depths of 60 - 90m

The maximum REMUS operating depth for missions between April 15, 2010 and December 8, 2010 was 70 m. (Recall that the PLOO outfall discharges at an approximate depth of 93 m.) Rise height model predictions generally ranged between 20 – 40 m from April 2010 through November 2010 which led to consistent detections of the plume above 70 m. The depth range was extended to 80 m for missions from December 8, 2010 to February 8, 2011 and finally to a maximum depth of 90 m for the remainder of the missions. The range increase was in response to lower observed plume rise heights due to the change in stratification conditions from December 2010 to January 2011 (Table 6).

1. Summary of AUV Plume Survey Findings

Visualizations of the PLOO plume provide some examples of plume detection and spatial distribution. The August 3, 2010 mission successfully tracked the plume over 5 km downstream of its source in a low-current regime (Figure 20). The maximum mission depth was chosen at 70 m to maximize spatial coverage of the plume in the far-field. Backscatter at 650 nm also distinguishes the plume from the surrounding waters, however as distance increases from the outfall, the signature significantly diminishes, making plume tracking difficult (Figure 21). The February 25, 2011 mission was designed to track the plume nearer to its source (< 1 km) in a high current regime and was sampled to 90 m depth (Figure 22). The datasets encapsulate a wide range of oceanographic conditions, making them ideal illustrators of the AUV's plume monitoring capabilities using the natural tracer CDOM.

Temperature and salinity (T-S) diagrams colored by CDOM-based dilution values for each survey mission are shown in Figure 23. The salinity data was "de-spiked" using the recursive filter discussed by *Schmitt et al*. [2005]. Evaluation of the data using this method allows the

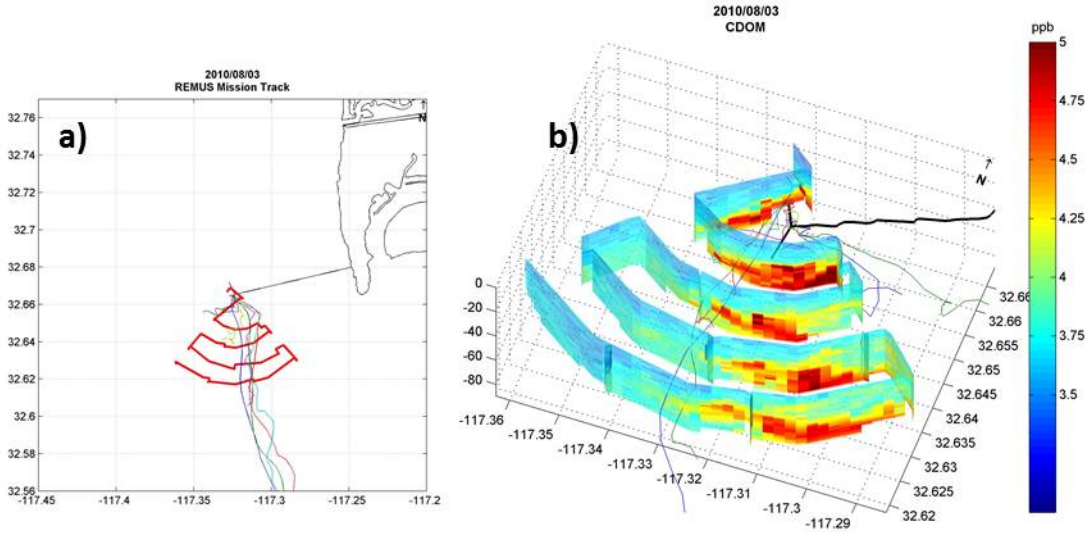

Figure 20. a) REMUS vehicle mission track (red) extending approximately 5 km south of PLOO (shown in black) for sampling conducted on August 3, 2010. Colored lines indicate the estimated plume trajectory based on PLOO buoy velocity profiles. b) Elevated values of CDOM (>4 ppb) indicate high concentrations of organic matter in the PLOO plume. The PLOO is shown in black with the observed plume toward the south-southeast. The plume trajectory (colored lines) is estimated from the PLOO buoy velocity profiles.

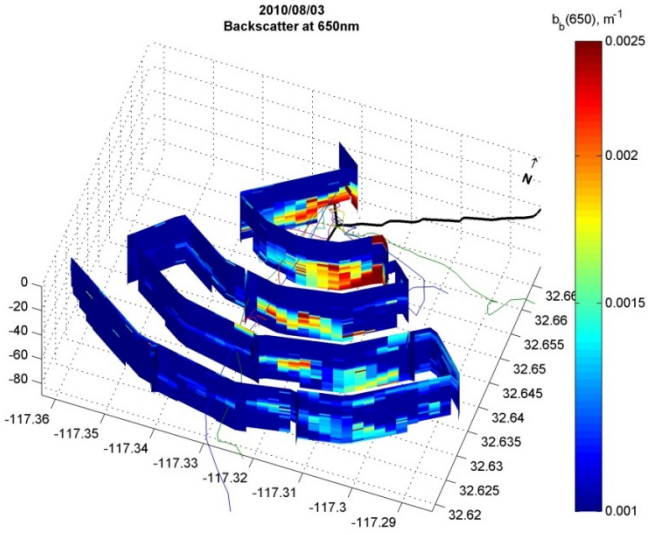

Figure 21. Elevated values (>0.0013m-1) of optical backscatter at 650 nm indicate elevated turbidity in the PLOO plume. The PLOO is shown in black with the observed plume toward the south-southeast. The plume trajectory (colored lines), estimated from the PLOO buoy velocity profiles, suggest the plume advects east until a depth of 60 m where the currents change to a southerly flow.

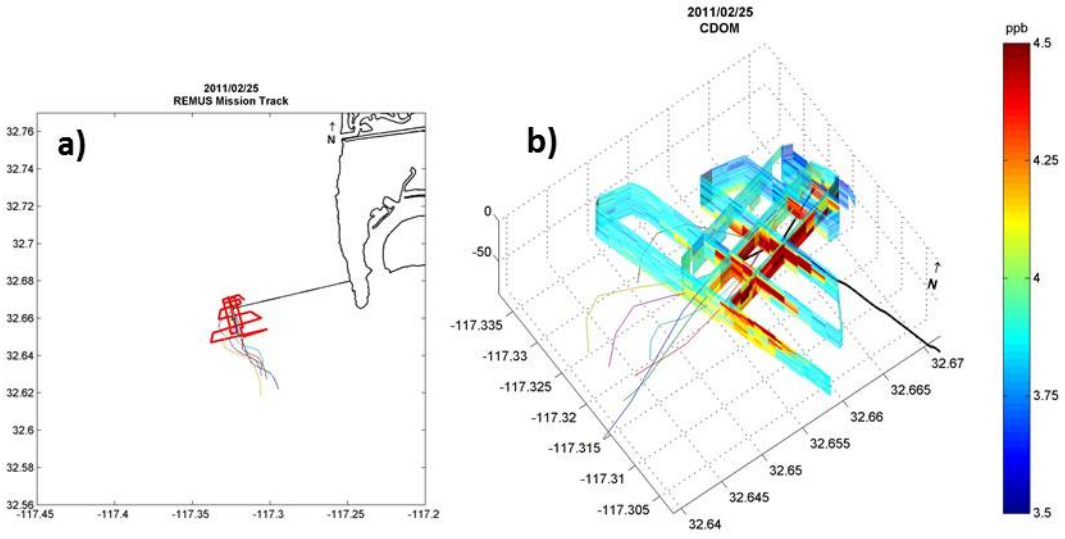

Figure 22. a) REMUS vehicle mission track (red) extending approximately 1 km south of PLOO (shown in black) for sampling conducted on February 25, 2011. Colored lines indicate the estimated plume trajectory based on PLOO buoy velocity profiles. b) Elevated values of CDOM (>4 ppb) indicate high concentrations of organic matter in the PLOO plume. The PLOO is shown in black with the observed plume toward the south. The plume trajectory (colored lines) is estimated from the PLOO buoy velocity profiles.

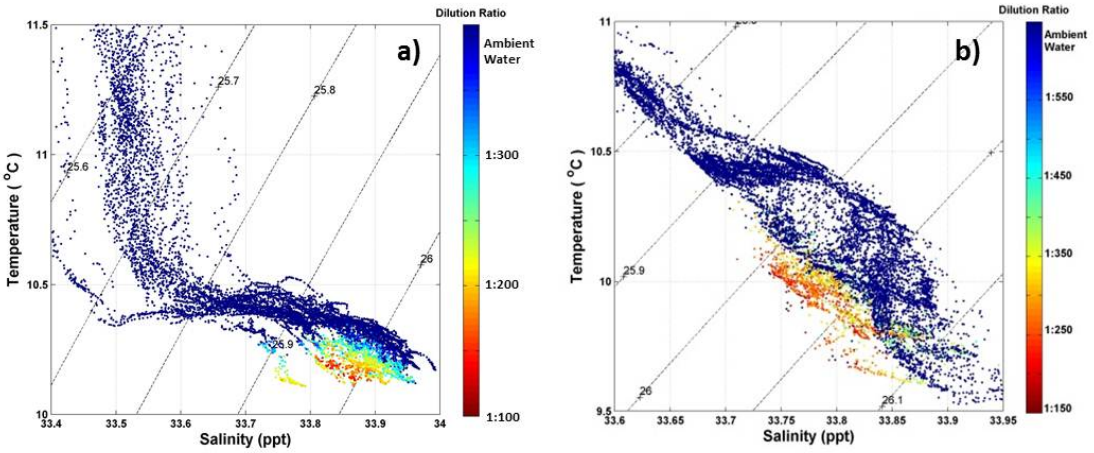

Figure 23. T-S diagram as a function of computed dilution ratios for the August 3, 2010 (a) and February 25, 2011 (b) PLOO missions. The dilution ratio (via CDOM measurements) clearly shows the plume's water mass properties as relatively fresh compared to ambient waters. The diagonal lines in each figure represent lines of constant density.

water mass associated with the plume to be easily identified as a distinct water mass, with the lowest dilution values (i.e. high CDOM) typically having low salinity. Previous work used these salinity signatures and initial mixing lines to estimate dilution near the diffuser [*Washburn et al*., 1992]. The plume water in the survey area typically mixed to the point of having little to no discernible density anomaly and while salinities within the plume are generally lower, their values fall within the distribution of background values making the use of initial mixing lines impractical. Dilution values obtained with the CDOM proxy in AUV monitoring missions do not have the same constraints as previous methods.

Once the plume characteristics have been identified in CDOM and salinity, samples falling within given thresholds identifying the water mass can be plotted to show the spatial distribution of the plume (Figure 24). The horizontal spatial distribution shows the August 3, 2010 plume advecting toward the southeast as far as sampling was conducted (5 km), while the vertical distribution shows the core of the plume centered at 62 m and a minimum rise height depth of 45 m. The spatial distribution of the February 25, 2011 PLOO plume is determined by selecting samples specific to the plume, in this case CDOM values greater than or equal to 4.3 ppb and salinity values less than or equal to 33.65 ppt (Figure 24b). The maximum REMUS depth was extended to 90 m for the February 25, 2011 monitoring mission which enabled mapping of the entire vertical structure of the plume with its core centered at 67 m and rising to a minimum depth of approximately 50 m. The horizontal distribution of the plume is strongly correlated with the estimated current trajectories based on the PLOO buoy velocity profile.

PLOO plume distributions based on water-mass characteristics in salinity and CDOM for all monitoring missions are presented in Figures 25 and 26. In all cases, there is good agreement between the estimated plume trajectory based on velocities measured by the buoy and the observed plume distribution. The horizontal distribution is much denser for missions near the diffuser (e.g. February 25, 2011 through April 22, 2011) while the distribution in the far-field

missions was sparser due to the resolution of the measurements. For the January 28, 2011 and February 8, 2011 monitoring missions, the higher velocity flow fields caused an advecting plume nearer to the bottom. The observations of these plumes were limited due to the AUV's maximum running depth of 80 m. The maximum operating depth was changed to 90 m for the remainder of the missions (February 25, 2011 through April 22, 2011) which consistently captured the full profile of the plume.

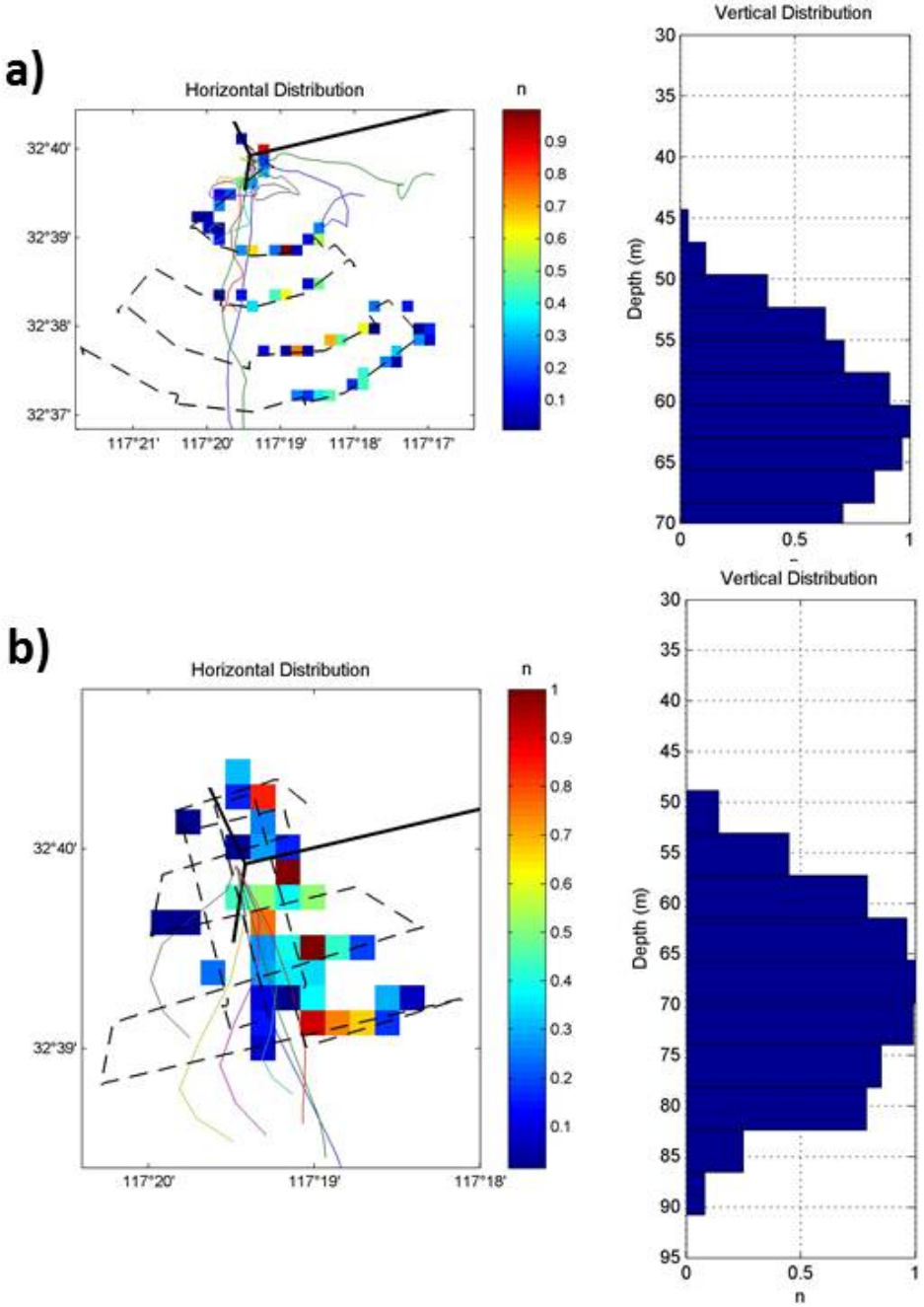

Figure 24. Horizontal (left) and vertical (right) distributions of the PLOO plume measured on August 3, 2010 (a) and February 25, 2011(b). Plume distributions are based on the number of samples with CDOM > 4.3 ppb and salinity < 33.65 ppt falling within each spatial bin (50 x 50 m horizontally and 1 m vertically) then normalized by the maximum number of samples observed in a single bin. On the horizontal distribution plot, the REMUS mission path is shown as a dotted black line, the estimated plume trajectory based on buoy velocity measurements are shown by colored lines and the PLOO outfall is shown in black.

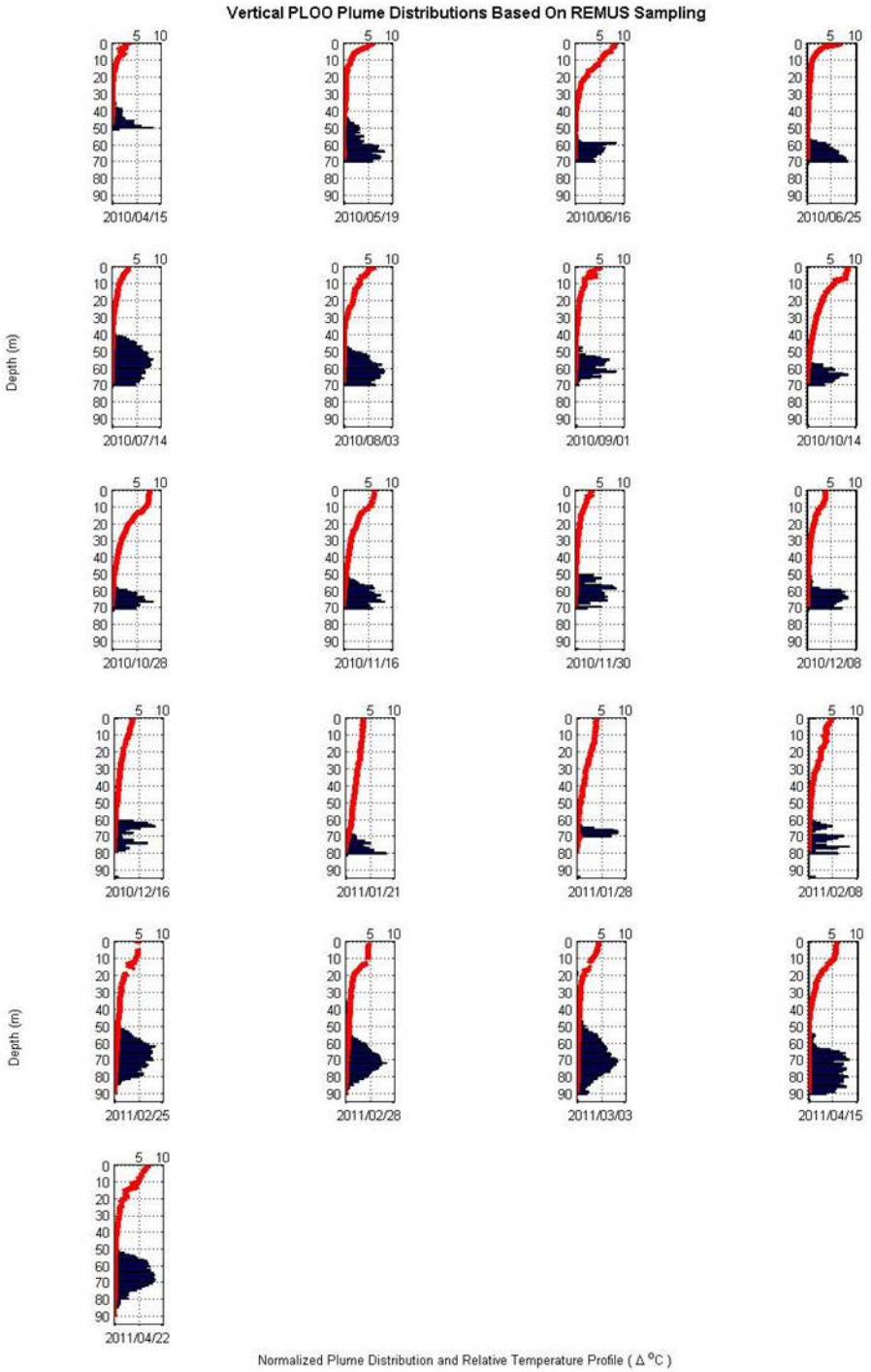

Figure 25. Plume distributions are based on the number of samples with characteristic CDOM and salinity values within 1 meter vertical bins. The number of samples is then normalized by the maximum number of samples observed in a single bin for each mission. The relative temperature profile (temperature profile relative to bottom water temperature) is plotted in red.

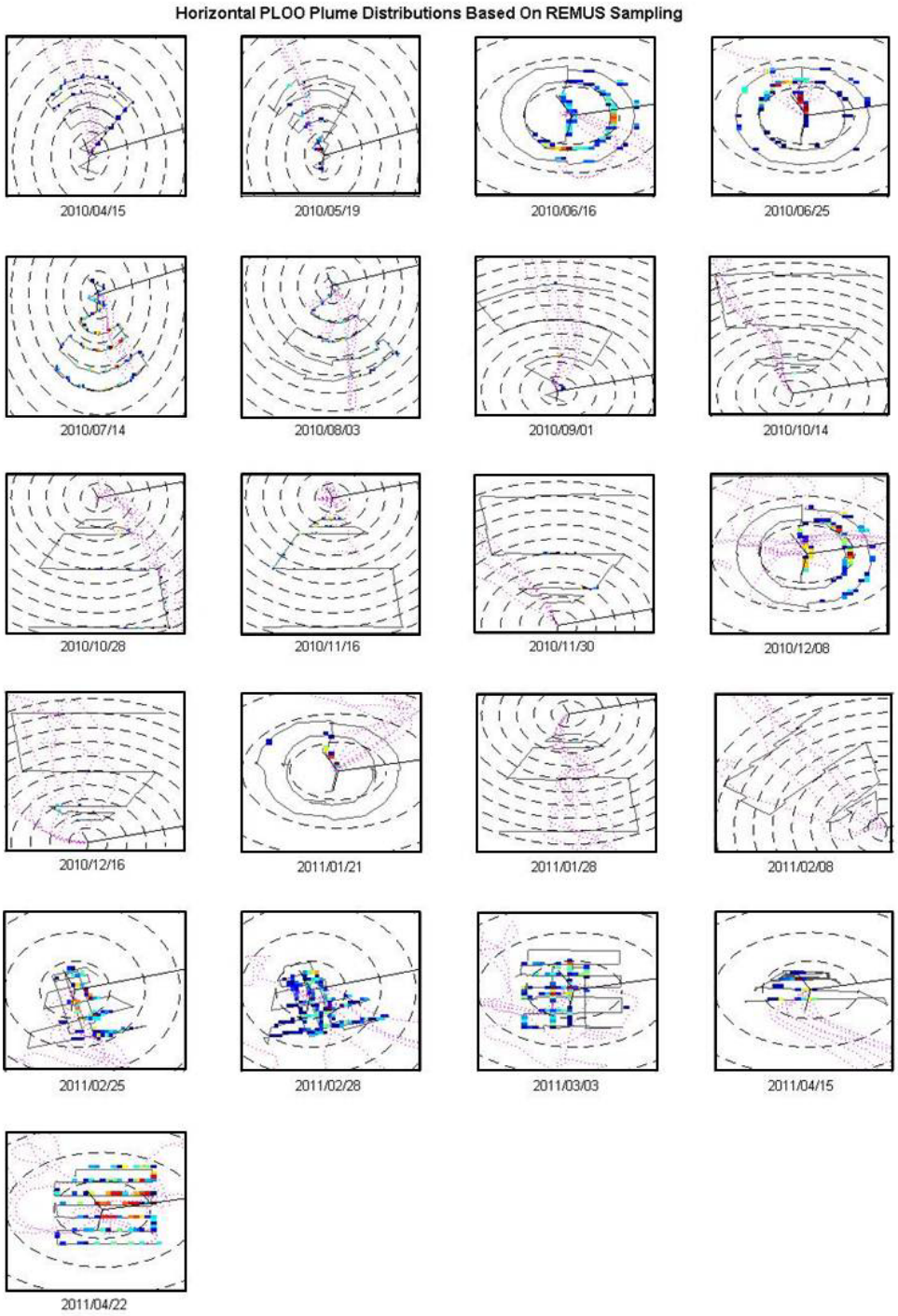

Figure 26. Plume distributions are based on the number of samples with characteristic CDOM and salinity values within spatial bins of 50 x 50 meters. The number of samples is then normalized by the maximum number of samples observed in a single bin for each mission. The REMUS mission path is shown in grey, the estimated plume trajectory based on buoy velocity measurements is shown in pink dashed lines and the PLOO outfall wye is shown in black.

2. Observed PLOO Plume Characteristics

Observed plume characteristics for each PLOO monitoring mission include plume rise height, thickness, width, and dilution. Observed plume rise height of each monitoring mission is compared to the predicted rise height in Figure 27. From April 2010 to April 2011, a minimum observed plume rise height to a depth of 35 m is observed during the February 28, 2011 mission. The observed plume rise height generally fluctuates between 40 – 60 m in depth. All observed plume rise height depths are listed in Table 7. **During the PLOO study, no surfacing events were predicted or observed due to the extreme depth of discharge**.

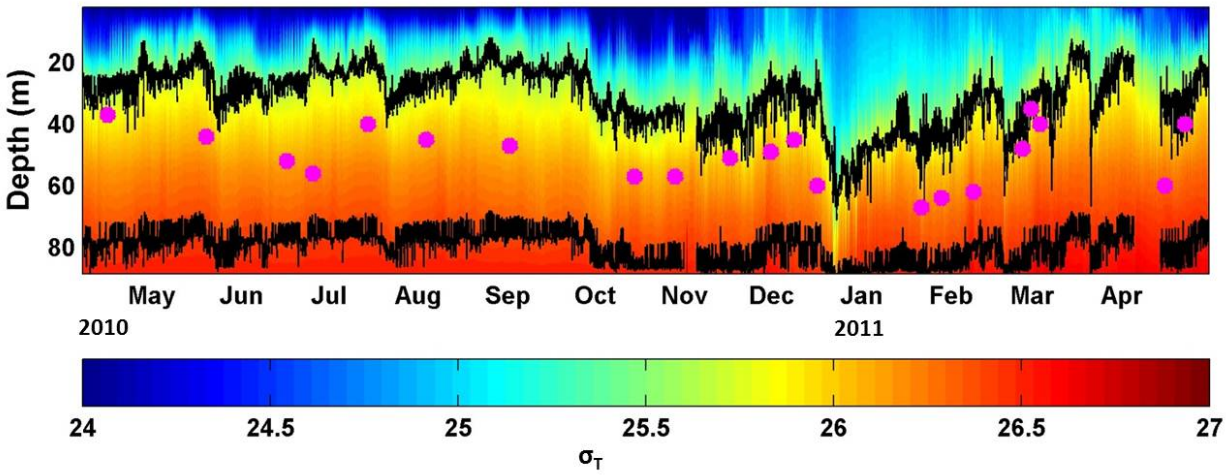

Figure 27. Density structure at the PLOO from April 2010 to April 2011. Also shown are the rise height and plume base estimated using the NRFIELD buoyant plume model. The estimated time-dependent depth extents of the plume are bound by these two black lines. No surfacing events were evident.

Velocity differences between missions explain differences observed in plume dilution and structure. Changes in plume structure and property distributions due to the increased current speed u may be parameterized by changes in the Froude number (F), defined as:

$$F = \frac{u^3}{b} \qquad \text{(Eq. 2)}$$

where u is the current speed and b is the flux of buoyancy per unit length of diffuser, or buoyancy flux, equal to $g(\frac{\Delta\rho}{\rho})(\frac{Q}{l})$ where g is the acceleration due to gravity, $\Delta\rho$ is the density difference between the plume water and seawater, ρ is the ambient seawater density at the diffuser depth, Q is the discharge flow rate, and l the diffuser length. This nondimensional parameter compares the competing effects of the ambient current to disperse and mix the plume (high Fr) with that of the buoyancy flux to concentrate and maintain the plume (low Fr) (Fischer et al. 1979; Roberts 1977; Washburn et al. 1992).

Elevated CDOM levels within the plume were used to calculate dilution values for each mission (eq. 1). Table 7 lists the average minimum dilution value of each mission and its corresponding Froude number. Higher current regimes increase the mixing between the discharge and its receiving waters causing increased levels of dilution. This is evident during the October 14, 2010, November 30, 2010, February 25, 2011, and April 15, 2011 missions with observed dilution values of 1:192, 1:304, 1:228, and 1: 204 respectively. Conversely, low current regimes account for the highest observed dilution levels of 1:117, 1:103, and 1: 109 for November 16, 2010, February 28, 2011, and March 3, 2011 missions respectively.

Table 7. REMUS survey summary including Froude number, minimum observed plume depth, and minimum observed dilution.

Date	Froude Number *	Min Observed Plume Depth (m)	Min Observed Dilution (1:N)
2010/04/15	**0.245**	37	141
2010/05/19	**1**	44	188
2010/06/16	**0.71**	52	177
2010/06/25	**0.71**	56	110
2010/07/14	**0.71**	40	125
2010/08/03	**0.245**	45	127
2010/09/01	**0.71**	47	193
2010/10/14	**3.45**	57	192
2010/10/28	**1.23**	57	184
2010/11/16	**0.09**	51	117
2010/11/30	**2.41**	50	304
2010/12/08	**0.52**	50	161
2010/12/16	**0.09**	60	248
2011/01/21	**1.57**	67	160
2011/01/28	**2.41**	64	162
2011/02/08	**1.23**	62	N/A
2011/02/25	**2.93**	58	228
2011/02/28	**0.02**	35	103
2011/03/03	**0.02**	45	109
2011/04/15	**2.41**	57	204
2011/04/22	**0.245**	50	157

* Average Froude number at depths of 60 - 90m

IV. DISCUSSION

A. Example AUV Missions

Our ability to synoptically evaluate the 3-dimensional spatial extent and hydrodynamic mixing of the plume during different seasonal conditions is best exemplified by presenting data from surveys conducted on August 3, 2010 and February 25, 2011. Plume mixing and its geometric evolution for each mission are illustrated by cross-sections of dilution at successive distances from the discharge (Figure 28a). To help delineate the contours, dilution values above 400 are not plotted.

The average velocity in the lower water column for the August 3, 2010 mission was 0.07 m/s, more than half of the average velocity estimated for the February 25, 2011 mission (0.16 m/s) yielding Froude numbers of 0.24 and 2.93 respectively (Table 8). The higher velocity current enhances near-field mixing and forms a narrow plume (Figure 28b) as it advects downstream with a width of 1.2 km at the last cross-section (1.5 km from the wye). Conversely, the plume shown in Figure 28a, dispersed by a low current regime is less mixed as it advects downstream and has a width of approximately 3 km. The differences in plume characteristics of each mission were compared at the 2 km cross-section (Figure 28a) and 1.5 km cross-section (Figure 28b) which were approximately co-located. In a parallel current (same direction as the outfall diffusers), the initial lateral plume spreads by a density current unrelated to turbulent diffusion [*Hunt et al*., 2010]. From laboratory experiments, it is predicted that the plume will spread linearly, in a V-shape according to:

$$\frac{w}{x} = 0.7F^{-1/3} \qquad \text{(Eq. 3)}$$

where w is the plume width at distance x from the source [*Roberts et al*., 1989]. Characteristics discussed in this section are summarized in Table 8. Equation 3 predicts a plume width of 2.8 km and 1.1 km for the co-located cross-sections of the August 3, 2010 and February 25, 2011 missions respectively; comparing well with measured values. We note that equation 3 was developed from straight-line diffuser tests, however the large angle (152 degrees) between the y-shaped diffusers located at PLOO make this a reasonable assumption for evaluating trends.

B. Far-Field Mixing

Plume models can reasonably predict bulk plume properties such as equilibrium depth, thickness, and dilution in the near-field. However, current plume models cannot accurately represent plume complexity, particularly the patchy nature of the wastefield [*Ramos et al*., 2005] and the role of oceanic turbulence in mixing the plume. The NRFIELD model assumes a uniform current, i.e., the current is constant in speed and direction over the rise height, however vertical shear in coastal currents will have potential to influence plume evolution. For the PLOO, currents are found to have significant vertical shear and temporal variability which introduces complexity in developing the sampling plan to efficiently track the plume from the near-field to the far-field; placing a requirement on environmental adaptation.

The importance of monitoring plume waters into the far-field is evident in the plume cross-sections depicted in Figure 28. Dilution of the plume in the far-field for a majority of the monitoring missions at the PLOO looked similar to the August 3, 2010 mission (Figure 28a) where mixing occurred slowly as distance increased from the diffuser. This result is expected since mixing in the far-field is due to background ocean turbulence, which typically produces much slower mixing than that in the near-field which is governed by buoyancy and momentum exchange processes from the diffuser jet. However, vigorous mixing in the far-field was observed in the February 25, 2011 monitoring mission (Figure 28b). As the plume progressed from the 0.25 km cross-section to the 1.5 km cross-section, the plume becomes virtually undetectable below a depth of 65 m, indicating significant mixing over the 1.25 km distance. In comparison to Figure 28a, the dilution only increased from 130 to 184 over a distance of 4 km. Figure 28b also shows an additional rise of the plume of approximately 10 m from a height of 60 m in the 0.25 km cross-section to 50 m at the 0.75 km and 1.5 km cross-sections.

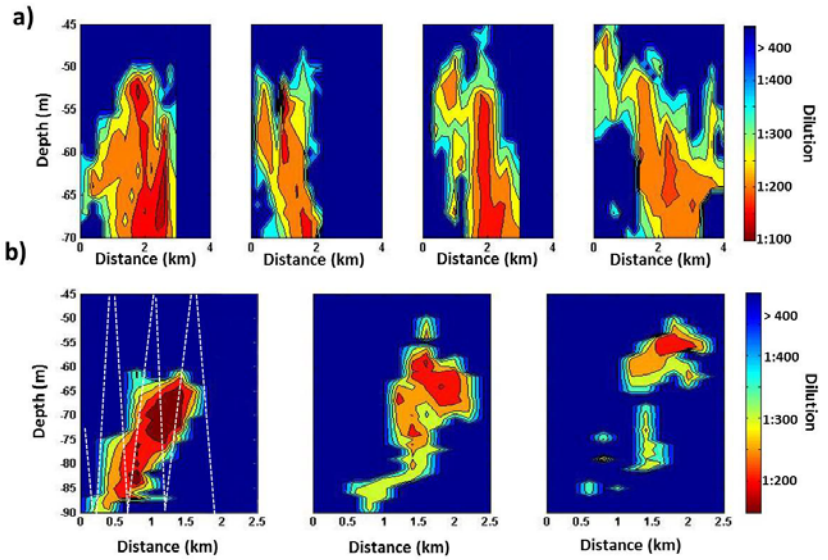

Figure 28. Cross-sectional dilution plots as a function of range from the outfall for (a) August 3, 2010 and (b) February 25, 2011 monitoring missions. The range is measured from the wye to each successive cross-section; (a) 2 km, 3 km, 4 km, 5 km and (b) 0.25 km, 0.75 km, 1.5 km. The figures show the distribution of the plume width and thickness as it progresses downstream. The sawtooth REMUS pattern is included in the 0.25 km cross-section, Figure 28b.

Table 8. Comparison of 8/3/2010 and 2/25/2011 background conditions and their effect on plume width.

Parameter	8/3/2010	2/25/2011
Average Current Velocity (m/s)	0.07	0.16
Froude number (F)	0.24	2.93
Plume width (km) *	3	1.2

* Measured at the 2 km cross-section (8/3/2010) and the 1.5 km cross-section (2/25/2011)

C. Computing Plume Dispersion

The cross-sectional plots shown in Figure 28b were used to estimate horizontal dispersion of the February 25, 2011 plume. Linear growth of the transverse dimension (x) of the plume over time (t), as measured from the contour plots, was used to estimate the bulk diffusivity coefficient K_x. Employing the methods described in *Elliott et al*. [1997], the plume distribution was assumed to be Gaussian in shape where K_x is related to the variance (σ_x^2) of the Gaussian-shaped relationship between concentration and the length scale:

$$\sigma_x^2 = 2K_x t \qquad \text{(Eq. 4)}$$

The method, more recently used to estimate horizontal dispersion for an oil transport model in *French-McCay et al*, [2007], assumes that a 4σ approximation of the length scale provides a realistic estimate of patch width. Therefore, the standard deviation (σ) was computed for each cross-section shown in Figure 28b. It was assumed that the plume at the 0.25 km cross-section was fully formed even though it is not located at the end of the diffuser. However, any difference in initial plume width from this point and the end of the diffuser will have a negligible effect on dispersion calculations.

The variance (σ^2) was plotted against diffusion time, and least squares was used to determine the value of the transverse diffusion coefficient K_x . Based on the three cross-sections seen in Figure 28b, K_x = 2.35 m^2/s (standard error = 0.77). This result falls in the range predicted by *Okubo* [1971] of 1-10 m^2/s for length scales of 1-10 km. The diffusion coefficient is commonly assumed to be related to the plume width (L) according to the "4/3" power law [*Hunt et al*., 2010]:

$$K_x = \propto L^{4/3} \qquad \text{(Eq. 5)}$$

where $\propto$ is a constant with typical values between 0.002 to 0.01 $cm^{2/3}/s$ for oceanic diffusion [*Fischer et al*., 1979]. Assuming an initial field width L of 1.2 km (from Figure 28b, 0.25 km cross-section), yields $\propto$ = 0.004.

A solution to the problem of horizontal turbulent diffusion from a finite line source in a uniform current is derived by *Brooks* [1960]. The solution ignores the effects of vertical diffusion and longitudinal dispersion; both are typically small when compared to their horizontal and transverse counterparts. Based on the 4/3 law, the resulting equation is:

$$\frac{c_{max}}{c_0} = \left[\text{erf}\left(\frac{3/2}{\left(1+8\propto L^{-2/3}t\right)^3-1}\right)^{\frac{1}{2}}\right]^{-1} \qquad \text{(Eq. 6)}$$

where erf is the standard error function, c_{max} is the maximum concentration at time (t), and c_0 is initial concentration. The ratio c_{max}/c_0 can be interpreted as the further dilution obtainable due to transverse diffusion in the far field during advective transport for a time t. For the February 25, 2011 mission, L = 120,000 cm, $\propto$ = 0.004, and an estimated travel time of 3 hours (10,800 s) to 1.5 km cross-section (based on t = x/U where x is distance from source and U is current velocity), yielding c_{max}/c_0= 1.01. Thus, we would expect the minimum dilution observed at the 0.25 km cross-section (Figure 28b) of 145 to increase only slightly to 147. However, our

observations reveal a significant increase of dilution from 145 at the 0.25 km cross-section to 232 at the 1.5 km cross-section. While, equation 6 should be used conservatively due to the assumptions of this solution [*Koh and Brooks,* 1975], such a large difference between predicted and measured dilutions implies that turbulent mixing is occurring leading to this increase in dilution.

D. Near- and Far-field Trends

Figure 29 presents the median of the dilution ratios for all missions that exhibited steady current regimes parallel to the diffusers (North/South). The median of the dilution ratio is based upon all the data sampled by the AUV both in the near and far-field at a particular range pass. The time estimates are based upon the advection time scale as computed from the current meter data. Higher current regimes (Fr > 0.11) were denoted by solid asterisks, while lower current regimes (Fr < 0.11) were denoted by hollow circles. The analysis indicates that the plume rapidly mixes in the near-field at an effective rate of t^2 before quickly adjusting to a slower rate of $\sim t^{1/10}$ in the far-field. The trend in the far-field is independent of current velocity as illustrated by each trendline at different Fr numbers. The rapid transition to slow mixing after initial mixing is expected since dilution in the far-field is dominated by lower background ocean turbulence levels compared to the near-field jet where buoyancy and momentum exchange processes dominate. Figure 29 illustrates both the dynamic range of discharge plume dilutions over which CDOM can be used as well as the effectiveness of the AUV sampling to characterize both near-field and far-field mixing.

Taylor's [1953, 1954] landmark papers on shear dispersion predicts tracer variance will grow linearly with time after an initial adjustment period, however, *Okubo* [1971], using the data from horizontal diffusion tracer experiments obtained prior to 1971, created diffusion diagrams for a time scale of diffusion between 2 hours and 1 month that indicated non-Fickian diffusion or a non-linear growth in variance with time. The observed plume characteristics used to compute median dilutions (Figure 29) also show this non-linear trend.

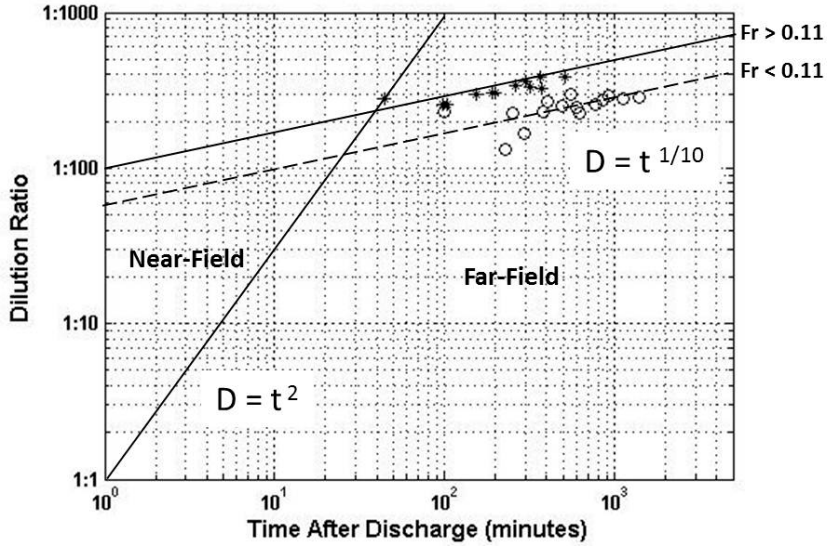

Figure 29. Median measured dilution ratios using the CDOM proxy as a function of time from PLOO. Data from missions with steady currents that were parallel to the diffusers (North/South) were combined to show the log-log trend in dilution as a function of time from the outfall. The trend based on missions performed in high Fr number regimes (defined as Fr > 0.11) compared to low Fr number regimes (F < 0.11) is also shown.

E. Comparison with Analytical Mixing Model

The observed dilution, plume thickness and height are compared with predictions made by the NRFIELD plume model and presented in Table 9. The data used for this comparison are the observed values measured at what was estimated to be the end of the near-field zone as characterized by the plume reaching its equilibrium depth. The August 3, 2010 mission was designed to track the plume in the far-field to a range of 5 km. Table 9 shows measured plume characteristics as estimated from Figure 28 compared with the NRFIELD predicted values. The plume thickness given in Table 9 is an estimated range as the vehicle surveyed to 70 m while the discharge originates at 90 m. The model predicts a dilution of 238 while dilution calculated from the average of the observed maximum values is 130. The same pattern holds for the February 25, 2011 mission with predicted dilution at the end of the near-field at 300 and observed at 206. Dilution values computed at increasing distances from the diffuser remained significantly less than NRFIELD predicted dilution values, leading us to believe the differences are not a result of misidentifying the boundary of the near-field mixing zone.

A 3-month analysis of the CDOM variability of the source effluent at the PLWTP provided a range of approximately +/- 15 ppb of the CDOM constant (121 ppb) used to calculate dilutions. These differences will not produce significant errors in the dilution calculations. Another potential explanation for the dilution mismatch may be a limitation of the model's parameterization of dilution as a function of Froude number (e.g. $D \sim u^{1/2}$) in addition to the assumptions of the discharge occurring in a uniform/constant current. For example, the model's predicted dilution will vary significantly across inputs ranging from 1-5 cm/s while natural variability of coastal currents can be an order of magnitude larger. In addition, to the challenges of going from laboratory to full-scale, the difference in dilutions may also be partially explained

by the mismatch between the discrete measurements provided by the AUV and the inherent spatial averaging implicit in the model output. However, it is unlikely that these sources of errors would account for the total difference between predicted and observed dilution values seen in Table 8.

The NRFIELD model assumes the submerged wastefield resulting from multi-port line diffusers forms a line plume in which individual plumes from each diffuser port merge before the terminal rise height [*Roberts et al*., 1989]. For the PLOO, the ratio of the port spacing to rise height is large, thus the diffuser port plumes do not fully merge before the terminal rise height, creating a point plume. The work of *Tian et al*., [2004] developed semi-empirical equations to predict the major near-field characteristics, including dilution of a submerged plume. However, they found that their results were not widely applicable for prediction of near-field dilution for a point plume, which suggests that the equations governing dilution of a line plume may not be practical for a point plume. Consequently, it is feasible that the NRFIELD line plume assumption could lead to the discrepancies between predicted and observed dilution at the PLOO [*P. Roberts*, personal communication].

Table 9. Comparison of REMUS field measurements and NRFIELD predictions for 8/3/2010 and 2/25/2011.

	8/3/2010		2/25/2011	
Parameter	**Measured**	**Predicted**	**Measured**	**Predicted**
Near-field dilution	130*	238	206*	300
Height of minimum dilution (m)	26	26.8	23	22.9
Plume thickness (m)	25-30	27.2	23	23.4
Plume height (m)	44	63	48	61

* Based on observations nearest to the end of the initial mixing zone.

F. Enhanced Far-Field Mixing and Plume Rise

The mechanism of the enhanced mixing and the additional plume rise illustrated in Figure 28b is not immediately evident. Analysis of the source effluent density prior to discharge did not reveal any significant differences. The NRFIELD model predicts the end of the near-field at 112 m from the effluent source while the first cross-section is located approximately 0.25 km from the source, thus minimal additional mixing or plume rise is expected beyond this point without an external mechanism. The dominant mechanism for converting fluid motion to mixing in the stratified ocean is shear instability in which shear overcomes the stability of stratification [*Geyer et al*., 2010]. A Richardson number ($Ri = N^2/S^2$, where N is the buoyancy frequency and S is the vertical shear) less than 0.25 is typically used as a critical value in which shear-related instabilities are thought to occur for a linearly varying current and density. *Abarbael et al*. [1984] included nonlinear interactions and concluded $Ri < 1$ is sufficient for instabilities to occur, while *Mack and Schoeberlein* [2004] found strong evidence of shear instabilities during high resolution tow measurements, but no critical Ri, rather a range from 1.3 to less than 0.25 that typically coincided with observed mixing.

Ri profiles were calculated along the horizontal AUV path using the current velocity observations from the buoy ADCP and AUV density observations, then compared with current velocity and shear (Figure 30). The February 25, 2011 mission experienced significantly higher current velocities than the August 3, 2010 mission. Friction with the seafloor caused adjacent velocities to slow creating the Bottom Boundary Layer (BBL) between the depths of 80 - 90 m for the higher velocity February 25, 2011 mission. The resulting low Ri number due to the increased shear implies turbulent mixing is likely occurring in the BBL. Several depths above the BBL also show a drop in the Ri number below its critical threshold of 1, most notably between 50 - 60 m. Changes in these regions are caused by decreased buoyancy frequency due to variations in the density field. Comparatively, the Ri number for the lower current regime observed by the August 3, 2010 mission did not drop below the critical value of 1 at any depth.

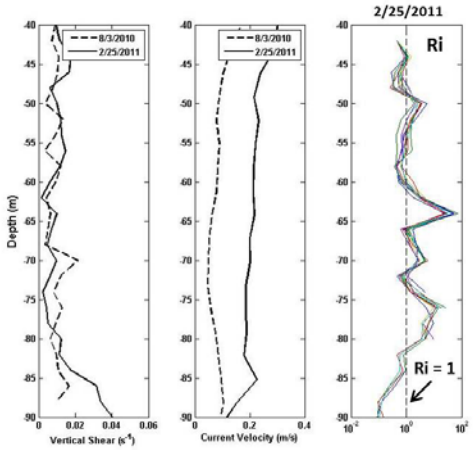

Figure 30. Profile plots of velocity shear and current velocity for August 3, 2010 (dotted line) and February 25, 2011 monitoring missions. The Ri profile plots of from the area of enhanced mixing seen in Figure 19b.

Closer examination of the statistics of the depth of the measured plume, the local salinity and temperature profile (REMUS measurements), and the Ri number profiles (Figure 30) gives a clue to the mechanism causing the additional plume rise and enhanced mixing. The bar graph shows the normalized plume density versus depth at the 0.25 km (hollow bars) and 1.5 km (solid bars) cross-sections. Since these cross-sections are beyond the initial mixing zone (near-field) and at their equilibrium height, the plume is not expected to rise and mix significantly without external influence. However, Figure 31 clearly illustrates an additional rise of 10 m over a distance of 1.25 km while Figure 28b shows significant mixing continues to occur beyond the initial-mixing zone. The temperature profile shows a temperature fluctuation between the depths of 50 - 55 m. The salinity profile also shows a small fluctuation from approximately 52 - 58 m. Observed isotherms from the buoy temperature chain at depths of 2 m, 31 m, and 55 m were analysed to determine the temporal temperature fluctuations in the region (Figure 32). The isotherms show significant temperature variations starting around February 19, 2011 and persisting through the February 25, 2011 monitoring mission. These variations are indicative of large amplitude internal waves propagating through the study area [*Phillips*, 1997].

Linear (small amplitude) and nonlinear (amplitude is a large fraction of the water depth) waves are prevalent features of coastal circulation in the region surrounding the PLOO [*Lennert-Cody and Franks*, 1999]. *Petrenko et al.,* [2000] was the first to show the influence of internal waves on an effluent plume. The Sand Island wastewater plume was shown to follow the vertical displacements of isotherms generated by a semi-diurnal internal tide. The authors found that displacements of 40 m yielded internal tides of the order of 15 m. Similarly, the isotherm displacements observed in this study after February 19, 2011 suggest internal waves with amplitudes between 10 to 15 m are present in the study area. For comparison, isotherms during the August 3, 2010 monitoring mission (Figure 32b) show no indication of internal wave activity which explains the plume's behaviour illustrated in Figure 28a (little additional mixing, no vertical displacement).

There is no shortage of proposed mechanisms capable of generating internal waves, including surface generation by the atmosphere through travelling pressure fields, variable buoyancy flux, or variable wind stress with the latter being most plausible; internal generation through the process of decay of large-scale circulations and mesoscale eddies by breaking or baroclinic instability; and bottom generation through interaction of the quasisteady currents advecting in a stratified ocean over bottom topography (lee waves) [*Thorpe*, 1975; *Garrett and Munk*, 1979]. In the PLOO region, the internal waves form as the tide moves over rough bottom topography offshore generating significant vertical shear of the horizontal currents through the water column. In shallow water the waves lose energy and can break causing vertical mixing [*Pineda*, 1994].

Based on the analysis presented in this section, a nonlinear internal wave generated by on-shore tidal flow over rough bottom topography is the most likely mechanism behind the enhanced mixing and vertical rise of the plume observed in Figure 28b. It is evident that vertical isothermal (and corresponding isopycnal) oscillations have a strong influence on the plume's mixing and position within the water column. Omission of the processes governing these variations is another possible source of discrepancies between in-situ observations and plume models results (*Petrenko et al*., 2000].

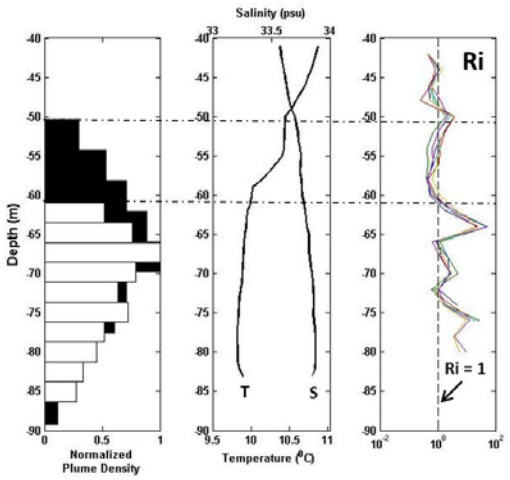

Figure 31. Normalized plume density plotted against depth for the 0.25 km cross-section (hollow bars) and the 1.5 km cross-section (black bars) illustrating a rise in plume height of 10 m in the far-field and profile plots of temperature, salinity and Ri number in the area of interest.

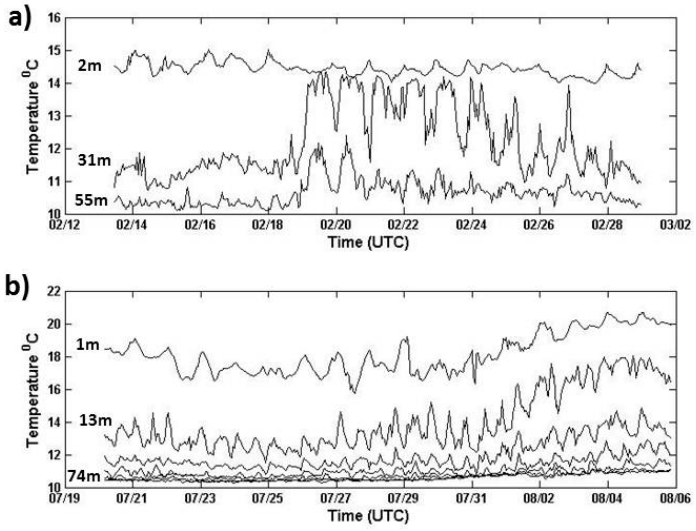

Figure 32. Observed isotherms at depths of (a) 2 m, 31 m, and 55 m from February 13, 2011 to February 29, 2011 and (b) 1 m, 13 m, 25 m, 38 m, 50 m, 62 m and 74 m from 20 July 2010 to 6 August 2010.

Internal waves also affected the PLOO study area beginning on December 22, 2010 and lasting for several days (Figure 33). The event was the maximum observed temporal temperature variability within the water column from April 2010 to April 2011 and suggests the presence of a large amplitude internal wave. The isotherms suggest the internal wave is significantly larger than the one illustrated in Figure 32 due to the temperature fluctuations at deeper depths. The sustained northwest current direction during the December 22, 2010 event was different than all other internal wave events throughout the PLOO study which suggests a different mechanism generated the observed internal waves. Figure 34a shows a 10-hour average profile plot of the currents on December 22, 2010. The currents are uniform in direction throughout the water column and have an average magnitude of 35 cm/s between the depths of 60 m and the surface. If these current conditions persist to the south, the northwesterly currents would intersect with the Coronado Islands before reaching the PLOO study area (Figure 34b). HF radar derived surface currents confirm that the surface currents direction are the same in the South Bay as observed at PLOO (Figure 35). If we assume that the current directions are also uniform with depth in the South Bay, we can conclude that the most plausible mechanism of the large amplitude non-linear internal waves observed at PLOO on December 22, 2010 is caused by the interaction of the currents with the Coronado Islands.

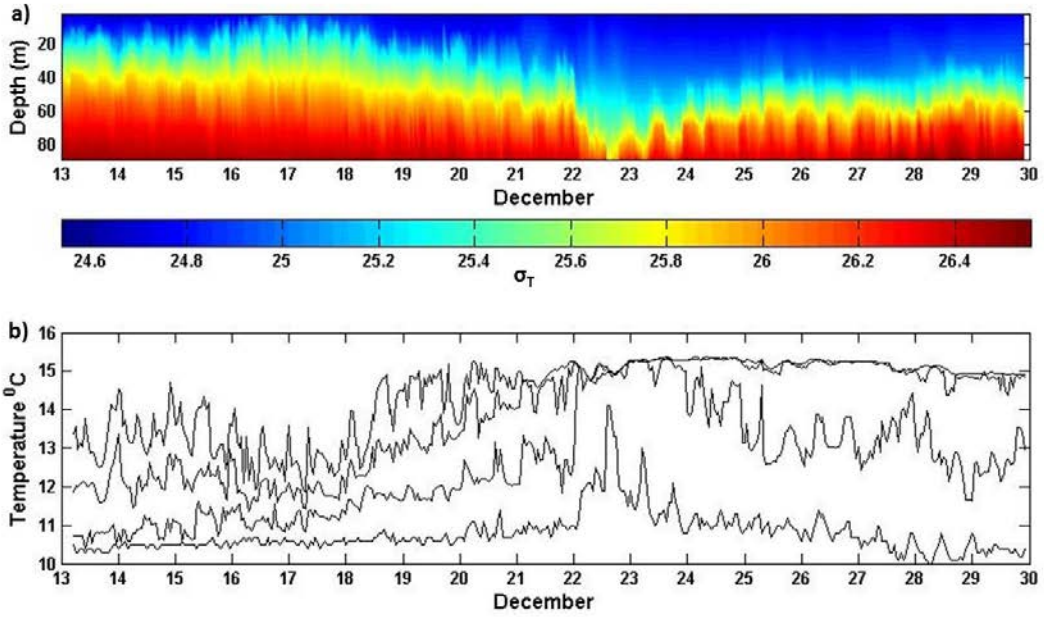

Figure 33. (a) Ocean temperature time series from December 13, 2010 to December 30, 2010. (b) Observed isotherms at depths of 19 m, 31 m, 54 m, 89 m from December 13, 2010 to December 30, 2010 .

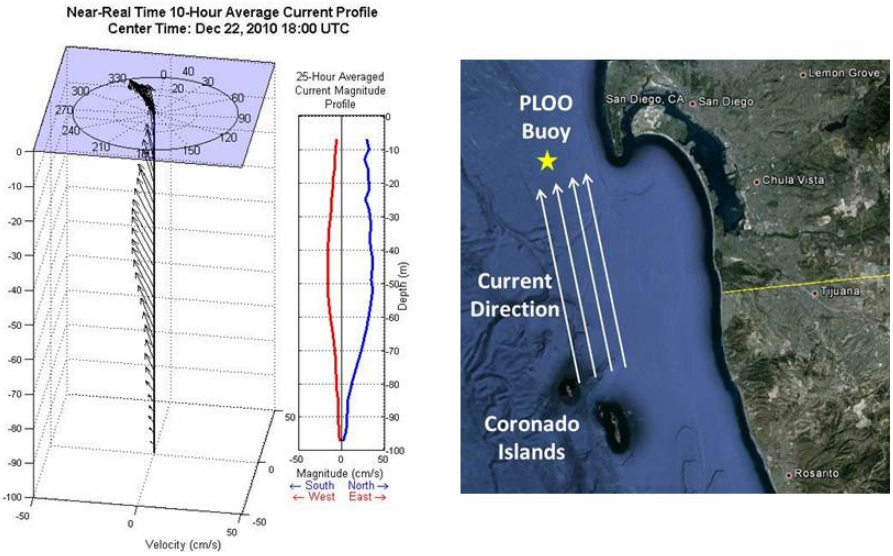

Figure 34. Uniform alongshore current direction that intersects the Coronado Islands and affects the PLOO study area on December 22, 2010.

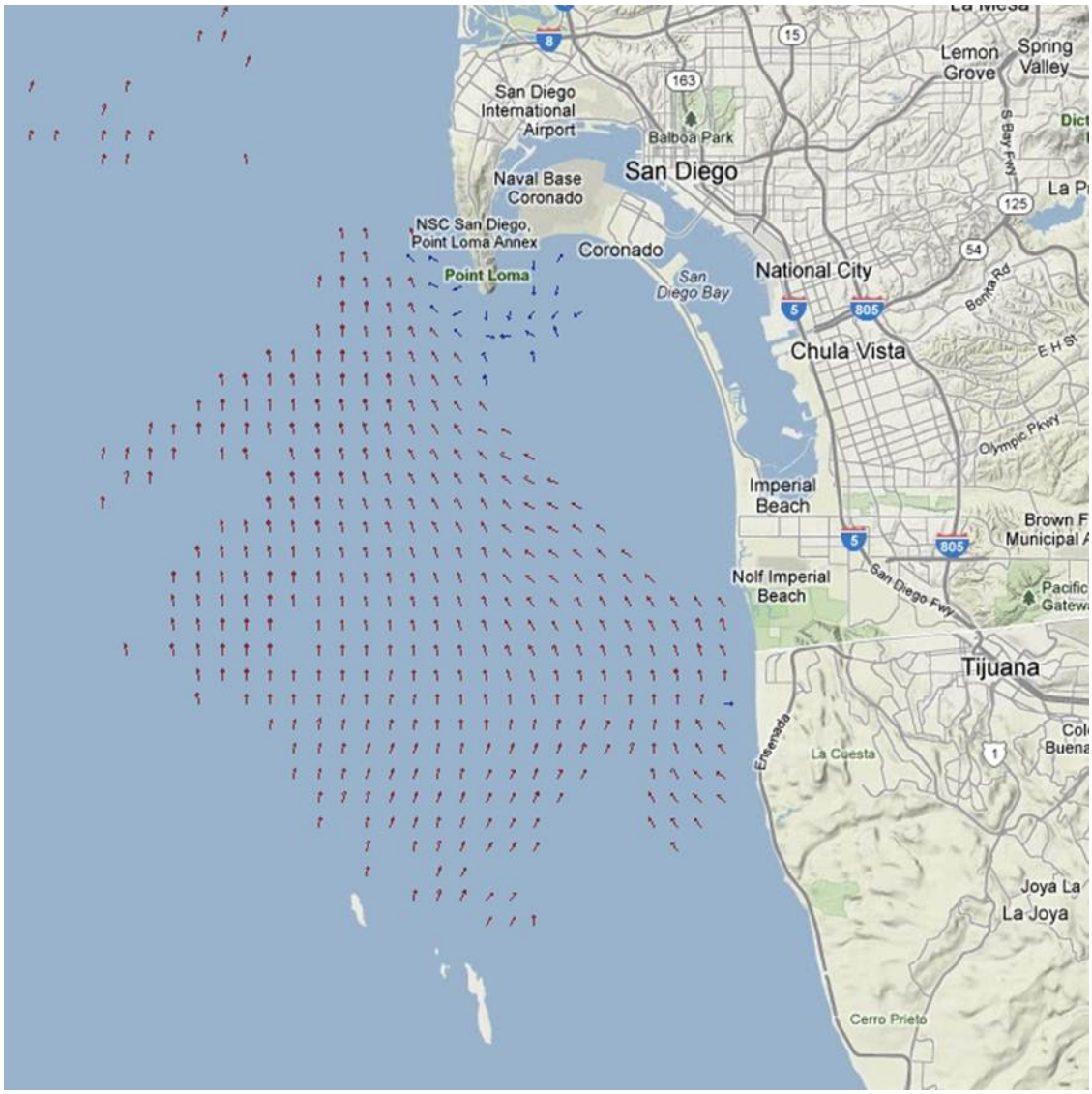

Figure 35. Online display of HF Radar derived surface currents in the South Bay on December 22, 2010. Sites maintained through this effort include Point Loma, Border Field State Park, and Coronado Islands.

V. CONCLUSIONS

Despite the political, ecosystem, and public health interests in coastal water quality, ocean monitoring of the physics responsible for the transport of a land-based or offshore wastewater discharge plume is difficult. Water quality sampling required of an NPDES permit holder in the receiving waters of their discharge typically is designed for assessing water quality on a statistical basis, not for assessing the fate and transport of their discharge. **The sampling required of an NPDES permit provides snapshots of ocean conditions, but under-samples the ocean in the time and space domains that are necessary to estimate the position of the plume.** In addition, the transport and orientation of discharge plumes are highly variable because

of ocean dynamics and can be elusive to track using a fixed grid of boat-based sampling stations. As a result, assessment of station data is often inconclusive. One reason sampling protocols for monitoring receiving water have not evolved significantly over the years is the lack of available tools that can provide appropriate monitoring at the appropriate scales required to accurately estimate the fate and transport of the discharge plume. Methods using vessel-based sampling at fixed grid sampling stations in the receiving waters have not changed significantly in 30 years.

A. Findings

Analysis of the data from this study has resulted in the following findings:

1. Measurements of ocean stratification at the PLOO and subsequent modeling of the behavior of the buoyant plume rise height, estimated that the discharge plume did not surface during the 12-month telemetry mooring monitoring period. The most likely mechanism that could cause the plume to surface would be a strong upwelling event, however the plume was never observed or predicted to rise to the surface even during such upwelling conditions. Thus, due to the deepwater depth of the discharge (~100m) and typical stratification conditions during the wet and dry seasons, it is unlikely oceanographic conditions at PLOO will be favorable for a surfacing plume.

2. The NRFIELD model predicts the PLOO plume to rise through the weakly stratified bottom layer until it intersects with the strongly stratified upper layer. A range of rise heights between the depths of 20-30 m was common during the months of April 2010 to October 2010, while warm waters extended to a depth of 30 m from October 2010 through November 2010 causing stronger stratification at these depths which suppressed the predicted rise height to a depth of approximately 40 m. For all monitoring missions, the observed plume rise height remained below the predicted rise height and generally fluctuated between 40 – 60 m in depth. The maximum observed rise height occurred during the February 28, 2011 monitoring mission when the plume rose to a depth of 35 m.

3. Subsurface currents measured by the oceanographic mooring at the outfall discharge site can be used to estimate the transport and orientation of the PLOO subsurface plume. Generally, the plume was advected either North or South for all missions, with exceptions for the February 28, 2011 and March 3, 2011 (minimal current), April 22, 2011 (variable - changing direction in the hours preceding a mission), and the June 16, 2010 and December 8, 2010 monitoring missions in which an on-shore flow was observed.

4. The AUV using a CTD probe, along with sensors for measuring changes in the ocean's optical properties, was able to effectively map out the location of the subsurface plume. With proper vehicle configuration and mission programming, the vehicle was able to detect the plume 100 percent of the time. The ability of the vehicle to sense the subsurface plume was enabled using proper mission planning of the vehicle track and consideration of plume transport estimates using PLOO mooring data in near-real time. The plume orientation measured by the AUV matched estimated trajectories from the ocean mooring velocity profile and stratification measurements for all missions. A total of 21 sampling missions were conducted. The mean observed dilution ratio of PLOO wastewater to seawater determined from AUV CDOM measurements was 1:170. However, the mean NRFIELD

predicted dilution based on the oceanographic conditions from the PLOO mooring was 1:357. The NRFIELD model assumes the submerged wastefield resulting from multi-port line diffusers forms a line plume in which individual plumes from each diffuser port merge before the terminal rise height. For the PLOO, the ratio of the port spacing to rise height is large, thus the diffuser port plumes do not fully merge before the terminal rise height, creating a point plume. This is the most feasible explanation for the difference between observed and predicted dilutions.

5. Linear (small amplitude) and nonlinear (amplitude is a large fraction of the water depth) waves are prevalent features of coastal circulation in the region surrounding the PLOO. In the region off Pt. Loma, the internal waves form as the tide moves over rough bottom topography offshore generating significant vertical shear of the horizontal currents through the water column. In shallow water the waves lose energy and can break causing vertical mixing. The February 25, 2011 monitoring mission showed that vertical isothermal (and corresponding isopycnal) oscillations have a strong influence on the plume's mixing and position within the water column and omission of the processes governing these variations is another possible source of discrepancies between in-situ observations and plume models results.

B. Published Work

The PLOO behavior study resulted in two peer-reviewed published journal articles:

1. Rogowski, P., Terrill, E., Otero, M., Hazard, L. and Middleton, W. (2012), Mapping Ocean Outfall Plumes and their Mixing using Autonomous Underwater Vehicles. *J. of Geo. Phys. Res*., **117**, C07016.

2. Rogowski, P., Terrill, E., Otero, M., Hazard, L. and Middleton, W. (2012), Ocean Outfall Plume Characterization using an Autonomous Underwater Vehicle. *Water and Science Tech*., (in press).

VI. MONITORING RECOMMENDATIONS

As a result of the findings reported herein for the Point Loma Ocean Outfall Plume Behavior Study, a recommended set of activities is proposed to assist with future receiving waters monitoring efforts for the PLOO discharge.

1. Continued operation of an oceanographic mooring system designed to measure subsurface velocity and ocean stratification is recommended to document the state of the receiving waters into which the PLOO discharges. Measurements conducted during this study showed that the probability of the PLOO plume surfacing is minimal. However, the subsurface velocity measurements proved invaluable for estimating the location of the plume so that it could be effectively sampled. Consequently, we recommend that the NPDES-mandated quarterly water quality sampling component of the City's ocean monitoring program be modified to use telemetered ADCP/temperature data from a permanent mooring located near the terminal diffuser wye structure of the outfall (discharge site) in order to design a more adaptive and optimized sampling grid pattern for these surveys.

2. The present offshore water quality sampling grid specified in the City's NPDES permit is too coarse in space to accurately identify where the submerged PLOO plume is located. If the goals of this component of the City's monitoring program are to sample the receiving waters to measure plume location and dilution levels, it is recommended that continued usage of a mobile AUV as described herein be in place and integrated with near-real-time reports of water column stratification and subsurface velocity. The approach used for the present plume behavior study involved programming an AUV to sample the ocean in locations probable for the PLOO plume to be present. The mission programming was guided by hourly reports of stratification and subsurface velocity provided by an ocean buoy located at the wye of the outfall (see Recommendation 1). This methodology allowed for observations of the dilution and fate of the effluent to a lateral distance of over 9 km from the diffusers. Dilution levels at these extents are similar to those nearer to the diffuser since mixing in the far-field is generally a slow process governed by oceanic turbulence. If NPDES monitoring goals include determination of the fate, extent, and dilution of the plume at large distances from the diffusers, utilization of an AUV will be essential.

VII. ACKNOWLEDGMENTS

Funding for this project was provided by NOAA Award No. NA08NOS4730441 to the City of San Diego Public Utilities Department by the National Oceanic and Atmospheric Administration. The work was conducted by the Scripps Institution of Oceanography under Contract H094679 between the City and UC San Diego.

VIII. LITERATURE CITED

Abarbael, H. D., D. D. Holm, J. E. Marsden, T. Ratiu (1984), Richardson number criterion for the nonlinear stability of three dimensional stratified flow, *Phys. Rev. Lett*., 52, 2352–2355.

Baumgartner, D. J., W. E. Frick, P. J. W. Roberts, (1994), Dilution models for effluent discharges, 3rd Ed., Rep. No. EPA/600/R-94/086. Office of Research and Development, U.S. Environmental Protection Agency, Washington, D.C.

Besiktepe, S., T. E. Ozsoy, M. A. Latif (1995), Sewage outfall plume in the 2-layer channel - An example of Istanbul outfall, *Water Sci. Technol*., 32, 2, 69-75.

Bratkovich, A. (1985), Aspects of the tidal variability observed on the southern California continental shelf, *J. Phys. Oceanogr*., 15, 225-239.

Brooks, N.H. (1960), Diffusion of sewage effluent in an ocean current, presented in First International Conference on Waste Disposal in the Marine Environment, University of California, Berkeley.

Chadwick, D. B., and J. L. Largier (1999b), Tidal exchange at the bay-ocean boundary, *J. Geophys. Res.,* 104, 29901–29924.

Ekman, V.W., (1905), On the influence of the earth's rotation on ocean currents. Arkiv foer Matematik Astronomi Och Fysik (Swedish), 2: 1–52.

Elliott, A. J., A. G. Barr, D. Kennan (1997), Diffusion in Irish Coastal Waters, Estuarine, *Coastal and Shelf Science*, 44 (Supplement A), 15-23.

Fischer, H. B., E. J. List, R. C. Y. Koh, J. Imberger, H. Brooks (1979), Mixing in inland and coastal waters, Academic Press, Inc.: New York, N.Y.

Fofonoff, N. P. and R. C. Millard (1983), Algorithms for computations of fundamental properties of seawater. UNESCO Technical Papers in Marine Science, No. 44, 53 pp.

French-McCay, D. P., C. Mueller, K. Jayko, B. Longval, M. Schroeder, J. R. Payne, E. Terrill, M. Carter, M. Otero, S. Y. Kim, W. Nordhausen, M. Lampinen, C. Ohlmann (2007), Evaluation of Field-Collected Data Measuring Fluorescein Dye Movements and Dispersion for Dispersed Oil Transport Modeling, paper presented at the 30th Arctic and Marine Oil Spill Program (AMOP). Technical Seminar, Emergencies Science Division, Environment Canada, Ottawa, ON, Canada.

Garrett, C. and W. Munk (1979), Internal waves in the ocean, *Ann. Rev. Fluid Mech*, 11, 339–369.

Geyer, W. R., A. Lavery, M. Scully, J. Trowbridge (2010), Mixing by shear instability at high Reynolds number, *Geophys. Res. Lett.*, 37, L22607.

Hendriks, T., and N. Christensen (1987), Current flow patterns in the San Diego Bight, annual report, pp. 27-31, *South. Calif. Water Res. Proj*., Westminster.

Hunt, C. D., A. D. Mansfield, M. J. Mickelson, C. S. Albro, W. R. Geyer, P. J. W. Roberts (2010), Plume tracking and dilution of effluent from the Boston sewage outfall, *Mar. Env. Res*., 70, 150–161.

Jones, B. H., A. Bratkovich, T. Dickey, G. Kleppel, A. Steele, R. Iturriaga, I. Haydock (1990), Variability of physical, chemical, and biological parameters in the vicinity of an ocean outfall plume, presented at the Third Int. Symp. on Stratified Flows, E. J. List and H. H. Jirka (eds.), ASCE, New York.

Jones, B. H., L., Washburn, Y. Wu (1991), The dispersion of ocean outfall plumes: physical and biological dynamics, presented at Coastal Zone '91, Proc. of 7th Symposium on Coastal & Ocean Management. ASCE, Long Beach, CA.

Jones, B. H., T. D. Dickey, L. Washburn, D. Manov (1993), Physical and biological dynamics of sewage outfall plumes in the coastal region: an integrated observational approach, Water Pollution 11: Modelling, Measuring, and Prediction, L.C. Wrobel and C.A. Brebbia (eds.), Computational Mechanics Publications, Southhampton. 527-534.

Koh, R. C. Y. and N. H. Brooks (1975), Fluid mechanics of waste water disposal in the ocean, *Ann. Rev. Fluid Mech*., 7, 187-211.

Lennert-Cody C. E., P. J. S. Franks (1999), Plankton patchiness in high-frequency internal waves, *Mar. Ecol. Prog. Ser*., 186, 59 – 66.

Mack, S. A. and H. C. Schoeberlein (2004), Richardson number and ocean mixing: Towed chain observations, *J. Phys. Oceanogr*., 34, 736–754.

Millero, F. J. and A. Poisson. (1981), International one-atmosphere equation of state of seawater, *Deep-Sea Res*., 28, 625-629.

Okubo, A., (1971), Oceanic diffusion diagrams, *Deep-Sea Res*., 18, 789-802.

Petrenko, A. A., B. H. Jones, T. D. Dickey (1998), Shape and initial dilution of Sand Island, Hawaii sewage plume, *J. Hydraulic Eng*., ASCE, 124, 565-571.

Petrenko, A. A., B. H. Jones, T. D. Dickey, M. LeHaitre, C. Moore (1997), Effects of a sewage plume on the biology, optical characteristics, and particle size distributions of coastal waters, *J. Geo. Phys. Res*., 102, 25061 - 25071.

Petrenko, A.A., B. H. Jones, T. D. Dickey, P. Hamilton (2000), Internal tide effects on a sewage plume at Sand Island, Hawaii, *Continental Shelf Res*., 20, 1–13.

Phillips, O. M., (1997), The Dynamics of the Upper Ocean, 2nd ed. London: Cambridge University Press.

Pineda, J., (1994), Internal tidal bores in the nearshore: Warm-water fronts, seaward gravity currents and the onshore transport of neustonic larvae, *J. Mar. Res*., 52, 427–458

Proni, J. R., H. Huang, W. P. Dammann (1994), Initial dilution of southeast Florida ocean outfall, *J. Hydraulic Eng*., ASCE, 120, 1409-1425.

Ramos, P., M. V. Neves, F. L. Pereira, I. Quintaneiro (2002), Mapping the Aveiro sea outfall plume: sampling strategy for an Autonomous Underwater Vehicle, presented at 2nd International Conference on Marine Waste Water Discharges, MWWD 2002, Istanbul, Turkey.

Ramos, P., S. R. Cunha, M. V. Neves, F. L. Pereira, I. Quintaneiro (2005), Sewage Outfall Plume Dispersion Observations with an Autonomous Underwater Vehicle, *Water Science and Techn.*, 52, 12.

Roberts, P. J. W. (1977), Dispersion of buoyant waste water discharged from outfall diffusers of finite length, thesis, presented to California Institute of Technology, at Pasadena, Calif., in partial fulfillment of the requirements for the degree of Doctor of Philosophy.

Roberts, P. J. W., W. H. Snyder, D. J. Baumgartner (1989), Ocean Outfalls. Parts I, II, and III. *J. Hydraulic Eng*., ASCE, 1–70.

Roberts, P. J. W. (1999a), Modeling Mamala Bay Outfall Plumes. I: Near Field, *J. of Hydraulic Eng*., ASCE. 125, 6, 564-573.

Roberts, P. J. W. (1999b), Modeling Mamala Bay Outfall Plumes. II: Far Field, *J. of Hydraulic Eng*., ASCE 125, 6, 574-583.

Roughan, M., E. J. Terrill, J. L. Largier, M. P. Otero (2005), Observations of divergence and upwelling around Point Loma, California, *J. Geophys. Res.*, 110, C04011.

Schmitt, R. W., R. C. Millard, J. M. Toole, W. D. Wellwood (2005), A double-diffusive interface tank for dynamic-response studies, *J. of Mar. Res.*, 63, 263-289.

Taylor, G. I. (1953), Dispersion of soluble matter in solvent flowing slowly through a tube, *Proc. R. Soc. Lond*., A219, 186-203.

Taylor, G. I. (1954), The dispersion of matter in turbulent flow through a pipe, *Proc. R. Soc. Lond*., 223, 446-468.

Terrill, E. (2009), IBWC Final Report - Coastal observations and monitoring in South Bay San Diego IBWC / Surfrider Consent Decree, February 25, 2009.

Thorpe, S. A., (1975), The excitation, dissipation and interaction of internal waves in the deep ocean, *J. Geophys. Res.*, 80**,** 328–338.

Tian, X., P. J. W. Roberts, G. J. Davero (2004), Marine Wastewater Discharges from Multport Diffusers II: Unstratifield Flowing Water, *J. of Hydraulic Eng*., 130, 12, 1147-1155.

Washburn, L., B. H, Jones, A. Bratkovich, T. D. Dickey, M. Chen (1992), Mixing, dispersion, and resuspension in vicinity of ocean wastewater plume, *J. of Hydraulic Eng*., ASCE, 118(1), 38-58.

Winant, C. D., A. W. Bratkovich (1981), Temperature and currents on the southern california shelf: a description of the variability, *J. Phys. Oceanogr.*, 11, 71–86.

Wu, Y. C., L. Washburn, B. H. Jones (1994), Buoyant plume dispersion in a coastal environment-evolving plume structure and dynamics, *Continental Shelf Res*., 14, 1001-1.

Appendix G
KELP FOREST ECOSYSTEM MONITORING REPORT

Renewal of NPDES CA0107409

APPENDIX G

KELP FOREST ECOSYSTEM MONITORING REPORT

January 2015

Appendix G

Kelp Forest Ecosystem Monitoring Report

Parnell, P.E, P. Dayton, K. Riser, and B. Bulach. 2014. Final Project Report (2010 – 2014): Evaluation of Anthropogenic Impacts on the San Diego Coastal Ecosystem. Prepared for City of San Diego Public Utilities Department by Scripps Institution of Oceanography, University of California, San Diego, CA.

EVALUATION OF ANTHROPOGENIC IMPACTS ON THE SAN DIEGO COASTAL ECOSYSTEM

Final Project Report (2010 – 2014)

By

P. Ed Parnell, Ph.D.

Paul Dayton, Ph.D.

Kristin Riser

Brenna Bulach

Scripps Institution of Oceanography, UC San Diego

Submitted to

City of San Diego Public Utilities Department

(UCSD Contract OO-19958/H074007)

November 2014

INTRODUCTION

The coastal shelf off San Diego is a premier recreational area with beaches that attract tourists from all over the world. The most charismatic of the marine communities that occur in the region are the highly productive giant kelp forests (*Macrocystis pyrifera*), especially the Point Loma Kelp Forest and the La Jolla Kelp Forest, which provide food and shelter for many species of marine fishes and invertebrates, and attract thousands of recreational divers and fishermen each year. These kelp forests also represent the most important fishing grounds for the commercial red sea urchin (*Strongylocentrotus franciscanus*) and spiny lobster (*Panuliris interruptus*) fisheries in all of California. Consequently, the potential for human-related impacts on these characteristic marine communities is critically important to understand.

Primary human impacts to San Diego's coastal waters and ecosystems include wastewater discharge via two large ocean outfalls, discharges of untreated waters, sediments and associated contaminants to the ocean via storm drains and surface runoff from local watersheds, and the transport and disposal of contaminated sediments originating from other sources (e.g., dredging from San Diego Bay). All of these stressors can have deleterious effects on kelp forest communities. These effects were most common prior to the period that wastewater and stormwater best practices were modernized beginning in the 1960's. The main sources of wastewater discharge off San Diego include the Point Loma Ocean Outfall (PLOO) and the South Bay Ocean Outfall (SBOO). The PLOO passes directly through the Pt. Loma kelp forest that occupies the nearshore shelf to depths of ~28m and discharges advanced primary treated wastewater ~7.3 km offshore in waters ~100 meters deep. The SBOO passes near the Imperial Beach kelp beds and discharges treated wastewater ~5.6 km offshore of Imperial Beach at a depth of ~30 meters. Surface runoff originates from several watersheds affected by human land

use such as agriculture, heavy industry, and general urbanization. Outflows of contaminated waters from such sources as the Tijuana River, San Diego Bay, Mission Bay, the North County lagoons, and the northern transport of contaminants along the coast originating from south of the US/Mexican border may also impact local water quality and kelp forest conditions in the region. Natural stressors such as ocean climate cycles ranging in period from years (El Niño Southern Oscillation) to decades (Pacific Decadal Oscillation) also greatly influence kelp forest communities at regional scales. The interaction of ocean climate variation and human disturbances can profoundly affect the stability and resilience of kelp forest communities.

The City of San Diego, as part of its enhanced ocean monitoring objectives for the San Diego coastal region, has contracted with Scripps Institution of Oceanography to monitor the status and dynamic forcing of kelp forests off San Diego from below the southern tip of Point Loma to North County (Fig. 1). This represents a continuation of more than 40 years of research and monitoring of kelp forests off San Diego (Dayton et al., 1984). This report summarizes the findings of a 4-year project agreement covering the period 2010 to 2014 and continuing this long-term study of the health of the giant kelp forests off San Diego (UCSD Contract OO-19958/H074007).

METHODS

Study Sites and Monitoring Strategy

The kelp forests monitored in this study include the large kep beds off Pt. Loma and La Jolla, and several smaller beds off North San Diego County (Fig. 1). The Point Loma kelp forest, measuring approximately 8-10 km long by 1 km wide, is located on a broad, mudstone-sandstone terrace offshore of San Diego, California. The La Jolla kelp forest occupies two broad

Cretaceous sandstone shelves that extend ~1 ¾ km offshore before they grade down below the depth where giant kelp can grow. The North County forests include several smaller isolated forests off Del Mar, Solana Beach, and Cardiff-by-the-Sea. These forests occupy low relief outcrops that are extensions of onshore terraces separated by numerous river eroded estuaries. The North County forests are shallower than the Pt. Loma and La Jolla kelp forests and are surrounded by sandy sediments comprising the Oceanside Littoral Cell.

The main components of the kelp forest ecosystem monitoring program include assessments of (1) algal density, growth, reproductive condition and recruitment, (2) invertebrate densities, (3) sea urchin demography (size distributions to monitor for episodic recruitment), and (4) temperature (a proxy of ocean nutrient status). Monitoring of the kelp forests was conducted at 21 permanent study sites distributed among the kelp forests off Point Loma, La Jolla, Del Mar, Solana Beach, and Cardiff (see Figs. 2-4). Study site selection was stratified by depth and alongshore distance, as well as the inclusion of characteristic ecological features and habitats.

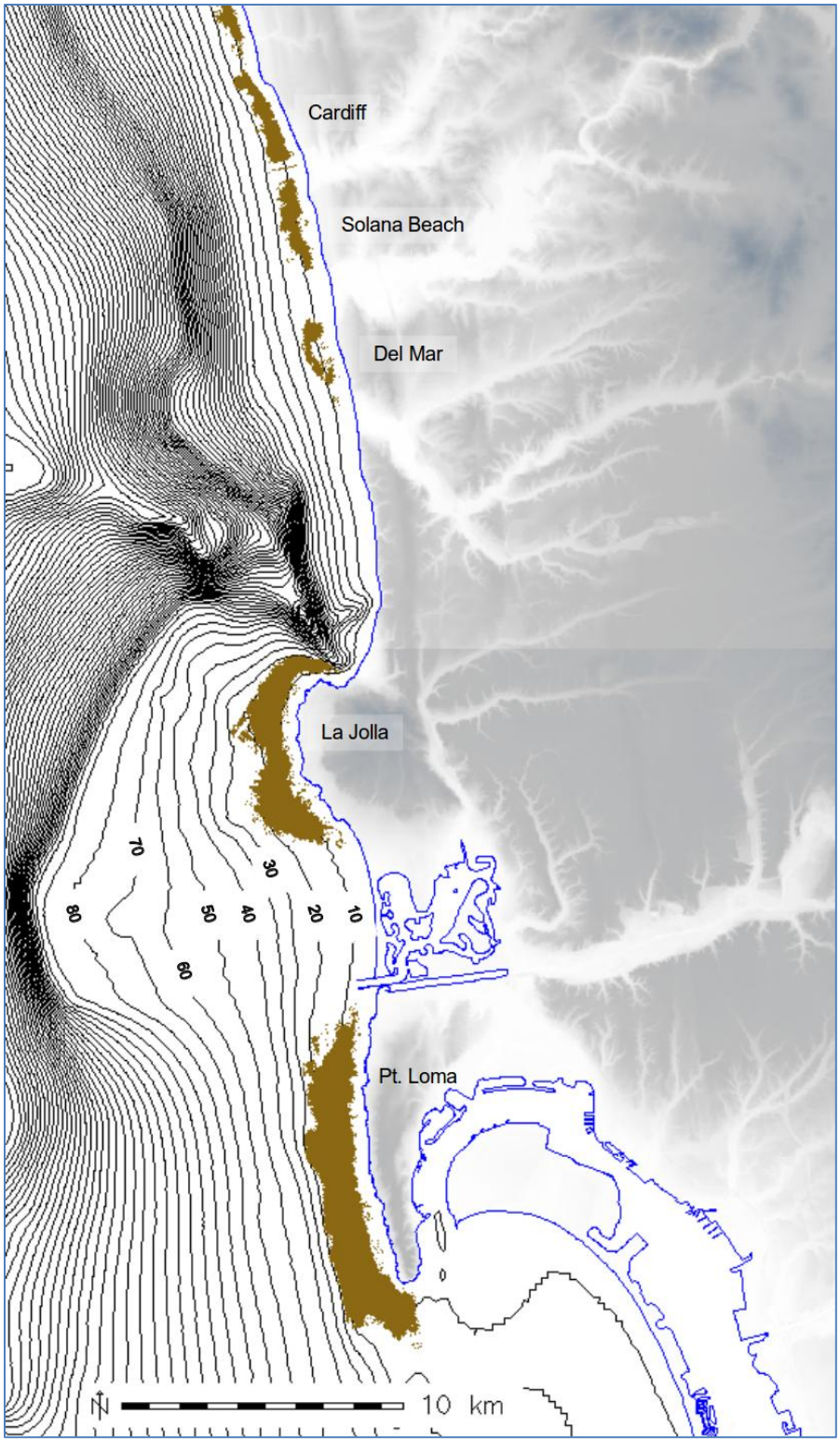

Figure 1. The kelp forests off San Diego that were part of this study. Depth units are meters.

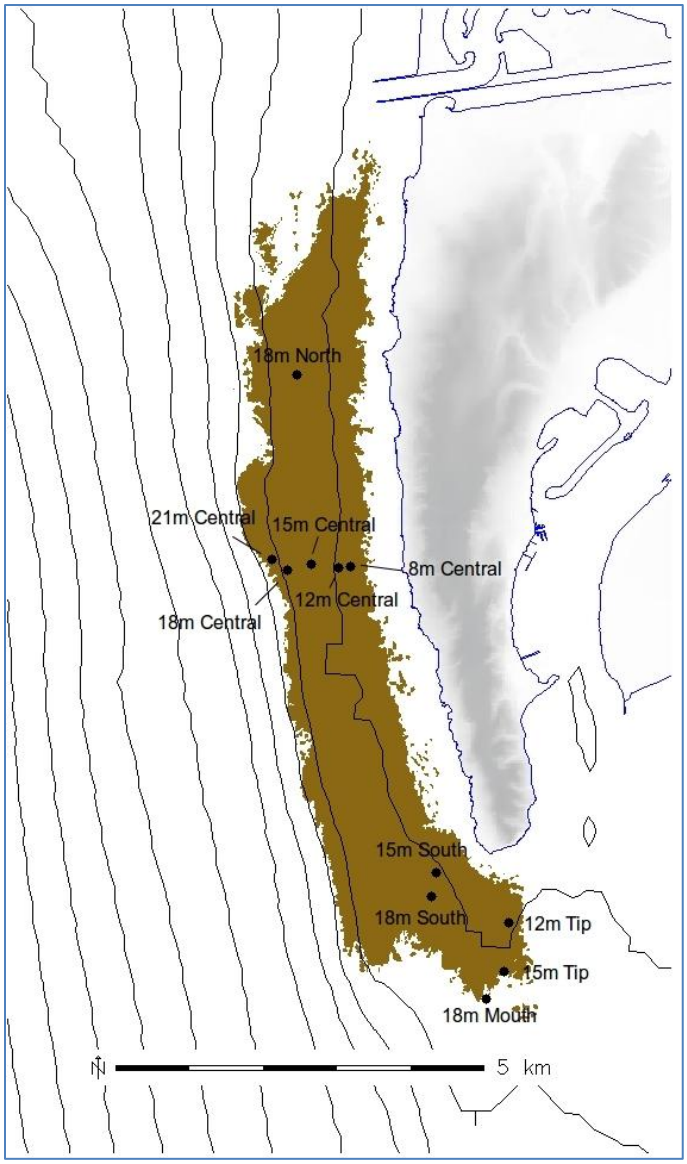

Figure 2. Map showing 11 study sites in the Pt. Loma kelp forest.

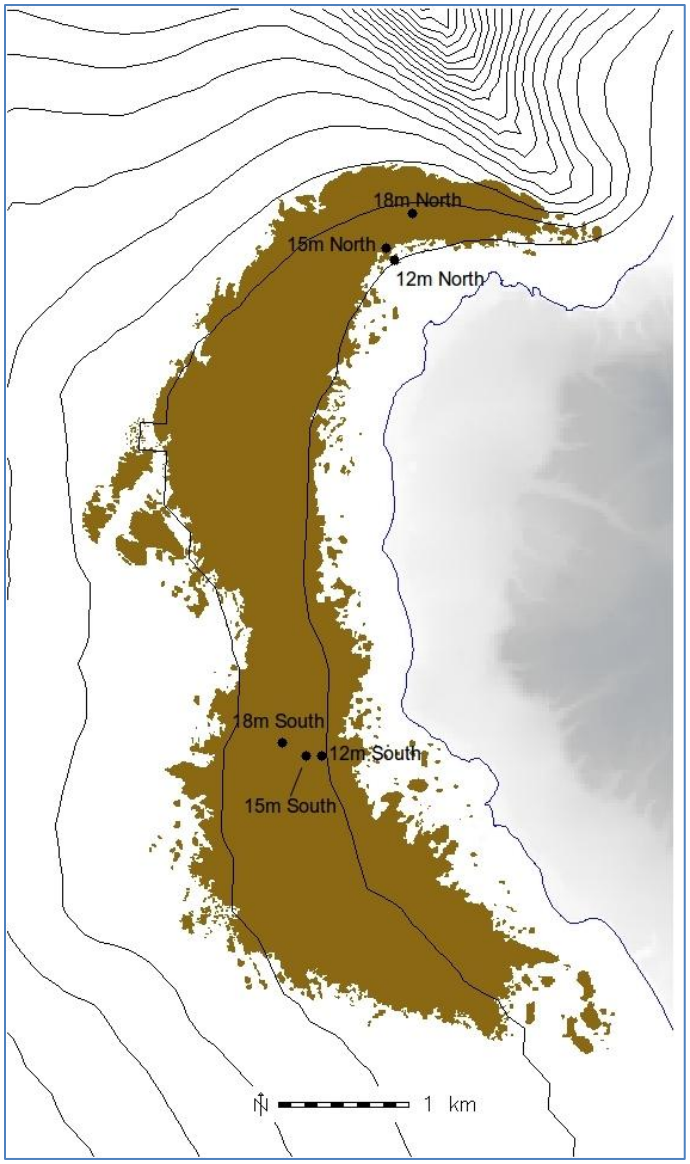

Figure 3. Map showing six study sites in the La Jolla kelp forest.

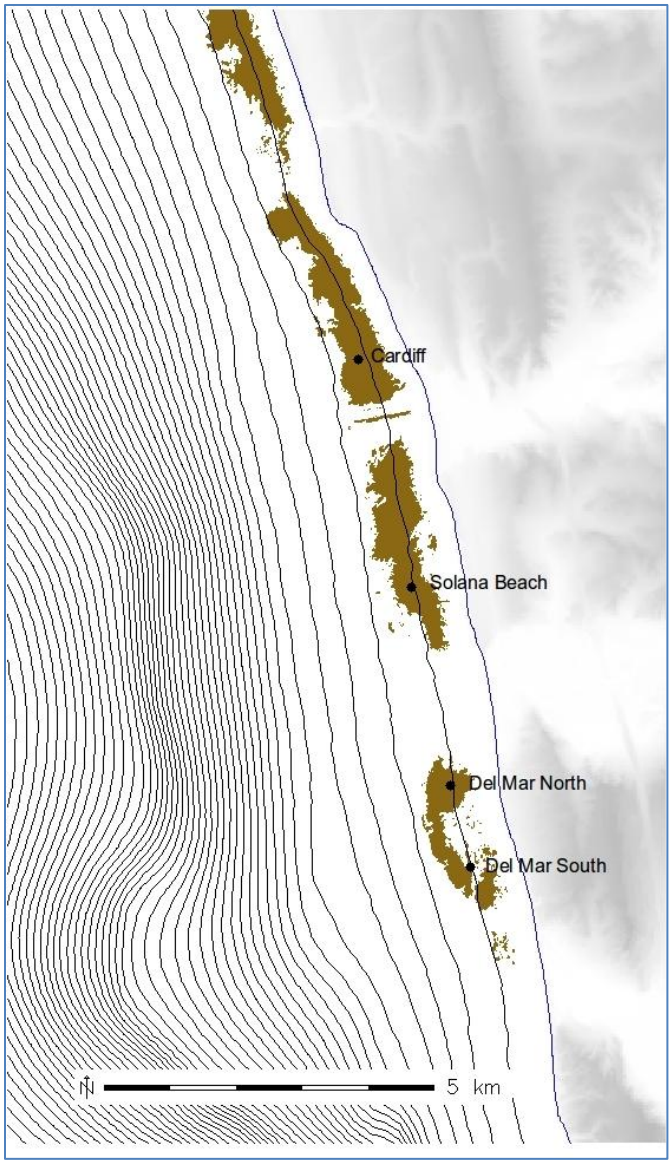

Figure 4. Map showing four study sites among the North San Diego County kelp forests.

Algae and invertebrates are censused along four permanent band transects at each study site. Band transects are oriented across-shore and are 25 m in length. Algae and invertebrates are censused within 2 m of both sides of each line. Therefore, the total area surveyed at each site is 400 m^2. Due to its small size, the Del Mar kelp forest band transects are divided among two locations, Del Mar North and Del Mar South (Fig. 4), each having two permanent 25 m band

transects. Algal densities are monitored at all study sites on a quarterly basis (once each season). Algal reproduction and growth for the three most common large kelp species (*Macrocystis pyrifera*, *Pterygophora californica*, and *Laminaria farlowii*) are monitored monthly at all of the central Pt. Loma stations.

Growth of *M. pyrifera* is monitored by counting the number of stipes on each plant at a height of 1 m above the substratum. Reproductive state is represented by the size of the sporophyll (germ tissue) bundle at the base of each plant. The volume is calculated as a cylinder based on the height and diameter of each bundle. This is an indirect measure of reproductive effort, but Reed (1987) has shown that sporophyll biomass is closely related to zoospore production. We ranked the reproductive state for each plant on the following scale:

0 = No sporophylls present.

1 = Sporophylls present but no sorus (site of active reproduction) development.

2 = Sporophylls with sori only at the base of sporophylls.

3 = Sporophylls with sori covering most of the surface.

4 = Sporophylls with sori covering the entire surface.

5 = Sporophylls with sori covering the entire sporophyll surface and releasing zoospores.

Growth of *Pterygophora californica* was determined by the method of DeWreede (1984). A 6mm diameter hole is punched in the midrib of the terminal blade 30mm from the base of the blade, and every month another hole is punched at the same location. The distance between the two holes represents the linear growth of each blade. Reproductive effort for *P. californica* is evaluated by a count of the total number of sporophyll blades on each plant and the number with sori.

Growth of *Laminaria farlowii* is determined in a similar manner to *P. californica*. A 13mm diameter hole is punched 100mm from the base of each blade, which is repeated each visit. The distance between the two holes represents the linear growth of each blade. The reproductive potential of *L. farlowii* is evaluated as the percent of each blade covered by sori.

Temperature and Nutrients

Kelps require adequate nutrients for growth and reproduction. Off southern California, nitrogen is the most limiting nutrient for giant kelp. There is a strong relationship between temperature and nitrate (Fig. 5). Fluctuations in ocean temperature occur at seasonal, internannual (El Niño), and decadal time scales (e.g. Pacific Decadal Oscillation). Nitrate has been less abundant for kelp growth off San Diego since the 1977-78 oceanographic regime shift (Fig. 6) in which the nitrate climate switched from mainly replete conditions to depleted conditions relative to the nitrate threshold for kelp growth.

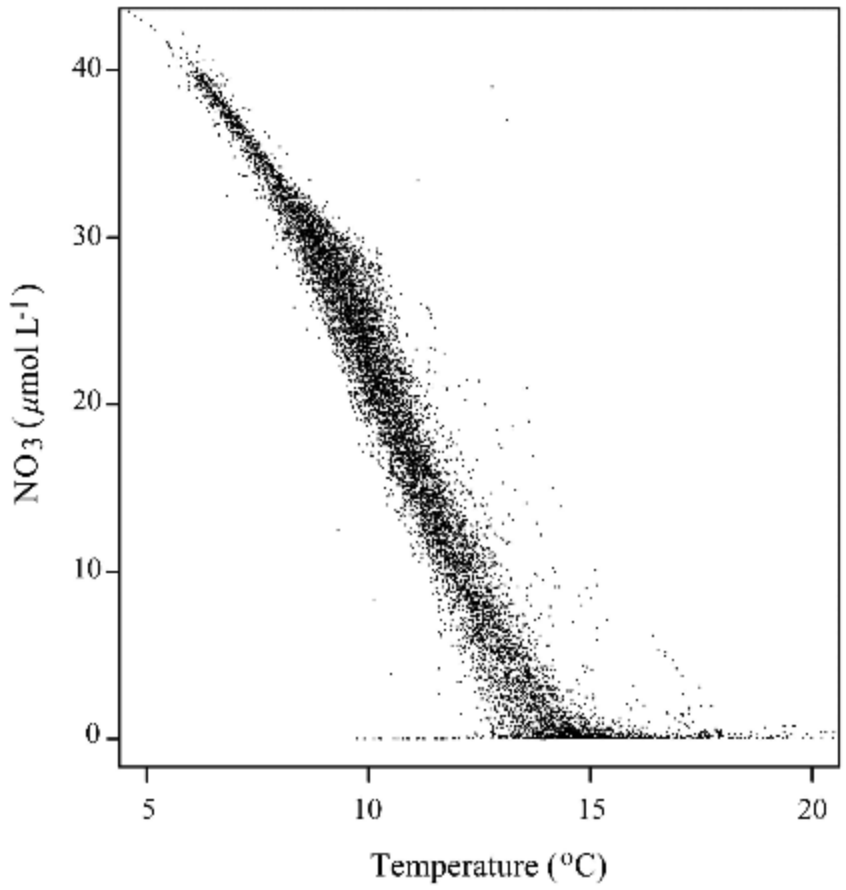

Figure 5. Nitrate concentration as a function of temperature off southern California (from Parnell et al., 2010).

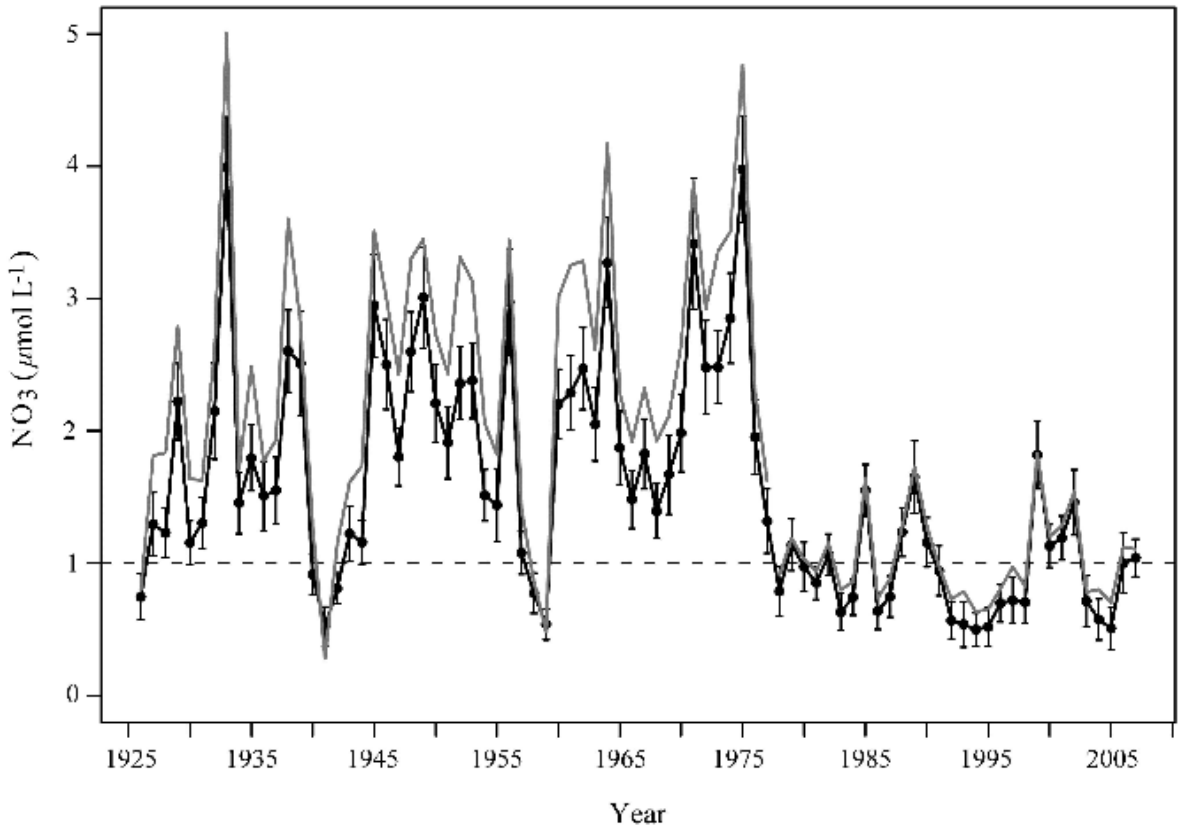

Figure 6. Estimated mean nitrate concentrations across the 1977-78 oceanographic regime shift. Nitrate values were estimated using a statistical fit of nitrate as a function of seawater density (from Parnell et al., 2010). Dashed line indicates the lower level of nitrate necessary for giant kelp growth and reproduction.

Bottom temperatures were recorded at all of the study sites using Onset Tidbit temperature recorders (http://www.onsetcomp.com/products/data-loggers/utbi-001). The sampling frequency was 10 minutes and accuracy and precision of the temperature recorders is ~0.2˚ C and ~0.3˚ C, respectively. There are occasional gaps in bottom temperature time series due to instrument loss or malfunction.

Sea Urchins

Sea urchins, mainly the red urchin *Strongylocentrotus franciscanus* and the purple urchin *S. purpuratus* that occur locally off San Diego, are primary grazers on kelps and are capable of completely grazing large areas of the bottom so little kelp is left. These areas are termed sea

urchin barrens, and can persist for long periods of time. An example is the sea urchin barren off South Pt. Loma that has persisted since at least the 1940's. The area affected has varied considerably over this period. We conducted an acoustic survey utilizing a single beam sonar system in 2012 to delineate the coverage of the sea urchin barrens at that time. The acoustic survey also covered the entire La Jolla and Pt. Loma kelp forests for bottom elevations and canopy coverage (giant kelp canopy, understory canopy, and *Pelagophycus porra* – elkhorn kelp).

Figure 7. Red (*Strongylocentrotus franciscanus*) and purple (*Strongylocentrotus purpuratus*) sea urchins grazing in an established barren.

The importance of sea urchins for the ecology of kelp forest communities dictates that understanding processes that affect their abundance are paramount for long term monitoring studies. Consequently, these and other invertebrates are counted annually along permanently fixed transect lines. Additionally, the recruitment of both red and purple sea urchins was estimated semi-annually at all of the sites in Pt. Loma and La Jolla by measuring the sizes of at least 100 sea urchins for each species at each site. In contrast, there are too few sea urchins in the north county kelp forests to facilitate sea urchin recruitment estimates. For the Pt. Loma and La Jolla estimates, sea urchins are collected in 1 m^2 PVC quadrats placed haphazardly in suitable sea urchin habitat near each study site. All sea urchins are exhaustively removed from cobbles and rocks and additional quadrats are placed as necessary to reach an adequate sample size of

>100 sea urchins. The sea urchin census and recruitment methods provide two different types of data that enable the evaluation of the relative impacts of sea urchin migration vs. recruitment of new individuals on kelp stands. We also monitor for evidence of sea urchin disease that can lead to mass mortality events, and which in turn can release large areas of the kelp forest from grazing pressure resulting in the redevelopment of giant kelp surface canopy.

Sedimentation in North County Kelp Forests

The North County kelp forests are supported by small outcrops of bedrock that exhibit low vertical relief and are relatively shallow compared to the La Jolla and Pt. Loma kelp forests. The large amount of sediment surrounding each of these kelp forests makes them vulnerable to kelp losses due to sediment redistribution covering the hard grounds. This has been the case in the past after periods of beach replenishment when sand migrates naturally from the beaches to the subtidal where the kelp forests are located. Therefore, sand levels or sand coverage are monitored at all North County study sites. This is done by measuring the exposed length of rebar that has been hammered into the hard ground at the Cardiff and Del Mar sites. Percent sand cover along the permanent transects is tracked at Solana Beach as the rebar has been repeatedly dislodged at this site.

RESULTS AND DISCUSSION

Bottom Temperature

The temperature record at the central Pt. Loma study sites extends back to 1984 just after the extensive 1982-83 El Niño event. The largest temperature signal in the time series is the 1997-98 El Niño event (Fig. 8) when much of the kelp forests disappeared due to nutrient stress

and large storm waves that coincided with that El Niño as storm tracks in the central Pacific switched southward. Relatively smaller warm water events have occurred since. Most notable was the 2005/2006 El Niño when much of the surface giant kelp canopy disappeared but plants were still growing below the thermocline where nutrients were more abundant. Bottom temperatures decrease with depth and nutrients are therefore more abundant at depth. This phenomenon physically controls space competition between the understory and canopy kelps. Strong El Niño's such as the 1997/98 El Niño penetrate to the bottom at the offshore edge of the forest at 25 m depth and stress the understory as well as the canopy kelps. In contrast, milder El Niño's do not typically penetrate to the bottom of the forests and therefore stress the surface canopy more than the understory where temperatures are cooler. Repeated cycles of mild El Niño's over many years in the absence of large storm waves leads to increasing understory domination at the expense of giant kelp canopy cover. The temperature climate off San Diego during the study period began moderately warm but cooled to the extent that even the bottom temperatures at the shallow 8 m station were below the 15˚C nitrate threshold. Temperatures increased by the end of the study period and a mild to moderate El Niño is forecast for this upcoming fall and winter.

Figure 8. Bottom temperature trends at the central Pt. Loma study sites ranging in depths from 8 to 21 m. The 33 m site is located just off the hard ground shelf supporting the Pt. Loma kelp forest where only bottom temperature data are collected. The horizontal line at 15˚C indicates the temperature above which nitrate concentrations begin to stress giant kelp growth and reproduction.

Macroalgae

The general trend in algal composition at the central Pt. Loma study sites over the last ~30 years mainly reflects cycles of temperature and wave disturbances followed by giant kelp recruitment and recovery mostly in discreet cohorts which are subsequently outcompeted by understory kelps whose reproduction and growth increases as giant kelp cohorts senesce or are disturbed in local patches. Larger scale *Macrocystis pyrifera* die-offs result in enhanced underwater light levels conducive for subsequent cohorts of giant kelp. Understory bottom cover typically increases with increasing time since the last large wave and/or temperature disturbance. This is graphically shown in Figure 9 for the 15 m central Pt. Loma study site. The graphed lines show the time series of the first three factors produced by a factor analysis of all algal species and species groups counted along the transect lines. Factor analysis transposes multi-dimensional data (in this case each species represents a dimension) into a lower dimensional representation (factors, plotted in Fig. 9). In this case, the factors are based on similarities between the species over time. The factors represent a combination of several species/groups

weighted by their importance (loading) for each species/group. Loadings for species/groups that are highly positively correlated with each factor have greater positive loadings while the converse is true for negatively correlated loadings (see Table 1). The first factor in Figure 9 (red) indicates giant kelp recovery after major disturbances periods - when giant kelp recruits, turf algae, and the early-colonizing brown alga *Desmerestia ligulata* were most common. The second factor (green) demonstrates canopy dominance between understory kelps and giant kelps. Values <0 indicate dominance by *Macrocystis pyrifera* and positive values indicate dominance by understory kelps. Factor 3 (blue) indicates dominance by turf algae.

Figure 9 clearly indicates that the algal stands off central Pt. Loma are highly dynamic. *Macrocystis pyrifera* mostly dominated after the major 1982/83 El Niño wave and nutrient disturbance and continued to dominate until the strong 1997/98 El Niño after which it appeared to recover. However, turf algae began to occupy more of the bottom beginning in the late 1990s so that by the mild El Niño of 2005/2006, the post-recovery *Macrocystis* cohort did not survive in high enough densities to preclude understory species. This appeared to facilitate understory domination by 2007 which has continued through the present study period. A small *Macrocystis* recruitment event was observed during the study period in 2012/2013 but was small relative to past historical recruitment events (Fig. 10). The same dynamic pattern was observed at all of Pt. Loma and La Jolla study sites with greater understory domination occurring earlier in shallow and eventually progressing to deeper areas of the forests where the reproductive capacity of understory algae is not as great. The exception to this pattern has consistently been observed at the south Pt. Loma study sites which have been repeatedly disturbed by episodes of sea urchin overgrazing.

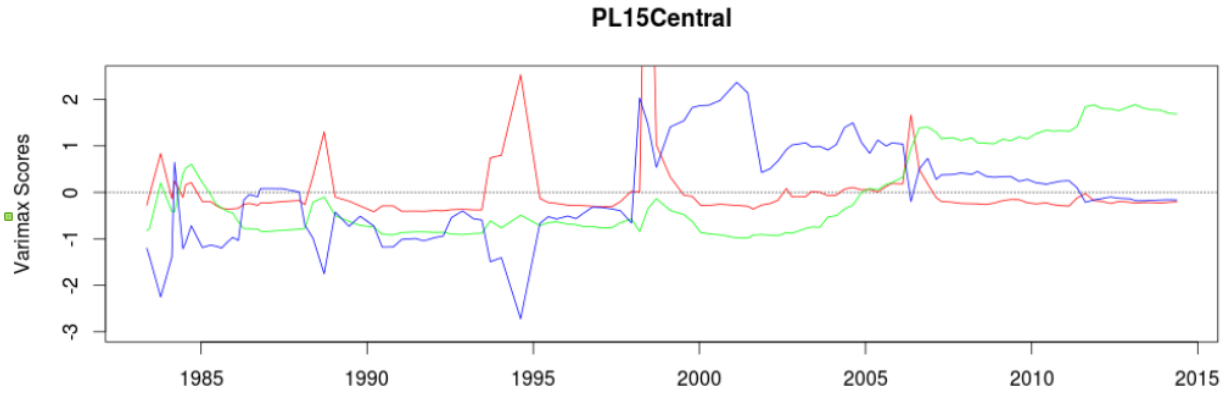

Figure 9. Scores for the first three factors resulting from a factor analysis of algal species/groups at the central Pt. Loma 15 m study site. Red=Factor 1, Green=Factor 2, Blue=Factor 3.

Table 1. Factor loadings for the first 3 factors resulting from a rotated (Varimax rotation) principal components analysis (factor analysis). The first 3 factors accounted for ~56% of the variability. Canopy guilds (surface, understory, and turf) are indicated for each species/group. Species with higher positive scores for a particular factor are positively correlated with the factor while scores that are negative are negatively correlated with that factor. Blank cells indicate species/groups that did not contribute significantly for a particular factor. The abbreviations used in factor analysis figures for each species/group are also listed.

Species or Species Group	Canopy	Abbreviation	Factor 1	Factor 2	Factor 3
Macrocystis pyrifera Adults	Surface	Macro		-0.377	-0.223
Macrocystis Pre-Adults	Surface	Macro PA	0.228		-0.286
Macrocystis Bifurcates	Surface	Macro Recs	0.374		-0.366
Macrocystis Pre-Bifurcates	Surface		0.939		
Pterygophora californica	Understory	Ptery	0.138	0.525	0.261
Laminaria farlowii	Understory	Lam		0.956	
Eisenia arborea	Understory	Eis		-0.120	-0.200
Cystoseira osmundacea	Understory	Cys	-0.102	0.852	
Articulate coralline algae	Turf	AC	0.145	0.415	0.756
Brown turf algae	Turf	BT	0.930		
Red turf algae	Turf	RT	0.595	0.170	0.782
Desmerestia ligulata	Understory	Des	0.660	0.173	
Cumulative Variance			0.233	0.425	0.557

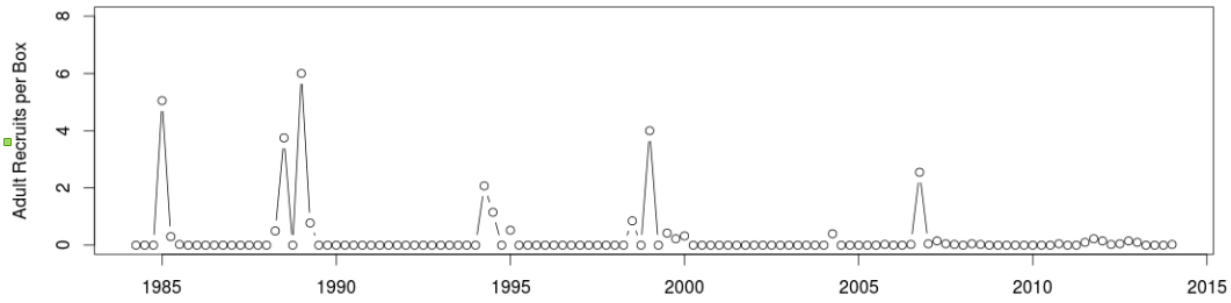

Figure 10. *Macrocystis* recruitment per 10 m^2 transect box at the central 15m Pt. Loma study site. Recruitment events were similar at the other central Pt. Loma sites.

A factor analysis was also conducted for all of the study sites for data gathered specifically during the study period (Fig. 11). Factors 1 and 4 are plotted on the 'x' and 'y' axes respectively. Factor 1 indicates the continuum from turfs to understory to *Macrocystis* (right to left). Factor 4 reflects site-relative *Macrocystis* recruitment during the study period (increasing recruitment from bottom to top). The shallow central Pt. Loma and La Jolla sites are turf and understory dominated while the deeper sites in all areas are less understory-dominated having

relatively more *Macrocystis* plants. Recruitment of giant kelp has been greatest in North County and the deeper south Pt. Loma sites where there has been recruitment following sea urchin overgrazing events. The least *Macrocystis* recruitment was observed at the 15 m central Pt.Loma site. Mean study site scores for the study period were plotted in Figure 11 whereas the range of study site scores observed during the study period are plotted as polygons in Figures 12-15 for central and northern Pt. Loma (Fig. 12), southern Pt. Loma (Fig. 13), La Jolla (Fig. 14), and North County (Fig. 15). Similarly, time series of adult *M. pyrifera* densities during the study period across the similar study site groupings are plotted in Figure 16. *Macrocystis pyrifera* increased due to recruitment events between 2011 and 2012 at the northern 18 m Pt. Loma site, the central Pt. Loma sites at 21 and 18 m, the southern Pt. Loma site at 18 m, and the north La Jolla site at 15 m. Kelp decreased due to sea urchin overgrazing at the Pt. Loma Tip site at 12 m.

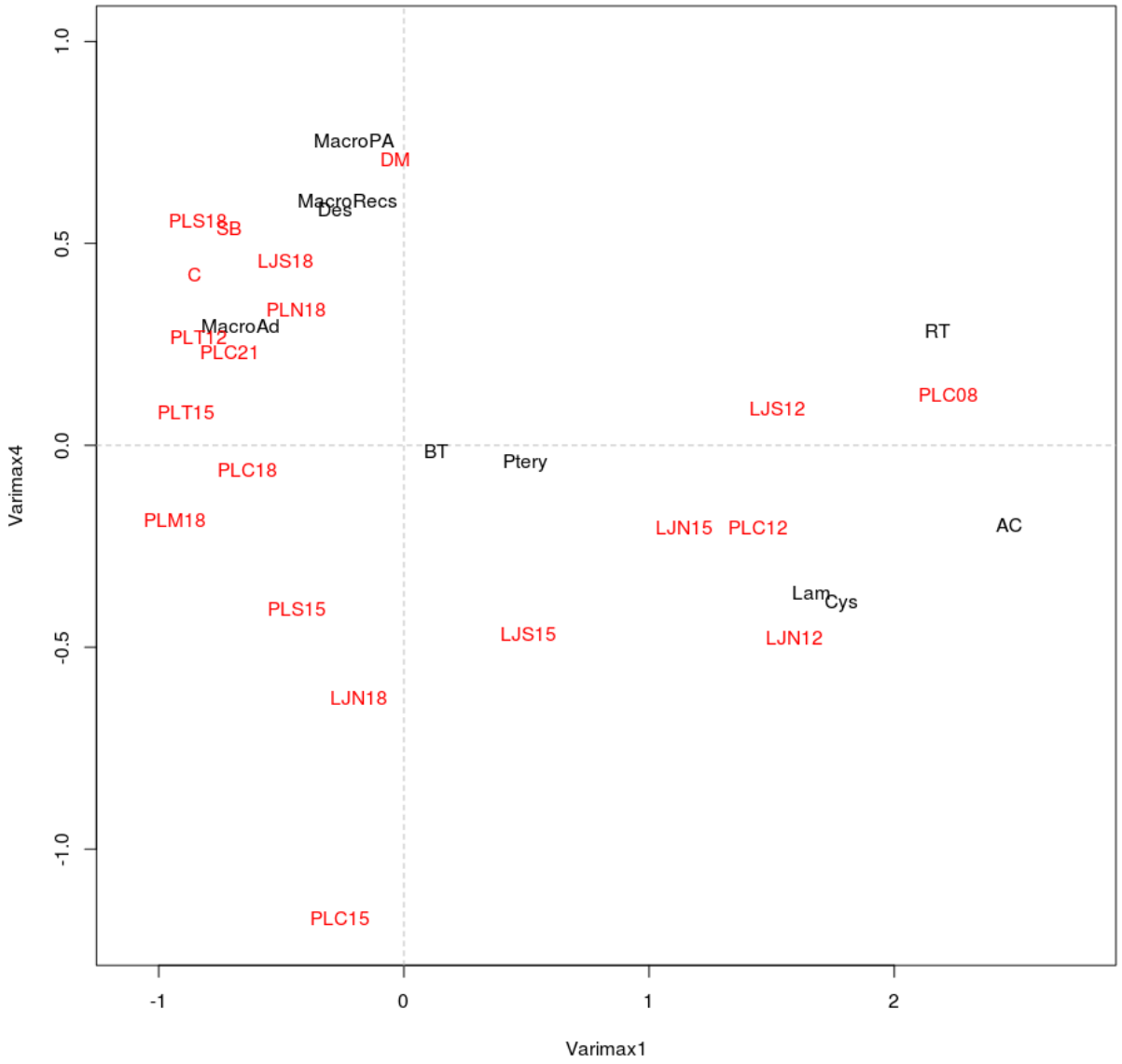

Figure 11. Factor analysis of all algal species/groups data at all of the study sites throughout the Pt. Loma, La Jolla, and North County kelp forests. Black text refers to species/group loadings (Abbreviations defined in Table 1) of Factor 1 ('Varimax 1') which quantifies the continuum from turf species, to understory species, to giant kelp. Factor 4 ('Varimax 4') indicates the occurrence of *Macrocystis* recruitment during the study period. Red text indicates site names. 'C' = Cardiff-by-the-Sea, 'SB'= Solana Beach, 'DM'=Del Mar, LJN (18, 15, and 12)= north La Jolla study sites at 18, 15 and 12 meter depths, 'LJSxx' refer to south La Jolla, 'PLN18' refers to north Pt. Loma 18 meters site, 'PLCxx'=central Pt. Loma sites at 21, 18, 15, 12, and 8 m, 'PLSxx'=south Pt. Loma 15 and 18 m sites, "PLTxx'=PL Tip stations at 12 and 15 m, 'PLM18'=Pt. Loma Mouth (of Bay) site 18 m deep.

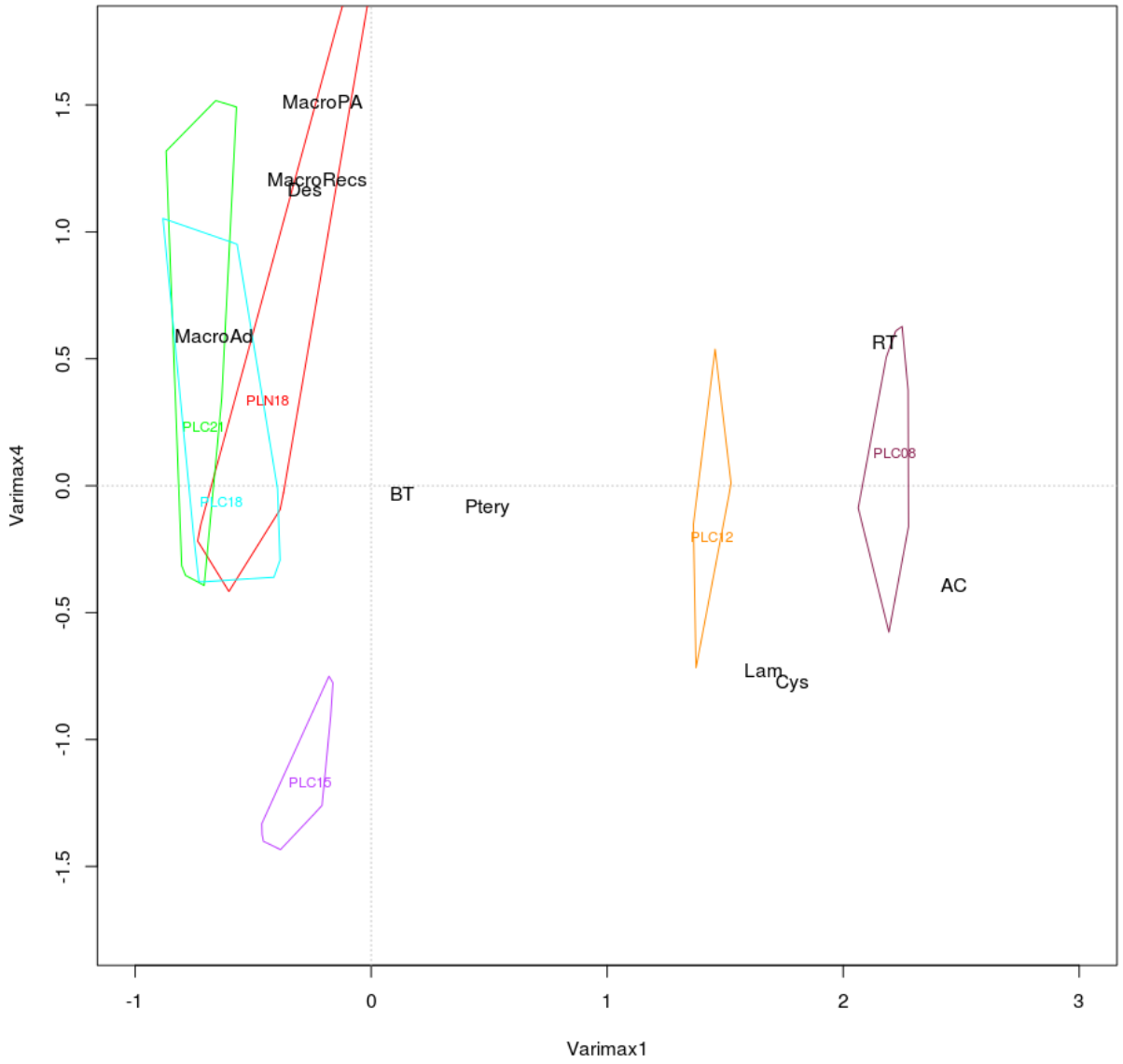

Figure 12. Factor analysis of all algal species at all sites during the study period for the northern and central Pt. Loma Stations. Polygons indicate the range of study site within the 2-dimensional ordination space over the course of the study period. Station names and species are described in the caption for Figure 11.

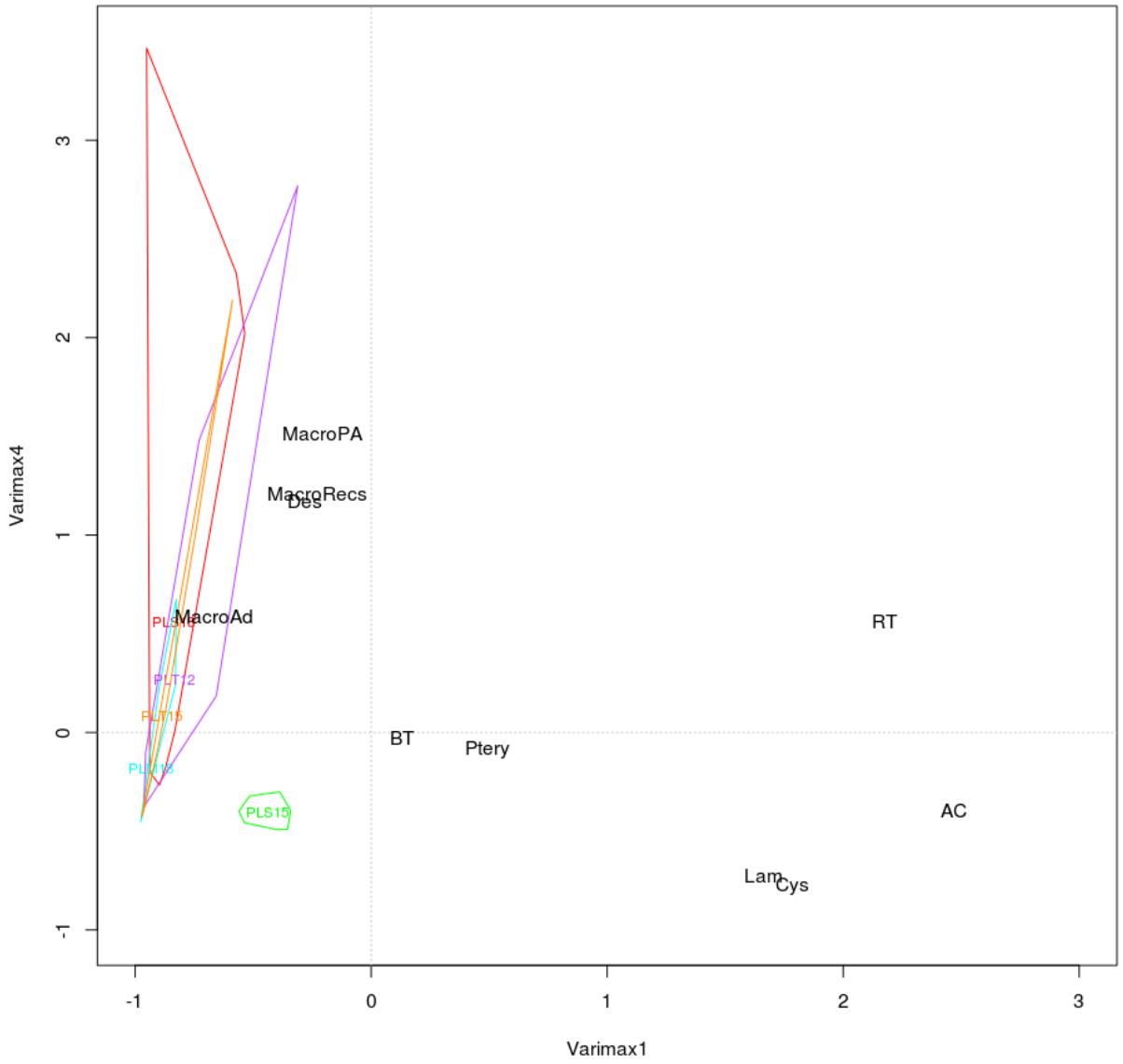

Figure 13. Factor analysis of all algal species at all sites during the study period for the southern Pt. Loma study sites. Polygons indicate the range of study site within the 2-dimensional ordination space over the course of the study period. Station names and species are described in the caption for Figure 11.

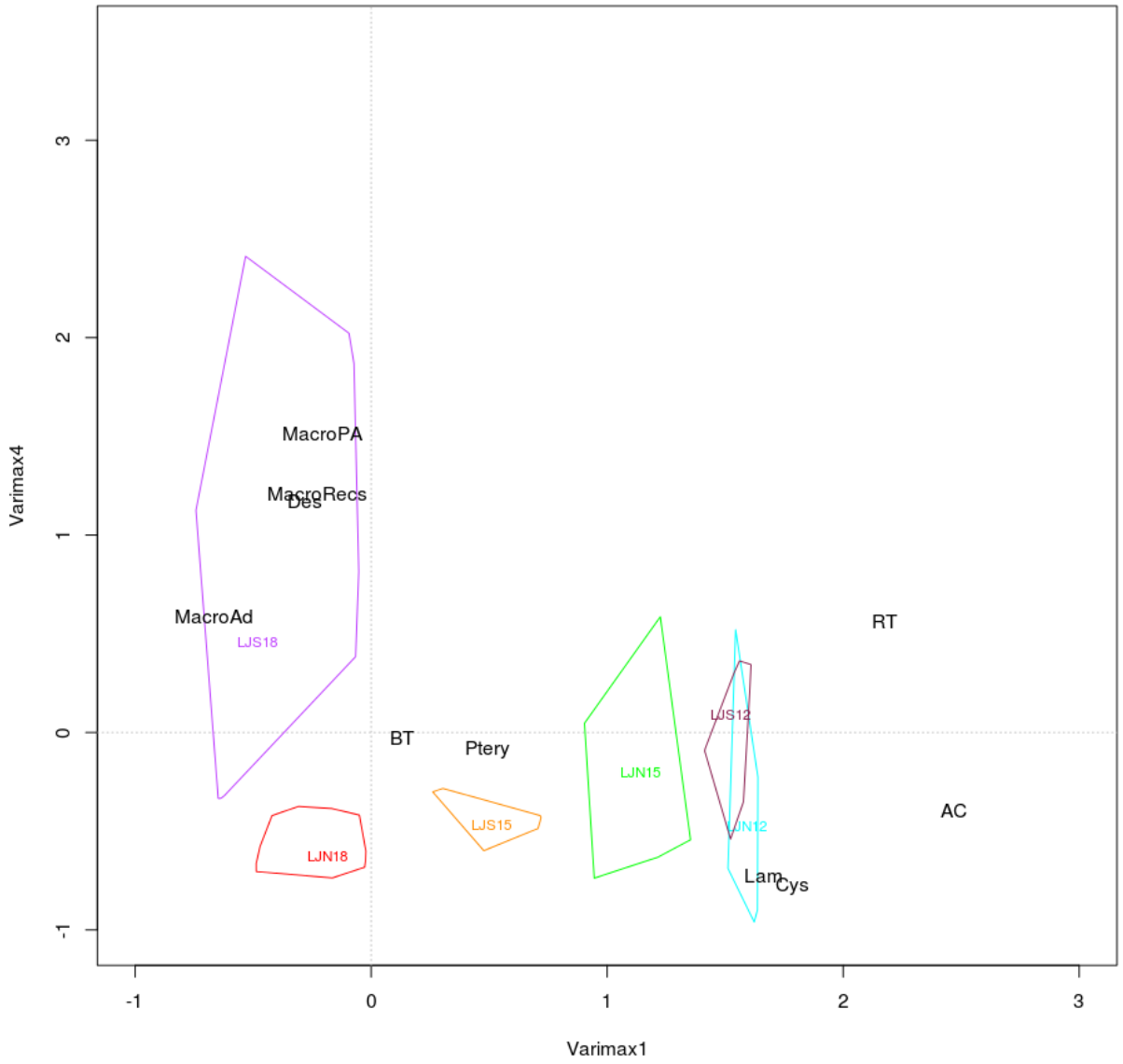

Figure 14. Factor analysis of all algal species at all sites during the study period for the La Jolla kelp forest study sites. Polygons indicate the range of study site within the 2-dimensional ordination space over the course of the study period. Station names and species are described in the caption for Figure 11.

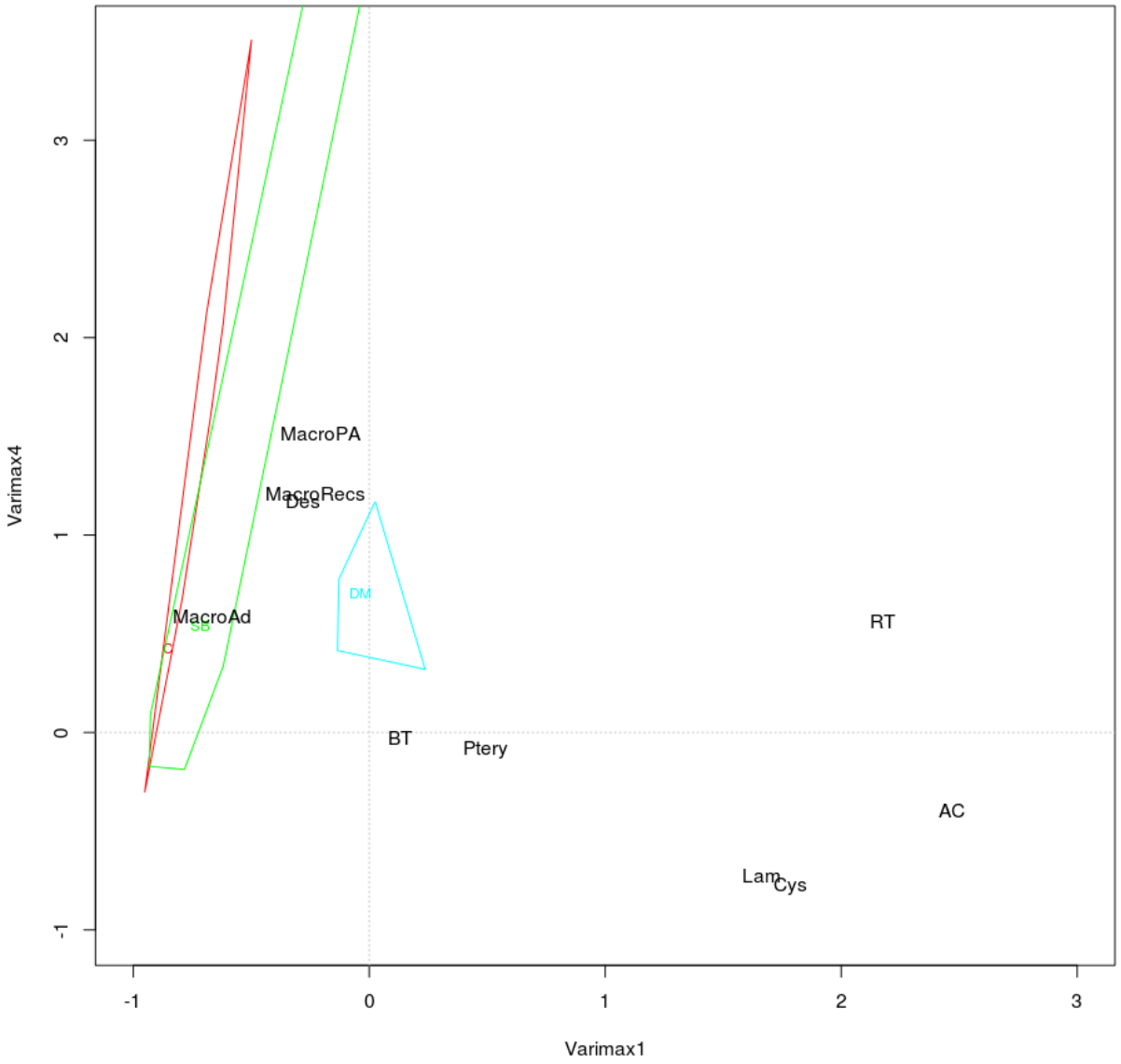

Figure 15. Factor analysis of all algal species at all sites during the study period for the North County study sites. Polygons indicate the range of study site within the 2-dimensional ordination space over the course of the study period. Station names and species are described in the caption for Figure 11.

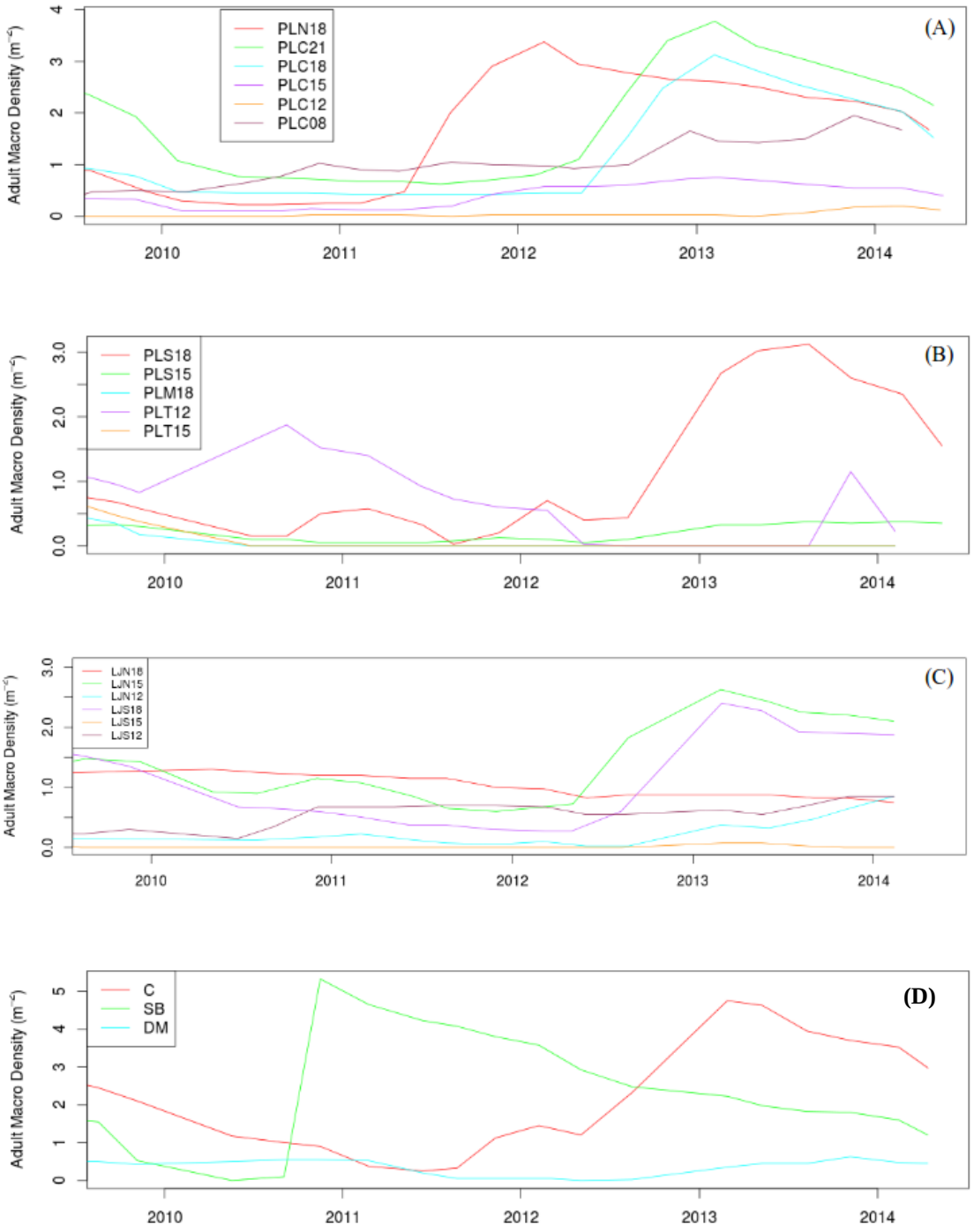

Figure 16. Densities of adult *Macrocystis pyrifera* during the study period at the (A) north and central Pt. Loma, (B) south Pt. Loma, (C) La Jolla, and (D) North County study sites.

Algal canopy guild structure resulting from the acoustic surveys of Pt. Loma and La Jolla are shown in Figures 17 and 18, respectively. The annual canopy forming kelp *Pelagophycus porra* was only mapped for La Jolla as the shelf structure supporting the Pt. Loma kelp forest condensed *M. pyrifera* with *P. porra* to the same areas making acoustic discrimination of the two species difficult in dense mixed stands. These plots demonstrate the mutually exclusive nature of the canopy and understory guilds at spatial scales of hundreds to thousands of meters. The core portions of both forests include the topographic highs at scales of hundreds of meters. If disturbances are extreme, most of both forests recovers as *M. pyrifera*, but with increasing time, understory species gradually outcompete *M. pyrifera* beginning mostly in the topographically low areas and gradually progressing onto the flanks and interior of the topographic highs.

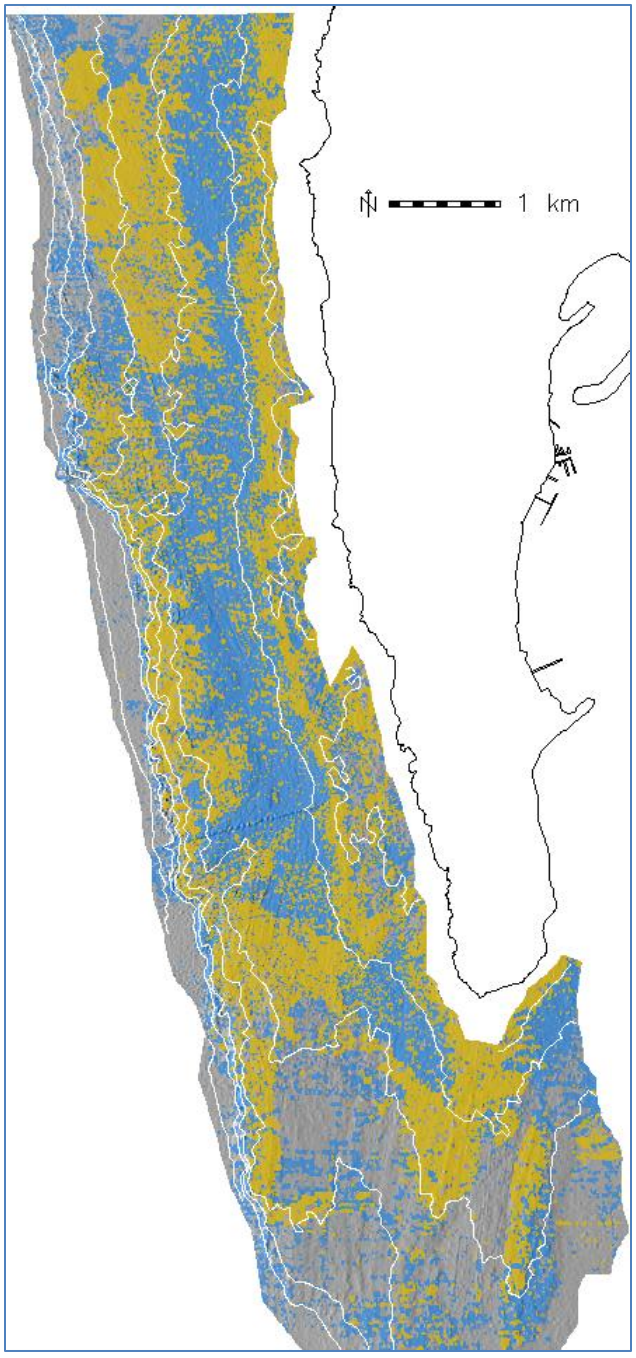

Figure 17. Algal distributions within the Pt. Loma kelp forest: blue=understory kelps (mainly *Pterygophora California, Eisenia arborea, Laminaria farlowii, Agarum fimbriatum, Desmerestia ligulata, and Sargassum muticum*) and surfgrass (*Phyllospadix torreyi*), gold=*Macrocystis pyrifera* (giant kelp). Distributions were determined from sonar surveys conducted in 2012.

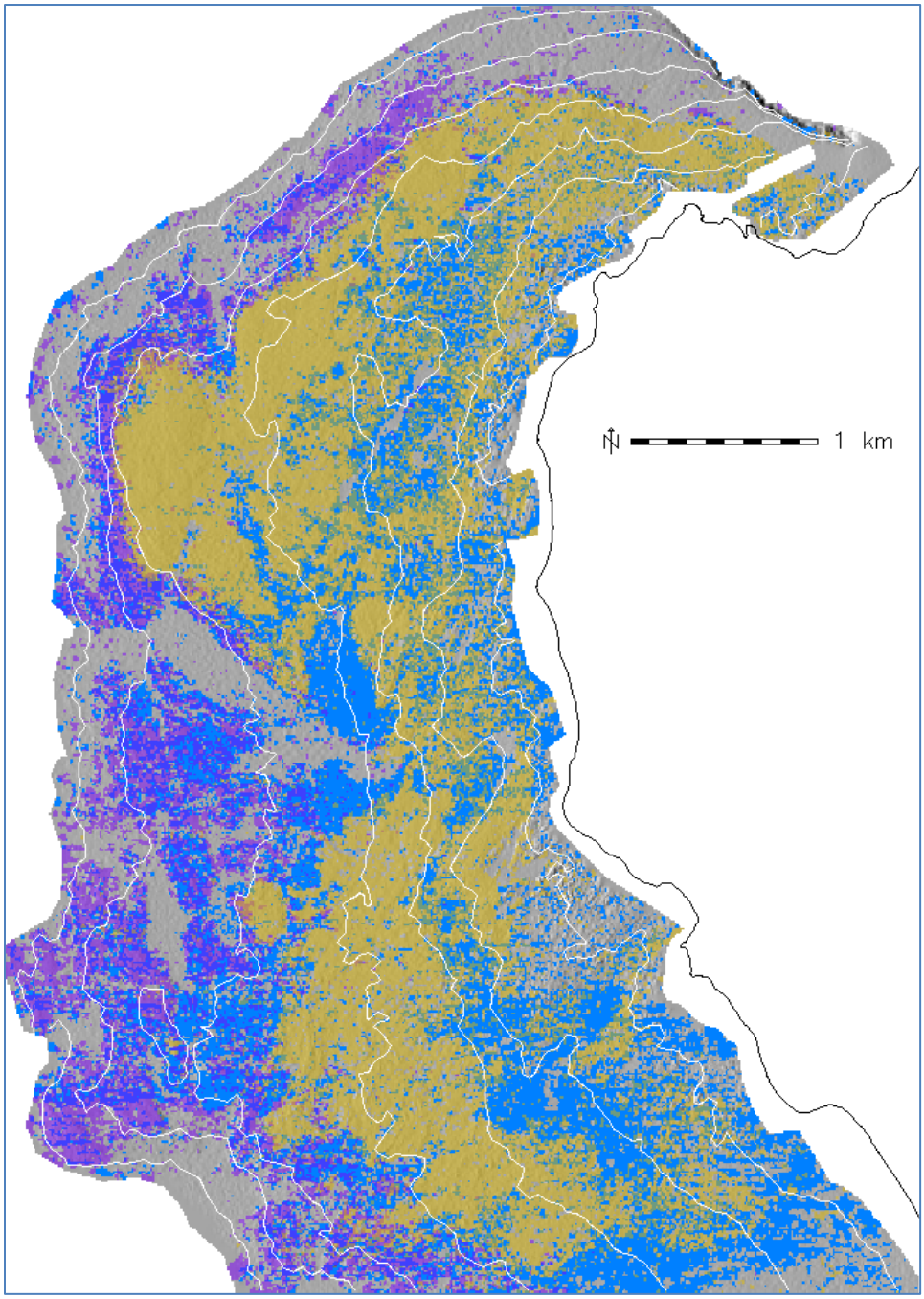

Figure 18. Algal distributions within the La Jolla kelp forest: purple=*Pelagophycus porra*, blue=understory kelps (mainly *Pterygophora California, Eisenia arborea, Laminaria farlowii, Agarum fimbriatum, Desmerestia ligulata, and Sargassum muticum*) and surfgrass (*Phyllospadix torreyi*), gold=*Macrocystis pyrifera* (giant kelp). Distributions were determined from sonar surveys conducted in 2013.

Algal Reproduction and Growth at Central Pt. Loma

As previously mentioned in the 'Methods' section, algal reproductive condition and growth were followed at the central Pt. Loma sites. There were large fluctuations in *M. pyrifera* sporophyll volume at all of these sites during the study period (Fig. 19) with no evidence of seasonality. This is typical for *M. pyrifera* throughout its range. Periods of greater variability were observed when there were very low stipe densities, which increase the light field at depth where the sporophyll bundles are located. Sporophyll volumes were close to zero at the 12 m study site throughout much of the study period but began to increase within the last few months of the study period as the number of giant kelp plants increased at this site due to a recent recruitment event. The continuing low densities of giant kelp at the 12-m site will likely continue since local spore output is so low and the site continues to be dominated by turf algae and understory.

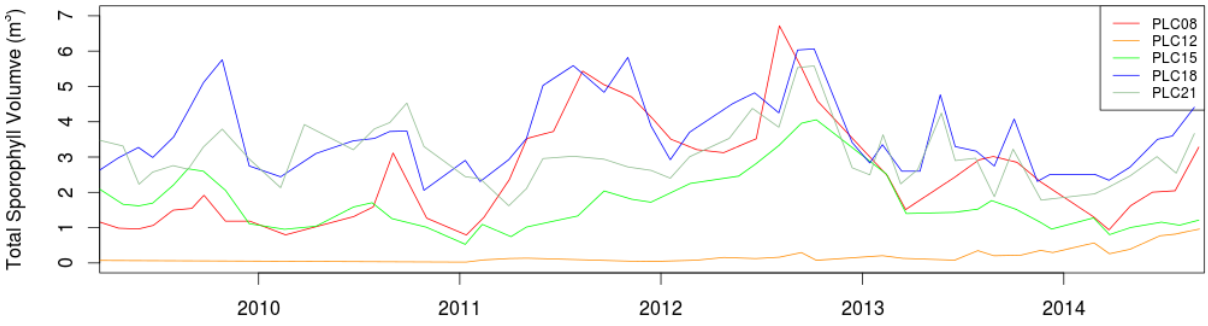

Figure 19. Total *M. pyrifera* sporophyll volume (m^3), measured monthly, at the central Pt. Loma study sites.

Growth and reproduction *of Pterygophora californica* are distinctly seasonal. In southern California, growth typically peaks during summer, with reproductive maxima occurring during the late fall and winter (McPeak 1974, Reed 1990). In our study, the reproduction of

Pterygophora californica continues to be highly seasonal with growth rates greatest during spring and summer (Fig. 20A). Soral condition (Fig. 20B) is completely out of phase with growth with maximal soral condition during fall and winter. The number of sporophyll per plant varies somewhat but relatively little compared to growth and soral condition and exhibits no apparent seasonal pattern (Fig. 20C). Interannual variability is also virtually non-existent. There is however great spatial variability in reproduction and growth among the sites. There have been historically few *P. californica* plants at the deeper sites (21 and 18 m) and when they have been present, these plants exhibit relatively little reproductive output. Presently there are no plants at the 21 m central and very few plants at the 18 m sites. Soral condition and growth are presently the greatest at the 12 m site where there are few giant kelp plants.

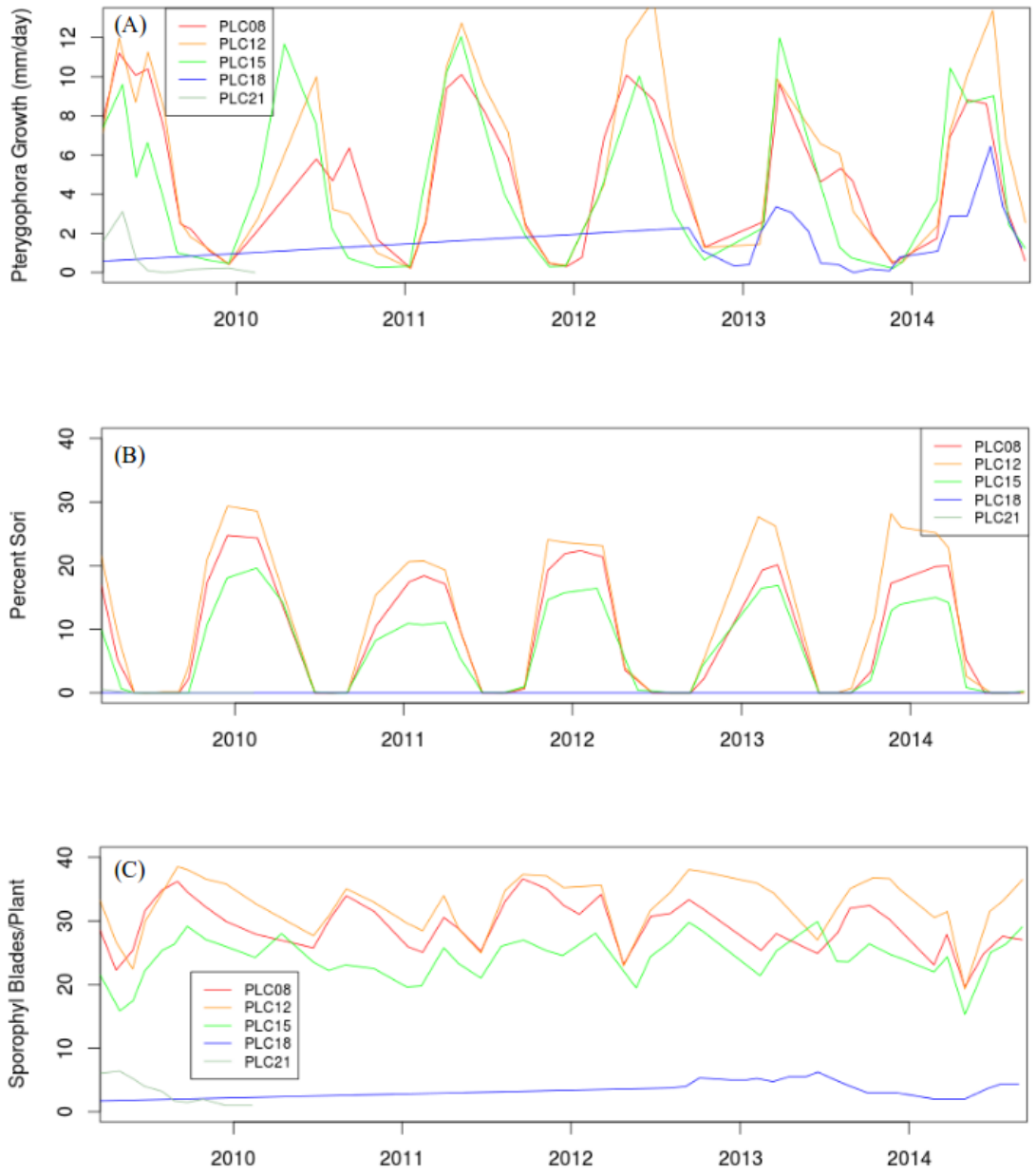

Figure 20. (A) Growth rates, (B) percent soral cover, and (C), mean number of sporophyll blades per plant for the understory kelp *Pterygophora californica* at the central Pt. Loma study sites during the study period.

Laminaria farlowii also exhibits distinct seasonal growth and reproduction that are out of phase with one another. Maximal growth rates occur in spring and summer (Fig. 21A) and maximal reproductive condition occurs in winter and fall (Fig. 21B). The same depth gradient observed for growth and reproduction of *P. californica* is also observed for *L. farlowii*. Both growth and reproduction decrease with depth. There were no apparent interannual fluctuations during the study period, though previous interannual fluctuations have been observed during past El Niño events when both growth and reproduction were greater due to release from light competition with giant kelp which is reduced during warm events. The understory algae are more persistently exposed to adequate nutrient levels during El Niños and therefore suffer less mortality.

Figure 21. (A) Mean growth rates and (B) mean soral percent cover (reproductive tissue) of the understory kelp *Laminaria farlowii* at the central Pt. Loma study sites during the study period (2010-2014).

Invertebrates

Sea Urchins

Red sea urchins, *Strongylocentrotus franciscanus*, support a major commercial fishery off California and both the La Jolla and Pt. Loma kelp forests support the areas with the largest harvest off southern California. During the study period, red sea urchin densities and recruitment varied greatly among sites and over time (Figs. 22 and 23). Most notable, were large increases in red urchin densities at the southernmost sites off Pt. Loma (PL Mouth 18m and PL 15 m) beginning in 2012 where densities were well above historic high densities ever observed at any site since the establishment of the core permanent sites in the early 1980s. Purple sea urchins, *Strongylocentrotus purpuratus*, were also observed near historic high densities at southern Pt. Loma sites (Fig. 24). Red and purple sea urchin densities approached 2 and 10 per square meter respectively at these sites during the study period. Recruitment of both species was also highest at these sites as well as the outermost sites in central and southern Pt. Loma (central Pt. Loma 21 and 18 m, and south Pt. Loma at 18 m – Figs. 23 and 25).

Figure 22. Densities of the red urchin, *Strongylocentrotus franciscanus*, along the permanent band transects at the (A) northern and central Pt. Loma study sites, (B) southern Pt. Loma study sites, (C) La Jolla study sites, and (D) North County study sites.

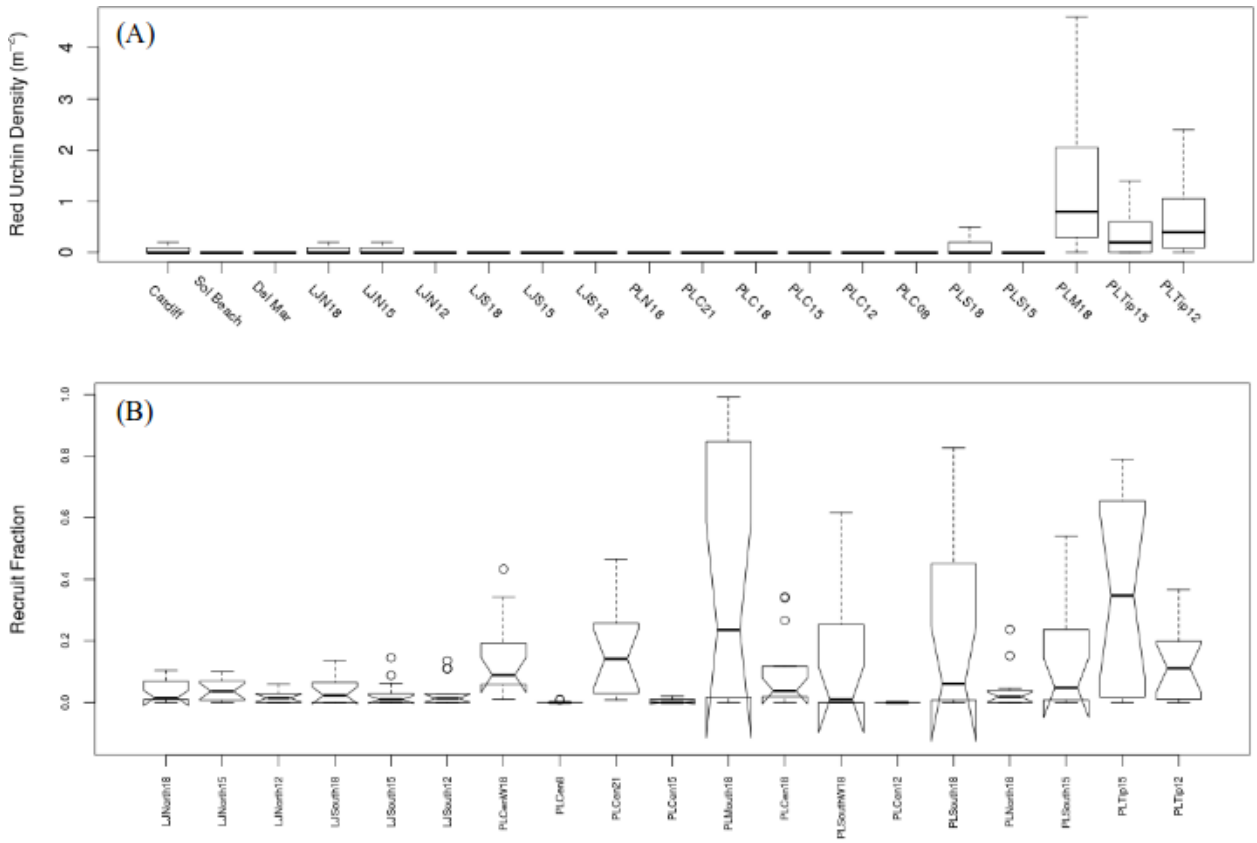

Figure 23. Boxplots of (A) densities and (B) fractional recruitment for the red sea urchin, *Strongylocentrotus franciscanus*, at all of the study sites during the study period (2010-2014). Bold lines indicate medians, boxes indicate the 25th and 75th percentiles, feathers indicate 5th and 95th percentiles.

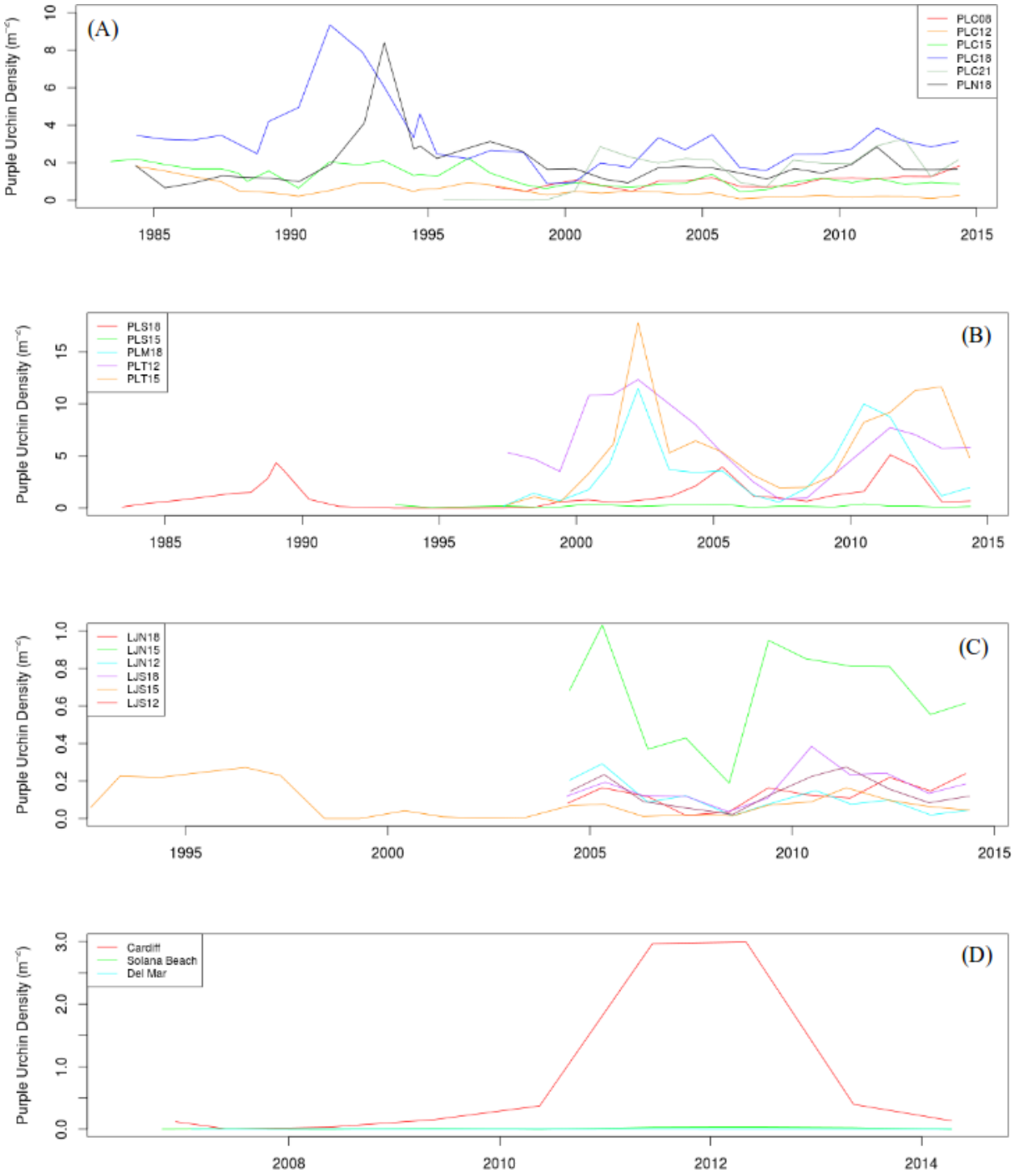

Figure 24. Densities of the purple sea urchin, *Strongylocentrotus purpuratus*, along the permanent band transects at the (A) northern and central Pt. Loma, (B) south Pt. Loma, (C) La Jolla, and (D) North County study sites.

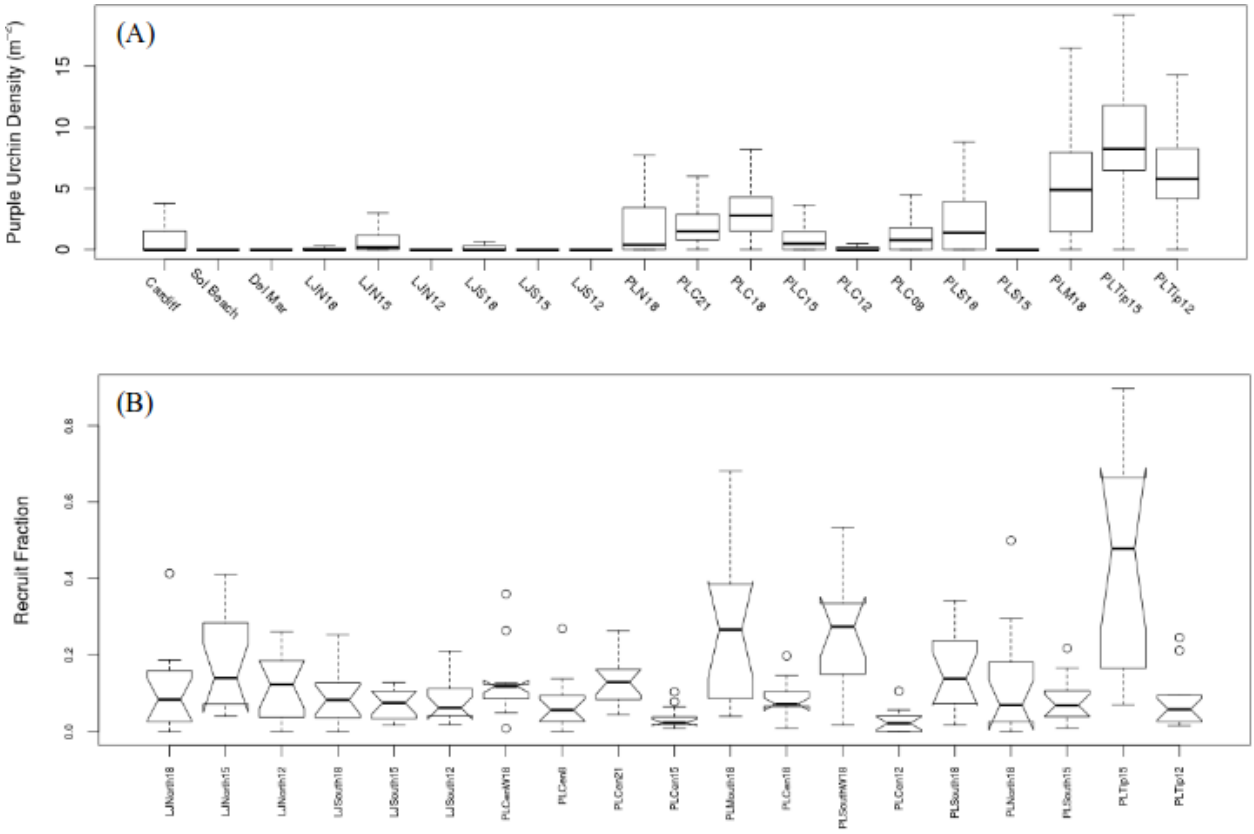

Figure 25. Boxplots of (A) densities and (B) recruit fraction (fraction < 25 mm) for the purple sea urchin, *Strongylocentrotus purpuratus*, at all of the study sites during the study period (2010-2014). Bold lines indicate medians, boxes indicate the 25th and 75th percentiles, feathers indicate 5th and 95th percentiles.

The distribution of the sea urchins barren in southern Pt. Loma covered ~2.16 hectares in 2012 and was centered between major ridge systems (Fig. 26). The edges of the barrens area remained stable during the study period with no major storm or disease perturbations. Densities of both sea urchin species were ~10-100 times greater at the edges of these barrens areas than observed at our study sites. These barrens will likely continue to remain stable without the occurrence of an El Nino, extreme storm or wave event.

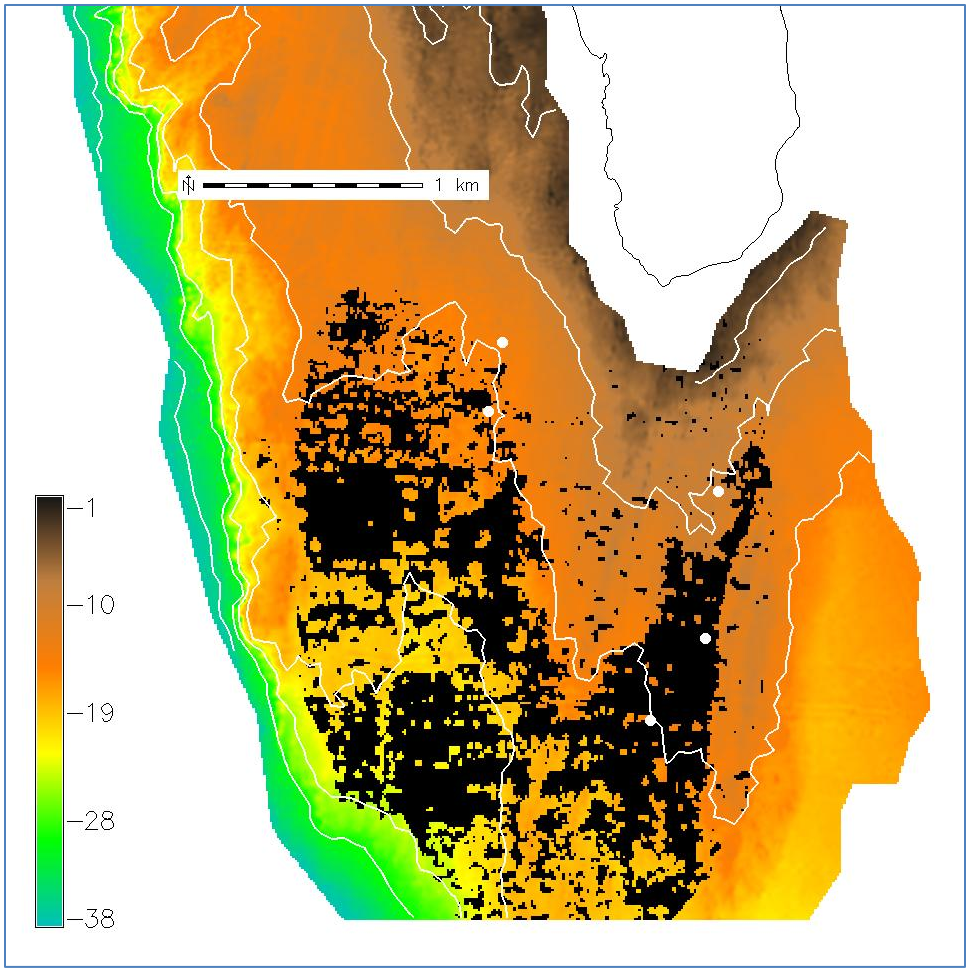

Figure 26. Distribution of persistent sea urchin barrens (black area) in the southern portion of the Pt. Loma forest. The distribution is based on a sonar survey conducted in 2011-2012. Urchin barrens area was ~2.2 hectares when survey was conducted. Southern Pt. Loma study sites are indicated by white circles. Legend indicates depth colors in meters.

Sea Stars

Seastar wasting disease was first observed off Washington state early in 2014. The disease progressed southward eventually appearing off south and central Pt. Loma beginning this spring. The first species affected were in the genus *Pisaster* (*P.giganteus and P. ochraceus*). Later this summer, it became apparent that the bat star, *Asterina miniata,* was exhibiting signs of wasting off central Pt. Loma. Seastars are major benthic predators and the effects of predator release in these areas could extend to sea urchins and pholads which are common prey species for these sea stars. Densities of *Pisaster* spp. crashed to zero or near zero at all of the study sites where they have been previously observed (Fig. 27). However, recruitment of *Pisaster* spp. was observed before, during, and after the adult die off on kelp blades in both Pt. Loma and La Jolla. These species may therefore recover within a couple of years.

Figure 27. Densities of *Pisaster* spp. seastars at the (A) central and northern Pt. Loma, (B) south Pt. Loma, and (C) La Jolla study sites.

Sedimentation at the North County Study Sites

Sediment levels at the North County study sites fluctuated mildly during the study period (Fig. 28). The sediments ranged no greater than ~12 cm at both Cardiff and Del Mar. Percent sand inundation at the Solana Beach site, the site that has historically been subjected to burial, was not observed along the permanent transect lines. Therefore, the North County study sites

have not been significantly affected by sand burial due to natural sediment movements (bedload and gravity wave resuspension) nor by beach replenishment activities.

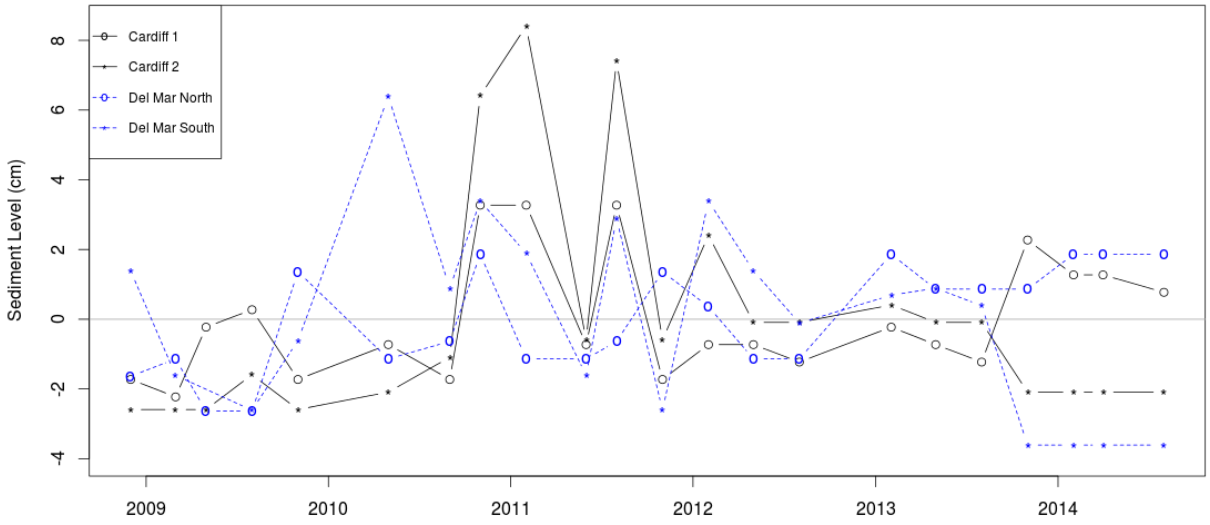

Figure 28. Scaled sediment heights at the Cardiff and Del Mar study sites off North County.

Conclusions

The kelp forests off San Diego during the study period (2010-2014) have been bathed by cooler nutrient rich waters most of the time until late this summer with the onset of what is predicted to be a mild El Niño. Therefore, conditions for giant kelp and understory species have been conducive for kelp growth. Giant kelp (*Macrocystis pyrifera*) canopy and density continues to be moderate at most sites with the exception of the south Pt. Loma study sites which continue to be subjected to repeated cycles of sea urchin recruitment and overgrazing. The reasons for the persistent sea urchin domination at these sites is still not fully understood but turbidity from tidal flows emanating from San Diego Bay and increased larval flux are likely contributing factors. Superimposed on the pattern of continued giant kelp persistence at the remaining study sites has

been a gradual shift from giant kelp canopy to understory and turf algal dominance that is most pronounced at the shallower sites and this pattern appears to be encroaching to deeper depths. Low bottom light levels at these depths >16 m limits understory reproduction and therefore understory dominance will likely slowly progress into the deeper sites unless an extended El Niño occurs. The gradual onset of understory dominance in the shallower halves of the forests results from a lack of large wave and nutrient disturbance which would lead to an understory die-off and thus release giant kelp to recruit and grow. The growth rate of giant kelp allows it to dominate in these systems given adequate levels of physical disturbance. A mild to moderate El Niño is predicted for this fall and winter (2014-2015). The fate of the kelp forests off San Diego depends on how long water temperatures remain above 15˚C and whether powerful winter storm wave events also occur. Powerful storm wave events are common during El Niño periods. The subsequent recruitment of giant kelp within the forests will depend on how much understory and turf is disturbed and the fate of *M. pyrifera* recruits will depend on subsequent nutrient conditions in the spring, summer, and fall of 2015. Overall, there continues to be no evidence that wastewater discharged from either the Pt. Loma or the South Bay ocean outfalls has affected the kelp forests off Pt. Loma, La Jolla, or North County.

References

Dayton, P. K., V. G. Currie, T, et al. (1984). "Patch Dynamics and Stability of Some California Kelp Communities." Ecological Monographs 54(3): 253-289.

DeWreede, R. E. (1984). "Growth and age class distribution of Pterygophora *californica* (Phaeophyta)." Marine Ecology Progress Series 19: 93-100.

McPeak, R. H. (1974). Fruiting in several species of Laminariales from southern California. Eighth International Seaweed Symposium, Bangor, North Wales, The Marine Science Laboratories, Menai Bridge.

Parnell, P. E., E. F. Miller, C. E. Lennert-Cody, P. K. Dayton, M. L. Carter, and Timothy D. Stebbins. (2010). "The Response of Giant Kelp (*Macrocystis pyrifera*) in Southern California to Low-Frequency Climate Forcing." Limnology and Oceanography 55 (6): 2686–2702.

Reed, D. C. (1987). "Factors affecting the production of sporophylls in the giant kelp *Macrocystis pyrifera.*" Journal of Experimental Marine Biology and Ecology 113: 61-69.

Reed, D. C. (1990). "The effects of variable settlement and early competition on patterns of kelp recruitment." Ecology 71(2): 776-787.

Appendix H
COASTAL REMOTE SENSING ANNUAL REPORTS

Renewal of NPDES CA0107409

APPENDIX H

COASTAL REMOTE SENSING ANNUAL REPORTS

January 2015

APPENDIX H

Coastal Remote Sensing Annual Reports

Table of Contents

APPENDIX H.1 – 2009 Ocean Imaging Report

Svejkovsky, J. 2010. Satellite and Aerial Coastal Water Quality Monitoring in the San Diego/Tijuana Region. Annual Summary Report, 1 January 2009 – 31 December 2009. Ocean Imaging, Solana Beach, CA. (30 April 2010)

APPENDIX H.2 – 2010 Ocean Imaging Report

Svejkovsky, J. 2011. Satellite and Aerial Coastal Water Quality Monitoring in the San Diego/Tijuana Region. Annual Summary Report, 1 January 2010 – 31 December 2010. Ocean Imaging, Solana Beach, CA. (30 April 2011)

APPENDIX H.3 – 2011 Ocean Imaging Report

Svejkovsky, J. 2012. Satellite and Aerial Coastal Water Quality Monitoring in the San Diego/Tijuana Region. Annual Summary Report, 1 January 2011 – 31 December 2011. Ocean Imaging, Solana Beach, CA. (30 April 2012)

APPENDIX H.4 – 2012 Ocean Imaging Report

Svejkovsky, J. 2013. Satellite and Aerial Coastal Water Quality Monitoring in the San Diego/Tijuana Region. Annual Summary Report, 1 January 2012 – 31 December 2012. Ocean Imaging, Solana Beach, CA. (13 February 2013)

APPENDIX H.5 – 2013 Ocean Imaging Report

Svejkovsky, J. 2014. Satellite and Aerial Coastal Water Quality Monitoring in the San Diego/Tijuana Region. Annual Summary Report, 1 January 2013 – 31 December 2013. Ocean Imaging, Solana Beach, CA. (April 30, 2014)

Appendix H.1

2009 Ocean Imaging Report

Satellite & Aerial Coastal Water Quality Monitoring in The San Diego / Tijuana Region

By Jan Svejkovsky

Annual Summary Report
1 January, 2009 - 31 December, 2009

This draft to become final in sixty days.

17 March, 2010

Ocean Imaging

201 Lomas Santa Fe Drive, suite 370, Solana Beach, CA 92075 Phone: 858-792-8529 Fax: 858-792-8761 www.oceani.com

Table of Contents

1.0 Introduction & Project History 1

2.0 Technology Overview 1

2.1 Imaging in the UV-Visible-Near InfraRed Spectrum 1
2.2 Imaging in the Infrared spectrum 2
2.3 Data Dissemination and Analysis 2

3.0 The Southbay Ocean Outfall Region 2

3.1 Highlights of 2009 Monitoring 2
3.2 Historical Analysis of Outfall Plume Dispersal Patterns 7

4.0 The Point Loma Outfall Region 19

4.1 Highlights of 2009 Monitoring 19

Appendix 27

1. Introduction and Project History

Ocean Imaging Corporation (OI) specializes in marine and coastal remote sensing for research and operational applications. In the 1990s, OI received multiple research grants from NASA's Commercial Remote Sensing Program for the development and commercialization of novel remote sensing applications in the coastal zone. As part of these projects, OI developed methods to utilize various types of remotely sensed data for the detection and monitoring of stormwater runoff and wastewater discharges from offshore outfalls. The methodology was initially demonstrated with collaboration of the Orange County Sanitation District. The NASA-supported research and demonstration led to a proof-of-concept demo project in the San Diego region co-funded by the EPA in 2000. Those results led, in turn, to adding an operational remote imaging-based monitoring component to the San Diego region's established water quality monitoring program, as stipulated in discharge permits for the International Wastewater Treatment Plant and Pt. Loma outfalls. The project was spearheaded by the State Water Resources Control Board (SWRCB), EPA Region 9, and continues to be jointly funded by the International Boundary Waters Commission and the City of San Diego.

The first phase of the project was a historical study utilizing various types of satellite data acquired between the early 1980s and 2002. The study established, among other findings, the prevailing near-surface current patterns in the region under various oceanic and atmospheric conditions. The current directions were deduced from patterns of turbidity, ocean temperature and surfactant slicks. In some cases, near-surface current velocity could be computed by tracking recognizable color or thermal features in time-sequential images. The historical study thus established a baseline data base for the region's current patterns, their persistence and occurrence frequency, and the historical locations, size and dispersion trajectories of various land and offshore discharge sources (e.g. the offshore outfalls, Tijuana River, Punta Bandera Treatment Plant discharge in Mexico, etc.).

In October, 2002 the operational monitoring phase of the project was initiated. This work utilizes 500m resolution Moderate Resolution Imaging Spectroradiometer (MODIS) color imagery (available near-daily), and 27m & 60m Thematic Mapper TM5 & TM7 color and thermal imagery (available 4 times per month). In addition, the project relies heavily on acquisition of multispectral color imagery with OI's DMSC-MKII aerial sensor and thermal infrared (IR) imagery from a Jenoptik thermal imager integrated into the system (see details in the "Technology Overview" section). These aerial image sets are most often collected at 2m resolution. The flights are done on a semi-regular schedule ranging from 1-2 times per month during the summer to once or more per week during the rainy season. The flights are also coordinated with the City of San Diego's regular offshore field sampling schedule so that the imagery is collected on the same day (usually within 2-3 hours) of the field data collection. Additional flights are done on an on-call basis immediately after major storms or other events such as sewage spills.

This report summarizes observations made during the period 1/1/2009 – 12/31/2009.

2. Technology Overview

OI uses several remote sensing technologies to monitor San Diego's offshore outfalls and shoreline water quality. Their main principle is to reveal light, heat or microwave signal patterns that are characteristic of the different discharges. Most often this is due to specific substances contained in the effluent but absent in the surrounding water.

2.1 Imaging in the UV-Visible-Near Infrared Spectrum

This is the most common technique used with satellite images and the DMSC aerial sensor. Wavelengths (colors) within the range of the human eye are most often used but Ultraviolet (UV) wavelengths are useful for detecting fluorescence from petroleum compounds (oil, diesel, etc.) and near-IR wavelengths can be useful for correcting atmospheric interference from aerosols (e.g. smog and smoke).

The best detection capabilities are attained when several images in different wavelengths are acquired simultaneously. These "multispectral" data can be digitally processed to enhance features not readily visible in simple color photographs. For example, two such images can be ratioed, thus emphasizing the water features' differences in reflection of the two wavelengths. A multi-wavelength image set can also be analyzed with "multispectral classification algorithms" which separate different features or effluents based on the correlation relationships between the different color signals.

The depth to which the color sensors can penetrate depends on which wavelengths they see, their sensitivity and the general water clarity. In the San Diego region, green wavelengths tend to reach the deepest and, as elsewhere, UV and near-IR wavelengths penetrate the least. Generally, OI's satellite and aerial sensor data reveal patterns in the upper 15-40 feet.

The color channels on satellite sensors cannot be changed, so they tend to be relatively broad, separating red, green, near-IR, and sometimes blue parts of the spec-

trum. OI's DMSC aerial 4-channel sensor has the added advantage of allowing each channel wavelength to be precisely customized. Through experimentation, OI has determined the exact wavelength relationships that maximize the detection of the offshore sewage outfall plumes and nearshore discharges such as the Tijuana River. With this channel configuration it is possible to monitor the plumes even when they are not visible to the naked eye.

2.2 Imaging in the Infrared Spectrum

Some satellite and aerial sensors image heat emanating from the ground and the ocean. They thus reveal patterns and features due to their differences in temperature. Since infrared wavelengths are strongly absorbed by water, the images reveal temperature patterns only on the water's surface. Such images can help detect runoff plumes when their temperatures differ from the surrounding ocean water. Runoff from shoreline sources tends to be warmer than the ocean water, although the reverse can be true during the winter. Plumes from offshore outfalls can sometime also be detected with thermal imaging. Since the effluent contains mostly fresh water, it is less dense than the surrounding salt water and tends to rise to the surface. If it makes it all the way, it is usually cooler than the surrounding sun-warmed surface water. If it is constrained by a strong thermocline and/or pycnocline ("vertical stratification"), it sometimes tends to displace some of the water above it in a doming effect. This displacement pattern is revealed in the thermal surface imagery.

2.3 Data Dissemination and Analysis

The satellite and aerial imaging data are made available to the funding agencies, the San Diego County Department of Health and the EPA through a dedicated, password-protected web site. Although it is possible to process most of the used data in near-real-time, earlier in the project the funding agencies decided that the emphasis of this project is not on providing real-time monitoring support and the extra costs associated with the rapid data turn-around are not warranted. Most satellite data is thus processed and posted within 1-2 days after acquisition and the aerial sensor imagery (which requires the most labor-intensive processing), within 2-5 days. OI has, however, in a number of cases, made some imagery available to the CDH and others in near-real time when observations were made that appeared to be highly significant for the management of beach closures or other sudden events.

3. The South Bay Ocean Outfall Region

3.1 Highlights of 2009 Monitoring

The South Bay Ocean Outfall (SBOO) wastewater plume generally remains well below the surface between approximately late March and November due to vertical stratification of the water column. During that period it usually cannot be detected with multispectral aerial and satellite imagery which penetrate the upper 7 to 15 meters (depending on water clarity). The plume also cannot be detected with thermal IR imaging which does not penetrate below the surface. Seasonal breakdown of the vertical stratification results in the plume's rise closer to the surface or to actually reach the surface between approximately late November and late March, when it can often be detected with aerial and satellite imaging. In 2009 the SBOO plume was visible throughout January and into 3/16/09. The plume was detected again on a 11/3/09 DMSC flight and remained traceable through the rest of the year.

Figure 1 shows vertical profiles at sampling station I14 (we chose to showcase this location because while it is close to the active wastewater release sites along the SBOO wye, it is usually not affected by the plume itself). The vertical profile characteristics correspond closely to the near-surface plume signature trends in our imagery: The January and February density profiles show an unstratified water column (corresponding to persistent plume detection in the imagery), with a pycnocline once again developing in the 4/8/09 profile. The vertical stratification began to decrease from October through November and the water column was again completely destratified by early December, corresponding to the plume's initial near-surface detection in early November and its persistent observation through December.

As in previous years, during the rain season months the coastal region in the vicinity of the SBOO is subject to rain runoff from the Tijuana River, which is characterized by turbid waters that often exhibit high indicator bacteria counts (see Appendix for more details). In some cases, the runoff plume is large enough in the offshore direction to overtake the area over the SBOO wye. Rain events during 2009 were dominated by multiple significant rainstorms from late January through February, 2009, and by another rain episode that occurred from the last few days of November into the first week of December, 2009. **Figure 2** shows the rain patterns as recorded at the National Estuary Research Reserve System's (NERRS) rain gauge located in the Tijuana Estuary, and discharge flow of the San Diego River to the north (no data were available for the Tijuana River).

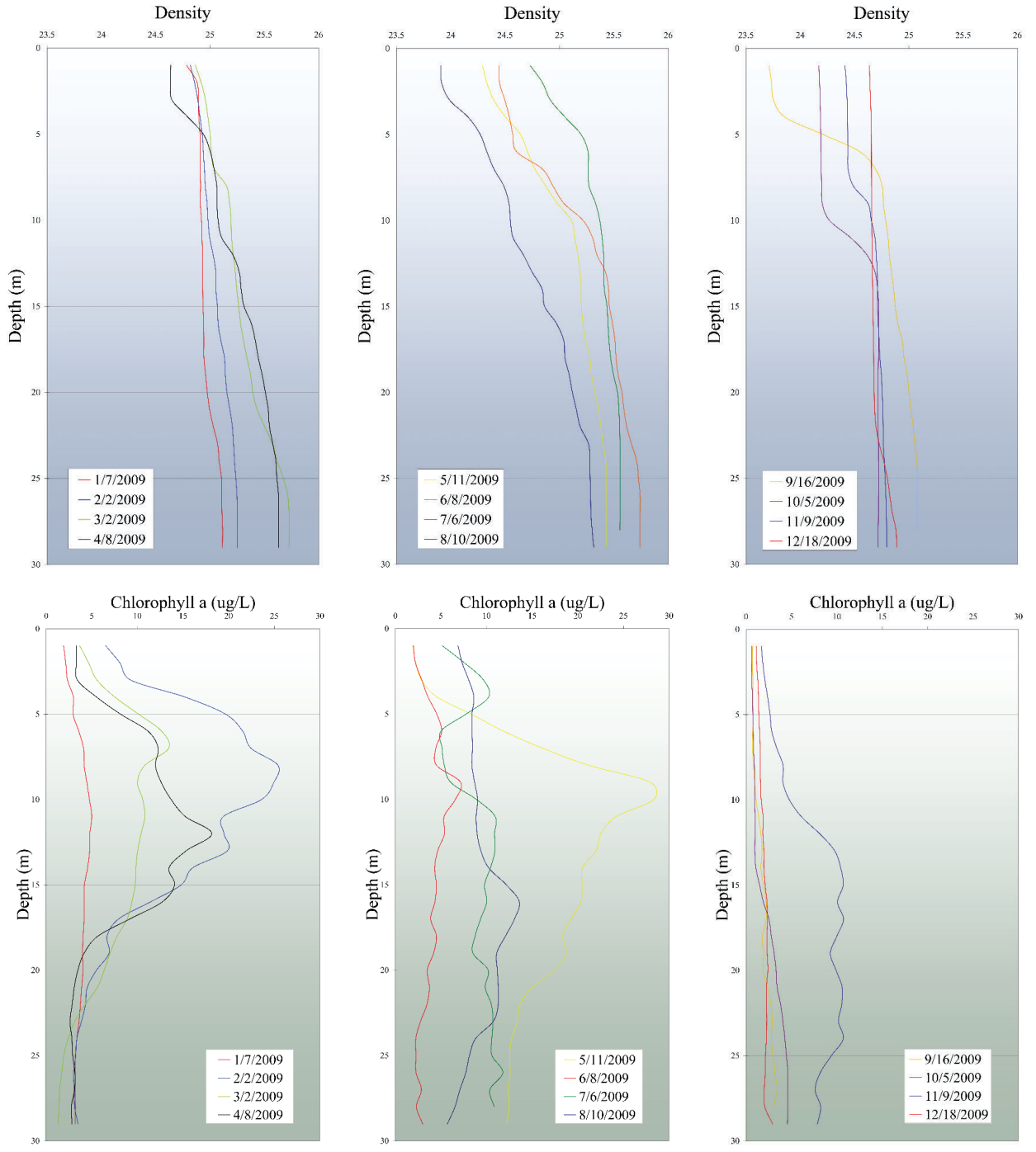

Figure 1.

Vertical profiles of Density (top) and Chlorophyll (bottom) at offshore station I-14 obtained during San Diego Metropolitan Wastewater Department's monthly offshore sampling program during 2009. The density profiles show lack of vertical stratification in the winter months, a rebuilding of a pycnocline in March and April and its gradual disappearance from October through November. Strong subsurface chlorophyll maxima existed during the spring months of 2009.

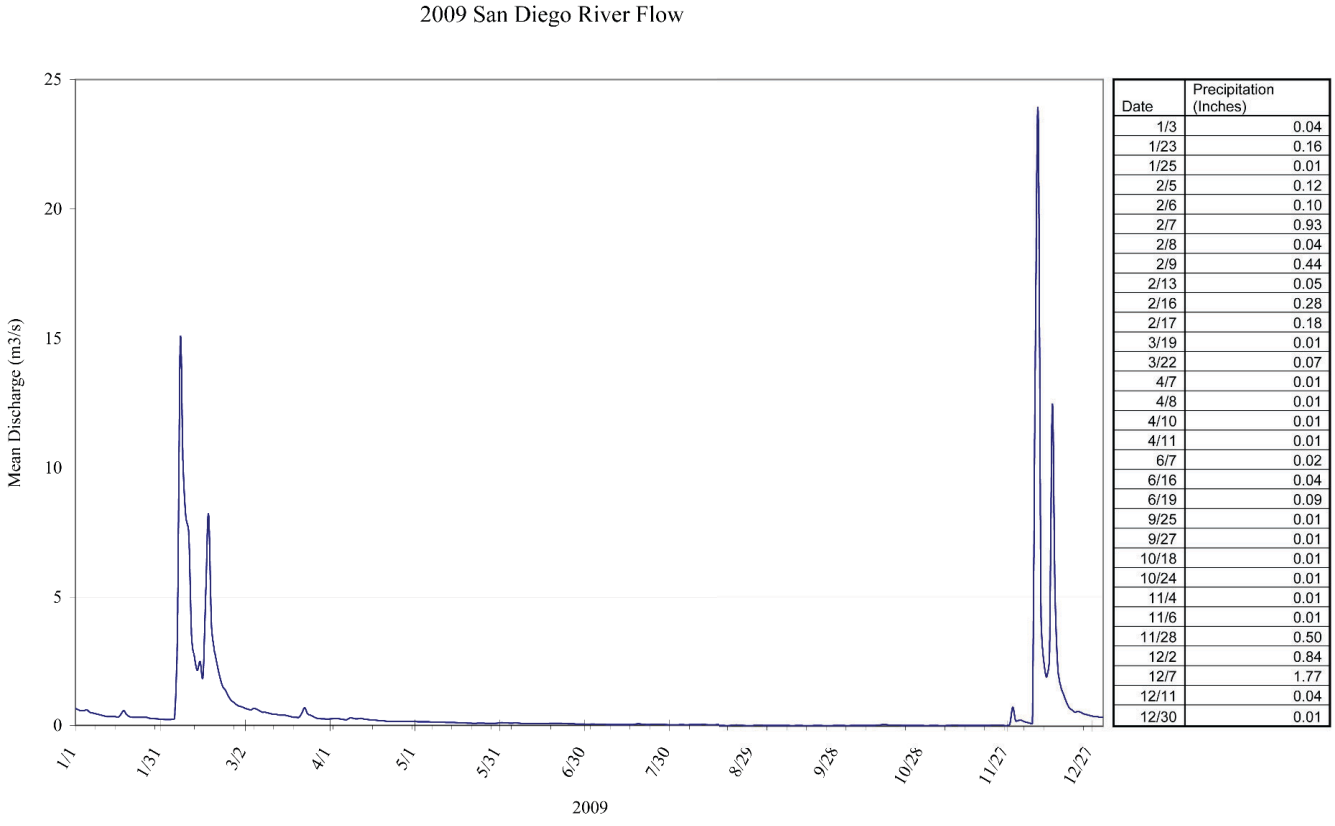

Date	Precipitation (Inches)
1/3	0.04
1/23	0.16
1/25	0.01
2/5	0.12
2/6	0.10
2/7	0.93
2/8	0.04
2/9	0.44
2/13	0.05
2/16	0.28
2/17	0.18
3/19	0.01
3/22	0.07
4/7	0.01
4/8	0.01
4/10	0.01
4/11	0.01
6/7	0.02
6/16	0.04
6/19	0.09
9/25	0.01
9/27	0.01
10/18	0.01
10/24	0.01
11/4	0.01
11/6	0.01
11/28	0.50
12/2	0.84
12/7	1.77
12/11	0.04
12/30	0.01

FIGURE 2.

GRAPH OF MEAN DAILY DISCHARGE OF THE SAN DIEGO RIVER DURING 2009 (MEASURED AT FASHION VALLEY). THE TABLE ON RIGHT SHOWS DAILY RAINFALL TOTALS AT THE NATIONAL ESTUARY RESEARCH RESERVE SYSTEM'S GAUGE LOCATED IN THE TIJUANA ESTUARY.

The rain events in January, 2009 caused polluted river discharge to enter the nearshore waters around the River mouth, resulting in beach closures. The offshore extent of the plume was not large enough to reach the outfall wye, however. Additional rainfall in early February extended the River plume size in all directions and, as was recorded by aerial imagery on 2/10/09 (**Figure 3**), the River runoff expanded over the area of the SBOO wye. The effects can also be seen in satellite TM imagery (which also shows the outfall plume signature) and coarser resolution MODIS imagery (**Figure 4**).

We believe the turbid, freshwater runoff surface layer tends to be rather thin – 1-2 meters. This is supported by several observations, including the common lack of expected low salinity and suspended sediment values in the City's vertical sampling data (which begin at 1 meter depth), and observations of the displacement of the turbid layer by small boat engines traveling through the area. The outfall plume also displaces the turbid layer when it has spread over the area. In that case, the plume signature appears dark in multispectral imagery relative to the more reflective, sediment-laden surrounding waters (**see Figures 3 and 4**). If the plume signature is detectable in thermal IR imagery, the outfall effluent waters have fully reached the surface (since the thermal signal originates in the very surface layer) – as was the case on 2/10/09.

A DMSC aerial survey on 3/16/09 (**Figure 5**) revealed a relatively small plume signature over the main riser group. The thermal IR image revealed no plume signature, suggesting that the plume waters were no longer reaching the actual ocean surface.

The South Bay region was subject to relatively strong and frequent plankton blooms during the 2009 spring and early summer months. Vertical chlorophyll concentration profiles at offshore sampling station I-14 (**Figure 1**) show low chlorophyll values in the January cast but a marked subsurface chlorophyll maximum is recorded in the Febru-

ary cast. Elevated subsurface values also existed in the March and April data sets, and another large subsurface maximum existed in early May. **Figures 6 and 7** exemplify these conditions with aerial DMSC and satellite MODIS imagery. The initial blooms in February corresponded to the rain periods and the spread of the Tijuana River plume offshoreward, covering the outfall wye and including sampling station I-14.

Southward flow patterns dominated the region in the summer months. A feature commonly revealed in the imagery was a current frontal zone seemingly related to the effects of Pt. Loma on the southward flow field. The front was characterized by internal waves, the appearance of cooler, upwelled water south of Pt. Loma and changes in water color/turbidity characteristics. The front tended to pass 500 – 1000 meters west of the SBOO wye, as can be seen in satellite TM imagery from 7/22/09 (**Figure 8**).

Unlike during some previous years, the South Bay region was not subject to major red tide events during 2009. The few, transient events that did occur were quite weak. **Figure 9** shows one such weak event from 15-16 September, occurring in waters within 2 km of the shoreline south of the Tijuana River mouth.

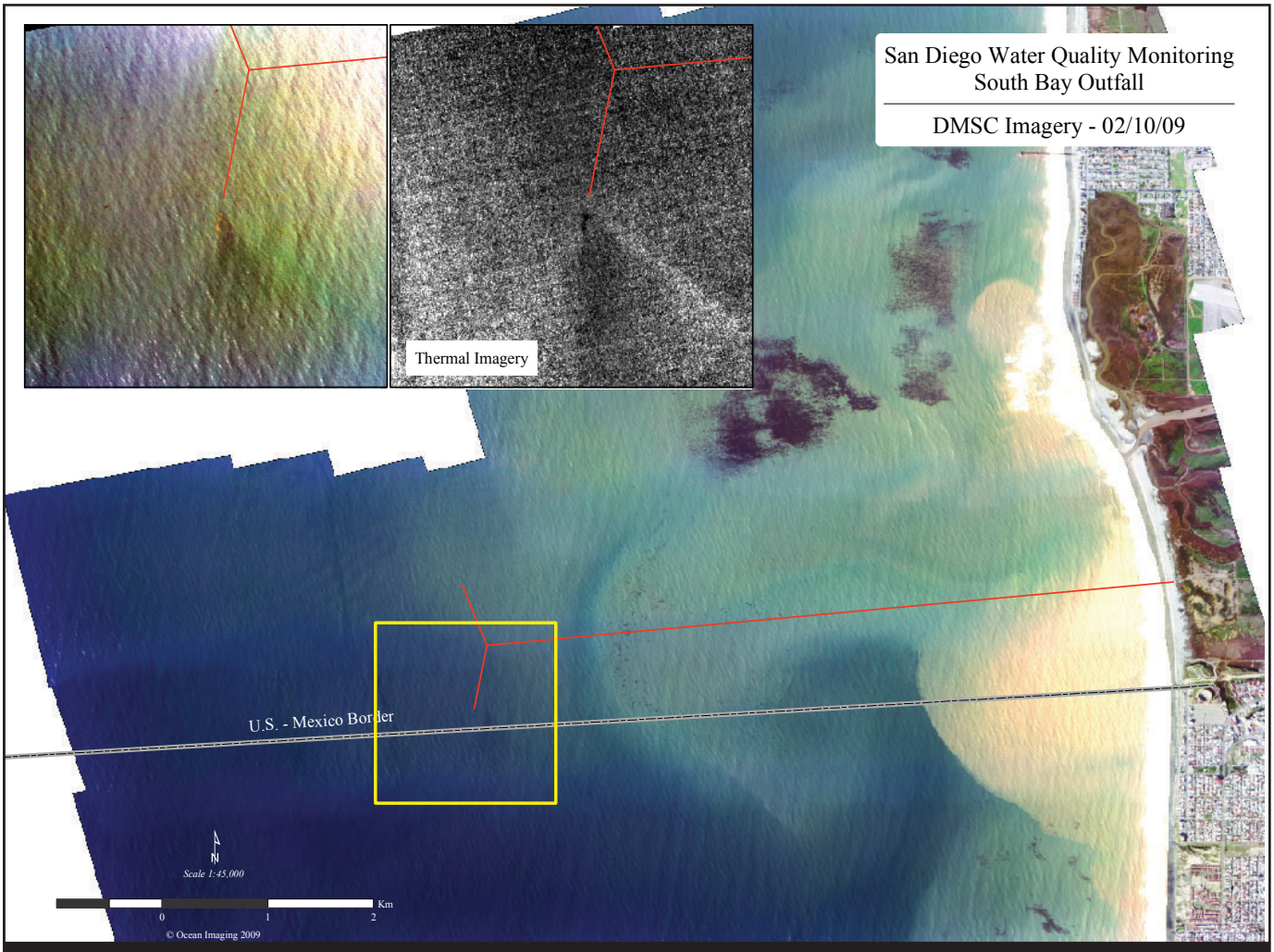

Figure 3.

DMSC aerial imagery of the Tijuana River mouth and South Bay Ocean Outfall region, acquired on 2/10/09. Several significant rain storms preceded this date in February, causing the Tijuana River to discharge large quantities of suspended sediment-laden fresh water runoff (yellow and green). By 2/10/09 it had overtaken the SBOO wye area. The inset images show the outfall plume manifestations in multispectral visible and thermal imagery (cooler water is darker). The dark brown areas in the large color image are kelp beds.

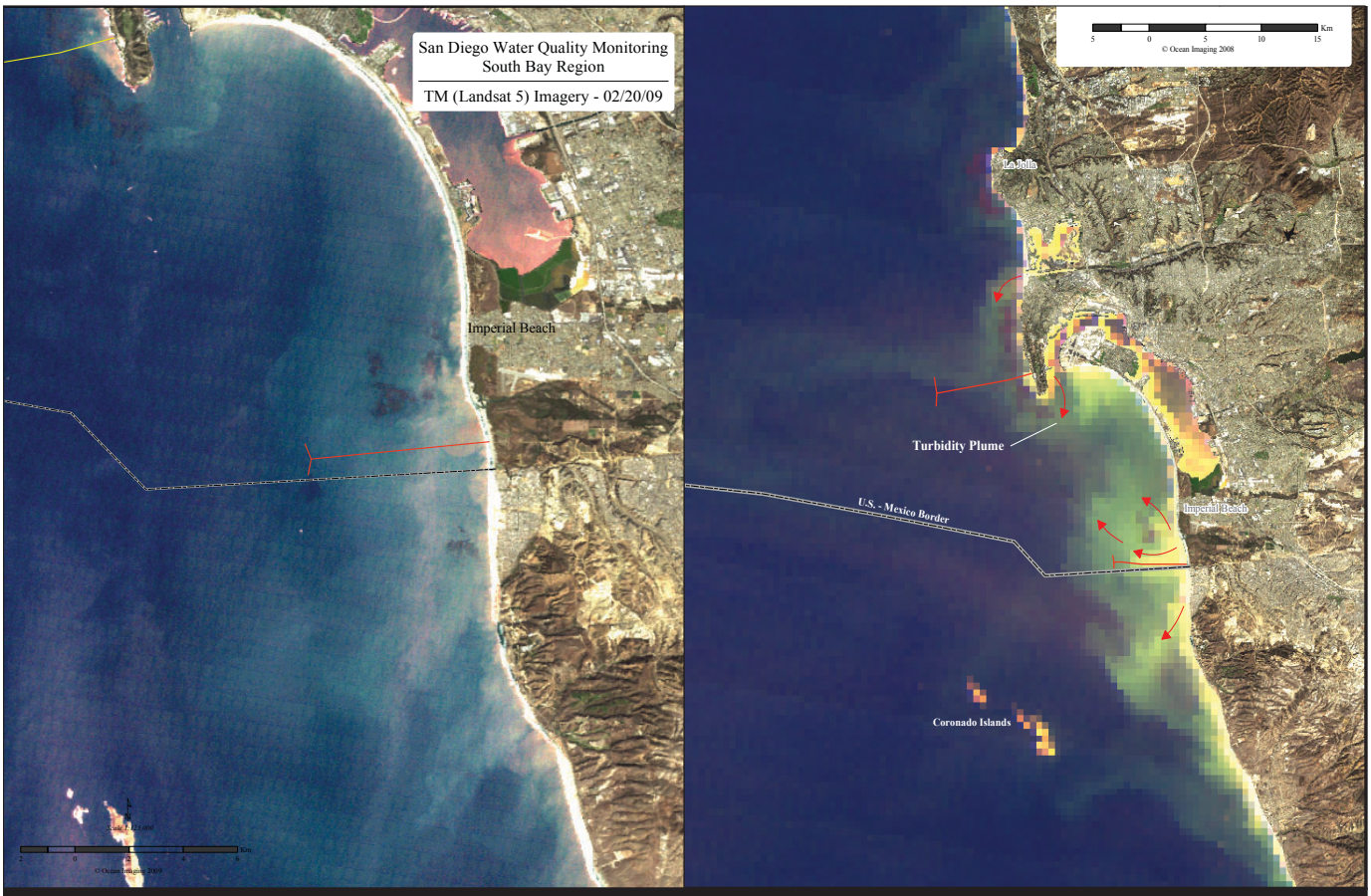

Figure 4.

Multispectral visible imagery of the South Bay region acquired by Thematic Mapper on 2/20/09 (left) and MODIS on 2/19/09 (right). The data were acquired after persistent rain events through February and show extensive turbid stormwater runoff affecting the South Bay nearshore waters. The larger-scale MODIS image also shows southward directed storm runoff from the San Diego River surrounding Pt. Loma.

The SBOO plume became directly observable in aerial imagery on 11/3/09, shown in **Figure 10**. As can be seen from the vertical profiles at station I-14 (**Figure 1**), the water column was still slightly stratified with a pycnocline at approximately 8 meters. However, the strong thermal plume signature recorded by the IR imager indicates that the densest portion of the plume did reach the ocean surface. It is interesting to note that the plume manifestation is very intense in both the multispectral and IR data, but is limited to the area immediately over and slightly south of the S28-85 riser group which traditionally accounts for the largest discharge volume. The overall size of the plume signature is small compared to many other image data sets from other years when the plume was surfacing. We postulate that, with some vertical stratification still in-place in November, 2009, most of the outfall discharge remained well below the surface but a small, highly concentrated portion retained sufficient buoyancy as it rose through the water column to break through the weak pycnocline and reach the ocean surface.

Aerial imaging of the SBOO in early December, 2009 showed the outfall plume with relatively typical southeastward trajectories and outside the influence of the Tijuana River discharge. Following very heavy rains on 12/7/2009 (1.77" at the NERRS station in the Tijuana Estuary) the River plume enlarged greatly in size and enveloped the offshore area of the SBOO wye. Areal imaging of the outfall on 12/14/09 revealed its plume's displacement influence as was already observed in February – the plume waters reached the surface and displaced the more reflective, sediment-laden upper layer (**Figure 11**).

It should also be noted that during the entire 2009, the Imperial Beach kelp bed remained quite large and even expanded into additional areas northward. This trend

began in 2005 (see Ocean Imaging's 1 July, 2005 – 30 June, 2006 Annual Report) and has continued since.

3.2 Historical Analysis of Outfall Plume Dispersal Patterns

The growing catalog of aerial and high resolution satellite imagery of the SBOO region enables us to make some conclusions on the behavior of its effluent plume in near-surface waters. We thought this report opportune to highlight some of the observed characteristics:

As has been discussed in previous reports, the SBOO is most commonly influenced by a southward-directed current field in the area of the outfall's wye. Based on historical data from Scripps Institution of Oceanography's CODAR high frequency radar data (which measure surface currents), surface current velocities most commonly range from 0 to 20 cm/s, although transient, higher velocities do sometimes occur. **Figure 12A** shows the outfall plume's near-surface dispersion pattern under typical southward flow conditions. The buoyant effluent appears to rise to the surface quickly and near-vertically under the majority of current conditions encountered on the image acquisition days. It then spreads in a triangular shape toward the south-south-east. Except for the southernmost plume extents, the edges of the plume tend to remain very sharply defined as the effluent is advected away from the wye, suggesting limited horizontal (vs. vertical mixing). The sharpness of the plume outline near the outfall has been shown to have effects on the detection of the effluent at sampling station I-12, located closest to the wye's southern end: In some cases multi-depth samples taken at the station location showed no near-surface manifestation of the plume. A time-coincident image showed the plume to indeed be surfacing, but its boundary was just outside the I-12 location. In other cases, vertical measurements detected the plume effluent at some depths but not others. This was linked to the sampling vessel's relatively small (but significant) drift movements while the samples were being collected, as the vessel drifted in and out of the plume's sharp boundaries (see Ocean Imaging's December 2003 – January 2004 progress report for more details).

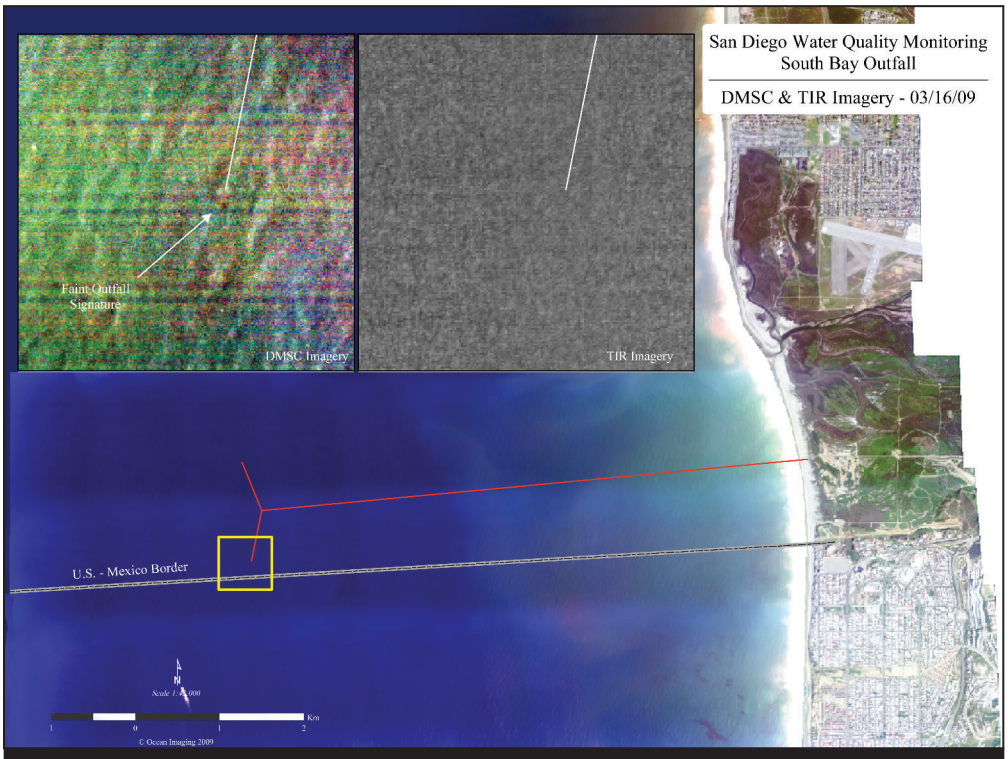

Figure 5.

DMSC aerial imagery of the South Bay Ocean Outfall region, acquired on 3/16/09. The inset images show the outfall wye's southern portion in multispectral visible and thermal imagery (cooler water is darker). A very small outfall signature is detectable in the color imagery but not in the thermal data, indicating the outfall plumes waters no longer reach the surface.

The SBOO is also affected by periodic northward current episodes. These events usually last from less than 24 hours to 2-3 days. In such conditions, observations of the outfall plume show it to be advected northwestward, as is exemplified in **Figure 12B**. TM satellite observations have shown it to be detectable up to several kilometers from the outfall wye, curving northwestward. We believe the reason for the westward motion component corresponds to the general offshore veering of the region's flow pattern as waters from the south become deflected by the shallower bottom topography of the Tijuana River's alluvial fan. More immediate mixing appears to occur along the plume's edges since they are usually considerably less sharp than in the southward flowing patterns. During the northward flow conditions, evidence of the effluent's near-surface manifestation is also commonly seen in time coincident field

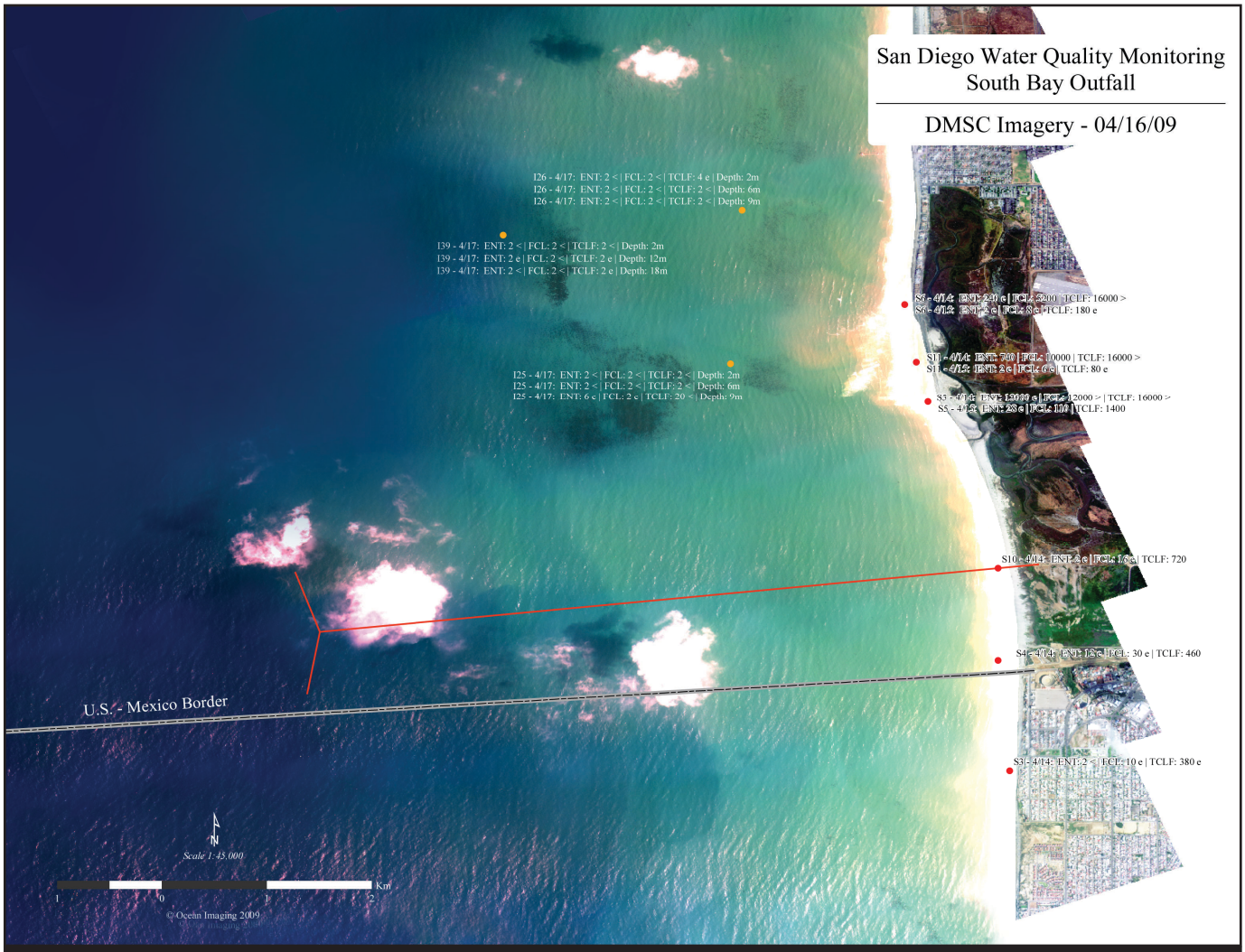

FIGURE 6A.

DMSC aerial imagery of the Tijuana River mouth and South Bay Ocean Outfall region, acquired on 4/16/09.

samples at stations I-12 and I-16 and/or I-14 to the north.

Under conditions of insignificant currents, the outfall plume has been observed to rise directly over the wye and spread out in a circular or oblong pattern, sometimes being constrained on the offshore side by an oceanic front. This is exemplified by DMSC data from 1/7/2009 in **Figure 12C**. During such no-current conditions we have occasionally observed the outfall's outflow to create circular standing wave patterns around the wye. Two of these instances are shown in Figure 13.

Since this project's aerial and satellite image-based monitoring of the SBOO began in 2003, we have observed the plume to disperse in the three patterns discussed above. We have also witnessed the plume's trajectory to be directly westward (offshore) on a few rare occasions when offshore-directed Santa Ana winds caused a relatively anomalous strong offshore forcing of the surface waters. We have, however, never witnessed the SBOO plume to be directed east or shoreward. The only possible exception to this are DMSC aerial data acquired on 2/6/2003, shown in **Figure 14**. The elliptical pattern of the discharge situated directly over the outfall wye indicates little or no current influence, as was described earlier. The core of the discharge actually shows individual discharge signatures from the different riser groups (see zoom-in section in **Figure 14**) and these indicate trajectories toward the northeast. We examined hourly wind records for that day collected at the NERRS station in the Tijuana Estuary

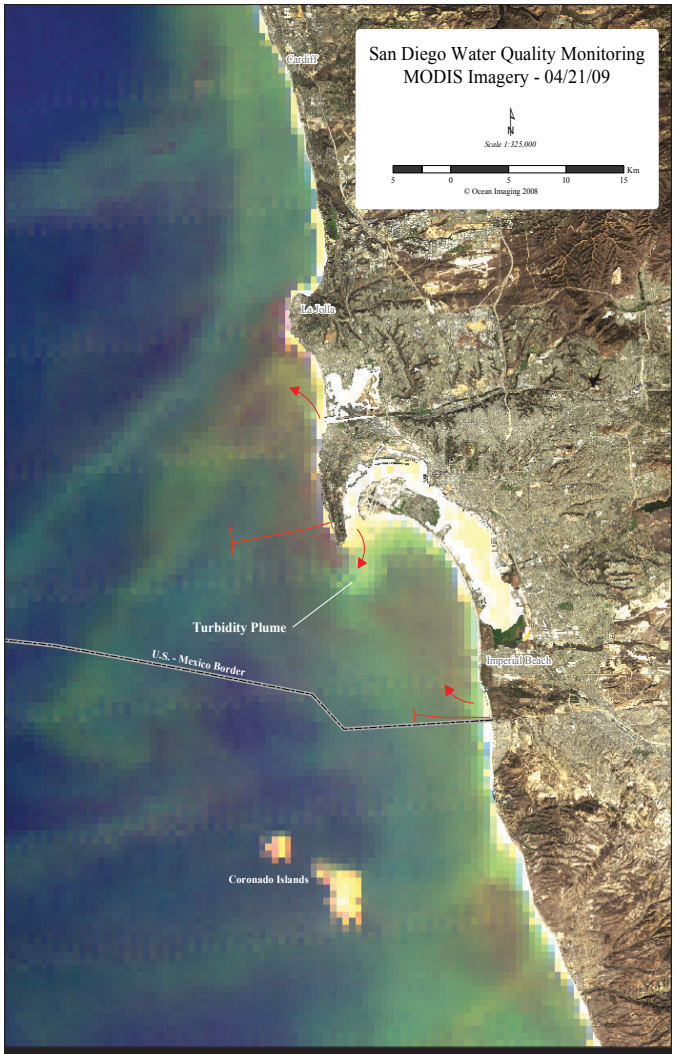

FIGURE 6B.

MODIS satellite image of the San Diego region acquired on 4/21/09. Both images show extensive plankton blooms affecting the coastal waters. The blooms continued into May, 2009 and correspond with the high subsurface chlorophyll measurements at offshore Station I-14 shown in Figure 1.

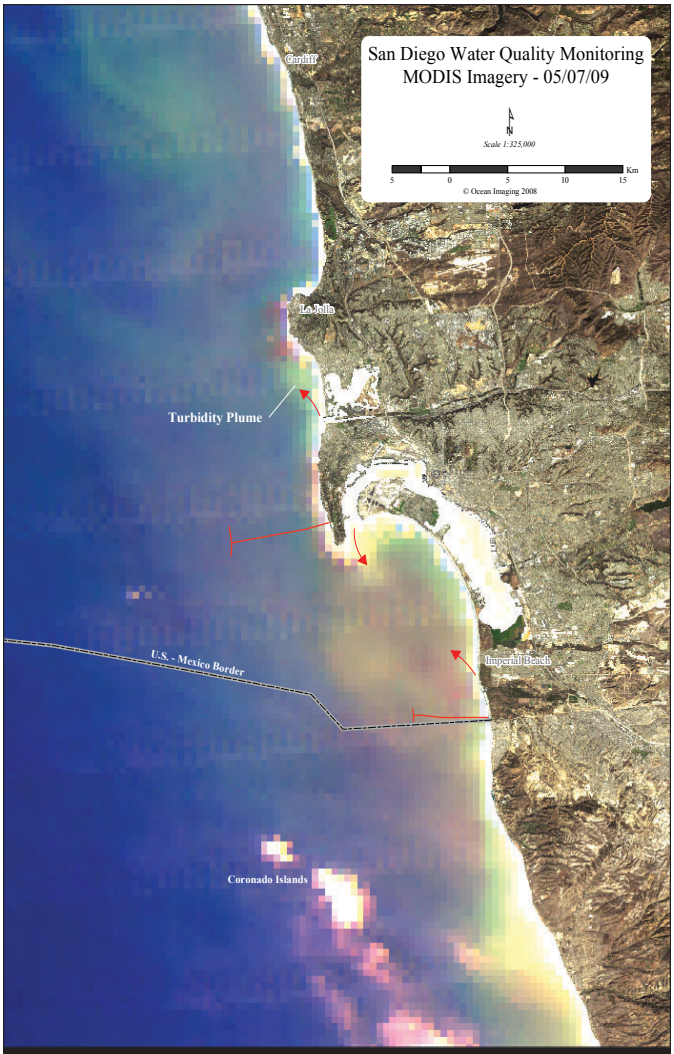

FIGURE 7.

MODIS satellite image of the San Diego region acquired on 5/7/09. Extensive plankton blooms are visible affecting San Diego's nearshore waters.

and found that very weak offshore-directed winds existed in the night and morning hours of 2/6/2003, but for the 3-4 hours before the image was acquired, strong (4+ m/s) winds blew from approximately 210-220° direction, i.e. from the south-south-west. Sustained winds of that magnitude from that direction are not common in the area (see Tijuana River study in the Appendix). SIO CODAR data from that time period show northeastward currents strengthening, which can be assumed to be the ocean surface response to the wind forcing. We thus interpret the aerial imagery as showing the initial lack of current forcing on the surfacing plume, which spread into a relatively large area above the outfall. This pattern is reflected in field samples collected earlier that morning: I-12, I-16 and I-14 all show elevated bacterial concentrations in the upper depths. Station I-23 is located directly in the northeastward trajectory of the imaged plume but does not show elevated bacteria concentrations. Since the field data were collected in the early morning before the strong winds began, it is likely that the plume had not yet reached the I-23 location.

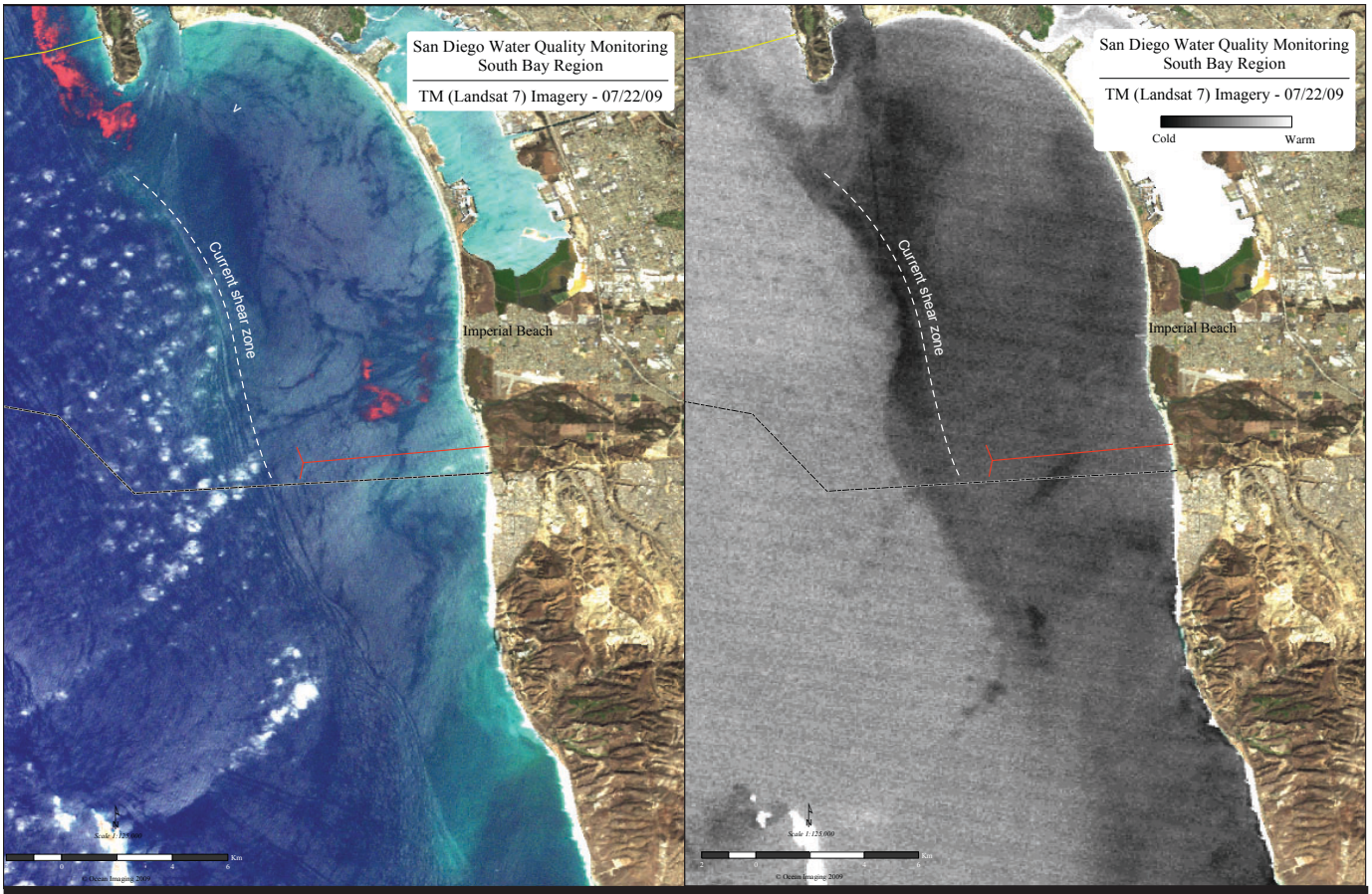

Figure 8.

TM satellite image of South Bay region acquired on 7/22/09. The multispectral visible image (left) shows surfactant features (dark elongations) aligned with a current shear zone extending south from Pt. Loma. The thermal image (right) shows the shear zone also as a thermal front.

The aerial imagery from 2/6/2003 show the SBOO plume reaching the closest to US shores that we have ever observed it. It must be noted that the plume's most shoreward detectable traces were still several kilometers distant from any point of the shoreline. The 2/6/2003 case represents an apparently rare co-occurrence of no initial current field effecting the entire region, followed by strong southwesterly winds that drove the offshore waters toward the northeast.

Since this monitoring project was initiated, the SBOO daily out flow volume has not changed significantly, totaling approximately 25 million gallons per day (MGD). The suspended sediment load within this volume has changed significantly, however. **Figure 15** shows SBOO daily effluent volume and total suspended sediment as monthly averages since 2006 from data provided by the IBWC. The data indicate that between early 2006 and 2008 the effluent's sediment load was reduced by approximately 50% and remained at that level thereafter. We were interested whether the sediment load reduction affected the plume signature's characteristics in the remotely sensed imagery. Most logically, one could expect a reduction in the size extents of the plume in the multispectral imagery because the reduction in sediment could make the plume's spectral signature less intense in a shorter amount of time as it is mixed with surrounding ocean waters while being advected away from the source. We thus measured the total discernible plume area in DMSC aerial image sets in all archived imagery from December, January and February when the outfall plume is most likely to reach the surface. In some cases a distinguishable plume signature reached into Mexico past our imaging system's field of view (we do not have permission to fly into Mexico), resulting in an incomplete total area measurement. No statistically significant relationship was found in the historical plume area measurements and the reduction in the SBOO's suspended sediment load reduction since 2006. Allowing for poten-

tially significant errors in the plume area measurements (which were done subjectively by creating polygons outlining the plume signal within each contrast-stretched data set), some of the largest plume signatures ever recorded occurred in the early months of 2010 (which were included in the analysis). The data are shown in **Figure 15**.

One possible explanation for these observations is that under oceanic and environmental conditions that are most advantageous for the formation of a large plume signature in the surface layer (southward-directed currents with low winds), the 50 mg/l Total Suspended Solids (TSS) concentration in the existing effluent is sufficient to resolve the plume signature by the DMSC multispectral instrument to the same extent as when the effluent contained twice the suspended solids. This could occur if the sediment load reduction was primarily due to the removal of larger, heavier particulates which will tend to precipitate out of the plume quickly, leaving the spectral reflectance effects of the finer particulates remaining in suspension virtually unchanged from those before the total load reduction. We do not have information on particle size composition changes (if any) related to the overall TSS reduction, so the hypothesis cannot be tested at this time.

As can also be surmised from the plume area data shown in **Figure 15**, the SBOO's plume signature size varies considerably even during each winter season. Our

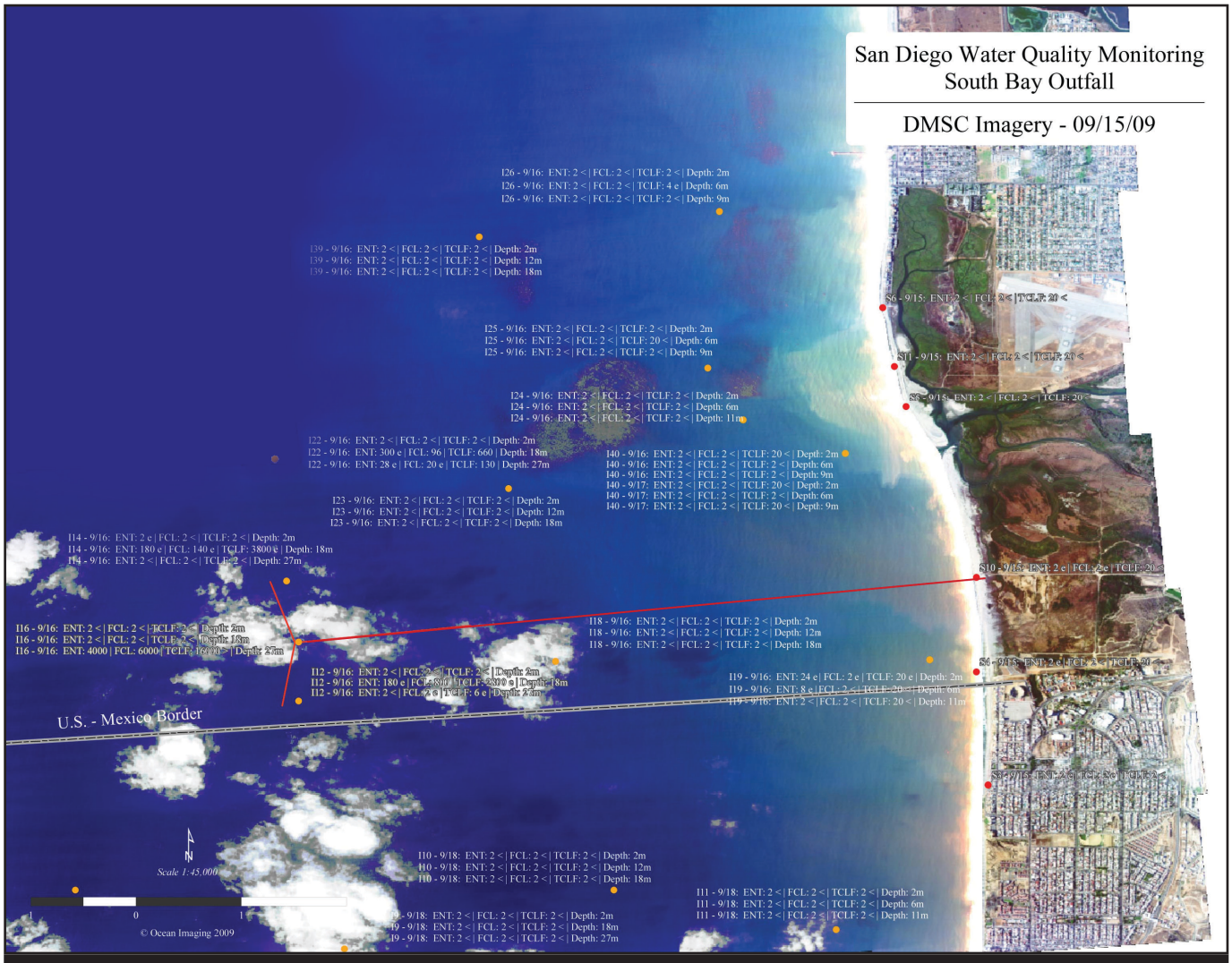

Figure 9A.

DMSC aerial imagery of the Tijuana River mouth and SBOO region on 9/15/09 showing localized, nearshore plankton blooms. Offshore bacterial sampling results from 9/16/09 are also shown.

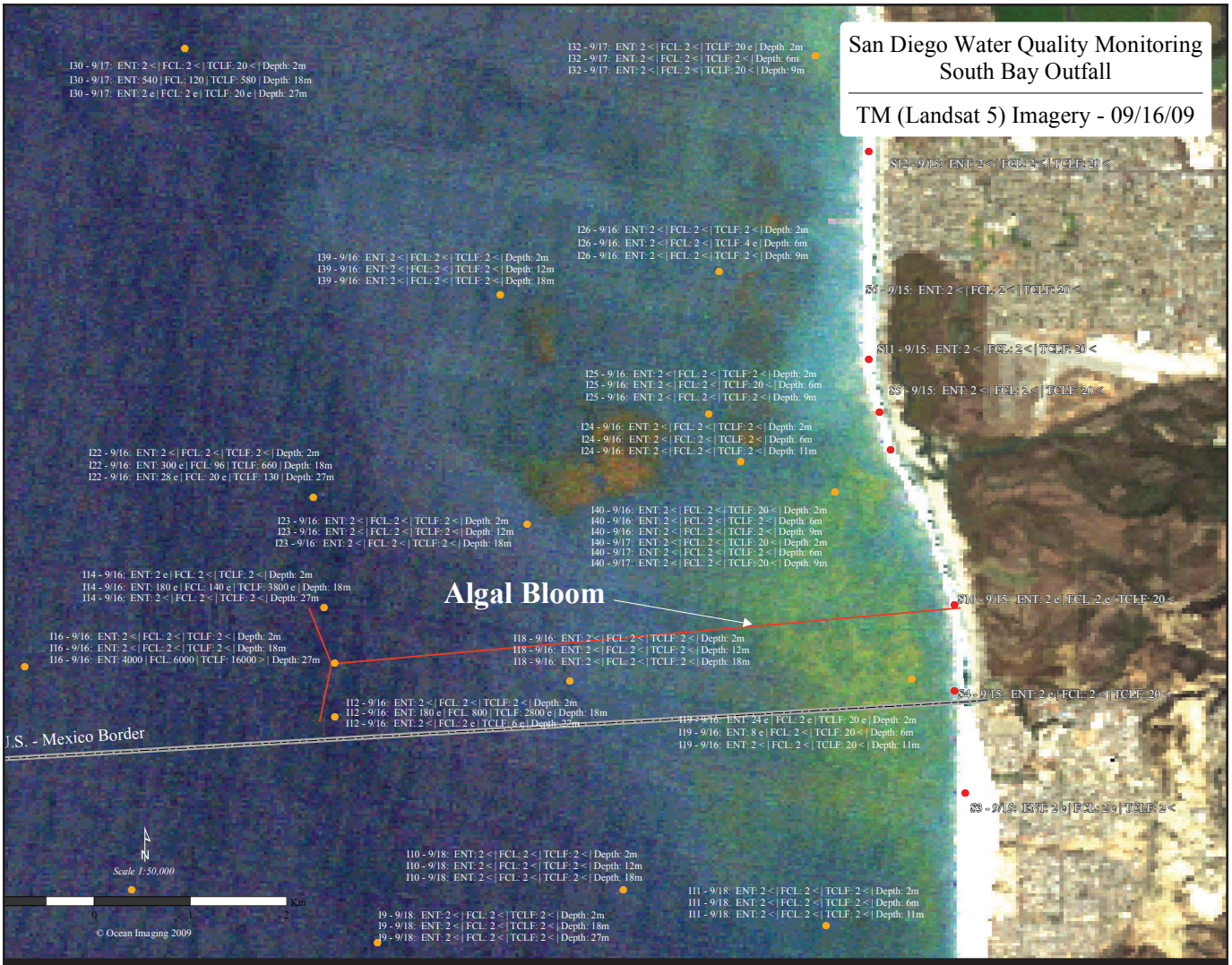

FIGURE 9B.

TM satellite imagery of the Tijuana River mouth and SBOO region on 9/16/09 showing localized, nearshore plankton blooms. Offshore bacterial sampling results from 9/16/09 are also shown.

image data archive accumulated to-date suggests that the plume does not continually surface during periods of the year when vertical stratification in the region is absent. **Figure 16** shows a 3 image sequence from DMSC aerial overflights in January, 2004. The water column was unstratified during the entire month (as judged by the City's vertical profile samples obtained in early January and again in early February). A survey on 1/5/04 showed one of the largest surface layer plume signatures yet recorded, with plumes from the individual riser groups easily distinguishable, and showing a typical shape and trajectory under a southward current regime. A similar, smaller pattern was also recorded in late January on 1/26/04 (**Figure 16C**). A survey in mid-January (**Figure 16B**) showed only a slight near-surface signature of the outfall plume, however. It is highly unlikely that the regional waters re-stratified in mid-January and destratified again within the next 13 days. Two other conditions can be deduced directly from the 1/13/04 data set that may help to provide an explanation for the variability in the plume's behavior: First, the orientation of the plume directly above the outfall wye and its omnidirectional shape indicates the existence of very weak or nonexistent currents; Second, the multitude of white "specs" in the image correspond to whitecaps, indicating rough seas. We posit that under such circumstances, enhanced vertical mixing causes the rising plume waters to intermix with the surrounding ocean waters much more rapidly, and a much smaller effluent volume actually

reaches the surface in a highly concentrated state.

The variability of the SBOO plume's reaching the ocean surface is enhanced in the fall-to-winter and winter-to-spring transition periods when the regional waters' vertical stratification weakens or begins to rebuild, respectively. As was already discussed for the 3 November, 2009 data set in Section 3.1, The plume's near-surface signature often is relatively small, and only the densest fraction of it actually reaches the surface. **Figure 17** shows two image pairs from 2004 and 2006 during the spring transition period in the first days of March. For each pair, the image data were acquired only a few days apart, however, while one image contains a surfacing plume signature, the other shows no surface (or near-surface) plume manifestation. The shapes of the visible plume signatures and coincident CODAR data suggest that on those days the ocean currents were very light, which (we believe) allowed the densest portion of the discharged effluent to break through the weak pycnocline (usually at 5-10 meters) and reach the surface. On the "no plume signature" days the surface layer currents were stronger and likely caused a more rapid vertical transport and mixing of any effluent reaching the shallow pycnocline layer. Our observations suggest that the number of days that the SBOO effluent actually reaches and affects the ocean surface is limited by current and vertical mixing conditions, especially during the seasonal transition periods.

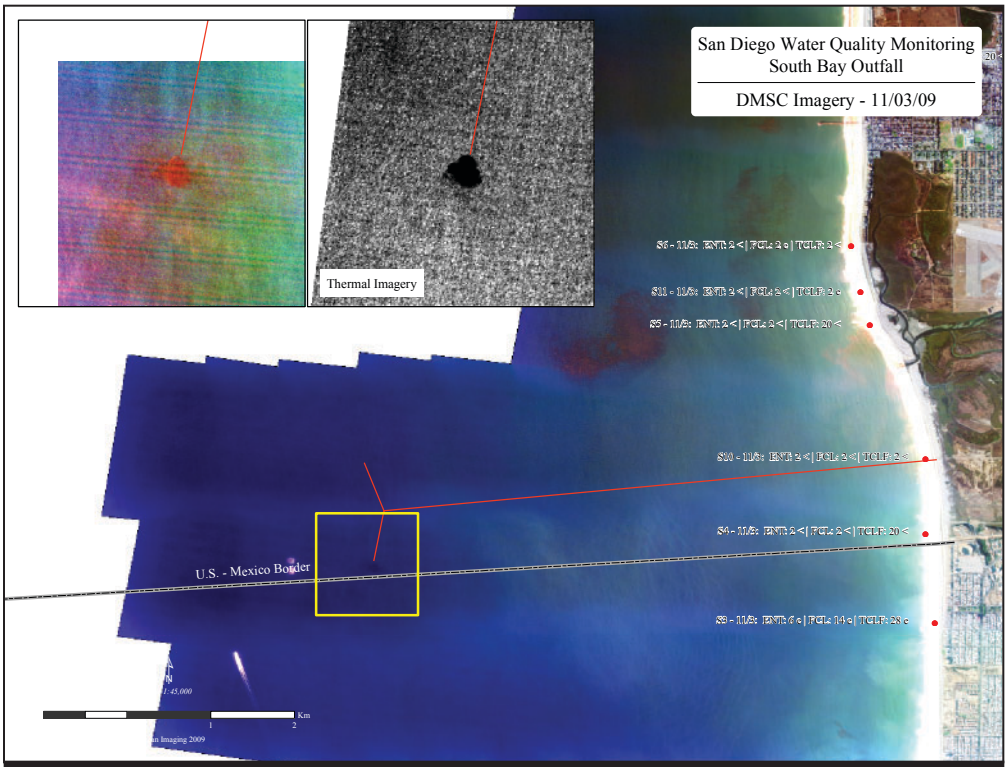

FIGURE 10.

DMSC AERIAL IMAGERY OF THE SBOO REGION ACQUIRED ON 11/3/09. THE INSETS SHOW THE FIRST SEASONAL SURFACE MANIFESTATION OF THE SBOO PLUME. THE PLUME WATERS ARE COOLER THAN THE SURROUNDING WATER IN THE THERMAL IMAGE.

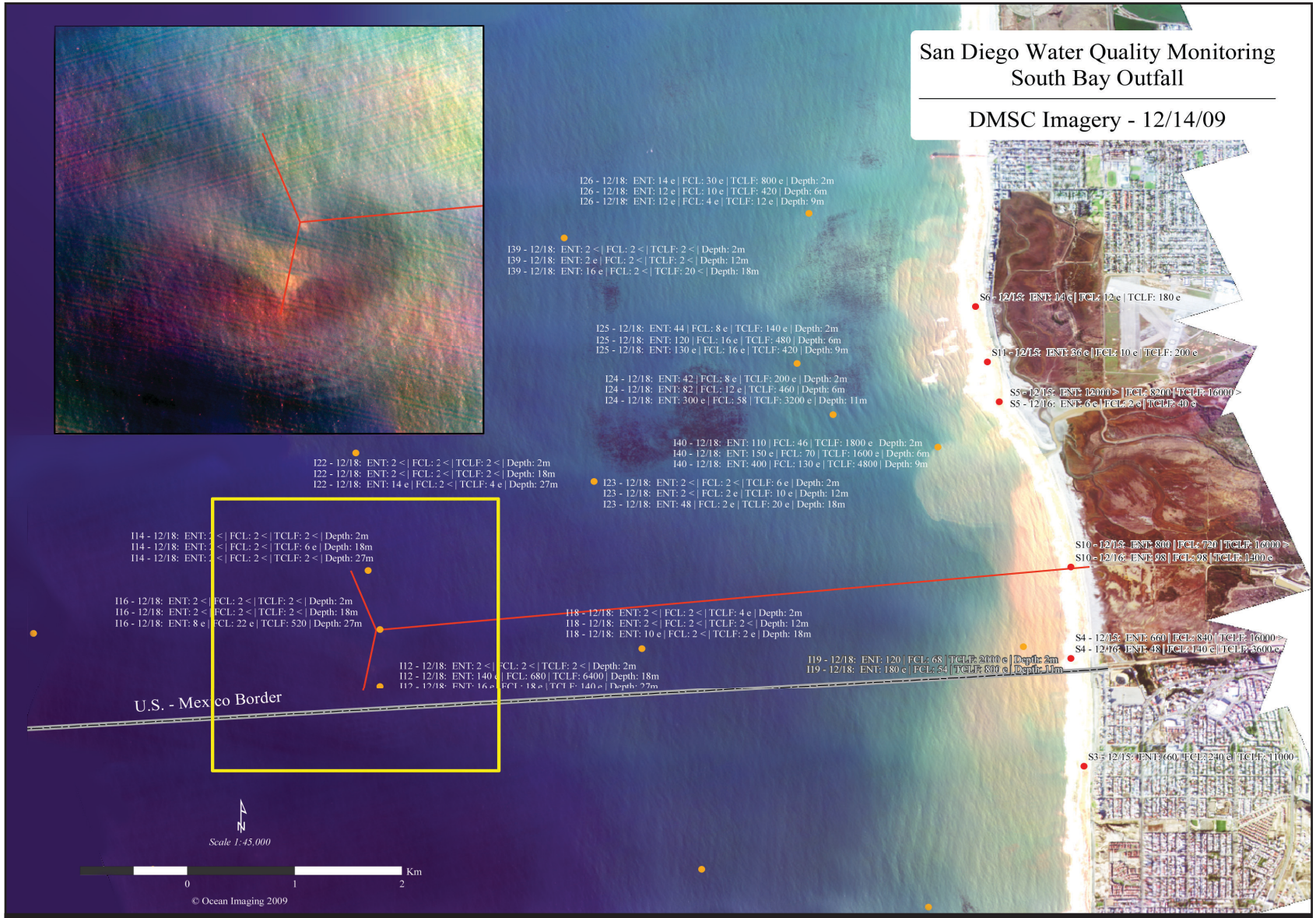

Figure 11.

DMSC aerial imagery of the SBOO region acquired on 12/14/09. The surfacing plume waters displaced the thin, turbid (brighter) layer of stormwater runoff from the Tijuana River which has expanded offshore over the outfall wye. Offshore bacterial sampling results from 12/18/09 are also shown.

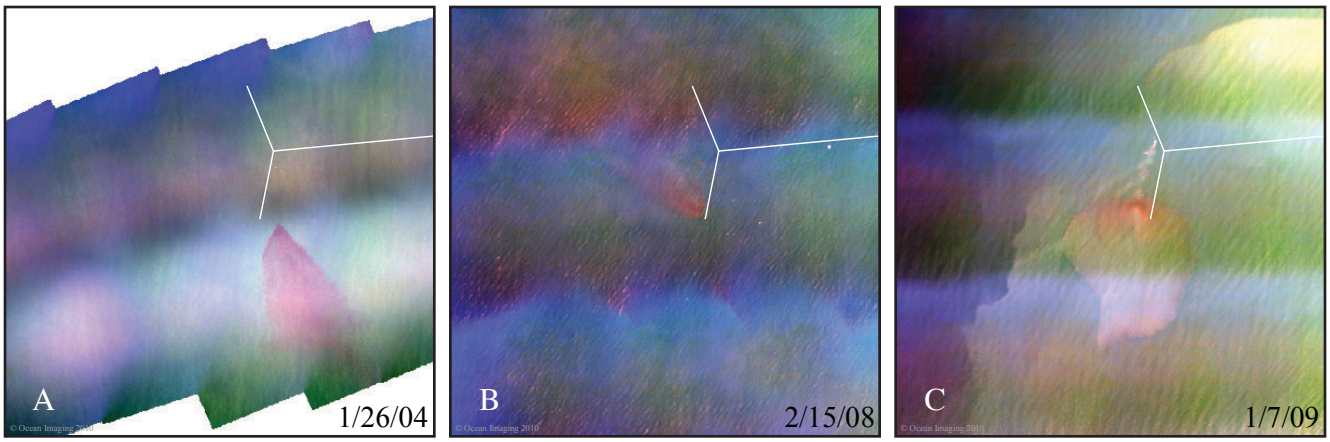

Figure 12.

DMSC aerial imagery of the SBOO showing three most commonly occurring dispersal patterns: during southward current flow (A), northward flow (B) and during weak or no currents (C).

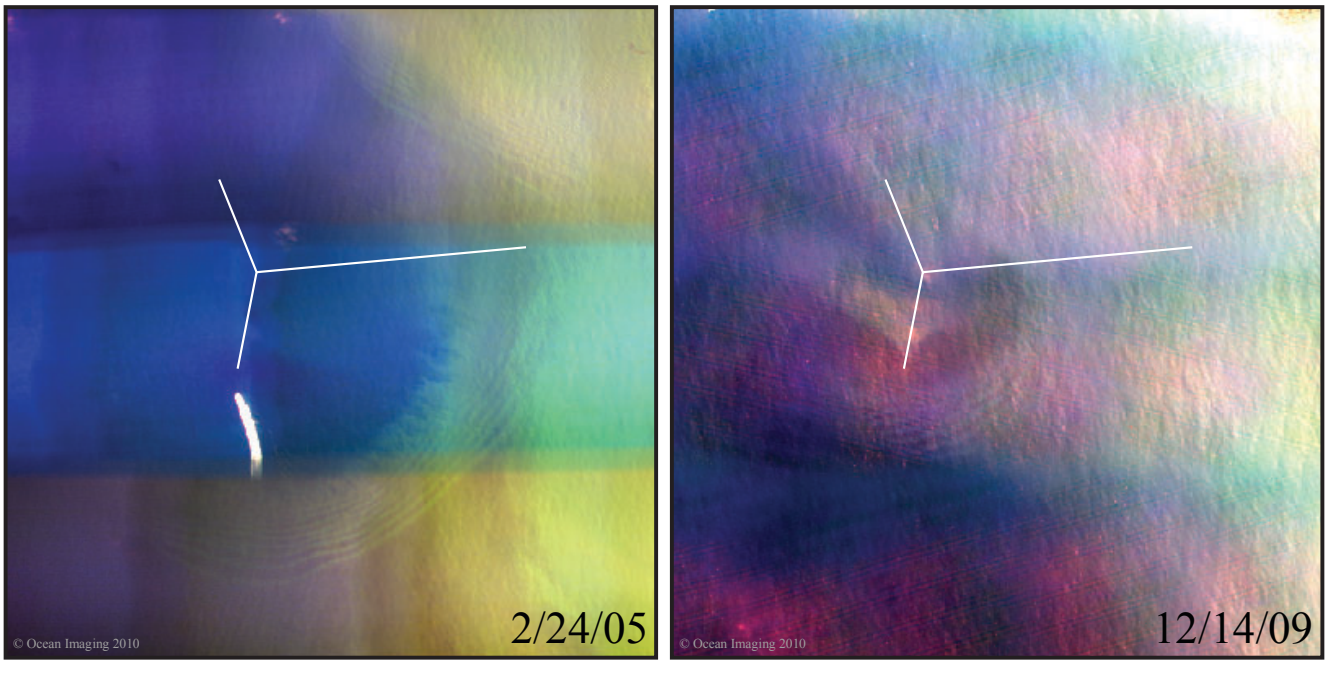

Figure 13.

DMSC aerial imagery of the SBOO plume signature during two lax-current events when circular standing wave patterns developed around the plume area.

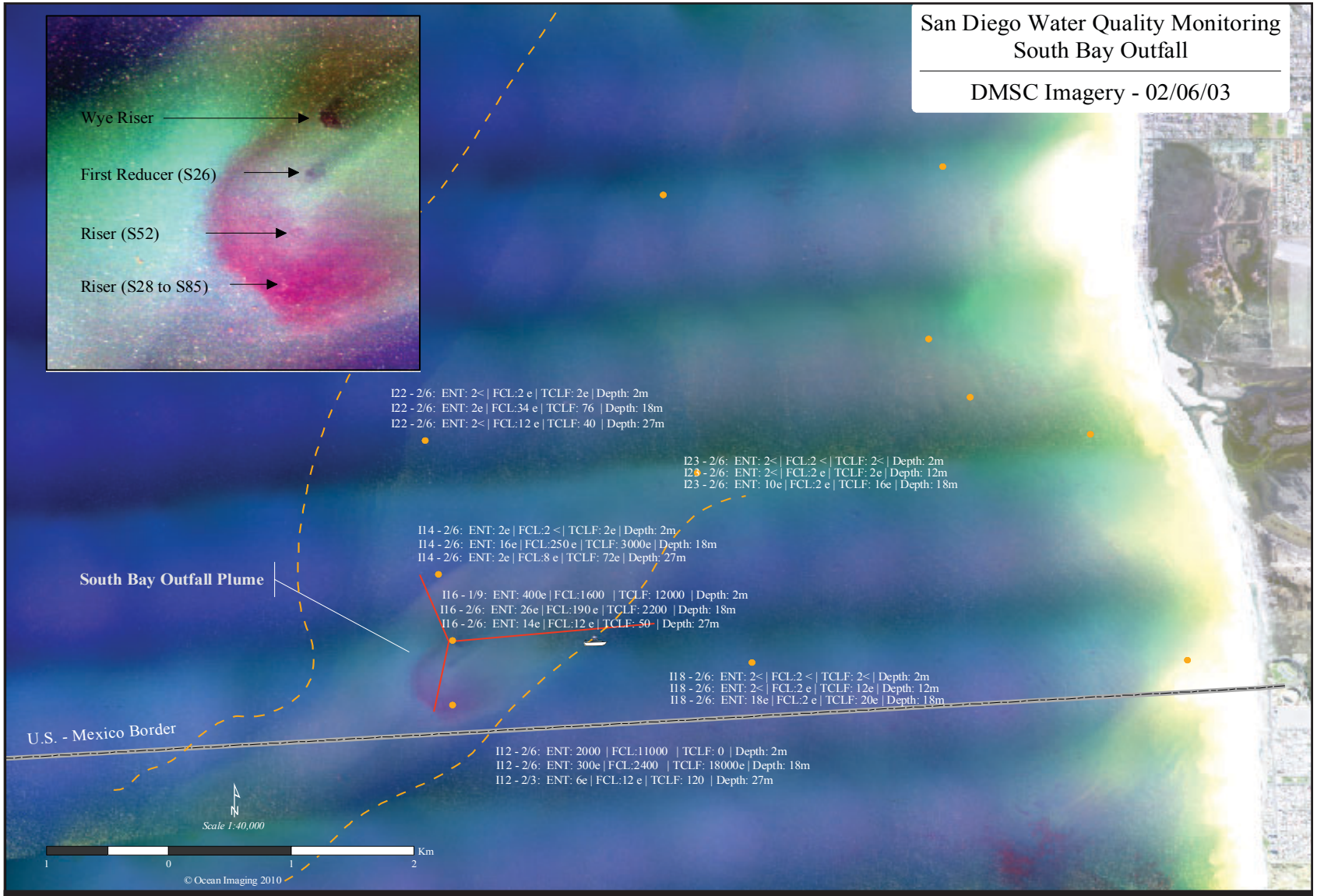

Figure 14.

DNSC aerial image of the SBOO region acquired in the afternoon of 2/6/03. Offshore bacterial sampling results obtained in the morning of the same day are also shown. The inset shows detail of the outfall plume core with separate plume signatures from each active riser group. The large plume pattern is associated with lax-current conditions and low morning winds, followed by southwesterly winds in the afternoon.

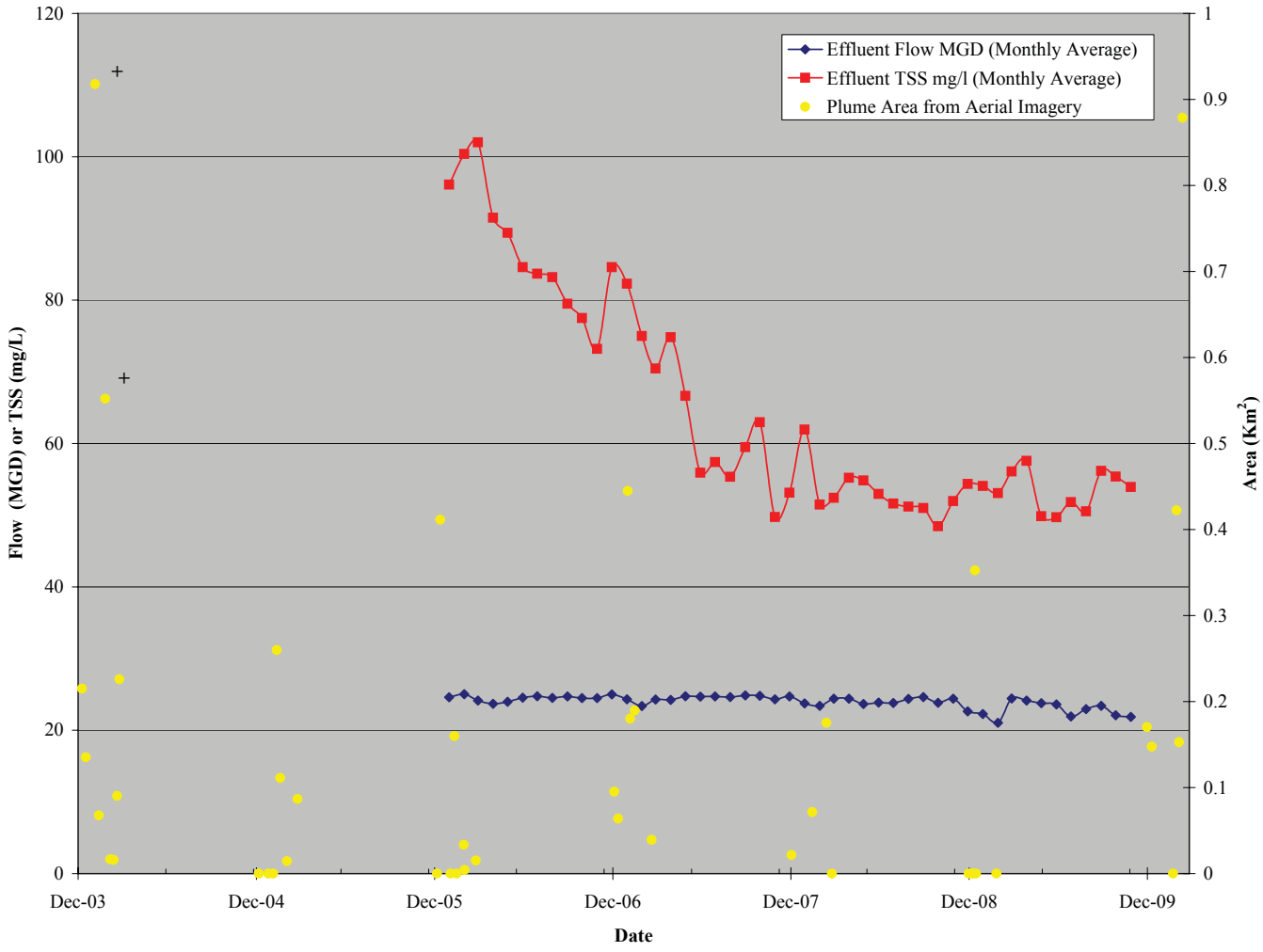

Figure 15.

SBOO monthly average daily discharge rate and total suspended sediment concentration shown with discharge plume sizes derived from individual DMSC image sets acquired in December, January and February of each year. The "+" symbol indicates the plume size extended outside the image.

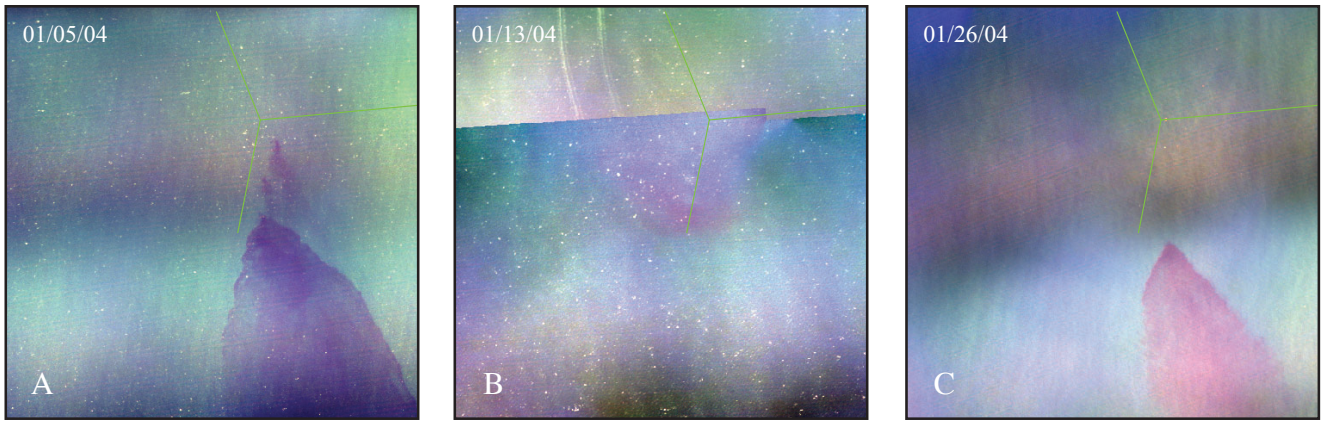

Figure 16.

DMSC aerial imagery of the SBOO wye area during January, 2004. The plume surface signature was very distinct on 1/5/04 but displayed only a very weak surface manifestation 8 days later on 1/13/04. It re-established its surface signature by 1/26/04 (see text for discussion).

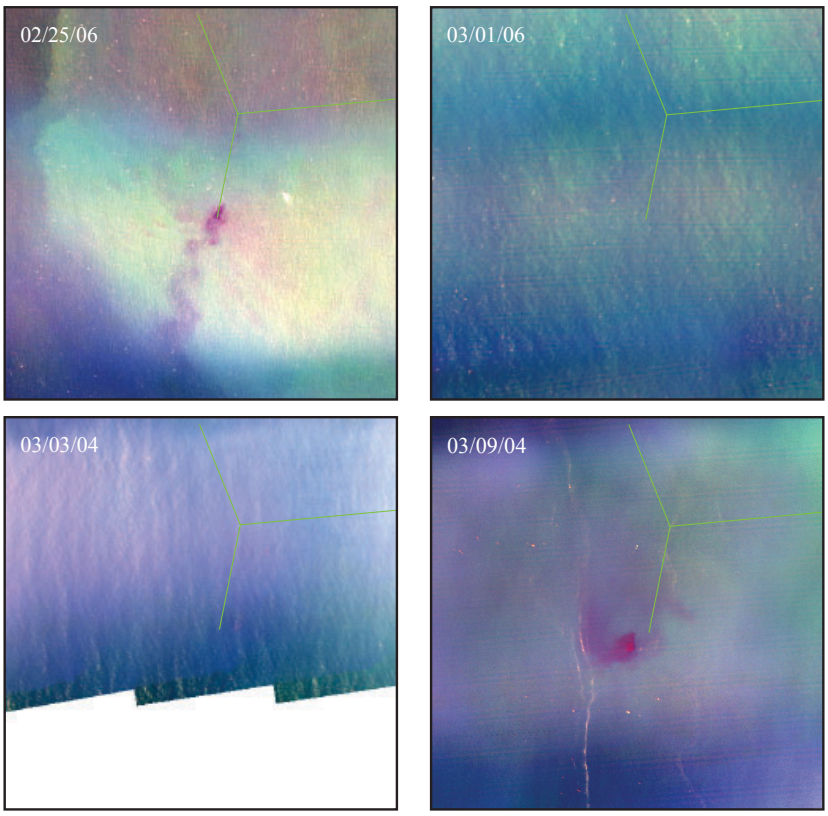

Figure 17.

DMSC aerial images of the SBOO wye area acquired 4 days apart in February-March, 2006 (top) and 6 days apart in March, 2004 (bottom). Each image pair exemplifies the transient nature of the outfall plume's reaching the surface during the spring transition months.

4. The Point Loma Outfall Region

4.1 Highlights of 2009 Monitoring

After its seaward extension in 1993, the Point Loma Outfall (PLO) is one of the deepest and longest wastewater outfalls in the world, discharging at the depth of 320 feet, 4.5 miles offshore. The outfall's plume is generally not observed directly with multispectral color or thermal imagery. It appears to not reach the surface waters, even during the winter months when the water column's vertical stratifications is weakened. We believe, however, that on some occasions we have observed the plume's extents indirectly in both image types through an anomalous lateral displacement of thermal or chlorophyll features around the outfall wye. This effect can be explained by the doming up of the discharged effluent and laterally displacing the near-surface waters above it.

Figure 18 shows 2009 vertical profiles of density and transmissivity at offshore station F19 which is located approximately 2km east (shoreward) of the PLO wye. The offshore sampling was done by the City on a quarterly basis during 2009. The density profiles show some vertical stratification remaining even in February. As in previous years, no direct near-surface manifestation of the discharged effluent was observed throughout 2009.

The rains in January and February did not affect the PLO region as strongly as the SBOO. MODIS satellite imagery from 1/28/09 (**Figure 19A**) show the waters off Pt. Loma to be relatively clear. Detailed nearshore imagery obtained with a DMSC aerial survey the following day (**Figure 19B**) actually penetrated the water column to show bottom substrate features between the shoreline and the kelp bed. Bacterial sampling done at nearshore stations on 1/30/2009 show, correspondingly, minimal near-surface bacteria levels.

The MODIS image in **Figure 19A** shows turbid waters that originated along North County to be flowing southward. As they reach La Jolla, they become deflected westward, then continue their southward or southwestward trajectory. This trend is often observed during the rain season and the trajectory tends to bring turbid runoff that originated from North County lagoons directly over the PLO. Conversely, a major portion of storm runoff from the San Diego River tends to remain closer to shore and flow southward into the region between the Pt. Loma kelp bed and the Pt. Loma shoreline. As is shown in **Figure 2**, however, the San Diego River had practically no discharge during January, 2009.

Because of the influence of North County's storm runoff on the PLO region, differences in rainfall between North County and more southern areas strongly affect water quality off Pt. Loma. **Figure 20** shows large-scale (MODIS) and detailed nearshore (DMSC) turbidity patterns on 2/10/09, after 5 days of rain. Total precipitation accumulation over the Tijuana Estuary was over 1.6" , 2.2" at Lindbergh Field but only 1.4" at North County's Oceanside Airport. These differences are reflected in the MODIS data which show significant runoff from the Tijuana River (see also Figure 3), relatively heavy runoff from the San Diego River, but relatively slight sediment-laden flows from North County. The DMSC imagery shows the majority of San Diego River's discharge (orange and light green areas) to spread southward close to the shoreline.

Following the rain influences in 2009's early months, the PLO region began to be influenced by upwelling-caused plankton blooms during March, 2009. **Figure 21** shows color and thermal images of the region on 3/16/09. The thermal imagery clearly shows a body of cool water, locally upwelled, which corresponds to a sizable green plankton bloom, as evidenced by the multispectral color image. The bloom had spread offshore to cover the PLO wye area and all waters closer to shore. Periodic plankton blooms continued to affect the PLO region through spring and summer, 2009. **Figure 22** shows plankton growth in a 15+km band along the entire San Diego County coastline on 5/7/09. These conditions are also reflected in the reduced transmissivity profile at Station F19 taken on 5/5/09 (corresponding to a subsurface chlorophyll maximum).

The plankton blooms ceased for the most part in September and waters along Pt. Loma and the PLO offshore area remained quite clear through the rest of the year. **Figure 23** shows two detailed nearshore DMSC examples, along with near-coincident nearshore bacteria sampling results. **Figure 24** shows regionwide conditions after relatively heavy rains in early December. While significant stormwater discharges existed along South Bay and Mexican shorelines, the Pt. Loma region was only marginally affected by runoff from the San Diego River. No major discharges were recorded from North County. It should be noted that MODIS-recorded turbidity plumes emanating from the San Diego River/Mission Bay outlet area in November and December, 2009 are directed northwestward, indicating relatively frequent northward current episodes along the Pt. Loma region at the end of 2009.

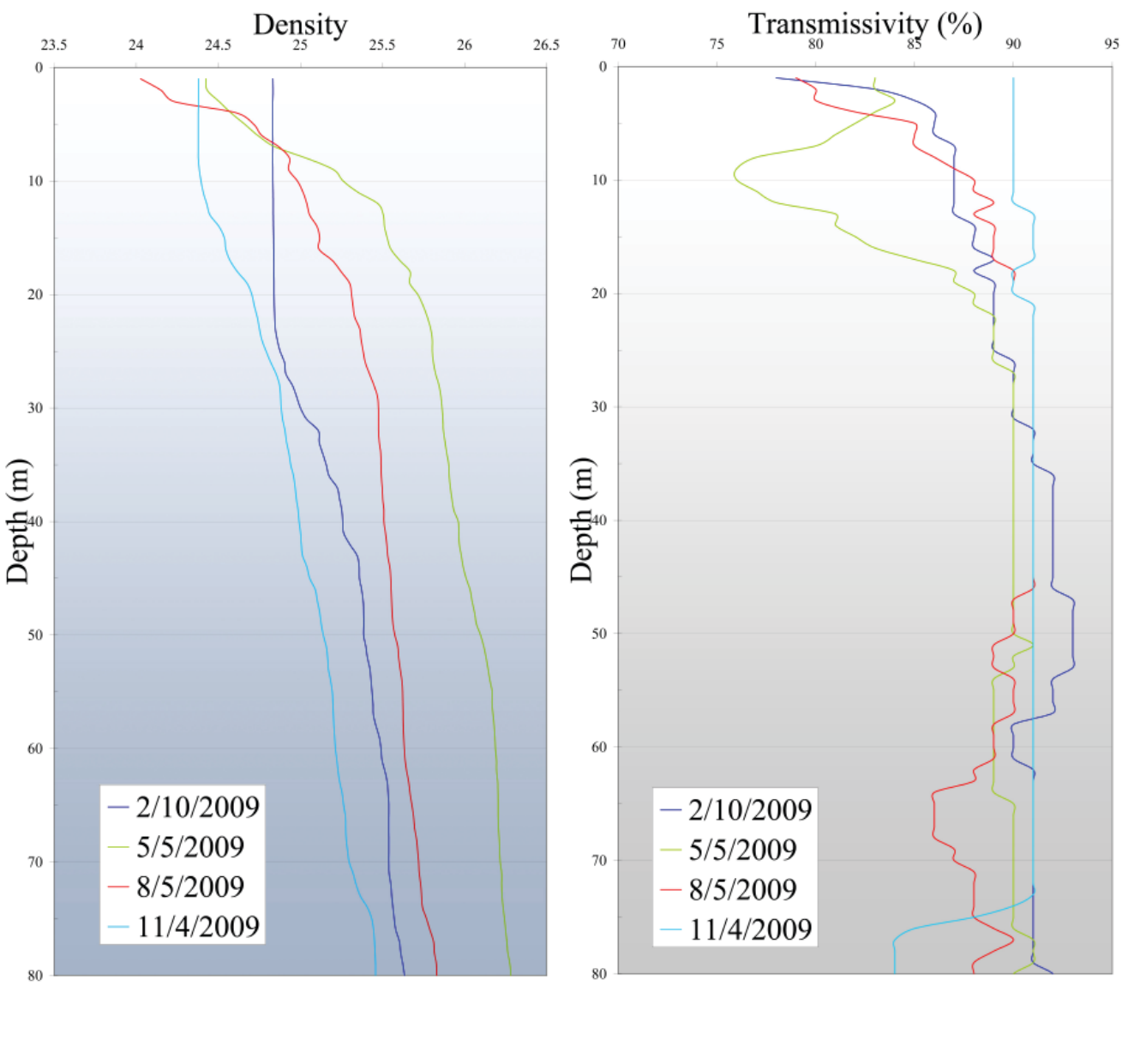

Figure 18.

Vertical profiles of density (top) and transmissivity (bottom) collected quarterly during 2009 by the City at Pt. Loma offshore station F19.

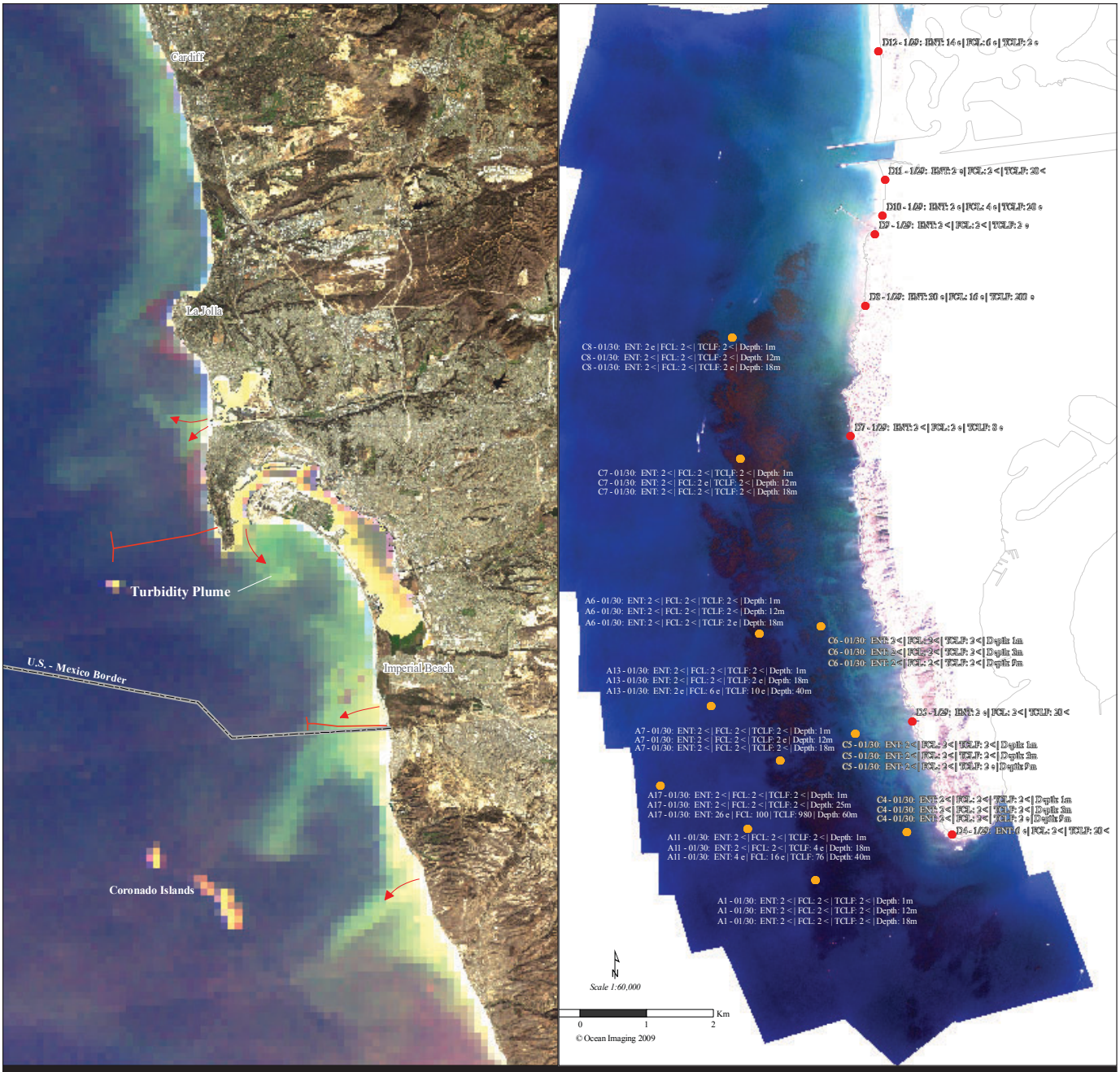

Figure 19A. Figure 19B.

MODIS satellite image of the San Dieo region (A), and DMSC aerial multispectral imagery of the Pt. Loma region (B) from 1/28/09 and 1/29/09, respectively. The large-scale MODIS data show turbid runoff originating in North County to be advected southward over the PLO. The high resolution DMSC image shows high clarity in the nearshore waters along Pt. Loma, allowing clear views of bottom substrate between the shoreline and kelp bed offshore (sandy areas appear bright, algae-covered rock bottom appears dark).

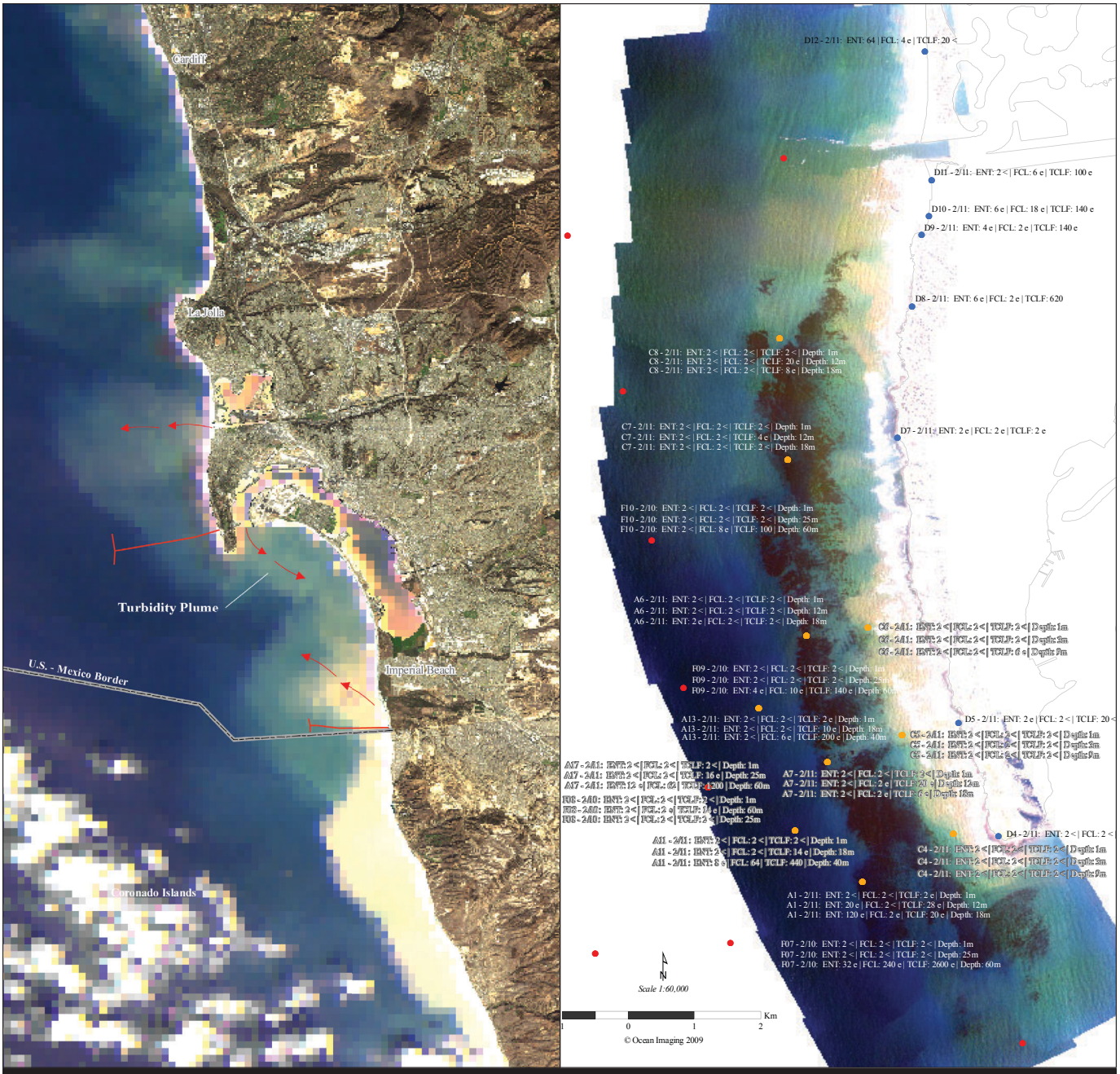

Figure 20.

MODIS satellite image of the San Dieo region (A), and DMSC aerial multispectral imagery of the Pt. Loma region (B) from 2/10/09 after 5 days of rainfall. North County received significantly less rain than central San Diego and South County, resulting in lower runoff volumes. The DMSC data show the most concentrated runoff from the San Diego River to fill the nearshore areas inside and around the Pt. Loma kelp bed.

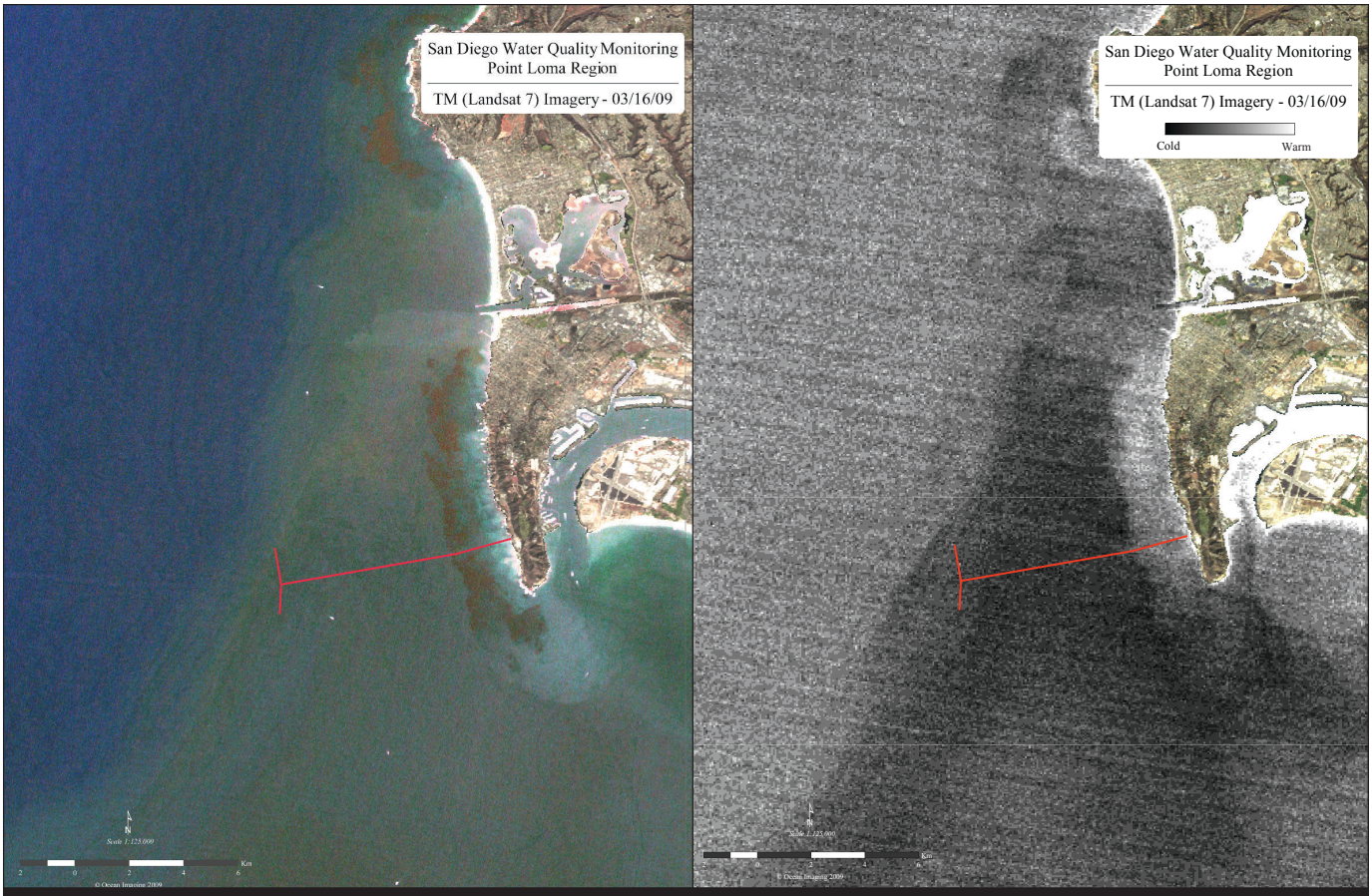

Figure 21.

TM satellite imagery of the Pt. Loma region acquired on 3/16/09. The multispectral visible image (left) shows a large plankton bloom originating along the coast from La Jolla southward and spreading over the PLO. The thermal image (right) shows the corresponding cool, upwelled water signature.

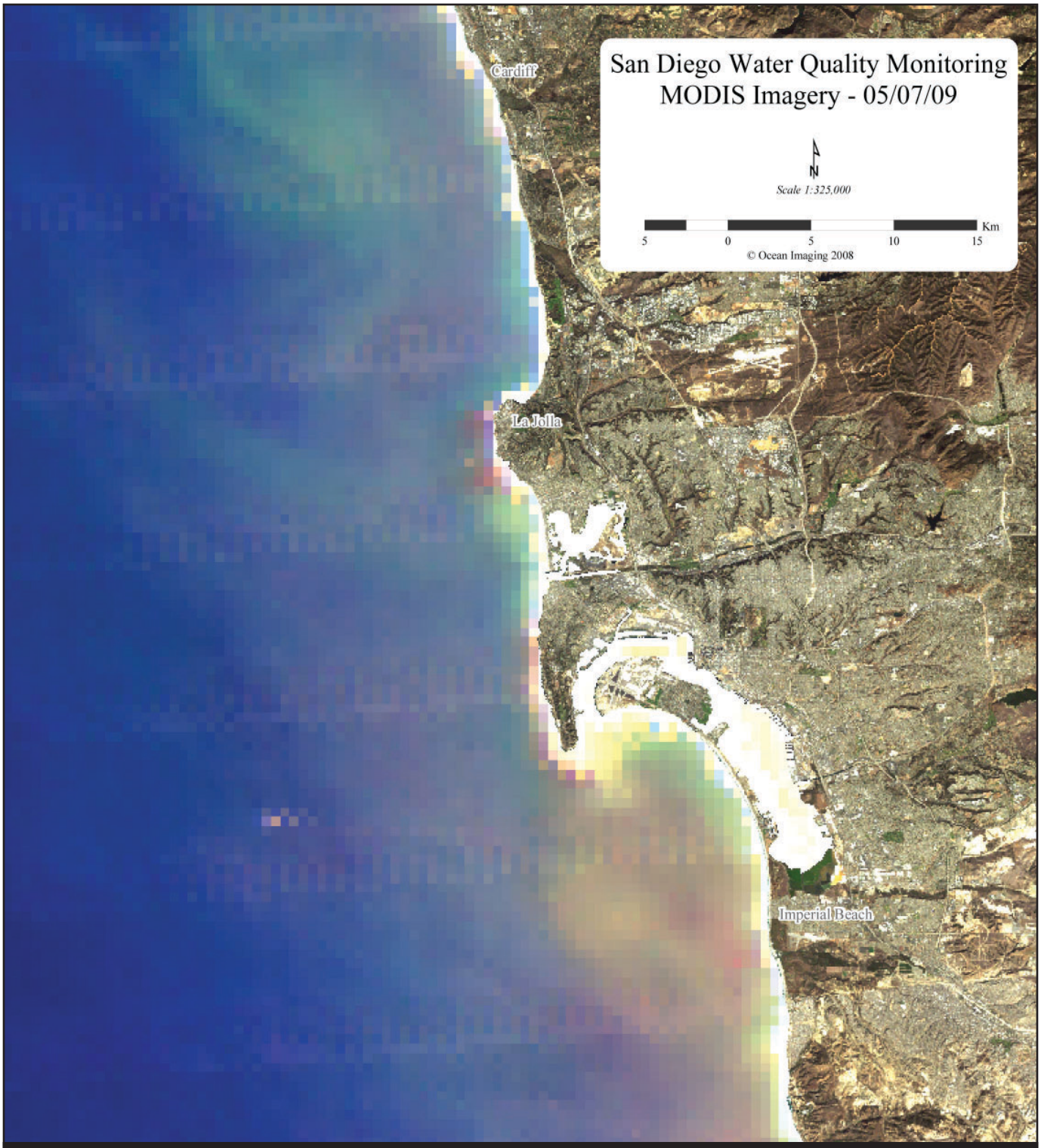

Figure 22.

MODIS satellite imagery of the San Diego County region acquired on 5/7/09 showing widespread plankton bloom conditions along the coast.

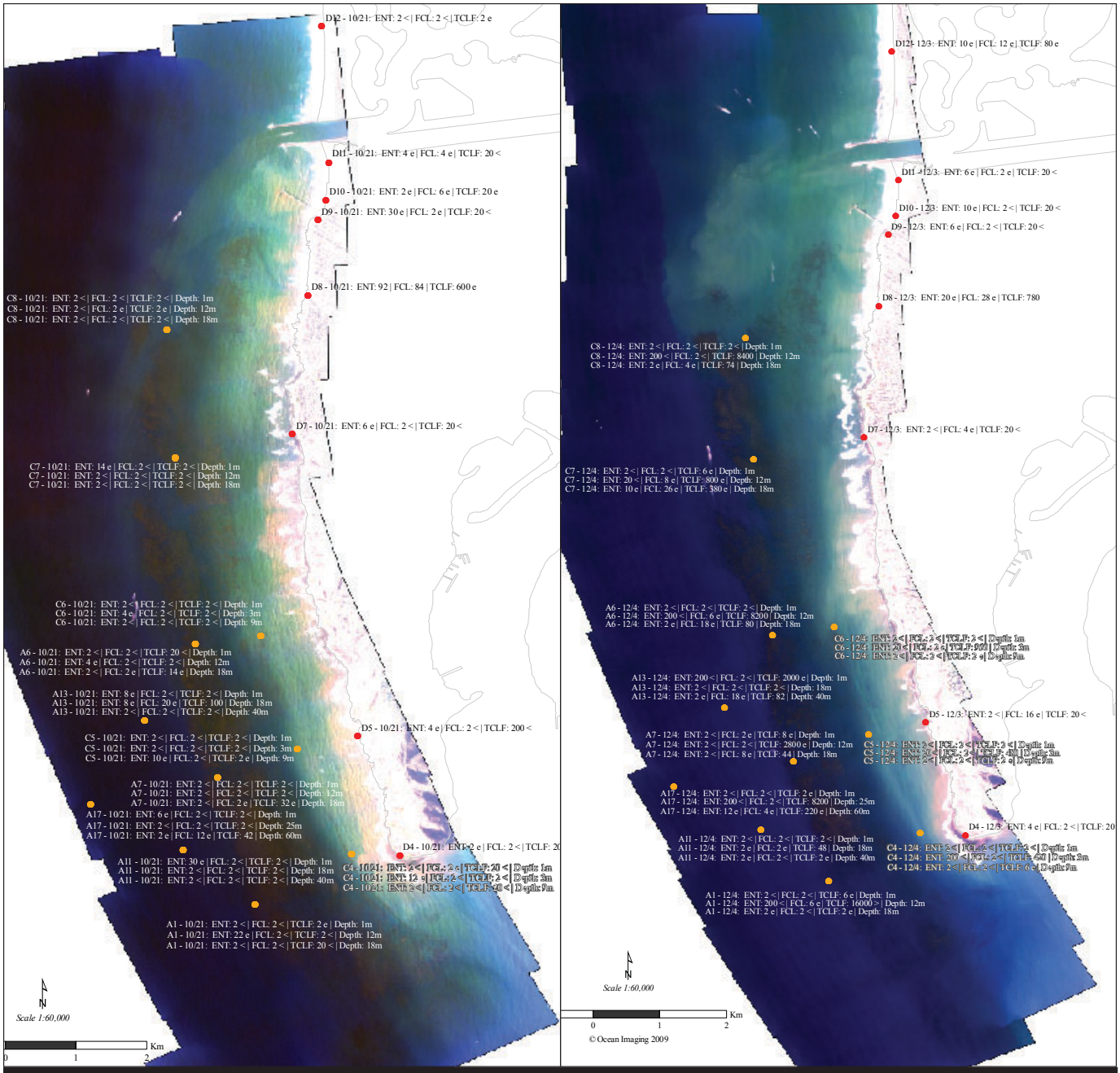

Figure 23.

DMSC aerial imagery of the Pt. Loma region from 10/21/09 (left) and 12/4/09 (right) showing relatively clear-water conditions. Corresponding shoreline and offshore bacterial sampling results also show minimal concentrations.

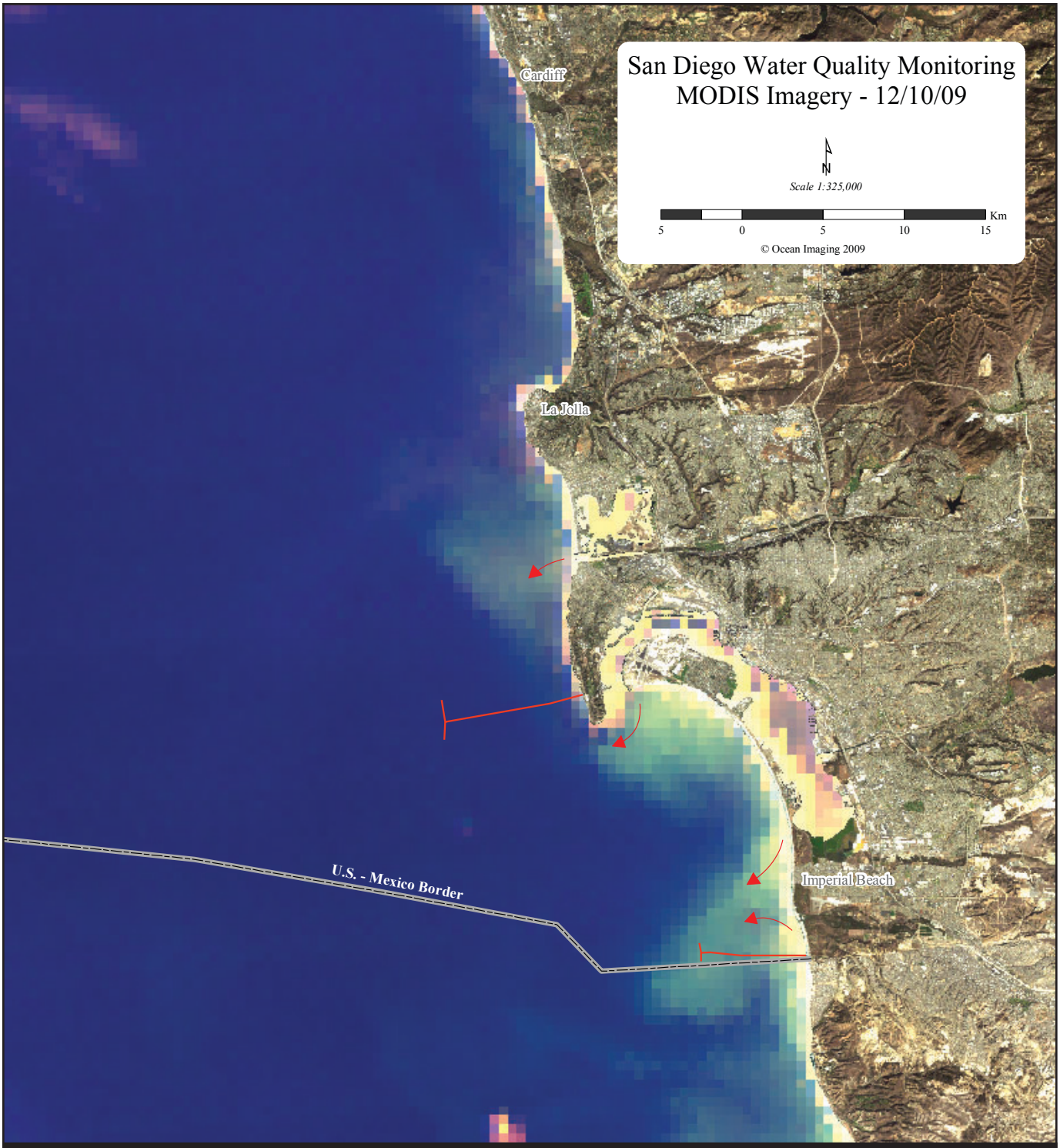

Figure 24.

MODIS satellite imagery of the San Diego County region acquired on 12/10/09 after relatively heavy rains. The PLO area was only marginally affected by stormwater runoff from the San Diego River/Mission Bay and no significant runoff from North County sources.

Appendix

This project's multi-year archive of highly detailed aerial image data over the South Bay region, coupled with frequent shoreline indicator bacteria sampling done by the City and the County Department of Health allowed us to undertake a thorough analysis of the spatial and contamination characteristics of the Tijuana River discharge plume. Stormwater discharge from the Tijuana River is commonly considered the largest source of shoreline pollution and beach closures in the San Diego region. We collaborated on the analysis with Dr. Nikolay Nezlin from the Southern California Coastal Water Research Project. At the time of this report, the results of the study are being published in the journal Estuarine, Coastal and Shelf Science. We present the proof pre-print of this article in the following Appendix.

Estuarine, Coastal and Shelf Science xxx (2010) 1–12

Contents lists available at ScienceDirect

Estuarine, Coastal and Shelf Science

journal homepage: www.elsevier.com/locate/ecss

Tracking stormwater discharge plumes and water quality of the Tijuana River with multispectral aerial imagery

Jan Svejkovsky [a,*], Nikolay P. Nezlin [b], Neomi M. Mustain [a], Jamie B. Kum [a]

[a] Ocean Imaging Corp., 201 Lomas Santa Fe Drive, Suite 370, Solana Beach, CA 92075, USA
[b] Southern California Coastal Water Research Project, Costa Mesa, CA 92626, USA

ARTICLE INFO

Article history:
Received 3 March 2009
Accepted 23 January 2010
Available online xxx

Keywords:
remote sensing
aerial surveys
plumes
water quality
USA, California, Tijuana River
32°25′–32°35′N, 117°15′–117°05′W

ABSTRACT

Spatial–temporal characteristics and environmental factors regulating the behavior of stormwater runoff from the Tijuana River in southern California were analyzed utilizing very high resolution aerial imagery, and time-coincident environmental and bacterial sampling data. Thirty nine multispectral aerial images with 2.1-m spatial resolution were collected after major rainstorms during 2003–2008. Utilizing differences in color reflectance characteristics, the ocean surface was classified into non-plume waters and three components of the runoff plume reflecting differences in age and suspended sediment concentrations. Tijuana River discharge rate was the primary factor regulating the size of the freshest plume component and its shorelong extensions to the north and south. Wave direction was found to affect the shorelong distribution of the shoreline-connected fresh plume components much more strongly than wind direction. Wave-driven sediment resuspension also significantly contributed to the size of the oldest plume component. Surf zone bacterial samples collected near the time of each image acquisition were used to evaluate the contamination characteristics of each plume component. The bacterial contamination of the freshest plume waters was very high (100% of surf zone samples exceeded California standards), but the oldest plume areas were heterogeneous, including both polluted and clean waters. The aerial imagery archive allowed study of river runoff characteristics on a plume component level, not previously done with coarser satellite images. Our findings suggest that high resolution imaging can quickly identify the spatial extents of the most polluted runoff but cannot be relied upon to always identify the entire polluted area. Our results also indicate that wave-driven transport is important in distributing the most contaminated plume areas along the shoreline.

1. Introduction

Storm and dry weather runoff from coastal metropolitan areas have been increasingly recognized as a major source of marine pollution. Runoff escaping into the ocean through storm drains, rivers and creeks includes bacteria, viruses, and anthropogenic components from sewage, as well as fuel, oil, break, tire and asphalt-related compounds from roadways, and industrial and agricultural substances. Unlike sewage outfalls that release their wastewater offshore, effluent from storm drains and river mouths is released directly into the surf zone. The resultant health hazards cause temporary beach closures and possible long-term effects on coastal habitats through the accumulation of pollutants in near-shore sediments.

In southern California (SC) and other arid coastal regions, stormwater discharge is highly seasonal and episodic, and is associated with turbid plumes of polluted water emerging from river mouths after storm events. The climate of southern California is of the Mediterranean type, with distinct dry (summer) and wet (winter) seasons. The majority of annual water and sediment loads entering the ocean from land sources are linked to winter storms (Inman and Jenkins, 1999). The accumulation of pollutants on terrestrial surfaces during the dry season, which then get swept into the ocean during the first few annual storms, results in a "First Flush Effect" that has been well documented with field measurements (Bertrand-Krajewski et al., 1998; Cristina and Sansalone, 2003; Tiefenthaler and Schiff, 2003) and even from space with satellite imagery (Svejkovsky and Jones, 2001).

Because of the significance of the region's stormwater discharges on human health and nearshore ecosystems, the ability to better understand the spatial extents, concentration and potential pollution risk of the stormwater discharge plumes is important. High winds and rough seas following a storm often

* Corresponding author.
E-mail address: jan@oceani.com (J. Svejkovsky).

0272-7714/$ – see front matter © 2010 Published by Elsevier Ltd.
doi:10.1016/j.ecss.2010.01.022

make ship-based field sampling of the formed plumes difficult (see Nezlin et al., 2007). Additionally, the sampling station grids that can be reasonably sampled are often not large enough to contain an entire plume and/or detailed enough to adequately resolve different characteristics within it. For this reason satellite remote sensing has been used to resolve terrestrial runoff plumes and relate their patterns to a variety of oceanic and atmospheric variables.

The most commonly used satellite data for river plume observations have included images from NOAA's Advanced Very High Resolution Radiometer (AVHRR) (Prangsma and Roozekrans, 1989; Stumpf and Goldschmidt, 1992; Stumpf et al., 1993), NASA'a Sea-viewing Wide Field-of-view Sensor (SeaWiFS) (Nezlin and DiGiacomo, 2005; Nezlin et al., 2005), and Moderate Resolution Imaging Spectrometer (MODIS) (Miller and McKee, 2004; Warrick et al., 2007; Nezlin et al., 2008). AVHRR, SeaWiFS and MODIS provide imagery at 1-km spatial resolution. MODIS also has channels with 250-m and 500-m resolutions that can be useful for observing river plumes. These channels provide significantly increased spatial resolution but pose problems with corrections of atmospheric attenuation which is important for any quantitative assessments. Some researchers have thus used the 250-m imagery only qualitatively from a visual standpoint (Ahn et al., 2005). Others have extended the MODIS 1-km atmospheric correction algorithm to the 500-m channels (Shutler et al., 2007) or utilized a simple clear water "dark pixel" subtraction method on a single 250-m channel (Miller and McKee, 2004). Some work has also been done using satellite sensors with higher spatial resolutions such as Landsat Thematic Mapper (30 m) (Lira et al., 1997), and SPOT (10 m) (Ouillon et al., 1997). Although the increased spatial resolution provides vastly greater structural detail within the plume signatures, the relatively low satellite revisit frequency (approximately twice per month), makes image availability after a storm event a major limitation. Imagery from these and similar sensors is also more difficult to calibrate and correct for atmospheric attenuation.

Previous post-storm studies of the SC region have utilized 1-km resolution multispectral imagery from SeaWiFS and MODIS. The studies examined satellite signatures around several major SC stormwater runoff sources and reached a number of general conclusions: the plume size estimated from the backscattering coefficient was highly correlated with the amount of rainwater precipitated over the entire watershed area and accumulated during the period preceding the plume (Nezlin and DiGiacomo, 2005); the discharges tended to be advected southward, with alongshore movement being more prevalent than across-shore transport, remained clearly distinguishable as a water mass for at least 5 days, and appeared to be primarily forced by wind stress (Warrick et al., 2007); the influence of tidal circulation on the plume area was insignificant (Nezlin and DiGiacomo, 2005). The former studies generally utilized a backscattering limit value to make a binary "plume" versus "no plume" classification for the region's waters (e.g., Nezlin et al., 2008). This approach, coupled with the relatively coarse spatial resolution of the satellite imagery (1000 m), obscured potentially important details of structure and suspended sediment load patterns within the plumes. The spatial resolution limitation also tended to blend numerous point source discharges from sources near the dominant discharge into one coherent "plume", thus distorting the spatial extents and apparent transport of the actual discharge signatures from sources targeted by the studies.

Tracking plumes from aircraft provides much higher spatial resolution than satellite imagery. A number of river plume and wastewater investigations have been done using aerial photography (St John and Pond, 1992; Ruffin, 1998; da Silva et al., 2002) and videography (Webster et al., 2004). Digital multispectral imagery was also utilized by (Jorgensen and Edelvang, 2000) to map suspended sediment concentrations and aid in hydrodynamic modeling. These previous studies generally related field-collected parameters to a single image set or a very limited number of aerial images, thus limiting their observations to the discharge rate, and atmospheric and plume composition parameters existing at a particular point in time. To-date no long-term aerial imaging database has been available for examining the response of a river discharge plume to different atmospheric and oceanic conditions.

Since 2003, Ocean Imaging Corporation has been providing aerial remote sensing imagery of shoreline and offshore discharges in southern San Diego County as part of the regional water quality monitoring program. The project utilizes Ocean Imaging's multispectral aerial sensor which, when flown at an altitude of 3800 m provides 2.1-m spatial resolution data in 4 spectral bands. The aerial imagery was collected on a relatively regular schedule (approximately every 10 days) but additional acquisitions were also made following storm events. The imagery included the coastal region surrounding the Tijuana River (TJR) mouth – one of the most contaminated and polluting runoff sources in California (SCCWRP, 1992; DEH, 2007). The archived aerial image data thus provide uniquely detailed and relatively frequent documentation of the TJR plume patterns. In addition to resolving intensity variations within the plume in great detail, the imagery also allows direct observations of other variables such as wave direction. We utilized this archive to relate the plume's distribution patterns to various oceanic and atmospheric forcing parameters at spatial resolutions not possible with satellite data. Surf zone bacterial samples available at high spatial and temporal frequency over the entire study area enabled us to examine the contamination characteristics of the runoff plume components. We thus also investigated the potential for directly using high resolution aerial imaging to establish public health risk beach closure boundaries.

2. The Tijuana River watershed

The TJR watershed is approximately 4465 km^2 in size. It straddles the United States and Mexico border, with about 72% in Mexico and 28% in the United States. More than 70% of its area is undeveloped. Near its terminus in the Pacific Ocean, the watershed's streams enter an urbanized area, mostly within the Tijuana, Mexico metropolis (Fig. 1). Within this area, 40% of the watershed's channels are unlined, while 60% constitute of concrete channels. The final 8 km are again natural, passing through the TJR Estuary and emptying into the ocean through a single opening. Four major dammed reservoirs above the urbanized region capture an estimated 70% of the watershed's runoff volume (Englert, 1997). Most of the runoff actually reaching the ocean therefore originates in the urbanized section of the watershed.

During the dry season (approximately April through September) none or only minimal flow tends to reach the TJR Estuary and no appreciable discharge thus enters the ocean. Following rain events, however, the TJR discharges excess runoff into the ocean in a highly turbid plume, readily discernible in aerial imagery. In addition to high-suspended solids concentrations, the runoff waters have been repeatedly shown to contain high levels of toxic contaminants (Gersberg et al., 2004), bacteria, and hepatitis and enteroviruses (Gersberg et al., 2006). Public health hazards posed by the TJR effluent result in beach advisory postings or downright closures for up to 4 km or more northward along the U.S. shoreline and lasting from several days to weeks. The closures are enacted by the San Diego County Department of Environmental Health (DEH) who base their decisions on exceedances of "AB 411 Standards" (State Water Resources Control Board, 2005) of indicator microorganisms in water samples collected in the surf zone.

Please cite this article in press as: Svejkovsky, J., et al., Tracking stormwater discharge plumes and water quality of the Tijuana River with..., Estuar. Coast. Shelf Sci. (2010), doi:10.1016/j.ecss.2010.01.022

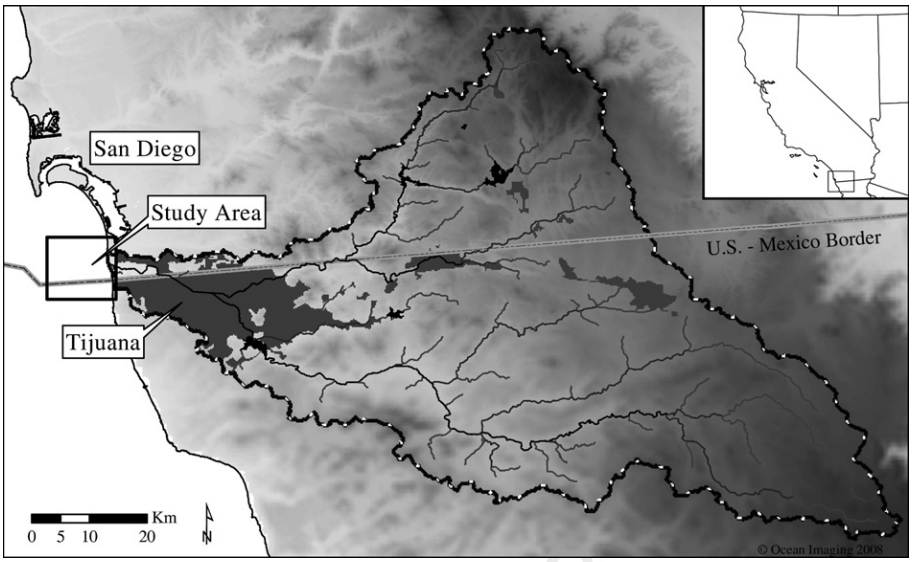

Fig. 1. The Tijuana River watershed with urbanized regions shaded in dark grey. (For interpretation of the references to colour in this figure legend, the reader is referred to the web version of this article.).

The frequent shoreline contamination problems associated with stormwater runoff from the TJR prompted the U.S. to construct the International Wastewater Treatment Plant (IWTP), which began operation in January, 1999. Each day the plant processes approximately 95 million liters of sewage from Tijuana's sewer system to advanced primary level and discharges it into the Pacific Ocean through an offshore outfall. The plant is connected to the TJR directly through a diverter channel system above the TJR Estuary, which diverts up to 49 million liters per day of flow from the river into the plant for treatment. The diverter system thus delays somewhat the initial entry of runoff into the Estuary and the ocean following a storm, and lessens the total volume of effluent entering the ocean during the TJR active flow. Although the benefit of the IWTP on the region's shoreline contamination is a continuing point of contention, recent analysis did find some decrease in bacterial exceedances at surf zone sampling stations near the TJR mouth (Gersberg et al., 2008).

3. Materials and methods

3.1. Aerial imagery

The multispectral imagery was acquired with a Digital Multispectral Camera (DMSC-Mk2) aerial imager manufactured by SpecTerra Ltd. in Australia. Thirty nine images were collected during rain seasons from February 2003 to February 2008. The DMSC collects 1024 by 1024 pixel image frames at 12-bit radiometric resolution with 4 separate camera channels whose imaging wavelength can be customized with narrow-band interference filters. For this analysis, a filter combination of 451/551/640/675 nm was utilized. The bandwidth for all channels was 10 nm, centered on the given wavelength. The imagery was acquired at an altitude of 3810 m, resulting in spatial resolution of 2.1 m. The system is integrated with a differential GPS/Inertial Measurement Unit, allowing automatic georeferencing of the captured image frames.

The imagery was collected along overlapping (by 40%) flight lines flown from west to east, with 60% image frame overlap. Flight times were chosen to minimize sun glint effect by imaging during 20°–35° sun angles. Most of the image acquisitions were done in the afternoon but some were done in the morning, as is discussed further below.

Following acquisition, the image frames were merged together to form a single image. The individual frames were first corrected for vignetting effects and approximately 25% of the perimeter of each frame was discarded. The trimmed image frames were then merged together using a "feathering" routine in ERDAS image processing software. Although it was possible to radiometrically calibrate each data set with an in-flight and post-flight calibration routine utilizing a white Teflon standard target, this procedure was not performed during many of the earlier archived overflights. Therefore, an alternate calibration method had to be used to allow direct comparisons between images acquired on different days and times. A number of calibration methods have been devised and evaluated for multispectral aerial imagery. These include normalization to a spectrally flat target (Schott et al., 1988; Ben-Dor et al., 1994), empirical relationships between radiance and reflectance (Dwyer et al., 1995), and radiative transfer models. Radiative transfer models require measurements or approximations of atmospheric variables at the time of data acquisition and empirical relationships require ground reflectance measurements of targets within the imaged area, neither of which were available for the Tijuana River image data. We thus opted for the normalization approach. We utilized a grey concrete runway located at an airfield just inland of the TJR mouth as a standardization target. Concrete surfaces have been shown to represent suitable image normalization targets at visible wavelengths in previous studies (Staenz and Itten, 1982; Lawless et al., 1998). After examining the digital number (DN) values of the runway in several representative images, a 625 m^2 portion was used as the calibration target. An image with the target's DN values in each wavelength channel falling within the midrange of values of all other images was chosen as the normalization standard. For each image set the mean DN values of the target were then computed and the entire image was scaled to the standard values on a channel-by-channel basis. The intent was to equalize the overall intra-image brightness differences due to differences in sun angle and atmospheric conditions.

The effectiveness of the procedure was tested by recomputing the runway brightness over a larger area in each image as well as computing the average brightness of 3 differently colored flat

Please cite this article in press as: Svejkovsky, J., et al., Tracking stormwater discharge plumes and water quality of the Tijuana River with..., Estuar. Coast. Shelf Sci. (2010), doi:10.1016/j.ecss.2010.01.022

Table 1
Digital numbers (DN) for each DMSC channel used for image-to-image calibration and statistics from 39 calibrated images.

DMSC channel		451	551	640	675	551/451	640/451	675/451
Calibrated to		1400	1600	1350	1850	1.143	0.964	1.321
Runway	Average	1406	1530	1263	1850	1.090	0.915	1.300
	σ	69	67	45	66	0.058	0.030	0.036
Roof #1	Average	1246	1381	1225	1597	1.107	0.988	1.269
	σ	78	81	68	108	0.053	0.042	0.037
Roof #2	Average	1141	1172	852	1098	1.029	0.756	0.952
	σ	90	105	59	96	0.059	0.030	0.030
Roof #3	Average	1737	2019	1794	2190	1.164	1.008	1.298
	σ	126	160	123	151	0.072	0.090	0.063

building roofs along the shoreline. The statistics are shown in Table 1. They indicate that the calibration procedure was quite effective in normalizing the intra-image reflectance brightness range, allowing quantitative image-to-image DN profile comparisons.

The ocean regions of each image were then classified to separate the TJR plume from surrounding "clear" water and to differentiate the plume waters into several classes based on their spectral differences. Through experimentation, we found a threshold approach using different channel ratios to be the most effective and robust. Past analysis of the image data as well as extensive visual observations of TJR outflows during aircraft overflights indicated that the TJR plume tends to be composed of three components with distinctly different color (i.e. spectral reflectance) characteristics. The spectral contrast of each plume component was further enhanced by comparing band-to-band ratios, specifically 551/451 nm, 640/451 nm and 675/451 nm, or using the 451/551/640 nm bands as RGB components in a color image. The distinct changes in spectral reflectance were most likely due to time-dependant precipitation of specific size and material composition suspended sediment particles. The best fitting ratio thresholds for separating non-plume waters from the plume and distinguishing the three classes within the plume were determined on a subset of images and the classification procedure was then applied to the entire image data set. We classified ocean surface into four classes: "clean ocean", "old plume" (OP), "old plume core" (OC), and "fresh plume core" (FC). The threshold values are shown in Table 2. We chose to classify the plume waters into three classes (versus less or more) because they represented the most robust ratio changes over the entire image set and coincided with visually distinct color changes in the RGB images. A final image-processing step was the application of a 300-m mask along the shoreline to mask out whitewater areas in the surf zone and exposed sand due to tidal differences.

3.2. Environmental data

TJR discharge data were obtained from the International Boundary Waters Commission's database in the form of daily flow rates. The daily rate was measured at a flow gauge located downstream from the IWTP diverter, immediately before the TJR enters the estuary.

Wave height and direction data were obtained for the buoy 46 086 (32°29′54" N; 117°59′57" W; depth 1856.2 m) owned and maintained by National Data Buoy Center (NDBC) (http://www.ndbc.noaa.gov). Wind direction and velocity were also available from this sampling platform. The buoy is located offshore, 81 km due west of the TJR terminus. Our analysis of the influence of wave height on the plume size (E_w) was based on the equation

$$E_w = W^{*}\exp(-K_w{}^{*}t), \quad (1)$$

where W is the wave height measured at the buoy, t is the time interval between the W measurement and the plume area size and K_w is the "forgetting factor". According to this coefficient, the influence of wave height decreased with time in accordance with an exponential equation with negative power coefficient. The coefficient K_w was estimated on the basis of maximum correlation between the plume size and the wave height effect $\sum E_w$ accumulated during 10 days before the flight (the contribution of waves after a period >10 days was considered negligible). Thirty six images of 39 were used for this analysis because wave data were available only after November 2003.

Tidal fluctuation data were obtained from the NOAA "Tides and Currents" website managed by the Center for Operational Oceanographic Products and Services (CO-OPS). The tidal level was measured at hourly time intervals in San Diego (station ID: 9410170 located at 32°42′48″ N, 117°10′24″ W) in meters referred to Mean Lower-Low Water (MLLW) datum level. Our analysis of the influence of tidal circulation on the plume size was based on the following model. We assume that each ebb tide contributes to the plume size and this influence (E_t) is proportional to the difference between high (H_h) and low (H_l) tides ("tidal prism"). The effect of each ebb tide (E_t) decreases with time interval between the ebb tide and the observation (t, days) according to equation

$$E_t = (H_h - H_l)^{*}\exp(-K_t{}^{*}t) \quad (2)$$

The "forgetting factor" K_t was estimated on the basis of maximum correlation between the plume size and the accumulated tide effect $\sum E_t$ during 10 days before the flight.

Wind speed and direction were obtained at NDBC offshore buoy 46086 and from a station within the Tijuana Estuary, maintained as part of the National Estuarine Research Reserve System (http://cdmo.baruch.sc.edu/QueryPages/realtime.cfm?Station_Code=tjrtlmet). The station is located in the estuary 2000 m north of the TJR terminus. The wind sensor is located on a 3.5 m high aluminum tower, corresponding to 7.5 m above sea level. Prior to July 2006 hourly wind values were available from averaged measurements taken every 5 s. After that date, 15 min wind values are available. We derived hourly speed and direction from the 15 min data by averaging the preceding 4 data values for each hour.

3.3. Bacterial data

Shoreline bacterial sampling results were obtained from the DEH. DEH personnel collect water samples within the surf zone at

Table 2
Threshold band ratios used to classify imagery.

Plume class	Band ratio (x)		
	551/451	640/451	675/451
Clear ocean	$x < 0.85$	–	–
Old plume (OP)	$0.85 \le x$	–	–
Old plume core (OC)	–	$0.45 \le x < 0.65$	$0.55 \le x < 0.75$
Fresh plume core (FC)	–	$0.65 \le x$	$0.75 \le x$

Please cite this article in press as: Svejkovsky, J., et al., Tracking stormwater discharge plumes and water quality of the Tijuana River with..., Estuar. Coast. Shelf Sci. (2010), doi:10.1016/j.ecss.2010.01.022

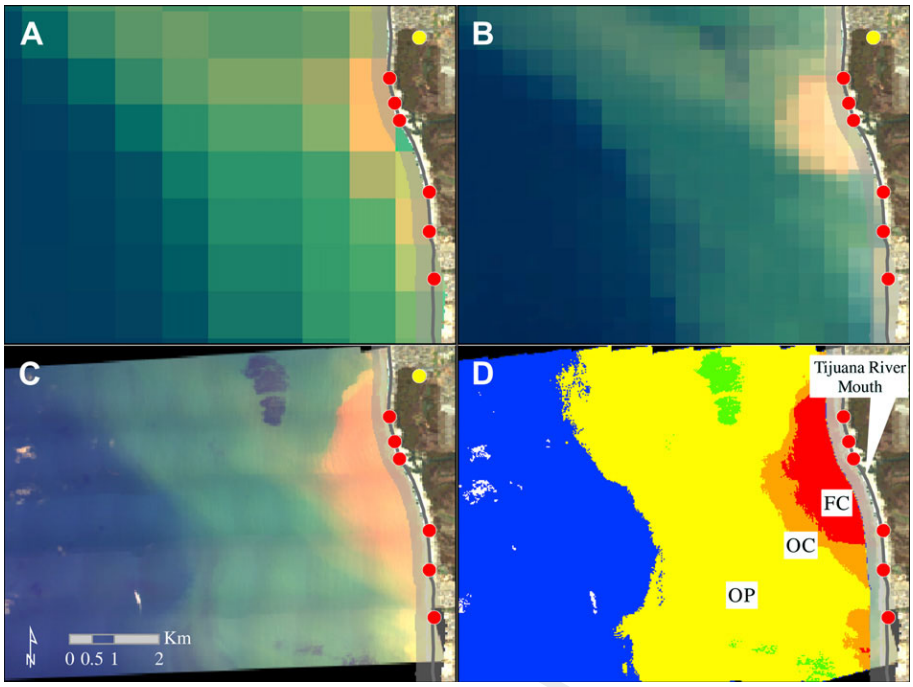

Fig. 2. MODIS 1-km true-color image (A) composed of bands 9 (blue), 12 (green) and 13 (red) and MODIS 500–250-m merge true-color image (B) composed of bands 4 (blue), 3 (green) and 1 (red) of the Tijuana River plume on February 24, 2005. Corresponding DMSC 2.1-m aerial image using 451/551/640-nm channels (C) and plume classification (D). Kelp growth is shown in green, DEH shoreline bacterial sampling locations are shown in red, Tijuana Estuary NERR Meteorological station location is shown in yellow. (For interpretation of the references to colour in this figure legend, the reader is referred to the web version of this article.).

established sampling locations (Figs. 2 and 3) in ankle to knee-deep water, 4–6 inches below the surface (DEH, 2007). The DEH Public Health Laboratory then utilizes the Multiple-tube Fermentation method to detect concentrations of total coliforms, fecal coliforms and enterococci. This method produces results after a 24–96-h incubation period. The DEH also utilizes the Enterolert test method for analyses of enterococci bacteria, which produces results in 24 h. As a beach closure indicator we used the California State Water Board "AB 411 Standards" (State Water Resources Control Board, 2005). The stations were classified as polluted when the FIB counts in single sample were either >10 000 "most probable number" (MPN)/100 mL for total coliforms, >400 MPN/100 mL for fecal coliforms, or >104 MPN/100 mL for enterococci.

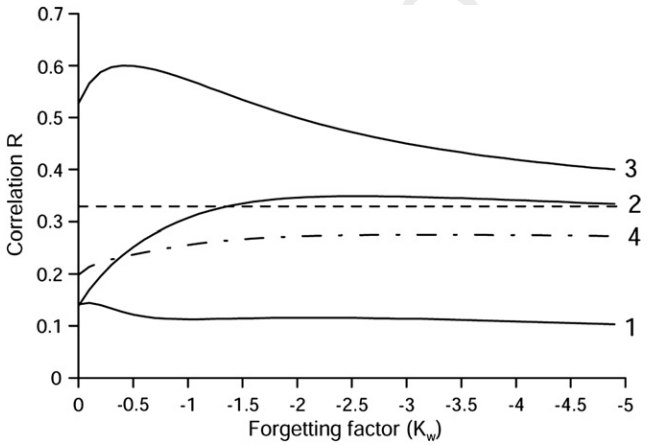

Fig. 3. Correlation between the size of fresh core (1), old core (2) and old plume (3) and wave height effect calculated using different "forgetting factors" (K_w). Dashed-dot curve (4) shows the correlation between the wave height effect and the TJR discharge. Horizontal dashed line indicates the 95% confidence level of correlation coefficient at $n = 36$.

Using each bacterial sample as an indicator of microbial contamination in nearshore waters around its sampling location allowed us to evaluate the contamination characteristics of each effluent plume class in the aerial imagery. To assess the possibility of directly utilizing the classified imagery for predicting beach closure extents around the TJR mouth, we used the following accuracy assessments: total accuracy (the percentage of correctly classified stations); commission error for "polluted" and "clean" stations (the chance to erroneously include a polluted station into the clean class or a clean station into the polluted class) and omission error (the chance to miss including a polluted station in the "polluted" class or miss including a clean station in the clean class) (see details in Congalton and Green, 1999; Lillesand et al., 2004).

4. Results

The 2.1-m resolution aerial imagery provides an important increase in detail over 1-km resolution MODIS or SeaWiFS satellite imagery utilized in previously published studies of runoff plumes in SC and elsewhere. Fig. 2 shows a representative example of the aerial imagery and resulting plume classifications, as well as 1-km and 250-m MODIS image data from the same day. Fig. 2A/B shows color composites of MODIS' 1-km and 500/250-m bands. In Fig. 2B, the 500-m data were "pan sharpened" with the 250-m band in ArcGIS software. This procedure results in the most spatial detail obtainable from MODIS imagery but, as was already mentioned, is difficult to use quantitatively due to difficulties in calibration and image-to-image normalization. The two most significant sources of error in defining the plume boundaries from satellite data are the spatial integration of plume intensities into 1 km (or 500 m) pixels and the contamination of nearshore pixels by land areas partially

Please cite this article in press as: Svejkovsky, J., et al., Tracking stormwater discharge plumes and water quality of the Tijuana River with..., Estuar. Coast. Shelf Sci. (2010), doi:10.1016/j.ecss.2010.01.022

contained in such pixels. The spatial integration effect can erroneously increase or decrease the core plume area. The shoreline contamination effect tends to increase the apparent longshore extents of the plume signatures, makes it difficult to correctly define the plume edges and obscures potentially important intensity variations within the plume in areas closest to shore. In addition to providing significantly increased detail of the plume features, the aerial data also provide greatly increased geolocation accuracy, which is important for spatially comparing field-gathered samples to the plume features.

4.1. Correlation between plume area and daily Tijuana River discharge

The TJR discharge rate (as measured on the day of the image acquisition) was the primary factor affecting the plume's size. TJR discharge explained 50–75% of the size of different parts of the plume (Table 3). Maximum correlation ($R^2 = 0.75$) was observed between the discharge and the size of "fresh plume core" (FC). The FC plume component exhibits a negative linear regression intercept. This can be explained by the buffering effect of the Tijuana Estuary, which can be expected to hold and absorb a portion of the incoming runoff volume. FC discharge was observed only when the TJR discharge rate measured at the TJR entrance into the estuary exceeded 0.30 $m^3\ s^{-1}$ (this value corresponds to 26 million liters per day). It must be noted that these rates represent runoff volume actually entering the estuary. Since the flow diverter above the estuary diverts up to 40 million liters of flow into the IWTP for processing, no flow will enter the estuary at the onset of a rain event until the upstream flow exceeds the diverter capacity. Likewise, subsequent flow into the estuary from upstream is correspondingly decreased by the diverter capacity.

The size of the older portions of the plume (OC and OP) was regulated by processes other than the TJR discharge. The inclusion of OC and OP into the total plume area decreased the correlation with TJR discharge. Adding the older plume components also caused the regression intercept to become positive (i.e. these plume components were observed even during no active TJR discharge). Under no discharge conditions, the plume area covered by the core portions (FC and OC) was 0.35 km^2; while the area of the entire plume (including FC, OC and OP) was significantly larger (5.67 km^2). It thus appears that while the fresh (FC) plume component is directly linked to the TJR discharge, the older portions of the plume are enhanced by other processes such as sediment resuspension in the surf zone and perhaps by tidal ventilation from the estuary.

Including the TJR discharge measured during the day prior to image acquisition did not improve the correlation. The reason was that the correlation between discharge during the day of flight and the previous day discharge was very high ($R^2 = 0.9915$).

4.2. Correlation between plume area and wave height

We found no correlation between the accumulated effect of wave height (E_w; Equation (1)) and the FC plume component (Fig. 3; curve 1). Similarly, the influence of wave height on OC was small (Fig. 3; curve 2). The old (OP) plume component area, however, was highly correlated ($R^2 = 0.3601$) with E_w (Fig. 3; curve 3). Maximum correlation corresponded to the forgetting factor $K_w = 0.4\ day^{-1}$. This corresponds to OP decreasing in size by a factor of 2.71 (i.e. exp (1)) during 2.5 days, i.e. daily decrease of the OP area was by a factor ~0.67. We interpret these results as indicating that a large part of the OP area resulted from wave-caused sediment resuspension, lasting a relatively short time.

Since storms are generally associated with both large waves and rainfall, it could be argued that the correlation between TJR overall plume size and wave height was fully or partially due to large river discharges occurring simultaneously with large wave conditions. To check this hypothesis, we utilized the same correlation methodology to compare wave height to TJR discharge. The correlation was small and insignificant (Fig. 3; curve 4).

4.3. Correlation between plume area and tidal circulation

The correlation between tidal effect (E_t; Equation (2)) and plume size was much lower than the effect of waves. Only for FC and OC the correlation coefficients were close to 90% confidence level (Fig. 4). The forgetting factor (K_t) resulting in maximum correlation was 0.3 day^{-1} for FC and 0.8 day^{-1} for OC. This implies that the fresh portion of the plume was more persistent than the old portion; FC decreased in size by a factor of 2.71 during 3.33 days and OC during 1.11 days (the first value was comparable to the forgetting factor for wave height effect K_w). The influence of tides on OC and FC was small (R^2 was 0.072 and 0.059, respectively). We conclude that only 6–7% of the plume core area can be explained by tidal effects.

4.4. Alongshore plume distribution

TJR plume alongshore extension was proportional to its area. The plume extended more to the south than to the north or offshore. This conclusion is based on the linear relationship (with zero intercept) between the plume area (S) and the plume extension to the north (E_n) and south (E_s) using the equation $E = A \times \mathrm{sqrt}(S)$, where A is a coefficient (Table 4). The coefficients characterizing the relationship between the plume area and the plume extension to the south were larger than to the north, indicating southward plume propagation. For the total plume area (FC + OC + OP) these coefficients were apparently underestimated, because the old portion of the plume extended beyond the image limits in about

Table 3
Linear regression statistics between TJR discharge ($m^3\ s^{-1}$) and the size (m^2) of plume including the classes: fresh core (FC), old core (OC), and old plume (OP). All regression equations were statistically significant ($P < 0.001$).

Plume classes	R^2	Slope	Intercept
FC	0.748	3.70×10^5	-1.13×10^5
FC + OC	0.586	9.27×10^5	$+3.07 \times 10^5$
FC + OC + OP	0.503	32.6×10^5	$+53.9 \times 10^5$

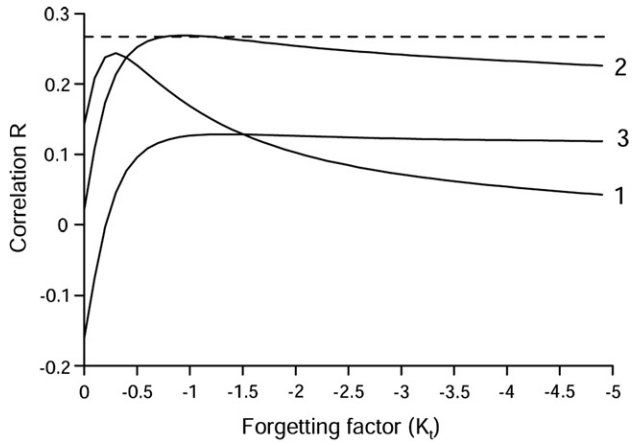

Fig. 4. Correlation between the size of fresh core (1), old core (2) and old plume (3) and tidal effect calculated using different "forgetting factors" (K_t). Horizontal dashed line indicates the 90% confidence level of correlation coefficient at $n = 39$.

Table 4
Linear (with zero intercept) regression between the square function of the plume size and plume extension to the north (N) and to the south (S). Plume classes: fresh core (FC), old core (OC) and old plume (OP). Statistics: slope (A), coefficient of determination (R^2), number of observations (n).

Plume classes	Direction	A	R^2	n
FC	N	0.767	0.696	37
	S	1.220	0.856	39
FC + OC	N	0.901	0.614	39
	S	1.086	0.801	38
FC + OC + OP	N	0.920	0.794	39
	S	1.055	0.786	39
FP + OC + OP after excluding observations exceeding the image coverage	N	1.636	0.840	19
	S	1.426	0.560	18

one-half of the data sets. After exclusion of these observations, the coefficients A increased. Assuming the hypothesis that the plume tends to extend equally in all directions, we expect the plume shape to be a half-circle with radius E and area S; as such, the coefficient $A = \text{sqrt}\,(2/\pi) = \sim 0.8$. The observed coefficients A for northward (E_n) plume distribution were close to this expected value. For southward plume distribution (E_s), the observed coefficients A were higher than expected, indicating that the TJR plume tended to be retained in the nearshore zone to the south from the TJR mouth rather than propagating offshore.

To investigate a possible relationship between the plume's alongshore propagation and wave direction, we utilized wave direction measurements at the NDBC buoy 46086, averaged over 6 h prior to image acquisition. Because the buoy is located approximately 80 km offshore from the TJR mouth, it was important to verify that the directions measured at the offshore locations corresponded to subsequent wave fields affecting the TJR plume. Since many of the high resolution aerial image sets directly revealed wave signatures, we compared the image-observed wave directions with wave directions measured at the buoy. Because some images provided clearer wave signatures than others (likely related to wave height) the image-derived observations were graded on a confidence of 0–4 (0 = low, 4 = high). The comparison results are shown in Fig. 5. We conclude that there is good correspondence between the 6-h mean wave direction measured at the buoy and subsequent wave direction observed directly from the imagery ($R^2 = 0.988$), especially when the accuracy confidence of the direct observations was high.

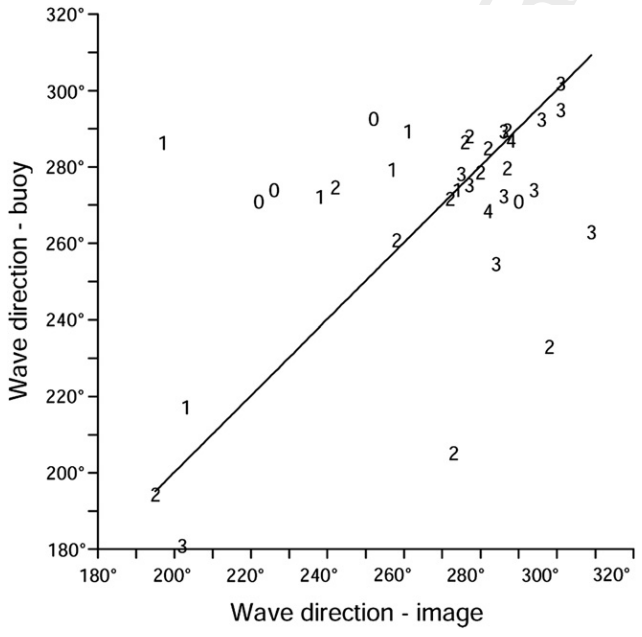

Fig. 5. Correlation between the wave direction measured at the offshore buoy and the wave direction estimated from the image. The numbers (0–4) indicate the quality (accuracy) of the wave direction estimated from the imagery (0–low; 4–high).

Using the buoy-derived wave direction, we examined its potential effect on alongshore (i.e. north-south) distribution of the TJR plume. Because the OP area extended past the imaged area boundaries in a large number of the available images, we only addressed distribution of the plume's core components (FC and OC combined). 14 images containing FC and/or OC signatures were available for analysis. We found that the core components exhibit influence of wave direction (Fig. 6). Waves from the northwest corresponded to longer southward extensions of the plume's core areas, while waves traveling from a southwestern direction generally corresponded to the plume's core being more northward directed. Waves directed from a westerly direction (i.e. more perpendicular to the coast) corresponded to the plume's core being more evenly distributed in both directions around the river mouth. The most common wave direction affecting the TJR shoreline is between approximately 275° and 290°, i.e. from the west-northwest, corresponding to the plume's core area most commonly having a southward distribution bias.

We also examined the relationship between wind direction and the plume's core components alongshore distribution. Winds from the Tijuana Estuary station exhibit a persistent diurnal pattern: during the night they are relatively light (<1 m/s) and easterly, corresponding to a "land breeze". After sunrise, between approximately 8 and 11 local time, they reverse direction and simultaneously increase in velocity, corresponding to a characteristic daytime "sea breeze". The winds revert back to a land breeze after sundown. The same diurnal cycle is also apparent in wind data from Lindbergh Field Airport, 19.5 km north of the estuary. The diurnal effect is not apparent, however, in wind records from the offshore buoy 46086. There is also a directional difference between winds at the shoreline stations and winds at the offshore buoy: the dominant wind direction for the 39 days with an available imagery was northwesterly at the buoy but southwesterly to westerly at the Tijuana Estuary station and at Lindbergh Field. Fig. 7 shows the relation between wind directions

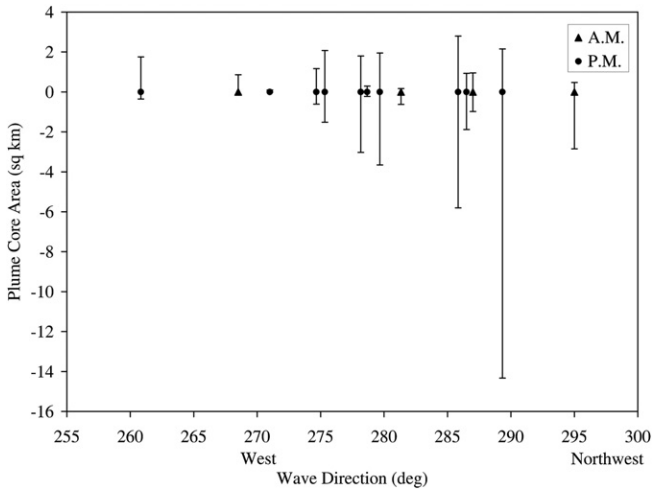

Fig. 6. Area of FC and OC plume components (km^2) to the north (positive) and to the south (negative) related to wave direction measured at NDBC buoy 46086 (averaged over 6 h prior to image acquisition). AM/PM refers to time of day when the imagery was acquired.

Please cite this article in press as: Svejkovsky, J., et al., Tracking stormwater discharge plumes and water quality of the Tijuana River with..., Estuar. Coast. Shelf Sci. (2010), doi:10.1016/j.ecss.2010.01.022

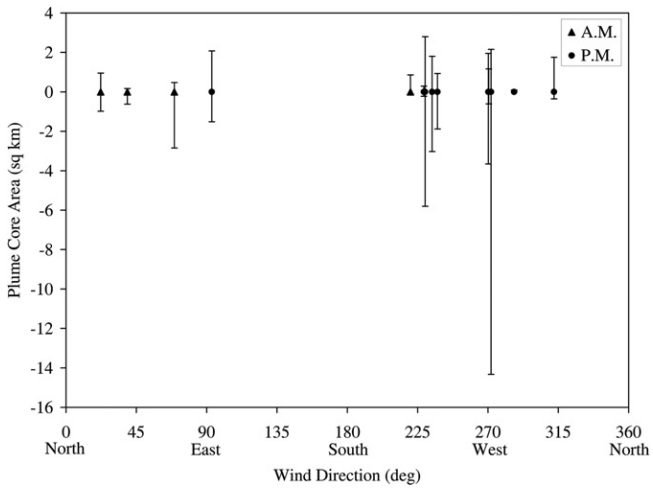

Fig. 7. Area of FC and OC plume components (km^2) to the north (positive) and to the south (negative) Related to wind direction measured at the Tijuana Estuary NERR (averaged over 4 h prior to image acquisition). AM/PM refers to time of day when the imagery was acquired.

and alongshore plume core distribution. The wind values represent 4 h averages prior to the time of each image. This time interval was chosen because longer time intervals for the afternoon image acquisitions would span through the diurnal direction (and velocity) shift and thus distort the true wind direction of the stronger daytime winds. Images acquired in the morning hours generally correspond to easterly winds but do not show a clear directional bias in plume direction. During the daytime sea breeze phase the plume area distribution also has no correspondence to the wind direction. The correlation results between plume distribution (as represented by percentage of total core area directed southward of the river mouth), and wave and wind direction are shown in Fig. 8. As was already noted, there is good correlation of the alongshore plume distribution with wave direction but no significant correlation with wind direction as measured by the nearby Tijuana Estuary sampling station.

Fig. 9 shows two examples when the wave and wind fields existing before the image acquisition were in opposing directions. In each case the core plume components were strongly directed upcoast or downcoast corresponding to the direction of the wave field and opposite to the wind.

We also considered utilizing High-Frequency (HF) Radar surface current data from the San Diego Ocean Observing System (SDCOOS) to assess the influence of surface currents on the plume dynamics. However, the unavailability of the data in digital format as well as the generally recognized limitation of HF radar-derived current accuracies very close to shore made us forego analysis of the imaged plume patterns relative to HF radar data.

4.5. TJR plume extents and shoreline bacterial pollution

The concentrations of indicator bacteria were highest in the FC plume area and gradually decreased with the age of plume components (Fig. 10). The shoreline areas encompassed in the plume core classes tended to have significantly increased bacteria concentrations, with the FC area always exceeding AB 411 standards (Table 5). The OP region showed much grater variability but tends to contain lower bacteria concentrations than the core areas, especially enterococci. Ocean waters classified as non-plume exhibited the lowest overall bacteria concentrations.

The accuracy of bacterial pollution detection using plume characteristics (Table 6) illustrates significant but loose correlation between plume optical characteristics and bacterial counts. The accuracy and error statistics were estimated on the basis of different combinations of plume classes derived from the aerial imagery (FC only, FC + OC, etc.) as "predicted" values versus shoreline bacterial sample counts as "observed" values. It is evident from these statistics, that a beach closure along the beach section in contact with the plume's FC component would never cause an unnecessary closure (0% commission error) because all samples within FC exceed California standards. Not including other, older portions of the plume in the closure boundary, however, results in 81.5% omission of polluted sample locations and is thus inadequate in minimizing public health risk. Conversely, including the entire plume area in the closure boundary results in only 3.3% omission of polluted waters (only 3 out of 92 shoreline samples were located

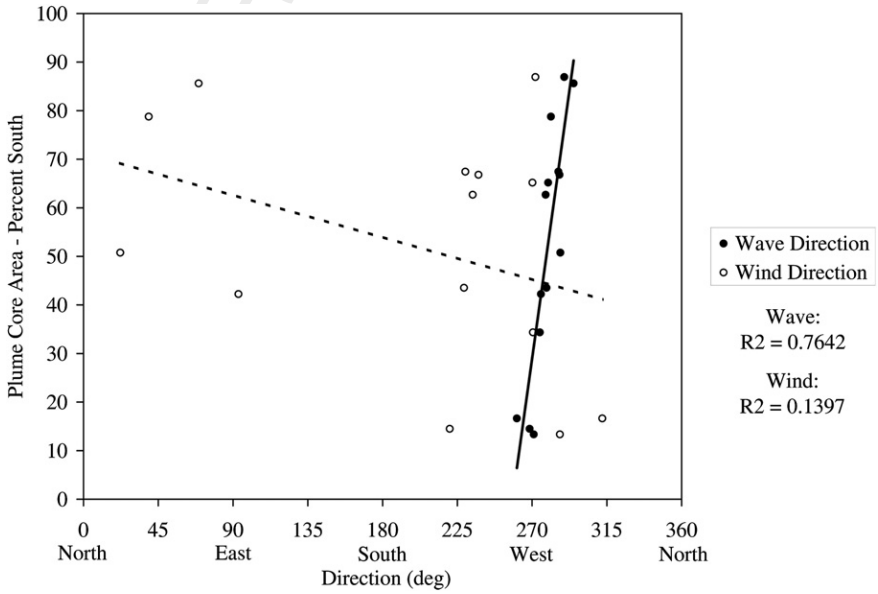

Fig. 8. Correlation between the alongshore plume distribution and wind and wave direction.

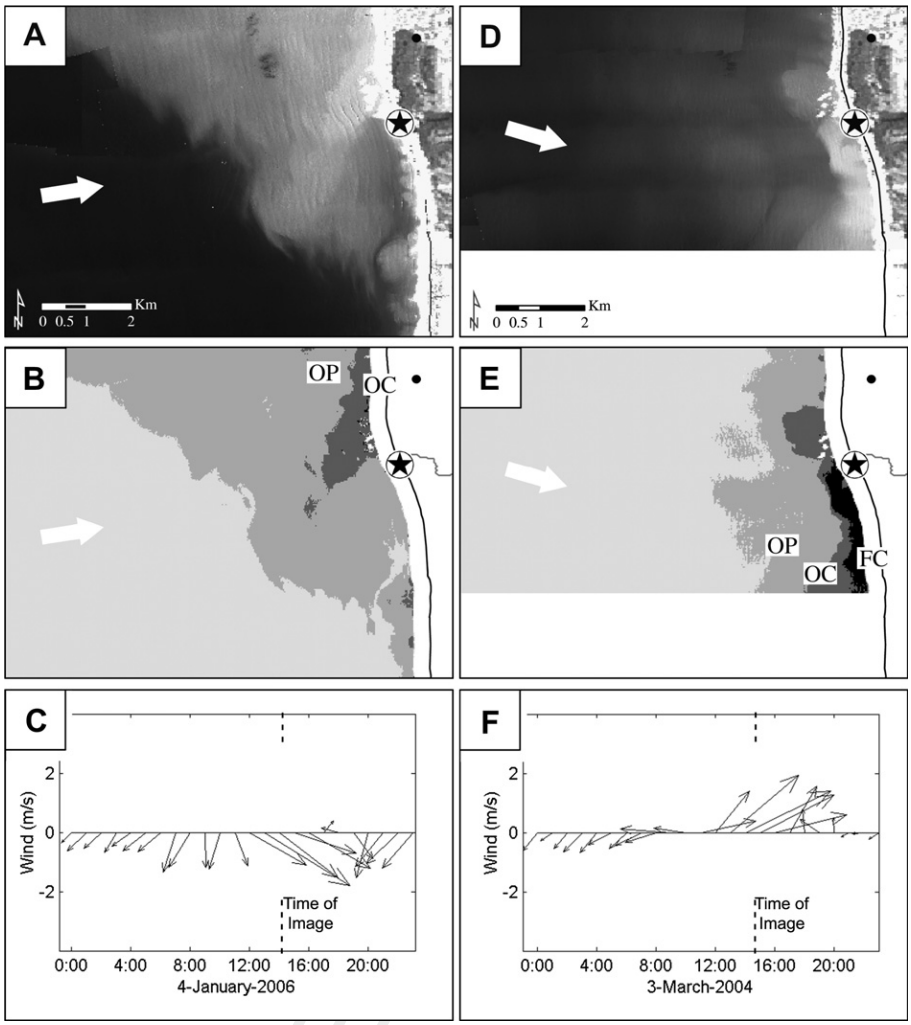

Fig. 9. Plume distribution, wave direction (6 h average) and hourly wind vectors on January 4, 2006 (A–C) and March 3, 2004 (D–F). Plume is shown as a grey-scale rendition of 451/551/640-nm composite image (A, D), and as classified into plume classes (B, E). Arrows at A, B, D, E indicate wave direction. Star symbol indicates TJR mouth and black dot shows location of Tijuana Estuary NERR wind measurement station. The bottom panels (D, F) show the diurnal variations of hourly wind velocity and direction, and the time of image acquisition.

outside the total plume area). This option, however, also results in 61.6% omission of unpolluted areas, i.e. a >60% overextension of necessary closure boundaries. Including only the two plume core classes to guide closure boundaries results in commission and omission errors between the two extremes.

5. Discussion

Different portions of the TJR plume, which we believe are related to different ages since discharge were accurately separated and mapped with the airborne imagery based on their spectral reflectance differences. Size of the most recently discharged effluent component within the TJR plume (FC) resulted directly from the TJR discharge volume, while the size of the "older" portions of the plume (OC and OP) was also regulated by factors other than the TJR freshwater flow, primarily wave resuspension. The different spectral reflectance properties of the "older" plume portions indicated lower concentrations of suspended sediment in those waters. Previous field studies of stormwater runoff plumes from rivers in southern California have shown that a large percentage of the initial suspended sediment load entering the ocean is quite rapidly precipitated out of the plume (Warrick and Milliman, 2003; Warrick et al., 2004a,b). The precipitation process alters the particle composition and size characteristics of the plume waters as they disperse from the river outlet. The gradual precipitation in turn alters the effluent's spectral reflectance characteristics which are apparent in our imagery. We therefore believe that the defined classes within the TJR plume reflect the relative age of each plume section. From multiple sequential flight observations we estimate the FC and OC portions represent effluent reaching the ocean within the past 12–36 h, while the effluent within the OP component is likely a combination of >2-day-old TJR discharge and sediments resuspended by surf waves.

The relationship between the plume area and the alongshore plume extension indicates that the plume tends to be retained in the nearshore zone, most commonly downcoast, rather than propagating offshore. This observation is in agreement with Warrick et al.'s (2007) observations of Southern California river plumes with satellite imagery.

Wave direction affected the shorelong distribution of the plume's core components. The possible influence of waves on the shorelong transport of river plumes has generally not been investigated in previous studies. It is recognized that along the SC coastline waves approaching the shore from the west or northwest are likely to yield down-coast surf zone currents, while waves from the south or southwest are likely to yield up-coast surf zone

Please cite this article in press as: Svejkovsky, J., et al., Tracking stormwater discharge plumes and water quality of the Tijuana River with..., Estuar. Coast. Shelf Sci. (2010), doi:10.1016/j.ecss.2010.01.022

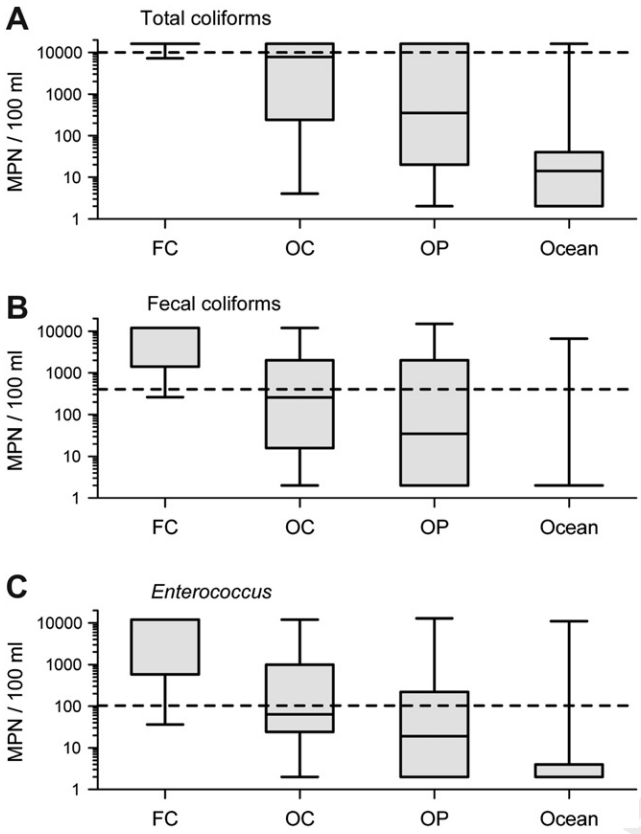

Fig. 10. Bacterial contamination at the surf zone sampling stations associated with the different plume classes. Box-whisker plots show medians, first and third quartiles, minima and maxima of total coliforms (A), fecal coliforms (B), and *Enterococcus* (C) in the fresh core (FC), old core (OC), old plume (OP), and ocean. Dashed lines indicate the California State Water Board "AB 411 Standards" exceedance limits.

currents (Inman and Brush, 1973; Kim et al., 2004). Studies of salinity and fecal indicator bacteria concentrations in runoff effluent from the Santa Ana River in SC indicated that contaminants tend to be transported parallel to shore by wave-driven currents (Ahn et al., 2005). This corresponds with our findings that the upcoast/downcoast distribution of the FC and OC plume components, which exhibit the highest bacteria concentrations and usually encompass the surf zone, correlate well with wave direction. In the TJR case, the wave influence is likely further enhanced by the shallow alluvial fan topography in front of the TJR mouth (Inman and Brush, 1973).

We found no correlation between wind direction and plume core alongshore distribution. This finding may appear inconsistent with earlier studies of river runoff plumes that identified wind forcing as the dominant plume-driving factor. For example, Walker et al. (2005) found the Mississippi River's plume to be very responsive to wind direction, and to reverse direction around the river delta rapidly upon the passage of wind-reversing cold fronts. Warrick et al. (2007), studied several SC river stormwater plumes and found that subsequent to the initial discharge momentum, the plumes' advection was dominated by winds. Pinones et al. (2005) linked alongshore river plume motion to wind-induced diurnal variability through salinity variations at a coastal station. These and other studies linking river plume distribution to wind forcing defined the runoff plume based on field sample grids extending out several kilometers from shore, and also utilized AVHRR, SeaWiFS or MODIS satellite imagery to visualize the plume patterns. We believe the lack of wind forcing influence in our observations is due

Table 5
Contingency table between the number of stations exceeding California water quality standards and the plume classes: fresh core (FC), old core (OC) and old plume (OP).

	Predicted (based on aerial imagery)				
	(1)	(2)	(3)	(4)	(5)
Observed (based on bacterial samples)	No plume	OP	OC	FC	Total
Polluted (exceeding CA standards)	3	49	23	17	92
Clean (not exceeding CA standards)	56	71	19	0	146
Total	59	120	42	17	238

to the size difference and nearshore location of the features studied. In the previous investigations "plume signatures" in the satellite imagery were identified as the total area of distinctly elevated turbidity – i.e. the entire area encompassed by FC, OC and OP classes in our aerial imagery. No effort was made to further subdivide the overall turbid region into sub-plume components. The overall plume signatures are commonly 10–50+ km in length and extend 5–10+ km offshore. Additionally, after major storms, turbidity signatures from multiple nearby point sources tend to be inseparable in the coarse resolution satellite imagery, thus enhancing the overall size of the "plume" feature. In contrast, the plume core signatures of the TJR plume in the high resolution aerial imagery that we examined with respect to wind and wave direction rarely extended offshore past 500–700 m and were anchored to the shore through the surf zone. Unlike the older (OP), more offshore-distributed plume areas, the plume core components were restricted to much shallower waters near the surf zone where wave energy can be expected to have more significant directional effects.

The diurnal cycle of winds at the river mouth versus the absence of this effect further offshore (as shown by wind fields at the NDBC buoy) should also be considered. The very light easterly winds during evening, nighttime, and early morning hours can be expected to have minimal effect on transport of the plume waters. Since we found that only 6–7% of the plume core area could be explained by tidal forcing, the dominant forces on the core plume's alongshore distribution during the land breeze hours are waves and, potentially, Coriolis accelerations which would cause an upcoast bias. This bias is not apparent in the 4 morning image acquisitions available for analysis of the plume core although, obviously, the small sample size is not sufficient to make firm conclusions about the Coriolis influence. The Tijuana Estuary station data show sea breeze conditions with increased wind speeds to span 4–6 h during the day. This contrasts markedly with wind profiles from the NDBC buoy offshore where the diurnal effects are not apparent and the wind field is usually stronger and much more persistent in speed and often in direction. Therefore, unlike the shore-anchored plume core components, the outer,

Table 6
Accuracy and error assessments of classification of coastal stations as "polluted" and "clean" on the basis of aerial imagery (Table 5). Plume classes: fresh core (FC), old core (OC) and old plume (OP). The statistics in row #1 (FC) were calculated assuming that only the plume class FC (column 4 in Table 5) was polluted and other classes ("No plume", OP and OC; columns 1–3 in Table 5) were clean. In row #2 (FC + OC) the plume classes FC and OC (columns 3–4 in Table 5) were considered polluted and two other classes (columns 1–2 in Table 5) were treated as clean. In row #3 (FC + OC + OP) all three plume classes (columns 2–4 in Table 5) were considered polluted and only the "No plume" class (column 1 in Table 5) was treated as clean.

Row #	Plume classes	Total accuracy (%)	Commission error (%)		Omission error (%)	
			Polluted	Clean	Polluted	Clean
1	FC	68.5	0	33.9	81.5	0
2	FC + OC	70.2	32.2	29.1	56.5	13.0
3	FC + OC + OP	60.9	50.3	5.1	3.3	61.6

older portions of the river plumes are subject to stronger and more persistent wind forcing which, as previous studies have shown, correlate well with wind direction.

The spatial detail in plume intensity and extents available from the aerial imagery is especially relevant in comparing the remotely sensed plume patterns and field-sampled bacteria concentrations. This also allows us to evaluate the possibility of utilizing high resolution aerial imagery for beach closure management, potentially in lieu of shoreline bacterial sampling. While the correlation in shoreline areas affected by the freshest effluent discharges is strong, the accuracy of predicting bacterial contamination from the imagery within the older portion of the plume is not very high. Our statistical results should be analyzed with several important considerations. First, the DEH sampled the shoreline stations approximately every 3 days, with daily sampling done at some stations on occasion. Although some of our aerial imagery was acquired on the same day as the field samples were collected, some of the data pairs available for analysis had an imaging-to-field sampling time difference of up to ±54 h. We limited the analysis to data pairs that had a time difference of <48 h. We also discarded data pairs when a rain event occurred within its time interval, i.e. when one variable was sampled before the rain and the other after the rain impact. Nevertheless, the sample time interval inherent in a number of the data pairs can be expected to negatively affect any correlations because the TJR plume extents and/or class component distributions may have been somewhat different at the time of the bacterial sampling. Second, indicator bacteria distributions in nearshore waters have been shown to be patchy (e.g., Boehm and Weisberg, 2005; Rosenfeld et al., 2006) and subject to dilution by rip cell currents (Ahn et al., 2005). Such conditions are not expected to greatly affect the outcome of sampling within the plume's fresh areas where the effluent is greatly concentrated and sample results always exceed maximum possible measurement. In the older, more spread-out and diluted parts of the plume obscured by sediment resuspension, however, spatial heterogeneity in bacteria concentrations could affect the correlation outcomes.

The results indicate that the greatest variability and hence error contribution is found in the old (OP) portion of the plume which may be relatively unpolluted in some instances but heavily polluted in others. There are several plausible explanations for this in addition to the temporal field sampling versus image acquisition differences. As we already noted, it appears that significant portions of the OP area are the result of particle resuspension which may extend the OP area in both time and space without direct effluent input from the river itself. This could result in relatively low bacteria concentrations within the OP extents. Since the OP plume portion is the oldest, bacteria in those waters have had the longest residency time in the ocean. Their concentration is expected to decrease with time due to die-off (Davies-Colley et al., 1994), and dilution and sedimentation (Kim et al., 2004). As was already mentioned, these processes favor patchy distribution and hence higher sampling variability. There are also processes that can cause anomalous or temporary increases in bacteria concentrations and thus contribute to the high variability within the OP section. For example, small contaminated runoff sources not associated with the TJR and not identifiable in the imagery can cause localized spikes in bacteria counts within the OP extents. This is especially relevant in the Playas de Tijuana area to the south and southern Coronado shores to the north, where single sampling station exceedances sometimes occur even when there is no outflow from the TJR. Another phenomenon that appears to cause exceedance bacterial concentrations in the OP section is the aforementioned "First Flush Effect". For example, imagery acquired on October 18, 2006 after the first significant rainstorm of the season showed only minimal discharge from the TJR whose spectral characteristics made it fall into the OP category. Shoreline samples taken on October 17–18 measured total coliform concentrations above the measurement limit at all stations up to 3400 m away from the river mouth. It cannot be ascertained if the microorganisms actually entered the ocean through the river effluent or were the result of the First Flush Effect in runoff directly from the surrounding beaches.

While previous studies in different world regions established wind forcing as the most common transport mechanism affecting the overall river plume patterns, our results show that, at least in the Tijuana River case, wave field direction is the most influential factor affecting the alongshore propagation of the freshest and most concentrated runoff effluent that pose the greatest public health hazard. This conclusion is likely applicable to other areas, as exemplified by Ahn et al.'s (2005) findings at the Santa Ana River where, during a field sampling effort, MODIS imagery showed the overall plume signature to be directed downcoast but the transport direction of fecal indicator bacteria in the surf zone was directed upcoast, in agreement with the existing wave field from the south.

The freshly discharged, most polluted plume waters can be readily identified and tracked in the aerial imagery, suggesting the possibility of utilizing such image data for setting beach closure boundaries to minimize public health risks. As was already noted, limiting the beach closures only to the FC and OC signature areas will result in few, if any, unnecessary closures. This strategy would be rarely adequate, however, since standard-exceeding indicator bacteria concentrations are very often found in the surf zone past the plume core boundaries. The alternate strategy – to close the entire beach zone impacted by FC, OC and OP signatures could, based on data available for our study, be a prudent choice if minimizing health risk is of prime importance and no other bacteriological data are available (only 3.3% of standard-exceeding samples were located outside the total plume boundary). Our analysis shows, however, that this strategy would likely result in significant (62% for the TJR data) overextension of the beach closure boundaries. Since beach closures can result in significant socioeconomic impacts for the affected regions (King, 1999) the desired strategy is to limit their extents as much as possible. The sole utilization of aerial remote sensing (or high resolution satellite imagery) for beach closure management thus carries important limitations and compromises. In areas where no field measurements are available, however, high resolution multispectral imaging could provide useful information for decreasing public health risk exposure to polluted runoff plumes.

Acknowledgements

We thank the International Boundary Waters Commission for TJR flow rates data, the National Data Buoy Center for wind and wave data, the Center for Operational Oceanographic Products and Services for tidal level data, and Clay Cliffton of the San Diego County Department of Environmental Health for bacterial pollution data. We also thank Dr. Steve Weisberg and two anonymous reviewers for their helpful comments on the manuscript. The aerial image acquisitions were co-funded by the City of San Diego, the International Boundary Waters Commission and the California State Water Resources Control Board. This study was supported by the City of San Diego Metropolitan Wastewater Department.

References

Ahn, J.H., Grant, S.B., Surbeck, C.Q., DiGiacomo, P.M., Nezlin, N.P., Jiang, S., 2005. Coastal water quality impact of stormwater runoff from an urban watershed in southern California. Environmental Science and Technology 39, 5940–5953.

Ben-Dor, E., Kruse, F.A., Lefkoff, A.B., Banin, A., 1994. Comparison of 3 calibration techniques for utilisation of GER 63-channel aircraft scanner data of Makhtesh-

Ramon, Negev, Israel. Photogrammetric Engineering and Remote Sensing 60, 1339–1354.

Bertrand-Krajewski, J.-L., Chebbo, G., Saget, A., 1998. Distribution of pollutant mass vs volume in stormwater discharges and the first flush phenomenon. Water Research 32, 2341–2356.

Boehm, A.B., Weisberg, S.B., 2005. Tidal forcing of enterococci at marine recreational beaches at fortnightly and semidiurnal frequencies. Environmental Science and Technology 39, 5575–5583.

Congalton, R.G., Green, K., 1999. Assessing the Accuracy of Remotely Sensed Data: Principles and Practices. Lewis Publishers, Boca Raton, p. 137.

Cristina, C.M., Sansalone, J.J., 2003. First flush, power law and particle separation diagrams for urban storm-water suspended particulates. Journal of Environmental Engineering-ASCE 129, 298–307.

Davies-Colley, R.J., Bell, R.G., Donnison, A.M., 1994. Sunlight inactivation of enterococci and fecal coliforms in sewage effluent diluted in seawater. Applied and Environmental Microbiology 60, 2049–2058.

da Silva, J.F., Duck, R.W., Hopkins, T.S., Anderson, J.M., 2002. Nearshore circulation revealed by wastewater discharge from a submarine outfall, Aveiro Coast, Portugal. Hydrology and Earth System Sciences 6, 983–988.

DEH, 2007. San Diego County 2006 Beach Closure and Advisory Report. County of San Diego Department of Environmental Health, Land and Water Quality Division, San Diego, 25 pp., available online at. http://www.co.san-diego.ca.us/deh/water/docs/bb_2006_bcr_summary.pdf.

Dwyer, J.L., Kruse, F.A., Lefkoff, A.B., 1995. Effects of empirical versus model based reflectance calibration on automated analysis of imaging spectrometer data: a case study from Drum Mountains, Utah. Photogrammetric Engineering and Remote Sensing 61, 1247–1254.

Englert, P.F., 1997. Characterizing Urban Storm Pollution in the Tijuana River Watershed. San Diego State University, 206 pp.

Gersberg, R., Tiedge, J., Gottstein, D., Altmann, S., Watanabe, K., Luderitz, V., 2008. Effect of the South Bay Ocean Outfall (SBOO) on ocean beach water quality near the USA-Mexico border. International Journal of Environmental Health Research 18, 149–158.

Gersberg, R.M., Daft, D., Yorkey, D., 2004. Temporal pattern of toxicity in runoff from the Tijuana River Watershed. Water Research 38, 559–568.

Gersberg, R.M., Rose, M.A., Robles-Sikisaka, R., Dhar, A.K., 2006. Quantitative detection of hepatitis a virus and enteroviruses near the United States-Mexico border and correlation with levels of fecal indicator bacteria. Applied and Environmental Microbiology 72, 7438–7444.

Inman, D.L., Brush, B.M., 1973. Coastal challenge. Science 181, 20–32.

Inman, D.L., Jenkins, S.A., 1999. Climate change and the episodicity of sediment flux of small California rivers. Journal of Geology 107, 251–270.

Jorgensen, P.V., Edelvang, K., 2000. CASI data utilized for mapping suspended matter concentrations in sediment plumes and verification of 2-D hydrodynamic modelling. International Journal of Remote Sensing 21, 2247–2258.

Kim, J.H., Grant, S.B., McGee, C.D., Sanders, B.F., Largier, J.L., 2004. Locating sources of surf zone pollution: a mass budget analysis of fecal indicator bacteria at Huntington Beach, California. Environmental Science and Technology 38, 2626–2636.

King, P., 1999. The Fiscal Impact of Beaches in Southern California. Final Report for California Department of Boating and Waterways. Public Research Institute, San Francisco State University, San Francisco, 29 pp., available online at. Q3

Lawless, K.P., Milton, E.J., Anger, C.O., 1998. Investigation of changes in the reflectance of ground calibration targets (asphalt and concrete), information for sustainability. In: 27th International Symposium on Remote Sensing of Environment. ERIM, Ann Arbor, Michigan, pp. 597–600.

Lillesand, T.M., Kiefer, R.W., Chipman, J.W., 2004. Remote Sensing and Image Interpretation, fifth ed. John Wiley & Sons, New York, 763 pp.

Lira, J., Morales, A., Zamora, F., 1997. Study of sediment distribution in the area of the Panuco river plume by means of remote sensing. International Journal of Remote Sensing 18, 171–182.

Miller, R.L., McKee, B.A., 2004. Using MODIS Terra 250 m imagery to map concentrations of total suspended matter in coastal waters. Remote Sensing of Environment 93, 259–266.

Nezlin, N.P., DiGiacomo, P.M., 2005. Satellite ocean color observations of stormwater runoff plumes along the San Pedro Shelf (southern California) during 1997–2003. Continental Shelf Research 25, 1692–1711.

Nezlin, N.P., Weisberg, S.B., Diehl, D.W., 2007. Relative availability of satellite imagery and ship-based sampling for assessment of stormwater runoff plumes in coastal southern California. Estuarine, Coastal and Shelf Science 71, 250–258.

Nezlin, N.P., DiGiacomo, P.M., Stein, E.D., Ackerman, D., 2005. Stormwater runoff plumes observed by SeaWiFS radiometer in the Southern California Bight. Remote Sensing of Environment 98, 494–510.

Nezlin, N.P., DiGiacomo, P.M., Diehl, D.W., Jones, B.H., Johnson, S.C., Mengel, M.J., Reifel, K.M., Warrick, J.A., Wang, M., 2008. Stormwater plume detection by MODIS imagery in the southern California coastal ocean. Estuarine, Coastal and Shelf Science 80, 141–152.

Ouillon, S., Forget, P., Froidefond, J.-M., Naudin, J.-J., 1997. Estimating suspended matter concentrations from SPOT data and from field measurements in the Rhone river plume. Marine Technology Society Journal 31, 15–20.

Pinones, A., Valle-Levinson, A., Narvaez, D.A., Vargas, C.A., Navarrete, S.A., Yuras, G., Castilla, J.C., 2005. Wind-induced diurnal variability in river plume motion. Estuarine, Coastal and Shelf Science 65, 513–525.

Prangsma, G.J., Roozekrans, J.N., 1989. Using NOAA AVHRR imagery in assessing water-quality parameters. International Journal of Remote Sensing 10, 811–818.

Rosenfeld, L.K., McGee, C.D., Robertson, G.L., Noble, M.A., Jones, B.H., 2006. Temporal and spatial variability of fecal indicator bacteria in the surf zone off Huntington Beach, CA. Marine Environmental Research 61, 471–493.

Ruffin, K.K., 1998. The persistence of anthropogenic turbidity plumes in a shallow water estuary. Estuarine, Coastal and Shelf Science 47, 579–592.

SCCWRP, 1992. Surface runoff to the southern California Bight. In: Cross, J.N., Francisco, C. (Eds.), SCCWRP Annual Report 1990–1991 and 1991–1992. Southern California Coastal Water Research Project Authority, Long Beach, pp. 19–28.

Schott, J.R., Salvaggio, C., Volchok, W.J., 1988. Radiometric scene normalization using pseudoinvariant features. Remote Sensing of Environment 26, 1–16.

Shutler, J.D., Land, P.E., Smyth, T.J., Groom, S.B., 2007. Extending the MODIS 1 km ocean colour atmospheric correction to the MODIS 500 m bands and 500 m chlorophyll-*a* estimation towards coastal and estuarine monitoring. Remote Sensing of Environment 107, 521–532.

St John, M.A., Pond, S., 1992. Tidal plume generation around a promontory: effects on nutrient concentration and primary productivity. Continental Shelf Research 12, 339–354.

Staenz, K., Itten, K.I., 1982. Reflective properties of asphalt and concrete surfaces. In: International Symposium of the ISPRS, vol. WG-VII. Toulouse, France, pp. 307–316.

State Water Resources Control Board, 2005. California Ocean Plan, 57 pp.

Stumpf, R.P., Goldschmidt, P.M., 1992. Remote sensing of suspended sediment discharge into the western Gulf of Maine during the April 1987 100-year flood. Journal of Coastal Research 8, 218–225.

Stumpf, R.P., Gelfenbaum, G., Pennock, J.R., 1993. Wind and tidal forcing of a buoyant plume, Mobile Bay, Alabama. Continental Shelf Research 13, 1281–1301.

Svejkovsky, J., Jones, B.H., 2001. Satellite imagery detects coastal stormwater and sewage runoff. Eos 82, 621–630.

Tiefenthaler, L.L., Schiff, K.C., 2003. Effects of rainfall intensity and duration on first flush of stormwater pollutants. In: Weisberg, S.B., Elmore, D. (Eds.), Southern California Coastal Water Research Project Annual Report 2001–2002. Southern California Coastal Water Research Project Authority, Westminster, CA, pp. 209–215.

Walker, N.D., Wiseman Jr., W.J., Rouse Jr., L.J., Babin, A., 2005. Effects of river discharge, wind stress, and slope eddies on circulation and the satellite-observed structure of the Mississippi River plume. Journal of Coastal Research 21, 1228–1244.

Warrick, J.A., Milliman, J.D., 2003. Hyperpycnal sediment discharge from semiarid southern California rivers: implications for coastal sediment budgets. Geology 31, 781–784.

Warrick, J.A., Mertes, L.A.K., Washburn, L., Siegel, D.A., 2004a. Dispersal forcing of southern California river plumes, based on field and remote sensing observations. Geo-Marine Letters 24, 46–52.

Warrick, J.A., Mertes, L.A.K., Washburn, L., Siegel, D.A., 2004b. A conceptual model for river water and sediment dispersal in the Santa Barbara Channel, California. Continental Shelf Research 24, 2029–2043.

Warrick, J.A., DiGiacomo, P.M., Weisberg, S.B., Nezlin, N.P., Mengel, M.J., Jones, B.H., Ohlmann, J.C., Washburn, L., Terrill, E.J., Farnsworth, K.L., 2007. River plume patterns and dynamics within the Southern California Bight. Continental Shelf Research 27, 2427–2448.

Webster, C.F., Fleischer, R.S., Everitt, J.H., Davis, M.R., Escobar, E., Repic, R.L., 2004. Assessing a wastewater discharge to the subtropical Rio Grande using aerial videography and in situ physicochemistry. Geocarto International 19, 41–48.

Please cite this article in press as: Svejkovsky, J., et al., Tracking stormwater discharge plumes and water quality of the Tijuana River with..., Estuar. Coast. Shelf Sci. (2010), doi:10.1016/j.ecss.2010.01.022

Appendix H.2

2010 Ocean Imaging Report

Satellite & Aerial Coastal Water Quality Monitoring in The San Diego / Tijuana Region

By Jan Svejkovsky

Annual Summary Report
1 January, 2010 - 31 December, 2010

This draft to become final in sixty days.

30 April, 2011

Ocean Imaging

201 Lomas Santa Fe Drive, suite 370, Solana Beach, CA 92075 Phone: 858-792-8529 Fax: 858-792-8761 www.oceani.com

Table of Contents

1.0 Introduction & Project History 1

2.0 Technology Overview 1

2.1 Imaging in the UV-Visible-Near Infrared Spectrum 1
2.2 Imaging in the Infrared spectrum 2
2.3 Data Dissemination and Analysis 2

3.0 Highlights of 2010 Monitoring 3

3.1 Atmosheric & Ocean Conditions 3
3.2 The South Bay Ocean Outfall Region 5
3.3 The Point Loma OCean Outfall Region 17

1. Introduction and Project History

Ocean Imaging Corporation (OI) specializes in marine and coastal remote sensing for research and operational applications. In the 1990s, OI received multiple research grants from NASA's Commercial Remote Sensing Program for the development and commercialization of novel remote sensing applications in the coastal zone. As part of these projects, OI developed methods to utilize various types of remotely sensed data for the detection and monitoring of stormwater runoff and wastewater discharges from offshore outfalls. The methodology was initially demonstrated with collaboration of the Orange County Sanitation District. The NASA-supported research and demonstration led to a proof-of-concept demo project in the San Diego region co-funded by the EPA in 2000. Those results led, in turn, to adding an operational remote imaging-based monitoring component to the San Diego region's established water quality monitoring program, as stipulated in discharge permits for the International Wastewater Treatment Plant and Pt. Loma outfalls. The project was spearheaded by the State Water Resources Control Board (SWRCB), EPA Region 9, and continues to be jointly funded by the International Boundary Waters Commission and the City of San Diego.

The first phase of the project was a historical study utilizing various types of satellite data acquired between the early 1980s and 2002. The study established, among other findings, the prevailing near-surface current patterns in the region under various oceanic and atmospheric conditions. The current directions were deduced from patterns of turbidity, ocean temperature and surfactant slicks. In some cases, near-surface current velocity could be computed by tracking recognizable color or thermal features in time-sequential images. The historical study thus established a baseline data base for the region's current patterns, their persistence and occurrence frequency, and the historical locations, size and dispersion trajectories of various land and offshore discharge sources (e.g. the offshore outfalls, Tijuana River, Punta Bandera Treatment Plant discharge in Mexico, etc.).

In October, 2002 the operational monitoring phase of the project was initiated. This work utilizes 500m resolution Moderate Resolution Imaging Spectroradiometer (MODIS) color imagery (available near-daily), and 27m & 60m Thematic Mapper TM5 & TM7 color and thermal imagery (available 4 times per month). In addition, the project relies heavily on acquisition of multispectral color imagery with OI's DMSC-MKII aerial sensor and thermal infrared (IR) imagery from a Jenoptik thermal imager integrated into the system (see details in the "Technology Overview" section). These aerial image sets are most often collected at 2m resolution. The flights are done on a semi-regular schedule ranging from 1-2 times per month during the summer to once or more per week during the rainy season. The flights are also coordinated with the City of San Diego's regular offshore field sampling schedule so that the imagery is collected on the same day (usually within 2-3 hours) of the field data collection. Additional flights are done on an on-call basis immediately after major storms or other events such as sewage spills.

This report summarizes observations made during the period 1/1/2010 – 12/31/2010.

2. Technology Overview

OI uses several remote sensing technologies to monitor San Diego's offshore outfalls and shoreline water quality. Their main principle is to reveal light, heat or microwave signal patterns that are characteristic of the different discharges. Most often this is due to specific substances contained in the effluent but absent in the surrounding water.

2.1 Imaging in the UV-Visible-Near Infrared Spectrum

This is the most common technique used with satellite images and the DMSC aerial sensor. Wavelengths (colors) within the range of the human eye are most often used but Ultraviolet (UV) wavelengths are useful for detecting fluorescence from petroleum compounds (oil, diesel, etc.) and near-IR wavelengths can be useful for correcting atmospheric interference from aerosols (e.g. smog and smoke).

The best detection capabilities are attained when several images in different wavelengths are acquired simultaneously. These "multispectral" data can be digitally processed to enhance features not readily visible in simple color photographs. For example, two such images can be ratioed, thus emphasizing the water features' differences in reflection of the two wavelengths. A multi-wavelength image set can also be analyzed with "multispectral classification algorithms" which separate different features or effluents based on the correlation relationships between the different color signals.

The depth to which the color sensors can penetrate depends on which wavelengths they see, their sensitivity and the general water clarity. In the San Diego region, green wavelengths tend to reach the deepest and, as elsewhere, UV and near-IR wavelengths penetrate the least. Generally, OI's satellite and aerial sensor data reveal patterns in the upper 15-40 feet.

The color channels on satellite sensors cannot be changed, so they tend to be relatively broad, separating red, green, near-IR, and sometimes blue parts of the spec-

trum. OI's DMSC aerial 4-channel sensor has the added advantage of allowing each channel wavelength to be precisely customized. Through experimentation, OI has determined the exact wavelength relationships that maximize the detection of the offshore sewage outfall plumes and nearshore discharges such as the Tijuana River. With this channel configuration it is possible to monitor the plumes even when they are not visible to the naked eye.

2.2 Imaging in the Infrared Spectrum

Some satellite and aerial sensors image heat emanating from the ground and the ocean. They thus reveal patterns and features due to their differences in temperature. Since infrared wavelengths are strongly absorbed by water, the images reveal temperature patterns only on the water's surface. Such images can help detect runoff plumes when their temperatures differ from the surrounding ocean water. Runoff from shoreline sources tends to be warmer than the ocean water, although the reverse can be true during the winter. Plumes from offshore outfalls can sometime also be detected with thermal imaging. Since the effluent contains mostly fresh water, it is less dense than the surrounding salt water and tends to rise to the surface. If it makes it all the way, it is usually cooler than the surrounding sun-warmed surface water. If it is constrained by a strong thermocline and/or pycnocline ("vertical stratification"), it sometimes tends to displace some of the water above it in a doming effect. This displacement pattern is revealed in the thermal surface imagery.

2.3 Data Dissemination and Analysis

The satellite and aerial imaging data are made available to the funding agencies, the San Diego County Department of Health and the EPA through a dedicated, password-protected web site. Although it is possible to process most of the used data in near-real-time, earlier in the project the funding agencies decided that the emphasis of this project is not on providing real-time monitoring support and the extra costs associated with the rapid data

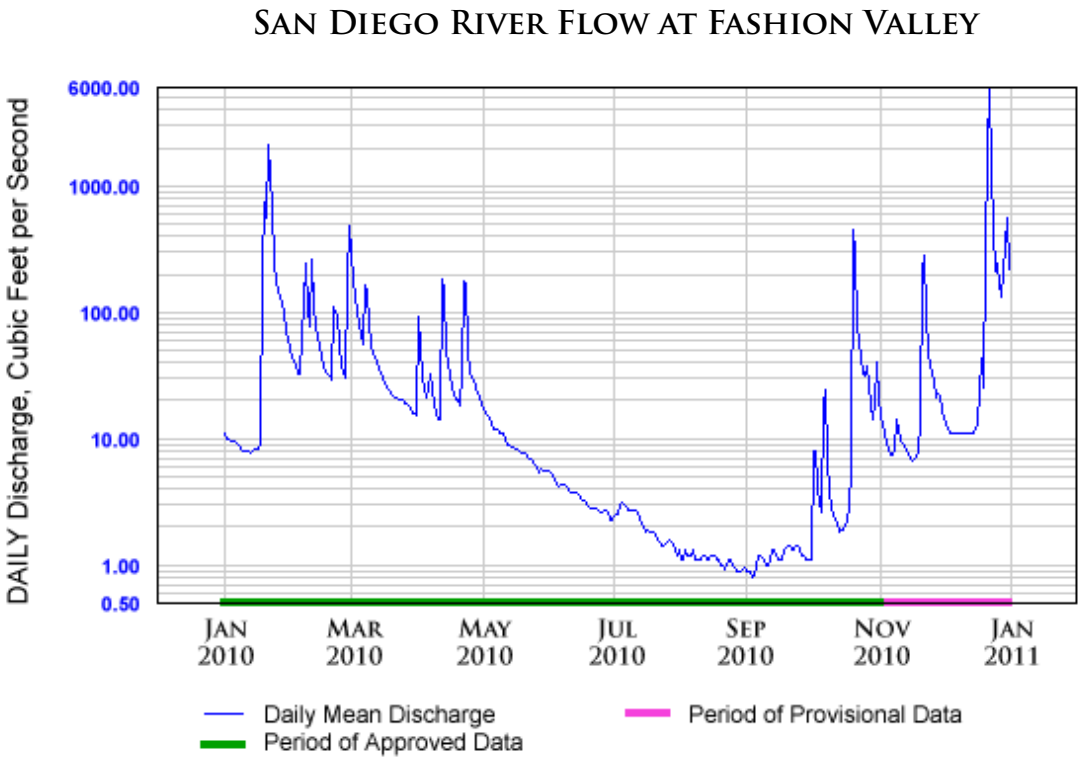

Lindberg Field Rainfall 2010	
January	3.38"
February	2.28"
March	0.68"
April	1.78"
May	0.01"
June	0.02"
July	0.02"
August	0.00"
September	0.03"
October	2.18"
November	0.88"
December	5.00"

Figure 1.

Graph of mean daily discharge of the San Diego River during 2010 (measured at Fashion Valley). The table on the right shows monthly rainfall totals at Lindbergh Field.

turn-around are not warranted. Most satellite data is thus processed and posted within 1-2 days after acquisition and the aerial sensor imagery (which requires the most labor-intensive processing), within 2-5 days. OI has, however, in a number of cases, made some imagery available to the CDH and others in near-real time when observations were made that appeared to be highly significant for the management of beach closures or other sudden events.

3. Highlights of 2010 Monitoring

3.1 Atmospheric & Ocean Conditions

The west coast of North America experienced numerous anomalous conditions during 2010 that also affected the coastal ocean regions around San Diego. Early in the year, a number of relatively powerful storms brought around 6" of rain to the region through February, as well as periods of very strong winds. On 20th January, 2010 the lowest-ever barometric pressure (29.21") was recorded at Lindbergh Field during one of these storms. **Figure 1** shows the monthly Lindbergh rainfall amounts and daily discharge patterns of San Diego River, and **Figure 2** shows the daily rainfall in the Tijuana Estuary for 2010.

The spring and summer months of 2010 were marked by significantly cooler than normal air and ocean temperatures. The abnormally cooler ocean temperatures were due to both, cooler air temperatures along Baja and California, and in early summer persistent marine layer that inhibited solar heating. By July -August, air temperatures were 4-5° below normal and nearshore sea surface temperatures (SSTs) were 2-4° below normal, as is shown in **Figure 3**.

The cool trend reversed in the fall, however, with numerous high temperature records being broken in Southern California (e.g. downtown Los Angeles reached 113°F on 26-27 September, 2010). October, 2010 has the distinction of being the 4th wettest on record in San Diego, November was the hottest on record (downtown San Diego reached 100°F on 11/4/2010), and December had the greatest rainfall total in San Diego's history.

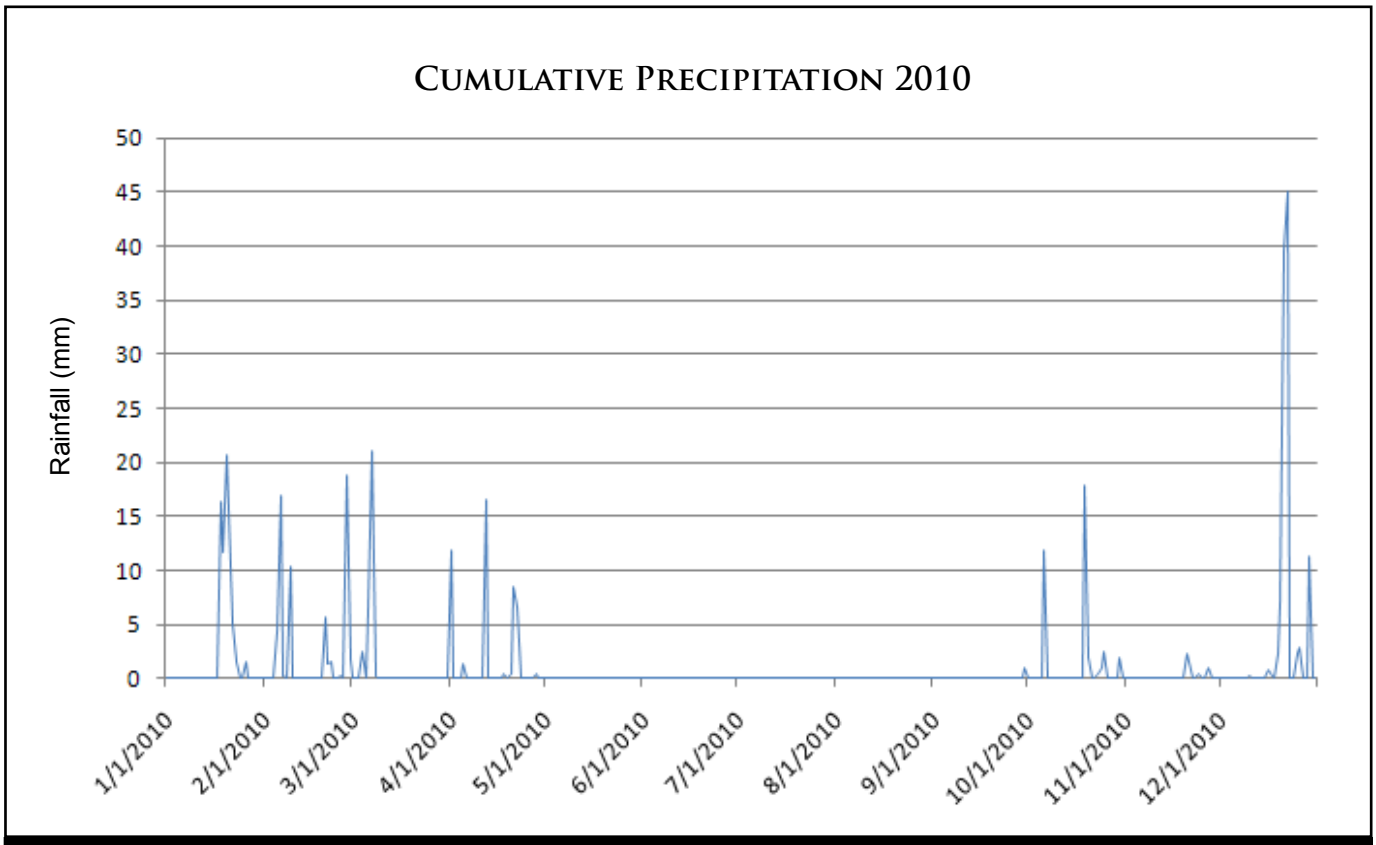

Figure 2.

Graph of daily cumulative daily rainfall in the Tijuana Estuary.

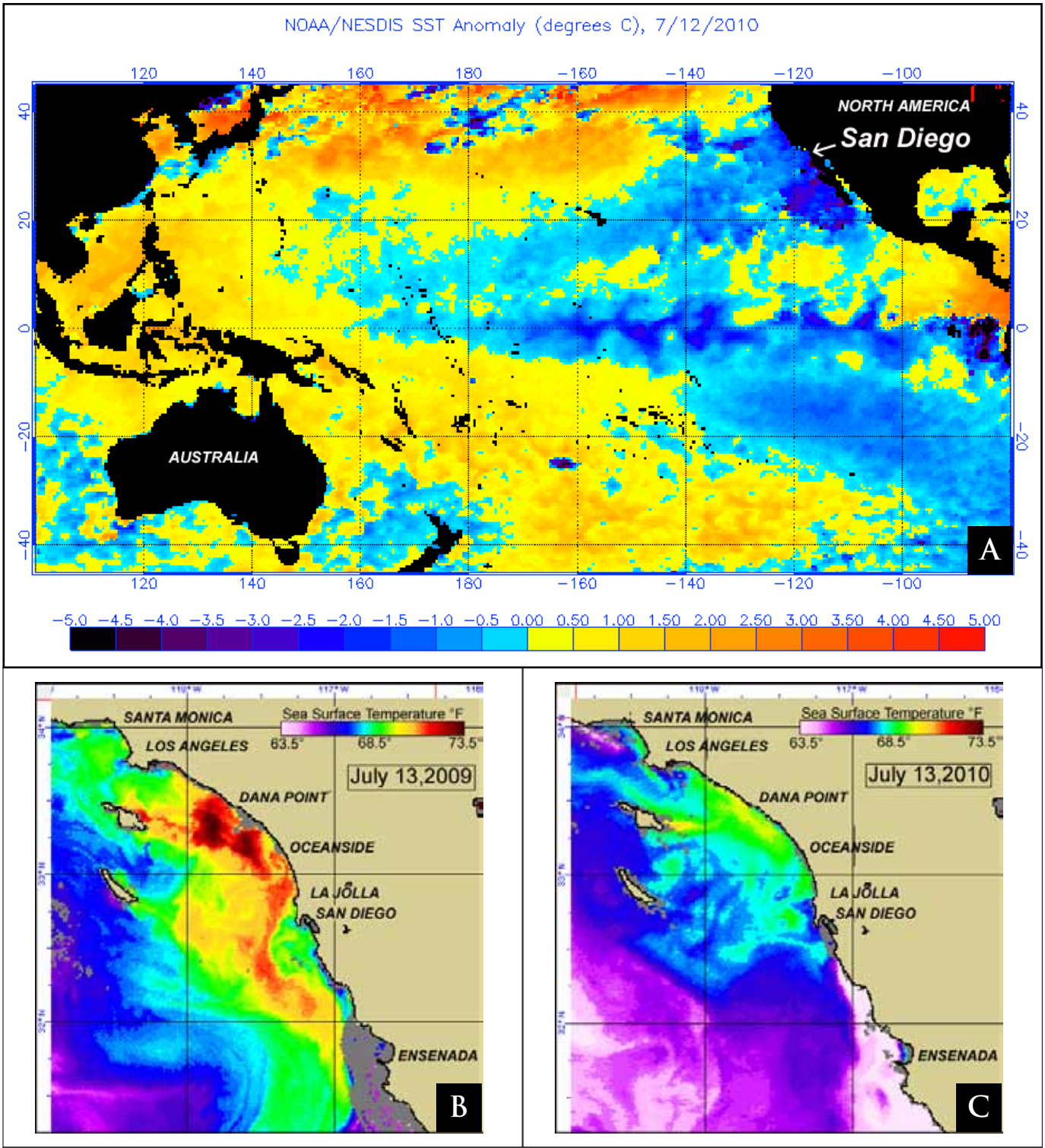

Figure 3.

A) surface temperature anomaly over the Pacific Ocean during July, 2010; B) AVHRR-satelite-derived sea surface temperatures along coastal Southern California on 7/13/2009, and C): 7/13/2010.

3.2 The South Bay Ocean Outfall Region

The South Bay Ocean Outfall (SBOO) wastewater plume generally remains well below the surface between approximately late March and November due to vertical stratification of the water column. During that period it usually cannot be detected with multispectral aerial and satellite imagery which penetrate the upper 7 to 15 meters (depending on water clarity). The plume also cannot be detected with thermal IR imaging which does not penetrate below the surface. Seasonal breakdown of the vertical stratification results in the plume's rise closer to the surface or to actually reach the surface between approximately late November and late March, when it can often be detected with aerial and satellite imaging. In 2010 the SBOO plume was visible through mid-February, then again in mid-March. The plume was detected again in mid-December (much later than normal) and remained traceable through the rest of the year.

As in previous years, during the rain season months the coastal region in the vicinity of the SBOO is subject to rain runoff from the Tijuana River, which is characterized by turbid waters that often exhibit high indicator bacteria counts. In some cases, the runoff plume is large enough in the offshore direction to overtake the area over the SBOO wye. During periods of northward flow, the river discharge plume is advected northward and, in some cases in the past, actually reached waters surrounding Pt. Loma where it caused increased indicator bacteria concentrations. In the early months of 2010 sustained northward flow events were relatively rare and, with the exception of 24-25 January, the river discharge plume was not advected significantly northward past its usual spread boundaries. Accordingly, the SBOO plume was observed to also be directed southward or southeastward, as is exemplified in **Figure 4**.

General advisories were issued by the County Department of Health (CDH) in response to the rain events in January and February. The CDH also issued actual beach closures at Imperial Beach and Coronado's Silver Strand on 5-12 February, 20-24 February and 27 February through 2 March. Analysis of our MODIS and aerial multispectral imagery can relate the late-February through March closures to post-storm effects of the polluted Tijuana River plume. The 5-12 February period deserves further note, however. Although some rain did fall on 5-6 and 9 February, no measureable rainfall occurred in the Tijuana region after that until the 20th. Both MODIS and aerial survey imagery show the Tijuana River plume to be relatively small in size and localized in the River mouth vicinity. A DMSC aerial survey on 2/8/2010 revealed a very large secondary plume anchored at the shoreline south of the US/Mexico border. As is shown in **Figure 5**, in addition to its high suspended sediment concentration, this feature exhibits a warmer-than-surrounding ocean thermal signature, suggesting it is of terrestrial origin. Shoreline bacteria samples collected the following day show very high indicator bacteria counts throughout the area. The DMSC data can be interpreted that the feature originated from the Tijuana River and was advected southward for a few kilometers within an extreme nearshore band, then radiated outward south of the border. Near-daily MODIS and 2/15 TM satellite data show that the feature persisted in that location at least through 2/15/2010. Based on previous, multi-year observations of the Tijuana River plume, the feature's location is very unusual and its persistence suggests that some other temporary but significant input of terrestrial-based discharge may have existed emptying at the beach in that area in early to mid February, 2010.

The spring 2010 months in the SBOO region exhibited relatively calm and good water clarity conditions, with a few General Advisories issued related to rain events in March and April. The SBOO plume was last directly observed at the surface (as indicated by the existence of a thermal signature, since the thermal signal does not penetrate the water column) on 3/15/2010 and is shown in **Figure 6**. In mid-May the entire San Diego region began to experience a series of strong plankton blooms which also affected waters in the SBOO region. A MODIS satellite image shows this effect on 5/28/2010 (**Figure 7**). The bloom was confined to the nearshore region, with the highest bloom densities generally being closest to shore. The large-scale plankton blooms continued through much of the summer, with another example shown from 7/16/2010 in **Figure 8**. The region's nearshore waters cleared somewhat during August. In mid to late September a red tide event developed nearshore along Coronado and temporarily affected the whole SBOO region, as can be seen in MODIS data from 9/25/2010 (**Figure 9**).

Our image data also revealed an anomalous condition in the nearshore waters south of the US/Mexico border in July, 2010. Because of high sun angles during the local image acquisition times, visible wavelength channels of the TM satellite imagery during the summer months tend to show high ocean surface reflectance, and hence reveal surface glint patterns rather than patterns of turbidity through the water column. Ocean surface areas with accumulations of surfactant materials (which tend to suppress the reflectance) appear dark. A TM image from 7/17/2010, shown in **Figure 10**, revealed a large area of surfactants along the immediate coast south of the US/Mexico border. The area also appeared warmer than surrounding water, due perhaps to the increased solar heating caused by the surfactant-related smoothing of the capillary wave field. Surfactant-related slick patterns are commonly seen in summer TM and other high resolution imagery but are usually in the shape of long strands (these are also seen in the 7/17 image further offshore). We have never observed such a large slick in this area before. Since same-day MODIS data do not show any signs of a massive, regionally-confined plankton bloom, and the area is not covered in kelp (both of which can cause a slick appear-

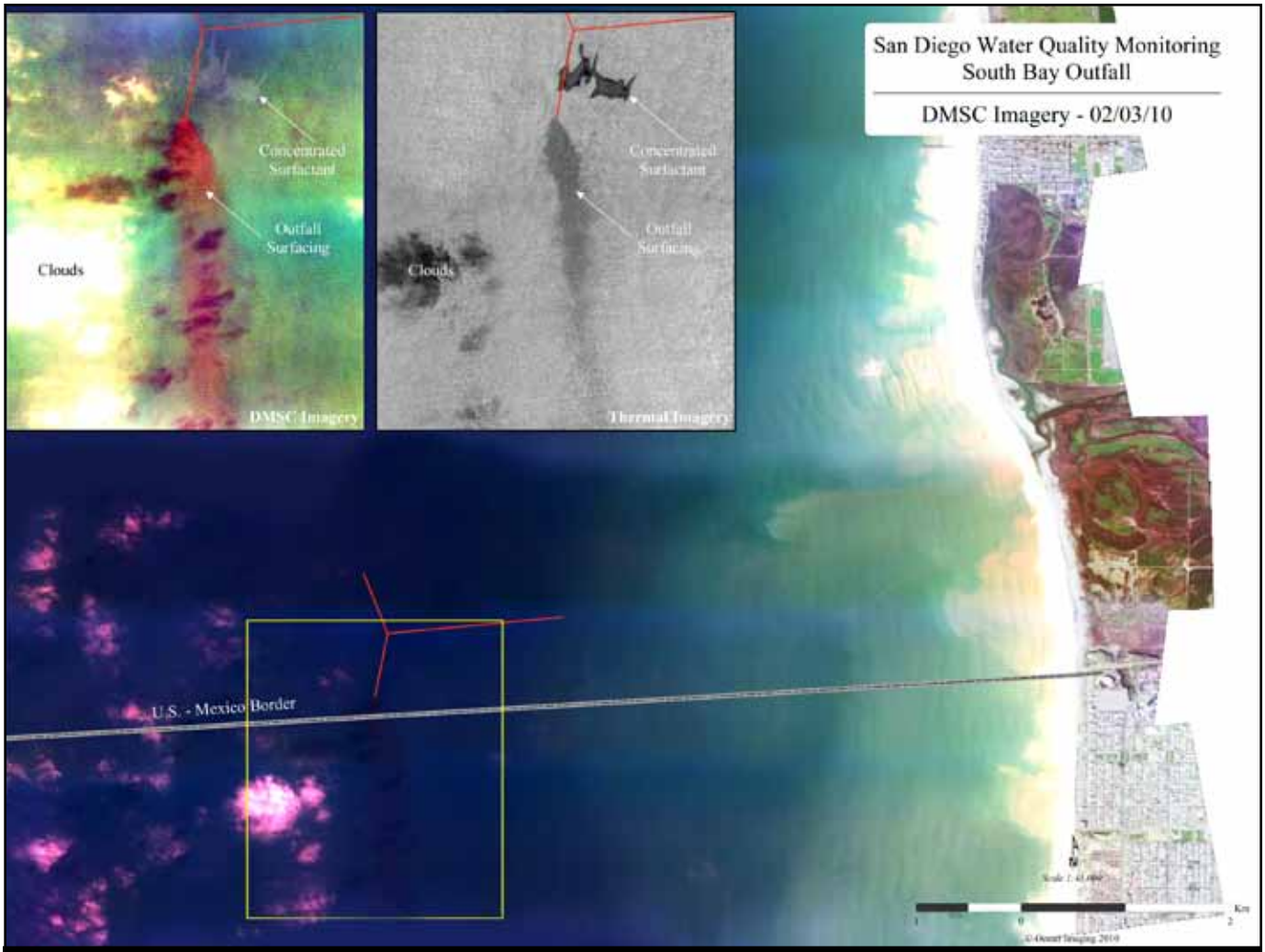

Figure 4A.

Multispectral color and thermal aerial imagery of the SBOO region acquired on 2/3/2010 showing southward and southeastward trajectories of the SBOO plume.

ance), it is logical to speculate about a possible anthropogenic cause. Substances such as oil and grease as well as detergents will cause surface slicks and we have documented in the past such effects during both, raw sewage spills and storm water runoff events. Two relatively large sewage spills occurred in Tijuana in summer 2010: a 2.1 million gallon event on 6/2-3/2010 and a 2.7 million gallon event on 7/7-8/2010. Neither of these was believed to reach the ocean, however. With no information as to the subsequent fate of the spilled sewage, it is not possible to postulate a connection between the spills and the large surfactant amounts along the shore in mid July. We do note the anomalous feature here, however, because of its unique nature in that location.

As was noted above, the atmospheric and ocean water cool trends dominating the region's 2010 spring and summer reversed in the fall to yield high temperature records in many parts of Southern California. Waters in the SBOO area remained relatively clear and stable. Rains in the mid to late part of October made it one of the wettest Octobers on record, however, unlike in previous years most of the rain fell gradually over several days. This may be reflected in the satellite imagery: the runoff plume from the Tijuana River remained relatively small and contained close to the coast. **Figure 11** shows it on 10/26/2010 after several days of light rains. This image comes from a new data source which we began using for the project in October, 2010 – a German multi-satellite constellation termed RapidEye, which provides multispectral imagery at

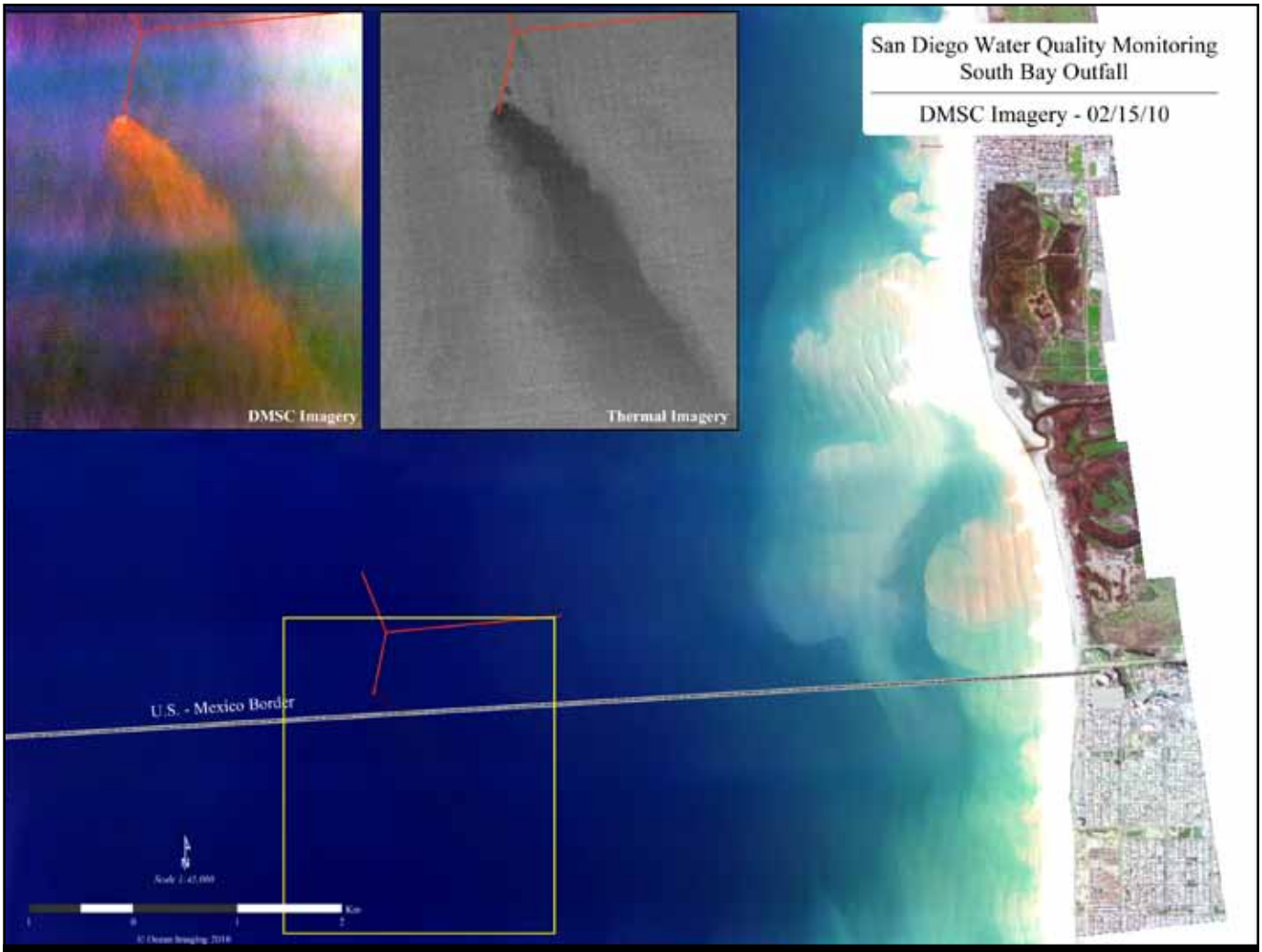

Figure 4b.

Multispectral color and thermal aerial imagery of the SBOO region acquired on 2/15/2010 showing southward and southeastward trajectories of the SBOO plume.

5m spatial resolution. The advantage of this system is that unlike other single high resolution satellites whose revisit orbits are separated by several days, the multiple RapidEye satellites can re-image a target of interest on a daily basis. Ocean Imaging negotiated a data collection contract with Rapid Eye specifically for this project, providing up to 4 cloud-free images per month during the rainy season and up to 2 per month during the dry season.

November 2010 experienced a major rain event, with more than 1.5" of rainfall recorded at the Tijuana Estuary on 11/21/2010 and another 1.8" on 11/22/2010. A MODIS image from 11/22/2010, acquired immediately after the skies cleared shows the Tijuana River plume reaching offshore to the SBOO wye. Similarly, large volumes of runoff can be seen flowing out of San Diego Bay. The runoff appeared to have dissipated quickly, however, since a RapidEye image acquired on 11/25/2010 (**Figure 12**) no longer shows major active flow from the River mouth, and the shorelong runoff waters have receded to within approximately 4km of the coast.

In past years, the SBOO effluent plume tended to be seasonally first detected in multispectral imagery in the later part of November, even earlier in some cases. In 2010, the plume was first detected in a RapidEye image acquired on 12/13/2010 (**Figure 13**). It is quite possible that the record heat occurring in the fall months of 2010 regionally acted to preserve vertical stratification in the water column later into the year than usual. Hence the SBOO plume

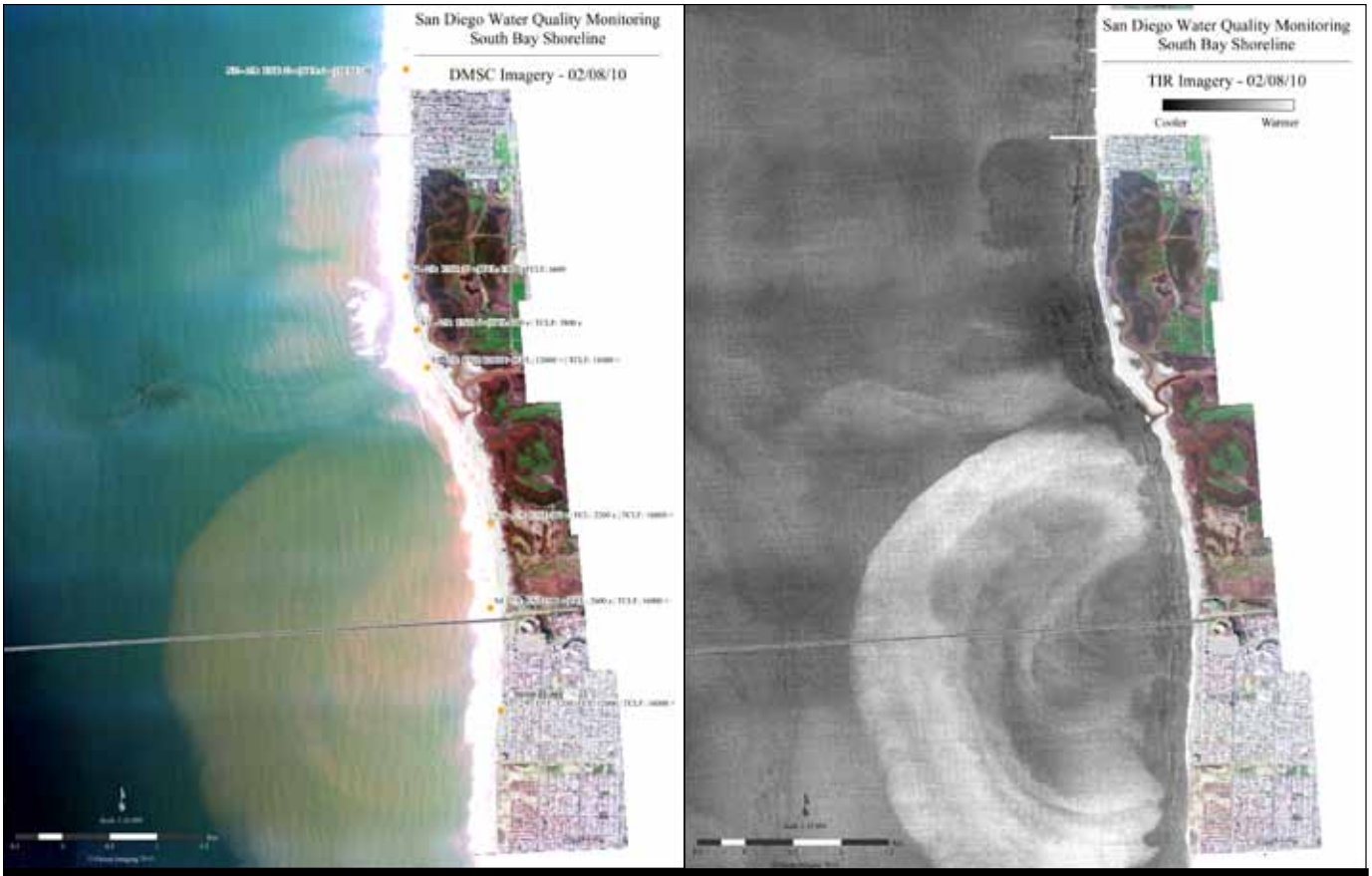

Figure 5.

Multispectral color and thermal aerial imagery of the South Bay and Tijuana shoreline region acquired on 2/8/2010.

may have remained trapped under the pycnocline seasonally longer than in previous years. The satellite data from 12/13/2010 also show an anomalous red tide occurring in the nearshore waters from Silver Strand southward to Rosarito Beach, Mexico.

Rains over the region in the later part of December, 2010 contributed to its accumulating the greatest rainfall total in history. **Figure 14** shows RapidEye satellite views of the SBOO region following persistent rains from 12/19/2010 to 12/22/2010. The Tijuana River plume extended westward well past the SBOO wye. As has been observed in such cases in the past, the highly turbid, freshwater runoff forms a relatively thin surface layer through which the less turbid outfall effluent breaks to the surface. In this case, the outfall's riser groups are clearly delineated through the contrasting patterns.

It should be noted that with the relatively infrequent occurrence of northward flow episodes during 2010 (they did increase in the last two months of the year), none of our aerial or satellite observations evidenced the discharge plume from Mexico's Los Buenos Creek to ever cross the US border or reach it in the nearshore area during 2010.

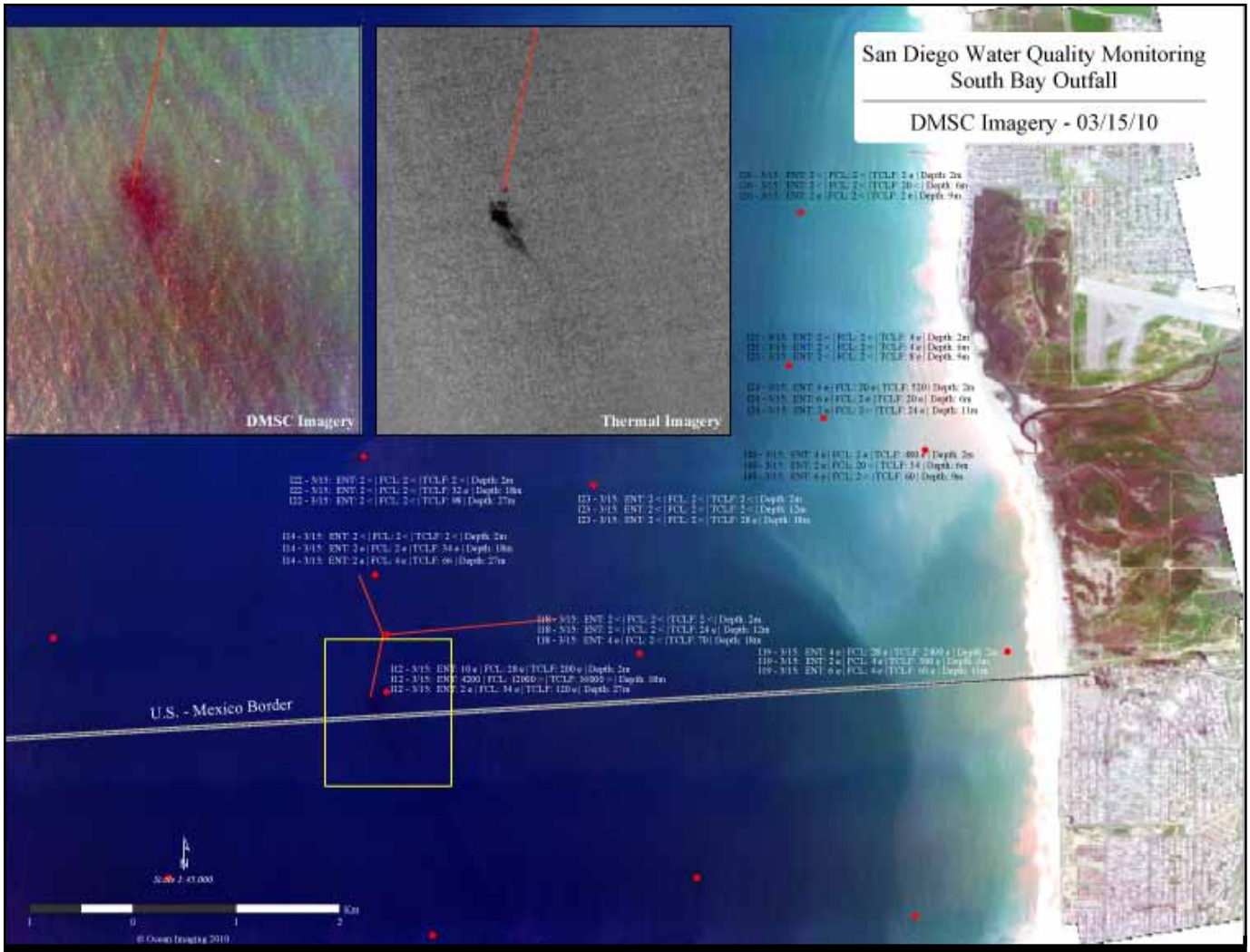

Figure 6.

color and thermal aerial imagery of the SBOO region acquired on 3/15/2010.

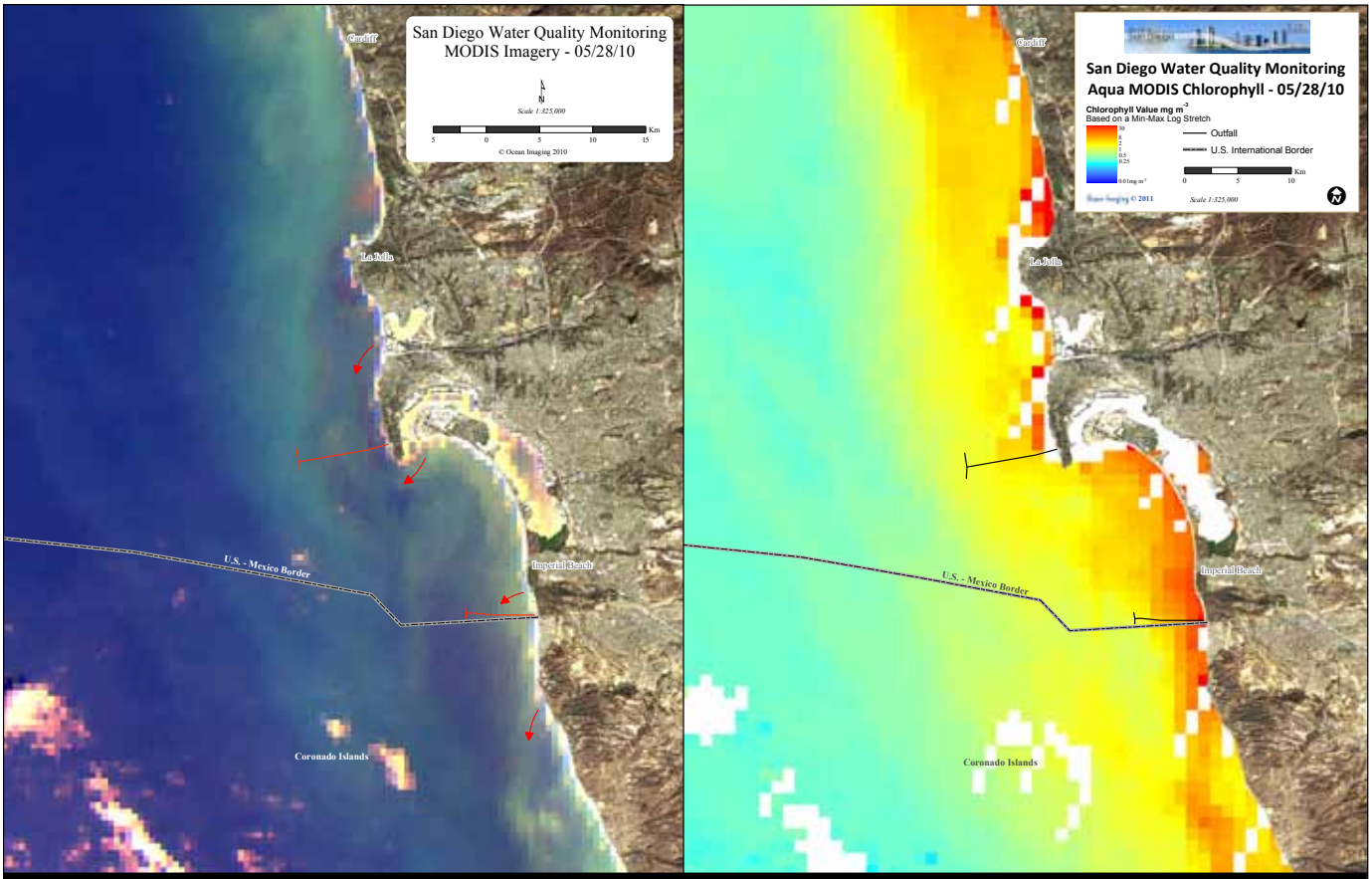

Figure 7.

MODIS satellite image of the San Diego region acquired on 5/28/2010 (left), and the same data processed for chlorophyll concentrations (right).

Figure 8.

MODIS satellite image of the San Diego region acquired on 7/16/2010 showing extensive nearshore plankton blooms.

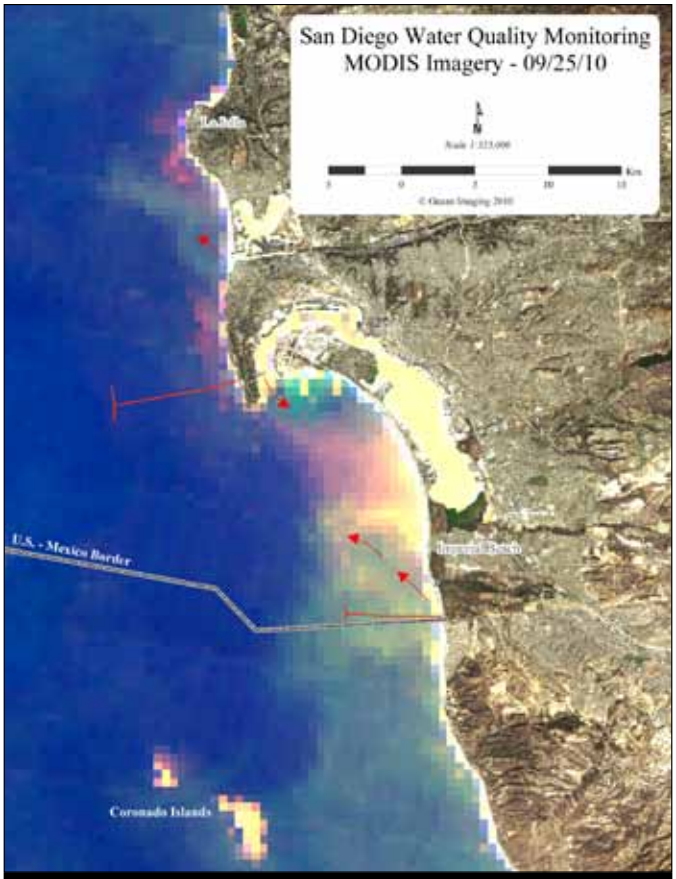

Figure 9.

MODIS satellite image of the South Bay region acquired on 9/25/2010 showing a localized red tide bloom in the area. The red features to the north by Pt. Loma and La Jolla are kelp beds.

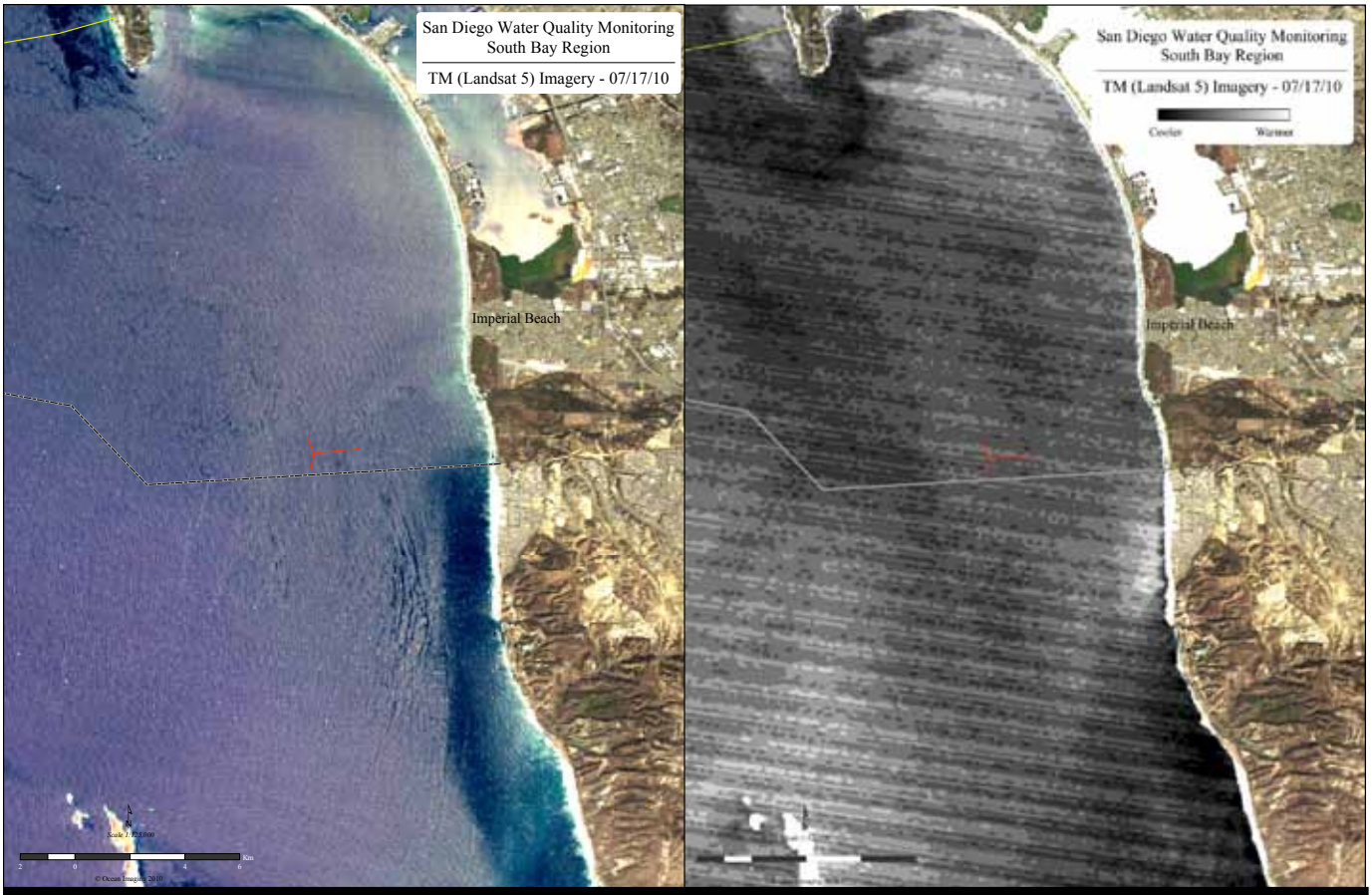

Figure 10.

Satellite TM image of the SBOO region acquired on 7/17/2010. Due to sunglint effects, the multispectral visible image (left) reveals glint reflectance patterns on the ocean surface. Dark features (less reflecting) correspond to surfactant accumulations. The thermal image (right) shows the large accumulation of surfactants along the Tijuana shoreline also exhibits a warm signature (see text for discussion).

Figure 11.

RapidEye satellite imagery of the SBOO region acquired on 10/26/2010 after several days of intermittent rain. Offshore and shoreline bacteria sampling results from the same day are also shown.

Figure 12.

RapidEye satellite image of the SBOO region acquired on 11/25/2010 after heavy coastal rains on 11/21-22/2010.

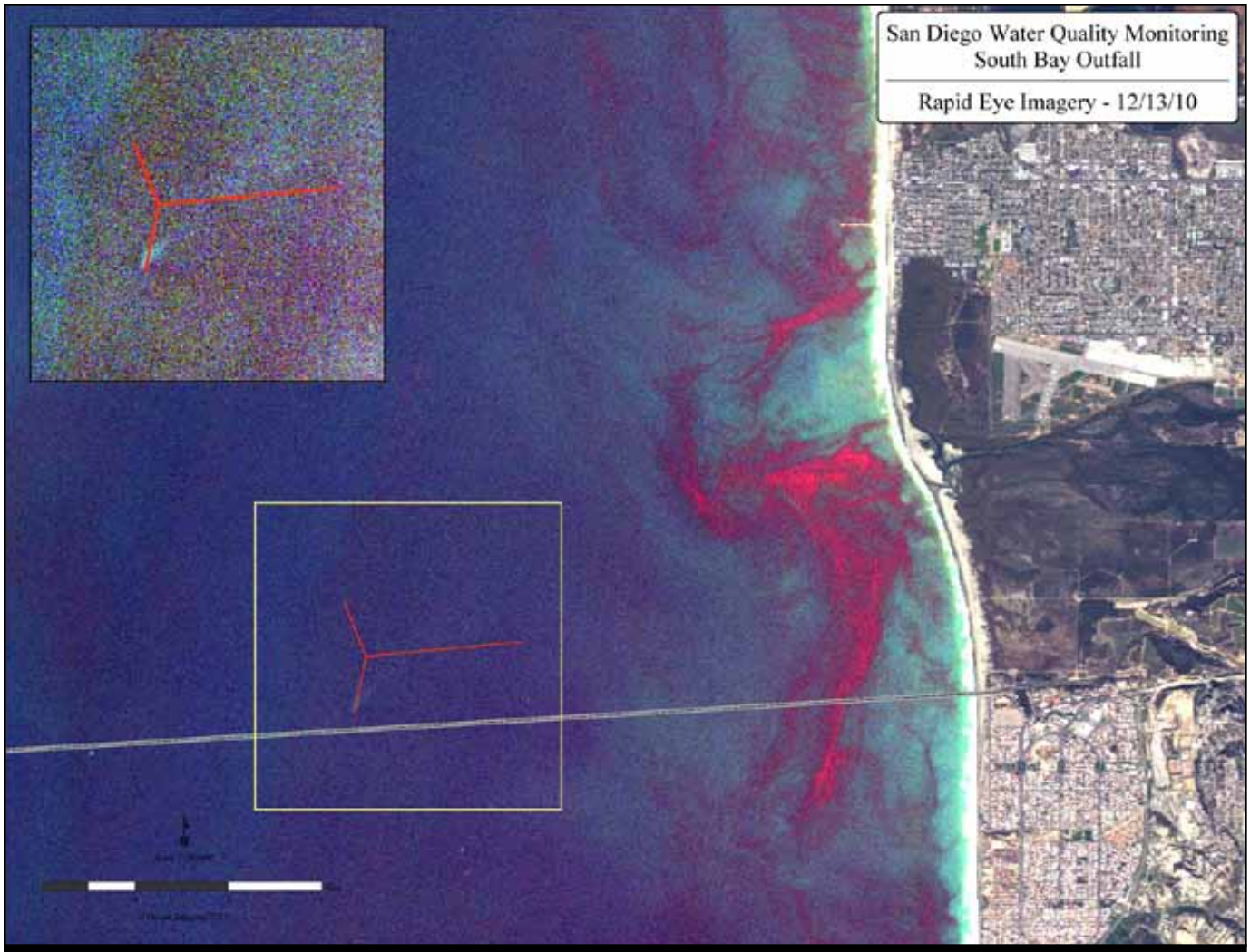

Figure 13.

RapidEye satellite image of the SBOO region acquired on 12/13/2010. The SBOO effluent plume signature had become visible near the surface. The red areas nearshore are a red tide that existed in this area and further south for several days.

Figure 14.

RapidEye satellite image of the SBOO region acquired on 12/24/2010. Highly turbid storm runoff waters from the Tijuana River have spread over the outfall wye area and the less turbid effluent breaks through it to the surface. The zoom-in shows effluent signatures from the outfall's individual riser groups.

3.3 The Point Loma Ocean Outfall Region

After its seaward extension in 1993, the Point Loma Outfall (PLO) is one of the deepest and longest wastewater outfalls in the world, discharging at the depth of 320 feet, 4.5 miles offshore. The outfall's plume is generally not observed directly with multispectral color or thermal imagery. It appears to not reach the surface waters, even during the winter months when the water column's vertical stratifications are weakened. We believe, however, that on some occasions we have observed the plume's extents indirectly in both image types through an anomalous lateral displacement of thermal or chlorophyll features around the outfall wye. This effect can be explained by the doming up of the discharged effluent and laterally displacing the near-surface waters above it.

During the first few (i.e. rain season) months of 2010 the PLO region experienced relatively mild conditions in terms of local runoff, contamination reaching the area from the Tijuana River, and similar events affecting water quality. An exception was during the later part of January, when multi-day rains briefly caused the San Diego River discharge (as measured at Fashion Valley) to exceed 1000 cubic feet per second. This period coincided with one of the few persistent northward current episodes of early 2010, and the flow regime thus advected much of the region's runoff northward – as is exemplified on 1/24/2010 (**Figure 15**). As can also be seen in the MODIS image, under high runoff conditions coupled with northward-directed currents, turbid waters exiting San Diego Bay tend to round the tip of Pt. Loma and expand into and around its kelp bed. From our observations, such waters tend to exhibit only very low or background indicator bacteria concentrations. This concurs with shoreline and offshore sampling results obtained on 1/28/2010, despite the continuance of a northward flow regime during that time (**Figure 16**).

Figure 15.

MODIS satellite image from 1/24/2010 showing a large stormwater runoff plume from the San Diego River being advected northwestward.

Additional but much less intense runoff episodes continued through February, March and April. The region's dominant current direction during those months was persistently southward. In some cases, the current patterns carried the sediment-laden runoff waters considerable distances offshore in the southwest direction, well outside the PLO wye. **Figure 17** shows MODIS data from 2/15/2010 that clearly show separate runoff features from two sources that most commonly affect the Pt. Loma region during the rain season: runoff from the San Diego River, and runoff from North County lagoons, most notably Penasquitos and San Dieguito. During spring 2010, local runoff along Pt. Loma tended to remain trapped between the shoreline and the kelp bed and generally contained low or background indicator bacteria concentrations (with the occasional exception at Imperial Beach's Dog Beach), as is exemplified in **Figures 18A and B**.

The last few rains of the 2009-2010 rain season occurred in April, 2010. During that month the San Diego region began experiencing strong plankton blooms in the nearshore waters from approximately La Jolla southward into Mexico. By May the blooms also affected North County. Good examples are shown in **Figure 19**. As was already noted, the 2010 summer was marked by anomalously low air and water temperatures, and excessive cloud cover. MODIS satellite imagery collected during occasional clear-sky days continued to show high nearshore plankton concentrations. In August high plankton conditions continued along the South Bay shoreline but the nearshore waters cleared significantly along Pt. Loma and North County.

The PLO wye region relatively often tends to be subject to increased suspended sediment and/or increased plankton concentrations contained in waters that originate

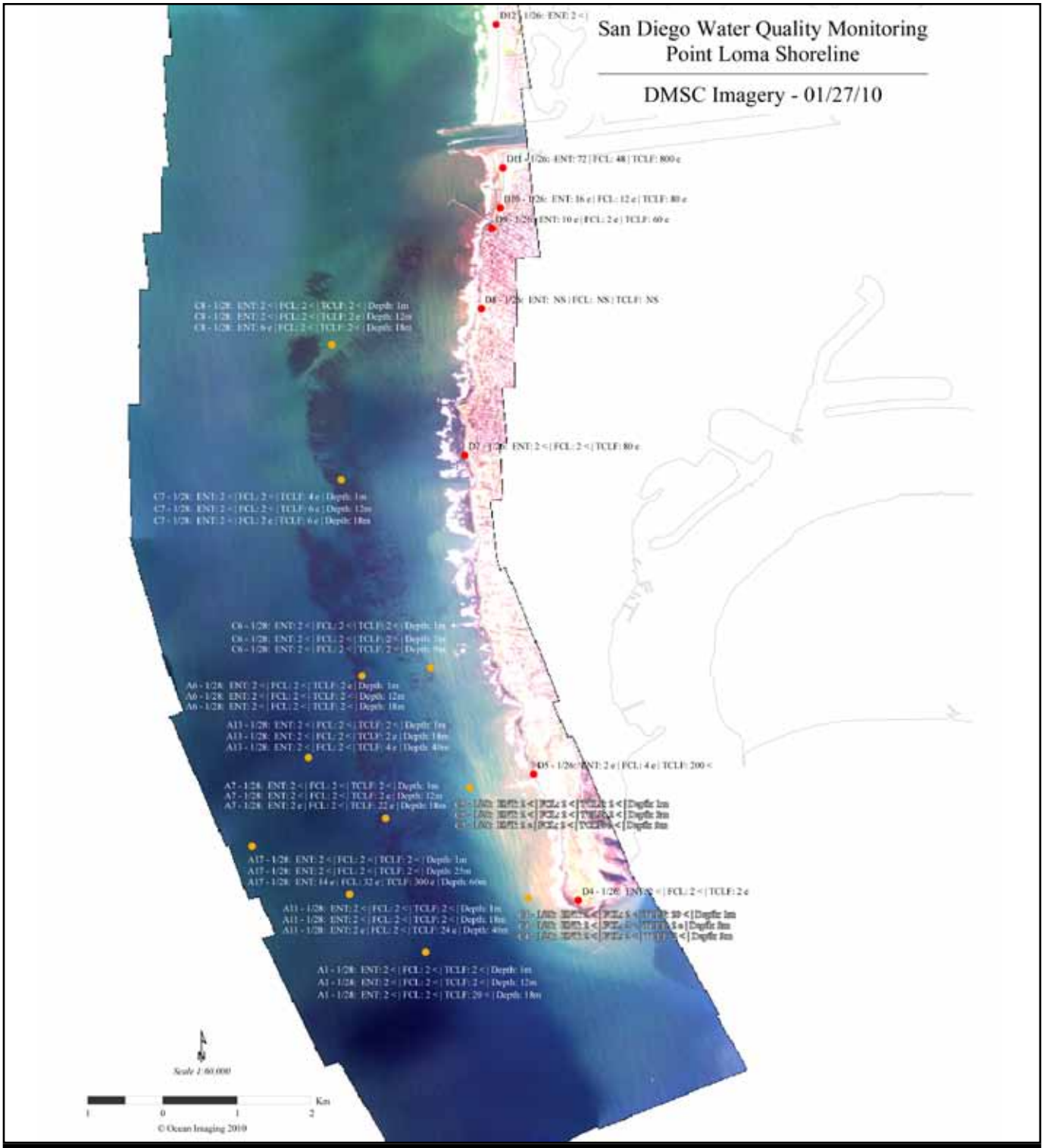

Figure 16.

DMSC aerial image of the Point Loma region acquired on 1/27/2010. Indicator bacteria sampling results collected on 1/28/2010 are also shown.

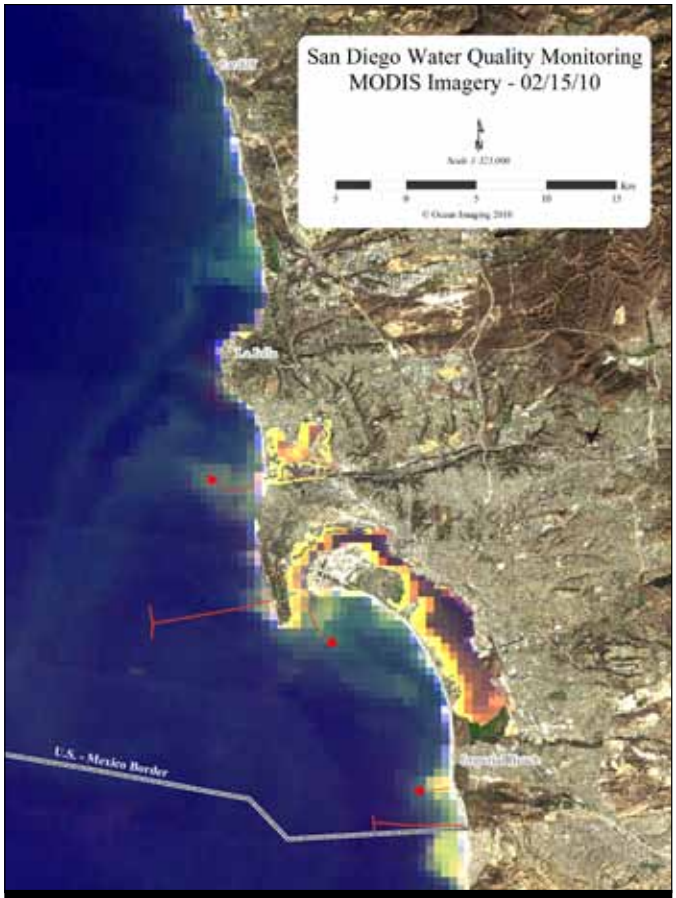

Figure 17.

MODIS satellite image from 2/15/2010 showing separated stormwater runoff plumes from North County lagoons and the San Diego River reaching west and south past the PLO wye.

along North County, Mission Beach or South Bay and become advected directly over the outfall wye. Sometimes, as is shown in **Figure 20A**, the effect can be highly localized and should be considered when interpreting offshore field sample data that may reflect such effects. The effect occurs throughout the year, most commonly with the anomalous waters originating north of the wye. Occasionally, however, a northward flow regime is persistent enough to drive such waters from the South Bay area over and past the wye, as occurred on 9/29/2010 (**Figure 20B**).

The Pt. Loma offshore region experienced persistently good water clarity through most of the last 3 months of 2010. Rain events in October and November, while significant, tended to deposit their precipitation over prolonged time periods rather than in heavy downpours. This appears to have limited the runoff impact of the San Diego River and similar sources to the very nearshore. **Figures 21A and B** show representative examples using the new RapidEye satellite imagery. The data from 11/1/2010 show a turbid plume emanating out of Mission Bay. This feature, and likely the surrounding turbidity along Ocean Beach, is not due to storm runoff. Rather, the turbidity is the result of dredge material disposal from an operation conducted in Mission Bay by the US Army Corp. of Engineers. As per the Regional Water Quality Control Board, the operation was not properly permitted and the disposal was not done in accordance with the appropriate protocols, thus impacting regional water quality.

As was mentioned in the previous section, the largest storm event of the year occurred between 12/19-22/2010. A regional RapidEye view from 12/24/2010 following the rains is shown in **Figure 22**. The satellite data reveal that runoff from the San Diego River contained relatively low suspended sediment loads (even though its mean daily discharge peaked at 6000 cubic feet per minute and remained above 300 cfpm through the rest of the year), as compared to the Tijuana River and other sources south of the US border. Similar to the situation on 9/29/2010 (**Figure 20B**), directed by a northward flow regime on 12/24/2010, highly turbid waters primarily of South Bay coast (and some San Diego Bay) origin flowed directly over the PLO wye location. The frequency of northward flow episodes during November and December 2010 was noticeably greater than earlier in the year. Unlike in some previous years, however, we did not observe the Tijuana River plume to directly reach the Pt. Loma region during 2010.

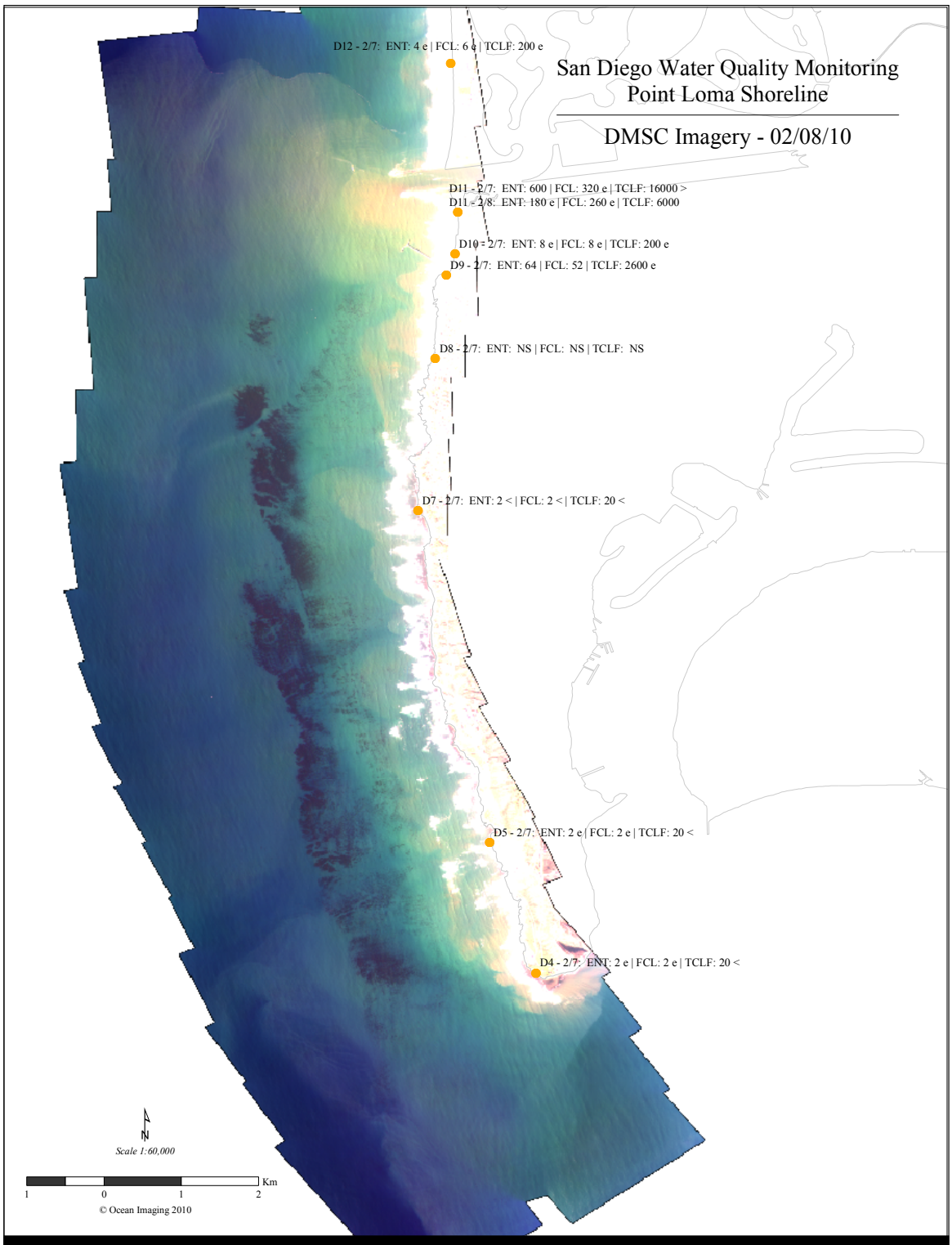

Figure 18a.

Aerial DMSC imagery of the Point Loma nearshore region acquired on 2/8/2010. Bacterial sampling results from 2/7/2010 are also shown.

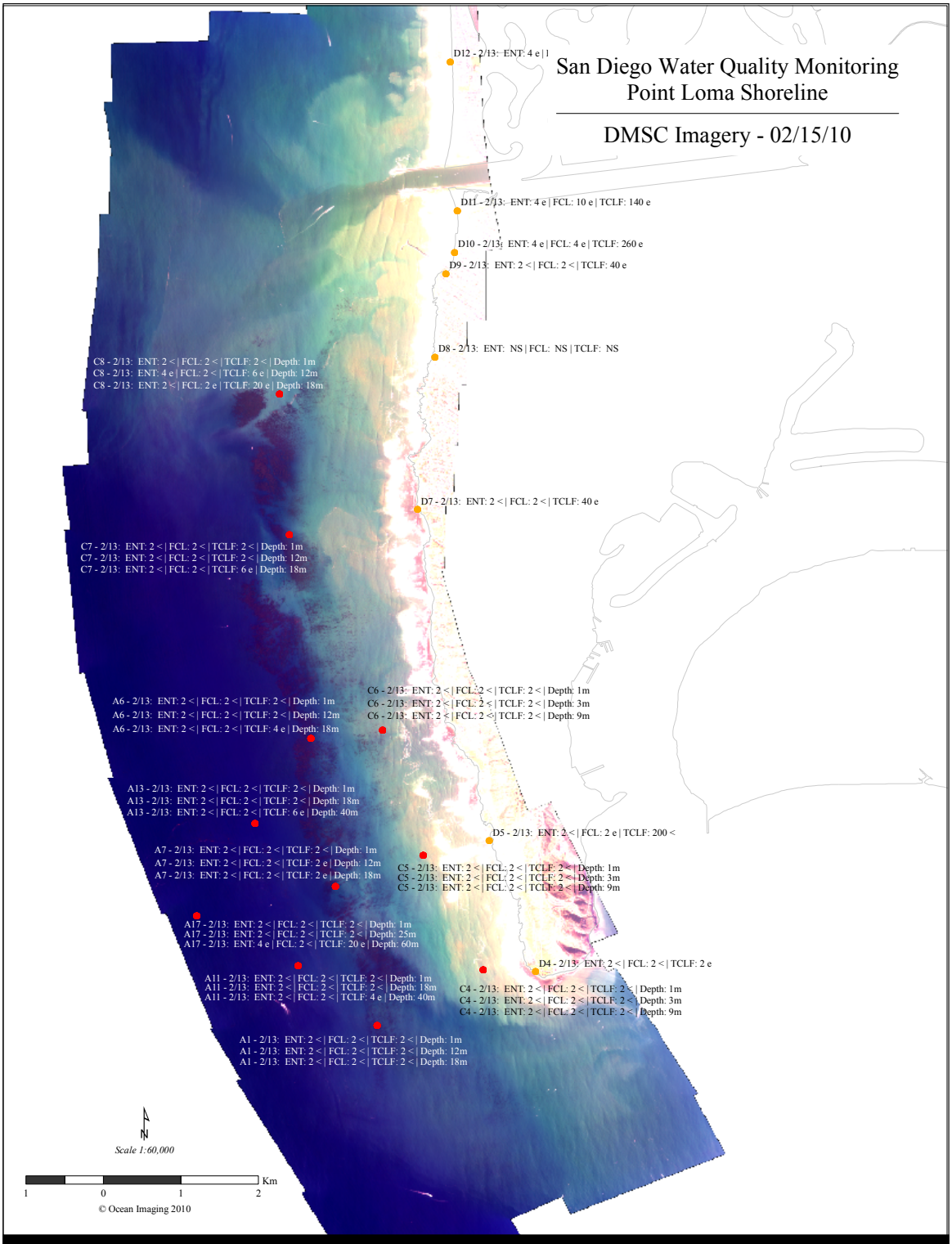

Figure 18B.

Aerial DMSC imagery of the Point Loma nearshore region acquired on 2/15/2010. Bacterial sampling results from 2/13/2010 are also shown.

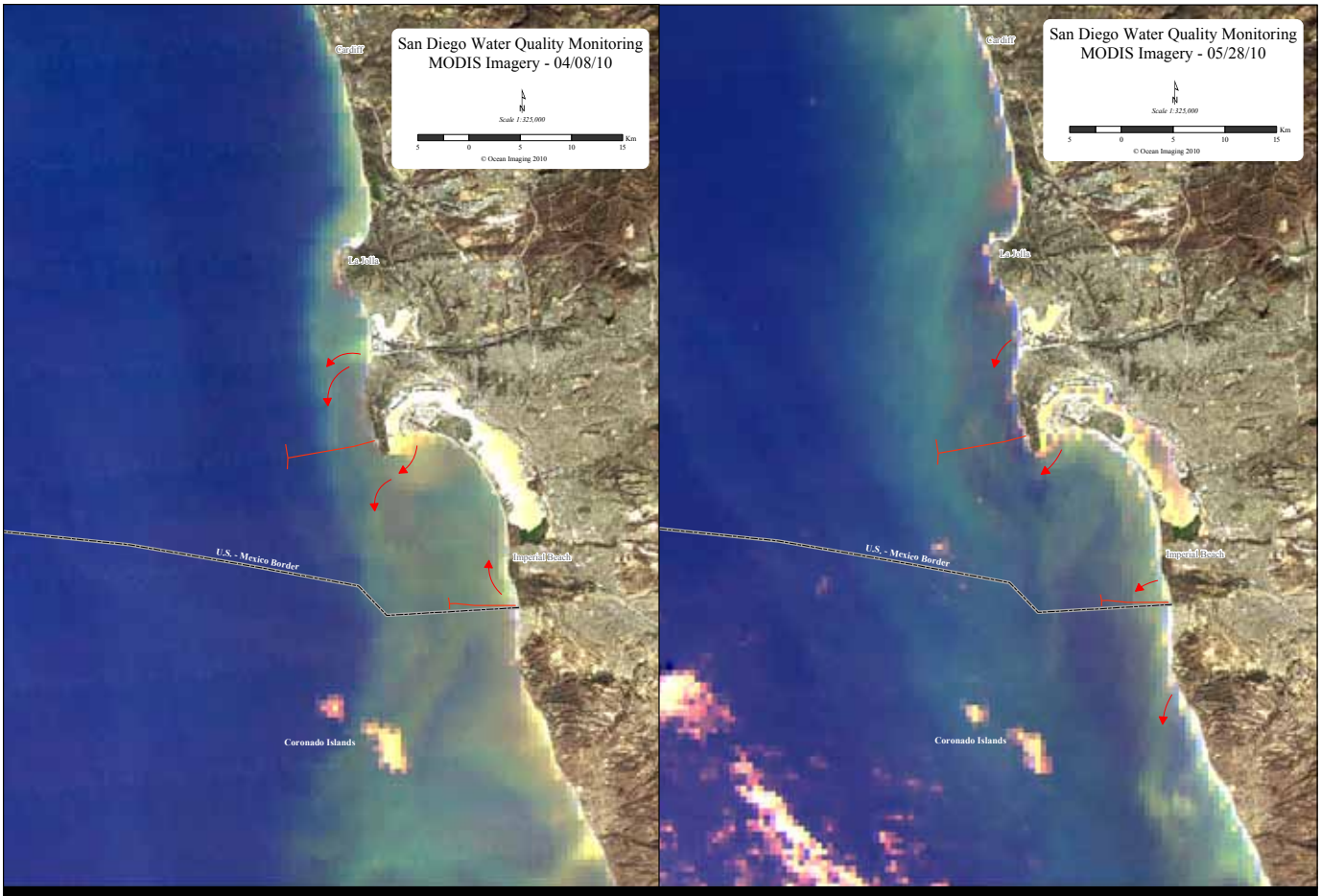

Figure 19.

MODIS satellite data from 4/8/2010 (left) and 5/28/2010 (right) showing extensive plankton blooms in San Diego's nearshore waters.

Figure 20.

(A) MODIS satellite imagery of the Pt. Loma region from 5/3/2010 showing a jet of turbid water originating nearshore to be advected directly over the PLO wye; (B) TM satellite image of the Pt. Loma region from 9/27/2010 showing turbid, high chlorophyll water originating off the South Bay coastline reaching over and past the PLO wye.

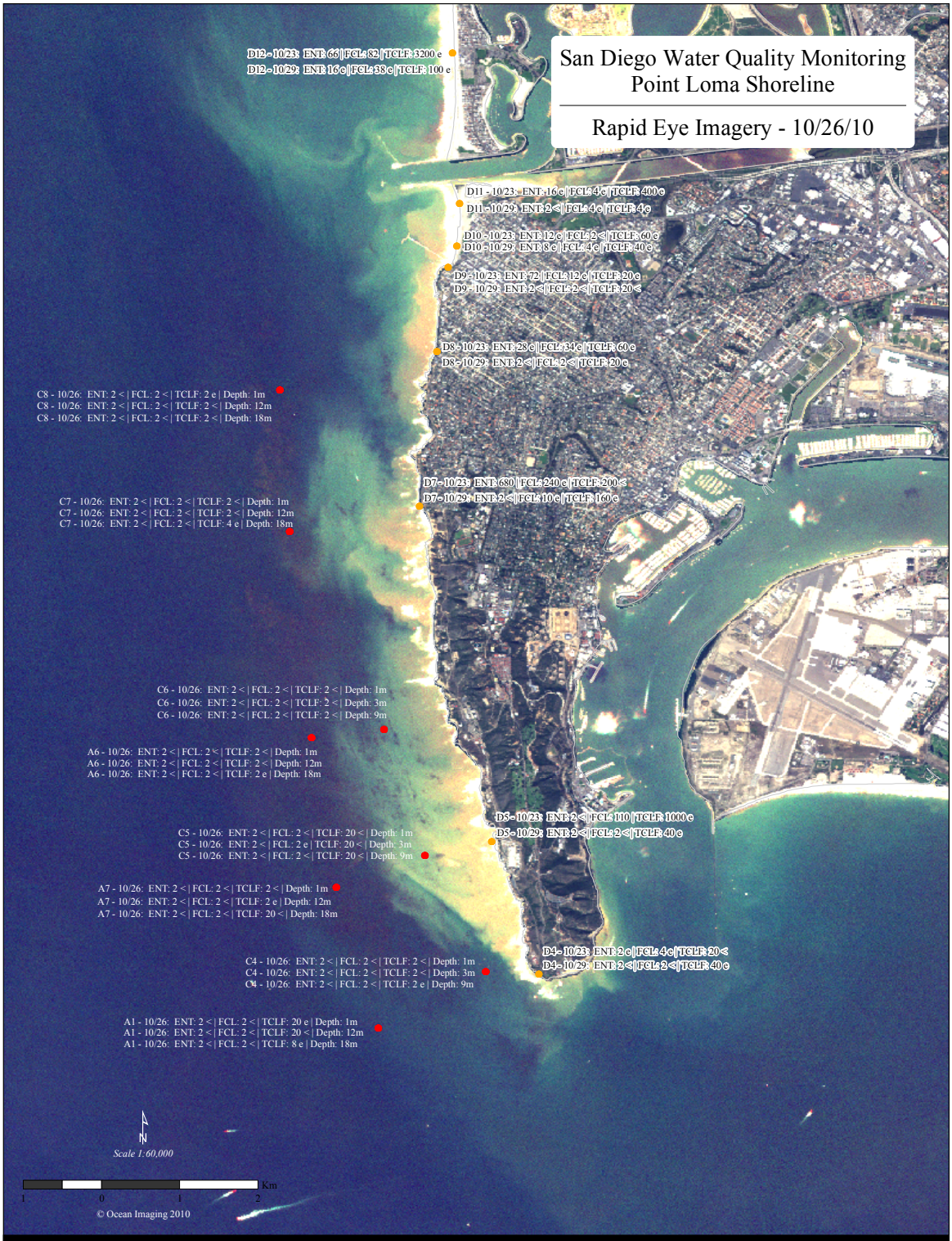

Figure 21a.

RapidEye satellite imagery from 10/26/2010 showing the Pt. Loma nearshore region after rains. Offshore bacterial sampling data from the same day are also shown.

Figure 21B.

RapidEye satellite imagery from 11/1/2010 showing the Pt. Loma nearshore region during dredging operations in Mission Bay (see text).

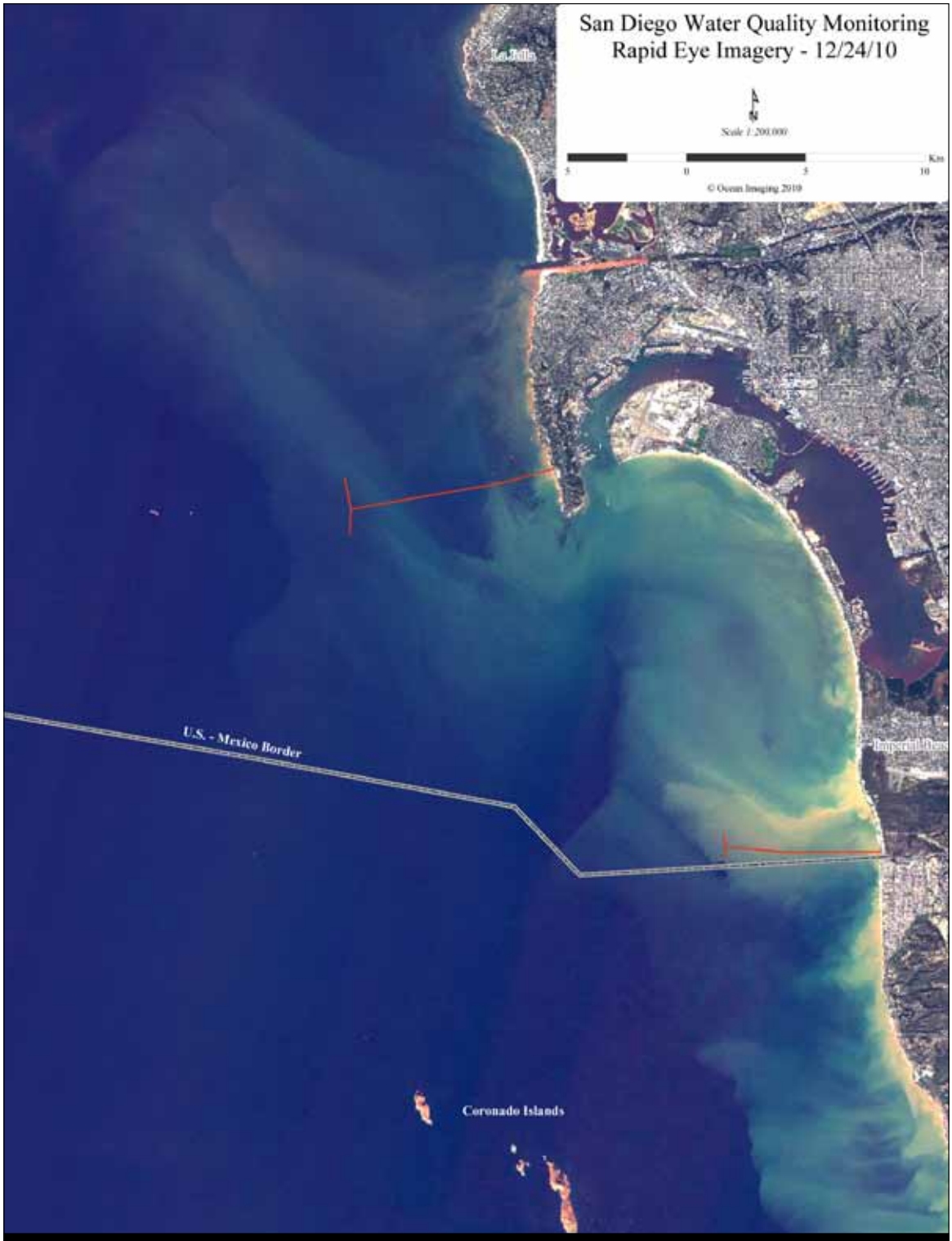

Figure 22.

RapidEye satellite image of the San Diego region from 12/24/2010 after the heaviest rains of the year.

Appendix H.3

2011 Ocean Imaging Report

Satellite & Aerial Coastal Water Quality Monitoring in The San Diego / Tijuana Region

By Jan Svejkovsky

Annual Summary Report
1 January, 2011 - 31 December, 2011

This draft to become final in sixty days.

30 April, 2012 (Revised 21 May, 2012)

Ocean Imaging

201 Lomas Santa Fe Drive, suite 370, Solana Beach, CA 92075 Phone: 858-792-8529 Fax: 858-792-8761 www.oceani.com

Table of Contents

1.0 Introduction & Project History 1

2.0 Technology Overview 1

2.1 Imaging in the UV-Visible-Near Infrared Spectrum 1
2.2 Imaging in the Infrared spectrum 2
2.3 Data Dissemination and Analysis 2
2.4 Existing and Future Enhancements of the Remote Sensing Monitoring Project 3

3.0 Highlights of 2012 Monitoring 3

3.1 Atmosheric & Ocean Conditions 3
3.2 The South Bay Ocean Outfall Region 3
3.3 The Point Loma OCean Outfall Region 12

1. Introduction and Project History

Ocean Imaging Corp. (OI) specializes in marine and coastal remote sensing for research and operational applications. In the 1990s, OI received multiple research grants from NASA's Commercial Remote Sensing Program for the development and commercialization of novel remote sensing applications in the coastal zone. As part of these projects, OI developed methods to utilize various types of remotely sensed data for the detection and monitoring of stormwater runoff and wastewater discharges from offshore outfalls. The methodology was initially demonstrated with collaboration of the Orange County Sanitation District. The NASA-supported research and demonstration led to a proof-of-concept demo project in the San Diego region co-funded by the EPA in 2000. Those results led, in turn, to adding an operational remote imaging-based monitoring component to the San Diego region's established water quality monitoring program, as stipulated in discharge permits for the International Wastewater Treatment Plant and Pt. Loma outfalls. The project was spearheaded by the State Water Resources Control Board (SWRCB), EPA Region 9, and continues to be jointly funded by the International Boundary Waters Commission and the City of San Diego.

The first phase of the project was a historical study utilizing various types of satellite data acquired between the early 1980s and 2002. The study established, among other findings, the prevailing near-surface current patterns in the region under various oceanic and atmospheric conditions. The current directions were deduced from patterns of turbidity, ocean temperature and surfactant slicks. In some cases, near-surface current velocity could be computed by tracking recognizable color or thermal features in time-sequential images. The historical study thus established a baseline data base for the region's current patterns, their persistence and occurrence frequency, and the historical locations, size and dispersion trajectories of various land and offshore discharge sources (e.g. the offshore outfalls, Tijuana River, Punta Bandera Treatment Plant discharge in Mexico, etc.).

In October, 2002 the operational monitoring phase of the project was initiated. This work utilizes 500m resolution Moderate Resolution Imaging Spectroradiometer (MODIS) color imagery (available near-daily), and 27m & 60m Thematic Mapper TM5 & TM7 color and thermal imagery (available 4 times per month)... In addition, the project relies heavily on acquisition of multispectral color imagery with OI's DMSC-MKII aerial sensor and thermal infrared (IR) imagery from a Jenoptik thermal imager integrated into the system (see details in the "Technology Overview" section). These aerial image sets are most often collected at 2m resolution. The flights are done on a semi-regular schedule ranging from 1-2 times per month during the summer to once or more per week during the rainy season. The flights are also coordinated with the City of San Diego's regular offshore field sampling schedule so that the imagery is collected on the same day (usually within 2-3 hours) of the field data collection. Additional flights are done on an on-call basis immediately after major storms or other events such as sewage spills.

This report summarizes observations made during the period 1/1/2011 – 12/31/2011.

2. Technology Overview

OI uses several remote sensing technologies to monitor San Diego's offshore outfalls and shoreline water quality. Their main principle is to reveal light, heat or microwave signal patterns that are characteristic of the different discharges. Most often this is due to specific substances contained in the effluent but absent in the surrounding water.

2.1 Imaging in the UV-Visible-Near Infrared Spectrum

This is the most common technique used with satellite images and the DMSC aerial sensor. Wavelengths (colors) within the range of the human eye are most often used but Ultraviolet (UV) wavelengths are useful for detecting fluorescence from petroleum compounds (oil, diesel, etc.) and near-IR wavelengths can be useful for correcting atmospheric interference from aerosols (e.g. smog and smoke).

The best detection capabilities are attained when several images in different wavelengths are acquired simultaneously. These "multispectral" data can be digitally processed to enhance features not readily visible in simple color photographs. For example, two such images can be ratioed, thus emphasizing the water features' differences in reflection of the two wavelengths. A multi-wavelength image set can also be analyzed with "multispectral classification algorithms" which separate different features or effluents based on the correlation relationships between the different color signals.

The depth to which the color sensors can penetrate depends on which wavelengths they see, their sensitivity and the general water clarity. In the San Diego region, green wavelengths tend to reach the deepest and, as elsewhere, UV and near-IR wavelengths penetrate the least. Generally, OI's satellite and aerial sensor data reveal patterns in the upper 15-40 feet.

The color channels on satellite sensors cannot be changed, so they tend to be relatively broad, separating red, green, near-IR, and sometimes blue parts of the spec-

trum. OI's DMSC aerial 4-channel sensor has the added advantage of allowing each channel wavelength to be precisely customized. Through experimentation, OI has determined the exact wavelength relationships that maximize the detection of the offshore sewage outfall plumes and nearshore discharges such as the Tijuana River. With this channel configuration it is possible to monitor the plumes even when they are not visible to the naked eye.

2.2 Imaging in the Infrared Spectrum

Some satellite and aerial sensors image heat emanatingSome satellite and aerial sensors image heat emanating from the ground and the ocean. They thus reveal patterns and features due to their differences in temperature. Since infrared wavelengths are strongly absorbed by water, the images reveal temperature patterns only on the water's surface. Such images can help detect runoff plumes when their temperatures differ from the surrounding ocean water. Runoff from shoreline sources tends to be warmer than th ocean water, although the reverse can be true during the winter. Plumes from offshore outfalls can sometime also be detected with thermal imaging. Since the effluent contains mostly fresh water, it is less dense than the surrounding salt water and tends to rise to the surface. If it makes it all the way, it is usually cooler than the surrounding sun-warmed surface water. If it is constrained by a strong thermocline and/or pycnocline ("vertical stratification"), it sometimes tends to displace some of the water above it in a doming effect. This displacement pattern is revealed in the thermal surface imagery.

2.3 Data Dissemination and Analysis

The satellite and aerial imaging data are made available to the funding agencies, the San Diego County Dept. of Health and the EPA through a dedicated, password-protected web site. Although it is possible to process most of the used data in near-real-time, earlier in the project the funding agencies decided that the emphasis of this project is not on providing real-time monitoring support and the extra costs associated with the rapid data turn-around are not warranted. Most satellite data is thus processed and posted within 1-2 days after acquisition and the aerial sensor imagery (which requires the most labor-intensive processing), within 2-5 days. OI has, however, in a number of cases, made some imagery available to the CDH and others in near-real time when observations were made that appeared to be highly significant for the management of beach closures or other sudden events.

2.4 Existing and Future Enhancements of the Remote Sensing Monitoring Project

Starting in 2011, Ocean Imaging has been providing the City with near-real-time access to daily imagery and multiple processed products from AVHRR and MODIS satellite sensors. As is discussed below, we are presently working on further integrating these as well as other satellite data and analysis products into the City's new GIS system:

Integration of Ocean Imaging-Generated Oceanographic and Weather Data with the EMTS web-based GIS "BioMap" Server: Since 2010 the City of San Diego Public Utilities Department's Environmental Monitoring and Technical Services (EMTS) Division has been developing a web-based GIS application to increase staff access to ocean monitoring data. The web application, called 'BioMap' has analytical tools which enable EMTS staff and others with access to the system to synthesize and explore large volumes of data dynamically via a web browser interface, in ways not possible in the past (Luostarinen, 2010). In order to make use of this web mapping technology and be compatible with BioMap, over the latter part of 2011 Ocean Imaging (OI) engaged in discussions with EMTS personnel about how to incorporate OI-supplied imagery and oceanographic data products into the BioMap system. It was determined that, compared to the existing methods (downloading from OI's password-protected San Diego Water Quality web site), the inclusion of OI data in BioMap via an OI-supported web map server will better facilitate the correlation of EMTS biological and water quality information to the environmental conditions visible in OI data products. Delivering and analyzing data using BioMap will greatly increase both the accessibility and utility of existing and future OI information products. As part of the plan to be compatible with BioMap OI intends to implement the following over the first three quarters of 2012:

- OI will determine the data formats of all of the existing raster and vector data products necessary for seamless incorporation into the BioMap server.
- The BioMap GIS application is served by ESRI's ArcGIS Server product, built in Adobe Flex using ESRI's API to enhance the end user interface. OI has decided to purchase ArcGIS Server and build an Open Geospatial Consortium-compatible (OGC) Web Map Service (WMS) which communicates directly and seamlessly with the BioMap server.
- Delivery of existing OI data products will be transitioned over to the OI-hosted WMS with links available only to BioMap for data access. OI will eventually house the WMS hardware and software at their Internet Service Provider's (ISP) facility deployed on a virtual machine cluster. The deployment via a computer cluster on a dedicated virtual private server will provide a higher level of availability to the end users, more computational power, enhanced scalability as well as increased security and system redundancy to avoid data loss and down time.

- The existing web site used for the delivery of OI data will remain in place and active during the transition to the OI WMS, however present plans are to eventually phase it out as EMTS and constituent users migrate to BioMap as their primary data repository and interface. OI will work with the City of San Diego and the International Water Boundary Commission (IWBC) to determine how long the existing web site will remain in place and active.

- As part of the transition to BioMap, OI will work with the EMTS staff to add new information products to the OI mix. Some of these products were not easily delivered and displayed prior to the existence of BioMap. Possible new OI data products include, but are not limited to:

    - Ocean surface current vector fields generated from the High Frequency Radar (HFR) system presently in place and active for the entire California coast out to 100 km. These data area available as 25 hour averages updated on an hourly basis. OI will extract a geographical subset of the entire data set and make available to BioMap on a temporal frequency decided on by OI and EMTS staff.

    - Oceanographic model-based ocean surface currents computed using both the Hybrid Coordinate Ocean Model (HYCOM) and geostrophic currents generated from satellite altimeter data (sea surface height anomalies)

    - Subsurface ocean currents generated from the Global Ocean Data Assimilation Experiment (GODAE) dataset.

    - Ocean mixed layer depth analyses generated from the HYCOM model (see example below).

    - Ocean salinity analyses generated from the HYCOM model

    - Local stream gauge data

    - Local rainfall data

- Following the successful installation of OI's WMS and its integration with BioMap, OI will work with the EMTS staff to optimize the fusion of these two systems and make a final determination as to which of the new and existing OI data products should remain as regular, ongoing deliverables.

With the OI data products available for display and analysis via BioMap the speed of availability, convenience to the end users and the decision-making power of the information will be dramatically increased. Combined with the addition of the new oceanographic and weather products, OI's service to the City of San Diego and the IWBC stands to significantly increase in value at little to no additional cost.

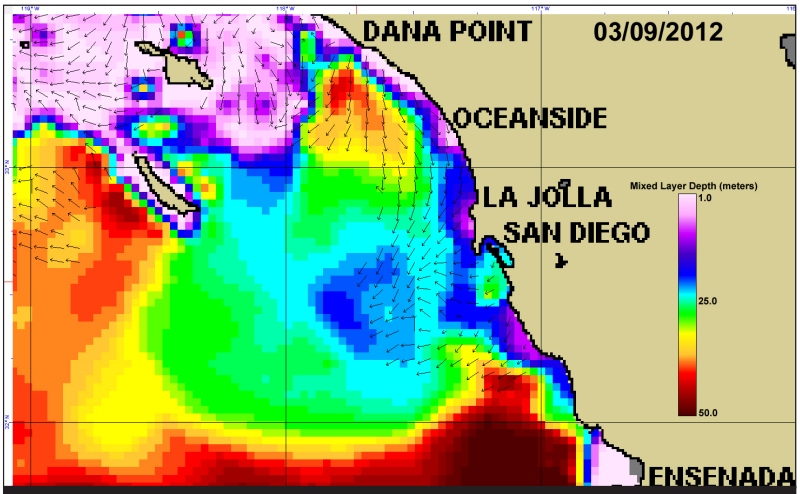

Sample HYCOM-generated ocean mixed layer depth analysis with HF Radar-derived surface currents overlaid.

Citations

Luostarinen, J. (2010). *BioMap_summary_for_ESRI_RegUG_Feb_final_sent.doc*. The City of San Diego Public Utilities Department's Environmental Monitoring and Technical Services (EMTS) Division. Received via email.

3. Highlights of 2011 Monitoring

3.1 Atmospheric & Ocean Conditions

Following a major rain period in late December, 2010, the San Diego region experienced relatively dry conditions through January and early February, 2011. The most rain fell in late February and March, then in November **(Figures 1 and 2)**, at the end of which San Diego seasonal rainfall was well above normal for the 2011/2012 season. This excess quickly disappeared, however, during a relatively dry December.

Below-normal sea surface temperatures (SSTs) around San Diego during the summer months paralleled conditions in 2010. **Figure 3** shows representative SSTs in mid-July during the last 4 years and highlights the region's cool trend in 2010 and 2011 versus the previous years. As always, San Diego's North County shoreline experienced the warmest regional SSTs, however, they barely

reached above 70°F on the warmest days. The North County nearshore waters were also a consistent source of red tides and phytoplankton blooms from spring through fall, which tended to be swept southward with the nearshore currents and thus affected coastal water clarity from North County to the Pt. Loma area.

3.2 The South Bay Ocean Outfall Region

The South Bay Ocean Outfall (SBOO) wastewater plume generally remains well below the surface between approximately late March and November due to vertical stratification of the water column. During that period it usually cannot be detected with multispectral aerial and satellite imagery which penetrate the upper 7 to 15 meters (depending on water clarity). The plume also cannot be detected with thermal IR imaging which does not penetrate below the surface. Seasonal breakdown of the vertical stratification results in the plume's rise closer to the surface or to actually reach the surface between approximately late November and late March, when it can often be detected with aerial and satellite imaging. In 2011 the SBOO plume was visible through the end of March. Vertical stratification **(Figure 4)** kept the plume from reaching the near-surface waters in the summer and early fall. A weak signature from the plume was detected again in mid-October **(Figure 13)**, which is the earliest such observation in recent years.

The heavy rainfall in late December, 2010 caused large runoff volumes from the Tijuana River, which spread in both directions along the coast and caused contamination to reach Coronado's beaches. **Figure 5A** shows these conditions on the first day of 2011. The SBOO region is most commonly subject to a southward current regime. **Figure 6** shows such conditions on 1/12/2011. The patterns of nearshore turbid waters indicate a relatively strong southward flow, and CODAR data from Scripps Institution of Oceanography's system recorded surface current velocities in excess of 20cm/s over that area. The satellite imagery shows no trace of the SBOO plume eventhough its surface signature is most commonly observed in January. This suggests that the SBOO effluent likely becomes highly dispersed within the water column before it reaches the surface under such current conditions.

As in previous years, occasional flow reversals to the north caused the SBOO plume to be advected northwestward, as is exemplified on 1/21/2011 in **Figure 6B**. That

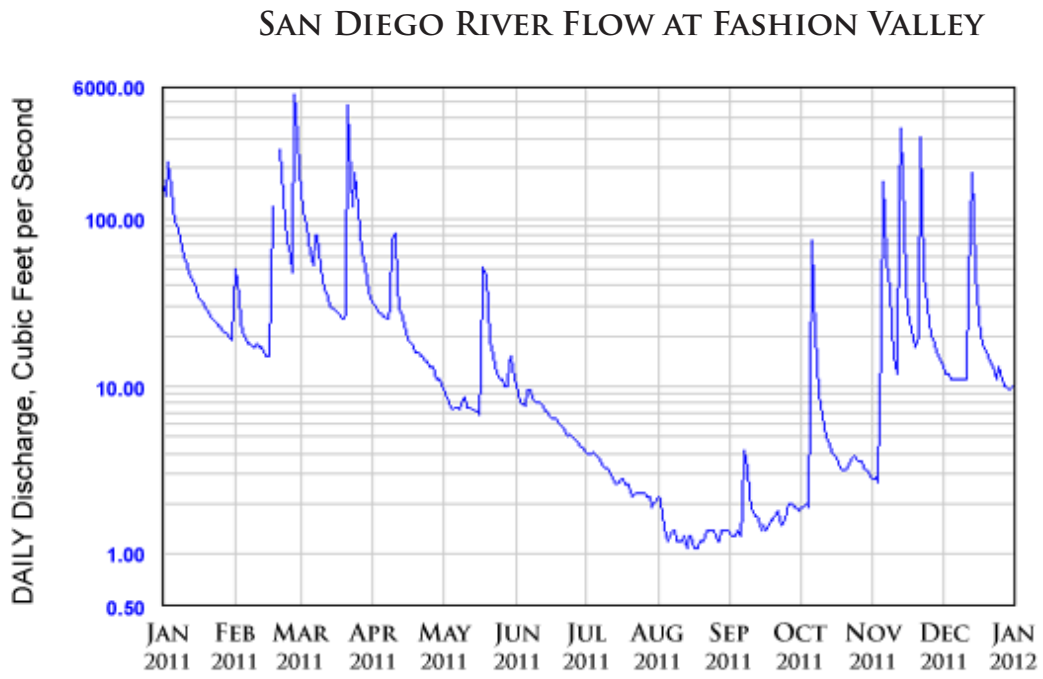

Lindberg Field Rainfall 2011	
January	0.30"
February	2.10"
March	1.46"
April	0.26"
May	0.36"
June	0.03"
July	0.00"
August	0.00"
September	0.13"
October	0.46"
November	3.12"
December	0.86"

Figure 1.

Graph of mean daily discharge of the San Diego River during 2010 (measured at Fashion Valley). The table on the right shows monthly rainfall totals at Lindbergh Field.

particular northward flow episode lasted several days. Under such persistent flow, satellite imagery has shown the Tijuana River runoff to reach as far as Pt. Loma where it can result in elevated indicator bacteria measurements around the Point. Satellite data obtained during the 21-23 January, 2011 period showed the Tijuana River plume to again reach the southern Pt. Loma area **(Figure 7)** although no time-coincident bacterial samples were available.

The relatively heavy rains in February greatly enlarged the Tijuana River runoff plume which expanded seaward over the SBOO wye **(Figure 8)**. With additional rain events, this condition continued through March **(Figures 9 and 10)**. The plume's waters corresponded to highly elevated near-surface bacterial measurements at some offshore stations **(Figure 9)**.

As is discussed in the next section, the SBOO region's nearshore waters during the 2011 summer months were actually clearer than areas to the north which were subject to persistent, intense plankton blooms. Due to seasonal sun angle versus orbit time geometry, several satellites tend to image the region's ocean in the sunglint area during the summer months. This reveals the patterns of surfactant slicks on the ocean surface, similar to those obtained with SAR instruments. In past years large slicks associated with Mexico's sewage discharge through los Buenos Creek have been commonly observed. The slicks were noticeably smaller in imagery collected during summer 2011, as is shown in **Figure 11**. We do not have information whether this observation is related to changes in treatment or output volume at the Punta Bandera plant. Additionally, the los Buenos plume was never observed to cross the U.S. border during 2011.

Figure 12 shows a major red tide that affected the entire San Diego County, including the SBOO region in September. Following this event the waters cleared and a Rapid Eye satellite image acquired on 10/11/2011 showed the first (albeit very weak) seasonal signature of the SBOO plume **(Figure 13)**. This is considerably earlier than in previous years. CTD casts at sampling stations I18 and I22 show a considerable breakdown of vertical stratification between September and October, 2011 **(Figure 4)** which, in addition to the relatively clear water conditions, may account for the plume's reaching near-surface and becoming detectable so early.

As was already noted, November 2011 was a very rainy month. Curiously, the Tijuana River runoff plume, as

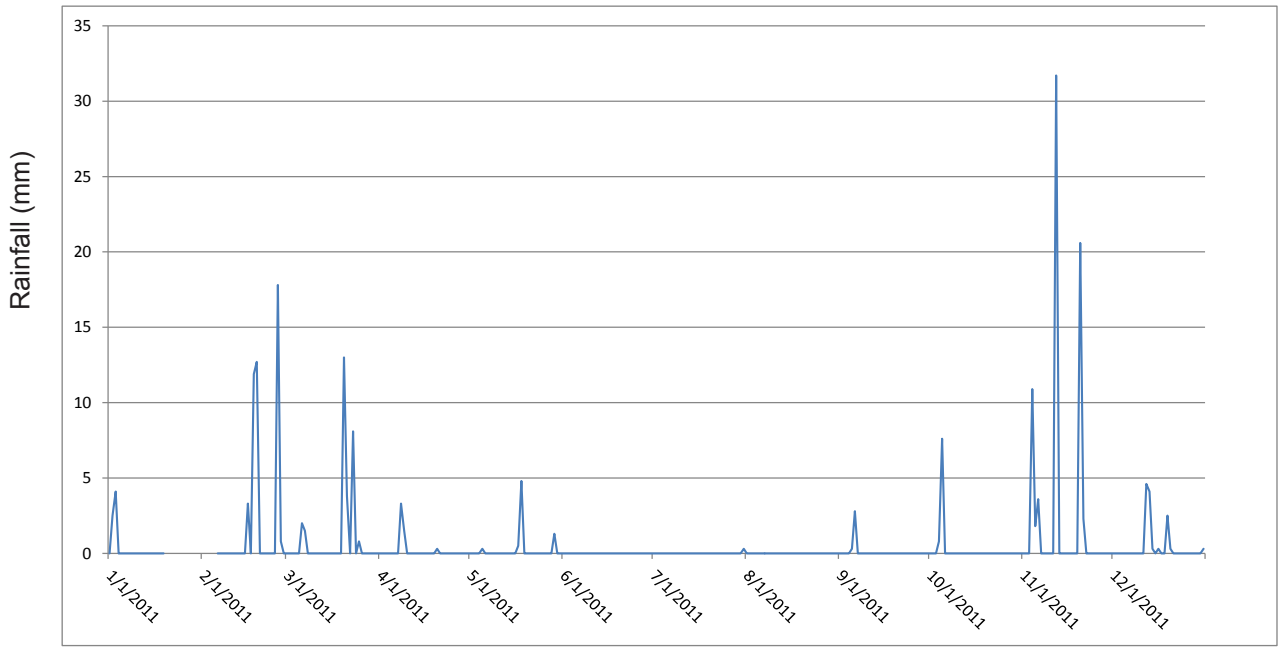

Figure 2.

Graph of daily cumulative daily rainfall in the Tijuana Estuary.

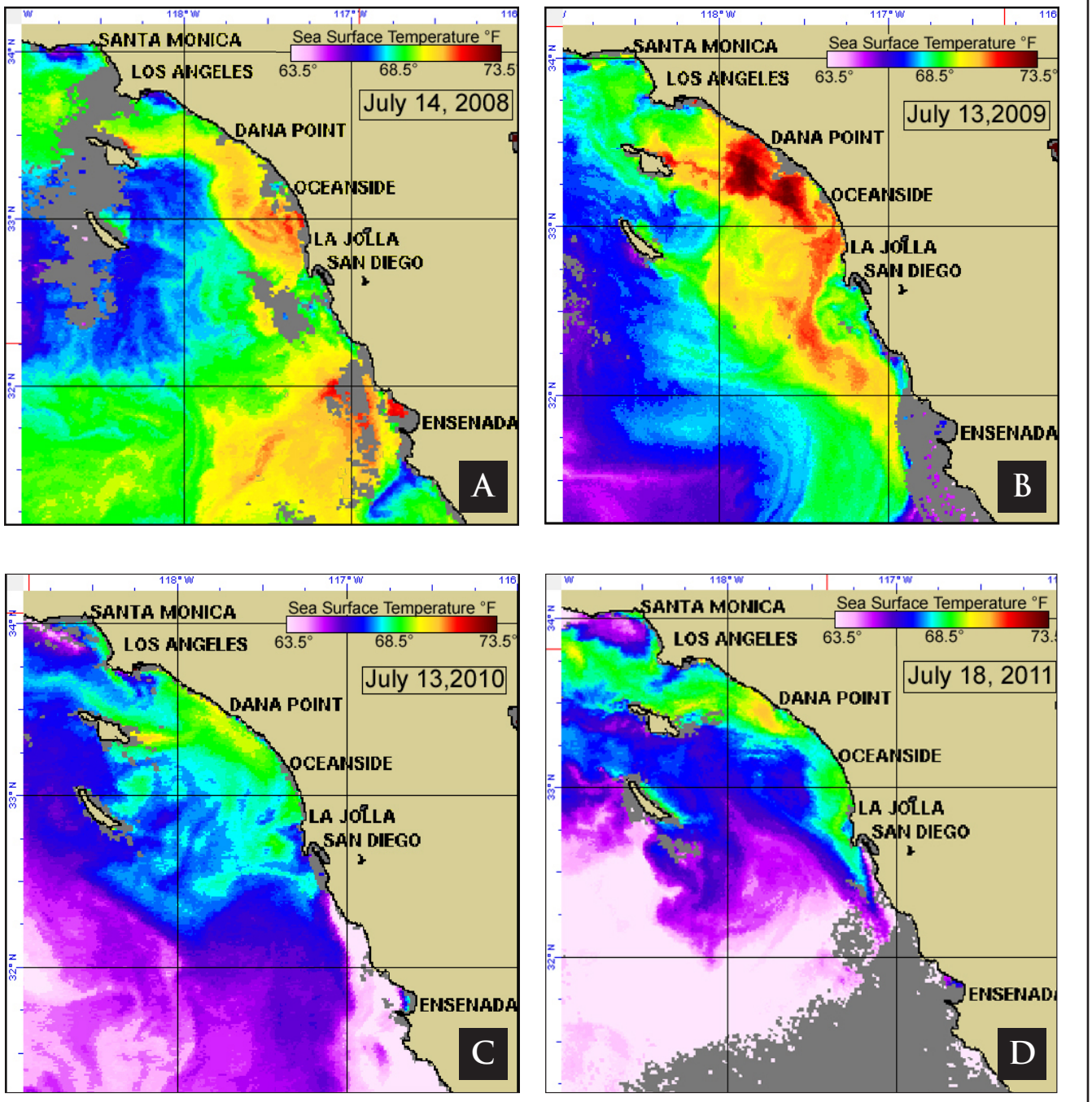

Figure 3.

AVHRR-satellite-derived sea surface temperatures over Southern California on 7/14/2008 (A), 7/13/2009 (B), 7/13/2010 (C) and 7/18/2011 (C). Note how much cooler the mid-July waters were during 2010 and 2011.

observed with remote sensing imagery, remained relatively small and nearshore. Similar conditions were observed from other runoff sources further north. One possible explanation is that many of the rain events consisted of steady yet relatively light rainfall which allowed much of the precipitation to be absorbed into the ground, versus sudden, heavy downpours which tend to result in greater runoff. This premise is supported by San Diego River flow and monthly rainfall data shown in **Figure 1**: although the November rainfall total was significantly larger than rain totals in previous February and March, November peak river flows were a mere fraction of peaks recorded the previous winter. Although reduced in volume and sediment load, the Tijuana River waters entering the ocean were significantly contaminated, as is exemplified by imagery and time-coincident bacterial sampling data in **Figure 14**.

Under mild current conditions during the winter months, the SBOO effluent rises directly up through the water column above the wye and separate plumes from the different riser groups are sometimes discernible in high resolution imagery. Such conditions existed in late December, 2011 and an example is shown in **Figure 15**.

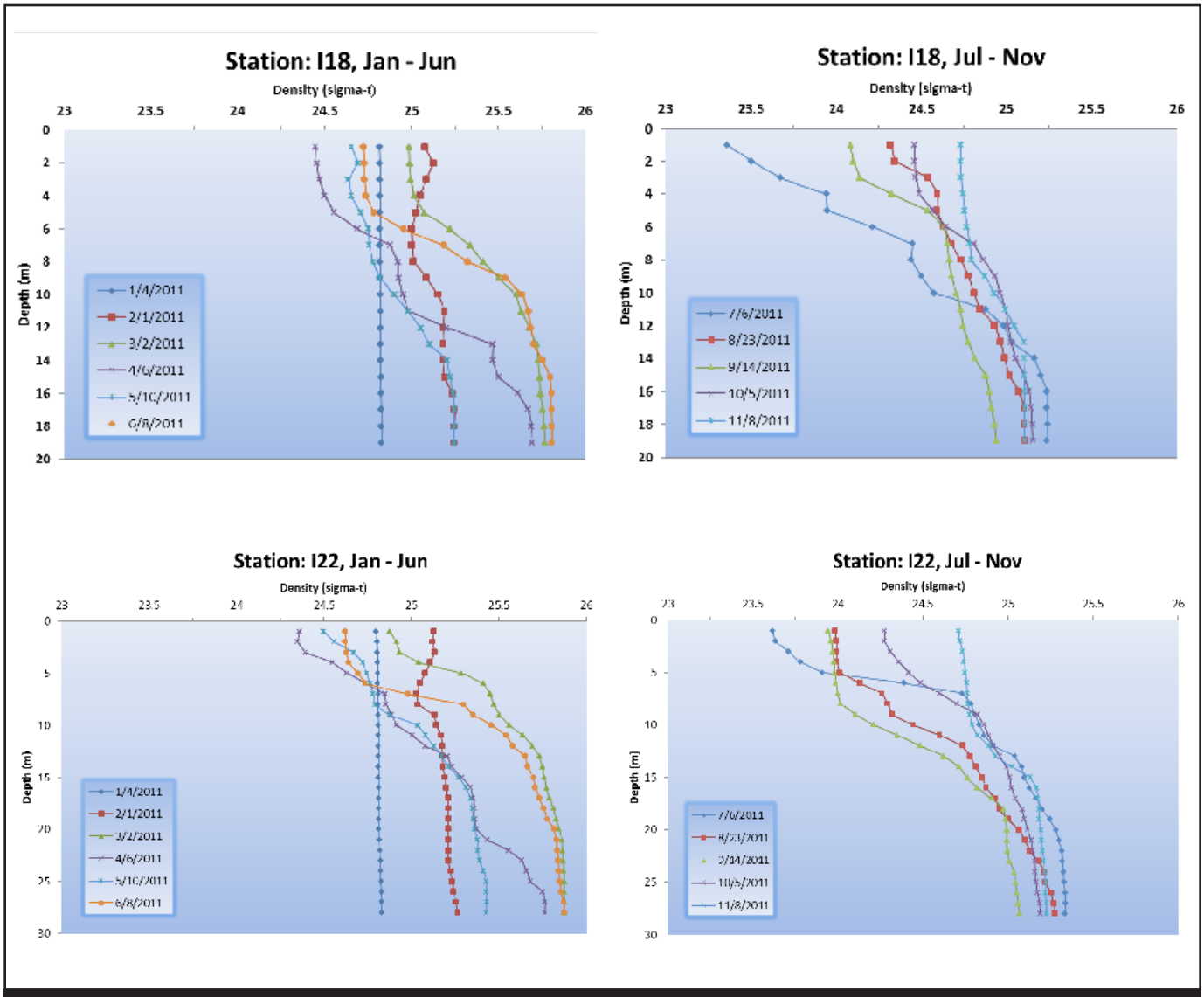

Figure 4.

Vertical density profiles from the City's monthly CTD surveys at sampling stations I18 (top) and I22 (bottom). (December data were not yet available at the time of this report's preparation.)

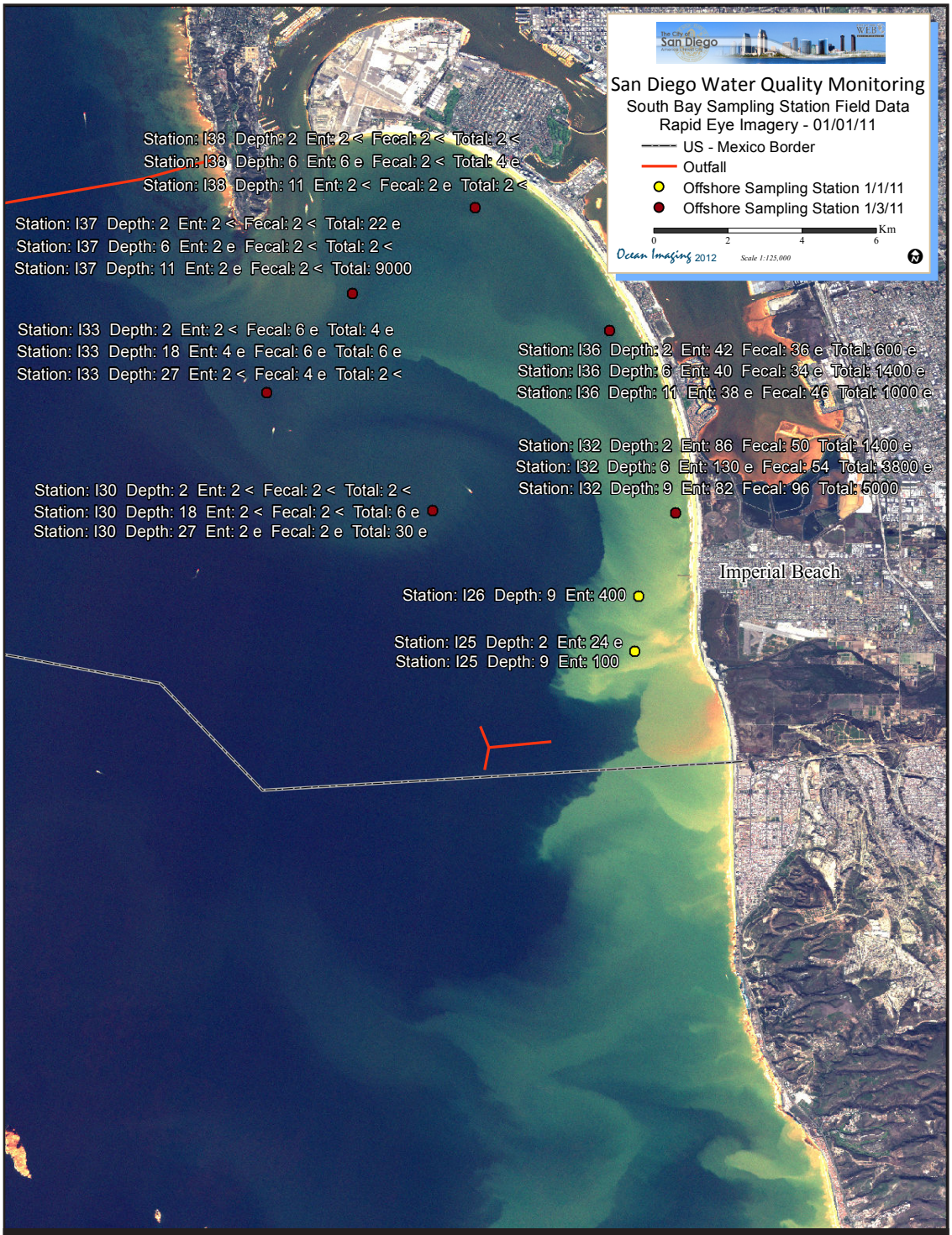

Figure 5.

RapidEye satellite imagery of the South Bay and Tijuana shoreline region acquired on 1/1/2011. Bacterial sampling results from 1/1/11 and 1/3/11 are also shown.

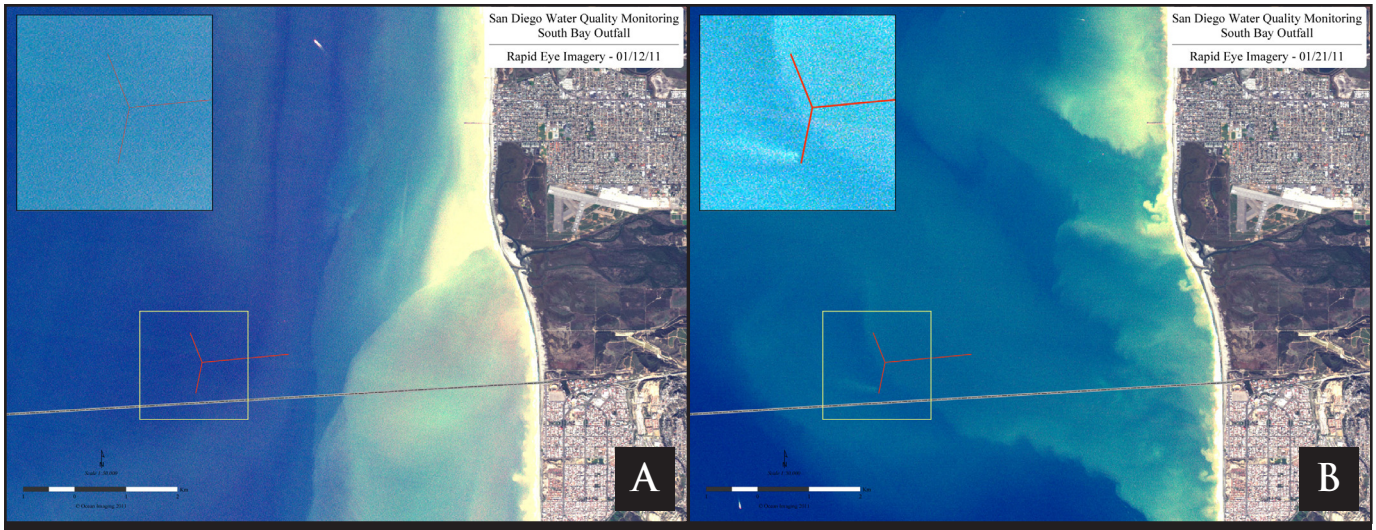

Figure 6.

RapidEye satellite imagery of the SBOO region from 1/12/2011 (A) and 1/21/2011 (B). Surface currents in excess of 20cm/s existed in the area on 1/12/2011.

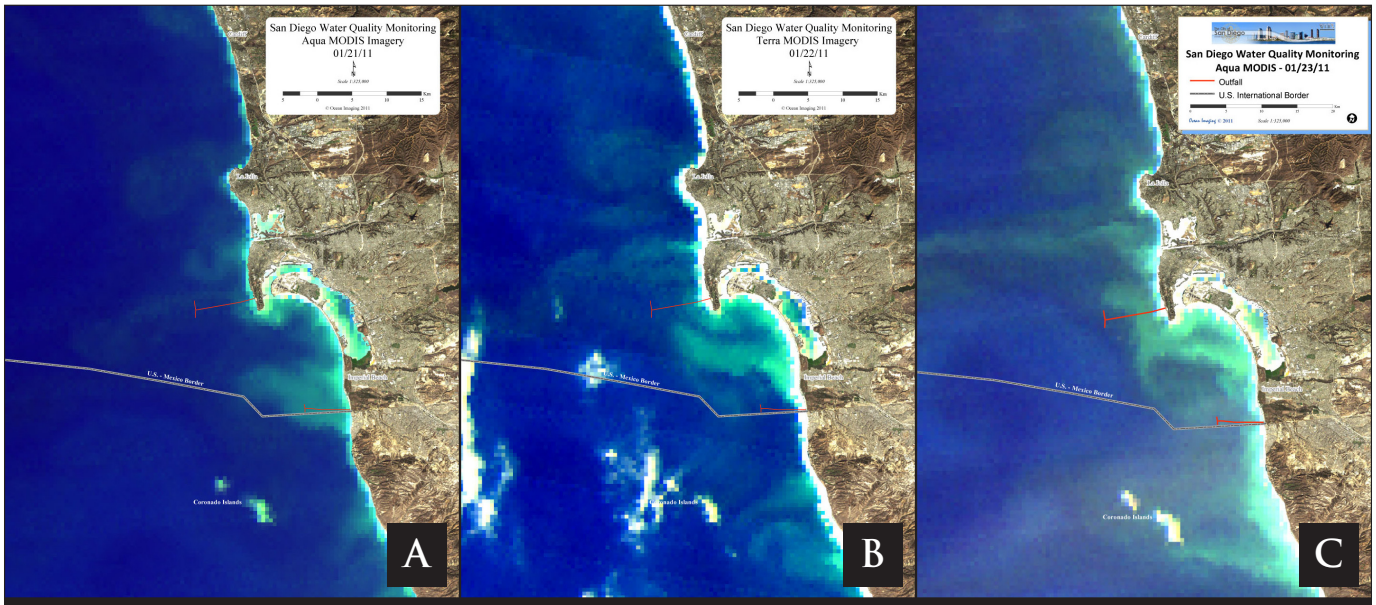

Figure 7.

MODIS satellite image of the San Diego region acquired on 1/21/2011 (A), 1/22/2011 (B), and 1/23/2011 (C), showing northward progression of the Tijuana River plume into the Pt. Loma area.

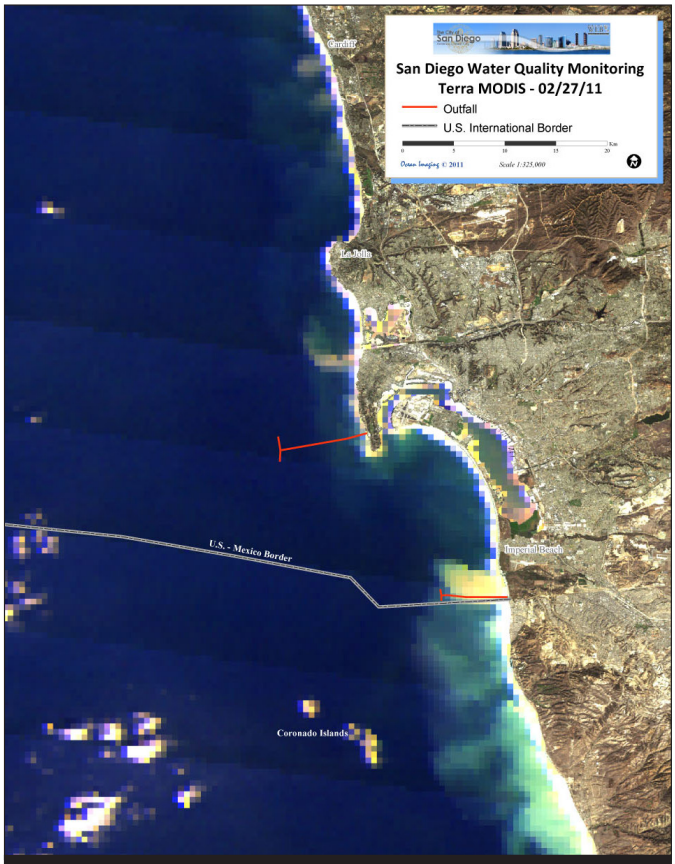

Figure 8.

MODIS color image from 2/27/2011 after relatively heavy rains showing a very large and sediment-laden Tijuana River plume (yellow feature).

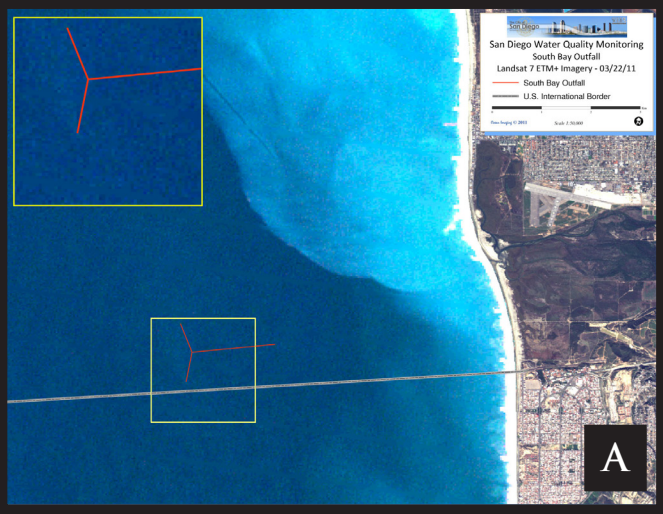

Figure 9.

Landsat e-TM satellite image of the South Bay region acquired on 3/22/2011 showing a surface signature of the SBOO plume due to increased turbidity (A), and lower temperature (B). Bacterial samples collected on the same day show high concentrations within the separate Tijuana Plume signature (C).

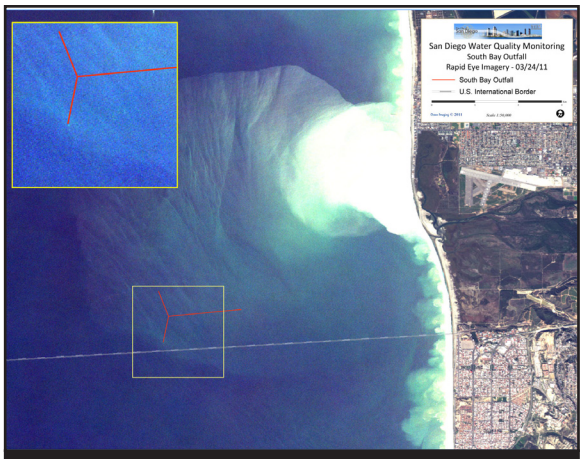

Figure 10.

RapidEye satellite image from 3/24/2011 showing the SBOO surface signature within turbid waters of the Tijuana River plume which extended past the outfall wye.

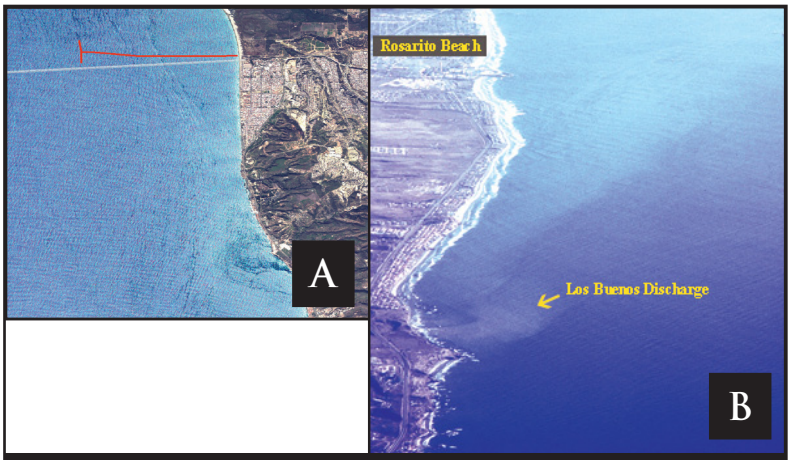

Figure 11.

RapidEye satellite imagery acquired on 6/18/2011 showing surfactant slicks in front of the Los Buenos Creek, Mexico within the sunglint pattern (A), and an oblique aerial photo of the slick from summer 2007 (B). Imagery collected during summer 2011 showed much smaller surfactant accumulations in the area than had been observed in previous years.

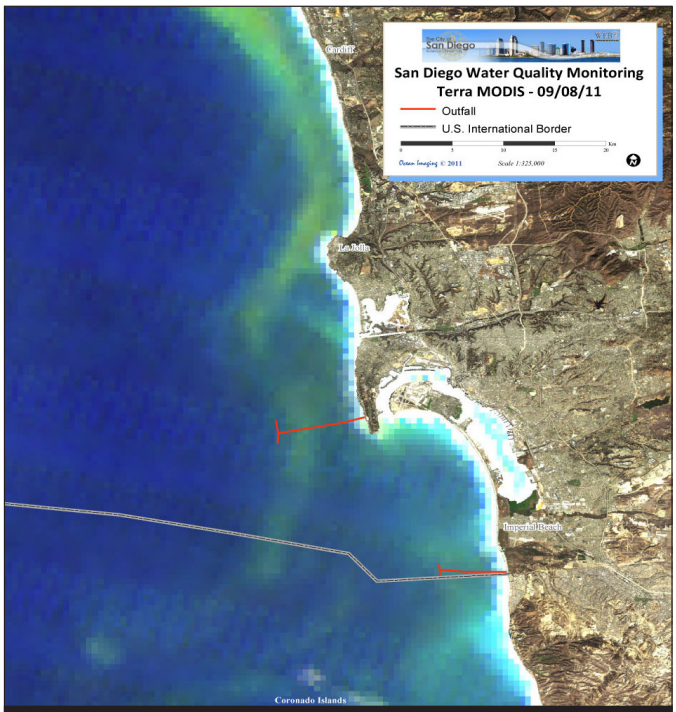

Figure 12.

MODIS satellite image of the San Diego region acquired on 9/8/2011 showing an extensive dinoflagellate bloom (red tide) along the coast.

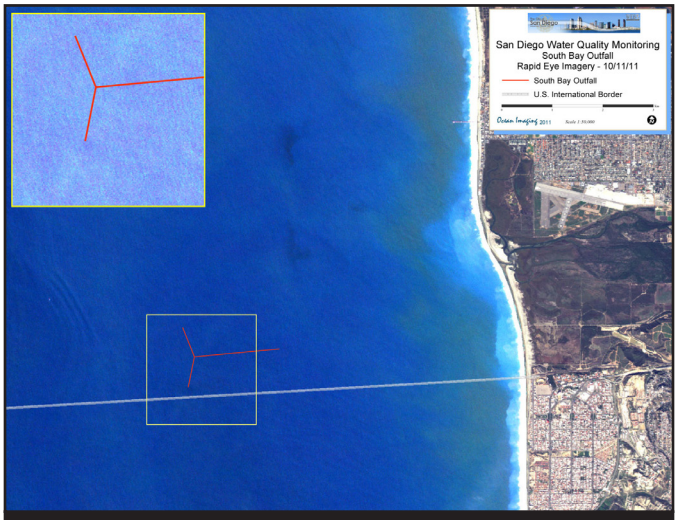

Figure 13.

RapidEye satellite image of the SBOO region acquired on 10/11/2011. The SBOO effluent plume signature had become weakly visible near the surface (darker circular feature over the end of the southern wye).

Figure 14.

RapidEye satellite image of the SBOO region acquired on 12/15/2011 and bacterial sampling results from the same day

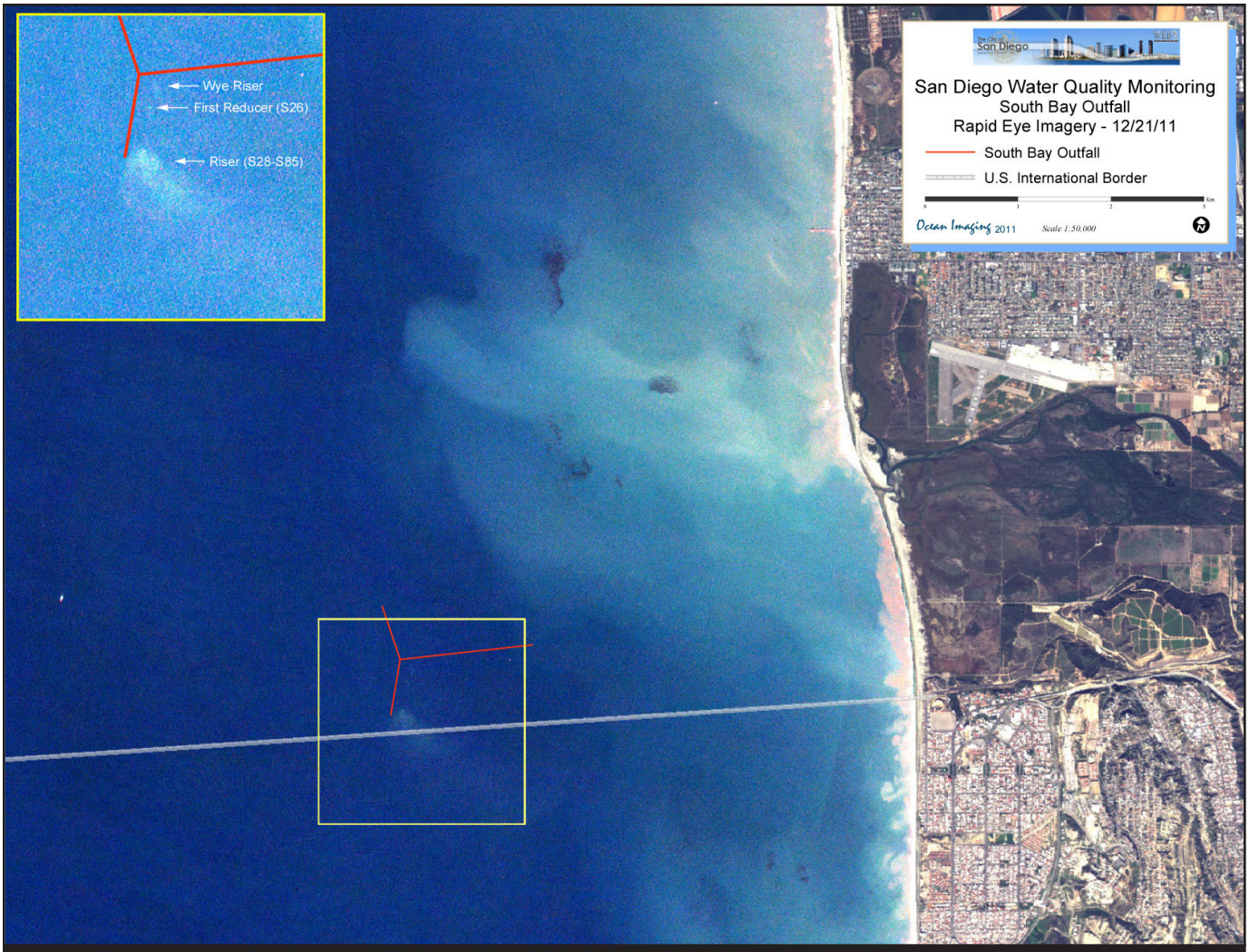

Figure 15.

RapidEye satellite image from 12/21/2011 showing SBOO plume signatures from individual riser groups.

3.3 The Point Loma Ocean Outfall Region

After its seaward extension in 1993, the Point Loma Outfall (PLO) is one of the deepest and longest wastewater outfalls in the world, discharging at the depth of 320 feet, 4.5 miles offshore. The outfall's plume is generally not observed directly with multispectral color or thermal imagery. It appears to not reach the surface waters, even during the winter months when the water column's vertical stratification is weakened. We believe, however, that on some occasions we have observed the plume's extents indirectly through an anomalous lateral displacement of thermal or chlorophyll features around the outfall wye. This effect can be explained by the doming up of the discharged effluent and laterally displacing the near-surface waters above it.

Early in 2011 the Pt. Loma region was influenced by the heavy rains in December 2010. **Figure 16** shows heavy turbid runoff features lining the shoreline and extending westward through the Pt. Loma kelp bed. Turbid runoff is also seen flowing from the San Diego River and Mission Bay, the latter being somewhat less sediment-laden. Both runoff plumes exhibit cooler-than-ocean thermal signatures. Conditions in the Pt. Loma region during an offshore sampling survey on 2/10/2011 are shown in **Figure 17**. No active shoreline runoff input sources are discernible and the bacteria sampling results show only background values in the upper part of the water column.

Beginning in early March and through June, the Pt. Loma region was consistently influenced by recurring red

tides and phytoplankton blooms which originated along the shoreline in Orange County and San Diego North County, then were swept southward past Pt. Loma. They tended to extend seaward over and past the PLO wye. Some examples are shown in **Figure 18 A-E**. The waters cleared in mid-July for a few weeks (**Figure 18 F**), but the plankton phenomena resumed in late summer and fall. **Figure 19** shows a TM-7 image of one such bloom on 8/29/2011. The sensor's thermal channel reveals the plankton bloom area off Pt. Loma to correspond to cool water (rendered as darker in **Figure 19B**). Also rendered within the cool (presumably upwelled) area are isolated, even cooler features that may correspond to localized divergence zones and vortices. This is the first time we have observed such structure in this area.

Figure 20A and B show more examples of plankton bloom events in September which originated along the North County coast and spread southward to cover the PLO area. **Figure 20C and D** show satellite views of a massive red tide event in October. It began along the shore north of Cardiff on 10/10-11/2011 and within 3 days swept past the San Diego coastline and south of the U.S./Mexico border. The frequency of the plankton blooms from spring through fall of 2011 was considerably higher than in most previous years. Because they began along the coast north of La Jolla and then were advected directly south along Pt. Loma, they generally did not affect the South Bay shoreline. Although the southern San Diego and northern Baja coast was affected periodically by localized upwelling and plankton blooms, water clarity was consistently better along that part of the coast than along Pt. Loma and areas to the north.

A notable sewage spill occurred in North County on 9/9/2011 when a city-wide power outage caused Pumpstation 64 to fail and spill sewage into Los Penasquitos Lagoon and out to sea. As is shown in **Figure 20A and B**, the latter spill occurred during one of the intense plankton blooms affecting the North County shoreline. No direct

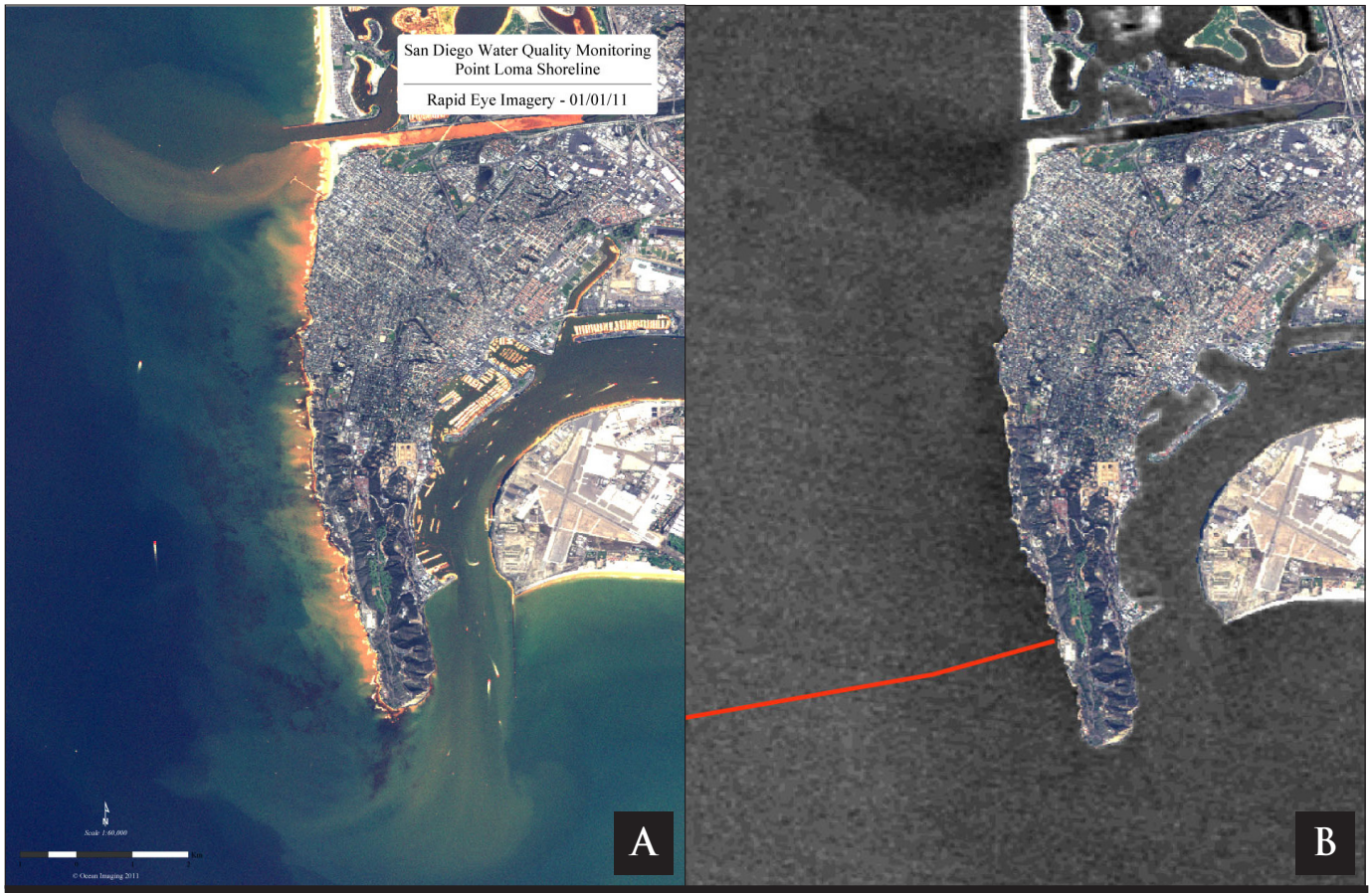

Figure 16.

Imagery of the Pt. Loma region on 1/1/2011 acquired with RapidEye multispectral (A) and TM-7 thermal (B) instruments.

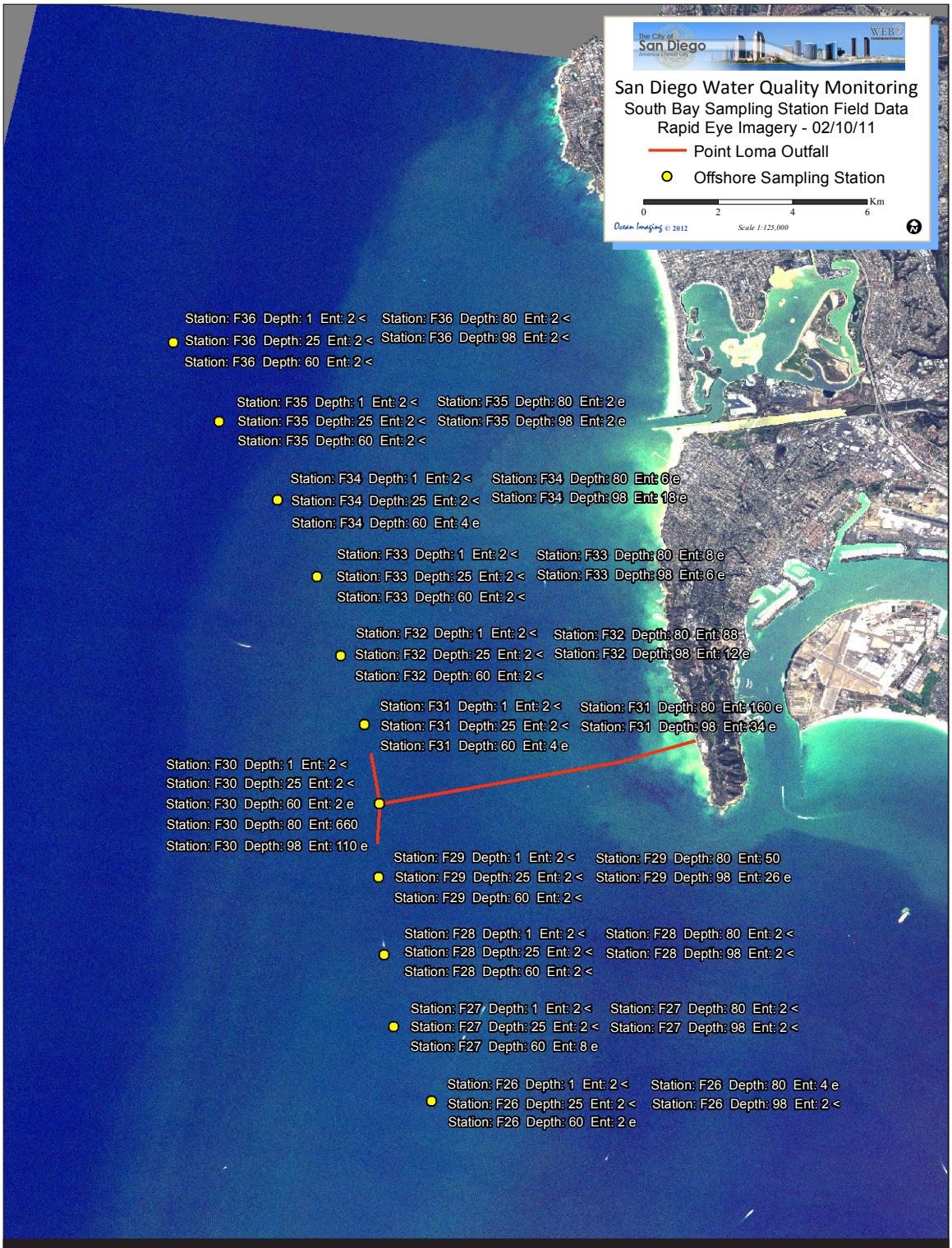

Figure 17.

RapidEye satellite image of the PLO region acquired on 2/10/2011 and bacterial sampling results from the same day.

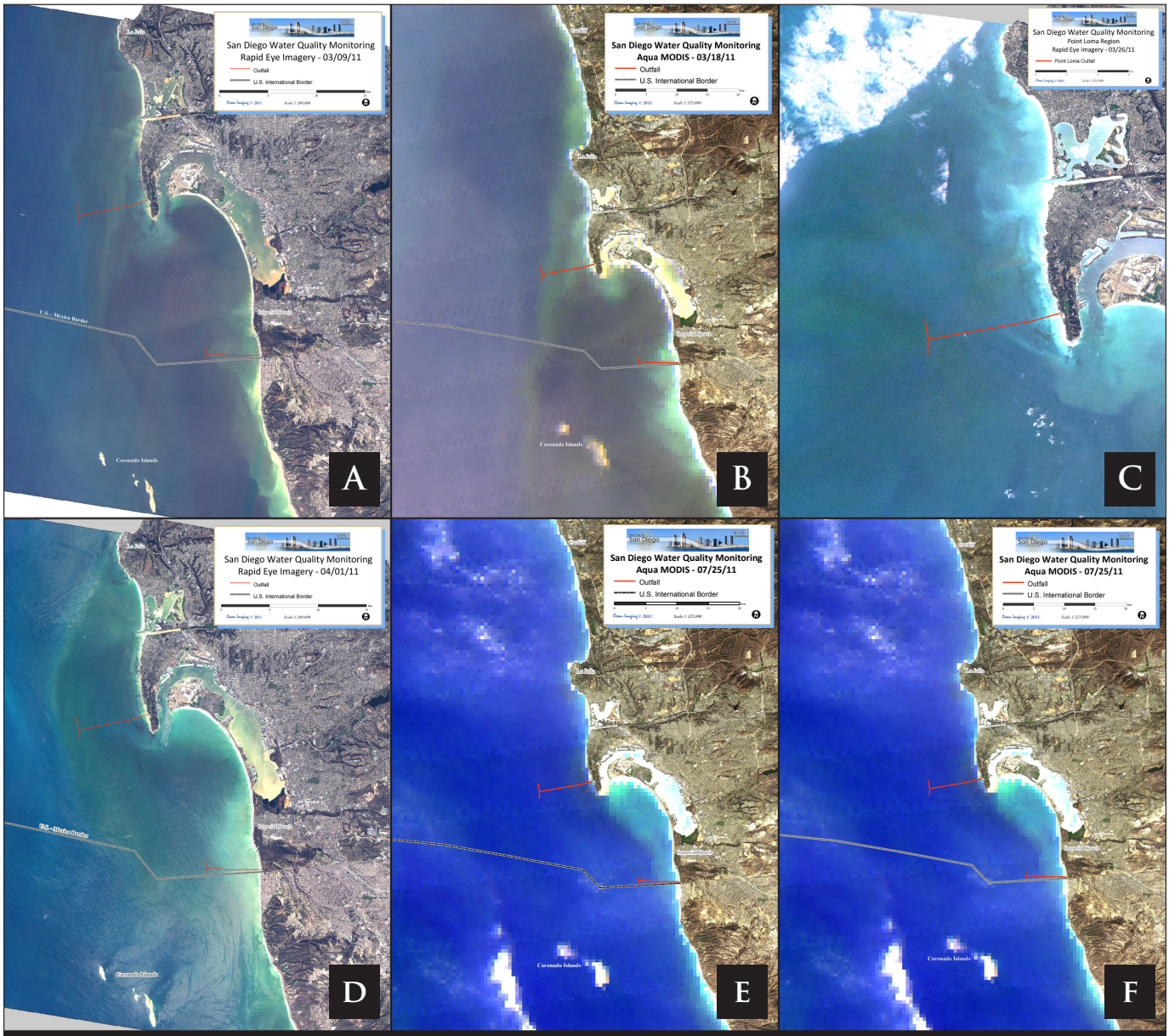

Figure 18.

Satellite imagery from 3/9/2011 (A), 3/18/2011 (B), 3/26/2011 (C), and 4/1/2011 (D) showing the PLO area to be consistently covered by southward-swept plankton blooms. The events eased somewhat in May but continued in June as shown on 6/5/2011 (E). The region finally cleared in mid-July as shown on 7/25/2011 (F).

observations of either spill were detected in the remote sensing data.

As was already noted, above average rainfall occurred in November, 2011. As was also already discussed, terrestrial runoff patterns into the ocean in the South County region, were considerably smaller than would have been expected, potentially due to the steady yet relatively light rain patterns which allowed much of the precipitation to be absorbed rather than lost as runoff. This same observation holds for runoff patterns along Pt. Loma and to the north, as exemplified by imagery shown in **Figure 21**. High resolution RapidEye data (**Figure 21A**) show a moderate plume of runoff from the San Diego River and Mission Bay. The runoff contained considerably less suspended sediment than, for example, the post rain conditions on

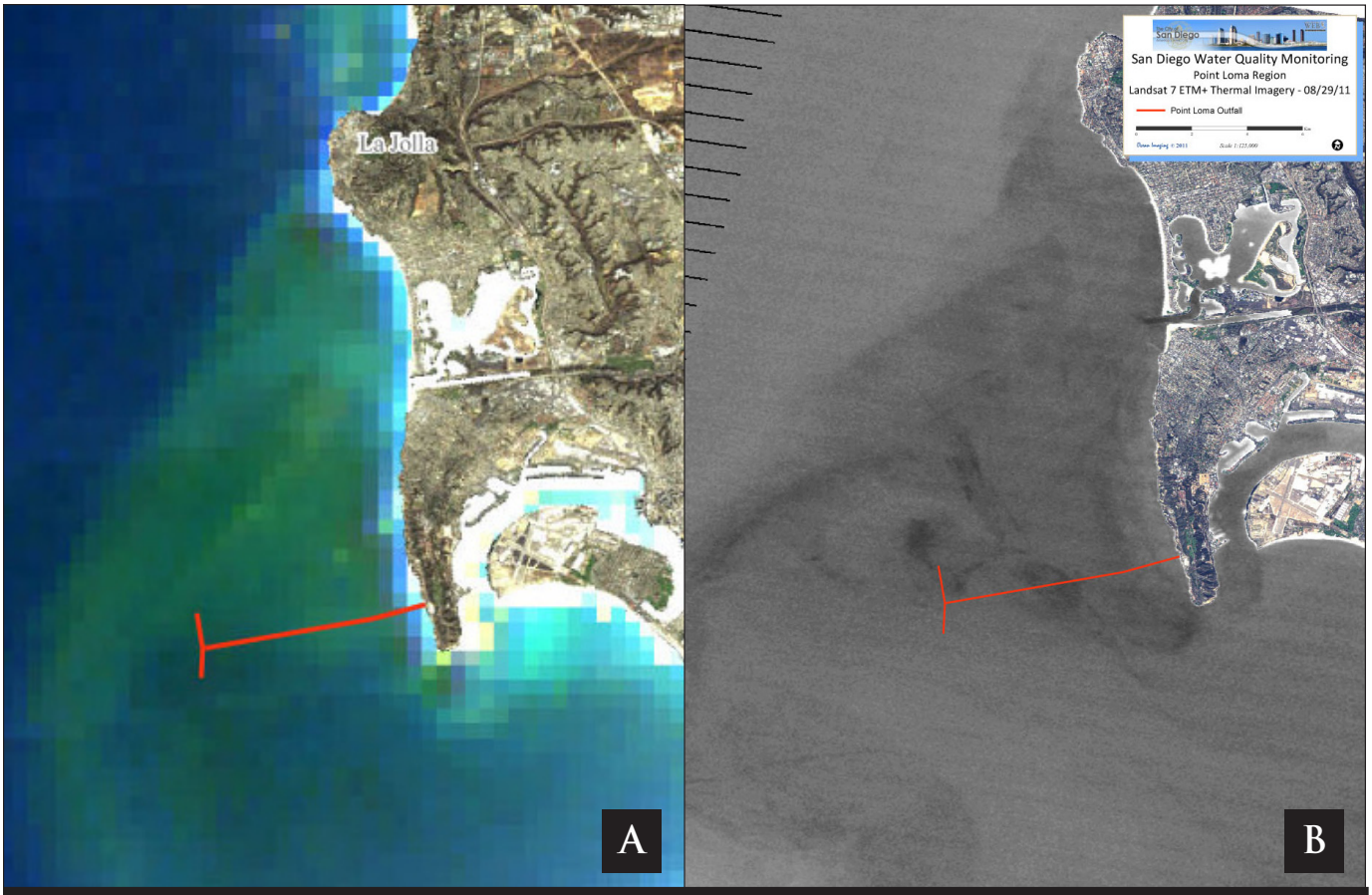

Figure 19.

The Pt. Loma region during a localized upwelling-caused plankton bloom shown on 8/29/2011 in color (left) and high resolution thermal (right) imagery (cooler water appears darker).

1/1/2011 shown in **Figure 16**. **Figure 21B** shows a larger scale view that includes North County, along which only minimal runoff signatures are discernible. Following the November rains, December 2011 was relatively dry and waters along San Diego County remained quit clear – as is exemplified in **Figure 22**.

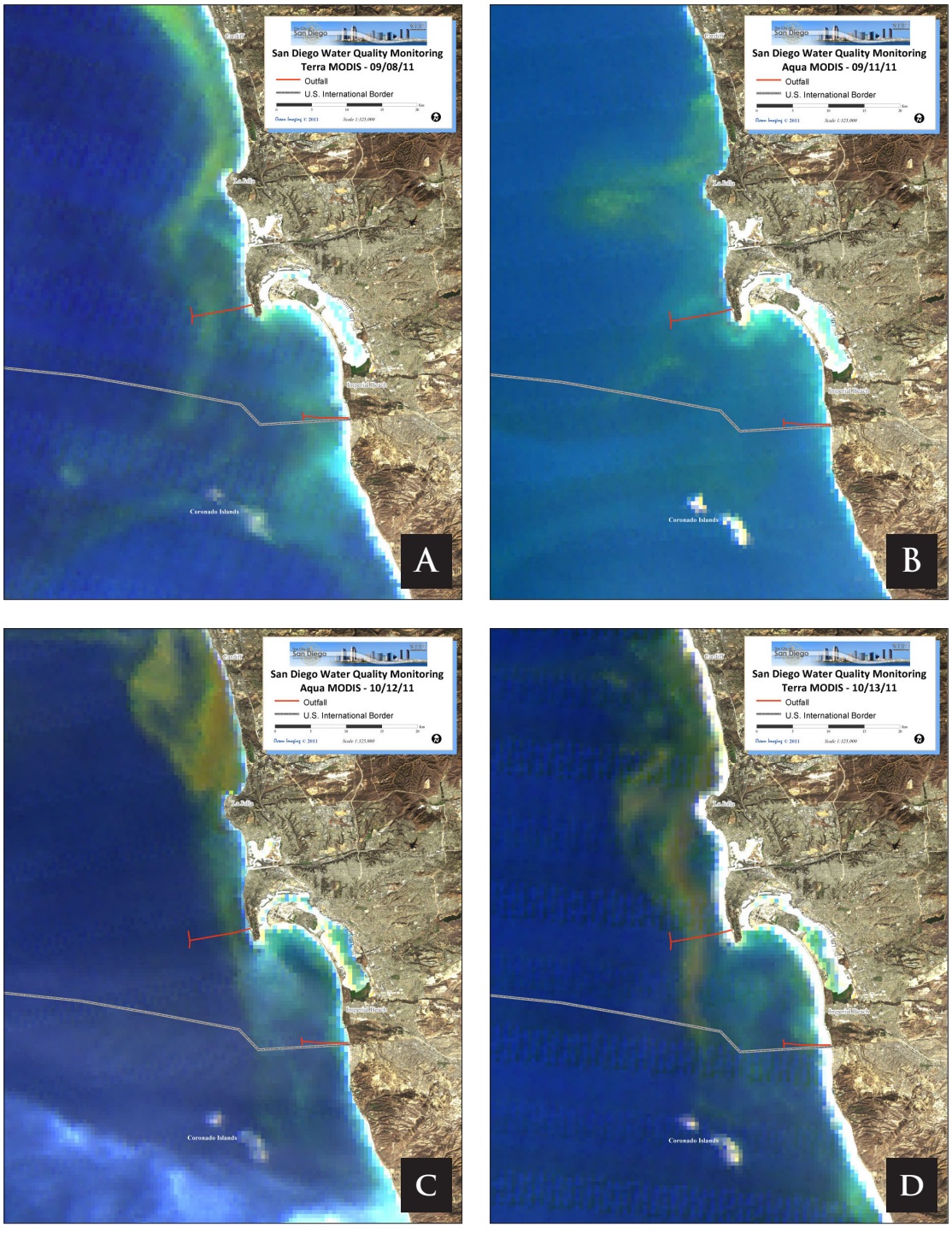

Figure 20.

Examples of continuation of frequent southward-swept phytoplankton (9/8/2011-A and 9/11/2011-B) and dynoflagellate (red tide) blooms (10/12/2011-C and 10/13/2011-D) affecting the Pt. Loma region.

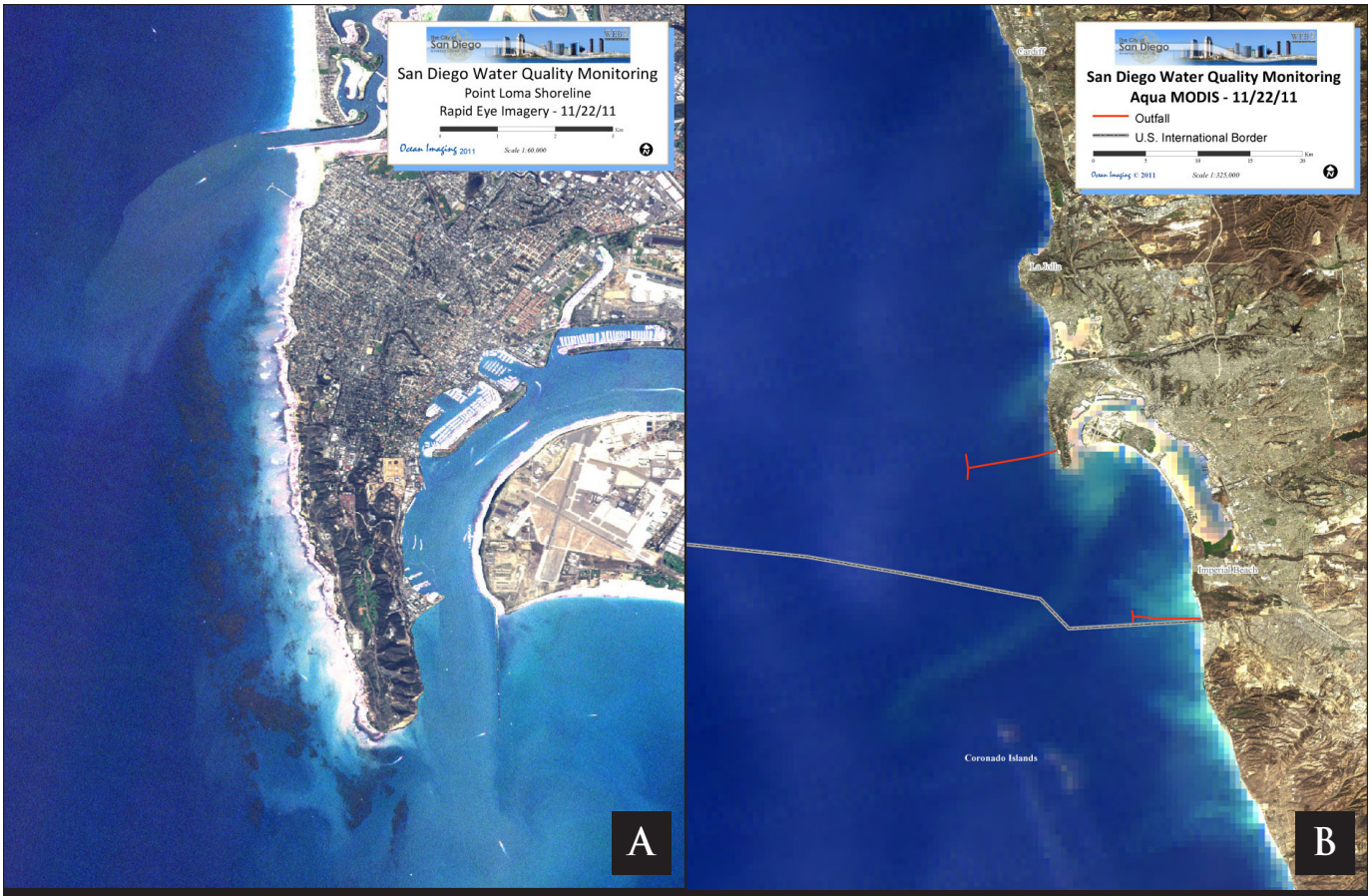

Figure 21.

RapidEye (A) and MODIS (B) imagery acquired on 11/22/2011 after consistent rains showing relatively moderate runoff from the San Diego and Tijuana Rivers and minimal turbid runoff from sources in North County (see text for discussion).

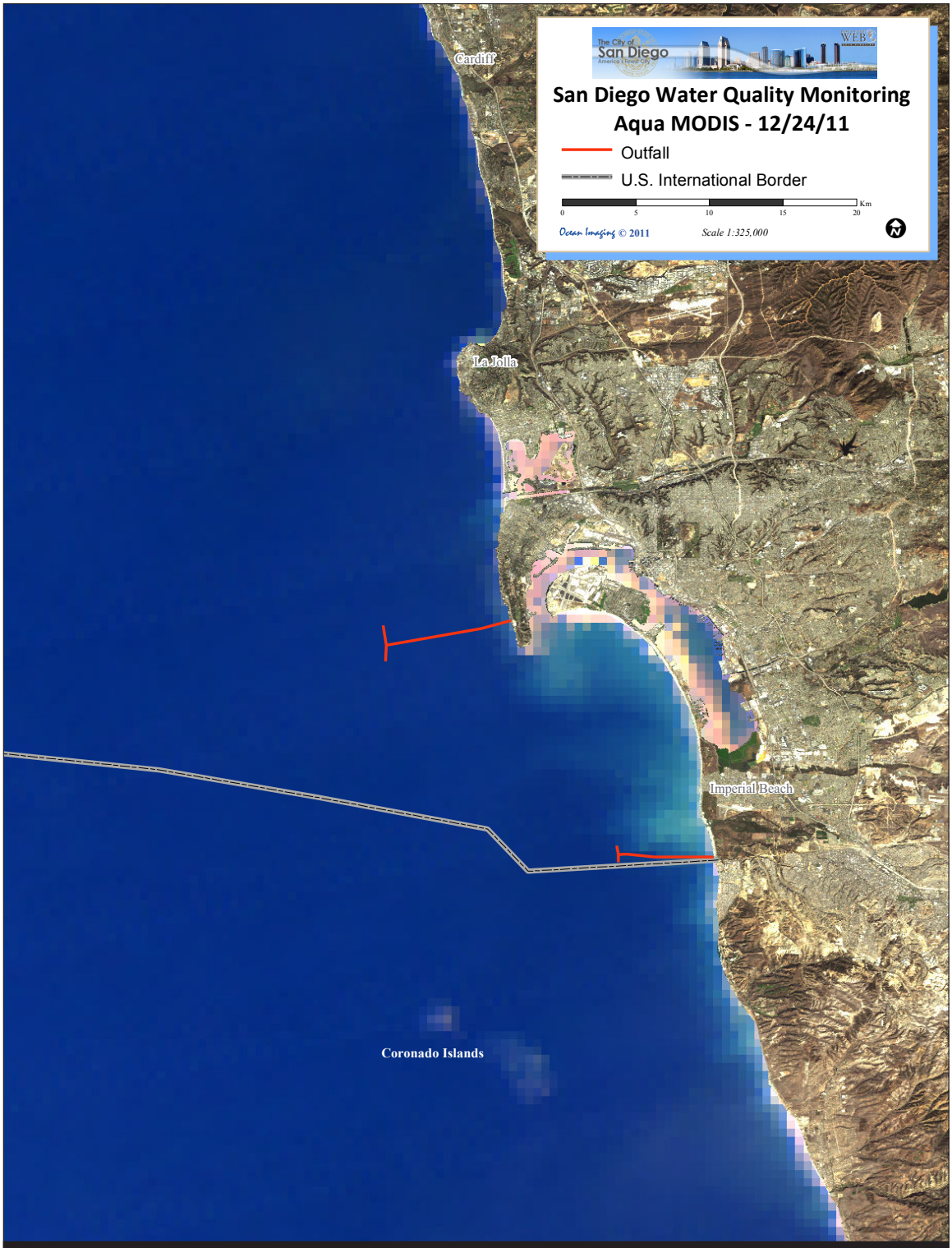

Figure 22.

MODIS imagery of the San Diego region acquired on 12/24/2011 showing clear water conditions along Pt. Loma and the North County coast.

Appendix H.4

2012 Ocean Imaging Report

Satellite & Aerial Coastal Water Quality Monitoring in The San Diego / Tijuana Region

By Jan Svejkovsky

Annual Summary Report
1 January, 2012 - 31 December, 2012

This draft to become final in sixty days.

13 February, 2013 (Revised 5 March, 2013)

Ocean Imaging

201 Lomas Santa Fe Drive, Suite 370, Solana Beach, CA 92075 Phone: 858-792-8529 Fax: 858-792-8761 www.oceani.com

Table of Contents

1.0 Introduction & Project History 1

2.0 Technology Overview 2

2.1 Imaging in the UV-Visible-NearInfrared Spectrum 2
2.2 Imaging in the Infrared Spectrum 2
2.3 Data Dissemination and Analysis 3

3.0 Highlights of 2012 Monitoring 4

3.1 Atmospheric & Ocean Conditions 4
3.2 The South Bay Ocean Outfall Region 5
3.3 The Point Loma Ocean Outfall Region 19
3.4 New Remote Sensing Products for the City's Biomap Server 25

1. Introduction and Project History

Ocean Imaging Corp. (OI) specializes in marine and coastal remote sensing for research and operational applications. In the 1990s, OI received multiple research grants from NASA's Commercial Remote Sensing Program for the development and commercialization of novel remote sensing applications in the coastal zone. As part of these projects, OI developed methods to utilize various types of remotely sensed data for the detection and monitoring of stormwater runoff and wastewater discharges from offshore outfalls. The methodology was initially demonstrated with collaboration of the Orange County Sanitation District. The NASA-supported research and demonstration led to a proof-of-concept demo project in the San Diego region co-funded by the EPA in 2000. Those results led, in turn, to adding an operational remote imaging-based monitoring component to the San Diego region's established water quality monitoring program, as stipulated in discharge permits for the International Wastewater Treatment Plant and Pt. Loma outfalls. The project was spearheaded by the State Water Resources Control Board (SWRCB), EPA Region 9, and continues to be jointly funded by the International Boundary Waters Commission and the City of San Diego.

The first phase of the project was a historical study utilizing various types of satellite data acquired between the early 1980s and 2002. The study established, among other findings, the prevailing near-surface current patterns in the region under various oceanic and atmospheric conditions. The current directions were deduced from patterns of turbidity, ocean temperature and surfactant slicks. In some cases, near-surface current velocity could be computed by tracking recognizable color or thermal features in time-sequential images. The historical study thus established a baseline data base for the region's current patterns, their persistence and occurrence frequency, and the historical locations, size and dispersion trajectories of various land and offshore discharge sources (e.g. the offshore outfalls, Tijuana River, Punta Bandera Treatment Plant discharge in Mexico, etc.).

In October, 2002 the operational monitoring phase of the project was initiated. This work utilizes 500m resolution Moderate Resolution Imaging Spectroradiometer (MODIS) color imagery (available near-daily), and 27m & 60m Thematic Mapper TM5 & TM7 color and thermal imagery (available 4 times per month). In addition, the project relied heavily on acquisition of multispectral color imagery with OI's DMSC-MKII aerial sensor and thermal infrared (IR) imagery from a Jenoptik thermal imager integrated into the system (see details in the "Technology Overview" section). These aerial image sets were most often collected at 2m resolution. The flights were done on a semi-regular schedule ranging from 1-2 times per month during the summer to once or more per week during the rainy season. The flights were also coordinated with the City of San Diego's regular offshore field sampling schedule so that the imagery was collected on the same day (usually within 2-3 hours) of the field data collection. Additional flights were done on an on-call basis immediately after major storms or other events such as sewage spills. In late 2010 OI negotiated a special data collection arrangement with Germany's RapidEye Corporation and this project began utilizing their multispectral imagery in lieu of most of the aerial DMSC image acquisitions. RapidEye maintains a unique constellation of 5 satellites which deliver 6.5 m resolution multispectral imagery. Unlike other single high resolution satellites, the multi-satellite constellation enables revisits of the San Diego region on a near-daily basis. Another advantage of using this imagery is the much larger spatial coverage available with each data set that was not possible using the aerial sensor. This enables a more regionally contiguous monitoring of events affecting the target areas. In 2012 OI also began operationally providing the City with a suite

of additional oceanographic products on a daily basis through the City's EMTS web-based GIS "BioMap" Server. These products range from atmospherically corrected satellite images of sea surface temperature and chlorophyll to radar and model-derived surface current fields.

This report summarizes observations made during the period 1/1/2012 – 12/31/2012.

2. Technology Overview

OI uses several remote sensing technologies to monitor San Diego's offshore outfalls and shoreline water quality. Their main principle is to reveal light, heat or microwave signal patterns that are characteristic of the different discharges. Most often this is due to specific substances contained in the effluent but absent in the surrounding water.

2.1 Imaging in the UV-Visible-NearInfraRed Spectrum

This is the most common technique used with satellite images and the DMSC aerial sensor. Wavelengths (colors) within the range of the human eye are most often used but Ultraviolet (UV) wavelengths are useful for detecting fluorescence from petroleum compounds (oil, diesel, etc.) and near-IR wavelengths can be useful for correcting atmospheric interference from aerosols (e.g. smog and smoke).

The best detection capabilities are attained when several images in different wavelengths are acquired simultaneously. These "multispectral" data can be digitally processed to enhance features not readily visible in simple color photographs. For example, two such images can be ratioed, thus emphasizing the water features' differences in reflection of the two wavelengths. A multi-wavelength image set can also be analyzed with "multispectral classification algorithms" which separate different features or effluents based on the correlation relationships between the different color signals.

The depth to which the color sensors can penetrate depends on which wavelengths they see, their sensitivity and the general water clarity. In the San Diego region, green wavelengths tend to reach the deepest and, as elsewhere, UV and near-IR wavelengths penetrate the least. Generally, OI's satellite and aerial sensor data reveal patterns in the upper 15-40 feet.

The color channels on satellite sensors cannot be changed, so they tend to be relatively broad, separating red, green, near-IR, and sometimes blue parts of the spectrum. OI's DMSC aerial 4-channel sensor has the added advantage of allowing each channel wavelength to be precisely customized. Through experimentation, OI has determined the exact wavelength relationships that maximize the detection of the offshore sewage outfall plumes and nearshore discharges such as the Tijuana River. With this channel configuration it is possible to monitor the plumes even when they are not visible to the naked eye.

2.2 Imaging in the Infrared Spectrum

Some satellite and aerial sensors image heat emanating from the ground and the ocean. They thus reveal patterns and features due to their differences in temperature. Since infrared wavelengths are strongly absorbed by water, the images reveal temperature patterns only on the water's surface. Such images can help detect runoff plumes when their temperatures differ from the surrounding ocean water. Runoff from shoreline sources tends to be warmer than the ocean water, although the reverse can be true during the winter. Plumes from offshore outfalls can sometime also be detected with thermal imaging. Since the effluent contains mostly fresh water, it is less dense than the surrounding salt

water and tends to rise to the surface. If it makes it all the way, it is usually cooler than the surrounding sun-warmed surface water. If it is constrained by a strong thermocline and/or pycnocline ("vertical stratification"), it sometimes tends to displace some of the water above it in a doming effect. This displacement pattern is revealed in the thermal surface imagery.

2.3 Data dissemination and Analysis

The satellite and aerial imaging data are made available to the funding agencies, the San Diego County Dept. of Health and the EPA through a dedicated, password-protected web site. Although it is possible to process most of the used data in near-real-time, earlier in the project the funding agencies decided that the emphasis of this project is not on providing real-time monitoring support and the extra costs associated with the rapid data turn-around are not warranted. Most satellite data is thus processed and posted within 1-2 days after acquisition and the aerial sensor imagery (which requires the most labor-intensive processing), within 2-5 days. OI has, however, in a number of cases, made some imagery available to the CDH and others in near-real time when observations were made that appeared to be highly significant for the management of beach closures or other sudden events. The BioMap Server-directed products are produced daily by OI and are automatically linked with the server when available.

3. Highlights Of 2012 Monitoring

3.1 Atmospheric and Ocean Conditions

From the standpoint of this project's focus on nearshore water quality monitoring, 2012 exhibited several relatively unique properties. Most notably, both rain season segments contained within 2012 had numerous rain events, however, the daily rainfall totals were relatively light, with each event often spread over several days. As is shown in **Figure 1** for the Tijuana Marsh region, coastal daily rainfall barely exceeded 1cm on only 3 occasions, with only one day exceeding 1.4cm. San Diego's coastal areas further to the north experienced similar conditions. The "gentle rain" trend extended into the county's inland areas as well. This can be readily seen in San Diego River flow data shown in **Figure 2**. The San Diego River encompasses a large watershed extending into the Cuyamaca Mountains. In 2012 the flow gauge at Fashion Valley in San Diego briefly reached 200 cubic feet per second on only 2 occasions, compared to multiple events reaching several thousand cubic feet per second in 2011 and over 500 cubic feet per second in 2010.

The general lack of high rainfall periods and hence low runoff volumes from point and nonpoint sources in the area are reflected in much of 2012 satellite imagery. With a few exceptions, the Tijuana River runoff plume post-rain event extents were suppressed from patterns usually seen in previous years. Waters along Point Loma and South Bay coasts tended to remain anomalously clear through both rain season periods in 2012.

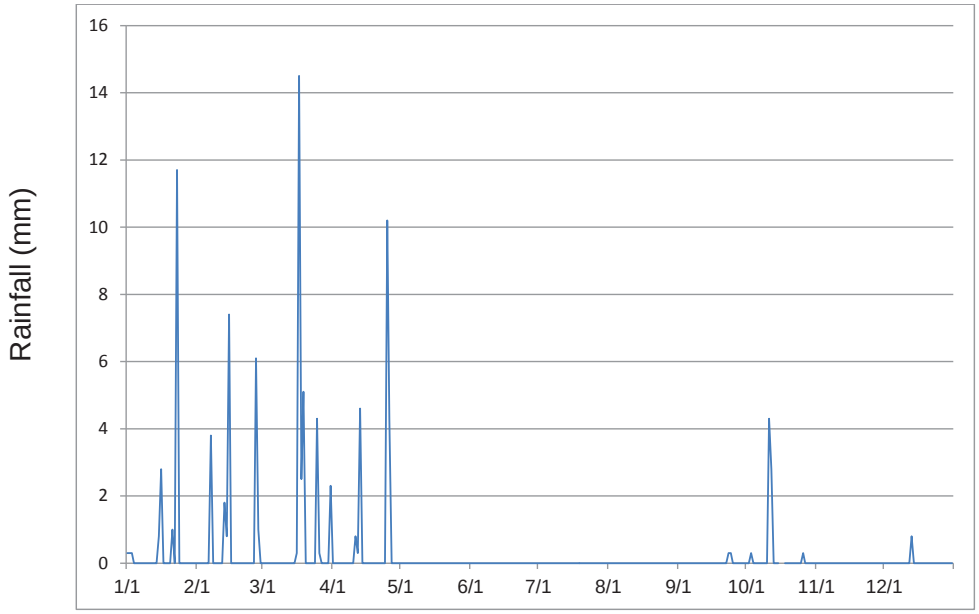

Date	Cum Prcp (mm)
1/1	0.3
1/2	0.3
1/3	0.3
1/15	0.8
1/16	2.8
1/21	1
1/23	11.7
2/7	3.8
2/13	1.8
2/14	0.8
2/15	7.4
2/27	6.1
2/28	1
3/16	0.3
3/17	14.5
3/18	2.5
3/19	5.1
3/25	4.3
3/26	0.3
3/31	2.3
4/11	0.8
4/12	0.3
4/13	4.6
4/25	10.2

Date	Cum Prcp (mm)
4/26	4.3
9/23	0.3
9/24	0.3
10/3	0.3
10/11	4.3
10/12	2.8
10/16	(No Data)
10/17	(No Data)
10/26	0.3
12/13	0.8

Figure 1.

Graph of daily cumulative daily rainfall in the Tijuana Estuary.

The region experienced two red-tide pulses from mid-February through the first week of March. Following those events relatively high water clarity returned to San Diego's coastal areas through the summer and fall.

3.2 The South Bay Ocean Outfall Region

The South Bay Ocean Outfall (SBOO) wastewater plume generally remains well below the surface between approximately late March and November due to vertical stratification of the water column. During that period it usually cannot be detected with multispectral aerial and satellite imagery which penetrate the upper 7 to 15 meters (depending on water clarity). The plume also cannot be detected with thermal IR imaging which does not penetrate below the surface. Seasonal breakdown of the vertical stratification results in the plume's rise closer to the surface or to actually reach the surface between approximately late November and late March, when it can often be detected with aerial and satellite imaging.

The SBOO treatment plant switched from advanced primary to secondary treatment in January, 2011. This change resulted, among other factors, in the reduction of total suspended solids (TSS) concentrations from an average of 60 mg/l for several years prior to the change, to 15 mg/l in 2011 and 2012 (S. Smullen/IBWC, pers. commun.). A reduction in TSS concentrations can be expected to have an effect on the reflectance intensity of the surfacing or near-surfacing effluent plume in the visible and near-IR imaging channels. Prior to 2011, a distinct plume signature was regularly detected in multispec-

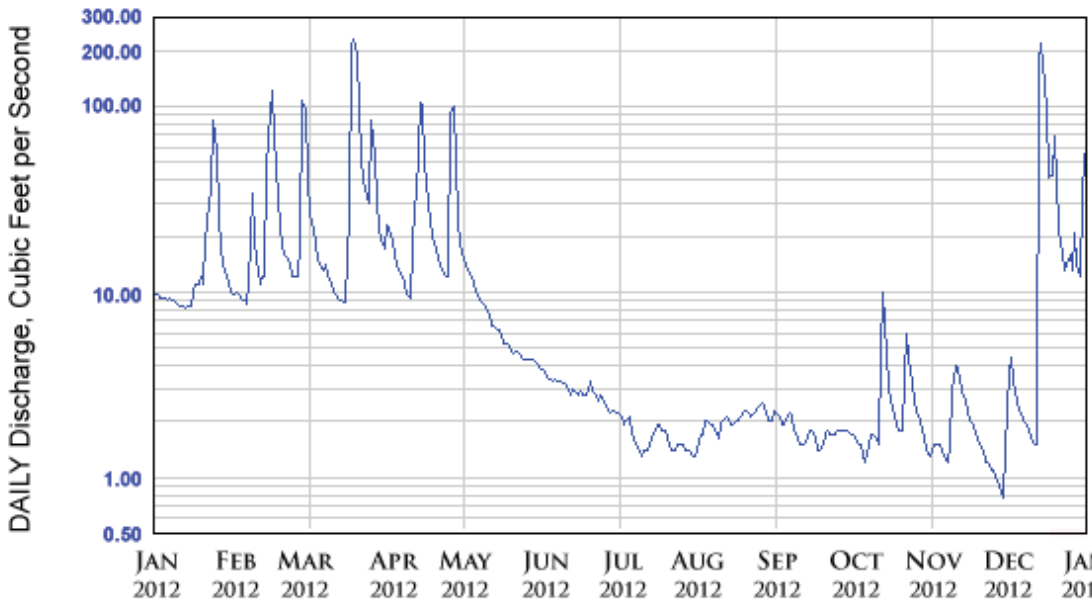

Lindberg Field Rainfall 2012

January	0.40"
February	1.19"
March	0.97"
April	0.88"
May	0.02"
June	0.00"
July	0.00"
August	0.00"
September	0.00"
October	0.70"
November	0.28"
December	2.19"

Figure 2.

Graph of mean daily discharge of the San Diego River during 2012 (measured at Fashion Valley). The table on the right shows monthly rainfall totals at Lindbergh Field.monthly rainfall totals at Lindbergh Field.

tral imagery as per the seasonal fluctuation described above. In 2011 the plume signature was also observed during the winter months, however, due to extensive rains its signature was often apparent as a "clear water" feature penetrating through the highly turbid storm runoff plume of the Tijuana River which was large enough to overtake the SBOO wye region offshore.

As is noted above, the region's waters were much clearer during 2012 and the Tijuana River plume generally did not affect the SBOO wye area. The SBOO plume was detected in some of the high resolution imagery, but more sporadically than in past years. For example, a RapidEye image acquired on 1/4/2012 shows a very clear SBOO plume signature with its characteristic triangular, southward-directed shape **(Figures 3A and 3B)**. It remains detectable for more than 4km from the outfall wye, making that instance one of the most extensive SBOO plume features recorded during this project. No traces of the SBOO plume are distinguishable, however, in RapidEye imagery acquired on 1/19/2012 and 1/26/2012 **(Figures 4A and 4B)**. A plume signature is once again apparent in 2/3/2012 imagery **(Figure 5)**. A TM-7 data set acquired on 2/5/2012 shows no plume signature in the multispectral visible channels but recorded a thermal signature over the southern wye **(Figure 6)**. A multispectral signature was recorded on 2/16/2012, but no signature was apparent on 2/22/2012 **(Figure 7)**.

It is unreasonable to assume that vertical stratification during January and February, 2012 varied so strongly and quickly as to cause the observed variability in the SBOO plume's reaching the ocean surface. We postulate that this high variability in the satellite observations is due to combined effects of the reduction in TSS loads of the plume and variability in dispersion rate due to subsurface currents existing on each observation day. Weak subsurface currents will allow the plume to rise directly to the surface in a relatively concentrated form, resulting in high spectral reflectance and thus high detectability in the multispectral imagery. Stronger subsurface currents will disperse the rising plume more quickly, lowering its spectral reflectance when it reaches the surface. Prior to the SBOO's switch to secondary treatment, the plume's TSS load (and hence spectral reflectance) was four times greater than in 2012. It is thus plausible that the much lower TSS loads in 2012 were below the detection threshold of the multispectral data when subject to dispersion under stronger subsurface conditions (but the plume would still exhibit a thermal signature on the surface as seen in the 2/5/2012 example). The imaging observations thus suggest that the SBOO's change to secondary treatment has documentable results as far as the reduction of TSS distributions reaching the surface in the winter months.

Following its complete disappearance from near-surface waters during the summer and fall of 2012, the SBOO plume was again first detected in high resolution imagery on 12/12/2012 **(Figure 8)**.

The South Bay region was subject to 3 reported sewage spills in 2012 that reached the ocean. On 4/4/2012 a software malfunction at an IBWC pump station caused a back-up of sewage which ultimately flowed into the Tijuana River. IBWC reports show the spill size as 2 million gallons over approximately 2.5 hours. Multiple subsequent news media reports report the spill size as up to 60 million gallons over 5 days, however, citing Surfrider and Wildcoast associations as the source of this estimate. A San Diego Union/Tribune article cites the 60 million gallon estimate included "treated sewage that typically is diverted to a plant in Mexico but is flowing to the Tijuana River while repairs are made in San Ysidro" (http://www.utsandiego.com/news/2012/apr/12/major-sewage-spill-hits-tj-river-again). From information available to OI, it is not clear whether any multiday discharge into the Tijuana River indeed

occurred. The event occurred between rain periods – one ending on 3/31/2012 and one beginning on 4/11/2012. A TM-7 image acquired on 4/9/2012 shows no distinct turbidity plume exiting the Tijuana River, but does show a well defined, relatively small thermal plume at the River mouth **(Figure 9)**. In the absence of rain, the lack of a turbidity plume and the fact that the image was acquired during a strong (-0.2 ft.) outgoing tide makes it likely (using past years' observation as a guide) that the thermal plume represents ebbing tide flushing of the Tijuana Estuary without any major additional runoff input. This is corroborated by 0 discharge measured at the Tijuana River flow gauge (IBWC data).

The next spill occurred on 4/24/2012 when 2 million gallons entered the Tijuana River from Mexico due to a pipeline rupture. The River was actively discharging at the time and a new rain event began the following day.

A spill of 5 million gallons on 8/25-30/2012 occurred in the Playas de Tijuana area, discharging sewage into the surf zone. A TM-7 image from 8/31/2012 is available but shows no features related to this event.

As was already noted, the Tijuana River discharge plumes in 2012 were, relative to previous years, quite reduced in size. Multiple General Advisories linked to rain events were issued by the County Dept. of Health, and several beach closures up to Imperial Beach were issued in March and April. The Silver Strand and Coronado were mostly spared of contamination in 2012, as per shoreline sampling results – which concurs with the remote sensing observations of the reduced River plume extents. The strongest outflows were measured 3/16-20/2012, corresponding to a 4-day rain event that also included the year's highest daily rainfall (14.5 mm) in the Tijuana Estuary. **Figure 10** shows the River's runoff plume on 3/21 – the only time it reached the SBOO wye location offshore. **Figure 11** shows the only example when, during a northward flow regime event, the Tijuana River plume was large enough to reach into the waters around southern Pt. Loma. Such events have been documented more frequently in previous years, in some cases resulting in elevated bacterial measurements in that area. **Figures 12A and 12B** show bacteria sampling results from the SBOO monthly offshore sampling in May and September, 2012 overlaid on time coincident and near coincident RapidEye imagery.

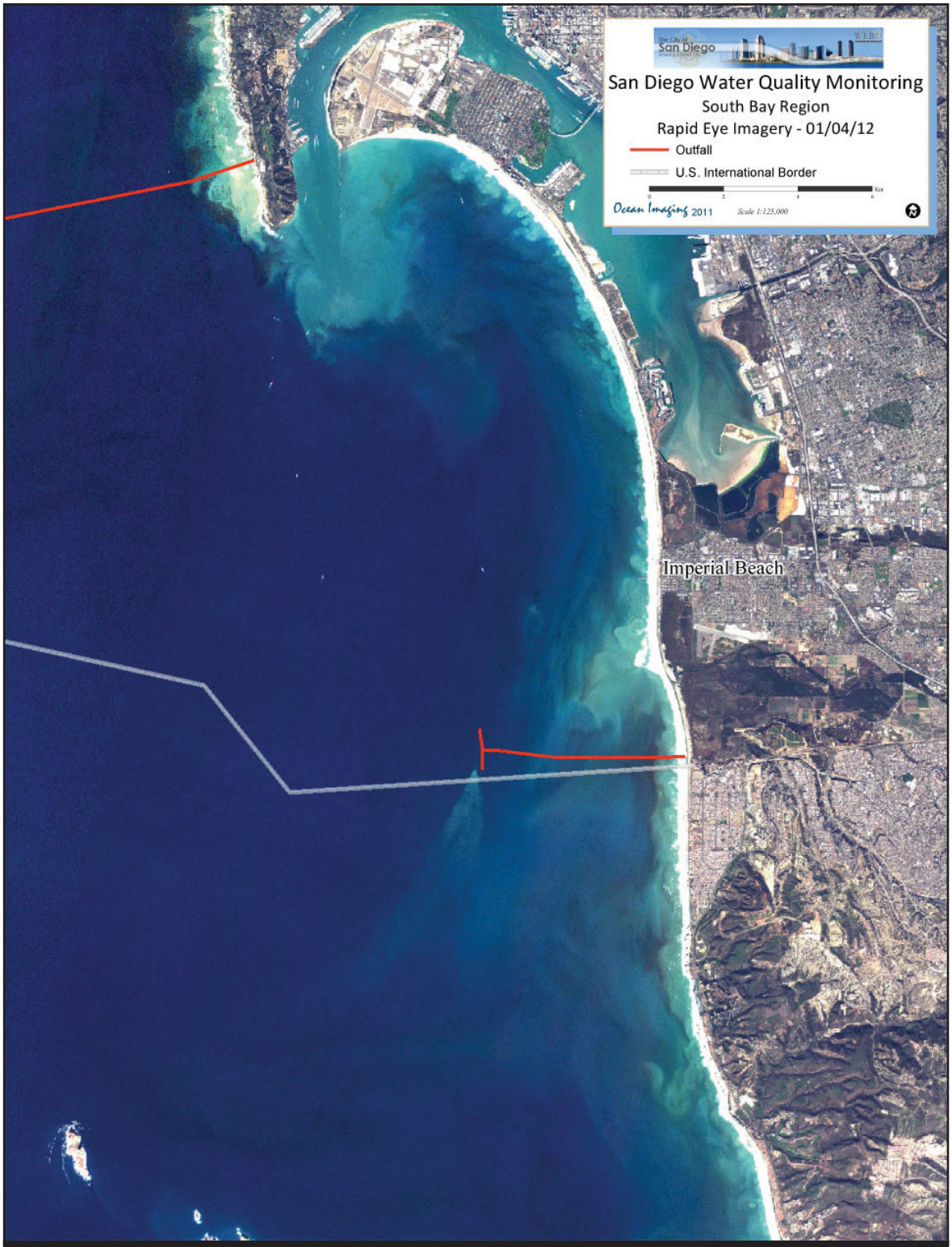

Figure 3A.

RapidEye satellite imagery of the South Bay and Tijuana shoreline region acquired on 1/4/2012.

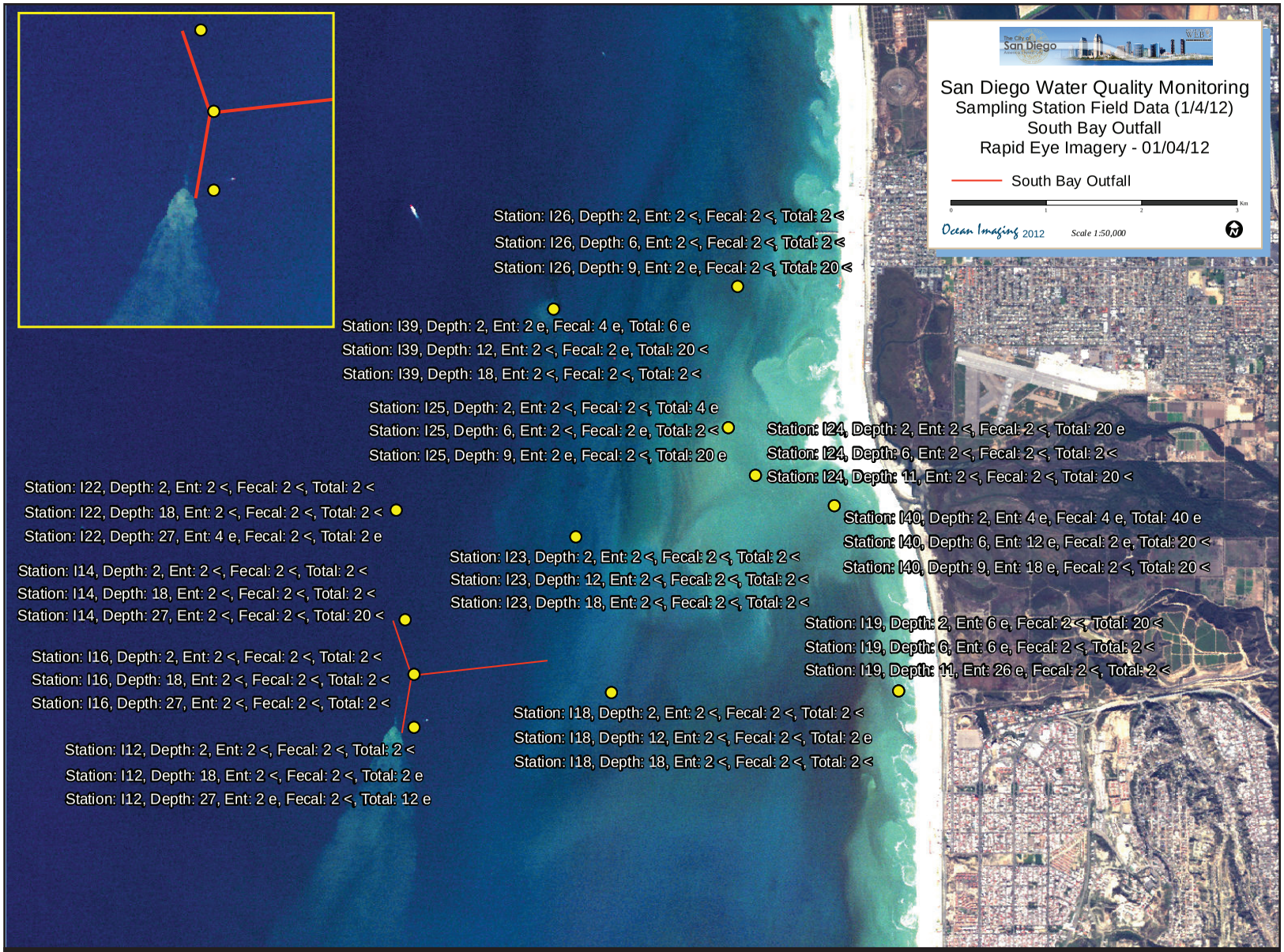

Figure 3B.

Same image as Figure 3A. with bacterial sampling results from the same day. The I12 station location was just outside the sharp plume boundary and thus did not record the surfacing plume.

Figure 4A.

RapidEye satellite imagery of the SBOO region from 1/19/2012.

Figure 4B.

RapidEye satellite imagery of the SBOO region from 1/26/2012. Near-time-coincident bacterial sampling results are also shown.

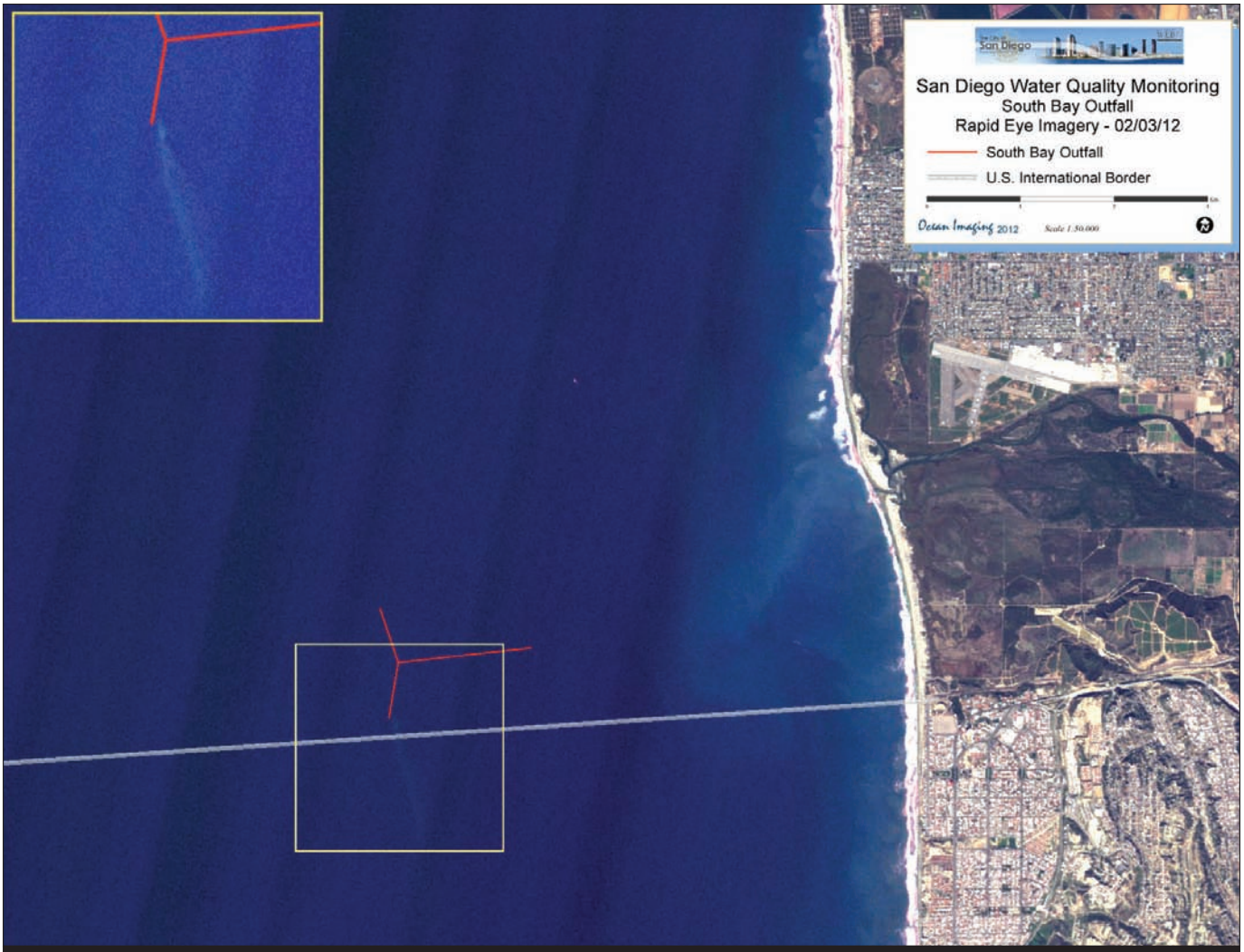

Figure 5.

RapidEye satellite imagery of the SBOO region from 2/3/2012.

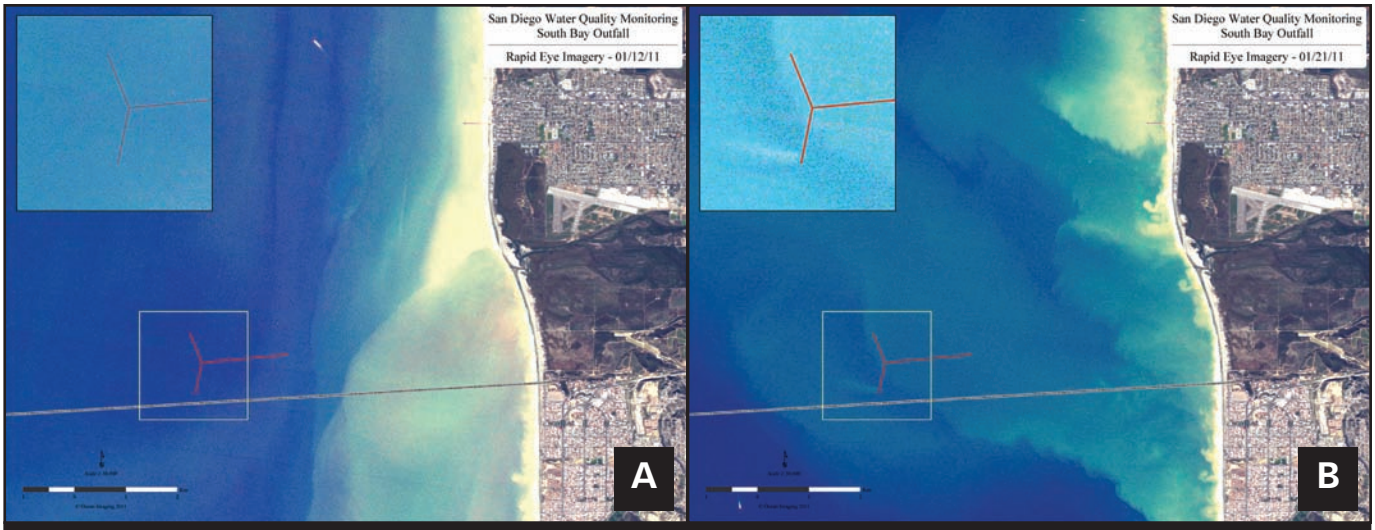

Figure 6.

Landsat e-TM satellite image of the South Bay region acquired on 2/5/2012 showing no surface signature of the SBOO plume in multispectral color (A), but a small signature in the thermal image seen as lower temperature (darker shade) at the tip of the southern wye extension (B). The striping is due to missing data lines due to a malfunction on the TM sensor.

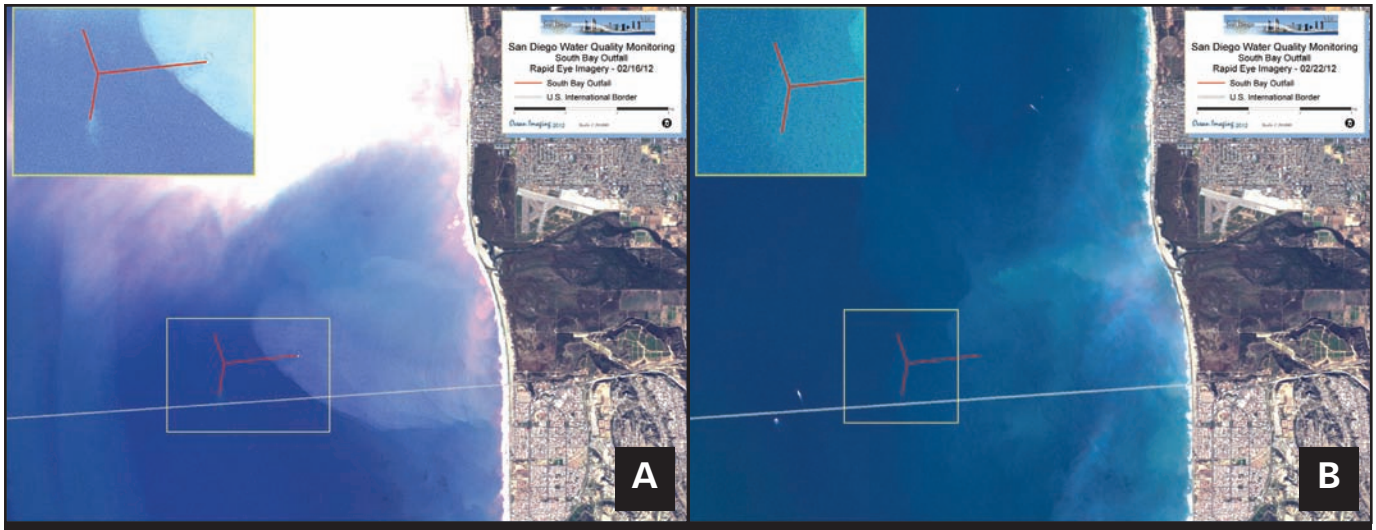

Figure 7.

RapidEye satellite imagery of the SBOO region from 2/16/2012 (A) with a distinct outfall plume signature, and 2/22/2012 (B) when no plume signature was evident.

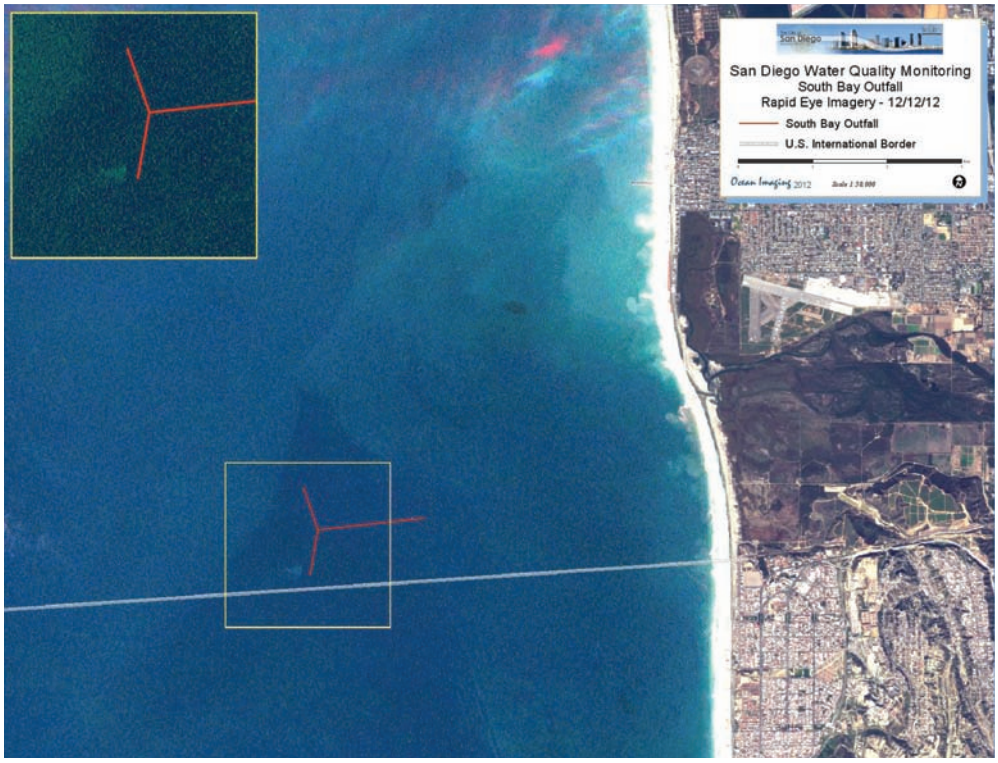

Figure 8.

RapidEye satellite imagery of the SBOO region from 12/12/2012 showing a small southwestward directed outfall signature.

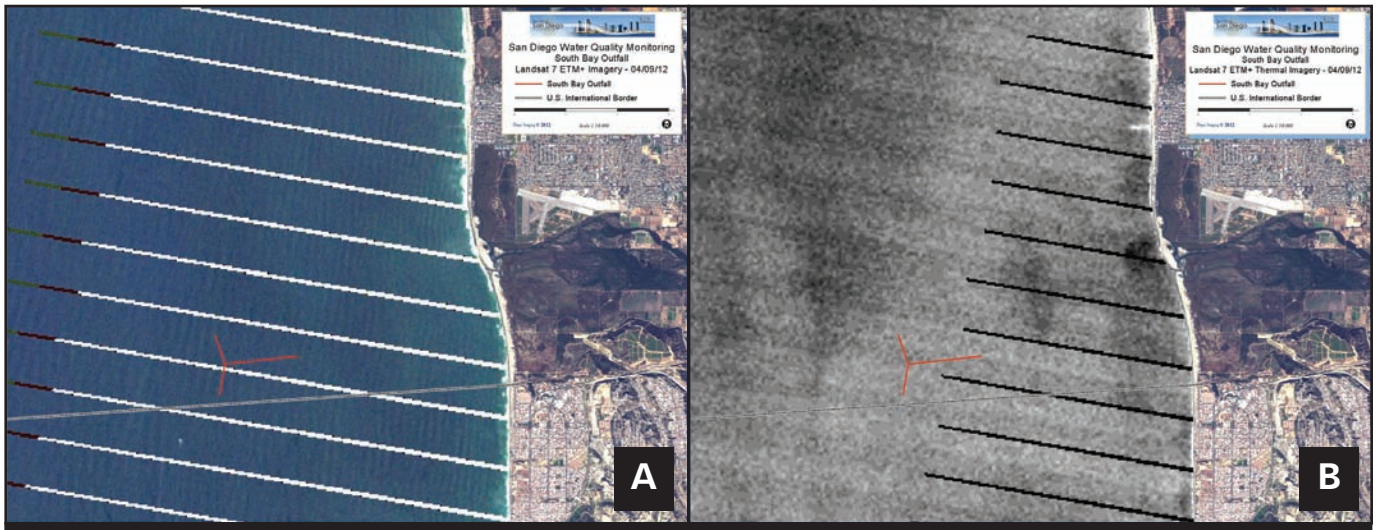

Figure 9.

Landsat e-TM satellite image of the South Bay region acquired on 4/9/2012 showing no high turbidity runoff plume from the Tijuana River in multispectral color (A), but a distinct signature in the thermal image seen as lower temperature (darker shade) circular feature in front of the River mouth (B). No SBOO plume signature is apparent in either data type. The striping is due to missing data lines due to a malfunction on the TM sensor.

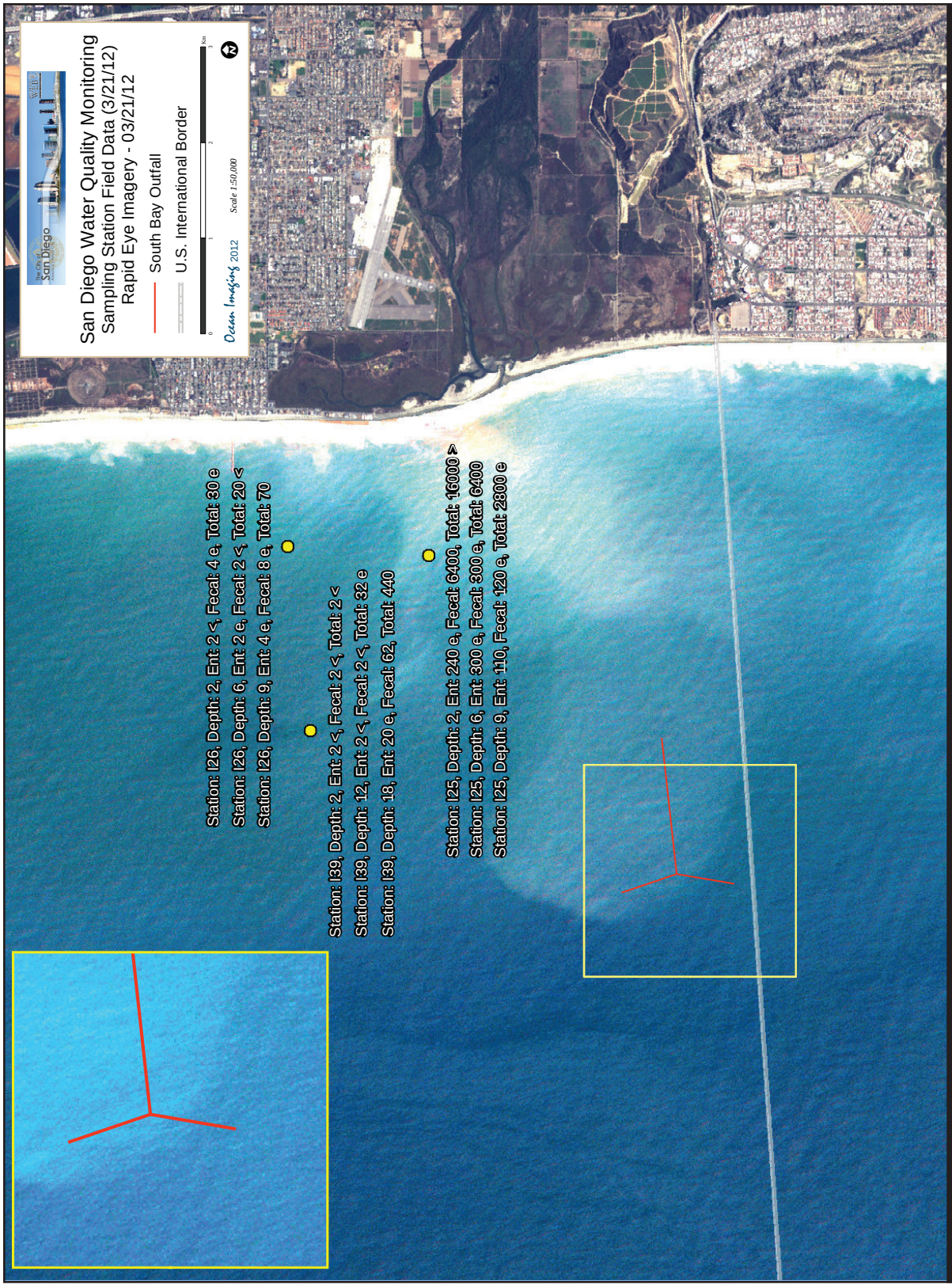

Figure 10.

RapidEye satellite imagery of the SBOO region from 3/21/2012 after the strongest rain event of the year. Part of the Tijuana River runoff plume had reached the SBOO wye area and same-day bacterial samples show elevated concentrations within the concentrated plume (Station I25).

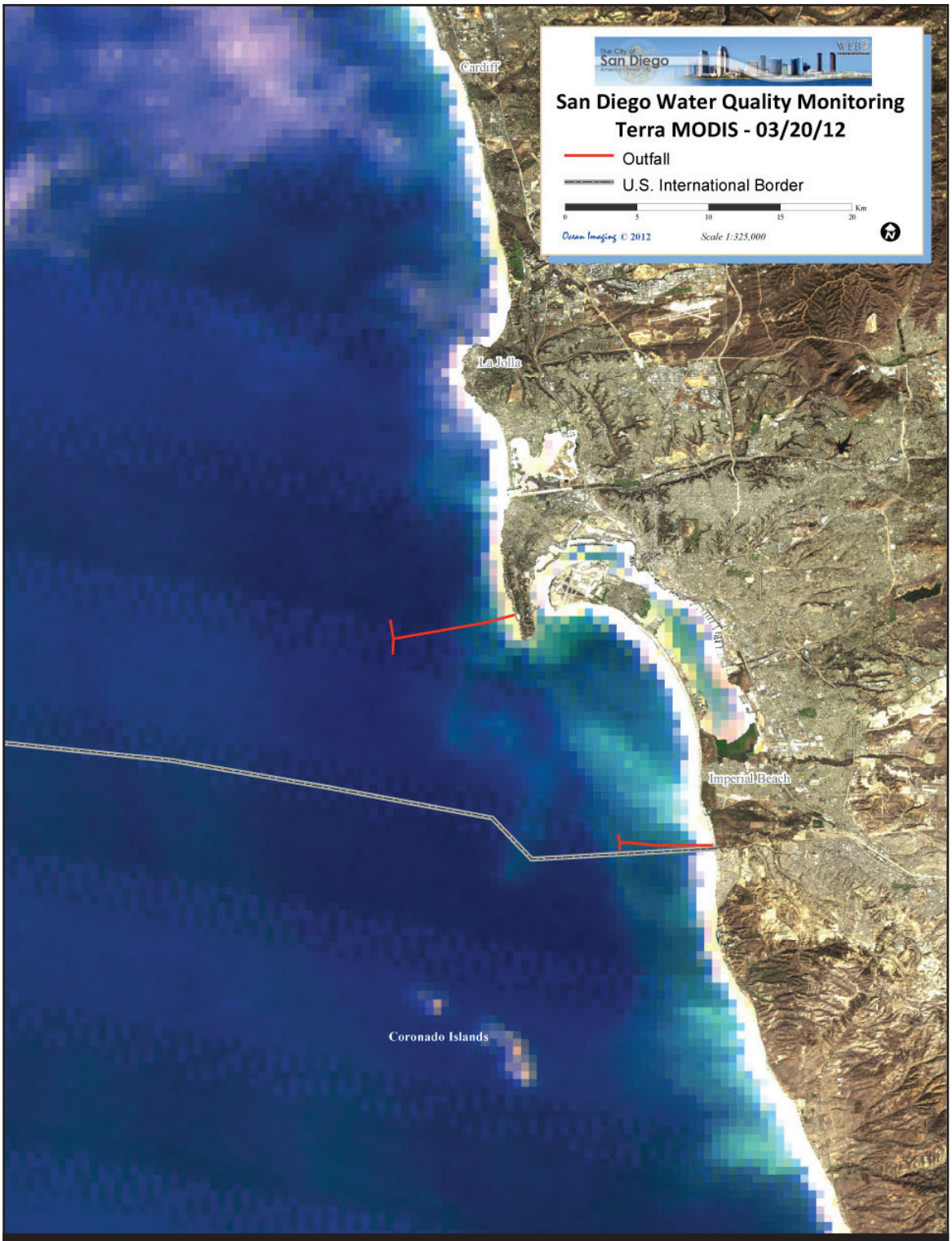

Figure 11.

MODIS satellite image of the San Diego region acquired on 3/20/2012 showing northward progression of the Tijuana River plume into the Pt. Loma area.

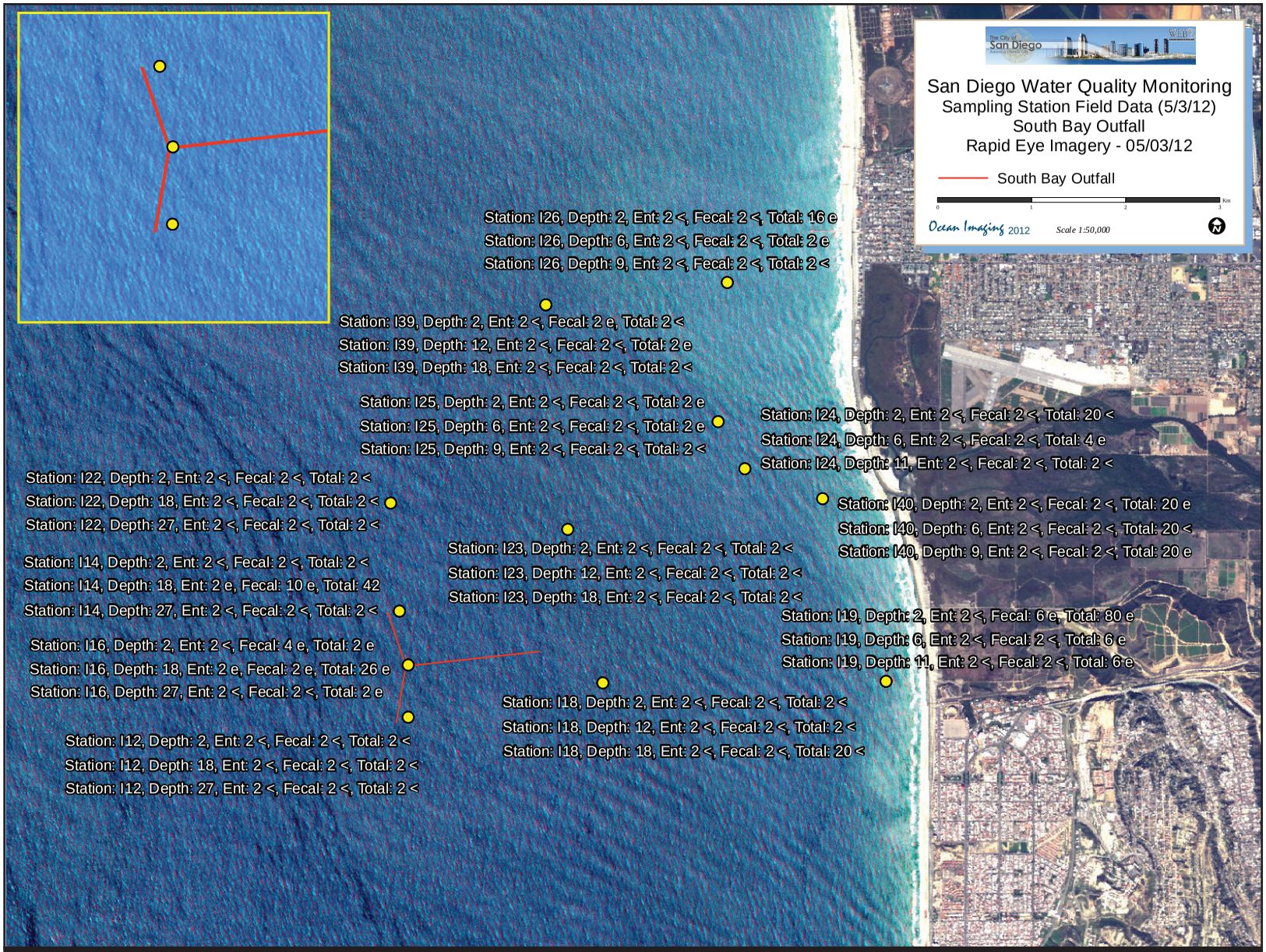

Figure 12A.

RapidEye satellite imagery of the SBOO region from 5/3/2012 with time coincident and near-coincident bacterial sampling results.

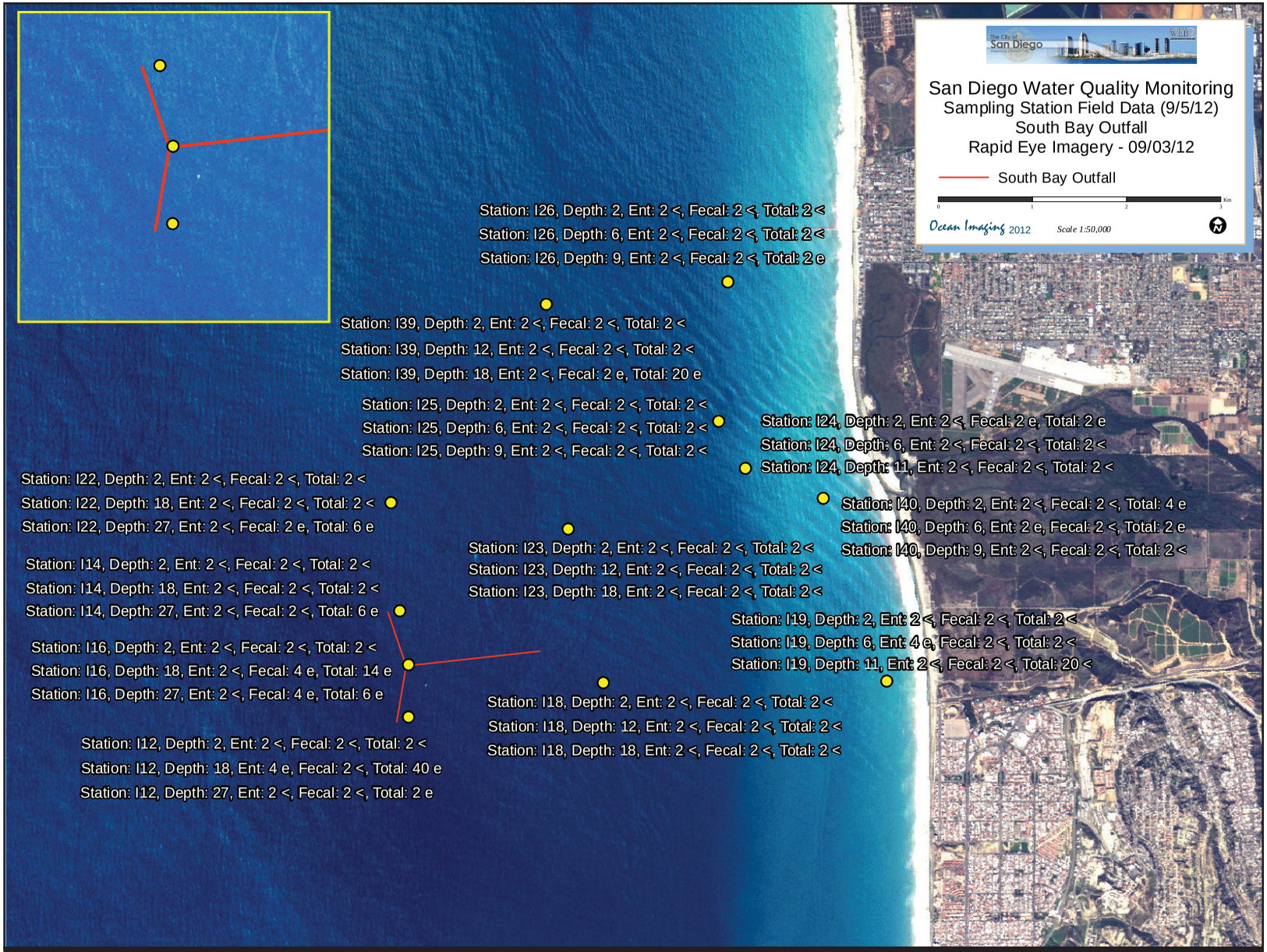

Figure 12B.

RapidEye satellite imagery of the SBOO region from 9/3/2012 with time coincident and near-coincident bacterial sampling results.

3.3. The Point Loma Outfall Region

After its seaward extension in 1993, the Point Loma Outfall (PLO) is one of the deepest and longest wastewater outfalls in the world, discharging at the depth of 320 feet, 4.5 miles offshore. The outfall's plume is generally not observed directly with multi-spectral color or thermal imagery. It appears to not reach the surface waters, even during the winter months when the water column's vertical stratifications are weakened. We believe, however, that on some occasions we have observed the plume's extents indirectly through an anomalous lateral displacement of thermal or chlorophyll features around the outfall wye. This effect can be explained by the doming up of the discharged effluent and laterally displacing the near-surface waters above it.

In 2012 the mild rain and runoff conditions that affected the South Bay coastal region had similar effects on the Pt. Loma area. Runoff from the San Diego River tended to be confined to the shoreline-to-kelp bed strip following most rain events. **Figure 13** shows conditions following one of the strongest rain events of the year, when the turbid runoff extended several kilometers offshore past the kelp, but this tended to be an exception during 2012. The Pt. Loma area got affected by 2 red tide events in February and early March. Both began along the coast of North County and were swept southward and over the PLO wye, as shown in **Figure 14**. Unlike in previous years, no major red tide or other plankton blooms occurred in the region during the summer months, with waters outside the kelp bed being generally very clear. Few mild rain episodes in September and October caused temporarily increased runoff and turbidity near the shoreline. Subsequently, no appreciable rainfall and mild wave conditions in November resulted in very clear waters even shoreward of the kelp bed, as is exemplified in **Figures 15A and 15B**.

The City conducted one of the Pt. Loma region's periodic offshore field sampling surveys during the February plankton bloom event on 2/22/2012 and OI was able to acquire a high resolution RapidEye image on the same day. As is shown in **Figure 16**, shallow depth bacterial sampling results show only background values throughout the region, however, chlorophyll concentrations reached up to 14.17 mg/m^3 (station F09 at 8m depth) – reflecting the regional plankton bloom.

Figure 13.

RapidEye satellite imagery of the Pt. Loma region from 1/26/2012 after one of the year's strongest rain events showing turbid runoff from the San Diego River covering the offshore region west of the Pt. Loma kelp bed.

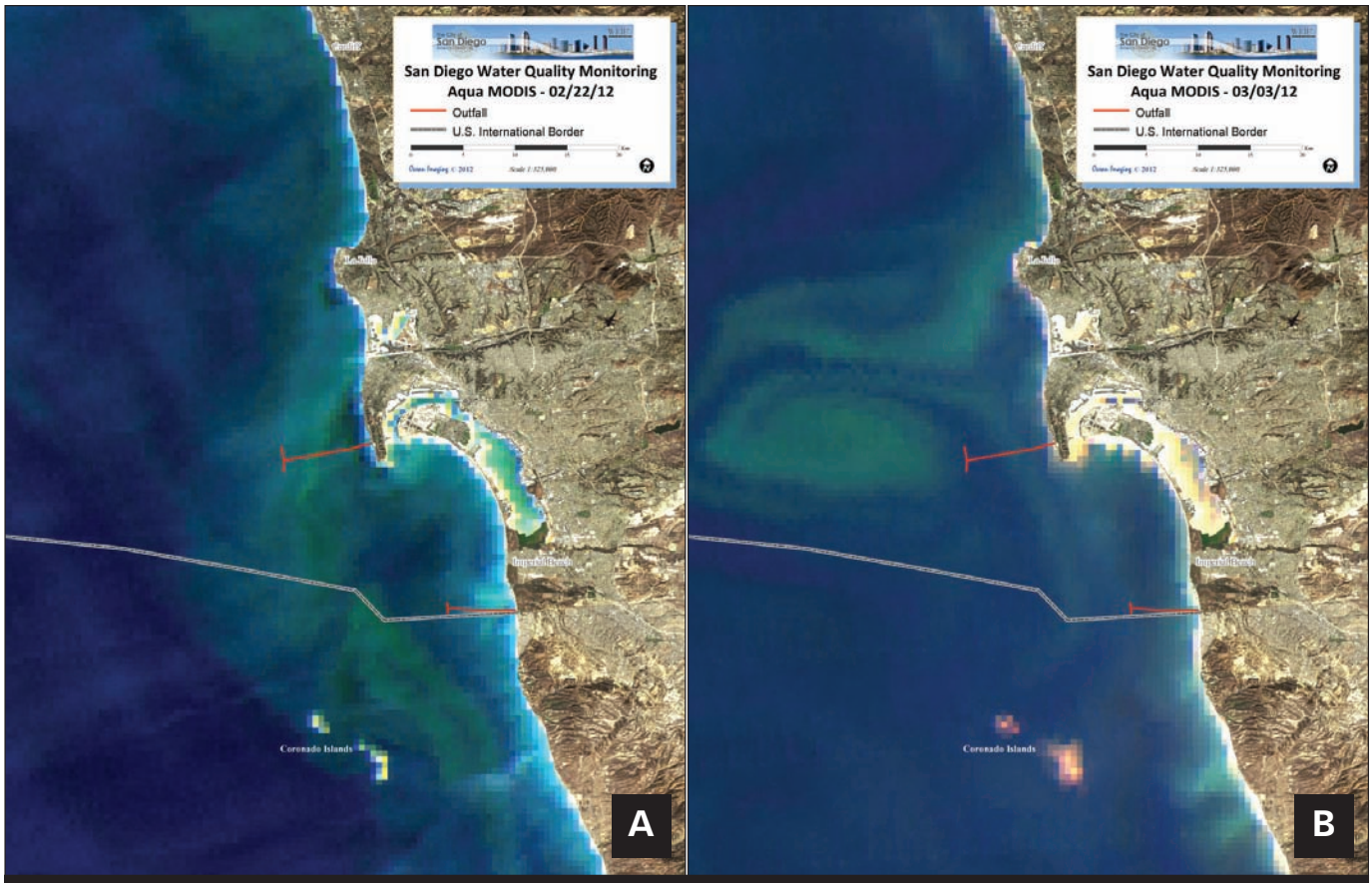

Figure 14.

MODIS satellite images of the San Diego region acquired on 2/22/2012 (A) and 3/3/2012 (B) showing two successive red tide events that swept southward through the Pt. Loma region.

Figure 15A.

RapidEye satellite imagery of the Pt. Loma region from 11/16/2012 showing very clear water conditions along Pt. Loma. The dark and light features between the kelp bed and the shoreline are bottom distributions of sand and vegetated reefs.

Figure 15B.

RapidEye satellite imagery of the Pt. Loma region from 12/12/2012 showing very clear water conditions along Pt. Loma. The dark and light features between the kelp bed and the shoreline are bottom distributions of sand and vegetated reefs.

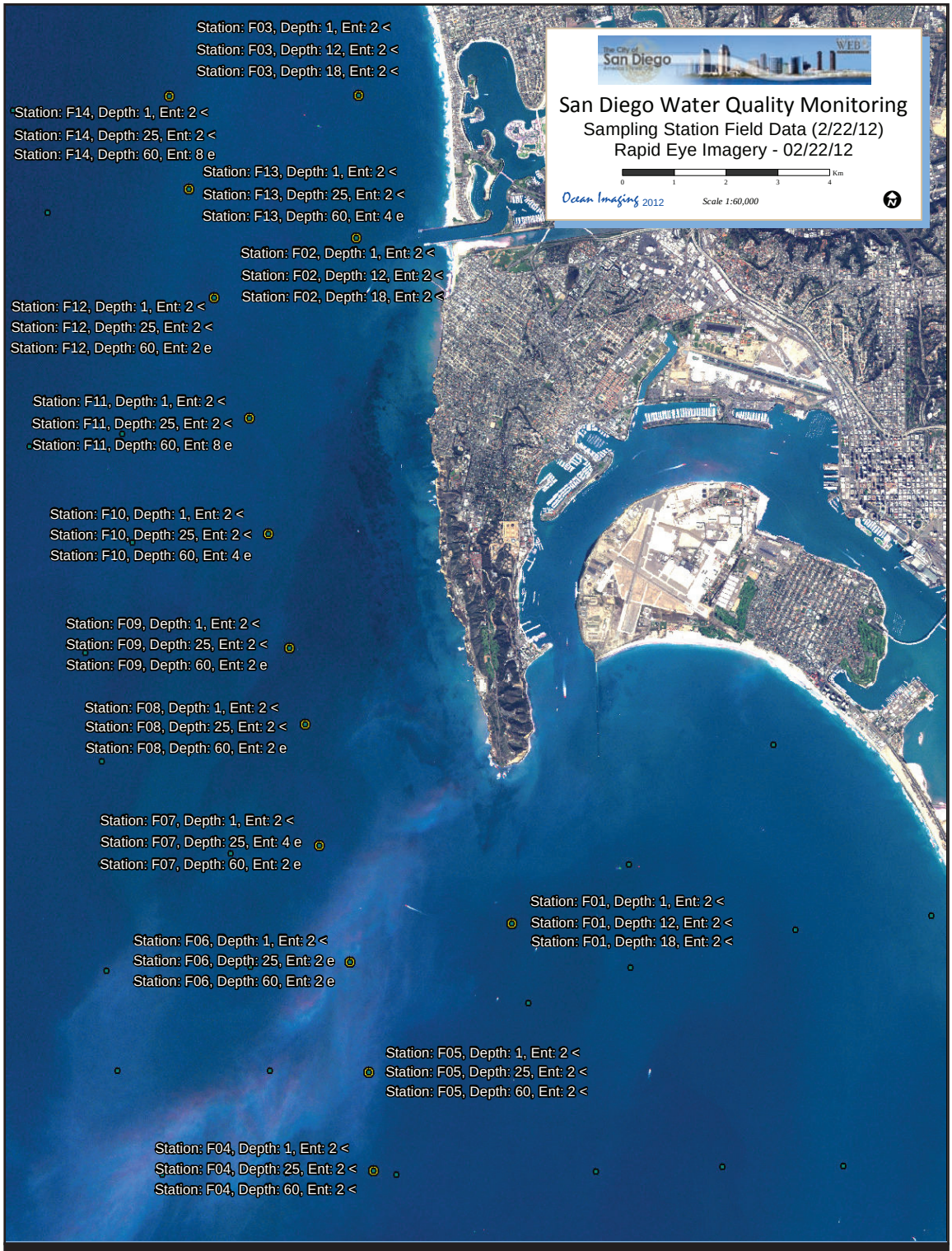

Figure 16.

RapidEye satellite image of the Pt. Loma region from 2/22/2012 with same-day offshore bacterial sampling results showing only background values throughout the region.

3.4 New Remote Sensing Products for the City's Biomap Server

As was already noted, in 2012 OI began operationally generating daily products for the City's BioMap server. These include satellite image based products such as Sea Surface Temperature and chlorophyll concentrations. They also include HF radar based currents and modeled currents generated from the Hycom model. **Figure 17** shows an example of a RapidEye image from 1/4/2012 with an overlay of HF radar surface currents averaged over the previous 24 hours. The trajectory of the SBOO plume corresponds well with the generated HF radar surface current field. OI plans to add additional products to the BioMap library, including mixed layer depth generated from models provided by the Navy.

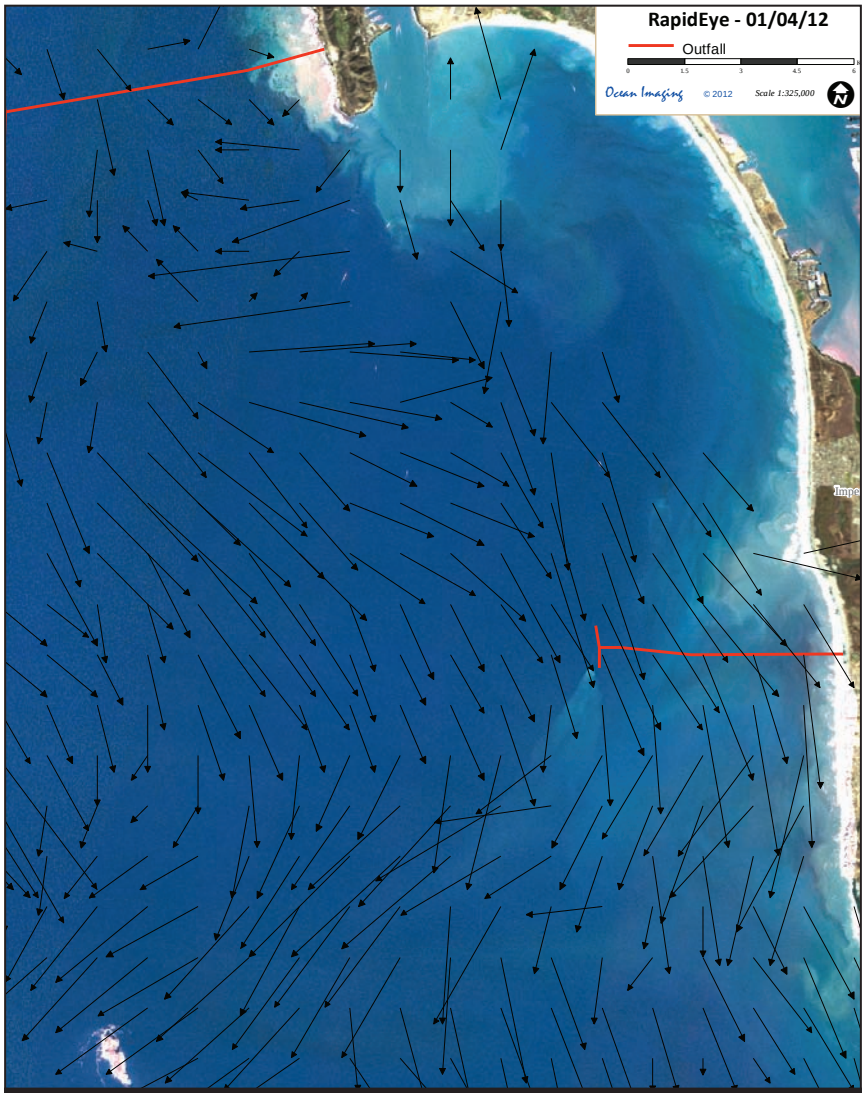

Figure 17.

RapidEye satellite image of the San Diego region from 1/4/2012 with an overlay of an HF radar surface current vector GIS product now being operationally provided to the City by OI on a daily basis.

Appendix H.5

2013 Ocean Imaging Report

Satellite & Aerial Coastal Water Quality Monitoring in the San Diego / Tijuana Region

By Jan Svejkovsky

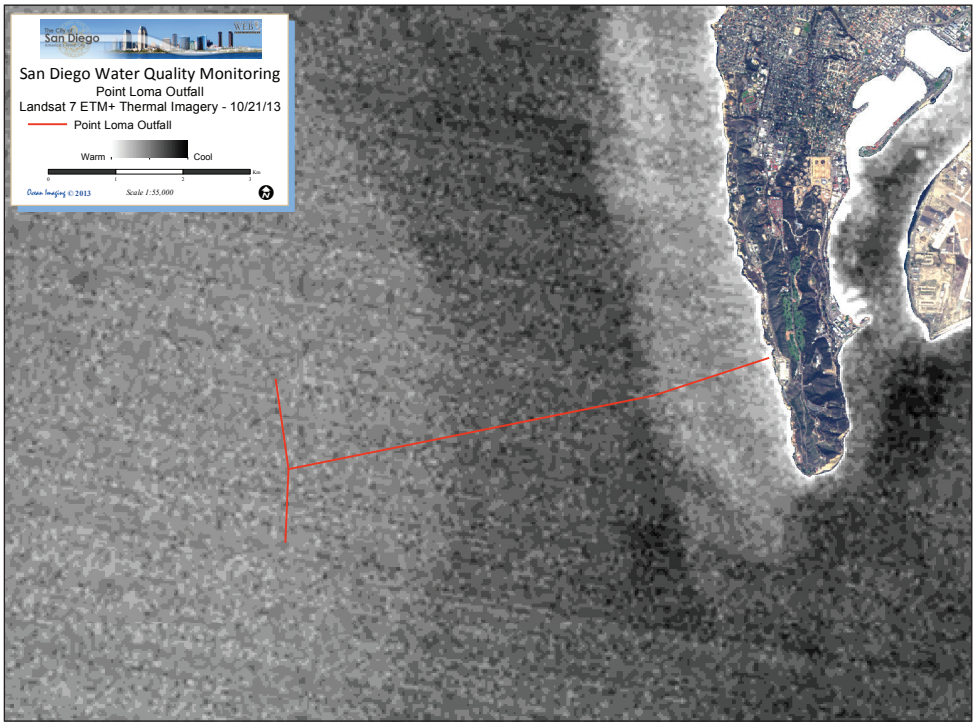

Annual Summary Report
1 January, 2013 - 31 December, 2013

This draft to become final in sixty days.

April 30, 2014

Ocean Imaging

201 Lomas Santa Fe Drive, Suite 370, Solana Beach, CA 92075 Phone: 858-792-8529 Fax: 858-792-8761 www.oceani.com

Table of Contents

1.0 Introduction & Project History 1

2.0 Technology Overview 2

2.1 Imaging in the UV-Visible-NearInfrared Spectrum 2
2.2 Imaging in the Infrared Spectrum 2
2.3 Data Dissemination and Analysis 3

3.0 Highlights of 2013 Monitoring 4

3.1 Atmospheric & Ocean Conditions 4
3.2 The South Bay Ocean Outfall Region 5
3.3 The Point Loma Ocean Outfall Region 11
3.4 Additional Data Products in 2013 14

1. Introduction and Project History

Ocean Imaging Corp. (OI) specializes in marine and coastal remote sensing for research and operational applications. In the 1990s, OI received multiple research grants from NASA's Commercial Remote Sensing Program for the development and commercialization of novel remote sensing applications in the coastal zone. As part of these projects, OI developed methods to utilize various types of remotely sensed data for the detection and monitoring of stormwater runoff and wastewater discharges from offshore outfalls. The methodology was initially demonstrated with collaboration of the Orange County Sanitation District. The NASA-supported research and demonstration led to a proof-of-concept demo project in the San Diego region co-funded by the EPA in 2000. Those results led, in turn, to adding an operational remote imaging-based monitoring component to the San Diego region's established water quality monitoring program, as stipulated in discharge permits for the International Wastewater Treatment Plant and Pt. Loma outfalls. The project was spearheaded by the State Water Resources Control Board (SWRCB), EPA Region 9, and continues to be jointly funded by the International Boundary Waters Commission (IBWC) and the City of San Diego.

The first phase of the project was a historical study utilizing various types of satellite data acquired between the early 1980s and 2002. The study established, among other findings, the prevailing near-surface current patterns in the region under various oceanic and atmospheric conditions. The current directions were deduced from patterns of turbidity, ocean temperature and surfactant slicks. In some cases, near-surface current velocity could be computed by tracking recognizable color or thermal features in time-sequential images. The historical study thus established a baseline data base for the region's current patterns, their persistence and occurrence frequency, and the historical locations, size and dispersion trajectories of various land and offshore discharge sources (e.g. the offshore outfalls, Tijuana River, Punta Bandera Treatment Plant discharge in Mexico, etc.).

In October, 2002 the operational monitoring phase of the project was initiated. This work utilizes 500m resolution Moderate Resolution Imaging Spectroradiometer (MODIS) color imagery (available near-daily), and 27m & 60m Landsat-5 & Landsat-7 color and thermal imagery (available 4 times per month). In addition, the project relied heavily on acquisition of multispectral color imagery with OI's DMSC-MKII aerial sensor and thermal infrared (IR) imagery from a Jenoptik thermal imager integrated into the system (see details in the "Technology Overview" section). These aerial image sets were most often collected at 2m resolution. The flights were done on a semi-regular schedule ranging from 1-2 times per month during the summer to once or more per week during the rainy season. The flights were also coordinated with the City of San Diego's regular offshore field sampling schedule so that the imagery was collected on the same day (usually within 2-3 hours) of the field data collection. Additional flights were done on an on-call basis immediately after major storms or other events such as sewage spills. In late 2010 OI negotiated a special data collection arrangement with Germany's RapidEye Corporation and this project began utilizing their multispectral imagery in lieu of most of the aerial DMSC image acquisitions. RapidEye maintains a unique constellation of five satellites which deliver 6.5 m resolution multispectral imagery. Unlike other single high resolution satellites, the multi-satellite constellation enables revisits of the San Diego region on a near-daily basis. Another advantage of using this imagery is the much larger spatial coverage available with each data set that was not possible using the aerial sensor. This enables a more regionally contiguous monitoring of events affecting the target areas. In 2012 OI also began operationally providing the City with a suite

of additional oceanographic products on a daily basis through the City's EMTS web-based GIS "BioMap" Server, and continued expanding the product selection and delivery through 2013. These products range from atmospherically corrected satellite images of sea surface temperature and chlorophyll to radar and model-derived surface current fields. Replacing Landsat-5 and Landsat-7 in 2013, Landsat-8 became operational with its Operational Land Imager (OLI).

This report summarizes observations made during the period 1/1/2013 – 12/31/2013.

2. Technology Overview

2.1 OI uses several remote sensing technologies to monitor San Diego's offshore outfalls and shoreline water quality. Their main principle is to reveal light, heat or microwave signal patterns that are characteristic of the different discharges. Most often this is due to specific substances contained in the effluent but absent in the surrounding water.

2.1 Imaging in the UV-Visible-NearInfraRed Spectrum

This is the most common technique used with satellite images and the DMSC aerial sensor. Wavelengths (colors) within the range of the human eye are most often used but Ultraviolet (UV) wavelengths are useful for detecting fluorescence from petroleum compounds (oil, diesel, etc.) and near-IR wavelengths can be useful for correcting atmospheric interference from aerosols (e.g. smog and smoke).

The best detection capabilities are attained when several images in different wavelengths are acquired simultaneously. These "multispectral" data can be digitally processed to enhance features not readily visible in simple color photographs. For example, two such images can be ratioed, thus emphasizing the water features' differences in reflection of the two wavelengths. A multi-wavelength image set can also be analyzed with "multispectral classification algorithms" which separate different features or effluents based on the correlation relationships between the different color signals.

The depth to which the color sensors can penetrate depends on which wavelengths they see, their sensitivity and the general water clarity. In the San Diego region, green wavelengths tend to reach the deepest and, as elsewhere, UV and near-IR wavelengths penetrate the least. Generally, OI's satellite and aerial sensor data reveal patterns in the upper 15-40 feet.

The color channels on satellite sensors cannot be changed, so they tend to be relatively broad, separating red, green, near-IR, and sometimes blue parts of the spectrum. OI's DMSC aerial 4-channel sensor has the added advantage of allowing each channel wavelength to be precisely customized. Through experimentation, OI has determined the exact wavelength relationships that maximize the detection of the offshore sewage outfall plumes and nearshore discharges such as the Tijuana River. With this channel configuration it is possible to monitor the plumes even when they are not visible to the naked eye.

2.2 Imaging in the Infrared Spectrum

Some satellite and aerial sensors image heat emanating from the ground and the ocean. They thus reveal patterns and features due to their differences in temperature. Since infrared wavelengths are strongly absorbed by water, the images reveal temperature patterns only on the water's surface. Such images can help detect runoff plumes when their temperatures differ from the surrounding ocean

water. Runoff from shoreline sources tends to be warmer than the ocean water, although the reverse can be true during the winter. Plumes from offshore outfalls can sometimes also be detected with thermal imaging. Since the effluent contains mostly fresh water, it is less dense than the surrounding salt water and tends to rise to the surface. If it surfaces fully, it is usually cooler than the surrounding sun-warmed surface water. If it is constrained by a strong thermocline and/or pycnocline ("vertical stratification"), it sometimes tends to displace some of the water above it in a doming effect. This displacement pattern is revealed in the thermal surface imagery.

2.3 Data dissemination and Analysis

The satellite and aerial imaging data are made available to the funding agencies, the San Diego County Dept. of Health and the EPA through a dedicated, password-protected web site. Although it is possible to process most of the used data in near-real-time, earlier in the project the funding agencies decided that the emphasis of this project is not on providing real-time monitoring support and the extra costs associated with the rapid data turn-around are not warranted. Most satellite data is thus processed and posted within 1-2 days after acquisition and the aerial sensor imagery (which requires the most labor-intensive processing), within 2-5 days. OI has, however, in a number of cases, made some imagery available to the CDH and others in near-real time when observations were made that appeared to be highly significant for the management of beach closures or other sudden events. The BioMap Server-directed products are produced daily by OI and are automatically linked with the server when available.

3. Highlights Of 2013 Monitoring

3.1 Atmospheric and Ocean Conditions

2013 was even drier than the previous year in the San Diego region. Only March and November had rainfall fractionally over 1" at Lindberg Field, and even less rain fell in Southern San Diego and Tijuana **(Figure 1)**. Additionally, the rain events were often localized rather than area-wide, resulting in rainfall totals that differed greatly between North, Central and South San Diego County. For example, North and Central areas experienced several rainy days in January, while the practically no rain was recorded in the Tijuana Estuary. Similarly, the most rain fell at Lindberg on 21 November (1.04") during a very localized convective rain shower, but that date produced only about 0.09" of precipitation in the Tijuana Estuary.

The 2012-13 season was characterized by neutral conditions in the equatorial Pacific (neither El Nino nor La Nina). Neutral conditions have been typically associated with below average rainfall in Southern California. As is shown in **Figure 2**, San Diego River flow – an indication of the overall watershed region's rainfall – reached and/or exceeded 100 cubic feet per second only twice in 2013 at the Fashion Valley gauging station, compared to 2012 when that value was exceeded 6 times. Very low runoff volume through 2013 also affected the Tijuana River, which resulted, in turn, in relatively few runoff-related beach closures with most limited to the immediate River-mouth area.

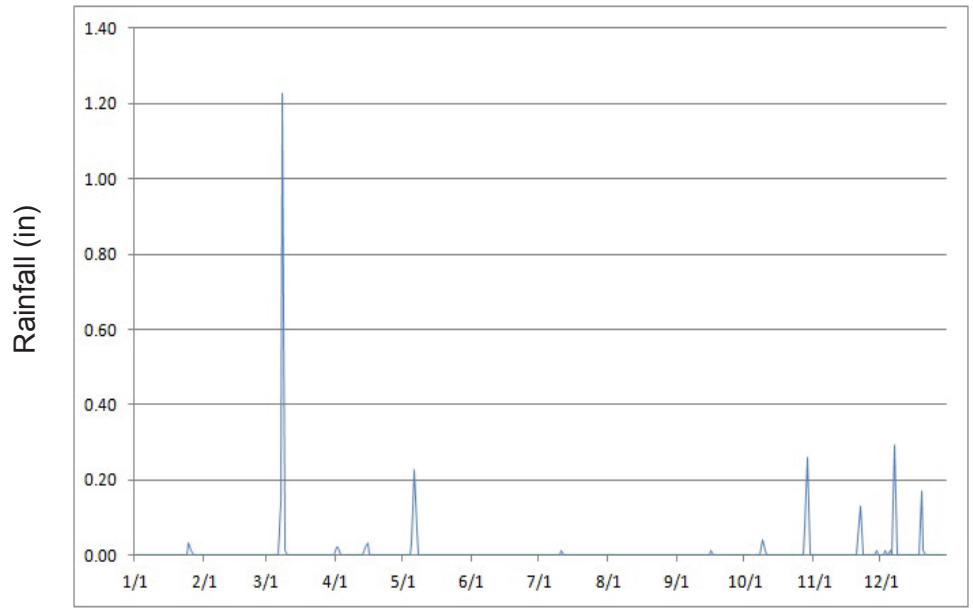

Date	CumPrcp (in)
1/25	0.03
1/26	0.01
3/7	0.14
3/8	1.23
3/9	0.01
4/1	0.02
4/2	0.02
4/14	0.02
4/15	0.03
5/5	0.03
5/6	0.23
5/7	0.07
7/11	0.01
9/16	0.01
10/9	0.04
10/10	0.01
10/28	0.08
10/29	0.26
11/21	0.09
11/22	0.13
11/29	0.01
12/3	0.01
12/5	0.01
12/7	0.29
12/19	0.17
12/20	0.01

Figure 1.

Graph of daily cumulative rainfall in the Tijuana Estuary.

3.2 The South Bay Ocean Outfall Region

The South Bay Ocean Outfall (SBOO) wastewater plume generally remains well below the surface between approximately late March and November due to vertical stratification of the water column. During that period it usually cannot be detected with multispectral aerial and satellite imagery which penetrate the upper 7 to 15 meters (depending on water clarity). The plume also cannot be detected with thermal IR imaging which does not penetrate below the surface. Seasonal breakdown of the vertical stratification results in the plume's rise closer to the surface or to actually reach the surface between approximately late November and late March, when it can often be detected with aerial and satellite imaging.

The SBOO treatment plant switched from advanced primary to secondary treatment in January, 2011. This change resulted, among other factors, in the reduction of total suspended solids (TSS) concentrations from an average of 60 mg/l for several years prior to the change, to 15 mg/l in 2011 and 2012 (S. Smullen/IBWC, pers. commun.). A reduction in TSS concentrations can be expected to have an effect on the reflectance intensity of the surfacing or near-surfacing effluent plume in the visible and near-IR imaging channels.

Prior to 2011, a distinct plume signature was regularly detected in multispectral imagery as per the seasonal fluctuation described above. In 2011 the plume signature was also observed during the

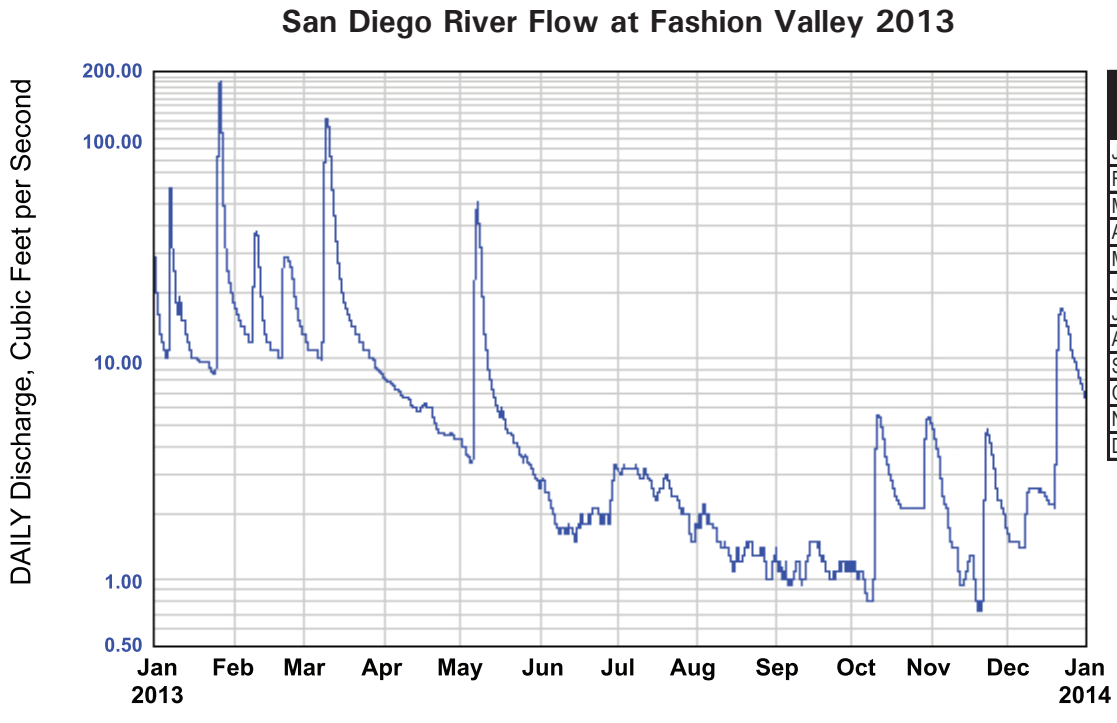

Lindberg Field Rainfall 2013	
January	0.70"
February	0.63"
March	1.22"
April	0.01"
May	0.26"
June	0.00"
July	0.05"
August	0.00"
September	0.00"
October	0.25"
November	1.48"
December	0.46"

Figure 2.

Graph of mean daily discharge of the San Diego River during 2013 (measured at Fashion Valley). The table on the right shows monthly rainfall totals at Lindbergh Field.

winter months, however, due to extensive rains its signature was often apparent as a "clear water" feature penetrating through the highly turbid storm runoff plume of the Tijuana River which was large enough to overtake the SBOO wye region offshore. As is discussed in our 2012 report, the SBOO plume turbidity signatures in data from the winter months of 2012 show high variability (visible on some days but not others) that was not experienced with imagery from earlier years of the project. Since it is unreasonable to assume that vertical stratification would have fluctuated so frequently and rapidly over the SBOO to cause the plume signature inconsistencies, we thus postulated that that this high variability in the satellite observations in 2012 was due to combined effects of the reduction in TSS loads of the plume and variability in dispersion rate due to subsurface currents existing on each observation day.

The SBOO plume was detected only intermittently in the satellite imagery during the first few months of 2013. On occasion, a surface thermal signature was apparent (the plume waters appear cooler than surrounding ocean sea surface temperatures [SSTs]) but no distinct turbidity plume signature was apparent in the same data set **(Figure 3 showing 2/23/13 data)**. This gives further support to our premise noted in the 2012 report – that the reduction in TSS loads is noticeable in the decade-long record of satellite and aerial multispectral imagery. While a thermal signature indicates the plume was fully surfacing, the lack of detectable turbid signature indicates relatively low TSS concentration in the surfacing effluent – a coincidence never noted in imagery from the earlier years of this project. On 3/1/13 a very faint plume signature revealing it as a less turbid feature than surrounding waters was detected in a RapidEye satellite image. The plume remained undetectable in the surface (thermal) and upper-column (multispectral visible) waters until it reappeared as a very distinct negative thermal anomaly in TM-8 imagery from 10/29/13, shown in **Figure 4**. Interestingly, the plume signature was again void of a turbidity signal, indicating relatively low TSS concentrations at and near the surface.

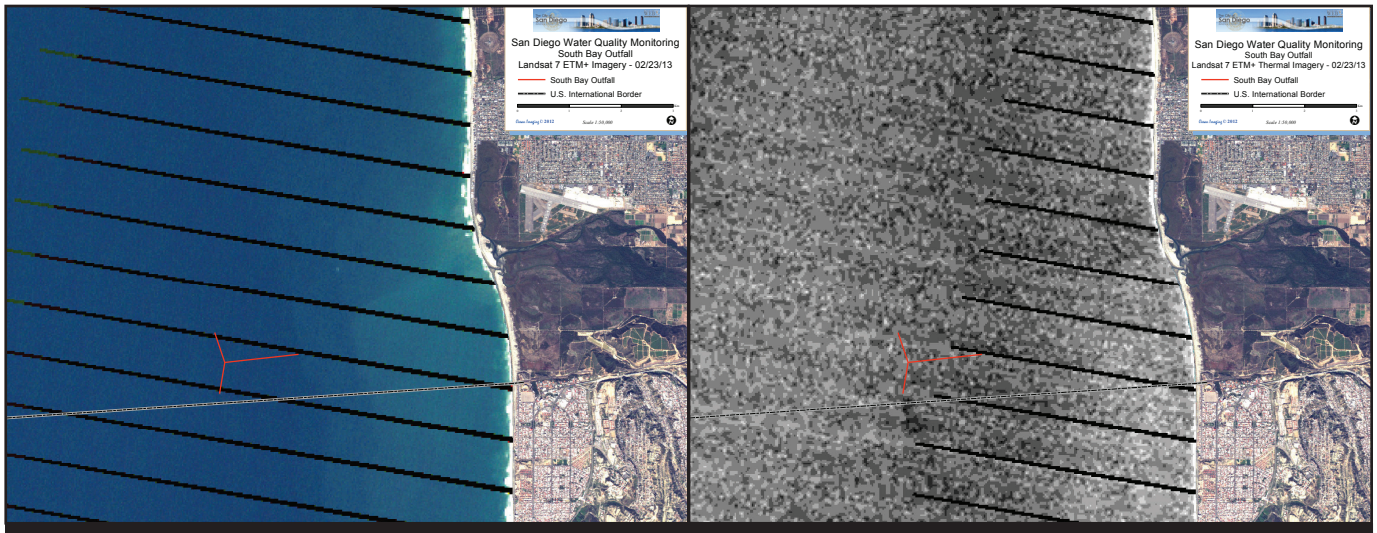

Figure 3.

ETM color (left) and thermal (right) imagery of the SBOO region acquired on 2/23/13. Cooler water appears darker in the thermal data.

This trend was noted further into November 2013, when multiple high resolution RapidEye acquisitions revealed no turbidity signature on, for example, 11/13/13 and 11/25/13 (RapidEye does not have a thermal channel), however the surfacing plume is detectable in a thermal image from TM-8 acquired on 11/14/13.

A TM-8 image acquired on 11/30/13 shows a historically very large signature of the SBOO plume both in the thermal and multispectral channels **(Figure 5)**. The plume is distinguishable along its southwestward trajectory for more than 2 kilometers from the SBOO's southern wye. Also noticeable in the multispectral color image is a relatively small but characteristically reddish runoff plume in front of the Tijuana River mouth. Correspondingly, shoreline bacterial sampling by the County Dept. of Health measured high indicator bacteria concentrations at the River Mouth station on 11/26/13-11/29/13. The river runoff signature indicates that there was sufficient stormwater runoff volume in the river to actively flow into the ocean. Although, as noted above, rain on 11/21/13 measured over 1" at Lindberg Airport, only about 0.09" was measured in the Tijuana Estuary. It is likely that the runoff volume was primarily enhanced from precipitation further inland in the watershed. It is not clear if the strong turbidity signature of the SBOO on 11/30/13 is directly related to the 11/21/13 rain event, but historically we do have examples when the plume signature was enhanced after major rains. During December, the SBOO plume once again showed a thermal signature in a TM-8 image from 12/16/13, but no turbidity signature on that day, or in high resolution satellite data from 12/12/13 and 12/24/13. A very slight signature is apparent in a RapidEye image from 12/21/13.

The relative lack of Tijuana River and other point and non-point source stormwater runoff during 2013 is reflected in the sparsity of greatly elevated indicator bacteria samples done along the SB shoreline by the County Dept. of Health, and hence also direct beach closures. Perhaps the most significant event was a combination of a rain event on 3/7/13-3/9/13 (which

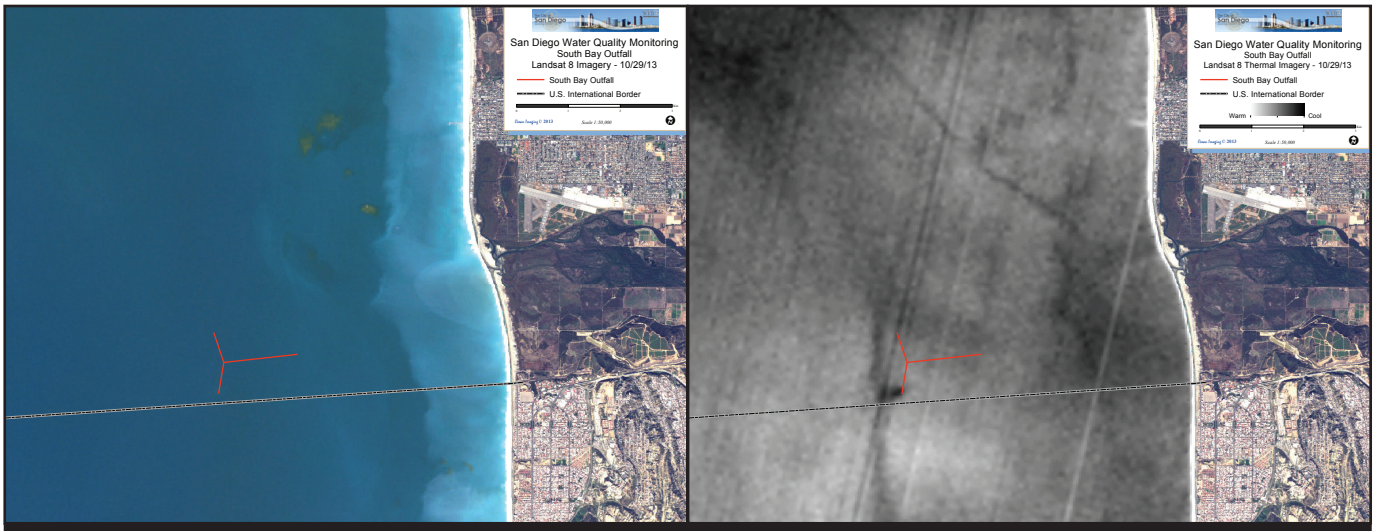

Figure 4.

OLI color (left) and thermal (right) imagery of the SBOO region acquired on 10/29/13. Cooler water appears darker in the thermal data.

included the greatest daily precipitation volume at the Tijuana Estuary for 2013) and a sewage spill that reached the ocean from Playas de Tijuana starting on 3/9/13 or 3/10/13. We obtained high resolution RapidEye imagery on 3/11/13 which is shown in **Figure 6**. The satellite data show a somewhat unusual cross-shore turbidity front feature extending approximately 1.5km directly west from the surf zone off the Tijuana Estuary, and trailing turbid water southward from its offshore edge. The shape indicates that a northward nearshore flow regime existed at least a day or so prior to the image acquisition, followed by a southward flow reversal during the day of the image. Also visible is the small but characteristically reddish fresh runoff plume in front of the river mouth north of the cross-shore feature. Shoreline bacterial sampling indicated elevated bacteria counts around the river mouth and northward up to the Imperial Beach Pier and Cortez Ave. between 3/19/13 and 3/21/13. Also affected were waters outside the surf zone, as sampled on 3/12/13 at stations I19, I24 and I40 **(Figure 7)**.

Another notable event was a late-season rain event on 5-7 May, which brought 0.33" of rain at the Tijuana Estuary and 0.26" at Lindberg Field. Shoreline sampling stations showed significantly elevated bacteria concentrations at the river mouth and at multiple stations along Imperial Beach on 5/7/13, but returning to background levels by 5/9/13. A MODIS satellite image from 5/9/13 shows no distinct river runoff plume.

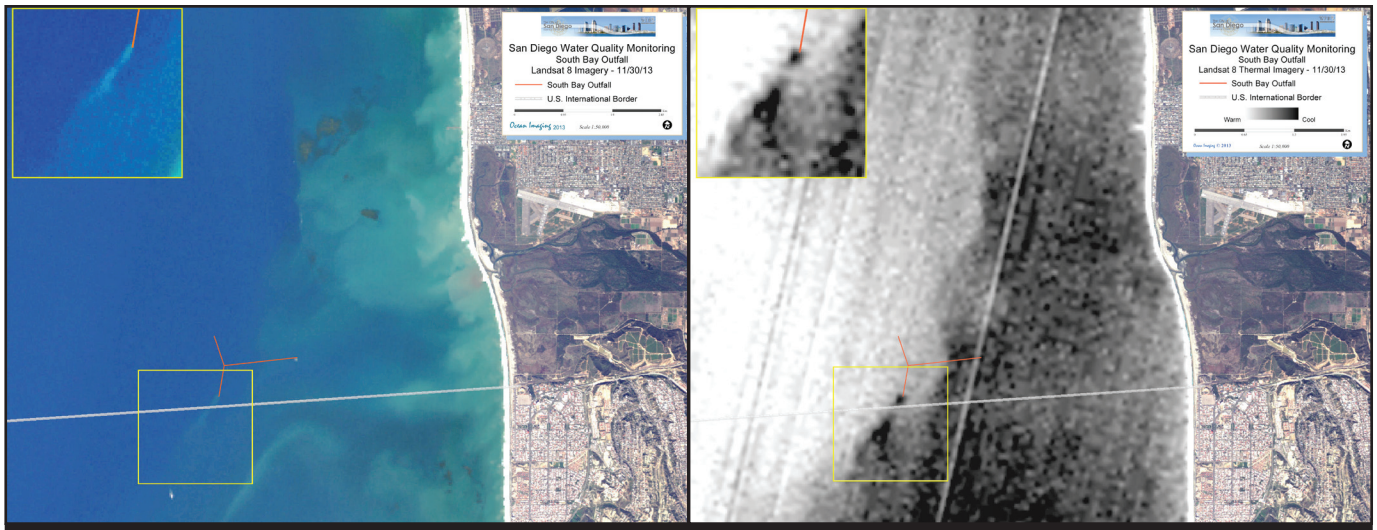

Figure 5.

OLI color (left) and thermal (right) imagery of the SBOO region acquired on 11/30/13. Large distinct turbidity and thermal SBOO plume signatures exist. Fresh, red-hued discharge from the Tijuana River is also detectable.

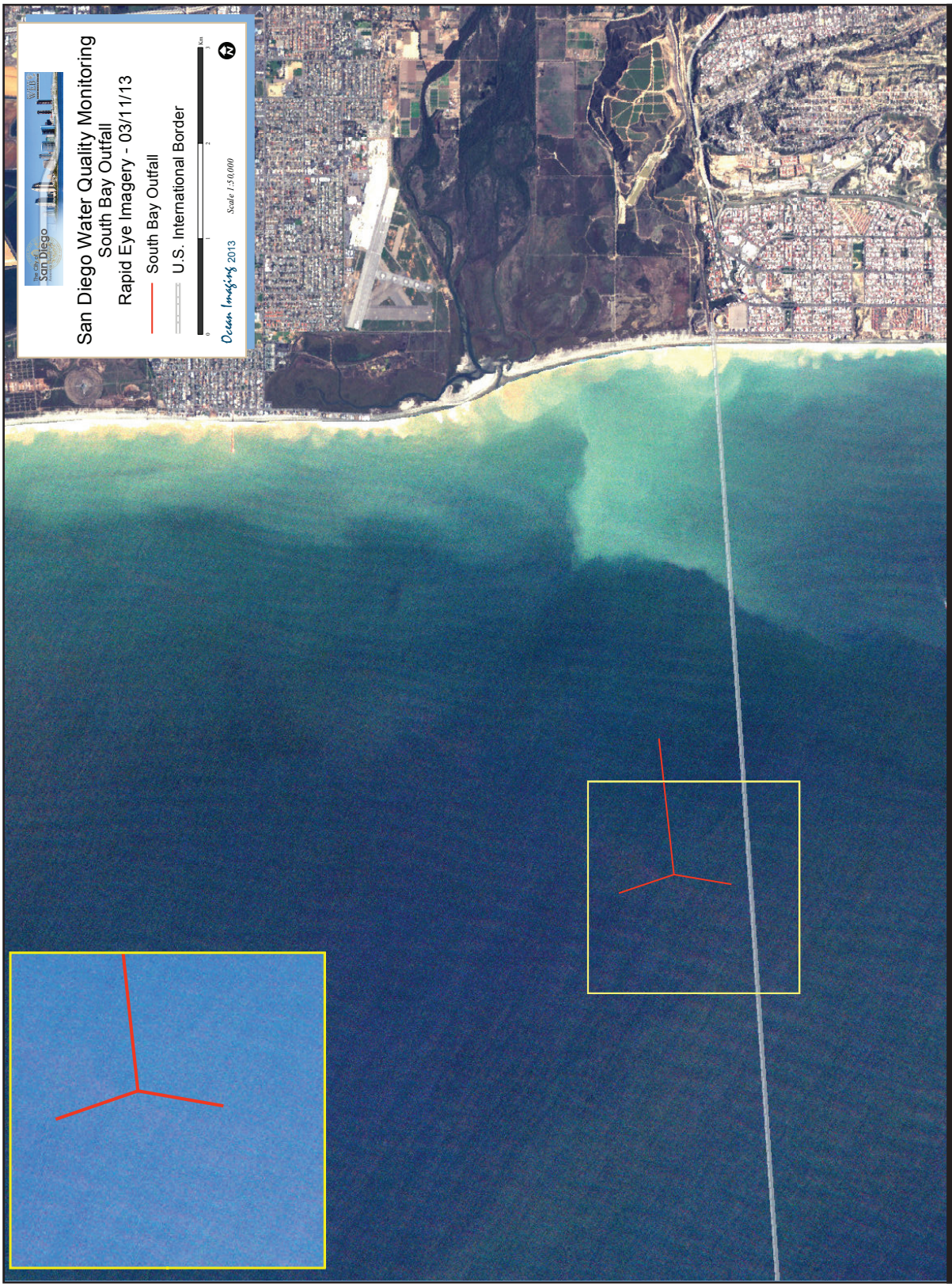

Figure 6.

RapidEye images of the SBOO region acquired on 3/11/13. No outfall turbidity signature exists but distinct turbidity features and some fresh (red-hued) Tijuana River discharge are apparent nearshore.

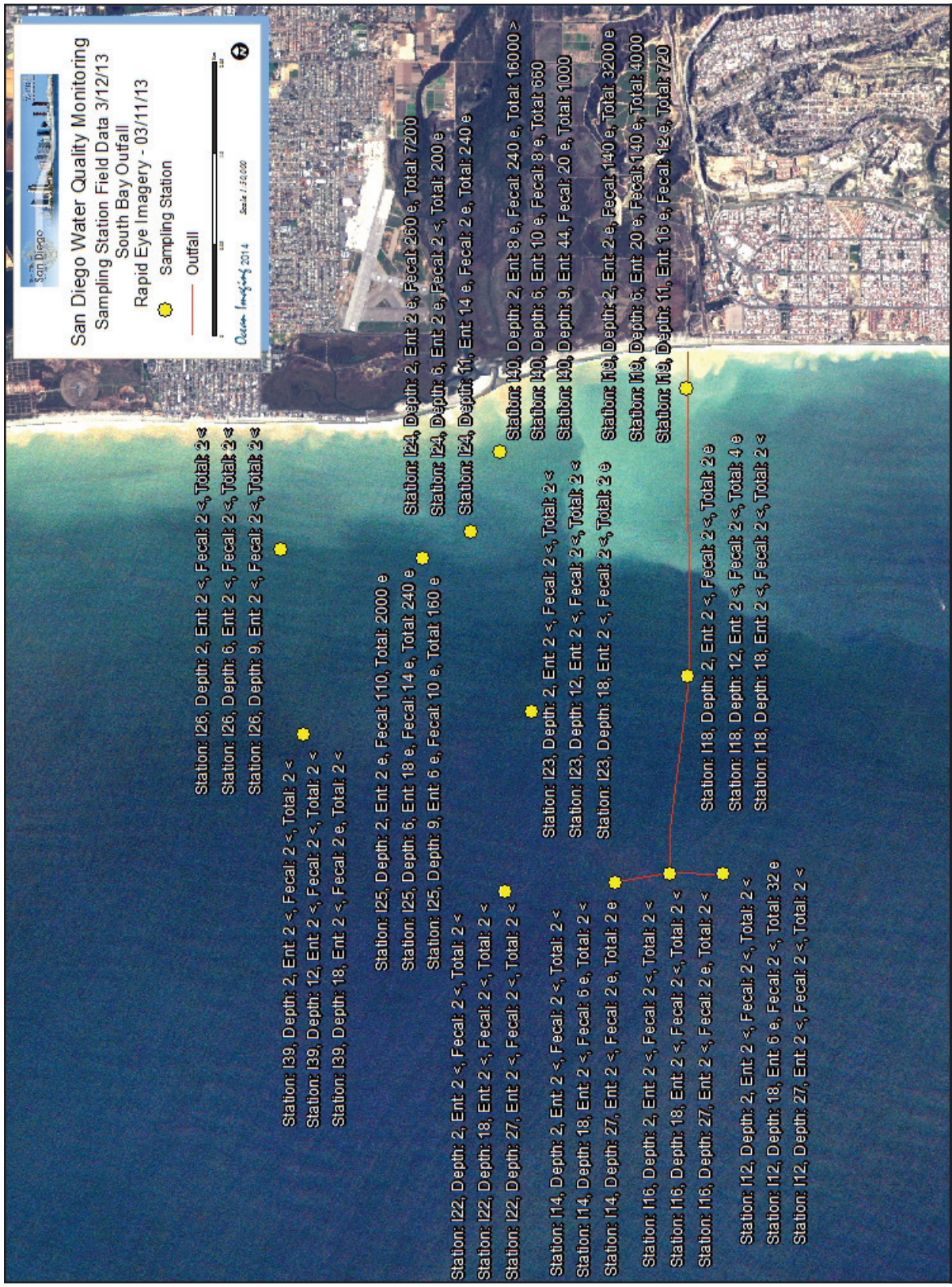

Figure 7.

RapidEye imagery of the SBOO region from 3/11/13 with offshore bacteria sampling results from 3/12/13.

3.3. The Point Loma Outfall Region

After its seaward extension in 1993, the Point Loma Outfall (PLO) is one of the deepest and longest wastewater outfalls in the world, discharging at the depth of 320 feet, 4.5 miles offshore. The outfall's plume is generally not observed directly with multi-spectral color or thermal imagery. It appears to not reach the surface waters, even during the winter months when the water column's vertical stratifications is weakened. We believe, however, that on some occasions we have observed the plume's extents indirectly through an anomalous lateral displacement of thermal or chlorophyll features around the outfall wye. This effect can be explained by the doming up of the discharged effluent and its lateral displacing the near-surface waters above it.

In 2013 the PLO region experienced conditions very similar to those already described for the SBOO further to the south: below average rainfall and thus point and non-point terrestrial runoff, and mostly clear-water conditions. Unlike in most previous years, the region did not experience any significant red-tide events or major plankton blooms. The most commonly observed phenomenon in the satellite data was the southward transport of waters with elevated TSS and plankton concentrations from nearshore areas of North County and La Jolla over the PLO wye area. After the main rain events and increased runoff from the San Diego River/Mission Bay outlets, that effluent often mixed with the North County waters and reached the PLO wye. An example is shown in **Figure 8**.

Early on in this project we noticed that the offshore location of the PLO wye often places it just outside a relatively stable upper-column water mass boundary that is detectable in satellite imagery and tends to represent a current shear zone as well. It separates more turbid waters filling areas along Pt. Loma inside, within and outside its kelp bed and clearer waters further (@ 4+ miles) offshore. **Figure 9A** shows this effect in RapidEye color imagery. This separation is difficult or impossible to detect in color imagery during clear-water nearshore conditions, which existed often during 2013 due to the lack of storm runoff and major plankton blooms. In such conditions high resolution thermal imaging continues to reveal the water mass boundary, however. Two examples from 2013 are shown in **Figure 9B and 9C**. Both show thermal patterns typical of the La Jolla – Pt. Loma region: surface waters between the shore and the kelp beds, as well as within the kelp bed tend to be several tenths of a degree or more warmer than waters outside the kelp beds. A region 2-4km wide with noticeably cooler SSTs rounds the outside of the beds, with a well defined front offshore that corresponds to the turbidity/color boundary discernible during lower inshore clarity conditions. Both shown examples and many others from imagery acquired for the project also show a region with the coolest SSTs just south of Pt. Loma, which we believe corresponds to locally driven upwelling modeled and field–validated by others (e.g. Roughan et al. 2005). Although satellite imagery only reveals patterns present on the ocean surface (thermal) and uppermost water column (color), the positioning of the PLO relative to the region's oceanographic and biological regimes as revealed in the remote sensing data provides important, broad synoptic insight and better understanding of potential interactions.

Roughan M, E. J. Terrill, J. L. Largier and M. P. Otero. 2005. Observations of divergence and upwelling around Point Loma, California. J. Geophys. Res. V110 (C04011).

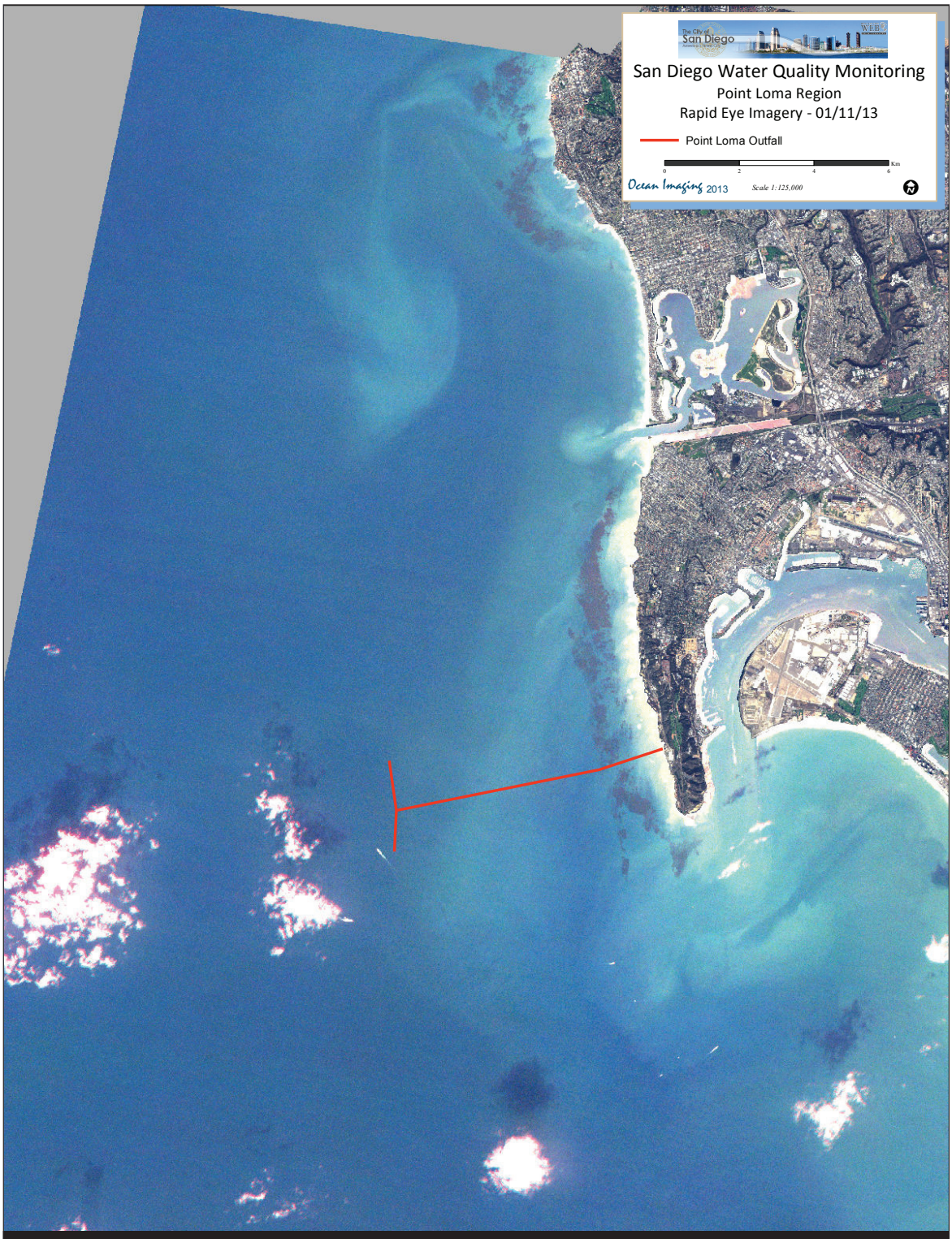

Figure 8.

RapidEye image from 1/11/2013 showing coastal turbid water mixed with San Diego River and Mission Bay runoff being advected southward over the PLO region.

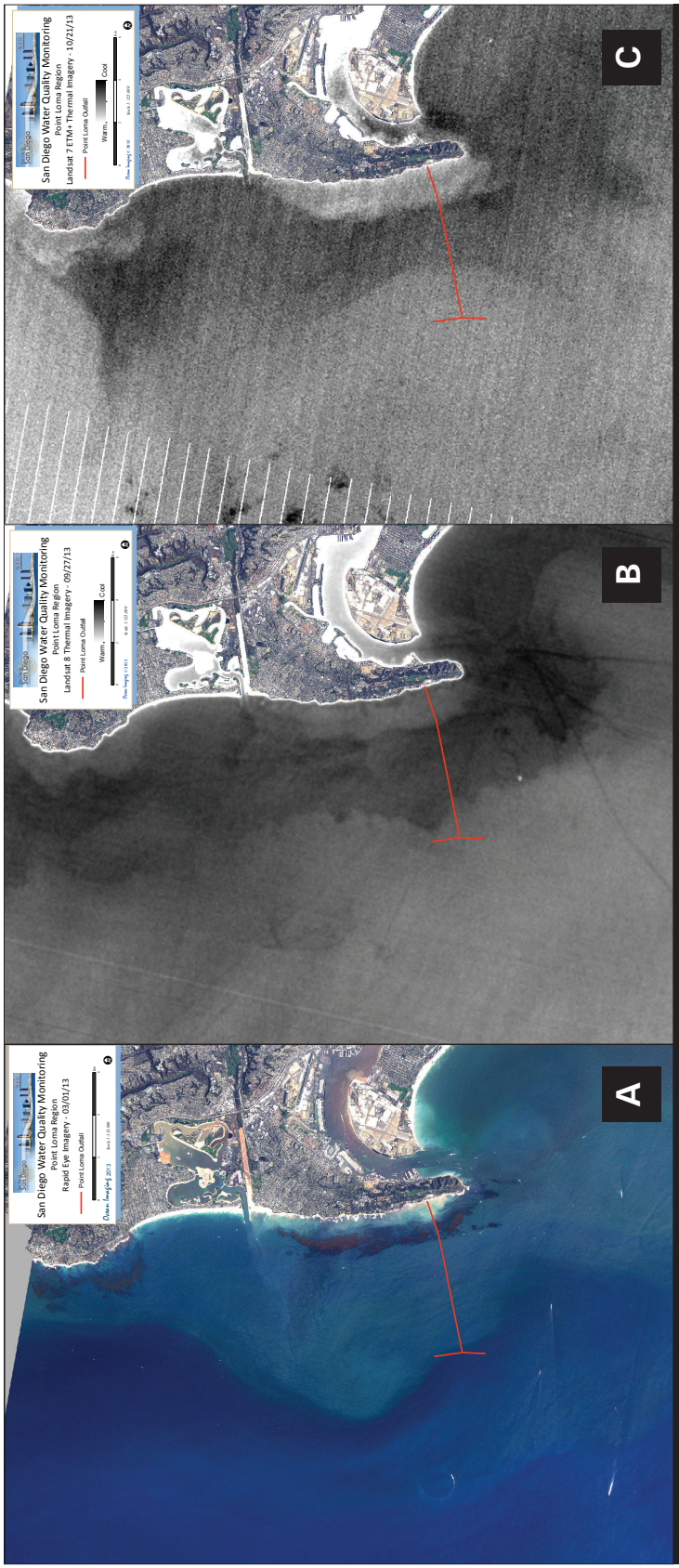

Figure 9.

(A) RapidEye image from 3/1/2013 showing the PLO wye located just west of a typically-positioned boundary between coastal turbid and offshore clear water masses.

(B) OLI thermal image from 9/27/2013 showing SST patterns in the PLO region, and its wye just west of a persistent water mass boundary (see text). The linear features are ship wakes.

(C) eTM thermal image from 10/21/2013 showing SST patterns in the PLO region, and its wye just west of a persistent water mass boundary (see text).

3.4 Additional Data Products in 2013

Since 2010 City of San Diego Public Utilities Department's Environmental Monitoring and Technical Services (EMTS) Division has been developing a web-based GIS application to increase staff access to ocean monitoring data. The web application, called BioMap has analytical tools which enable EMTS staff and others with access to the system to synthesize and explore large volumes of data dynamically via a web browser interface, in ways not possible in the past (Luostarinen, 2010).

In order to make use of this web mapping technology and be compatible with BioMap, over the latter part of 2011 and into early 2012, Ocean Imaging (OI) engaged in discussions with EMTS personnel about how to incorporate OI-supplied imagery and oceanographic data products into the BioMap system. It was determined that, compared to the existing methods (downloading from OI's password-protected San Diego Water Quality web site), the inclusion of OI data in BioMap via an OI-supported

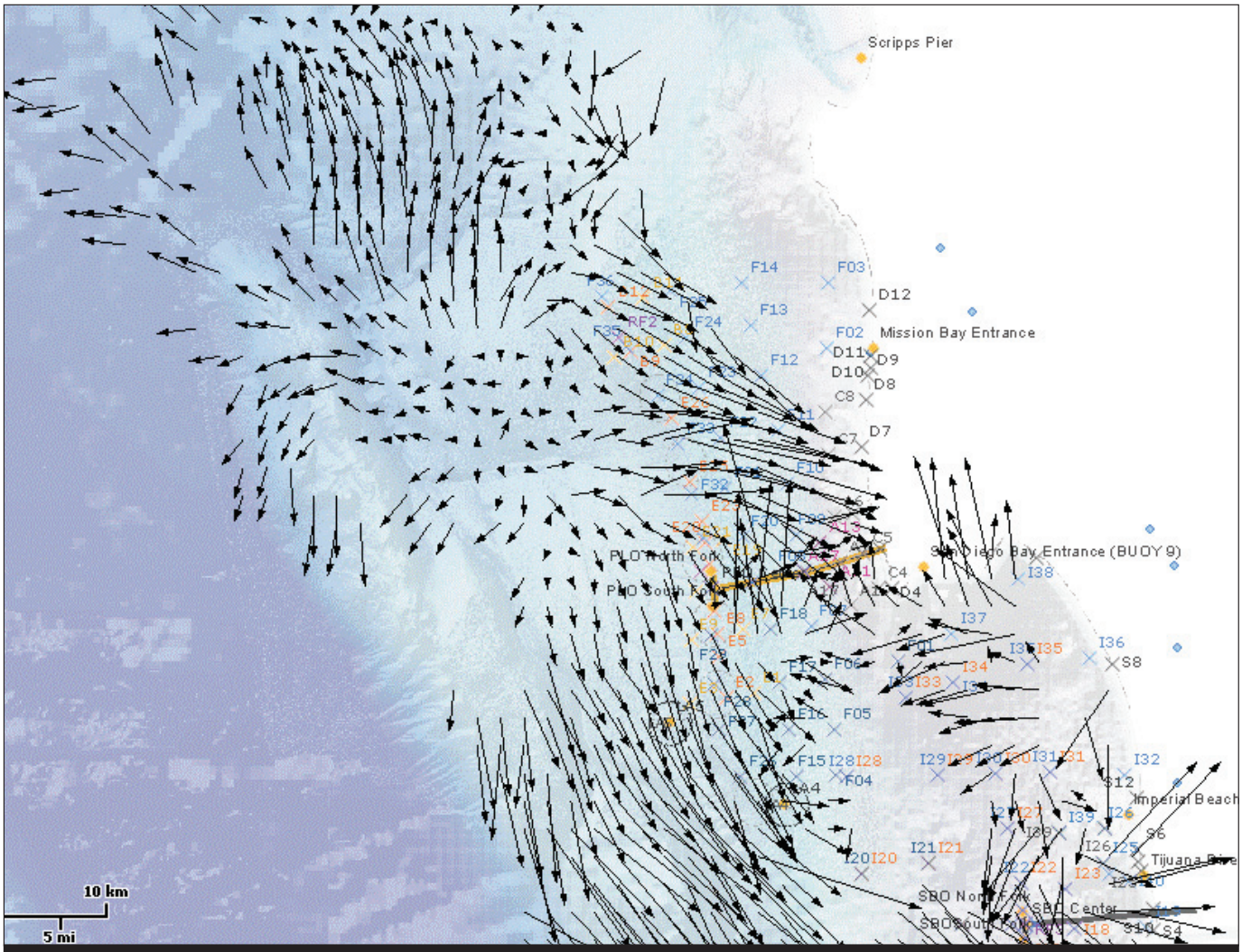

Figure 10.

Sample screen capture of HF Radar currents displayed via BioMap.

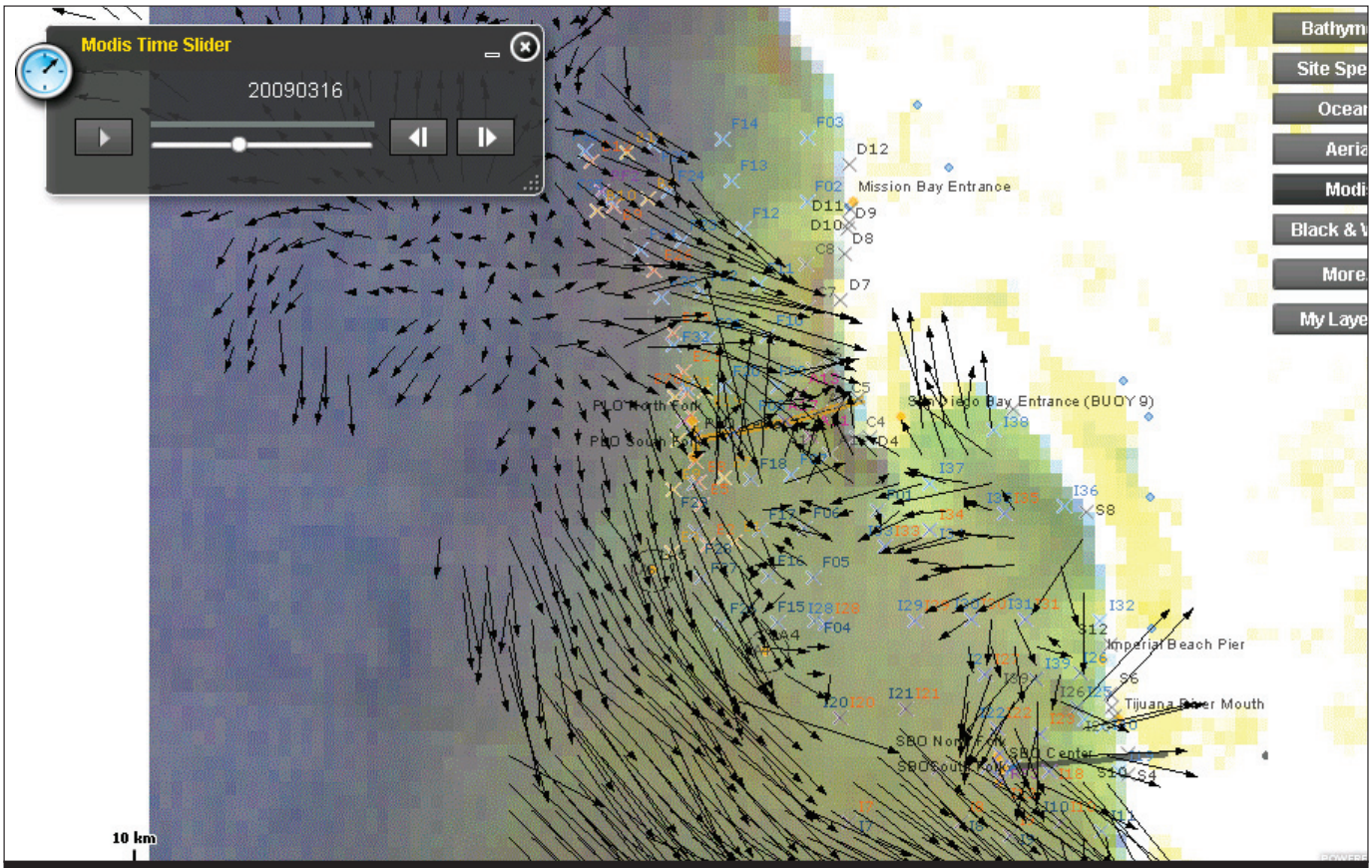

Figure 11.

Example screen capture of Time Slider tool now used for MODIS satellite data in BioMap.

web map server would better facilitate the correlation of EMTS biological and water quality information to the environmental conditions visible in many of the OI data products. Delivering and analyzing data using BioMap would greatly increase both the accessibility and utility of existing and future OI information products. In late 2012, as part of the plan to be fully compatible with BioMap, OI implemented an ArcGIS Server-based web mapping service (WMS) to seamlessly deliver a variety of new oceanographic products to the EMTS Division. This system was fully operational during the entirety of 2013 and continues to act as the primary delivery mechanism for select OI data products.

OI's ArcGIS Server is hosted at OI's Internet Service Provider's (ISP) secure, climate-controlled data center in San Diego, California. OI decided to purchase ArcGIS Server because of its Open Geospatial Consortium (OGC) compatibility and the ability to develop Web Map Service (WMS) which communicates directly and seamlessly with the BioMap server. ESRI's ArcGIS Server product is also built in Adobe Flex using ESRI's API to enhance the end user interface. OI's server is deployed on a virtual machine cluster running on the Windows 2008 R2 platform. The deployment via a computer cluster on a dedicated virtual private server provides a higher level of availability to the end users, more computational power, enhanced scalability as well as

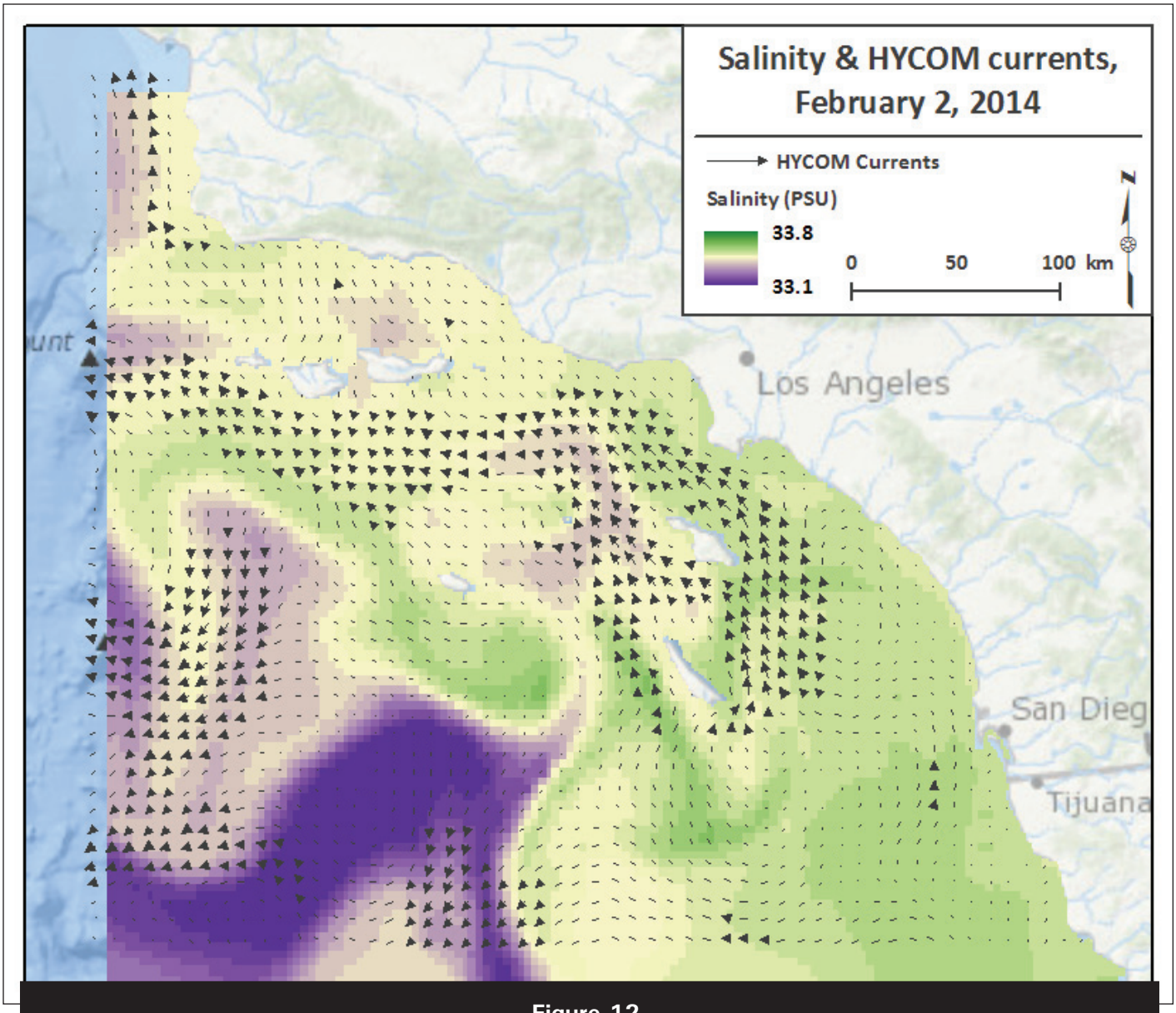

Figure 12.

HYCOM – Salinity, 3 kilometer spatial resolution. HYCOM ocean currents for the same day are overlaid on the imagery.

increased security and system redundancy to avoid data loss and down time.

As discussed in previous reports, beginning in late 2012, OI implemented the delivery of two types of ocean current products via ArcGIS Server and BioMap: High Frequency Radar-derived surface currents (HF Radar) and Hybrid Ocean Coordinate Model (HYCOM) model-derived surface currents (http://hycom.org). The raw data for the HF Radar currents are retrieved from National HF RADAR Network via the Scripps Coastal Observing Research and Development Center (CORDC) on an hourly basis and reformatted into ESRI-compatible shapefiles. The hourly products are averages of the previous 25 hours and generated at one and six kilometer

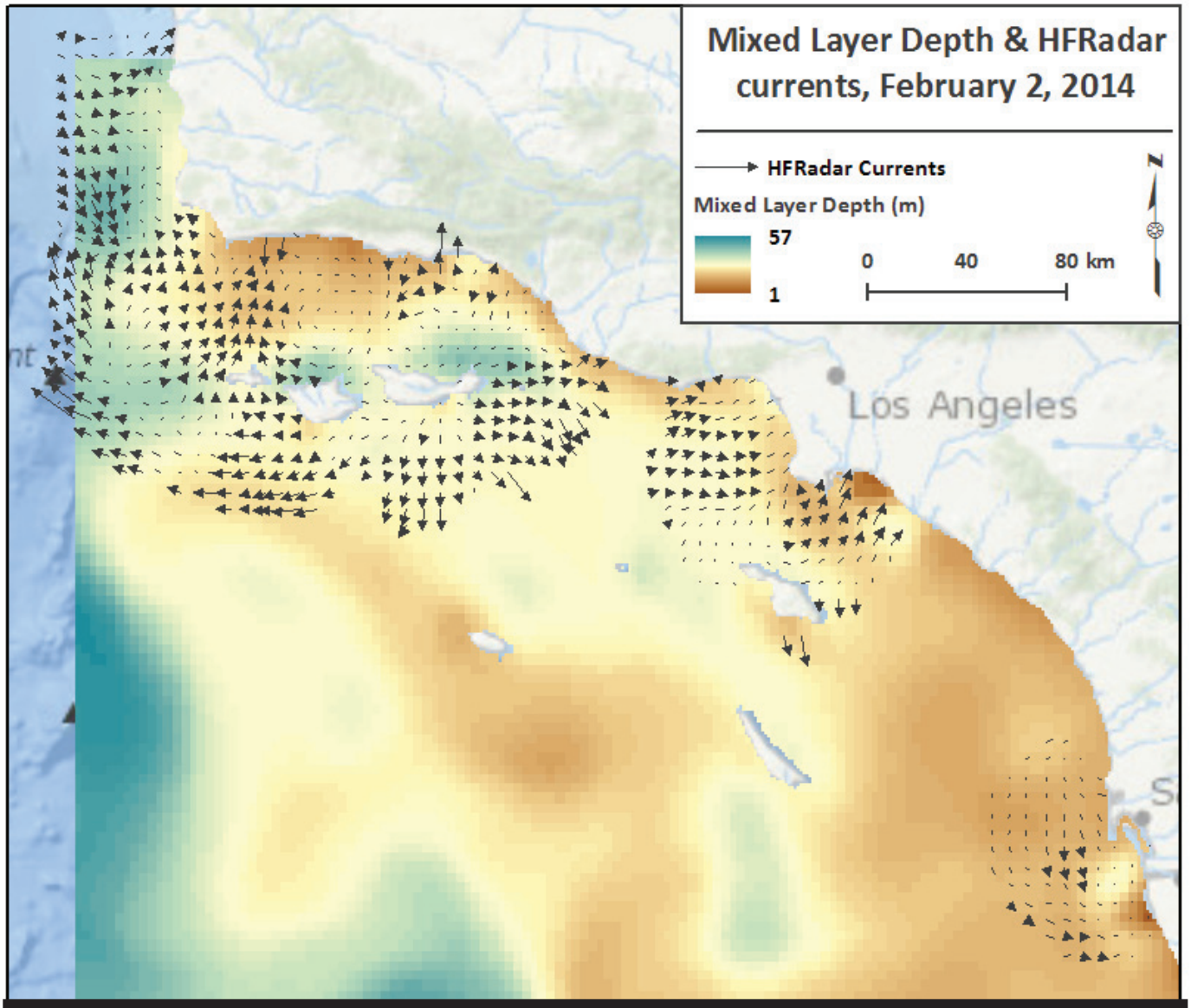

Figure 13.

HYCOM – Mixed Layer Depth, 3 kilometer spatial resolution. HF Radar ocean currents for the same day are overlaid on the imagery.

spatial resolutions **(Figure 10)**. Each hourly shapefile is then, in turn, packaged up as a REpresentational State Transfer architecture (REST) compatible 'web service' by which each 'service' contains one week's worth of hourly, dated shapefiles. Each weekly web service for the prior week is posted to the ArcGIS Server every Monday morning. As part of the continued development process which occurred in 2013, it was decided that the archived data services would be made available in monthly groupings (i.e. the web services are packaged/organized by month with service file names allowing easy access by BioMap - HFRadar_2013_Dec, HFRadar_2014_JAN). The HYCOM currents are daily products for which each web service contains one week's worth of daily, dated shapefiles. The archived web service packages

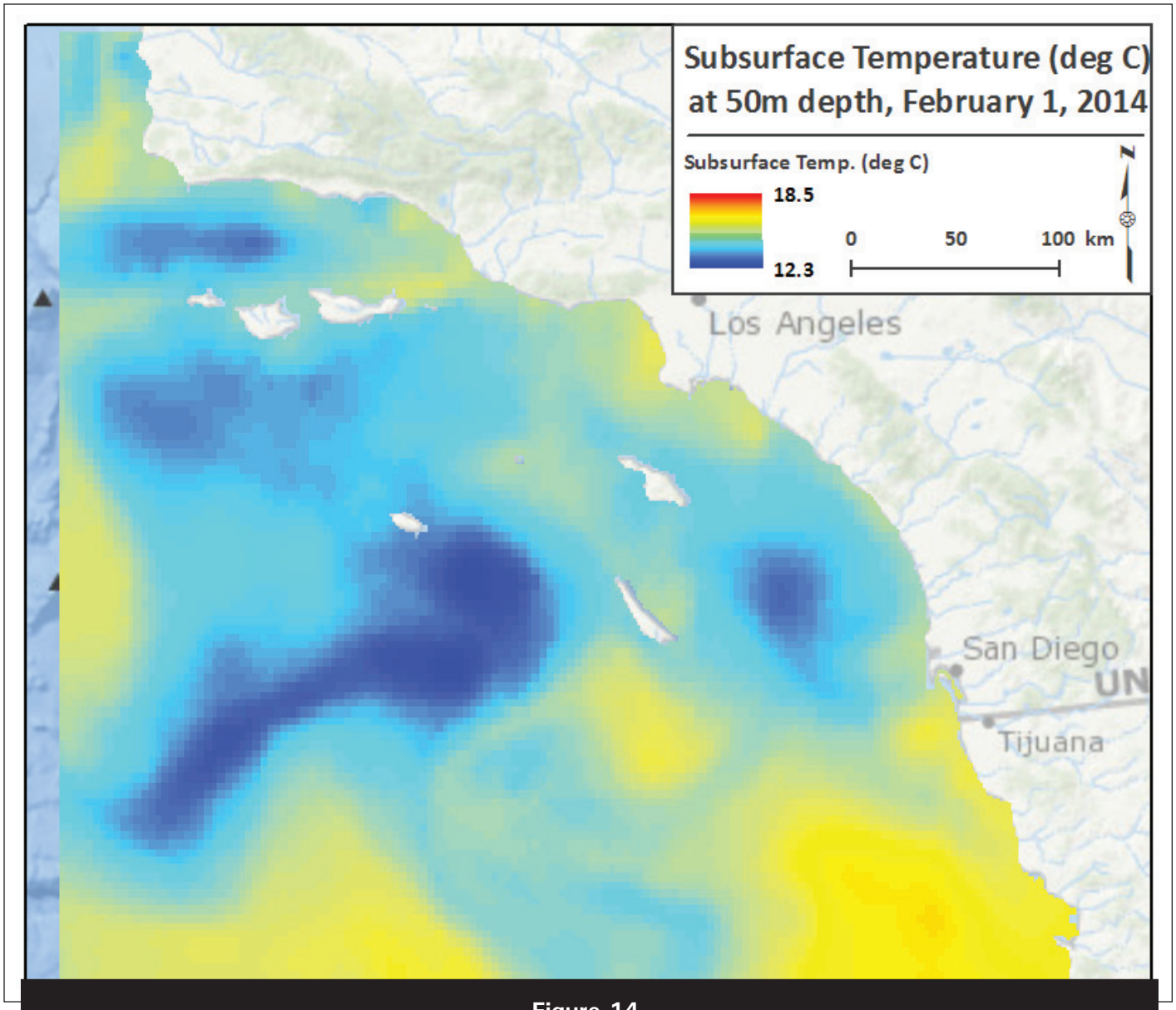

Figure 14.

HYCOM – Subsurface Temperature (50m), 3 kilometer spatial resolution.

are structured in the same fashion as the archived HF Radar products. Also in 2013, OI developed ability to deliver the currents in a format which would allow BioMap users to display the data on a 'Time Slider' within BioMap **(Figure 11)**. OI is waiting for word from EMTS staff as to when they would like to fully integrate this format into their system.

In October of 2013, OI initiated the delivery of HYCOM-derived raster image data products for BioMap display via our ArcGIS server. Several different image products are now generated on a daily basis: ocean salinity, mixed layer depth and subsurface temperature at 50 meters, 100 meters, 150 meters and 200 meters. All of the products are derived from the HYCOM model. The web service

packages for the mixed layer depth and salinity data contain all of the data produced since October of 2012 and are updated every Sunday at midnight. The web services for the subsurface temperature imagery are packaged up by month and also updated on the server every Sunday at midnight. These image products are delivered covering the entire Southern California Basin, however the BioMap user can zoom in to his/her local area to see more detail in the data. **Figures 12,13 and 14** show examples of these products.

At the present time, several of the legacy data products such as the MODIS true color imagery, RapidEye, Landsat TM7, Landsat TM8, AVHRR-SST, MODIS-SST and MODIS-Chlorophyll imagery are still only available via the OI password-protected web site (http://oceani.com/SanDiegoWater/). Discussions with EMTS staff in December of 2013 concluded that these data sets will remain only accessible via the web site until EMTS has finalized some improvements/changes presently being made to the BioMap system. OI will work to migrate some or all of these products to the ArcGIS server at that time if desired by EMTS and the International Boundary and Water Commission (IBWC).

Luostarinen, J. (2010). BioMap_summary_for_ESRI_RegUG_Feb_final_sent.doc.The City of San Diego Public Utilities Department's Environmental Monitoring and Technical Services (EMTS) Division. Received via email.

"HYCOM." HYCOM. N.p., n.d. Web. 05 Feb. 2014.